General Disclaimer

One or more of the Following Statements may affect this Document

- This document has been reproduced from the best copy furnished by the organizational source. It is being released in the interest of making available as much information as possible.

- This document may contain data, which exceeds the sheet parameters. It was furnished in this condition by the organizational source and is the best copy available.

- This document may contain tone-on-tone or color graphs, charts and/or pictures, which have been reproduced in black and white.

- This document is paginated as submitted by the original source.

- Portions of this document are not fully legible due to the historical nature of some of the material. However, it is the best reproduction available from the original submission.

GSC

GENERAL SOFTWARE CORPORATION

Sqt

GSC-TR8401

LANDSAT-4 HORIZON SCANNER

PERFORMANCE EVALUATION

Prepared for:

GOLDARD SPACE FLIGHT CENTER

By

Stephen Bilanow
Lily C. Chen
W. Minor Davis
John P. Stanley

Under

Contract No. NAS5-27664
Task No. 1

January, 1984

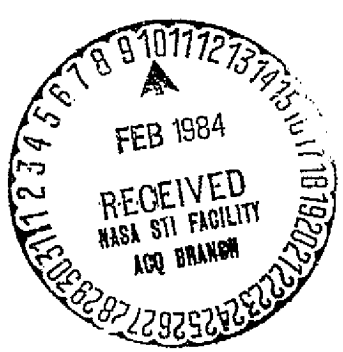

ABSTRACT

This document presents an analysis of the flight performance of a new design of horizon scanner flown on Landsat-4. The analysis is based on a study of representative data spans covering a little more than a year since the Landsat-4 launch. The salient features in the data are described and demonstrated by data plots. High frequency noise must be filtered out to achieve good accuracy, but this is effectively done by 128-point averaging. The effects of Earth oblateness and spacecraft altitude variations are modeled, and the residual systematic errors are analyzed. Most of the residual errors are apparently explained by the effects of Earth radiance variation, with the winter polar regions showing the highest variability in the attitude measurements due to winter stratosphere temperature variations. A model for the predicted radiance effects is compared with the flight data and deficiencies in the radiance effects modeling are noted. Correction coefficients are also provided for a finite Fourier series representation of the systematic errors in the data. An analysis of the seasonal dependence of the coefficients indicates the effects of some early mission problems with the reference attitudes which were computed by the onboard computer using star trackers and gyro data. The effects of sun and moon interference are discussed, and a few remaining unexplained anomolies in the data are noted. The sensor noise characteristics and their power spectrum are described and the variability of full orbit data averages are presented. A complete set of plots of the sensor data for all the available data spans is included in the Appendices.

TABLE OF CONTENTS

TABLE OF CONTENTS (CONTINUED)

LIST OF FIGURES

LIST OF FIGURES (CONTINUED)

LIST OF FIGURES (CONTINUED)

LIST OF TABLES

SECTION 1 - INTRODUCTION

1.1 PURPOSE AND DOCUMENT OVERVIEW

This document presents an analysis of the Landsat-4 horizon scanner flight performance. The Landsat-4 mission provides a unique opportunity to evaluate the flight performance because accurate reference attitudes are available from the Onboard Computer (OBC) which makes use of star tracker and gyro data. The Attitude Determination and Control Section (ADCS) at Goddard Space Flight Center (GSFC) is supporting this work with the goal of understanding the attitude accuracies obtainable from this latest generation horizon scanner. The Landsat-4 Project Office is also partially funding this work with particular interest in the results that may be used in the design and implementation of a backup control law utilizing corrected horizon scanner data. The initial planning for this scanner evaluation is provided in Reference 1 and the mathematical modeling of the scanner is given in Reference 2. Preliminary results on the scanner performance were provided in References 3 and 4 and this document updates and expands upon those results. In particular, a clearer picture of the systematic seasonal trends is presented with over a year of data now processed. Some early mission uncertainties in the reference attitudes are discussed with regards to their impact on the horizon sensor residual errors. More details of the Sun and moon interference effects are described. A detailed review of all of the currently available data spans was made and several unexplained anomolies in the measurements are noted. In addition, full orbit average variations are discussed as an indication of very low frequency noise.

This report reviews all the salient features in the data and discusses their known or probable causes. It also presents correction coefficients for the measurements based on fits to the systematic residual errors. Major topics discussed include the following.

- The effects due to Earth oblateness and orbit eccentricity
- Systematic effects due to seasonal radiance changes
- Correction coefficients and their seasonal dependence
- Analysis of the residual errors in the corrected measurements
- Sun and Moon interference effects and residual data anomolies
- Polar radiance variation and cold cloud effects
- The measurement noise characteristics and power spectrum
- Full orbit averages in the pitch and roll measurements

Section 1 of this report provides background information with regard to the mission and the scanner. It also provides an overview of the software used in the evaluation effort, and briefly describes the scanner modeling and nominal calibrations. Section 2 provides a summary of the data spans and an overview of the flight data characteristics. Section 3 describes the modeled systematic errors due to attitude perturbations, spacecraft altitude variations, and Earth oblateness effect. It also presents the residual errors in the data after these systematic errors are removed. These residual errors are then compared with the predicted systematic Earth radiance effects in Section 4. The radiance effects modeling deficiencies and the remaining residual error sources are discussed. Section 5 presents the Fourier series fits to the pitch and roll measurement errors for each data span. It also provides an analysis of the error sources indicated by the seasonal dependence of the correction coefficients. Section 6 discusses the Sun and Moon interferences, and other data anomolies. Section 7 dicusses the large scanner measurement variations in the winter polar region and the cold cloud effects on the scanner horizon measurements. Section 8 discusses the sensor noise characteristics and their power spectral densities. Section 9 discusses the variations in the full orbit averages which indicate a very low frequency noise. Finally, Section 10 summarizes the key results obtained in the current study.

1.2 MISSION OVERVIEW

Landsat is a program of the Office of Space and Science Applications managed by NASA Goddard Space Flight Center. The General Electric Company Space Division is the mission contractor responsible for Landsat-4 spacecraft design, integration and testing, as well as the design of the Data Management System, the Landsat Assessment System and the Operations Control Center.

The Landsat series of satellites provides multispectral imagery of the Earth's surface useful for Earth resources analysis. Landsat-4 is intended as a precursor to an operational system for global resource management. The improvements over previous Landsat spacecrafts include a higher data rate, a new more accurate sensor (the thematic mapper), and a more efficient operational ground support and-data management system.

The Landsat-4 spacecraft design is significantly different from the previous Landsats. Landsat-4 makes use of the Multimission Modular Spacecraft (MMS) design and the NASA Standard Onboard Computer (OBS) for spacecraft control and data handling. The MMS bus includes four momentum wheels, three electromagnetic coils, and three two-axis gyroscopes for 3-axis stability, orientation and momentum control. The MMS bus also includes two NASA standard star trackers, one fine sun sensor, and a 3-axis magnetome... for attitude determination.

Landsat-4 also has two Conical Earth Sensors for Earth direction determination. These sensors are used in control laws for the attitude acquisition sequence and used as backup attitude sensors by the analog "Safehold Electronics" to check for possible problems in the primary onboard attitude determination and control system. Plans are being made to develop a backup control law for the OBC which uses calibrated and corrected horizon scanner data rather than star tracker data.

Landsat-4 was launched on July 16, 1982. It flies in a sun synchronous, near polar, near circular orbit with about a 710 kilometer altitude. The orbit inclination is about 98.2 degrees. The orbit eccentricity is about 0.001, with about a 17 kilometer difference between apogee and perigee altitudes. Perigee always occurs near the maximum Northern latitude crossing. Periodic orbit adjust maneuvers maintain this orbit.

1.3 CONICAL SCANNER DESCRIPTION

This section briefly describes the horizon scanner design and its mounting geometry on the Landsat-4 spacecraft. A more detailed description of the scanner and its mathematical modeling is given in Reference 2. Specifications for the scanner are provided in References 5 and 6.

The instrument whose measurements are analyzed in this report is called a Conical Earth Sensor (CES) by its manufacturer, Ithaco Inc., and it is referred to as an Earth Sensor Assembly (ESA) by the mission contractor, General Electric. Conical scanner or horizon scanner are names commonly used for this type of sensor. This type of attitude sensor functions by sweeping a narrow field-of-view infrared detector in a conical path and detecting the Earth-in and Earth-out horizon crossings. One axis of the spacecraft orientation is measured by the width of the Earth scan. Another axis is measured by the phase of the scanner rotation at which the middle of the Earth scan is found.

The Landsat-4 CES design is significantly different from most previous horizon scanners flown by NASA. The changes were designed to achieve a higher accuracy than earlier models. The principal differences are a narrower spectral bandpass, a slower scan rate and a new horizon detection logic. A diagram of the CES is shown in Figure 1-1.

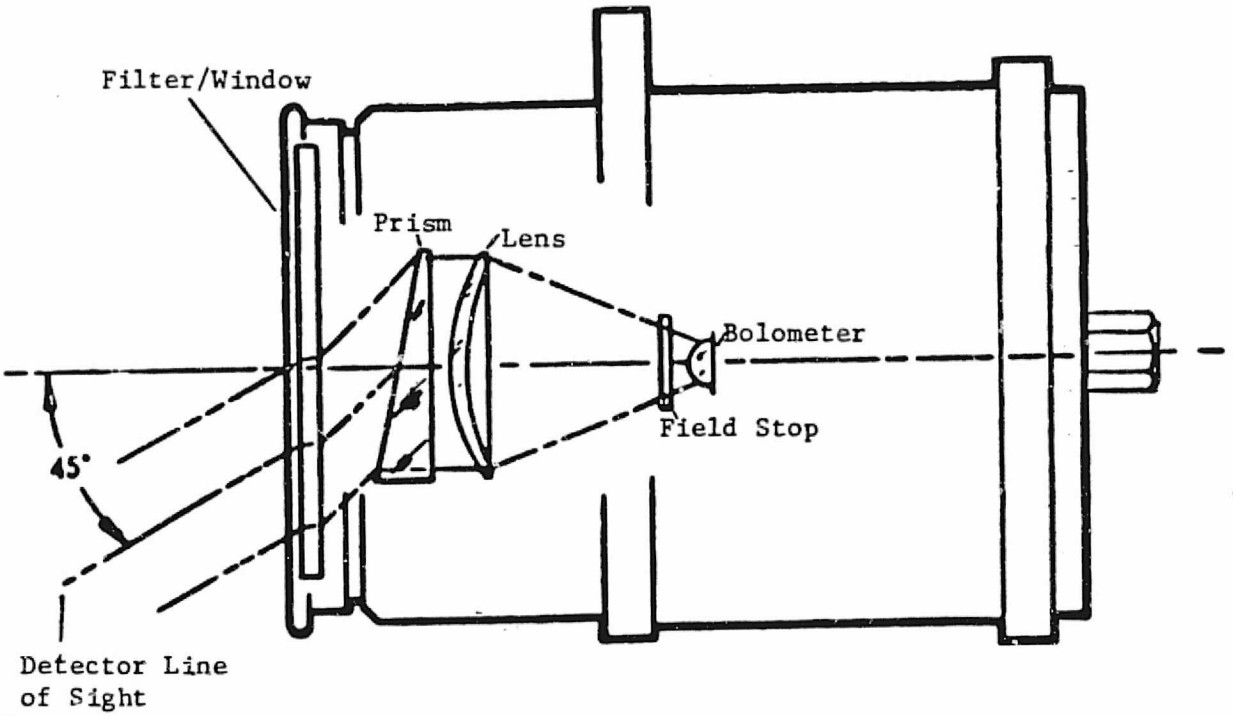

FIGURE 1-1. Diagram of the Earth Sensor Scanner Assembly (Adapted from Reference 5)

The spectral bandpass for Landsat-4 and several previous missions are compared in Figure 1-2. The narrower bandpass relative to previous missions reduces the scanner sensitivity to radiation outside the CO_2 absorption band and thereby reduces the sensitivity to lower atmosphere and surface temperature variations. Details of the Earth's infrared radiance are discussed in Section 4.1.

The spectral bandpass is achieved by an interference filter coated on the inside of the window which seals the unit, and is modified slightly by the transmission properties of the optics, which are made of germanium. The incoming radiation is focused by two lenses, with bolometer immersed in the second lens. The bolometer is a thermistor (thermally sensitive resistor) made of sintered oxides of manganese cobalt and zinc pressed into a thin flake.

Between the filter/window and the first lens is a prism which is designed to bend the incoming infrared radiation 45 degrees from the optic axis. The prism is rotated at 120 r.p.m. by a synchronously operated stepping motor to generate the scanning motion for the detector field of view.

Very high scan rates are common for horizon scanners because they are often built as an integral part of momentum wheels used for spacecraft control (e.g. the Ithaco Scanwheel which was flown on Seasat, Magsat, HCMM, SAGE, and earlier Landsats and the RCA Wheel Horizon Scanner flown on AE-C, D, E, and DE-B.) The relatively slower scan rate of the CES, 120 r.p.m., allows a better signal-to-noise ratio for the infrared detector and this makes more practical the horizon detection logic which uses the Earth signal derivative. Earth signal derivative horizon locator logics are more commonly found on spin stabilized geosynchronous satellites.

The Landsat-4 horizon detection signals are shown in Figure 1-3 and the horizon crossing determinations are illustrated in Figure 1-4. A

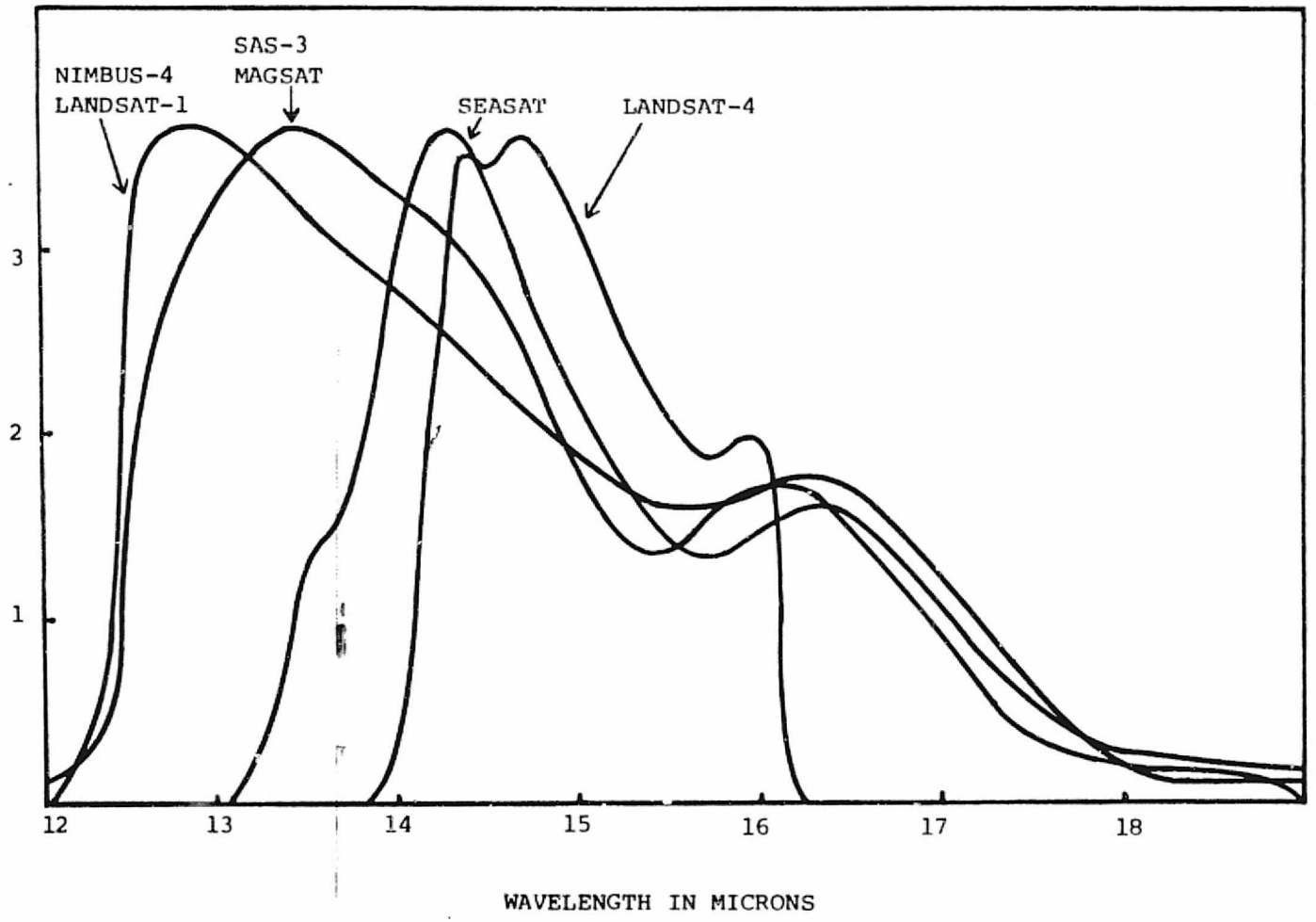

FIGURE 1-2. Comparison of Spectral Bandpass for Four Missions. Each curve is normalized to the same maximum height. The vertical scale has no significance.

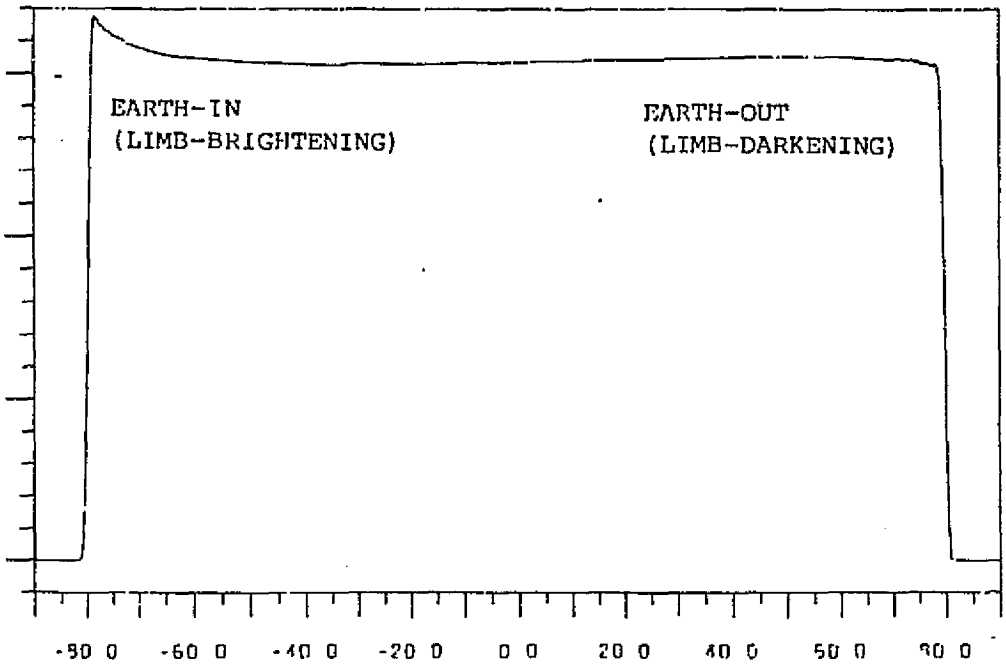

(a) Earth Radiance Input Signal vs. Scan Rotation Angle

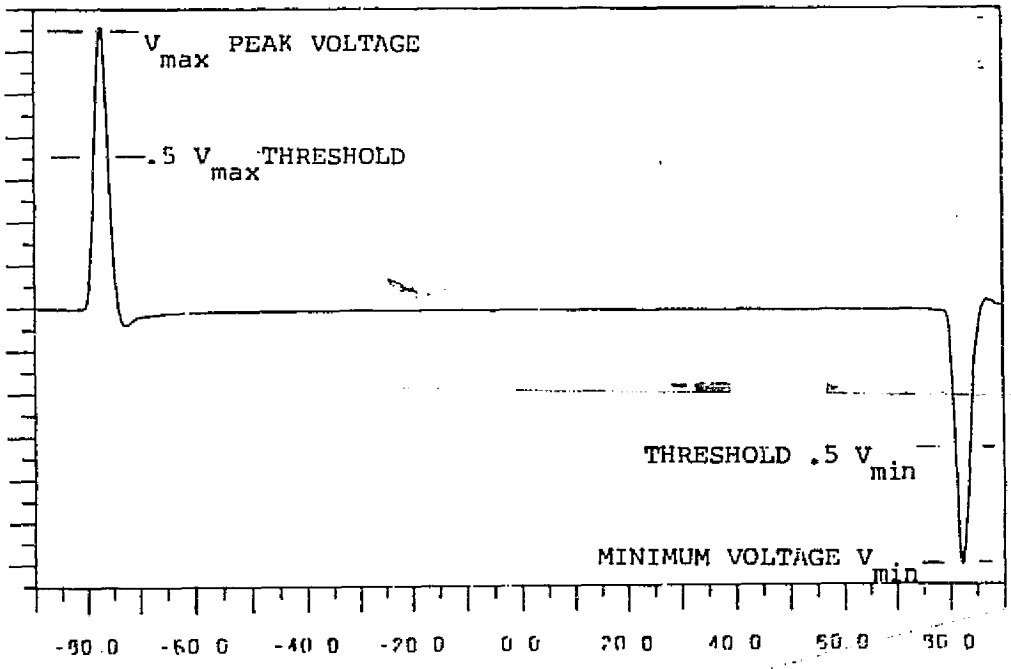

(b) Electronics Output Signal vs. Scan Rotation Angle

FIGURE 1-3. Simulation of Sensor Optical and Electronics Input/ Output Signals and Diagram of Threshold Levels

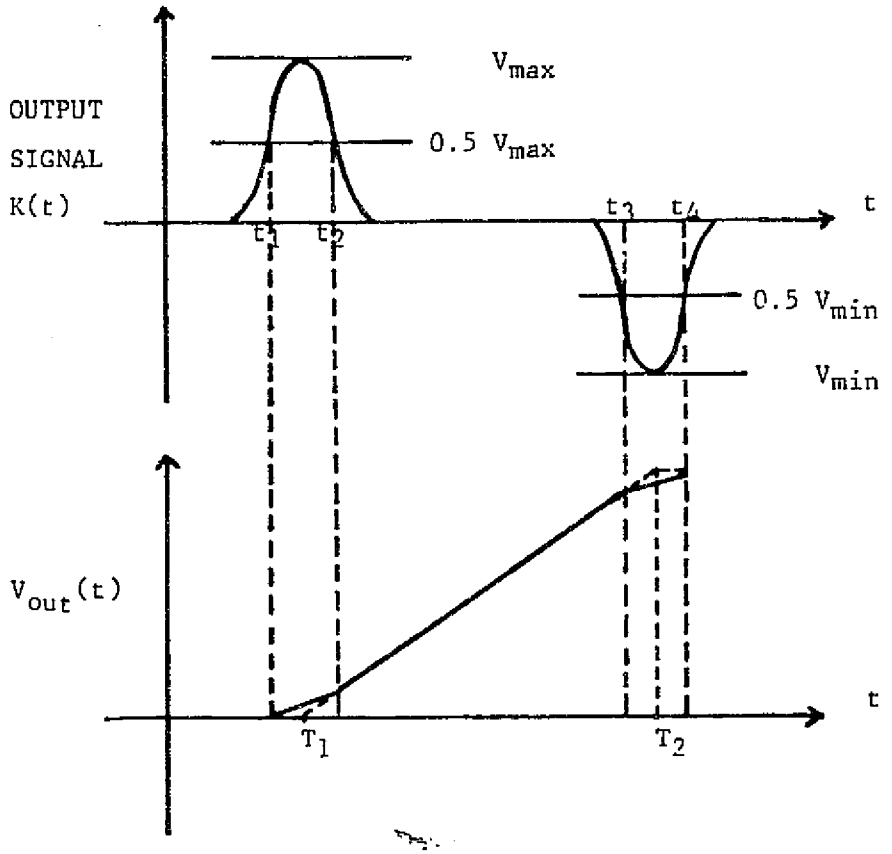

FIGURE 1-4. Conical Scanner E Voltage (Earth Width) Determination from the Bolometer Output Signal

sample of the incoming radiance signal as the scanner field-of-view sweeps across the Earth is shown in Figure 1-3(a). The sensor electronics process this signal to provide the voltage output shown in Figure 1-3(b). The electronics are effectively differentiating the filtered input signal to obtain the output voltage. Peak detectors are used to measure the amplitudes of the spikes in the output signal. Then threshold detectors set at half the peak voltages detect the times of these spikes. An anolog integrator measures the time span between the Earth-in and the Earth-out pulses. This integrator charges at half the normal rate while the threshold detectors are on, and thus the time between the middles of the two threshold detection periods is measured.

An analog sample and hold circuit stores this integrated voltage in an output buffer for each scan cycle. This is called the E channel or Earth width output. A second output voltage is computed which is proportional to the scanner rotation angle between a reference position and the middle of the Earth scan. This is called the H channel, or Earth phase output. Both of these voltages are stored in sample and hold circuits and are updated once each spin period, which is every 0.5 seconds. Under nominal geometry, the relationships between these voltages and the spacecraft pitch/roll angles are approximately linear.

Two Conical Scanners are onboard Landsat-4. The optic axis of Scanner 1, which is called the tail-side scanner, is oriented toward the negative spacecraft velocity direction tilting 24 degrees toward the Earth center. The axis of Scanner 2, which is called the right-side scanner, is mounted toward the negative orbit normal direction, also tilting 24 degrees toward the Earth center. With this mounting geometry, the attitude pitch component is measured by sensor 1 width and sensor 2 phase, and the attitude roll component is measured by sensor 1 phase and sensor 2 width. This relationship is shown in Table 1-1.

TABLE 1-1. Relationship Between Attitude Components and Earth Measurements

	Sensor 1	Sensor 2
Pitch	Width	Phase
Roll	Phase	Width

Figure 1-5 shows a diagram of the conical scanner ground tracks relative to the subsatellite point and flight path. This shows the path traced by the field of view over the surface of the Earth, assuming a nominal spacecraft altitude and attitude. Marks along the scan paths indicate one degree intervals of scanner rotation inside the horizon. Figure 1-6 shows the ground tracks of the scanner on the Earth at five minute intervals as the spacecraft moves around its orbit. These plots illustrate the horizon crossing geometry at various positions in the orbit.

1.4 EVALUATION SOFTWARE OVERVIEW

The software system developed for analyzing the Landsat-4 horizon scanner performance is called the Conical Scanner Evaluation System (CSES). The system consists of eight subsystems. Each subsystem performs distinct functions and they interface through several databases. The key features of the system are comprehensive modeling of predicted measurements to compare with the flight data and flexible data plotting and data fitting capabilities for analyzing the data and condensing large volumes of data to show the important orbit period systematic effects.

The structure and database interfaces of CSES are illustrated in Figure 1-7. The subsystems are indicated by boxes and the databases are indicated by either tape or disk dataset symbols. Detailed descriptions of CSES and its data bases are given in Reference 7. The purpose of each subsystem is described briefly in the paragraphs which follow.

Telemetry Reblocking Utility (TRU)

It was discovered that preprocessing of the telemetry data is necessary because of the way that data is written to tape by the

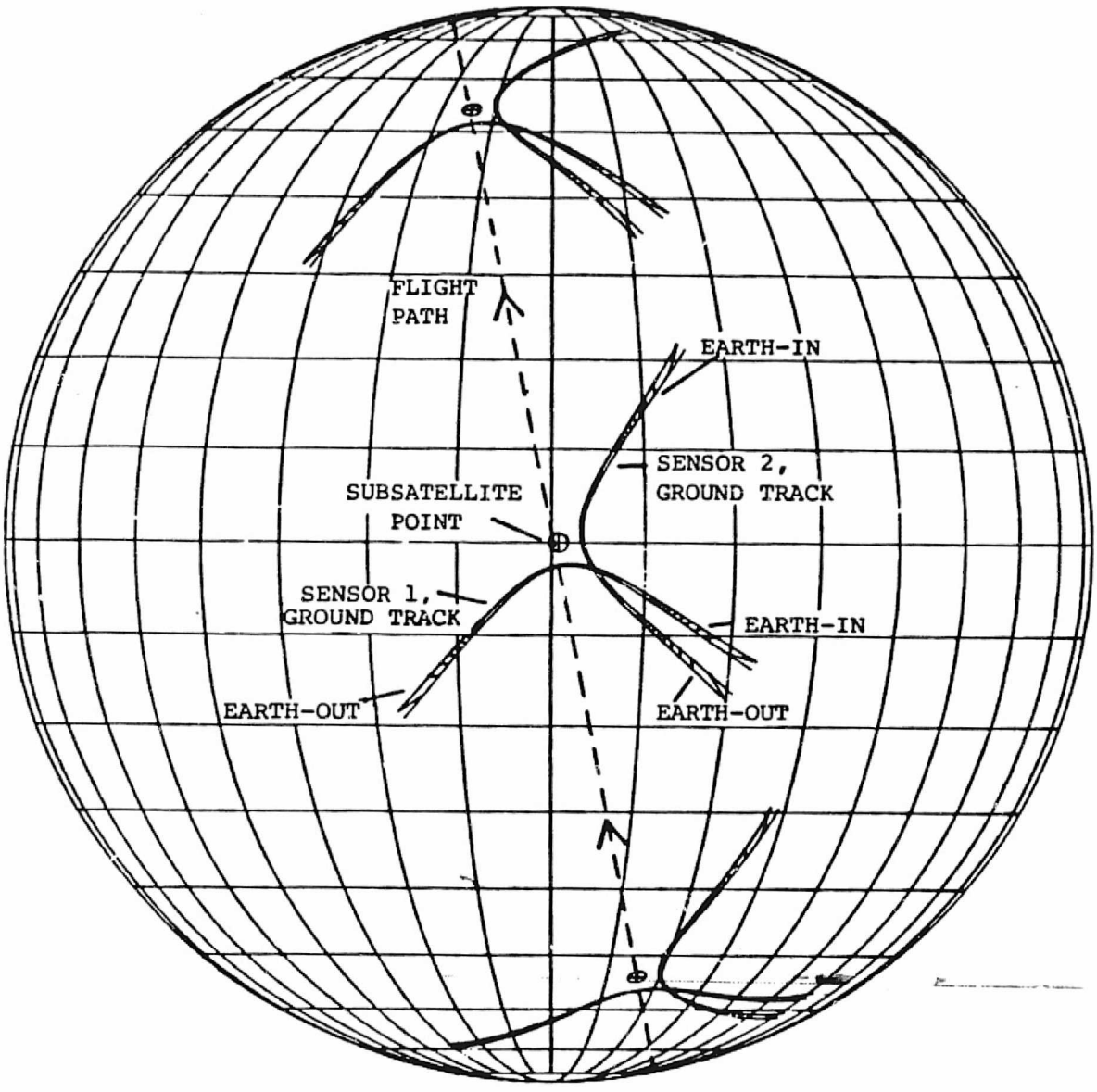

FIGURE 1-5. Scanner Ground Track

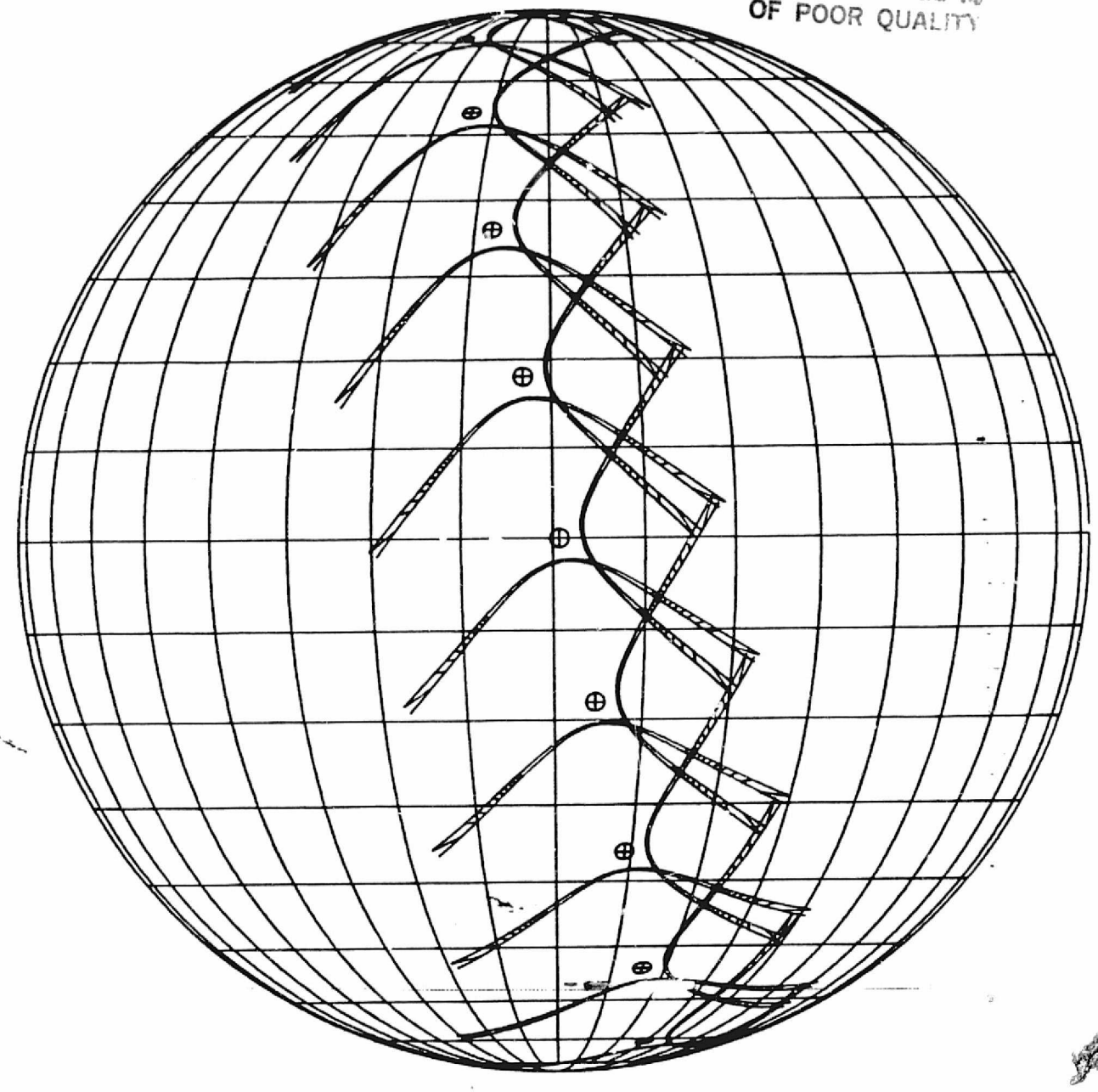

FIGURE 1-6. Landsat-4 Conical Scanner Ground Track on the Earth at 5 Minute Intervals; Ascending Node View (1 of 4)

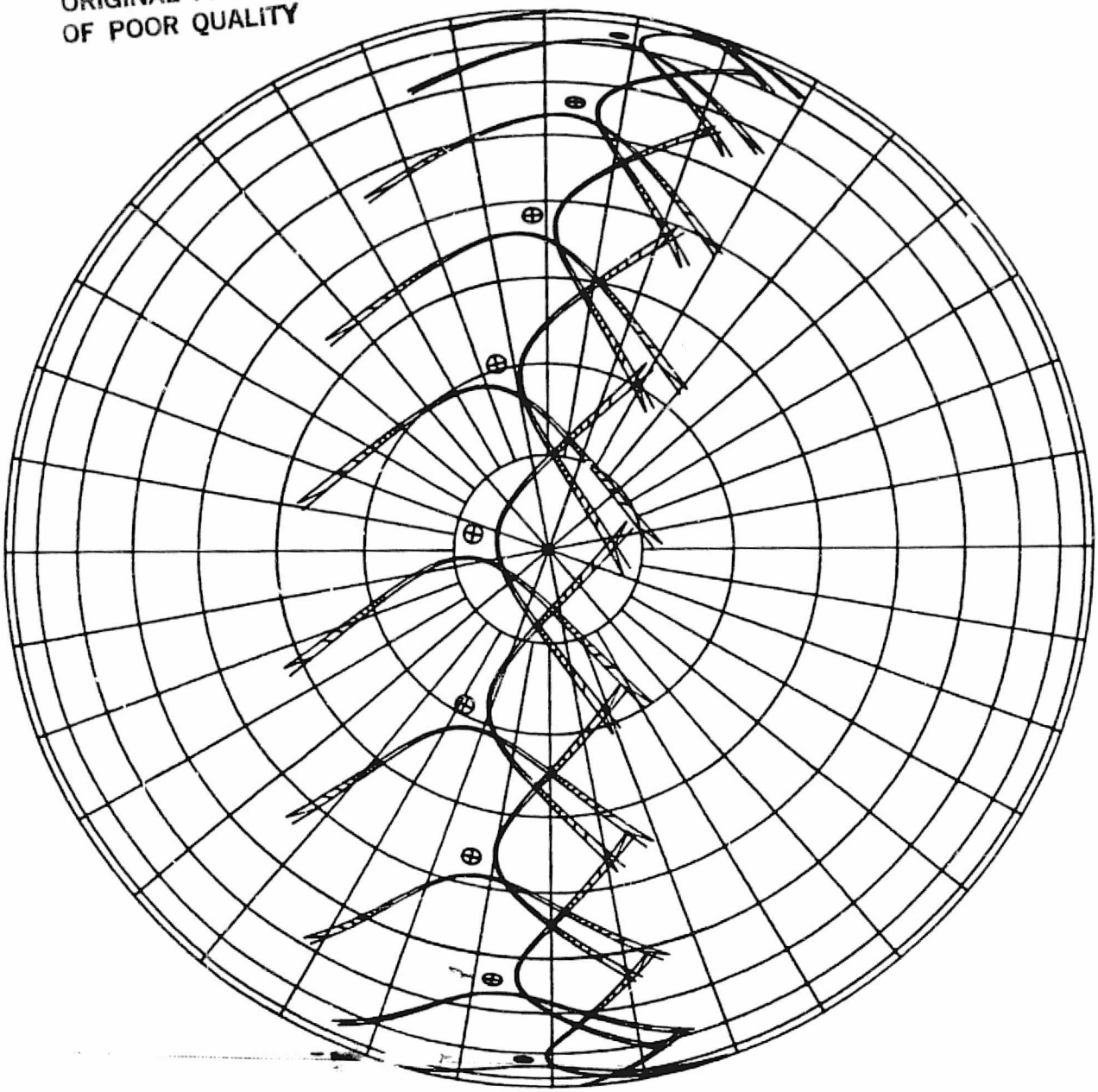

FIGURE 1-6. Landsat-4 Conical Scanner Ground Track on the Earth at 5 Minute Intervals, North Polar View (2 of 4)

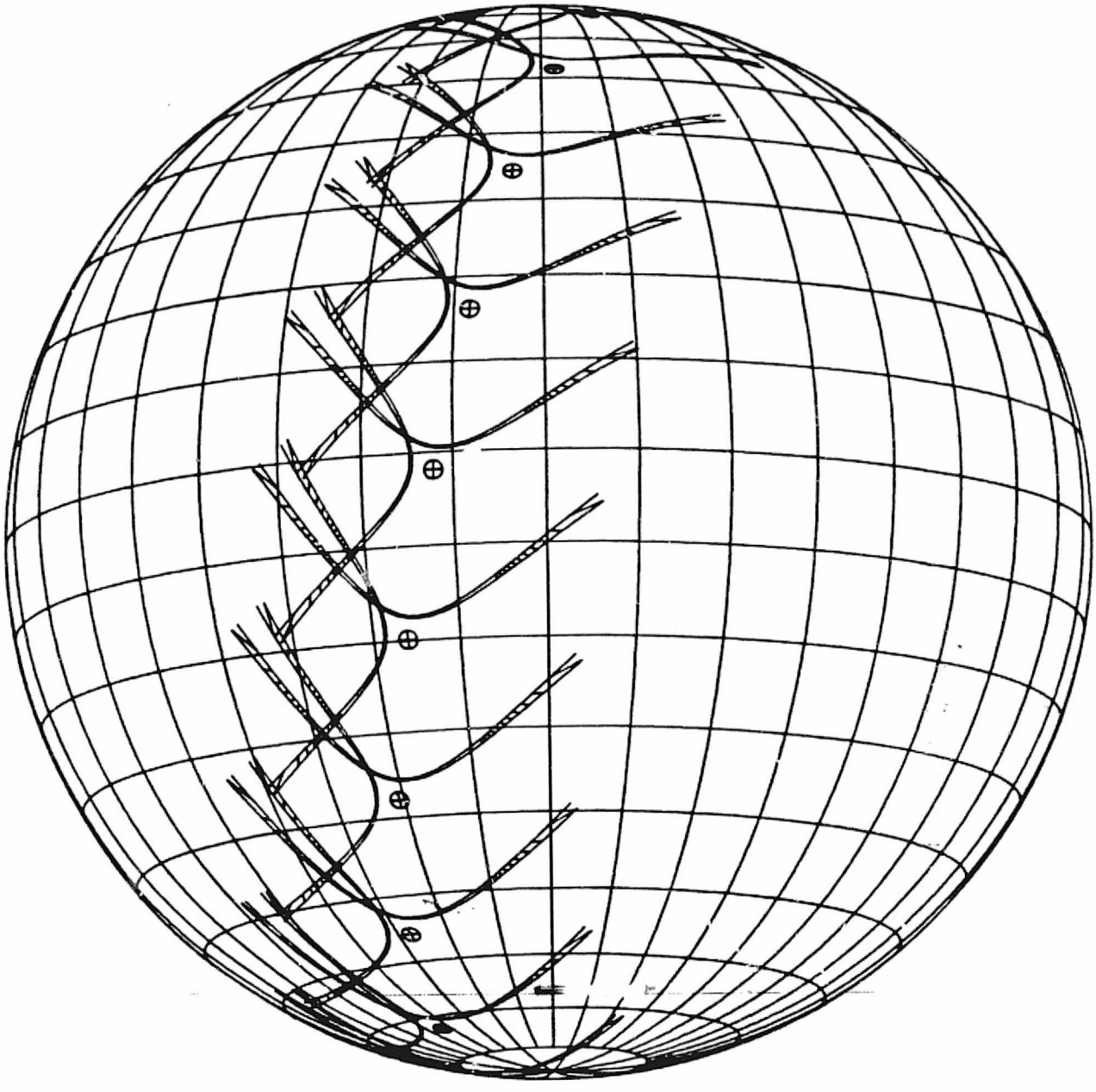

FIGURE 1-6. Landsat-4 Conical Scanner Ground Track on the Earth at 5 Minute Intervals, Descending Node View (3 of 4)

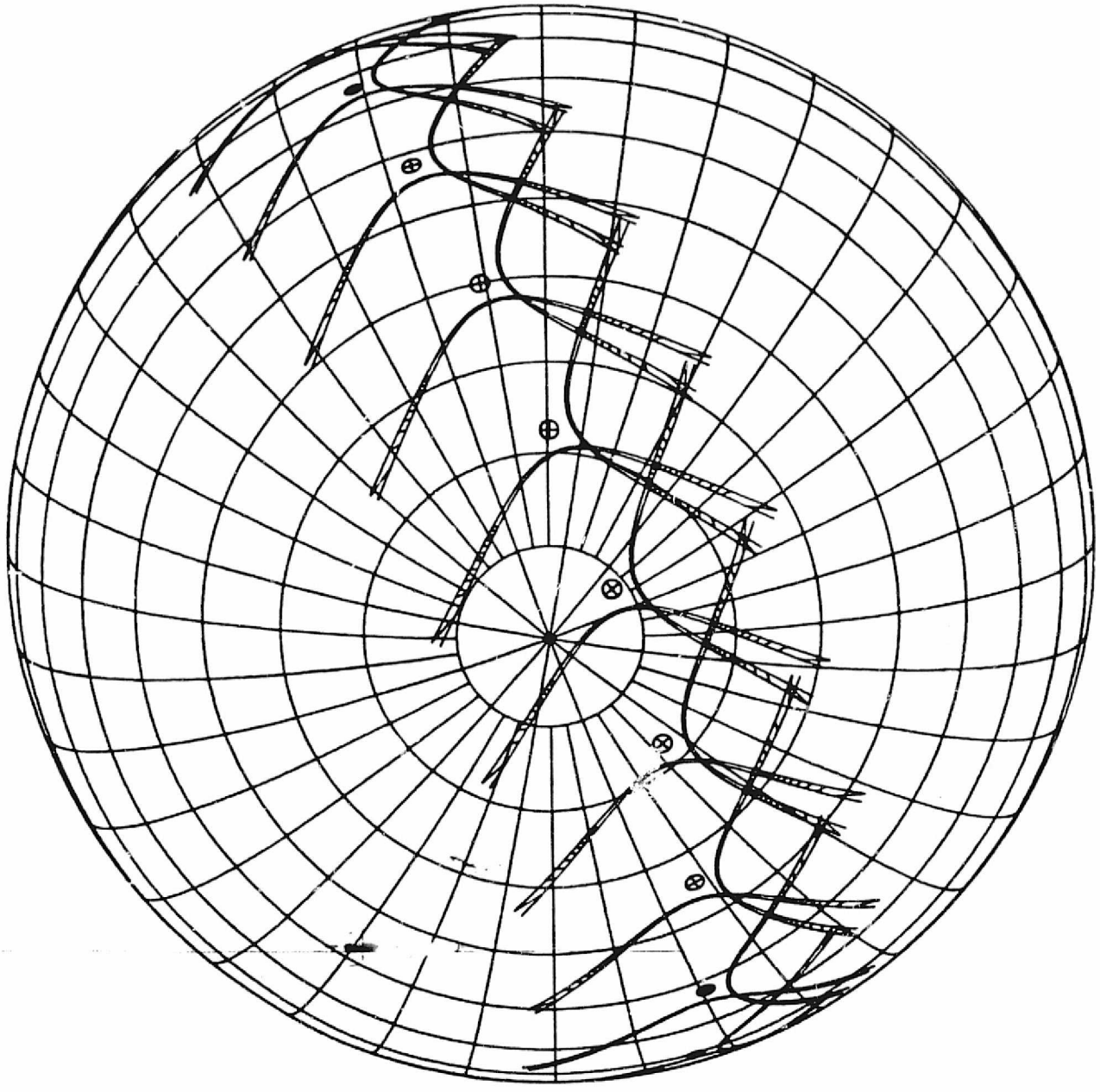

FIGURE 1-6. Landsat-4 Conical Scanner Ground Track on the Earth at 5 Minute Intervals, South Polar View (4 of 4)

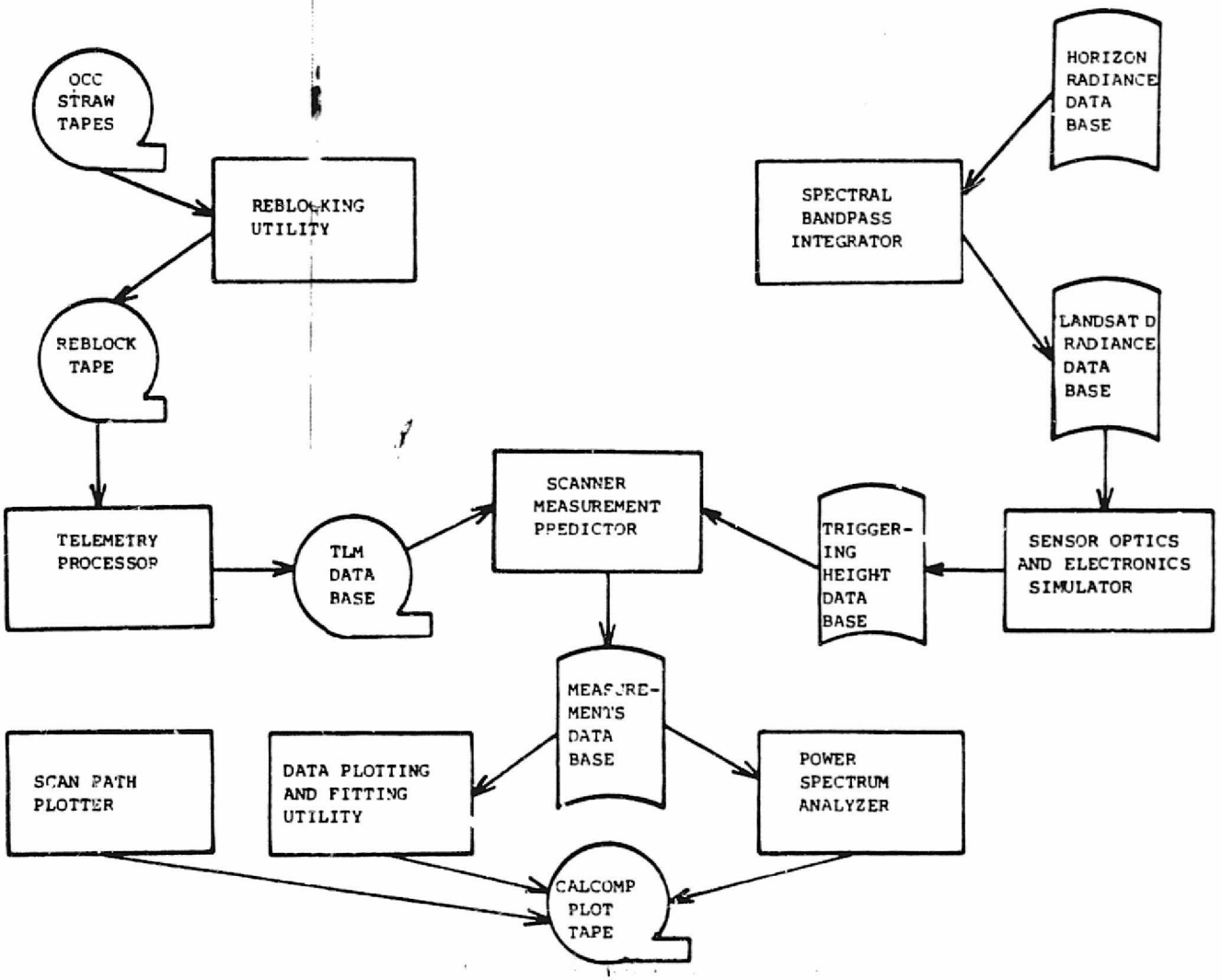

FIGURE 1-7. Conical Scanner Evaluation System (CSES) Relationship Between Subsystems and Data Bases

Landsat-4 Operations Control Center VAX 11/780 computer. When unpreprocessed data tapes are read by the IBM 360/95 it is found that each data block contains slightly less than one telemetry major frame, with the rest of the frame in the next block. The reblocking utility passes through the tape, and reblocks the data to one major frame per physical record so that it can be read by the telemetry processor. Both the received tape and the reblocked tape store the data in reverse time order, i.e., the first major frame of each data file on the tapes contains the end time in the data pass.

Telemetry Processor (TP)

The purpose of the Telemetry Processor is to extract from the raw mission format telemetry data those data words which are relevent to the Conical Scanner evaluation. The Telemetry Processor extracts this subset, which includes Conical Scanner sensor measurements, OBC attitudes, ephemeris, and timing information, from the spacecraft telemetry and stores it in the Telemetry Data Base.

Spectral Bandpass Integrator (SBI)

The Spectral Bandpass Integrator extracts Earth infrared radiance data from an existing data base called the Horizon Radiance Data Base (HRDB). The HRDB (Reference 12) contains Earth radiance data as a function of viewing angle, latitude, month, and wavelength. The Spectral Bandpass Integrator integrates the radiances over the specific spectral bandpass of the conical scanner. The resulting Earth radiance as seen by the scanner optics is stored in the Landsat-D Radiance Data Base. The radiance is retrieved from this data base for input to the Sensor Optics and Electronics Simulator.

Sensor Optics and Electronics Simulator (SOES)

The main function of the Sensor Optics and Electronics Simulator is to predict the Conical Scanner sensor reponses to seasonal, systematic variations in the Earth horizon radiance. This is done by first computing the radiance input signal as the scanner field-of-view sweeps across the Earth and then computing the electronics output signal using a linear model of the circuit response (Figure 1-3 illustrates sample data plots of these signals generated by the SOES). The horizon detection logic is then simulated to compute the horizon crossing position. The predicted responses are stored in the Triggering Heights Data Base (THDB) in the form of horizon triggering heights for both scanners at all orbit positions and seasons. The data are retrieved from the data base as needed for input to the Scanner Measurement Predictor (SMP). In addition, analysis of the sensor can be performed to study the sensitivity to various optics and electronics parameters.

Scanner Measurement Predictor (SMP)

The Scanner Measurement Predictor writes a Measurements Data Base (MDB) which contains the observed scanner measurements and the predicted scanner measurements (based on a detailed scanner and Earth model, and the spacecraft attitude and orbit), and a number of other key variables useful for correllation with the measurements. The other variables include the scanner temperatures, the reference attitudes, the spacecraft position in the orbit, and the horizon crossing latitudes. The SMP also has a "predicted-predicted" mode where it replaces the observed measurements with predicted measurements based on a second set of model parameters. This mode may be used to demonstrate the theoretical effects resulting from the adjustment of various model parameters.

Data Plotting and Fitting Utility (DPFU)

The Data Plotting and Fitting Utility produces Calcomp plots of selected data which is obtained from the Measurements Data Base (MDB). It computes polynomial and/or finite Fourier series fits to the data, and plots these fitting functions as well as residuals from the fits. It also computes statistics for the data and the fit residuals. The utility is designed so that any variable, which may be selected or computed from the MDB, can be plotted and/or fitted as a function of any other variable. The DPFU provides options for overlaying or stacking a series of plots. A special plot type called a serial stacked plot, can show several orbits of data stacked sequentially in order to clearly show variations from one orbit to the next.

These options provide a great deal of flexibility for analyzing and displaying various features in the data, particularly the orbit period effects. Definitions of the specific data variables that can be plotted and fit by the DPFU, and their plot label titles, are listed in Appendix A of Reference 3.

In addition, a number of routines utilized by the DPFU data fit processing were extracted for use in a separate utility in order to allow data fitting and plotting of namelist input data. The plotting capabilities in this utility includes both printer plots from an existing subroutine name GRAPH and Calcomp plots from a general plotting subroutine named GRAPHC, which was developed from the DPFU plotting subroutines. This utility was used to produce the plots of the pitch and roll fit coefficients and residual statistics of Section 5.

Scan Path Plotter (SPP)

The Scan Path Plotter plots the path of the scanner field-of-view across the Earth's surface. Sample plots from this utility were shown

in Figures 1-5 and 1-6. The scan path plot helps to provide a general understanding of the scan geometry. The plots can be overlaid on Geostationary Operational Environmental Satellite (GOES) Earth photographs to show the scan geometry in relation to meteorological conditions.

Power Spectrum Analyzer (PSA)

The Power Spectrum Analyzer obtains the autocorrelation function and power spectral density of the scanner measurements which are contained in the MDB. A data fit can be subtracted from the data to take out the general trend in the measurements, leaving the noise component to be analyzed. The spectrum is then obtained by taking a discrete Fourier transform of the mean lagged product or autocorrelation function estimate. A spectral window may be optionally applied to the autocorrelation function. The Power Spectrum Analyzer provides printouts and plots of the input time series, the autocorrelation function, and the power spectral density. The plots are made using the Wolf Plotting and Contouring Package.

1.5 SPACECRAFT TELEMETRY AND NOMINAL CALIBRATIONS

The spacecraft telemetry information retrieved by the CSES Telemetry Processor is summarized in Table 1-2.

The width and phase measurements are sent down once every 0.128 seconds as E-voltage and H-voltage counts respectively. The nominal conversions from counts to the pitch and roll angles and to the Earth width and phase angles are given in Table 1-3. The counts are obtained by an Analog-to-Digital converter in the Remote Interface Unit (RIU) onboard Landsat-4. A conversion factor of 50 counts per volt is employed by the RIU. The conversions between the voltages and the pitch/roll angles were calibrated by ground bench tests. The nominal calibration is 0.5 volts per degree. The conversions between the

TABLE 1-2. Telemetry Measurements Retrieved by CSES

Measurement	Sensor ID	Data Rate* (Sec)
Width (Pitch)	1	0.128
Width (Roll)	2	0.128
Phase (Roll)	1	0.128
Phase (Pitch)	2	0.128
Bolometer Temperature	1	16.384
Bolometer Temperature	2	16.384
Electronics Temperature	1	16.384
Electronics Temperature	2	16.384
OBC Attitude:		
Quaternion	N/A	4.096
OBC Ephemeris:		
Position Vector	N/A	4.096
Velocity Vector	N/A	4.096
Signal Status	1	0.128
Signal Status	2	0.128
Sensor Status	1	4.096
Sensor Status	2	4.096
DPU Time	N/A	16.384
Flight Software Times	N/A	4.096

* 1 major frame = 16.384 sec.
1 minor frame = 0.128 sec.

TABLE 1-3. Nominal Calibrations for Conical Scanner Measurements

Measurements	Sensor	Related Attitude Angle (Deg)	Nominal Calibration	Related Earth Angle (Deg)	Nominal Calibration
E-Voltage Count (C_E)	1	Pitch p	$p = 0.04\ C_E - 5.00$	Earth Width (Ω)	$\Omega = \frac{p}{0.539} + 155.64$
	2	Roll r	$r = 0.04\ C_E - 5.00$	Earth Width (Ω)	$\Omega = \frac{r}{0.539} + 155.64$
H-Voltage Count (C_H)	1	Roll r	$r = 0.04\ C_H - 5.00$	Earth Phase (Φ)	$\Phi = \frac{r}{0.914}$
	2	Pitch p	$p = 0.04\ C_H - 5.00$	Earth Phase (Φ)	$\Phi = \frac{-p}{0.914}$

pitch/roll and the Earth width/phase measurements are derived theoretically using linear approximations (Reference 2), assuming a circular orbit of 7086 km in radius, a spherical Earth of 6378.14 km in radius, and a constant horizon triggering height of 40 km. The error due to the non-linearity between the Earth measurements and the pitch/roll angles is negligibly small for the nominal range of attitude variations. However, the assumptions of circular orbit, spherical Earth, and constant horizon triggering height constitute the main sources of systematic errors in the attitude determination using Conical Scanner data. This is discussed in detail in the following sections of the document.

Note that the definition of Earth phase adapted for this document is a right hand rotation about the sensor boresight from the scanner reference axis (the nominal Earth direction at zero pitch, roll, yaw) to the mid point of the Earth scan. Reference 2 actually defines the phase in terms of the spin sense of the scanner but errorneously assumed the spin axis to be along the boresight whereas the spin vector is actually opposite the boresight 135 degrees from the scan cone. This spin sense definition of the phase can be adapted (as it currently is internally in the CSES software) by changing the sign of phase to pitch or roll conversion factors.

The bolometer and electronics temperatures are measured every 16.384 seconds. The conversion from the temperature counts to degrees centigrade is done by the fifth order polynomial defined below (Reference 8).

$$\begin{aligned} \text{Temperature} = {} & 164.4 - .47777\ C \\ & + .08178\ C^2 - .0007119\ C^3 \\ & + .000002888\ C^4 - .000000004401\ C^5 \end{aligned}$$

where C is the telemetry counts. A plot of this relation is shown in Figure 1-8. The bolometer temperatures are measured by thermistors

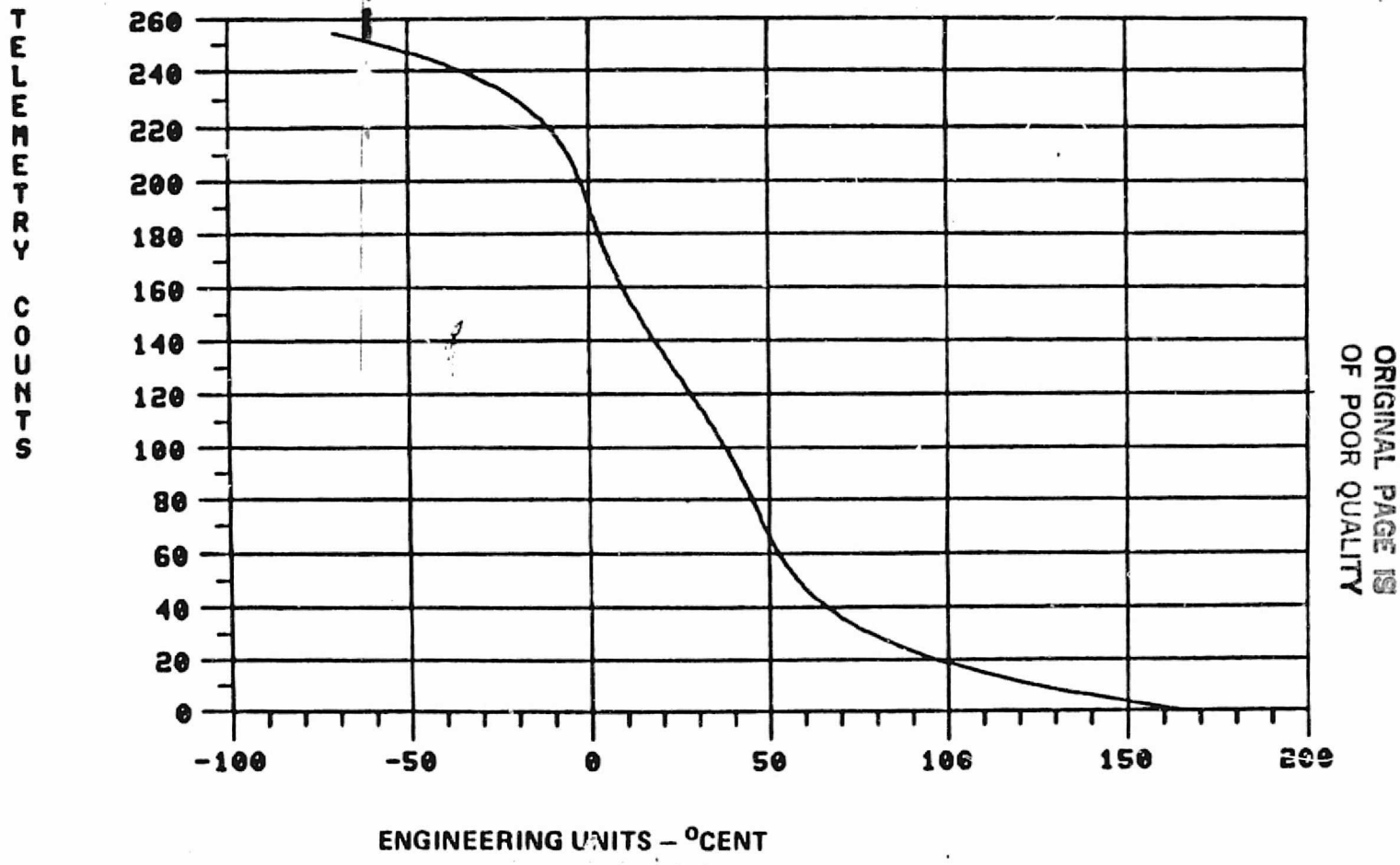

FIGURE 1-8. Conversion from Temperature Counts to Degree Centigrade
(Adapted from Reference 8)

located in the Conical Earth Sensor assembly. The temperature information is retrieved in order to identify possible temperature dependent errors in the sensor measurements.

The OBC attitude is sent down through the quaternion representation. The OBC also provides spacecraft position and velocity vectors. The OBC attitude and ephemeris information is updated every 4.096 seconds. The attitude is computed by the OBC using star tracker and gyro data. These attitudes are the reference attitudes used in analyzing and calibrating the Conical Scanner measurements in this study.

The OBC ephemeris information retrieved by the TP is used in the Scanner Measurements Predictor to locate the spacecraft positions in the orbit. The Flight Software times provide the reference times for the attitude and ephemeris information.

The signal and sensor status voltages are retrieved from the telemetry to identify any failure condition of the scanners. The signal status is updated once every 0.128 seconds and the sensor status is updated once every 4.096 seconds.

SECTION 2 - DATA CHARACTERISTICS OVERVIEW

This section summarizes the data spans used in this analysis, describes the general characteristics of the relevant Landsat-4 flight data, and serves as an introduction to the subsequent sections which discuss various aspects of the data in detail.

In this and subsequent sections all data plots are in units of degrees unless otherwise stated.

2.1 DATA SPAN SUMMARY

Data spans of about 24 hours duration were acquired at approximately two week intervals in order to accomplish this survey of the Landsat-4 scanner performance. This data volume was chosen to adequately represent the orbit to orbit changes over the course of a day, and demonstrate the seasonal variations over the course of the year. The data spans processed for this report span 13 1/2 months from August 1982 through September 1983. Additional data is being accumulated and will be used to update these results at a later date.

Table 2-1 provides a summary of all the data spans processed for this analysis. This table includes the start time and duration of each span, a list of the data gaps which are over ten minutes duration, and a count of the number of major frames which were rejected because they contained some flagged data.

Table 2-2 contains a summary of special features encountered in the available data spans. Each of these features are discussed later in the report. The Sun and moon interference and other scanner data anomolies are discussed in Section 7. The reference attitude anomolies are discussed in the next subsection.

TABLE 2-1. Summary of Data Spans

DATA PASS NO.	DATA SPAN			DATA GAPS OVER 10 MINUTES			NUMBER OF MAJOR FRAMES REJECTED
	Start Date YY-MM-DD	Time HH:MM	Duration HH:MM	Date MM-DD	Time HH:MM	Duration HH:MM	
1	82-08-10	21:54	22:38	08-11	09:03	00:29	53
				08-11	14:50	00:21	
2	82-08-25	01:08	26:17	08-25	02:38	02:12	31
				08-25	09:35	02:40	
3	82-09-08	04:33	24:45	09-08	12:30	00:12	467
				09-08	23:05	02:01	
				09-09	01:40	01:39	
4	82-09-22	00:33	25:27	09-22	06:07	00:19	39
				09-22	08:13	01:56	
				09-22	20:08	03:34	
5	82-10-05	15:31	25:13	10-06	03:16	01:12	135
				10-06	06:47	01:58	
6	82-10-20	05:12	24:43	10-30	20:23	05:32	80
7	82-11-02	23:07	23:58	11-02	07:12	01:58	52
8	82-11-16	06:33	24:51	(NO GAPS)			11
9	82-12-01	00:28	26:43	12-01	15:27	00:59	52
10	82-12-14	12:25	26:21	12-14	14:03	00:53	13
				12-14	20:42	04:25	
11	82-12-28	05:32	24:42	12-28	12:26	00:11	156
				12-28	14:13	02:04	
12	83-01-19	06:36	29:30	01-19	10:19	01:38	39
				01-19	13:39	01:15	
13	83-02-02	03:24	26:25	02-02	08:54	00:37	33
				02-02	21:23	00:14	
14	83-02-17	00:01	30:54	02-17	05:15	00:34	56
15	83-03-03	02:57	24:46	(NO GAPS)			51
16	83-03-14	13:45	27:17	03-14	19:20	01:46	56
17	83-03-29	23:54	24:45	(NO GAPS)			54
18	83-04-14	00:34	27:44	(NO GAPS)			16
19	83-04-26	02:04	25:03	(NO GAPS)			7
20	83-05-11	00:15	26:07	(NO GAPS)			11
21	83-05-23	00:39	27:45	05-23	20:26	00:45	12
22	83-06-06	00:23	26:37	(NO GAPS)			30
23	83-06-21	22:59	26:23	06-22	00:41	01:16	19
24	83-07-06	15:48	26:41	07-07	20:56	01:19	36
				07-07	06:38	01:20	
25	83-07-26	00:40	29:32	(NO GAPS)			8
26	83-08-06	13:45	28:00	(NO GAPS)			45
27	83-08-31	00:14	27:57	09-01	00:47	01:16	10
28	83-09-14	00:27	29:32	09-14	04:24	00:12	27

TABLE 2-2. Notes on Data Span Special Features

PASS NUMBER	START DATE	NOTES ON SPECIAL FEATURES
1	82-08-10	
2	8-25	
3	9-08	
4	9-22	Earth acquisition mode during first 70 minutes.
5	10-05	
6	10-20	
7	11-02	Moon interference in Sensor 2 on first 3 orbits. Two bad data points in the reference attitude.
8	11-16	
9	12-01	Moon interference in both sensors.
10	12-14	
11	12-28	
12	83-01-19	Sun interference in Sensor 1.
13	2-02	Sun interference in Sensor 1.
14	2-17	Sun interference in Sensor 1. Anomolous correlated noise in both pitch channels for 2 short periods (less than 15 minutes each). One bad data point in the reference ephemeris.
15	3-03	Sun interference in Sensor 1.
16	3-14	Anomolous noise in each pitch channel for separate 5 minute periods.
17	3-29	Moon interference in Sensor 2 on first 5 orbits.
18	4-14	Anomolous noise level in both pitch channels for about 40 minutes.
19	4-26	
20	5-11	
21	5-23	
22	6-06	
23	6-21	
24	7-06	
25	7-26	Earth acquisition mode during first 30 minutes. Moon interference in both sensors.
26	8-06	Two anomolous attitude excursions for 8 minute periods with poor reference attitudes during excursions.
27	8-31	
28	9-14	Moon interference in sensor 1 on last 3 orbits.

2.2 REFERENCE ATTITUDE

The available data spans were selected from periods when the spacecraft maintained a good reference attitude under control of the OBC. The OBC was generally using the star trackers and gyros to provide the reference attitude. For many of the data spans, only one star tracker was in use, but this did not degrade the system accuracy (in fact the one tracker was chosen to improve the accuracy when relative alignment errors between the trackers were recognized as causing less stability in the gyro drift rate estimates). Two of the available data spans, June 22 and July 26, come from periods when the spacecraft was under control using only the fine sun sensor and gyros, however the accuracy of the control for these data spans is believed to be very good.

Early in the Landsat-4 mission some problems were recognized in the OBC reference attitudes. The key symptom was orbit period variations in the star tracker residuals (differences between the observed and expected star positions) of about 220 arc seconds (0.06 degrees) amplitude. Several contributing error sources were located and the problem in the residuals was finally eliminated on February 15, 1983. The OBC reference attitude problems and their resolution are discussed in Reference 9. Reference 9 does not provide complete information on the direction or amplitude of the attitude errors vs. time. The apparent effect of the reference attitude problems based on analysis of the horizon scanner residual errors is discussed in Section 5.3.

For the data after February 15, the accuracy of the reference attitude was estimated to be about 8 arc seconds or 0.00225 degrees (Reference 9). Some questions may still exist about the reference attitude, but their accuracy is generally believed to be better than 36 seconds or 0.01 degrees.

Figure 2-1 shows the downlinked reference attitudes and spacecraft altitude above a spherical model Earth as a function of time for four orbits on November 3, 1982. The attitudes are in degrees and the altitudes are in kilometers. Figure 2-2 shows the same data plotted as a function of orbit phase from the ascending node. In these plots the four orbits are overlayed on top of each other. These plots demonstrate the consistency of the spacecraft attitude over several orbits.

The spacecraft is in precision Earth pointing mode, and the attitude stays very close to zero pitch/roll/yaw except for two brief excursions each orbit in roll and yaw. These disturbances are due to the reorientation of the solar panels which occur when the satellite enters or leaves the Earth's shadow. The amplitude of the attitude excursion is about 0.05 degrees. Otherwise the attitude variation is generally less than 0.02 degrees peak-to-peak and is within $\pm$ .02 degrees of zero pitch/roll/yaw. This same general pattern is seen in the reference attitudes in all the data which is included in the report with the exceptions discussed below. Appendix A provides a complete set of plots of the reference attitudes for the data spans used in this analysis effort.

Generally the spacecraft was in precision Earth pointing mode (flags MODE=4 and ICAL=3 in the OBC ACS telemetry report) for all the data spans. This control mode maintains the spacecraft at zero pitch-roll-yaw as illustrated in Figures 2-1 and 2-2. However two data passes, on 9/22/82 and 7/26/83, were received with the spacecraft in Earth acquisition mode at the beginning of the data spans (ICAL=2). Though the spacecraft was in Earth acquisition mode, the reference attitudes appear to be accurate before the Earth pointing mode is initiated (70 minutes after the start of the data span on 9/22/82 and 30 minutes after the start of the data span on 7/26/83).

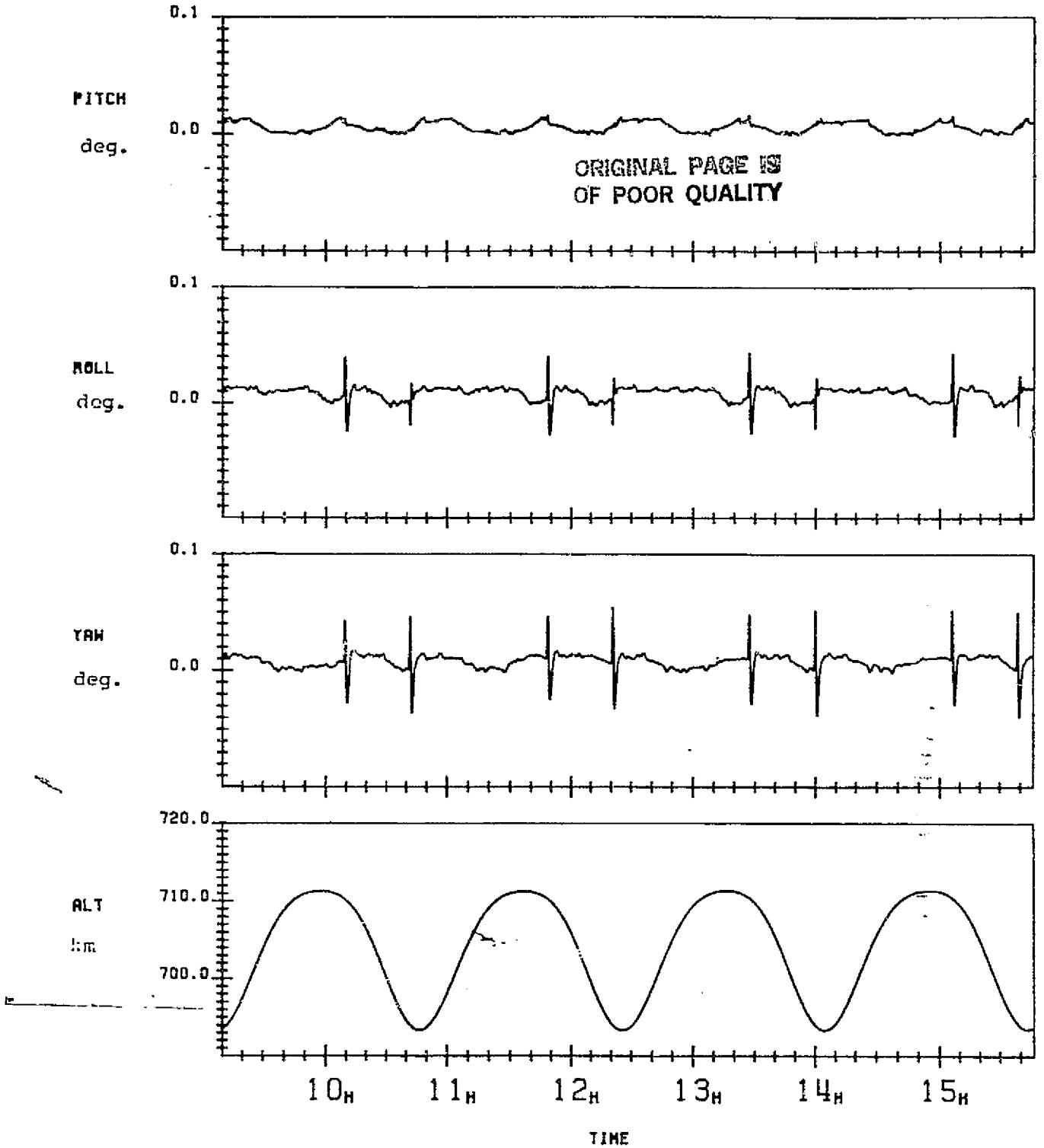

FIGURE 2-1. Landsat-4 On Board Computer Attitudes and Altitudes Above Earth Equatorial Radius as a Function of Time for Four Orbits

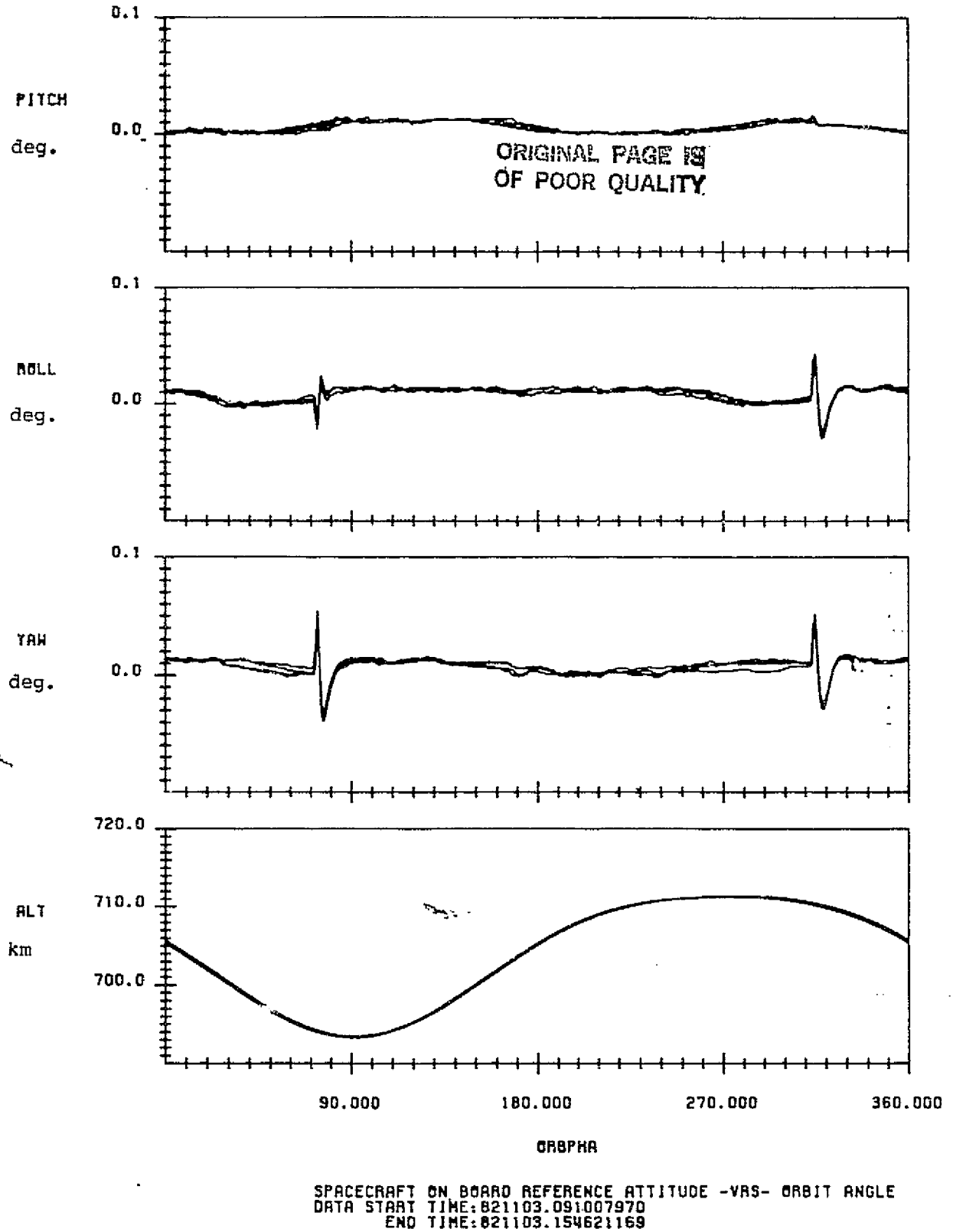

FIGURE 2-2. Landsat-4 On Board Computer Attitudes and Altitude Above Earth Equatorial Radius as a Function of Orbit Phase Angle from the Ascending Node

Many of the data spans show brief small excursions in pitch, roll, or yaw, always less than about 0.1 degrees amplitude. Small spikelike excusions of less than 0.03 degrees amplitude appear to become more frequent after April 1983. Two very large excursions greater than 0.1^{o} appear on August 7, 1983 in the pitch, roll and yaw measurements, and seem to indicate temporary losses of the reference attitude. A few other possible anomolies in the reference attitude indicated by the scanner data are discussed in Section 6.3.

A few spikes in the reference attitude data are due to spurious data in the attitude or ephemeris telemetry. Two spikes that can be seen in the reference attitudes on December 1 and one spike on February 17 are simply due to bad data points which were not rejected in the data processing.

2.3 SPACECRAFT EPHEMERIS

The Landsat-4 onboard ephemeris is computed in the OBC from the coefficients of a Fourier series which is uplinked daily from the ground. The peak position errors of the onboard ephemeris are generally less than a kilometer and practically always less than 2 kilometers, with the largest errors being along the satellite track. The radial and cross-track position errors are generally much less than 100 meters.

Figure 2-3 shows the downlinked spacecraft altitude as a function of orbit phase from the ascending node computed in two different ways. Figure 2-3(a) is the altitude computed above a spherical Earth with a radius of 6378.14 kilometers. This plot shows the spacecraft altitude variations which are due to the orbit eccentricity. Figure 2-3(b) shows the spacecraft altitude above the oblate Earth. It uses the standard oblate Earth model, which is an ellipsoid with a polar radius of 6356.76 km and an equatorial radius of 6378.14 km.

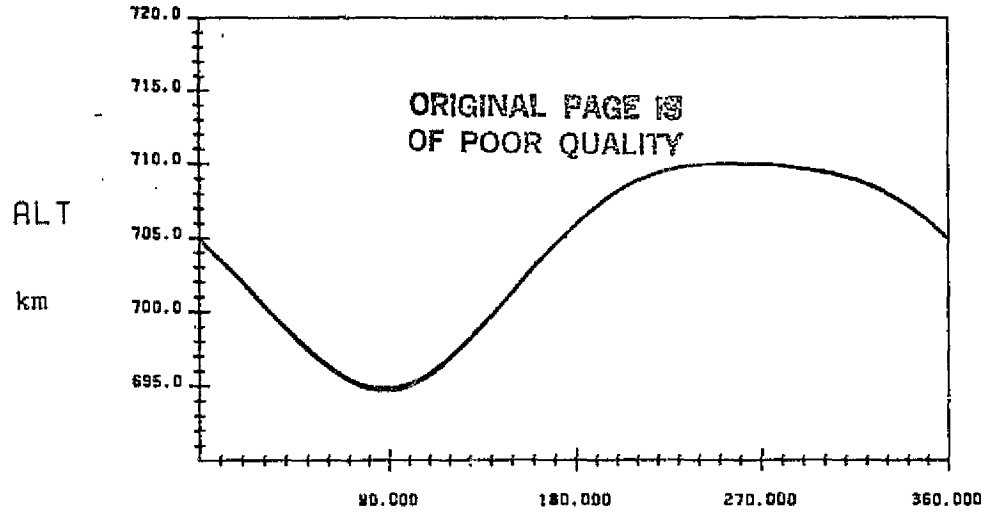

(a)

ALTITUDE ABOVE EARTH EQUATORIAL RADIUS OF 6378.14 KM
DATA START TIME:821214.122558872
END TIME:821214.204208615

RUN TIME: WED APR 13,1983 14.42.42.25

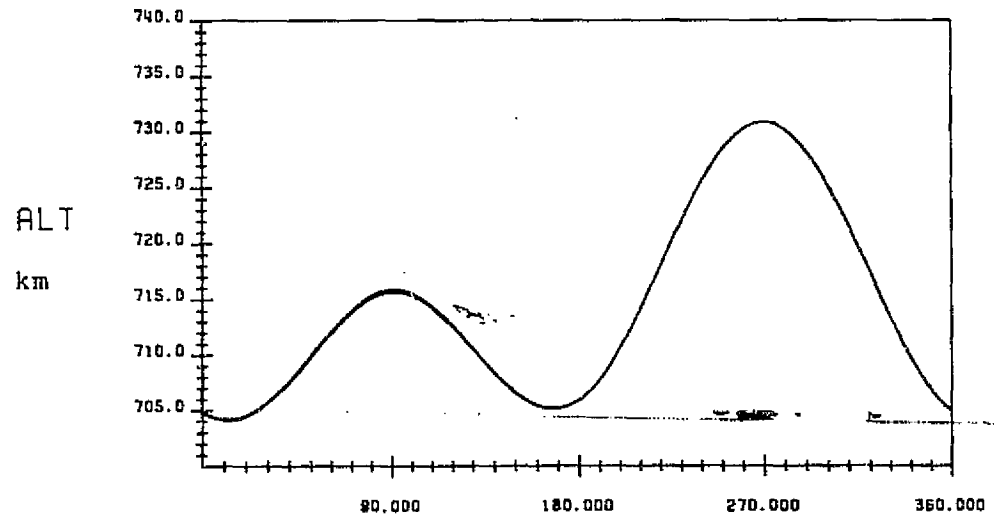

(b)

ALTITUDE ABOVE OBLATE EARTH
DATA START TIME:821214.122558872
END TIME:821214.204208615

FIGURE 2-3. Spacecraft Altitude in Kilometers as a Function of Orbit Phase from the Ascending Node (a) Above Earth Equatorial Radius and (b) Above Oblate Earth

The Landsat-4 orbit is being maintained with orbit adjust maneuvers every 4 to 6 weeks which raise the mean semi-major axis about 200 meters to compensate for the accumulated effects of atmospheric drag (Reference 10). The mean eccentricity of the orbit has stayed between 0.00095 and 0.0015. The semi-major axis and eccentricity are chosen so that perigee stays trapped over the North Pole by the effects of Earth oblateness. Therefore the spacecraft altitude variation shown in Figure 2-3 is typical of that seen throughout the mission.

The Landsat-4 orbit is sun-synchronous with a descending node at approximately 9:30 a.m. local time. The local decending node time varies slightly throughout the year because the right ascension rate of the sun changes due to the Earth's orbit eccentricity, while the node precession rate of the Landsat-4 orbit is nearly constant.

Table 2-3 provides Landsat-4 osculating orbital elements for descending node epoch times for two dates a year apart. Also provided is the node precession rate for the two dates. The orbit inclination and the node rate have both decreased a small amount gradually during the mission due to consistent torques on the orbit applied by solar gravity. This node rate can be used to estimate the node positions at other times throughout the year. The other orbit parameters vary slightly due to the orbit adjust maneuvers and orbit decay. The orbit period is approximately 98.88 minutes.

2.4 SCANNER TEMPERATURE DATA

Thermistors (thermally sensitive resistors) on board the spacecraft are used to monitor the temperatures of the scanner bolometers and certain positions within the Earth Sensor Assembly housing. The latter may be considered as indicators of the scanner electronics temperatures because they are somewhat near the location of the Earth Sensor Electronics Boxes. Figure 2-4 shows the temperature measurements, calibrated in degrees centigrade, for four orbits on

TABLE 2-3. Landsat-4 Osculating Orbital Elements and Node Rate

Date	8/1/82	8/1/83
Epoch Time (Descending Node)	01 hour 4 min. 29.9785 sec.	00 hour 36 min. 47.7184 sec.
Semi-Major Axis	7087.0239	7086.9227
Eccentricity	0.001313	0.001241
Inclination	98.2504	98.2006
Rt. Asc. of Asc. Node	273.947	274.524
Argument of Perigee	106.34	111.134
Mean Anomoly	73.515	68.733
Node Rate	0.990970	0.985067

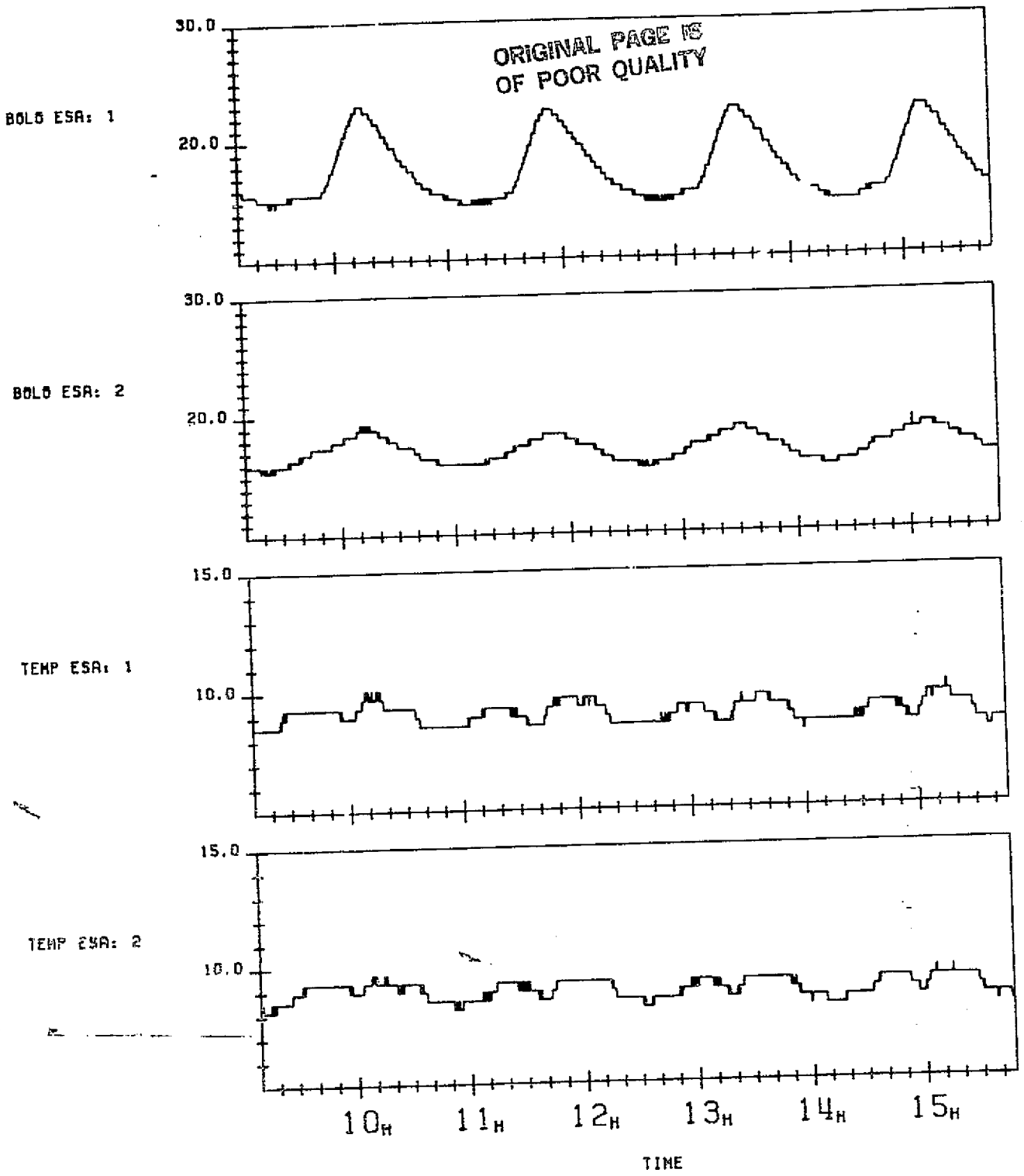

FIGURE 2-4. Scanner Temperatures in Degrees Centigrade as a Function of Time for Four Orbits

November 3, 1982. Figure 2-5 shows the same data plotted as a function of orbit phase from the ascending node. Both these plots demonstrate the quantization in the telemetry measurements.

The scanner 1 bolometer temperature varies more than any of the other temperatures. It shows a nearly linear rise in temperature starting just before the satellite passes the south pole and continuing for around 70 degrees of orbit anomoly, or 20 minutes. Then the temperature falls off more slowly than it rose until it reaches a steady state for the descending node portion of the orbit. The total temperature range spanned is about 8 degrees centigrade.

The scanner 2 bolometer temperature varies at orbit period also, but it varies more slowly and evenly, nearly sinusoidally. The scanner 2 temperature variations are in phase with those of scanner 1. The total temperature range spanned is about 3 degrees centigrade.

Both of the electronics temperatures stay nearly constant. There is some indication of an orbit period pattern, but it is a small variation and is barely above the level of the noise. The peak-to-peak variations in these temperatures is less than two degrees centigrade.

This same pattern of bolometer and electronics temperatures is seen in all the data examined for this report. Appendix B provides plots of the scanner temperatures for the data analyzed in this report.

An explanation for the observed temperature variations based on the flight geometry seems to be indicated. The region just past the South Pole is the part of the orbit where sunlight can be expected to shine on the bottom side of the spacecraft where the scanners are located. Scanner 1 may be warmed by exposure to sunlight over this part of the orbit. On the other hand, scanner 2 is located to the right side of the spacecraft, which is always the shady side due to the sun

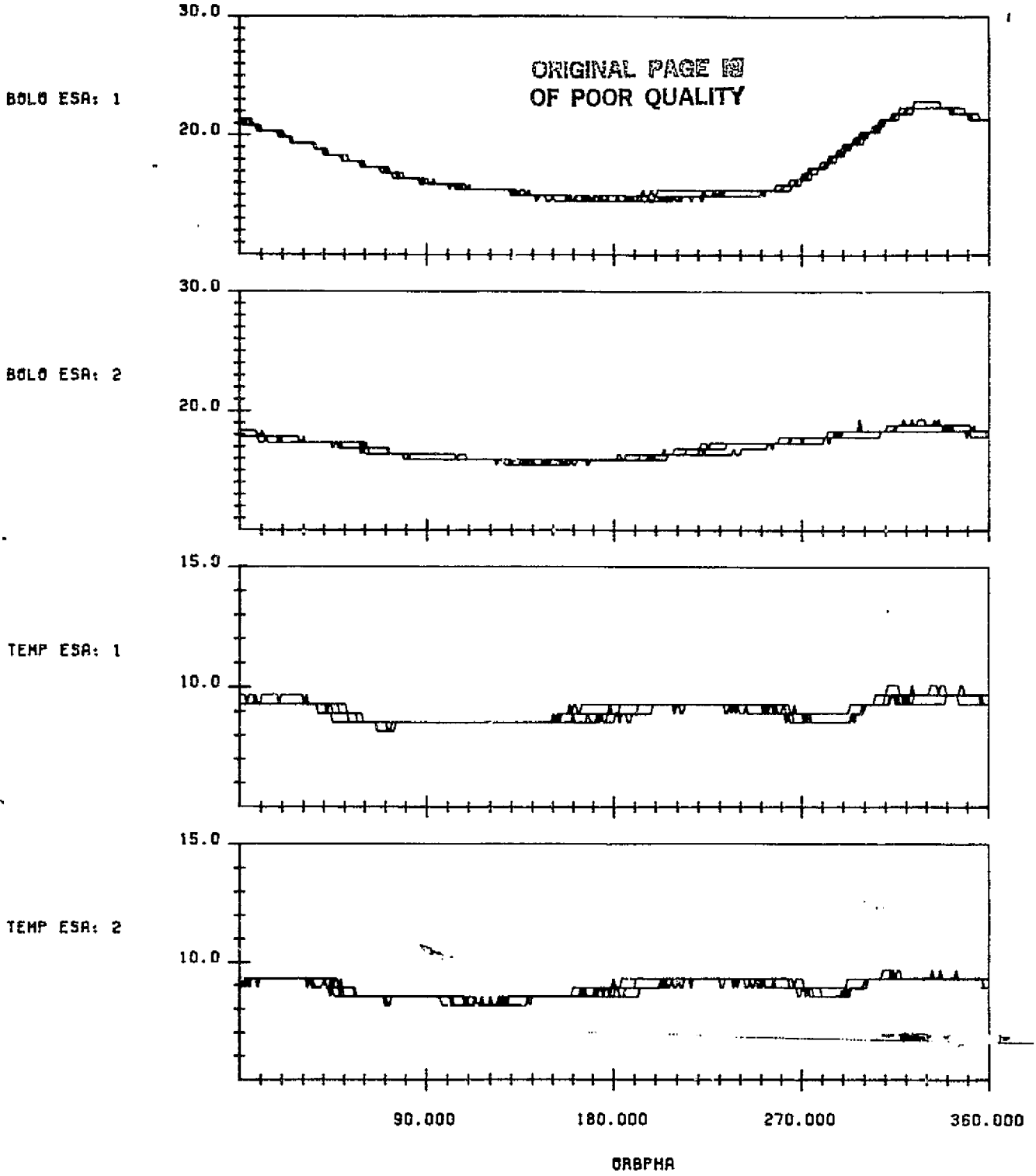

FIGURE 2-5. Scanner Temperatures in Degrees Centigrade as a Function of Orbit Phase for Four Orbits.

synchronous orbit. Thus scanner 2 can be expected to show less warming due to sun exposure. Moreover it seems likely that the comparatively small variations exhibited by the electronics temperatures is the result of the electronics being better insulated from the spacecraft exterior.

2.5 NOISE REDUCTION AND DATA AVERAGING

Before discussing the scanner attitude measurements, it will be useful to discuss the data volume and noise reduction which is applied. It is necessary to reduce the data volume to efficiently process and plot the data.

Figure 2-6 shows twenty minutes of horizon scanner Earth width and Earth phase measurements with every telemetry observation plotted. The scanner observations are made every 0.128 seconds. There is a high level of noise in the data, especially on the Earth phase. There are also some unusual noise distribution characteristics apparent in the Earth phase channels. The noise characteristics are discussed further in Section 8.

N-point averaging of the observations reduces the data volume, and also acts to reduce this high frequency point-to-point noise. The noise reduction helps in the analysis of the finer errors in the data. Therefore N-point averaging is used as the standard method for the reduction of most of the scanner attitude data which is plotted and analyzed for this report.

N-point averaging refers to taking a number, N, of consecutive observations and using its average as a single observation. The average of the next N observations are then taken as the next measurement. For most of the data plotted and fit in this report, one major frame of data, 128 observations, is taken and the average is used to represent the major frame time span (16.384 seconds). If a

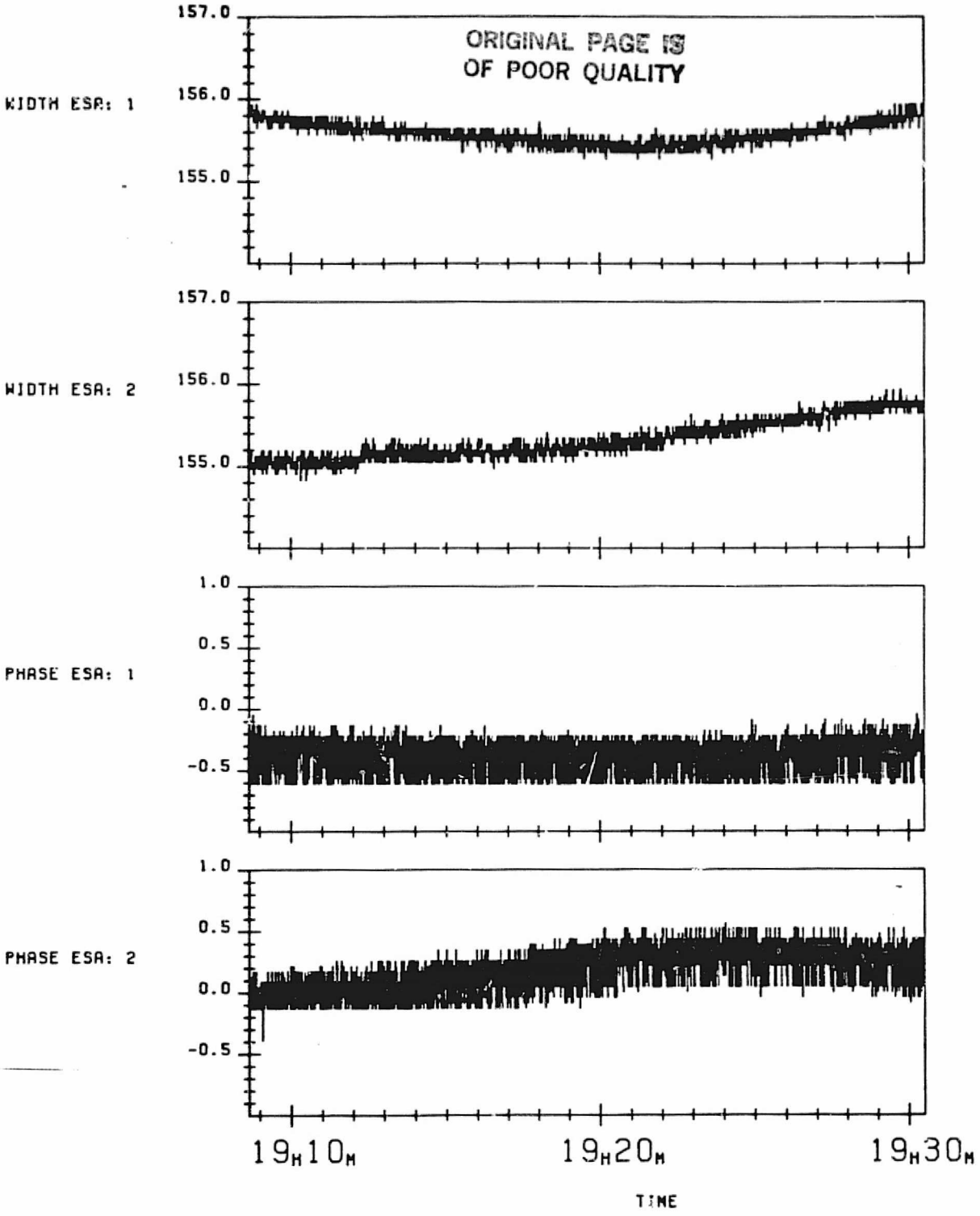

FIGURE 2-6. Twenty Minutes of Scanner Earth Width and Phase Measurements with Every Data Point Plotted

major frame is encountered with missing data, the whole major frame is thrown out. Since data dropout is not very common, this is a practical approach.

Figure 2-7 shows the effect of N-point averaging on the Earth width and phase measurements for a twenty minute data span. In these plots, the results from 1-point, 8-point, 32-point and 128-point averaging is shown for the same data span. The smooth line which is drawn through the data is a fifth order polynomial fit to the data. It helps to show the remaining noise amplitudes in the higher order averages.

2.6 SCANNER ATTITUDE MEASUREMENTS OVERVIEW

Figure 2-8 shows the Earth width and phase measurements as a function of time for the same four orbits on November 3 whose attitude and scanner temperature measurements were discussed previously. Figure 2-9 shows the same data as a function of orbit phase angle from the ascending node. 128-point averaging has been applied to reduce the data noise. The nominal calibration given in Section 1.5 is used.

Systematic orbit period and half orbit period variations are clearly present in the data. The Earth widths vary more than the Earth phase measurements. Earth phase for scanner one shows the least overall variation.

The general orbit period features of these measurements are explained by the effects of Earth oblateness and orbit eccentricity. Due to Earth oblateness, the Earth width measurements are largest when the spacecraft is near the equator and smallest when the spacecraft is over the poles. Due to the orbit eccentricity the Earth width is smaller around the South Pole, when near apogee, than at the North Pole, when near perigee. More details of the effects due to oblateness and eccentricity are discussed in Section 3.

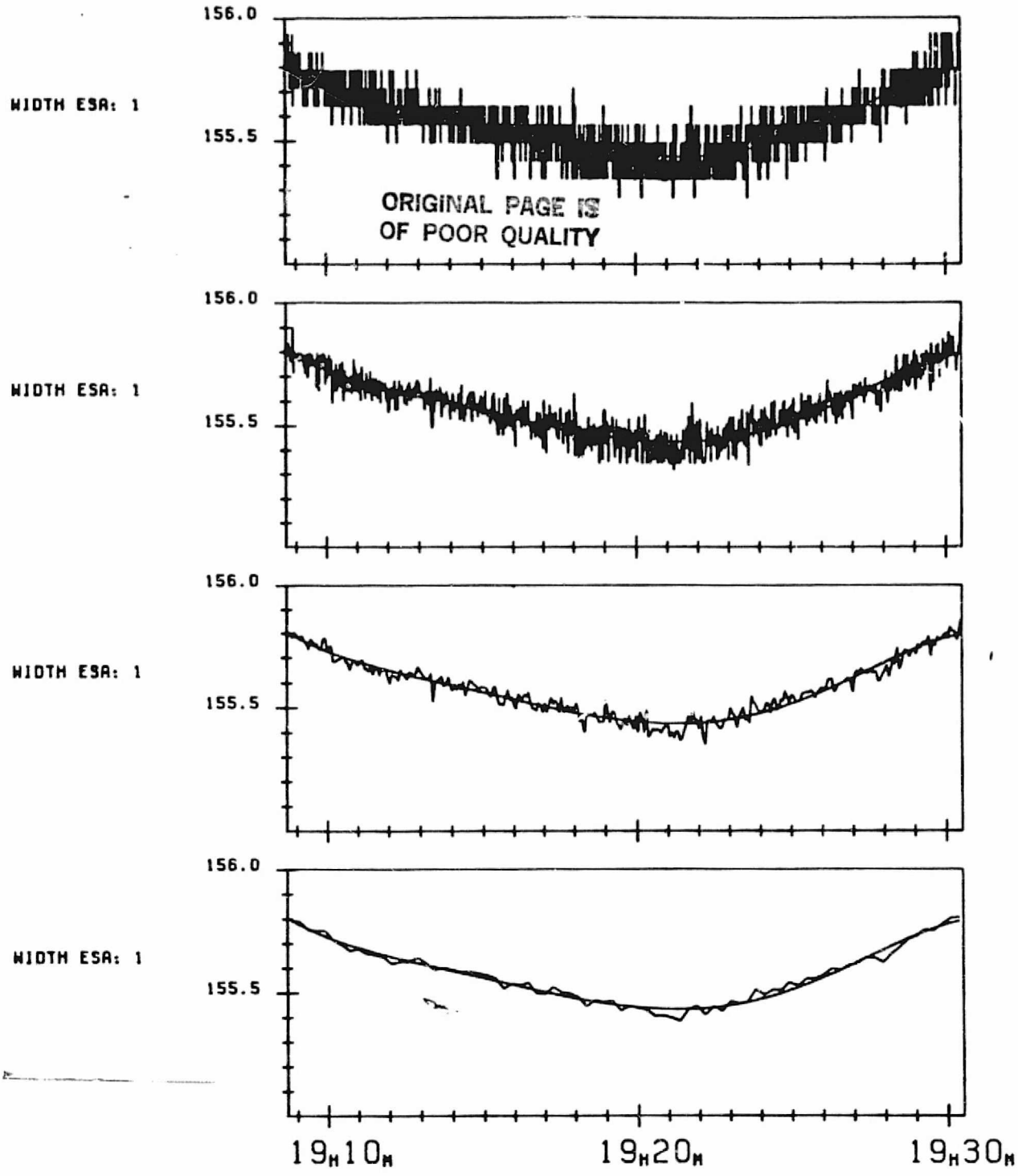

FIGURE 2-7. The Effect of N-Point Averaging on a 20 Minute Span of Data from Scanner 1. A Fifth Order Polynomial is Fit to the Data Span to Show a Smooth Reference Line (1 of 2, Earth Width Data)

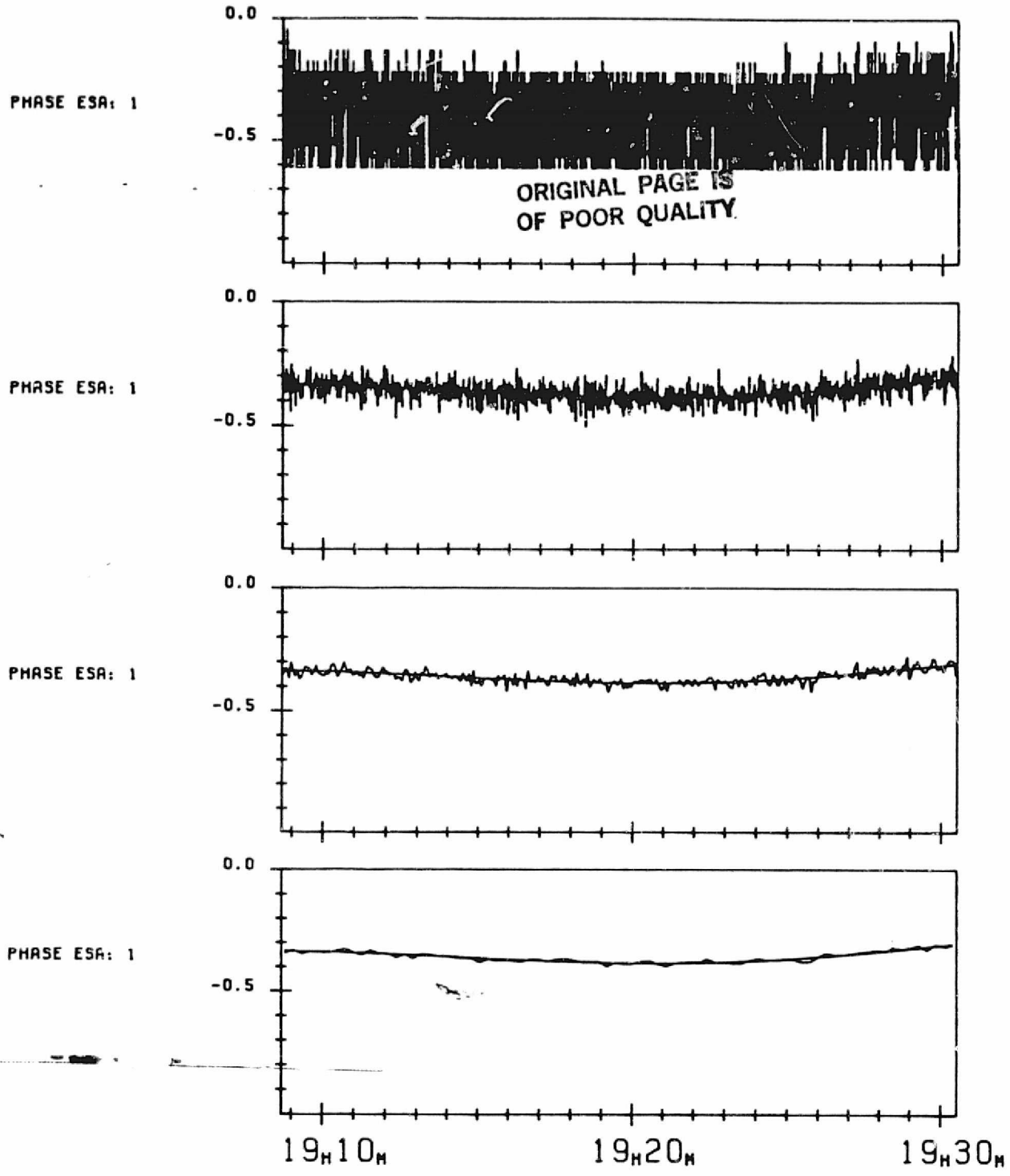

EARTH PHASE -VRS- TIME. THE FIT IS 5TH-ORDER POLYNOMIAL.
FROM TOP TO BOTTOM, THE DATA IS 1,8,32 AND 128 POINT AVERAGED
DATA SPAN: MDB TAPE: 31326
DATA START TIME:820930.190839969
END TIME:820930.193030180

FIGURE 2-7. The Effect of N-Point Averaging on a 20 Minute Span of Data from Scanner 1. A Fifth Order Polynomial is Fit to the Data Span to Show a Smooth Reference Line (2 of 2, Earth Phase Data)

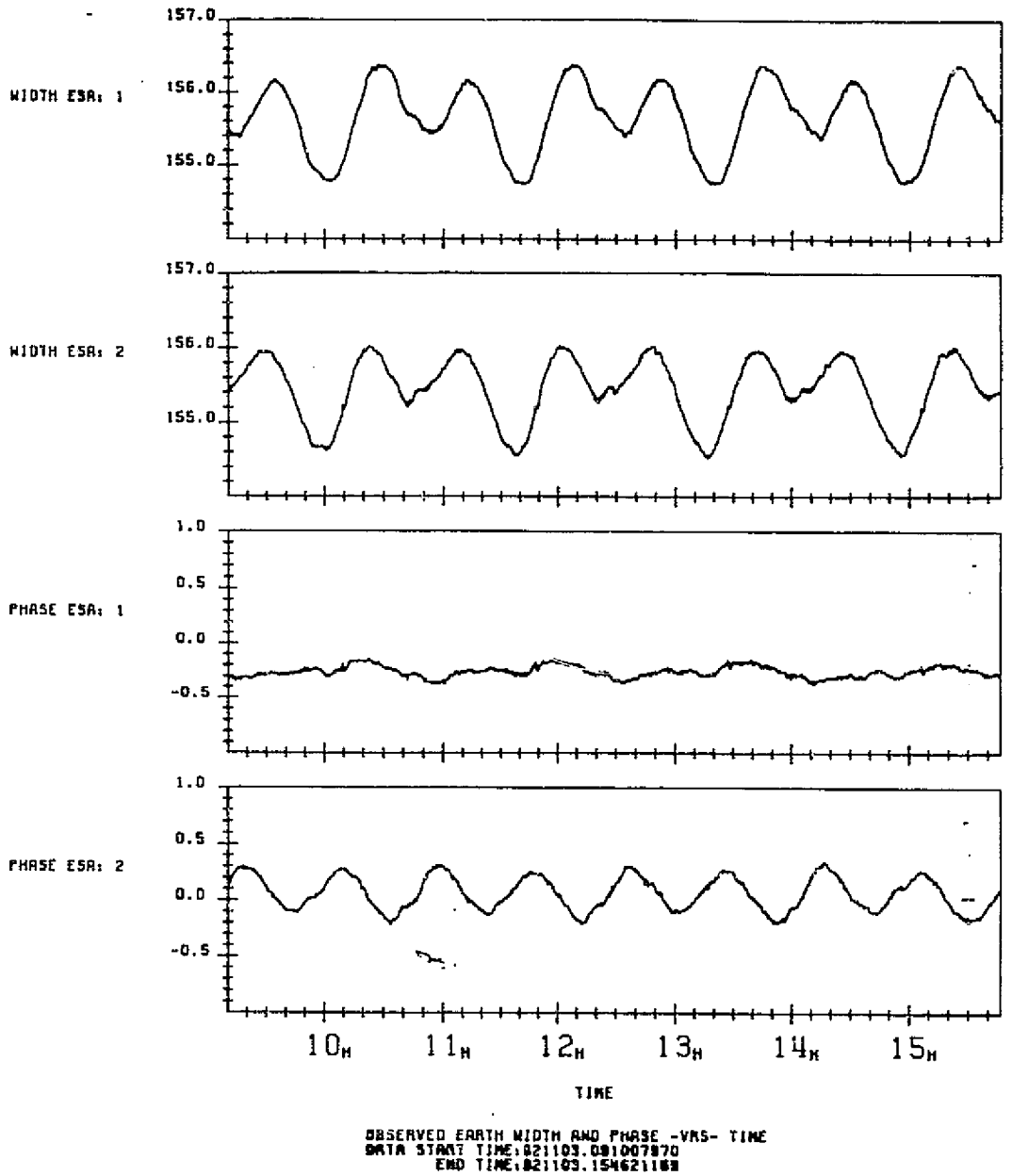

FIGURE 2-8. Scanner Earth Width and Phase Measurements as a Function of Time for Four Orbits, with 128 Point Averaging Applied

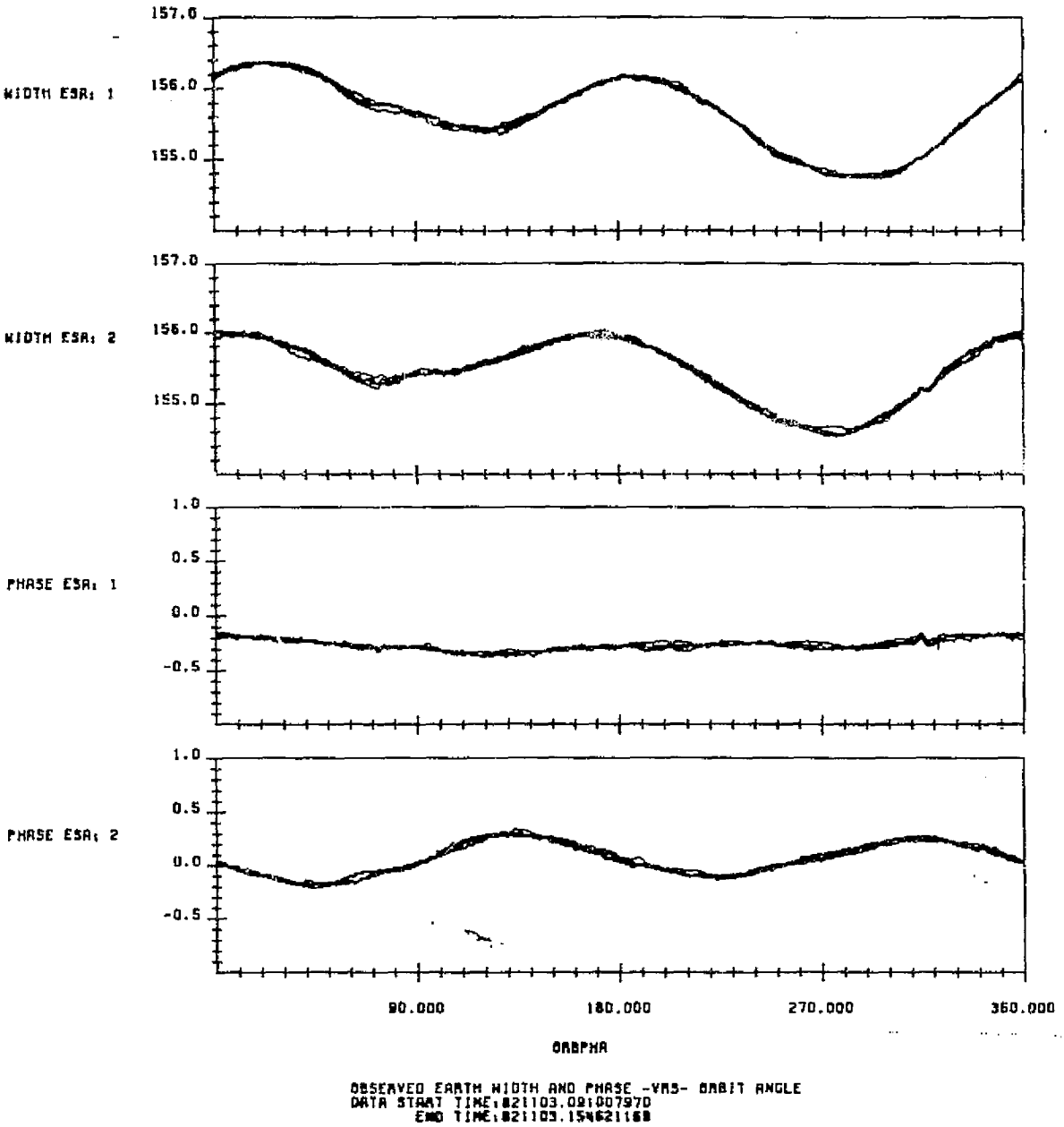

FIGURE 2-9. Scanner Earth Width and Phase Measurements as a Function of Orbit Phase Angle from the Ascending Node, for Four Orbits, with 128 Points Averaging Applied

Using a simple spherical Earth model and the assumption of a circular orbit, the Earth width and phase measurements are converted by a linear relationship to pitch and roll attitude measurements for use on board the spacecraft. Figures 2-10 and 2-11 show the scanner pitch and roll measurements computed using the nominal calibrations (see Table 1-3), for the same data span shown previously. Figure 2-10 shows the measurements as a function of time and Figure 2-11 shows the measurements as a function of orbit phase.

These are the pitch and roll measurements used by the safehold electronics for the backup analog control law. The spacecraft attitude measured by the OBC star tracker and gyro system at the same time is nearly zero pitch/roll/yaw (see Figures 2-1 and 2-2).

In this parameterization of the measurements, the pitch for scanner 1 and the roll for scanner 2 show the large systematic variation characteristic of the Earth width data. It is the roll measurements for scanner 1 that is the most constant.

Plots of the Landsat-4 on board horizon scanner pitch and roll measurements for the data spans analyzed in this report are provided in Appendix C.

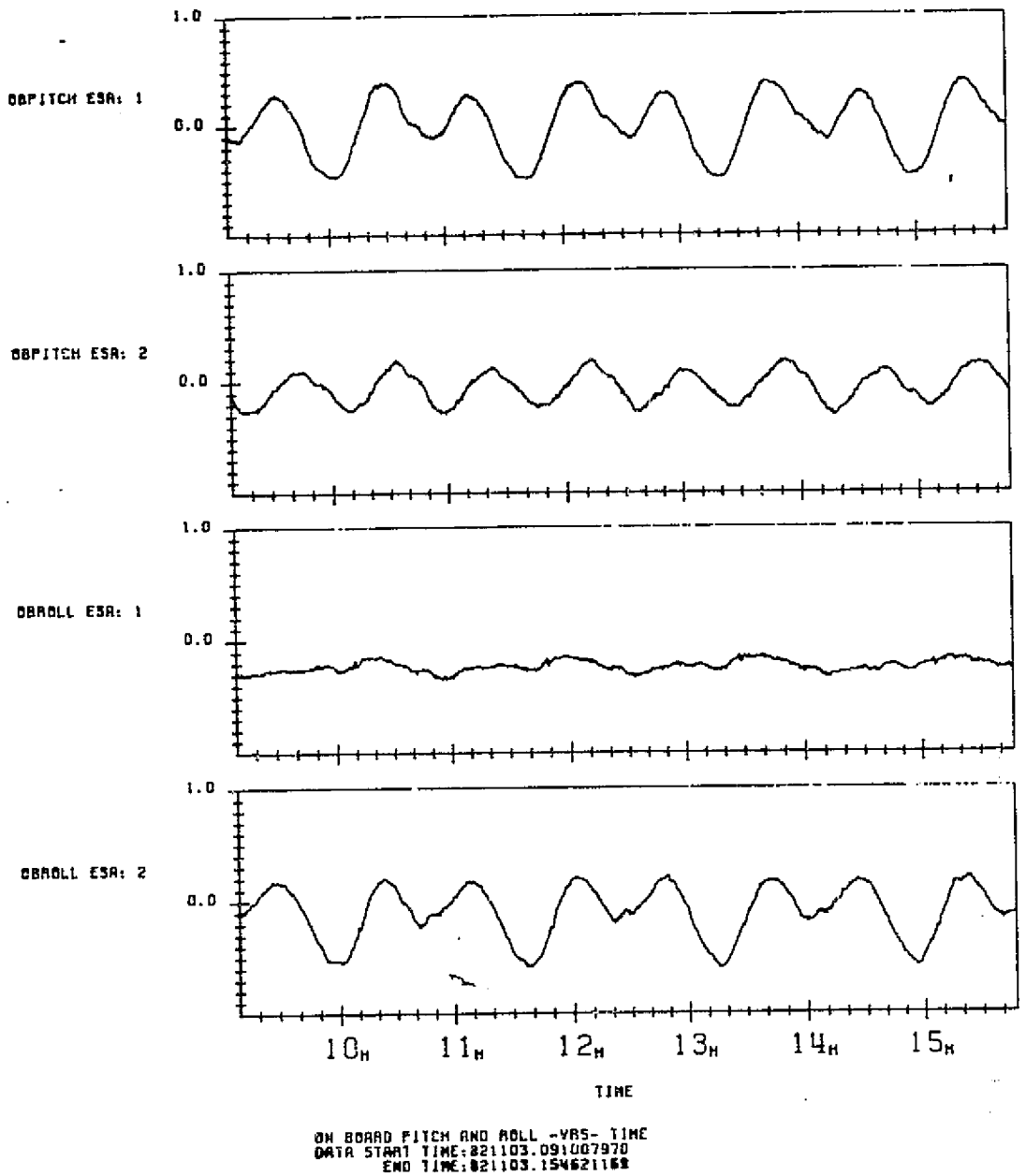

FIGURE 2-10. Scanner On Board Pitch and Roll Measurements as a Function of Time for Four Orbits with 128 Points Averaging Applied

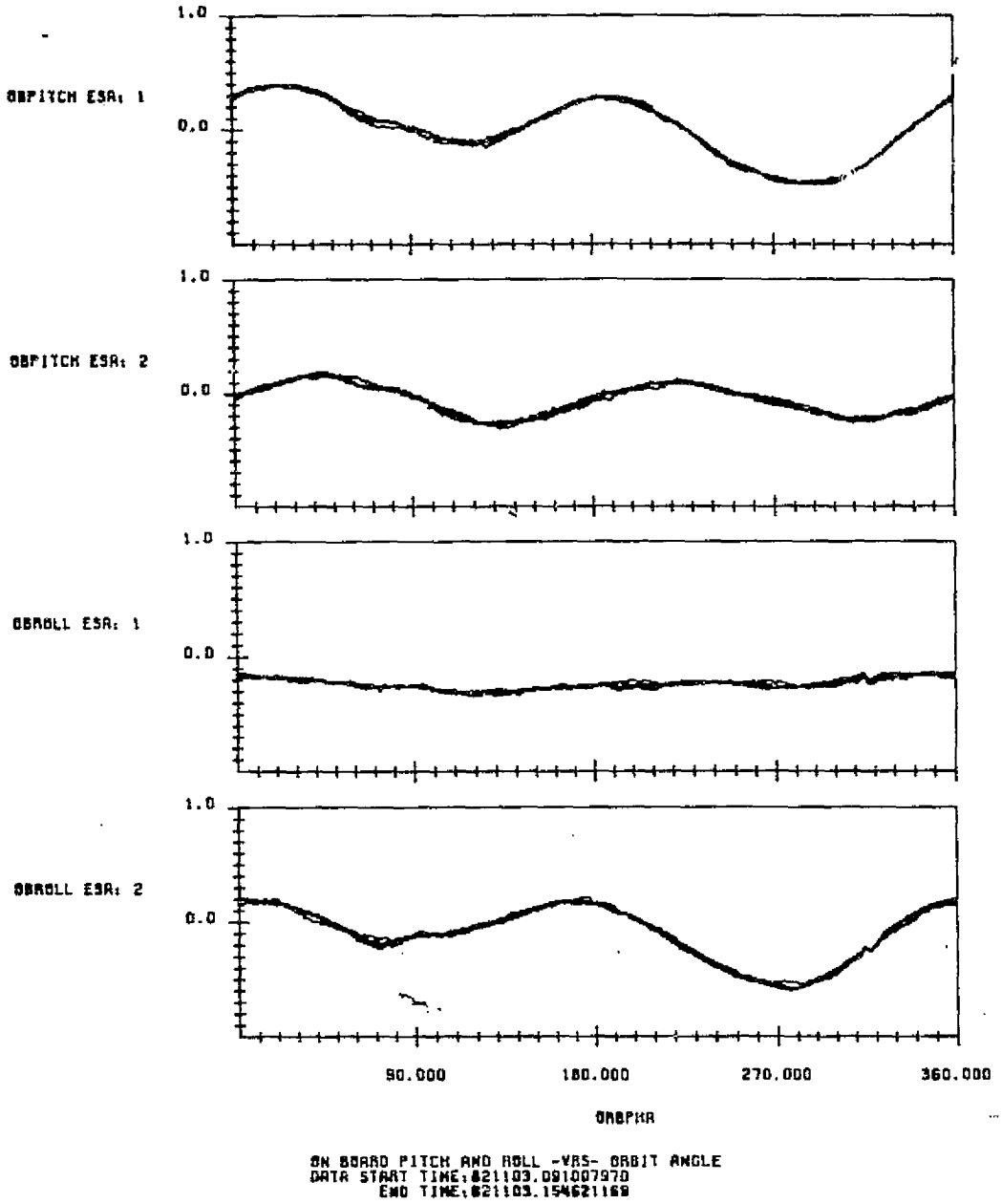

FIGURE 2-11. Scanner On Board Pitch and Roll Measurements as a Function of Orbit Phase for Four Orbits with 128 Points Averaging Applied

SECTION 3 - ATTITUDE, ORBIT, AND EARTH OBLATENESS EFFECTS

This section discusses the modeled systematic effects on the scanner measurements due to attitude variations, orbit eccentricity, and Earth oblateness. These effects are well understood and explain most of the systematic variations in the scanner measurement. Section 3.1 discusses the predicted scanner measurements that model all these effects. Sections 3.2, 3.3, and 3.4 briefly discuss the attitude, orbit, and Earth oblateness effects separately. Section 3.5 presents the residual errors after these effects are removed. Analysis of the residual errors is discussed further in the following sections.

3.1 PREDICTED SENSOR MEASUREMENTS

The Scanner Measurements Predictor subsystem generates a set of predicted scanner measurements based on the spacecraft orbit and attitude, an oblate Earth model, and various scanner model parameters. Therefore these predictions include the effects of orbit eccentricity, Earth oblateness, and also spacecraft attitude variations.

Figure 3-1 shows the predicted scanner data for the same four orbits for which flight data was plotted in Figure 2-8. Figure 3-2 shows the predicted data along with the flight data. Figure 3-3 shows the predicted data as a function of orbit phase angle. The predictions provided here use the nominal measurement calibrations (see Section 1.5), the orbit and attitude taken from the OBC, and standard oblate Earth coefficients.

Notice that the scanner 1 predictions show constant biases relative to the observed data. These biases can easily be corrected based on the average difference. However it was decided to leave the nominal calibrations for all the plots to avoid confusion in the parameters used. Notice that the predicted and observed data agree in their general features.

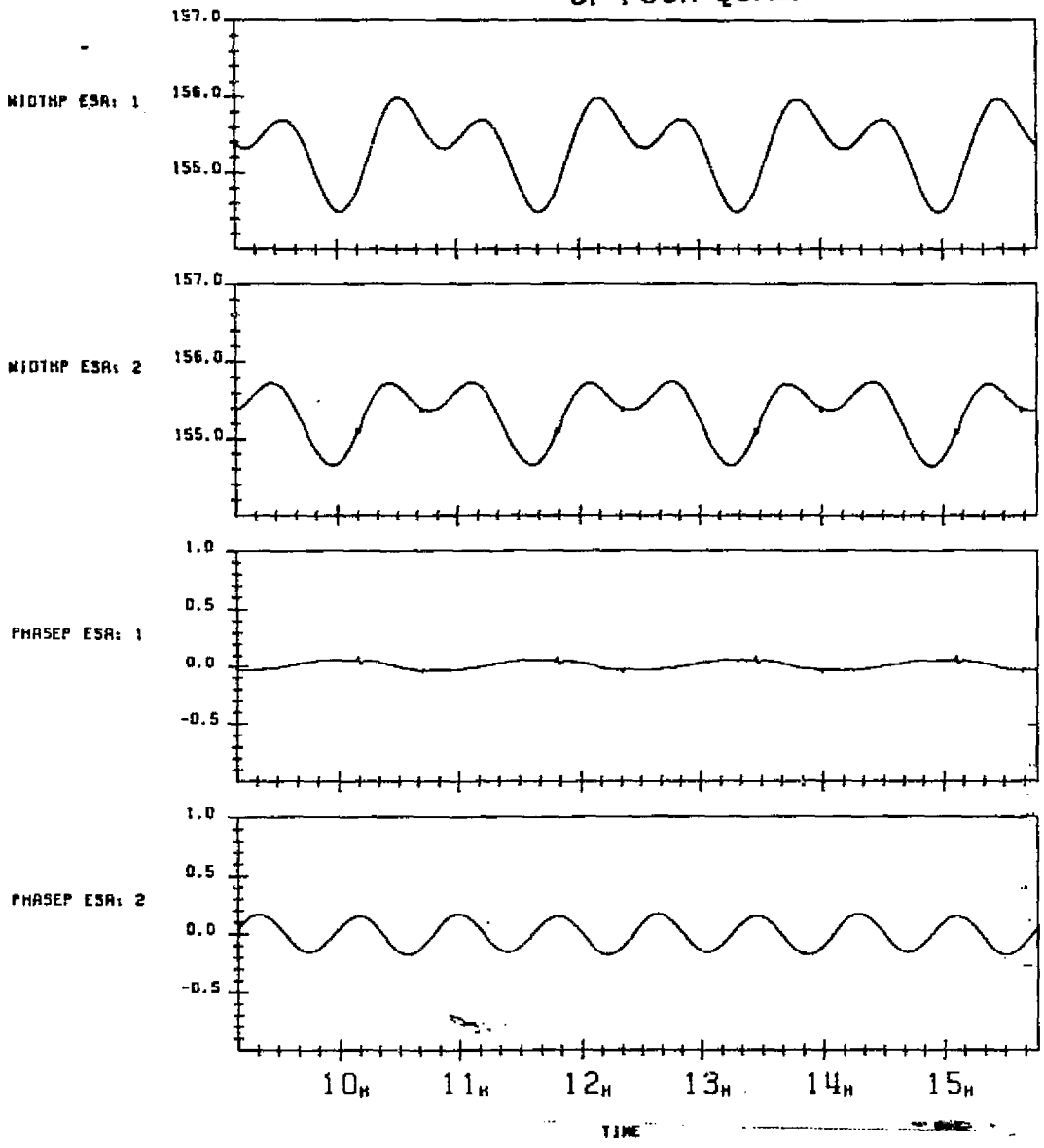

FIGURE 3-1. Predicted Scanner Measurements as a Function of Time for Four Orbits, Based on the OBC Attitude and Orbit and an Oblate Earth Model

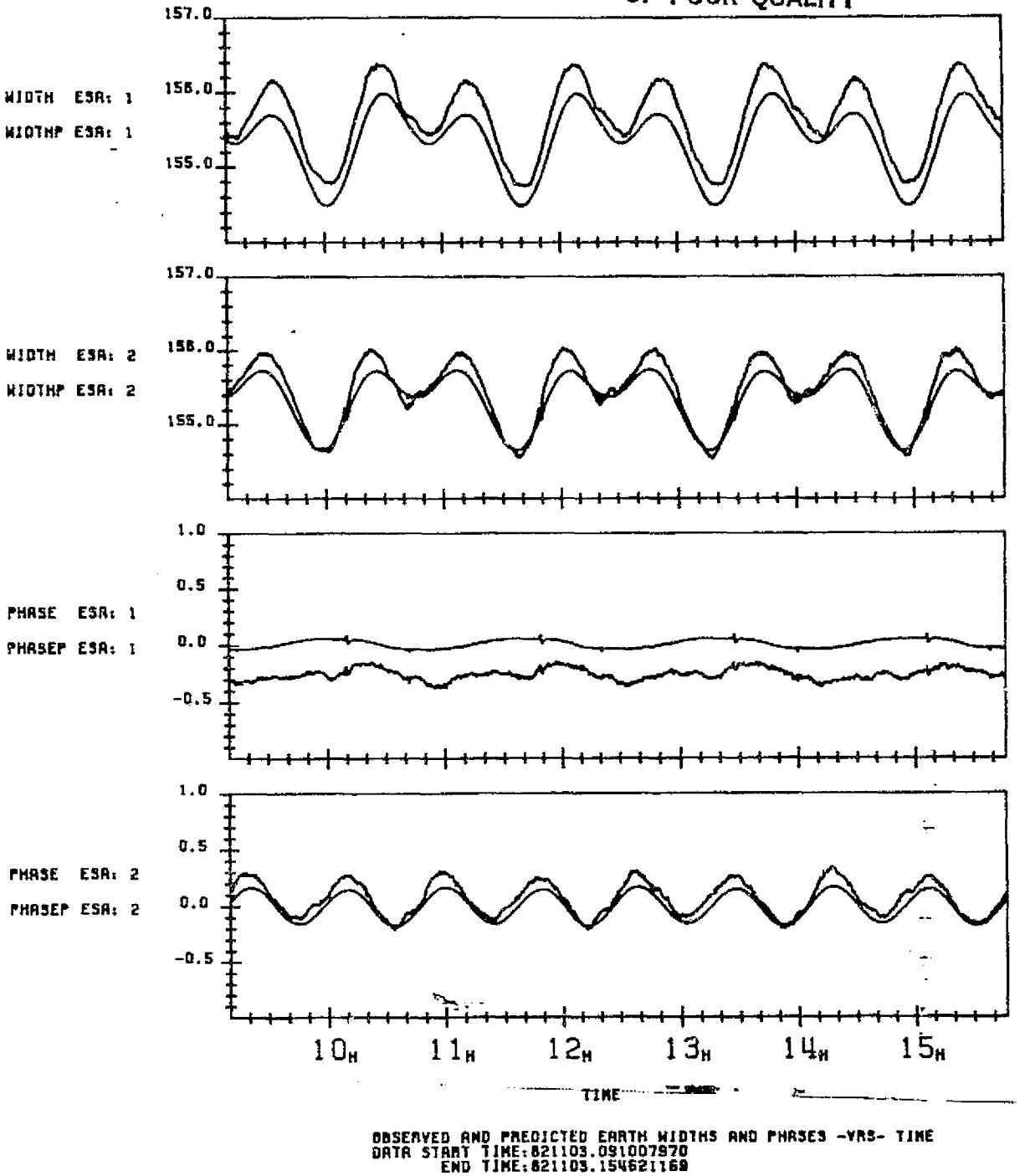

FIGURE 3-2. Predicted and Observed Scanner Measurements as a Function of Time for Four Orbits

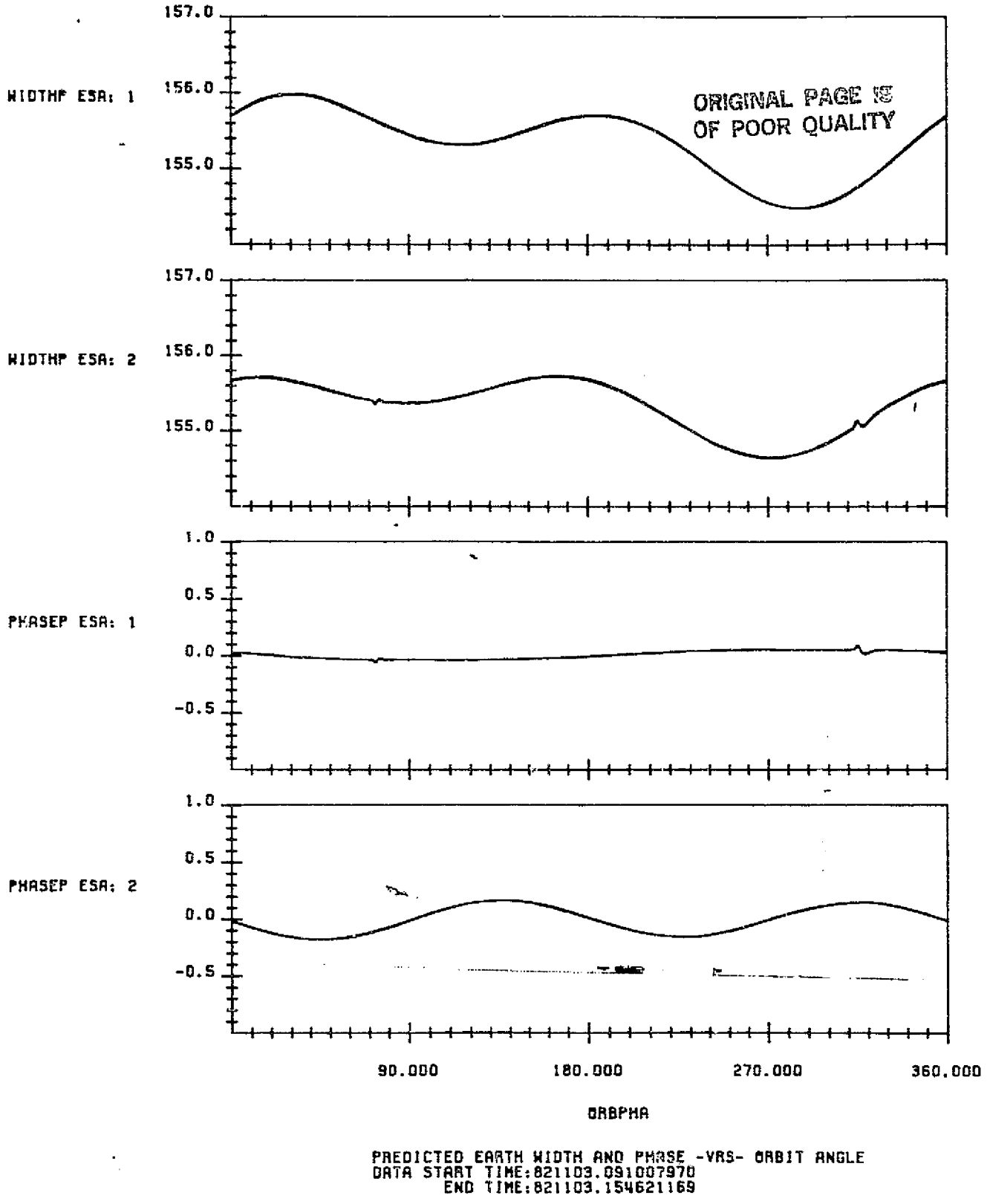

FIGURE 3-3. Predicted Scanner Measurements as a Function of Orbit Phase

3.2 ATTITUDE EFFECTS

For the data spans presented in this report, the spacecraft attitude computed by the OBC stays within 0.02 degrees of zero pitch, roll, yaw, except for small excursions in roll and yaw of about 0.05 degrees. These excursions, which occur twice per orbit regularly, are due to reorientations of the solar panels when the spacecraft enters and leaves the Earth's shadow. This effect is shown in both the predicted and the observed roll measurements (sensor 1 phase and sensor 2 width) in Figures 3-1 through 3-3. It shows up as small bumps in the measurements around 80° and 320° of orbit phase from the ascending node.

3.3 ORBIT EFFECTS

The effect on the Earth width measurements of an orbit eccentricity of 0.001 (which is typical for Landsat-4) is plotted in Figure 3-4. This plot was generated by predicting the change in the Earth width for the 0.001 eccentricity compared to the Earth widths for a circular orbit. Keplerian orbital elements with perigee at the North Pole and a spherical Earth model were used.

Due to the orbit the Earth width is smaller around the south pole (270° orbit angle), when near apogee, than at the North pole (90° orbit angle), when near perigee.

The spacecraft altitude does not impact the Earth phase measurement.

3.4 EARTH OBLATENESS EFFECTS

Figure 3-5 illustrates the effects of Earth oblateness on the Earth width and phase measurements. This plot was generated by predicting the change in the scanner measurements for the oblate Earth compared to a spherical Earth with a mean Earth radius.

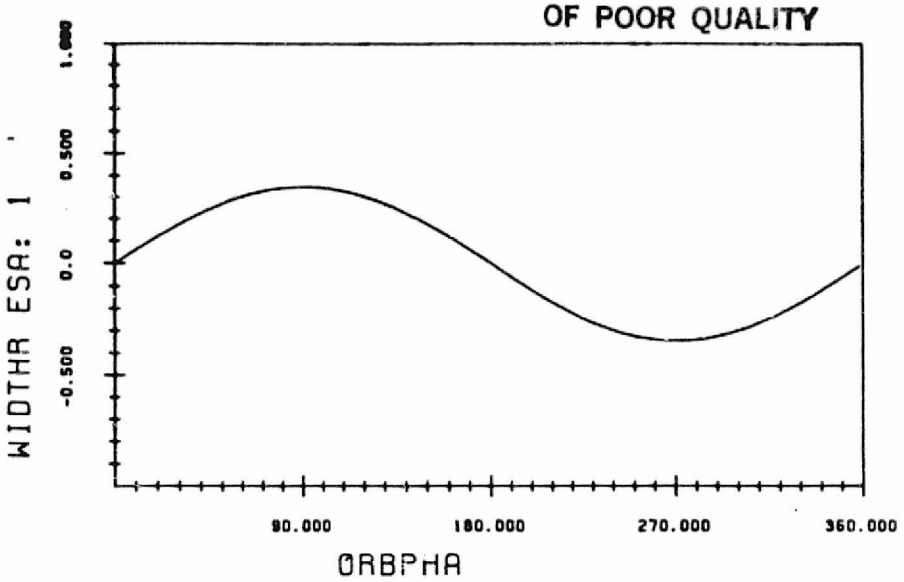

PREDICTED 1: CIRCULAR ORBIT
PREDICTED 2: ECCENTRICITY 0.001 (REPLACES OBSERVED DATA)
KEPLERIAN ORBIT, AXIS = 7087 KM, ECC. = 0.001, INC. = 98.2,
PERIGEE OVER NORTH POLE, SPHERICAL EARTH 6367 KM
DATA START TIME:820704.000000000
END TIME:820704.013900000

RUN TIME: THU APR 14,1983 06.39.36.45

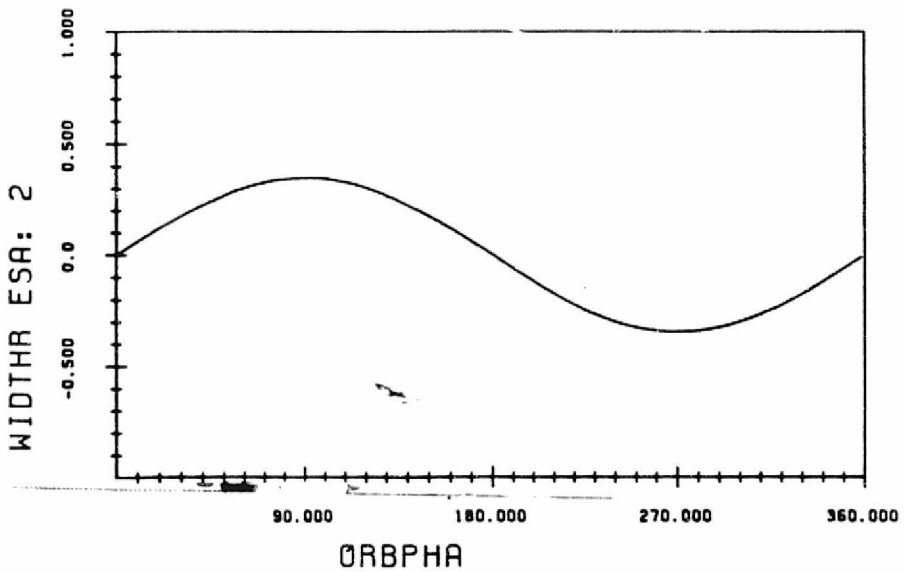

PREDICTED 1: CIRCULAR ORBIT
PREDICTED 2: ECCENTRICITY 0.001 (REPLACES OBSERVED DATA)
KEPLERIAN ORBIT, AXIS = 7087 KM, ECC. = 0.001, INC. = 98.2,
PERIGEE OVER NORTH POLE, SPHERICAL EARTH 6367 KM
DATA START TIME:820704.000000000
END TIME:820704.013900000

FIGURE 3-4. The Effects of Orbit Eccentricity on the Earth Width Measurements

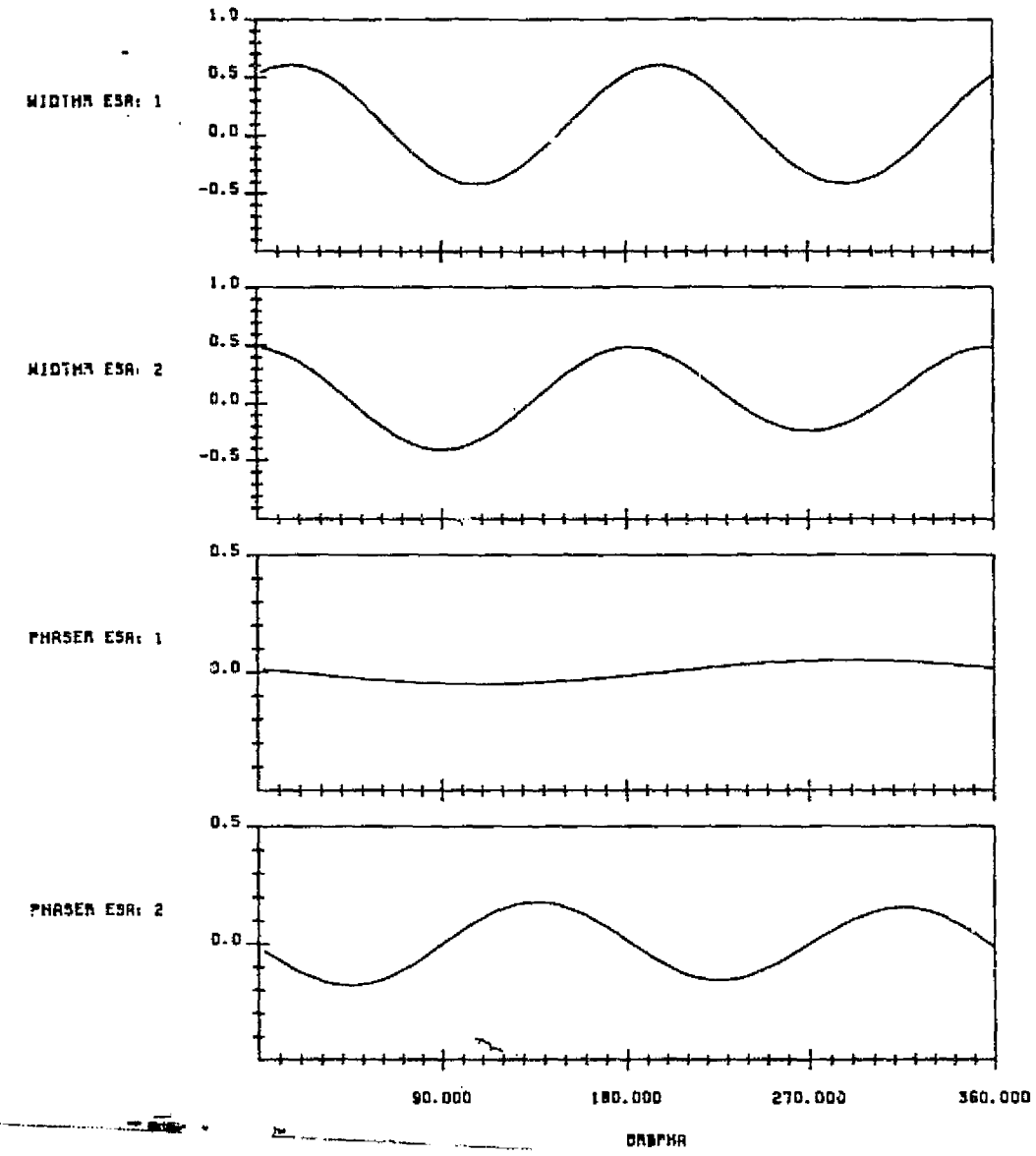

FIGURE 3-5. The Effect of Earth Oblateness on the Earth Width and Phase Measurements

Earth oblateness has its largest impact on the Earth width measurements. It is similar to a twice orbit frequency spacecraft altitude variation because the Earth is flattened at the poles. However more details of the Earth oblateness effect can be understood by looking at the difference in the Earth-in and Earth-out horizon crossing latitudes. The horizon crossing latitudes for the Landsat-4 scanner orientations are illustrated in Figure 1-6.

For scanner 1, both horizon crossings are located behind the subsatellite ground track, while scanner 2 has one horizon behind and the other symmetrically forward on the right side of the ground track (see Figure 1-5). Due to this, there is a phase lag in the oblateness effect on the scanner 1 Earth width relative to the oblateness effect on the scanner 2 Earth width.

Since the scanner 2 horizons are both to the right of the spacecraft, this scanner views horizons at higher latitudes over the North Pole than over the South Pole region. As a result, the oblateness effect on scanner 2 is smaller around the south pole.

The effects of oblateness on the Earth phase measurements results solely from the difference in Earth radius at the Earth-in and Earth-out crossing. Since the scanner 1 horizon crossings occur at nearly the same latitude, Earth oblateness has little effect on this measurement. Scanner 2 has the maximum effects when the spacecraft is at the mid latitudes where one crossing is closer to the pole and the other is closer to the equator.

3.5 RESIDUAL ERRORS

This section discusses the residual errors between the observed scanner measurements and the predicted scanner measurements where attitude, orbit, and Earth oblateness effects are modeled. An

overview of the residual error characteristics is presented utilizing representative data spans, and the standard plot formats used for analyzing the residual error characteristics are introduced. Specific features in the residual errors are analyzed in detail in subsequent sections.

Figure 3-6 shows a plot of the pitch and roll residual errors vs. time for the four orbits whose predicted and observed measurements were plotted in Figure 3-2. Figure 3-7 shows the residuals as a function of orbit phase for the orbits. Notice how the residual error tends to repeat at orbit period. This is typical of all the data. However, longer data spands covering a full day often show some gradual changes in the residual pattern over the day.

Figure 3-8 shows the pitch and roll residuals as a function of orbit phase for the complete data span on the same day. With the longer data span, more variability in the measurements is represented. This kind of figure is useful for showing the variability or consistancy in the measurements from orbit to orbit. Appendix D contains plots in the same format as Figure 3-8 for all the data spans.

Figure 3-9, which we refer to as a serial-stacked plot, shows another way to illustrate the orbit-to-orbit variations in the measurements. The serial-stacked plot presents consecutive orbits of data stacked sequentially. The time on the left of the plot gives the start time of each data segment. (Note that a data gap of more than one orbit appears in this plot starting around 7:15.) With the data presented in this way it is easy to see the changes in the orbit period pattern throughout the day, and on which orbits special features occur. For example, one can observe from these plots that the orbits with the unusually small Earth widths in scanner 2 for the south pole region of the orbit occur near the beginning of the data span.

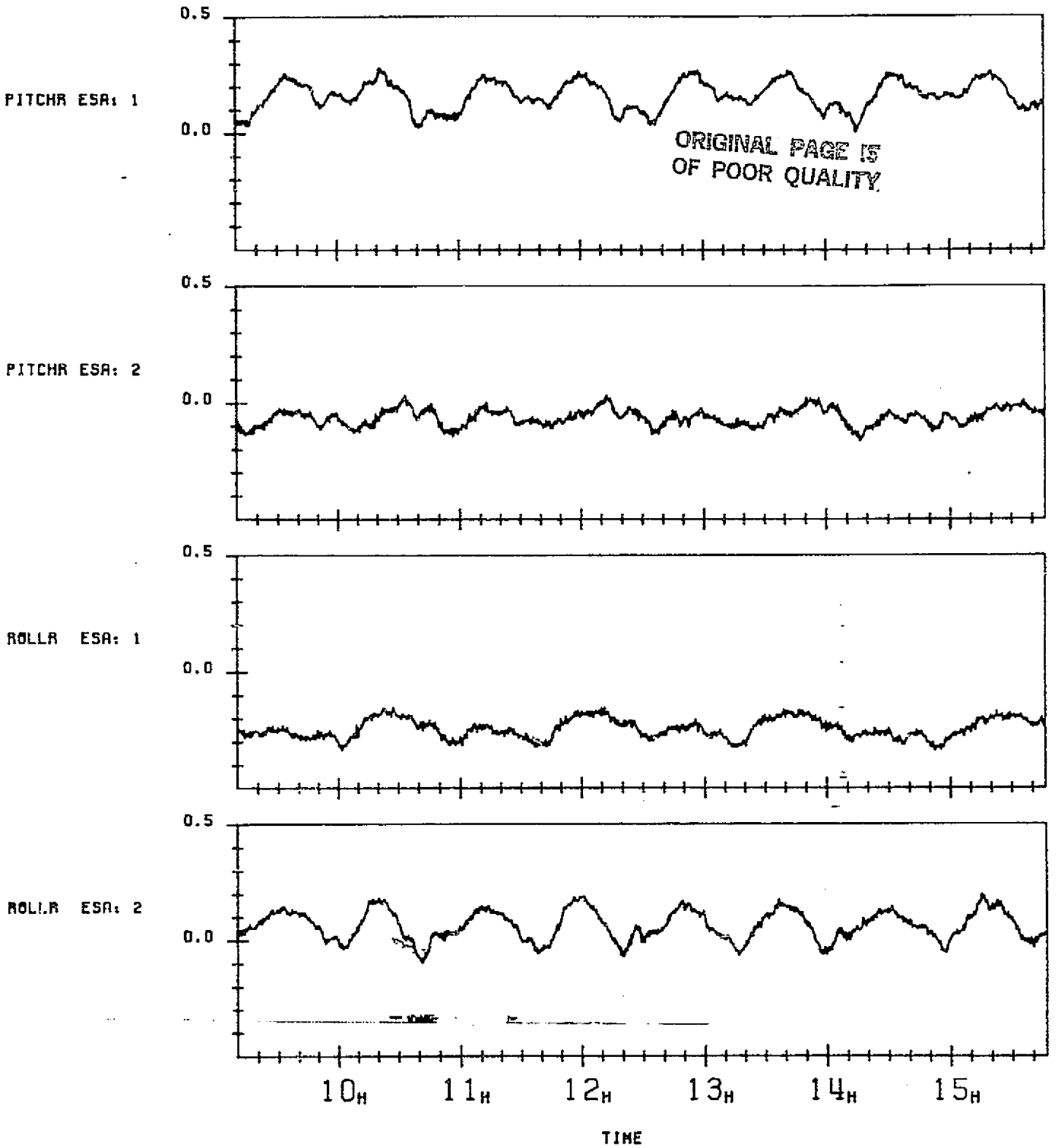

FIGURE 3-6. Residual Errors in Pitch and Roll as a Function of Time for Four Orbits

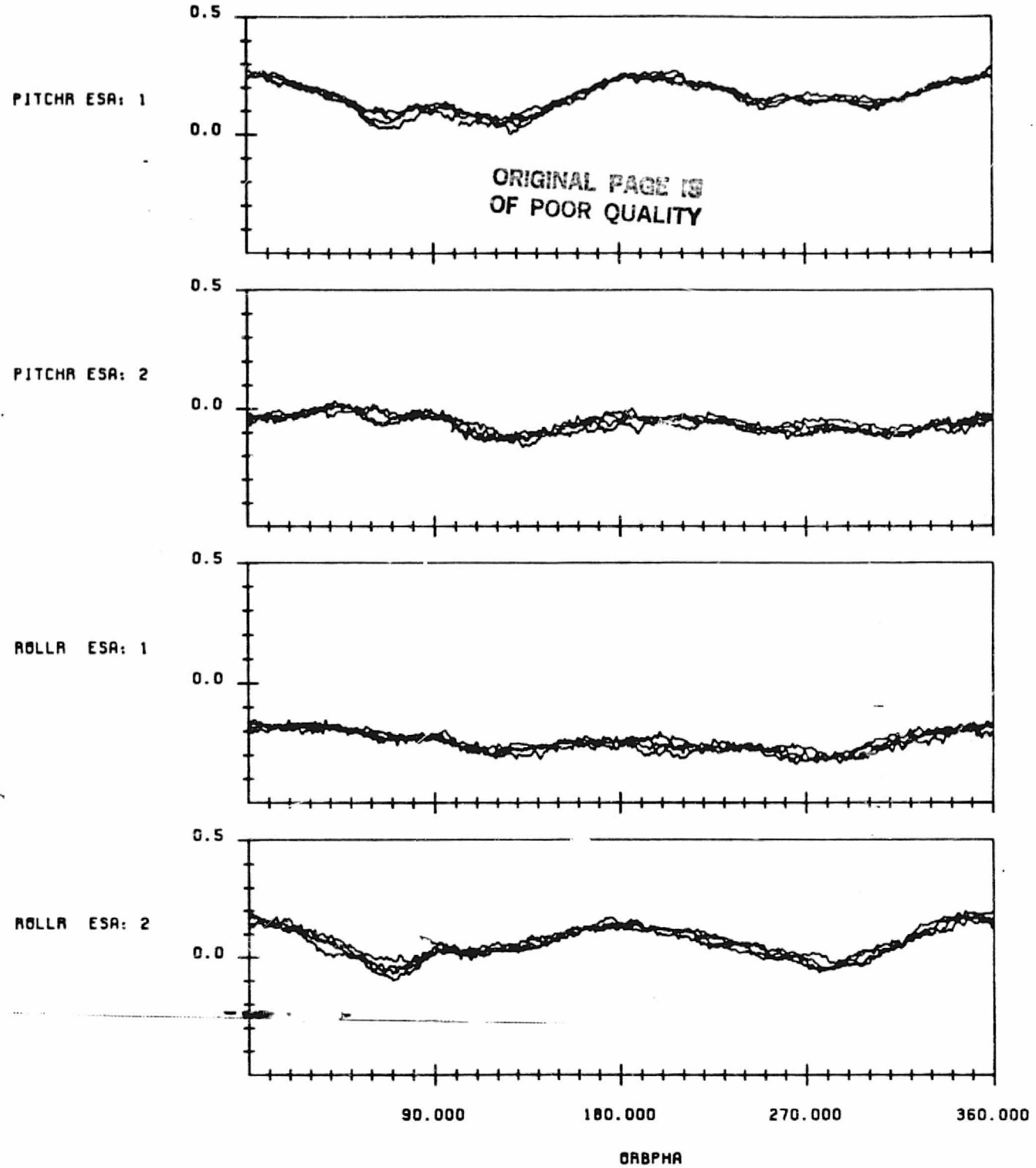

FIGURE 3-7. Residual Errors in Pitch and Roll as a Function of Orbit Phase for Four Orbits

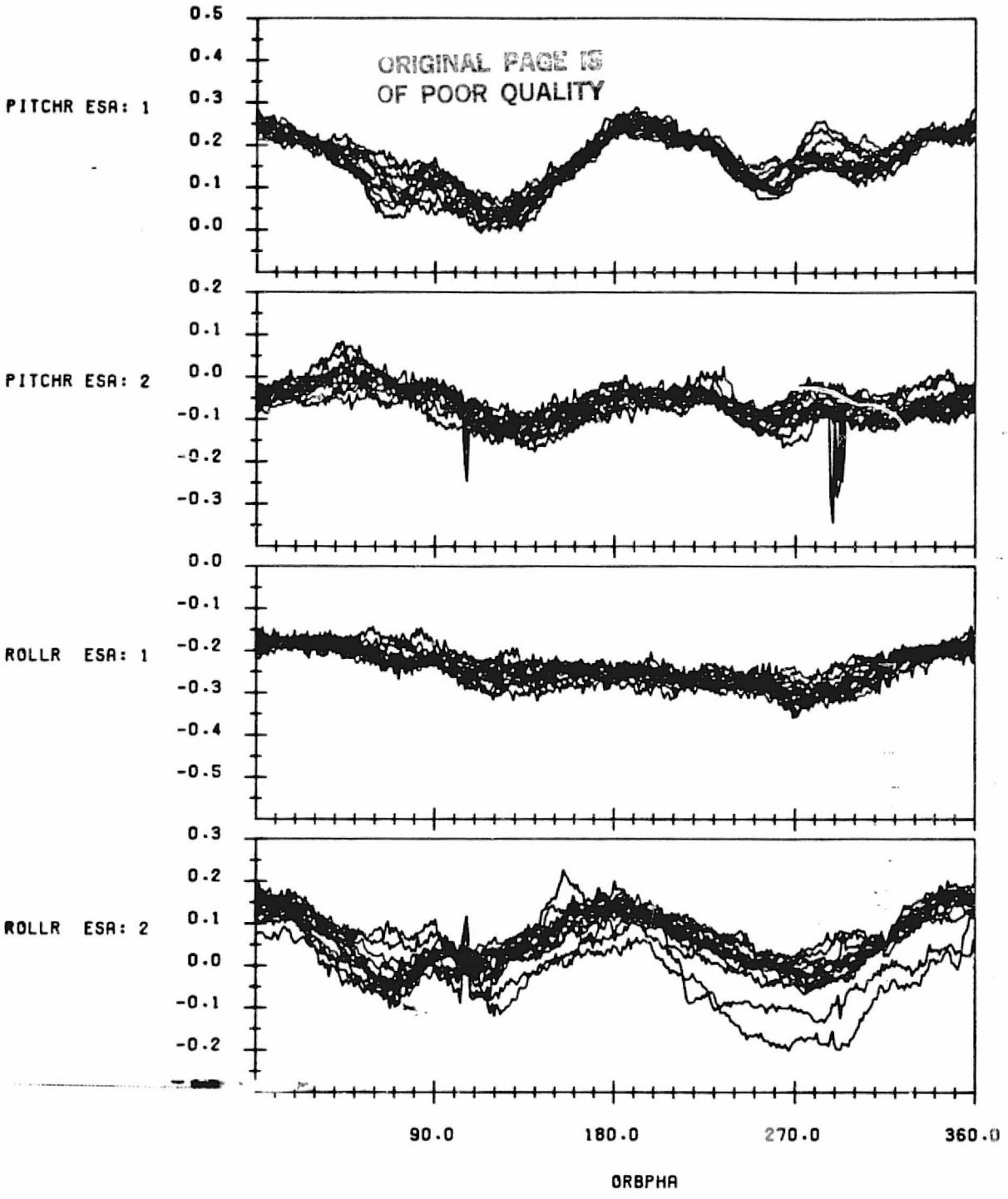

SCANNER RESIDUAL ERRORS IN DEGREES FOR NOMINAL CALIBRATION
WITH EARTH OBLATENESS, OBC ORBIT AND OBC REFERENCE ATTITUDE
EFFECTS MODELLED
DATA START TIME:821102.230736644
END TIME:821103.220936128

FIGURE 3-8. Residual Errors in Pitch and Roll as a Function of Orbit Phase for November 3, 1982

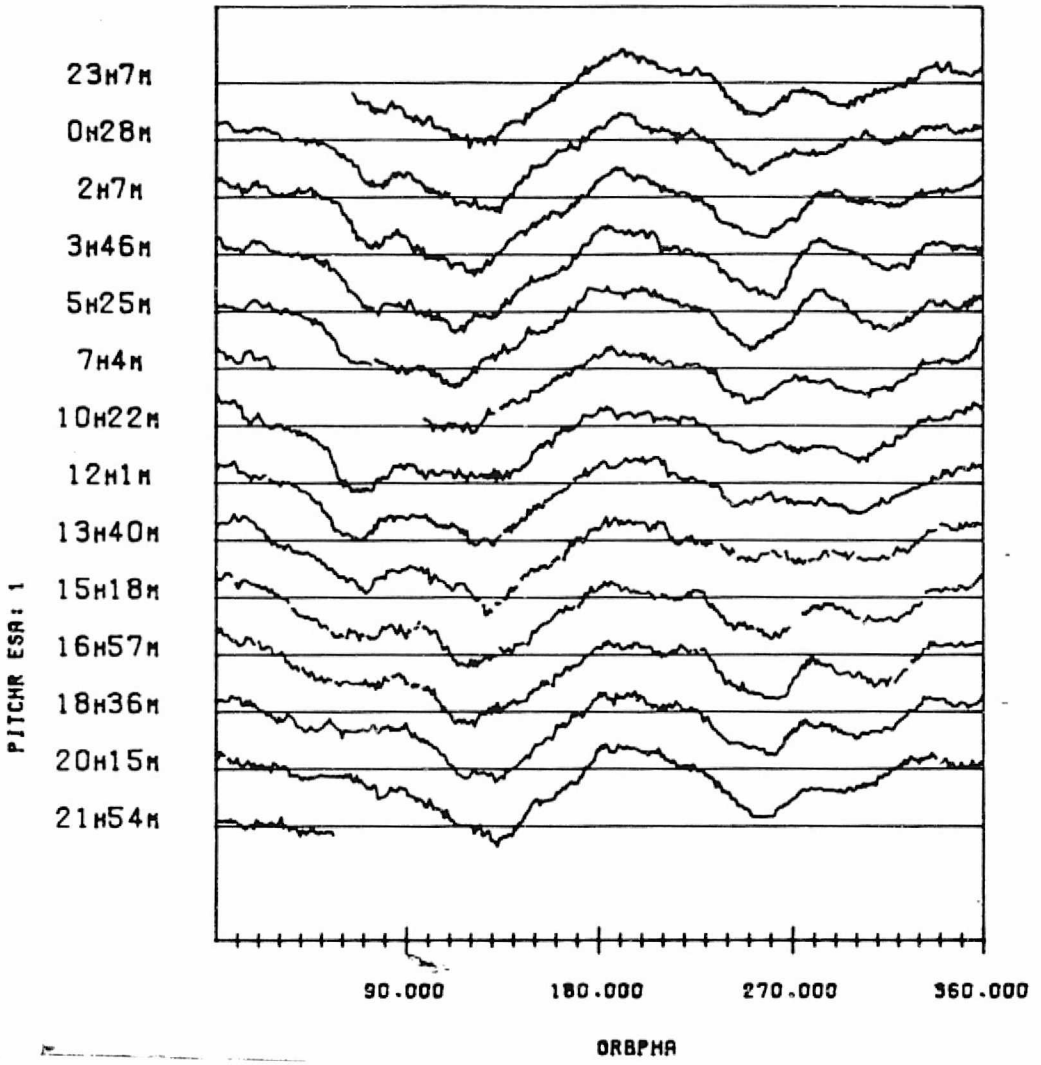

FIGURE 3-9. Residuals for Consecutive Orbits on November 3, 1982 (1 of 4, Sensor 1 Pitch)

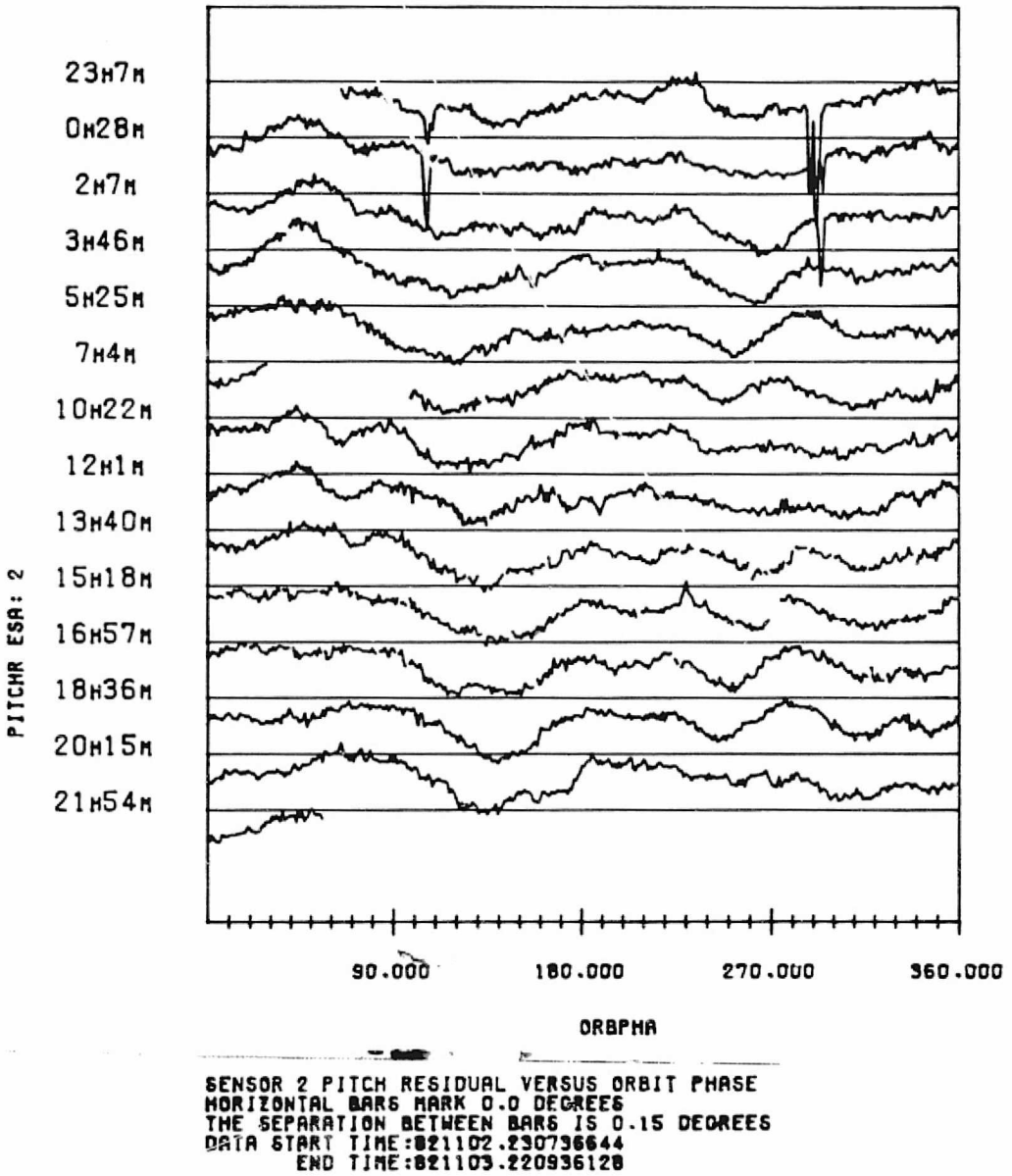

FIGURE 3-9. Residuals for Consecutive Orbits on November 3, 1982 (2 of 4, Sensor 2 Pitch)

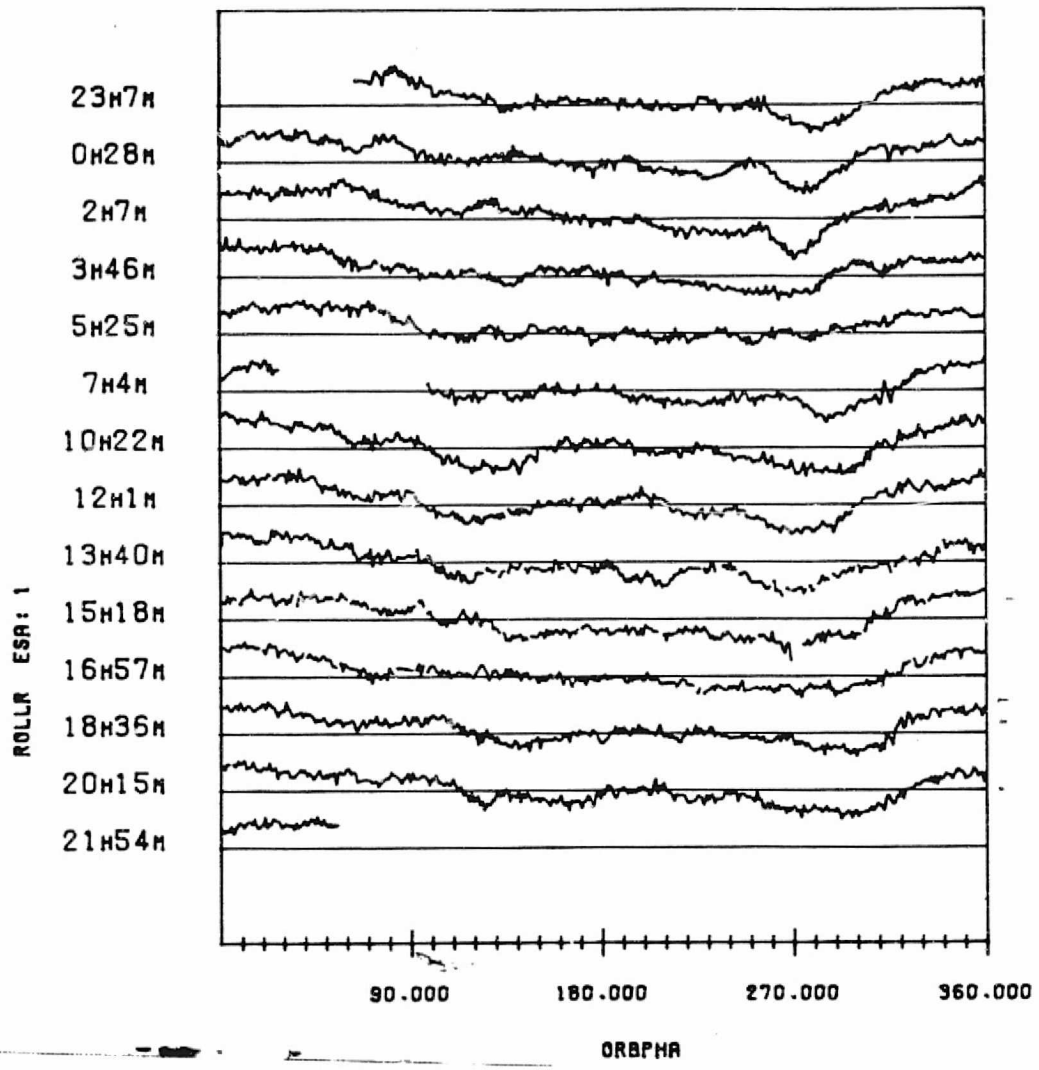

FIGURE 3-9. Residuals for Consecutive Orbits on November 3, 1982 (3 of 4, Sensor 1 Roll)

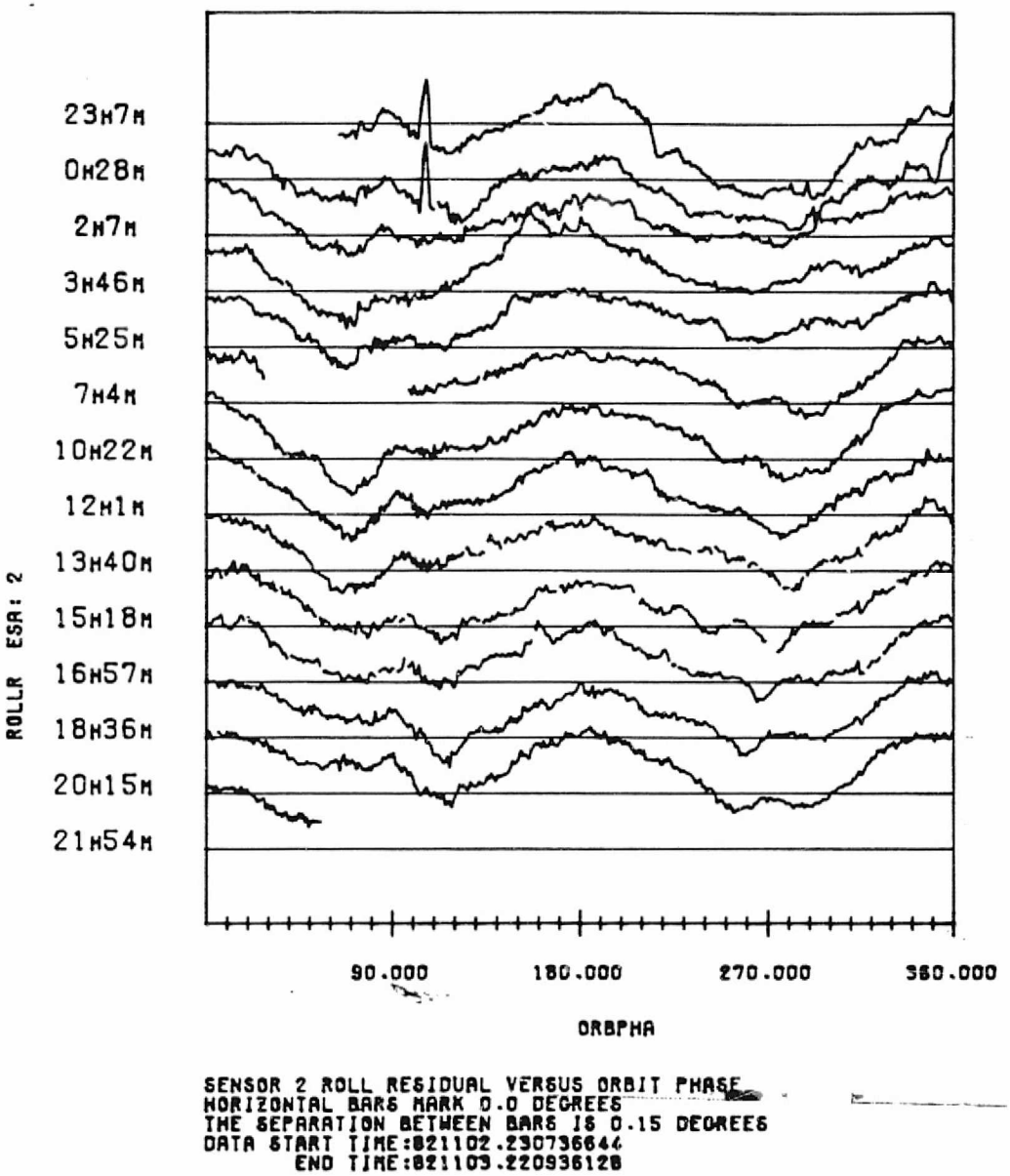

FIGURE 3-9. Residuals for Consecutive Orbits on November 3, 1982 (4 of 4, Sensor 2 Roll)

Glitches or bumps appear in the scanner 2 data at 105 and 290 degrees from the ascending node on the first few orbits of this data span. These glitches result from Moon irterference which is discussed in Section 6.2.

Figure 3-10 shows the residual errors as a function of orbit phase for 12 sample days representing all months of the year.

The most outstanding and curious feature is the large measurement variation from orbit to orbit that occurs at times in one polar region or the other. The peak-to-peak residual error spread in the polar region is often as high as 0.4 degrees. Aside from these polar region variations, the measurements generally show the same systematic error pattern each orbit with the peak-to-peak variation from orbit to orbit typically less than 0.1 degrees. The orbit period systematic error patterns change gradually throughout the year.

Particular features in some of the data spans in Figure 3-10 are noted as follows:

- Spikes in the sensor 1 measurements in January, February and March are due to sun interference effects as described in Section 6.1.

- The glitches in both scanner measurements on December 1, 1982 are due to moon interference effects as described in Section 6.2.

- Small excursions around the North pole on August 6, 1982 are due to the reference attitude anomoly mentioned in Section 2.2.

Constant biases are apparent in each of the measurement channels. The average biases for each channel are summarized in Table 3-1. These biases result from a combination of ground calibration errors and sensor modeling parameter adjustments. For example, the Earth width

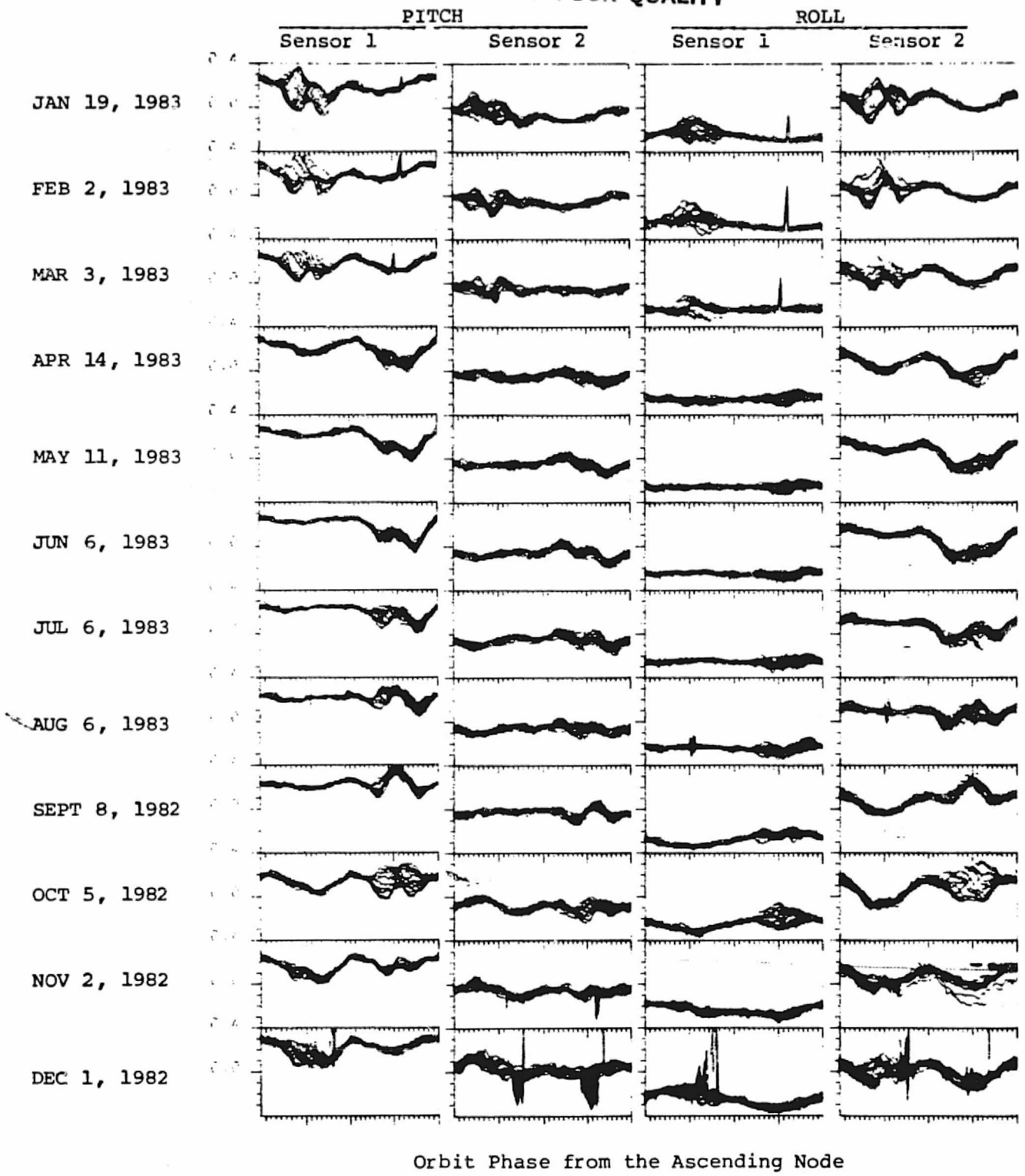

FIGURE 3-10. Residual Errors in Pitch and Roll with Nominal Calibration and Attitude, Orbit and Earth Oblateness Modeling for Sample Days from Each Month

TABLE 3-1. Constant Biases from the Nominal Oblate Earth Model

Measurement Channel	Average Bias
Sensor 1 Pitch (Width)	.19
Sensor 2 Pitch (Phase)	-.05
Sensor 1 Roll (Phase)	-.25
Sensor 2 Roll (Width)	.06

NOTE: The following key model parameters are assumed in obtaining the the above constant biases.

1. Nominal Sensor Calibration;
   0.0 degrees pitch and roll at 2.5 volts sensor output

2. Nominal 40 kilometer triggering height above the oblate Earth model for the predicted measurements.

channel biases are sensitive to the constant horizon triggering height which is assumed for the oblate Earth model predicted measurements. A 40 kilometer height was assumed for this processing. The constant biases in the width channels (sensor 1 pitch and sensor 2 roll) would decrease by about 0.03 degrees for each kilometer increase in the nominal constant triggering height used. The biases should remain constant throughout the mission. The small variations that occur in the average biases for each day are discussed in Section 5.3.

Appendix D contains plots of these residual errors with the constant biases removed for all the data spans processed for this report. One additional anomoly is apparent from the review of all these plots which has not yet been mentioned. The sensor 2 roll (width) channel shows a larger than usual spread in the orbit to orbit variations for several days early in the mission. This feature has not been seen any of the days since the beginning of 1983.

It is believed that the orbit period systematic errors and polar region measurement patterns result largely from the effects of Earth radiance variations. The Earth radiance variation and its effect on the scanner measurements is discussed in the next section. Details of the scanner measurement orbit-to-orbit variations in the polar region are discussed in Section 7.2. General features in the horizon scanner measurement errors are consistent with the hypothesis that large scale stratospheric radiance variations are influencing the measurements. These features are enumerated below.

1. The fact that the residuals variations are generally the largest around the winter pole is consistent with higher radiance variability observed there.

2. Both scanner Earth widths show similar residual patterns, with a slight phase lag for scanner 1. This suggests that the error may originate from the Earth's surface.

3. The Earth widths are more affected than the Earth phases, suggesting perhaps that the radiance variations are generally on a large enough scale that they effect both horizons the same way.

4. Around the winter pole, the effects change gradually from one orbit to the next in a manner that is generally consistant with a radiance feature rotating with the Earth. The residual pattern tends to repeat itself 24 hours later when the satellite ground track covers the same longitudes.

5. The residual error patterns change gradually over the year and repeat the same general pattern at dates one year apart.

SECTION 4 - PREDICTED EARTH RADIANCE EFFECTS

The main error source contributing to the residual errors presented in Section 3.5 is believed to be the Earth radiance variations. This section provides an overview of the general characteristics of the Earth radiance variations, and focuses the discussion on the systematic latitude dependent radiance effects which have been modeled by the Horizon Radiance Data Base (HRDB) and the Landsat-4 Sensor Optics and Electronics Simulator (SOES). The HRDB/SOES predicted effects are compared with the flight data and the residual errors from the predictions are presented. The HRDB model deficiencies and other possible unmodeled error sources which may contribute to this residual error are discussed.

4.1 EARTH RADIANCE CHARACTERISTICS OVERVIEW

This section discusses the general character of the systematic Earth radiance variations in a qualitative sense. Selected data from meteorological research is provided which displays these characteristics.

Figure 4-1 shows a spectrum of the Earth's outgoing infrared radiation for three sample views below Nimbus 4 observed by the IRIS experiment. Radiation is absorbed and reemitted by various constituents in the atmosphere. The strong CO_2 absorption band between 14 and 16 microns is generally chosen for attitude sensing horizon scanners because it is less dependent on surface conditions than other bands, and is generally more stable in brightness. In the center of this band, nearly all surface radiation is absorbed and reemitted in the stratosphere, and therefore the emissions in this band reflect stratospheric temperatures.

As one moves from the center of this band to the edge, one becomes sensitive to radiation originating at lower and lower altitudes. In

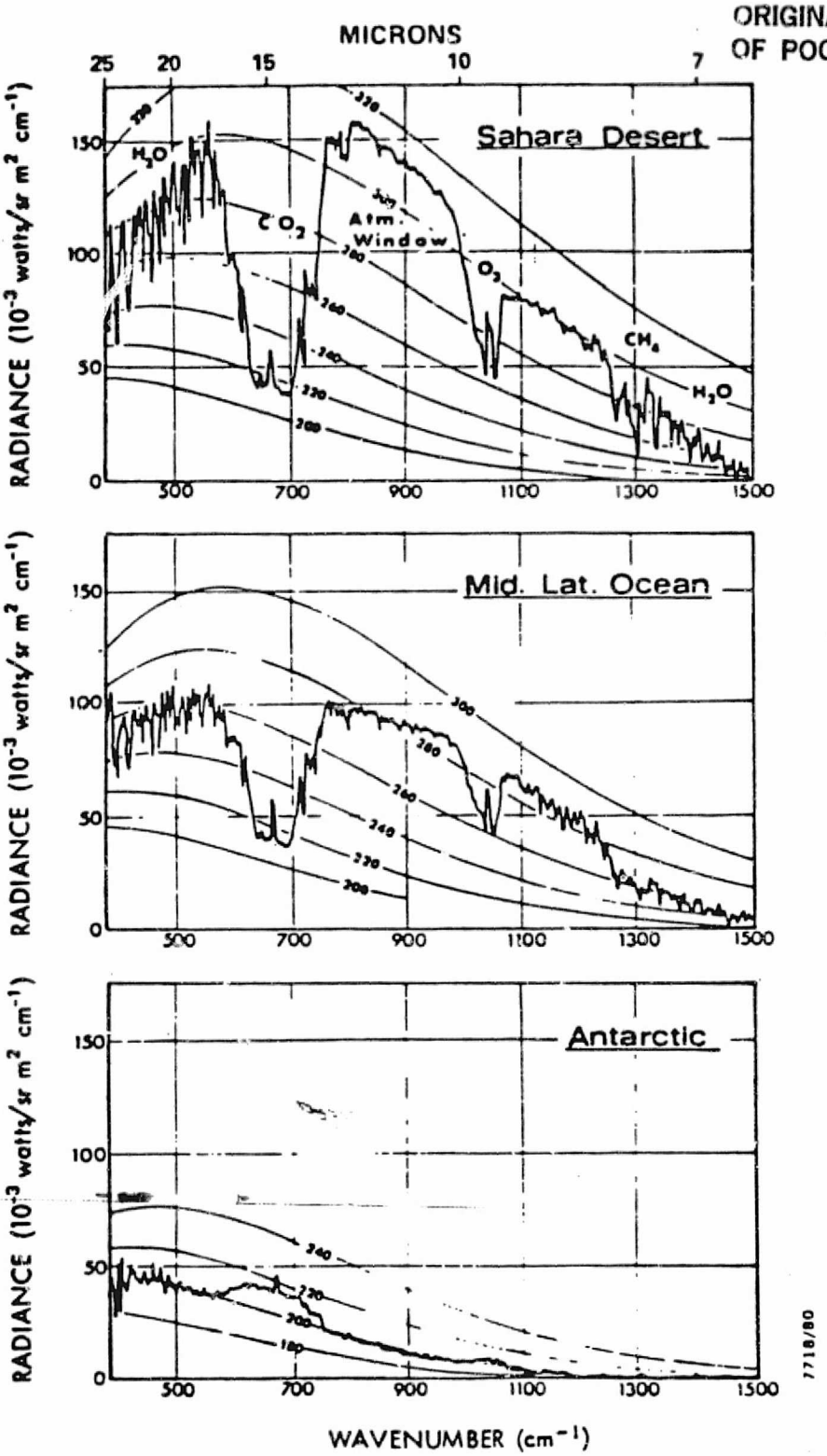

Thermal emission spectra (obtained from Nimbus 4 IRIS experiment during orbit 29, 10 April 1970) compared to curves of constant brightness temperatures (K).

FIGURE 4-1. Earth's Outgoing IR Radiation for Various Nadir Views

fact this sensitivity is used in many experimental meteorological satellite sensors to compute soundings of the atmospheric temperatures as a function of altitude. The lower atmosphere shows the same winter/summer temperature variations that we are familiar with on the ground, and there is also the permanent latitude dependent trend characterized by the equator always being warmer than the poles. Near the edges of the CO_2 absorption band, the outgoing radiance is strongly influenced by the temperatures of the surfaces or cloud tops which are viewed.

An excellent compilation of data on the Earth radiance at 15 microns (the center frequency of the CO_2 band) is presented by S. Fritz and S. Soules using Nimbus 3 Satellite Infrared Spectrometer. Fritz and Soules were interested in the systematic stratospheric temperature variations indicated by the data, but for us this data indicates the systematic patterns of Earth radiance variations to which the horizon scanners will respond. Figure 4-2 shows two figures extracted from one of their papers (Reference 15) which illustrate the seasonal variations in the 15 micron radiance.

Figure 4-2(a) shows the seasonal changes in the radiance for a range of latitudes. As might be intuitively expected, the Northern and Southern hemispheres each are warmer in the summer and cooler in the winter. There is a slight asymmetry between the hemispheres which is apparently explained by the eccentricity of the Earth's orbit: The Earth is closest to the Sun in December so the Southern hemisphere gets the warmest. Finite Fourier series fits were made to these seasonal changes, and the residuals from these fits are shown in Figure 4-2(b). A clear feature illustrated by these plots is the greater instability of the radiances in the winter hemispheres. Thus the Southern hemisphere shows more radiance variability in June through September while the Northern hemisphere shows more variability in December through March. The Northern hemisphere variability appears greater than the Southern.

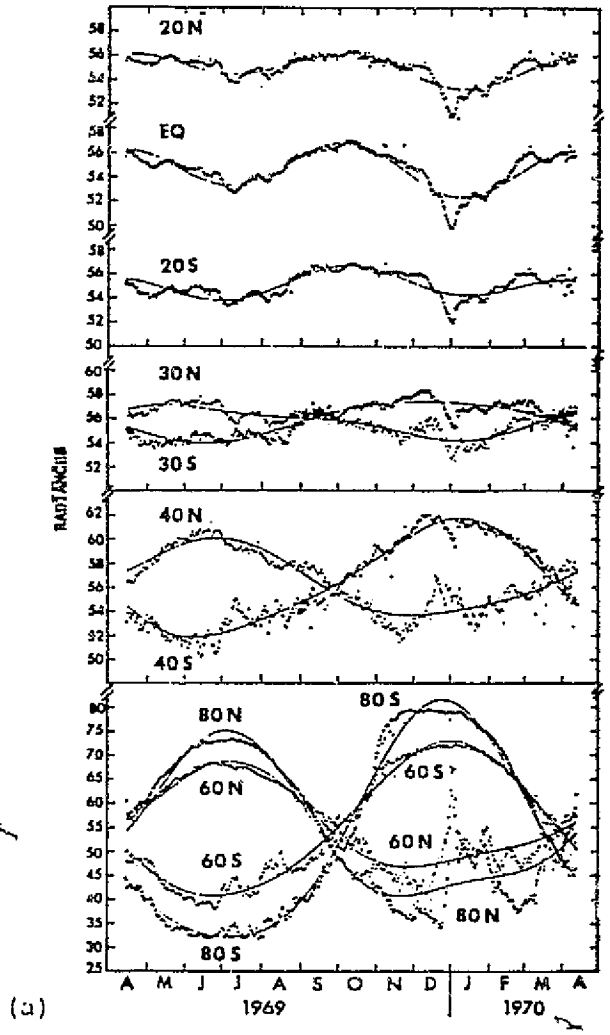

FIGURE 1.—Annual march of radiances at 669.3 cm^{-1} for selected latitudes showing the seasonal warming and cooling of the stratosphere. Smooth curves are radiance values [$mW \cdot m^{-2} \cdot (ster)^{-1} \cdot (cm^{-1})^{-1}$] calculated from the data by a finite Fourier-series method using annual and semiannual periods. Data at each latitude represent observations for a 4° latitude zone averaged daily around the latitude circle.

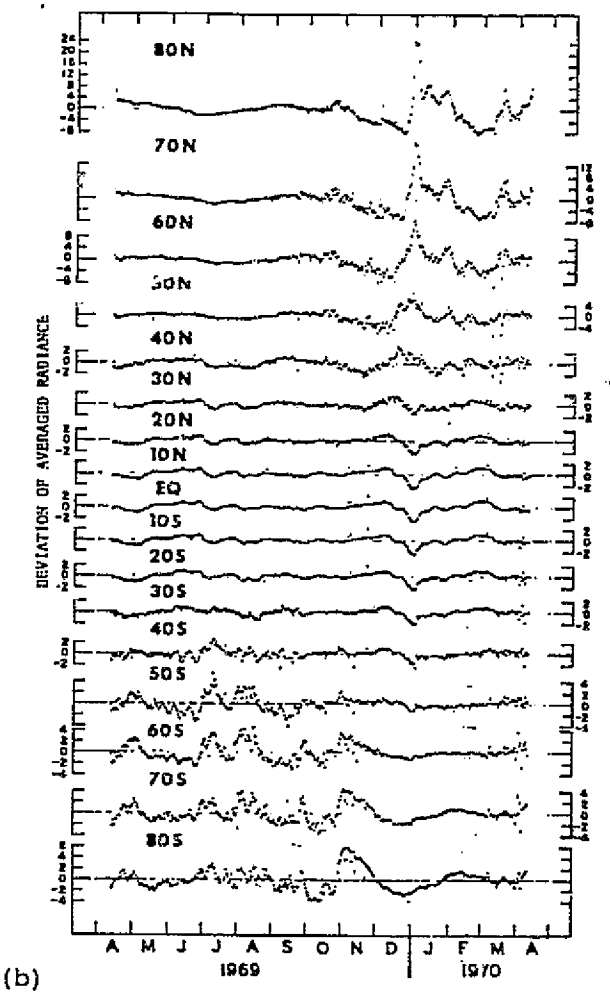

FIGURE 2.—Deviation of averaged latitudinal radiance [$mW \cdot m^{-2} \cdot (ster)^{-1} \cdot (cm^{-1})^{-1}$] from a finite Fourier-series fit for 80°N–80°S from Apr. 14, 1969, to Apr. 13, 1970.

FIGURE 4-2. Annual Variations in Latitude Averaged Earth Radiance at 15 Microns as Measured by the Nimbus III Satellite Infrared Spectrometer (Adapted from Reference 12)

While the Fritz ans Soules data represent the Earth radiance for the nadir view in the center of 15 micron band, it is actually the radiance viewed on the edge of the Earth which is more important for horizon sensing.

Measurements of the Earth limb radiance have recently become available from the Limb Infrared Monitor of the Stratosphere (LIMS) experiment onboard Nimbus-7. General Software Corporation has recently examined this data as part of an effort to understand the Earth radiance variability and the accuracy of the HRDB (Reference 11). The LIMS data includes measurements for a wide bandpass and a narrow bandpass both centered on the 15 micron CO_2 band. These spectral bandpasses are shown in Figure 4-3. The width of the Landsat-4 spectral bandpass falls between these two.

Figure 4-4 shows a plot of all the CO_2 limb profile measurements taken at several latitude bands, on January 17, 1979 with all the profiles available within a 2 degree latitude band overlayed. The latitude dependence of the Earth limb radiance is illustrated. Also, the greater variability of the winter hemisphere limb radiance is clearly demonstrated. Further discussion of the latitude dependence of the Earth radiance indicated by LIMS is given in Section 4.4, and the variability of the Earth radiance in the polar region is discussed later in Section 7.1.

4.2 SEASONAL SYSTEMATIC EFFECTS MODEL

Extensive efforts have been made to predict the effects of seasonal systematic latitude dependence of the Earth radiance. This effort requires a model of the sensor response as well as a model of the Earth radiance.

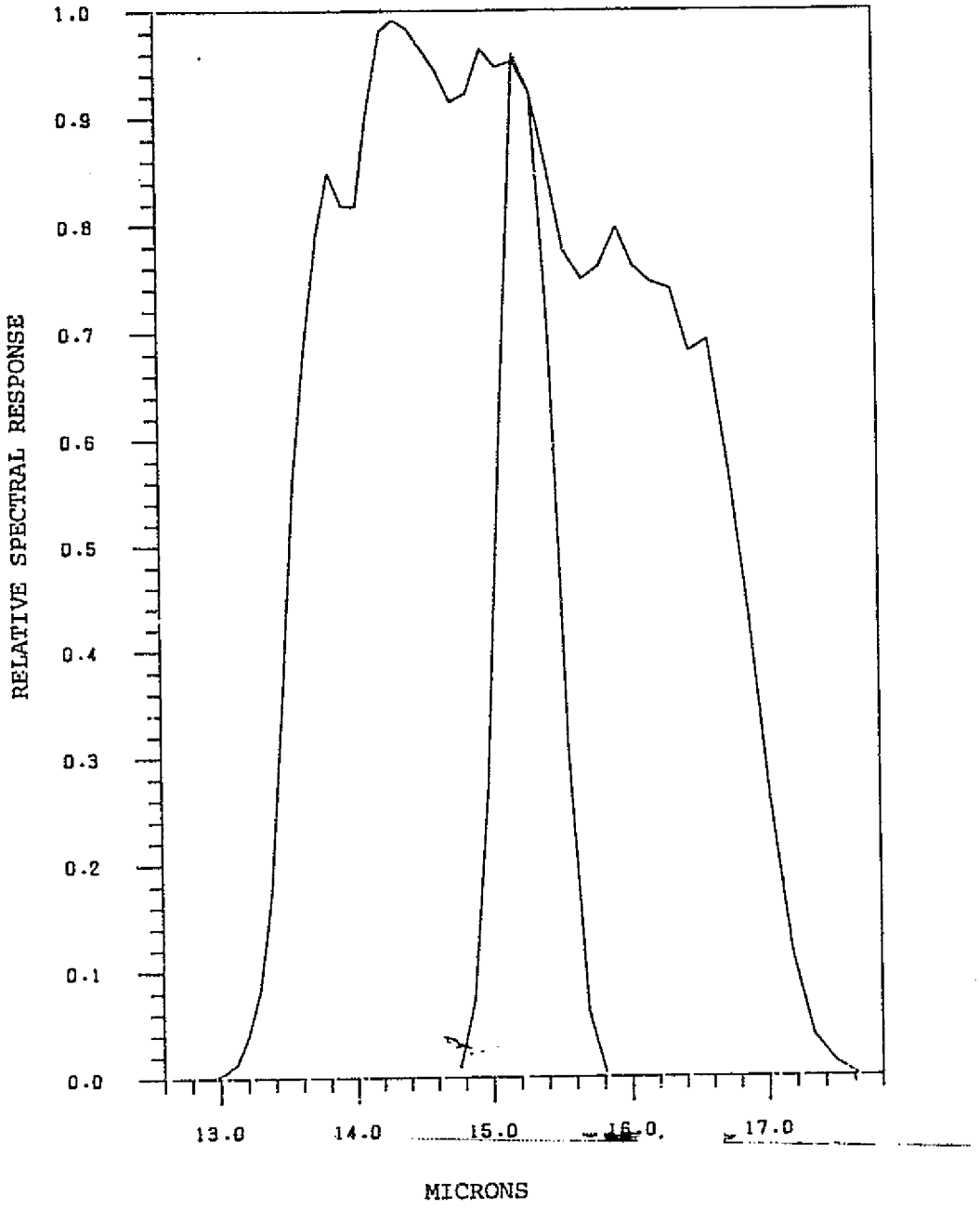

FIGURE 4-3. LIMS Narrow and Wide CO_2 Band Spectral Response as a Function of Wavelength

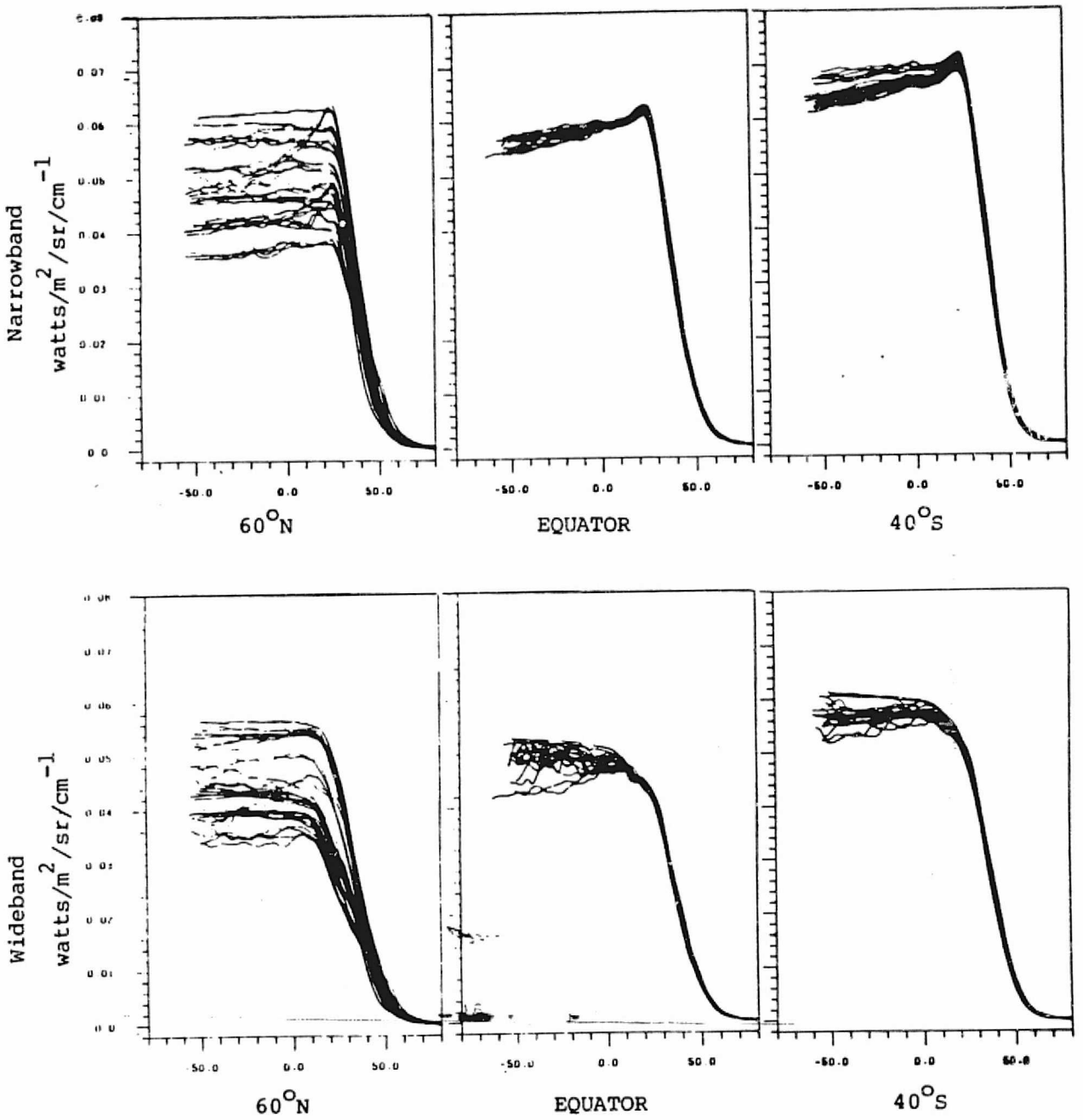

FIGURE 4-4. Overlaid Narrowband (Top) and Wideband (Bottom) CO_2 Profiles as a Function of Tangent Height (KM) for 60°N, the Equator and 40°S Latitudes from LIMS Data Measured on January 17, 1979

To model the sensor response to radiance changes, the Sensor Optics and Electronics Simulator (SOES) was developed. It computes the incoming radiance integrated over the bolometer field of view as it sweeps across the Earth. This input signal is convolved with the electronics impulse response function to compute the electronics output signal on which threshold detection is done. This linear system model of the electronics is based on a transfer function for the electronics provided by the scanner manufacturer, Ithaco, Inc. The output signal is computed at a representative number of points and then the horizon detection logic, described earlier (Section 1.3), is simulated, by parabolic interpolation for the peak detection, and linear interpolation for the threshold crossings. The scanner measurements are computed for the nominal flight geometry as the spacecraft moves around the orbit and receives the radiance signal from the various parts of the Earth.

The Attitude Determination and Control Section at Goddard Space Flight Center has recently supported the development of a Horizon Radiance Data Base (HRDB) which estimates the average monthly latitude dependence of the Earth radiance. The HRDB was developed by Computer Sciences Corporation (CSC) (Reference 12) as part of an effort to provide a global database of the Earth Infrared (IR) Radiance for use in evaluating systematic horizon scanner errors. The HRDB is based on a 1972 Radiosonde Observations (RAOBS) data base (Reference 13) which provides average atmospheric temperatures, and an adaptation of the United States Air Force LOWTRAN-5 computer program (Reference 14) for computing the radiation based on the atmospheric model.

The HRDB is a database of average Earth radiance spectra from 8 to 22 microns as a function of latitude, month of the year, and scanner viewing angle. The wavelength range spans the region commonly used by horizon scanners. To apply the HRDB to a particular sensor, the radiance data is integrated with the sensor spectral response function. The HRDB provides radiance spectra for 20 degree latitude

bands centered between 80° South and 80° North, for each month of the year. The viewing angles are parameterized as tangent heights when the line of sight is above the physical horizon, and as zenith angles when the line of sight intersects the Earth surface. More details about the HRDB are provided in Reference 12. An evaluation of the HRDB accuracy through a comparison between the HRDB and the Nimbus-7 Limb Infrared Monitor of the Stratosphere (LIMS) data is given in Reference 11. Pertinent results of the LIMS/HRDB comparison are discussed in the next section to explain some deficiencies in the HRDB/SOES modeling.

The HRDB/SOES predictions for the systematic Earth radiance effects are shown in Figure 4-5 for all 12 months of the year plotted against orbit phase from the ascending node. The largest predicted effects are in the Earth width measurement channels (sensor 1 pitch and sensor 2 roll). The two width channels show a similar predicted effect but there is a slight phase lag observable in sensor 1 relative to sensor 2 because both the sensor 1 horizons are looking behind the spacecraft. The next largest effect is in the phase measurement for sensor 2. The smallest effect is in the phase measurement for sensor 1 for the same reason that the Earth oblateness effect is smallest in this channel; both the scanner 1 horizons view nearly the same latitude and therefore the radiance effects cancel out for the phase measurements.

Reviewing the progression in the radiance effects over the 12 months, one can notice a particularly abrupt change in the systematic effects in the southern hemisphere between October and November. Around the minumum southern latitudes a notable rise in the width channel measurements appears in July and August and reaches a maximum amplitude in September and October. Then this feature abruptly disappears in November with only a small rise at the south pole appearing within a general drop in the Earth widths around the southern hemisphere. The predicted drop in Earth widths in the

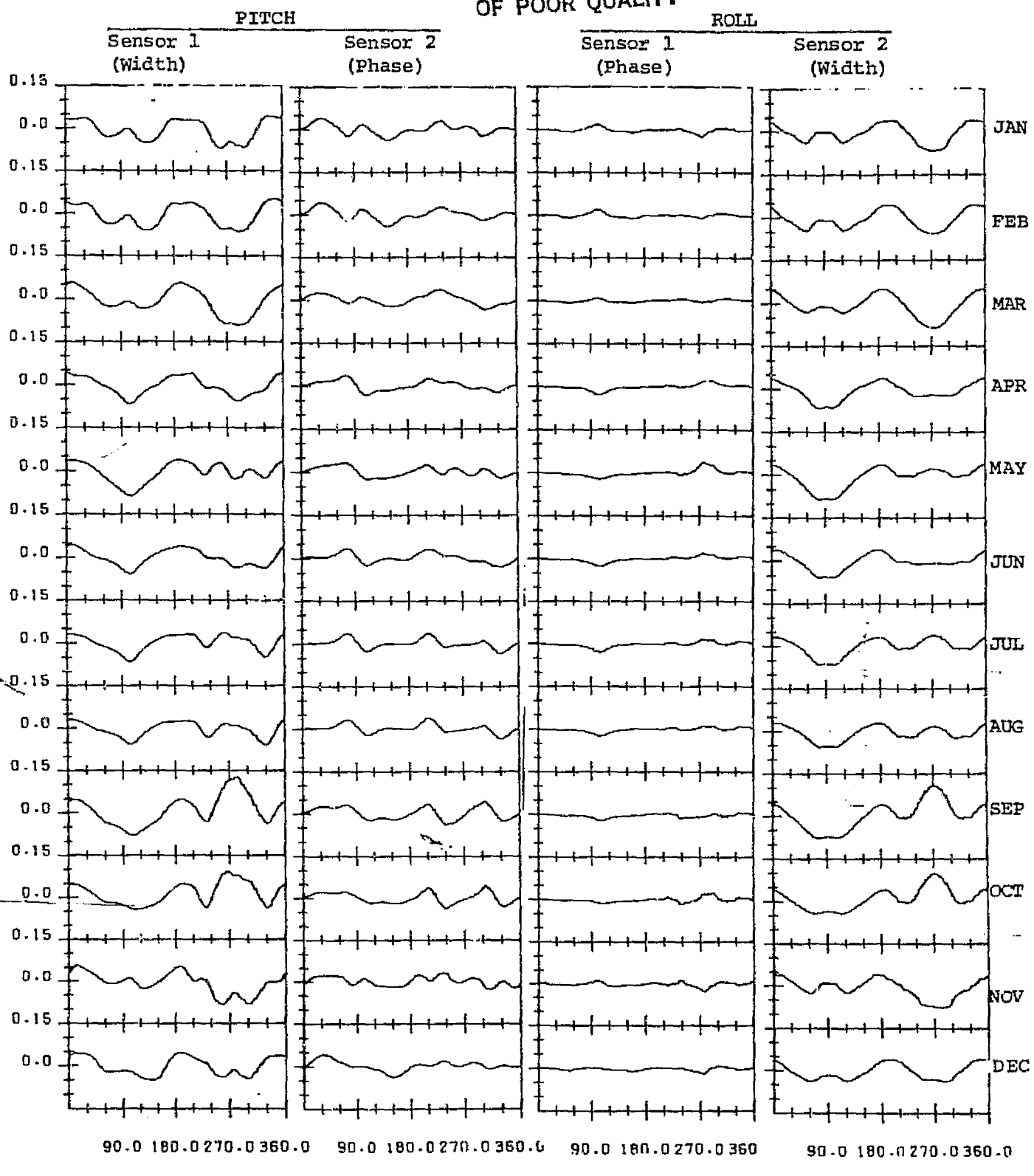

FIGURE 4-5. HRDB/SOES Predicted Horizon Radiance Effects for All Months

southern hemisphere reaches a maximum in March and then largely disappears in April, May, and June. The northern hemisphere shows less variation in the systematic effects predicted over the course of the year. A general reduction in both Earth widths around the northern hemisphere is predicted throughout the year, with the winter months showing a slight rise around the north pole within the general reduction. Notice the significant lack of symmetry between the effects predicted in the northern and southern hemispheres.

4.3 MODEL COMPARISON WITH FLIGHT DATA

The HRDB/SOES modeling successfully predicts many of the key features in the residual errors (see Figure 3-10 for comparison with the predicted effects in Figure 4-5). For example the large rise in the errors in the Earth widths due to radiance effects for the south pole region of the orbit in September is predicted and observed in the flight data residuals. Also this feature's fairly rapid disappearance by November is predicted and observed. The predicted general tendency of a drop in the Earth widths around both poles in November through June is observed. However many details of the amplitude and timing of the predicted effect show a mixture of sucesses and failures.

In order to clearly illustrate the comparison between the predicted radiance effects and the observed residual errors, Figure 4-6 shows the systematic errors predicted by SOES/HRDB plotted alongside the observed residual errors (with oblateness and attitude/orbit effects removed) for 15 sample data spans. In each of the plots, the predicted curves are placed above the data by a constant distance in order to show the systematic variations clearly. Figure 4-6 demonstrates that the HRDB and SOES successfully predict the general shape of the seasonal systematic errors in the Landsat-4 Conical Scanner measurements for most months. The smaller bumps predicted by the corrections sometimes clearly correlate with features in the data, however sometimes they do not correlate with any observable features

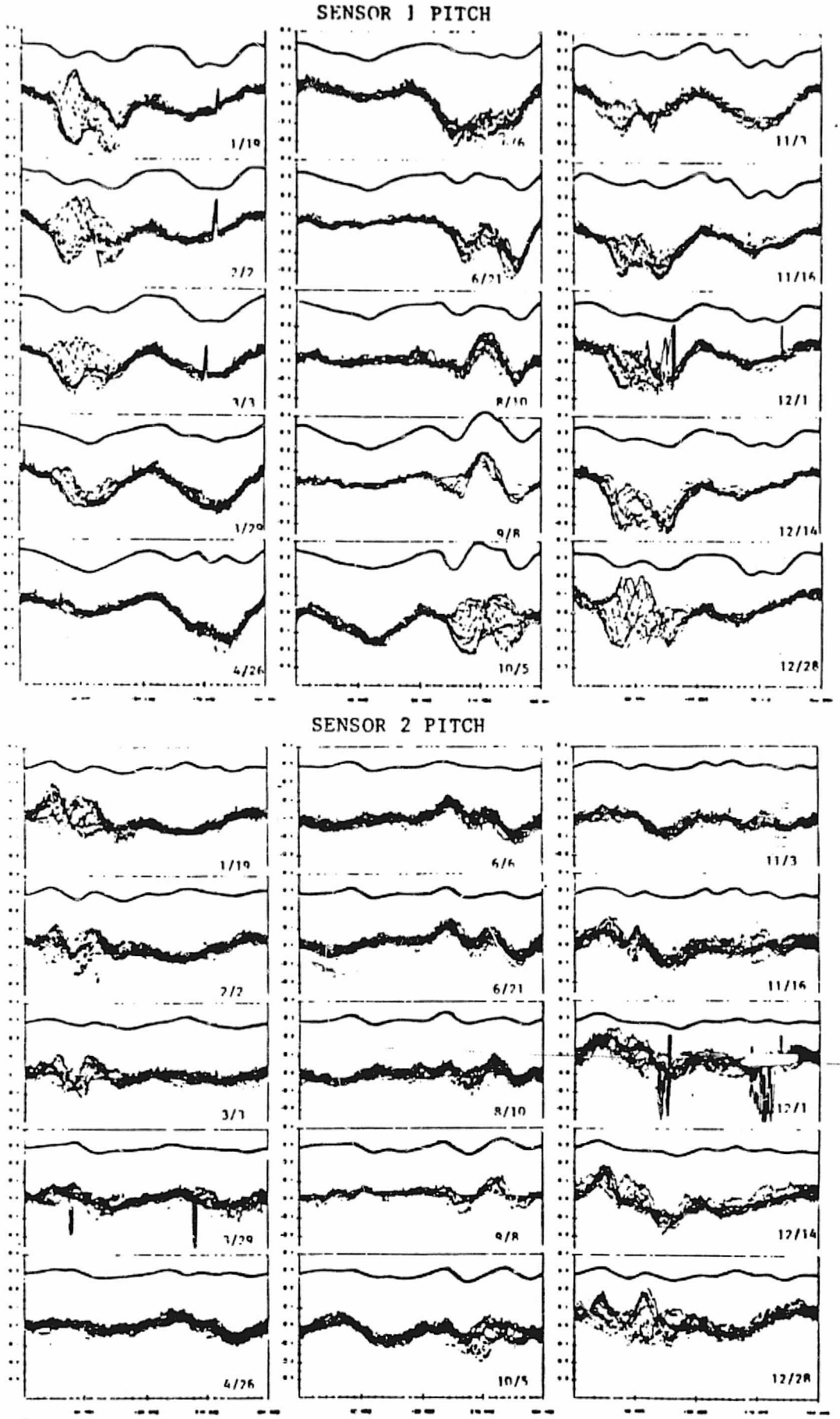

FIGURE 4-6. Residual Errors Compared to Predicted Radiance Effects (1 of 2)

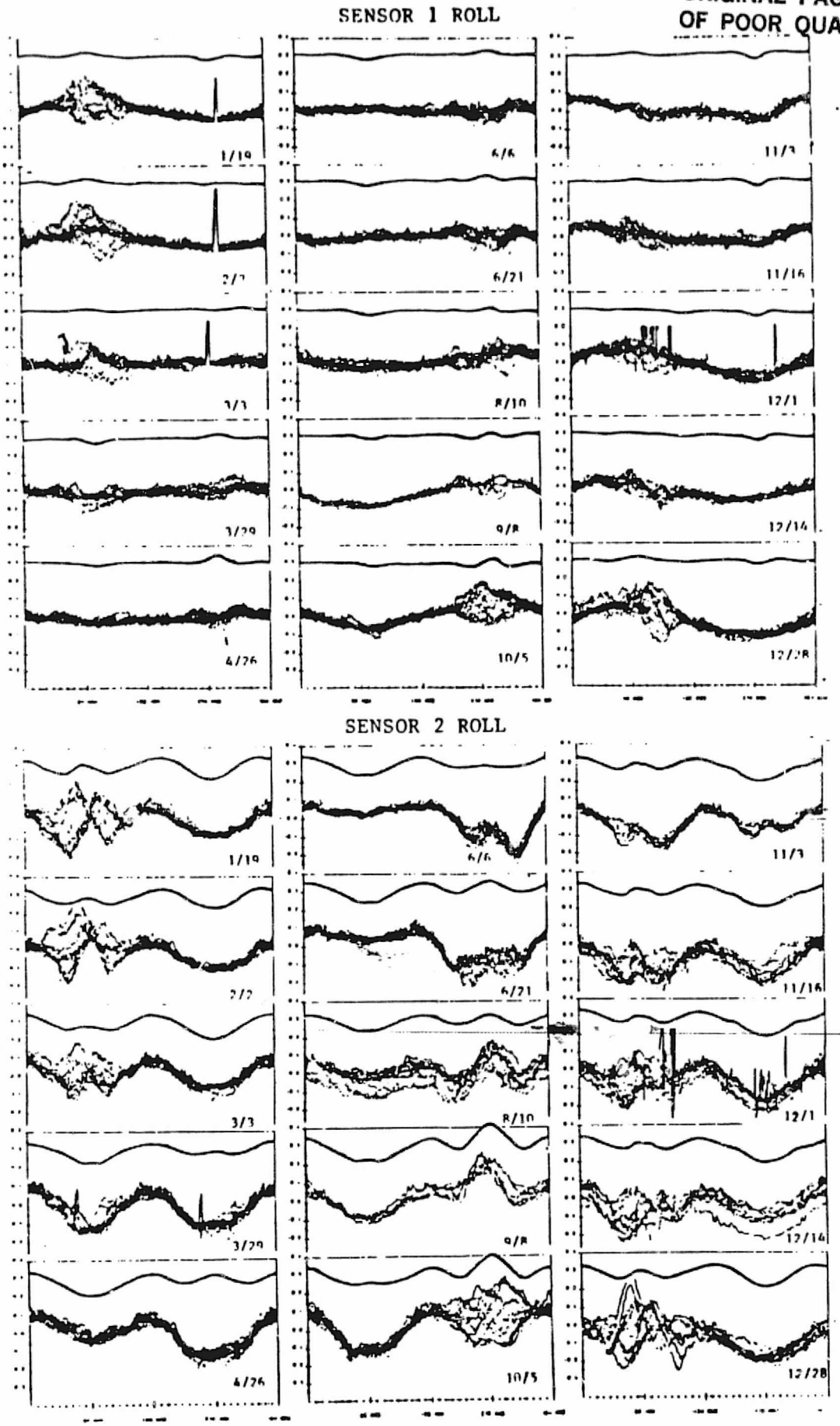

FIGURE 4-6. Residual Errors Compared to Predicted Radiance Effects (2 of 2)

in the data. For some months the HRDB predicts the proper amplitude for the corrections in Earth widths, most notably for March and September. The corrections are most noticably underestimated for April to June in the southern hemisphere and October to December in the northern hemisphere.

Figure 4-7 shows the residual errors plotted beside the predicted radiance errors and also shows the residual errors after the predicted radiance effects are removed from the data for sample spans from all months. This figure illustrates the success and deficiencies of the HRDB/SOES in removing the radiance effects from the data. Also illustrated is the fact that the HRDB may introduce additional errors to the data by making erroneous corrections. This occurs most noticably in the northern hemisphere in June and July.

In general, the averaged residual errors in the data are reduced after the HRDB/SOES corrections are applied. This will be further discussed in Section 5.4.

A complete set of plots for all the data spans of the residual errors after the predicted HRDB/SOES effects and constant biases are removed are provided in Appendix E.

4.4 HRDB MODEL DEFICIENCIES

Some of the errors in the HRDB/SOES modeling of the radiance effects are explained by deficiencies indicated in the HRDB by comparison with the LIMS data (Reference 11). Figure 4-8 shows the latitude dependence of the Earth radiance predicted by the HRDB and observed by LIMS for the narrow and wide bandpasses for the seven months in which the LIMS experiment operated. The HRDB generally underestimated the gradient in Earth radiance between the tropics and the poles. Thus the HRDB underestimates the summer hemisphere brightness and overestimates the winter hemisphere brightness.

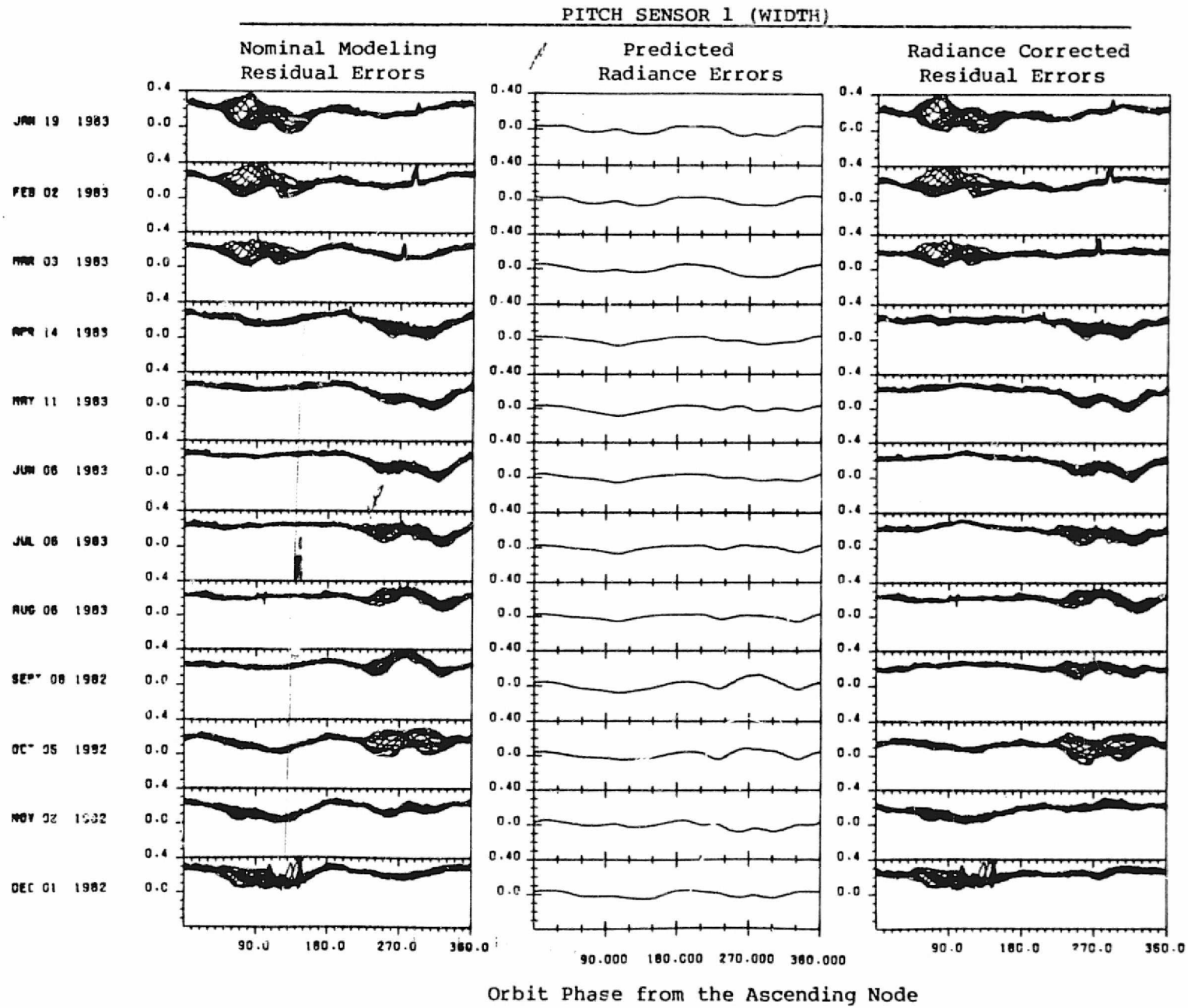

FIGURE 4-7. Residual Errors, Predicted Radiance Errors and Radiance Corrected Residual Errors for 12 Months (1 of 4, Pitch Sensor 1)

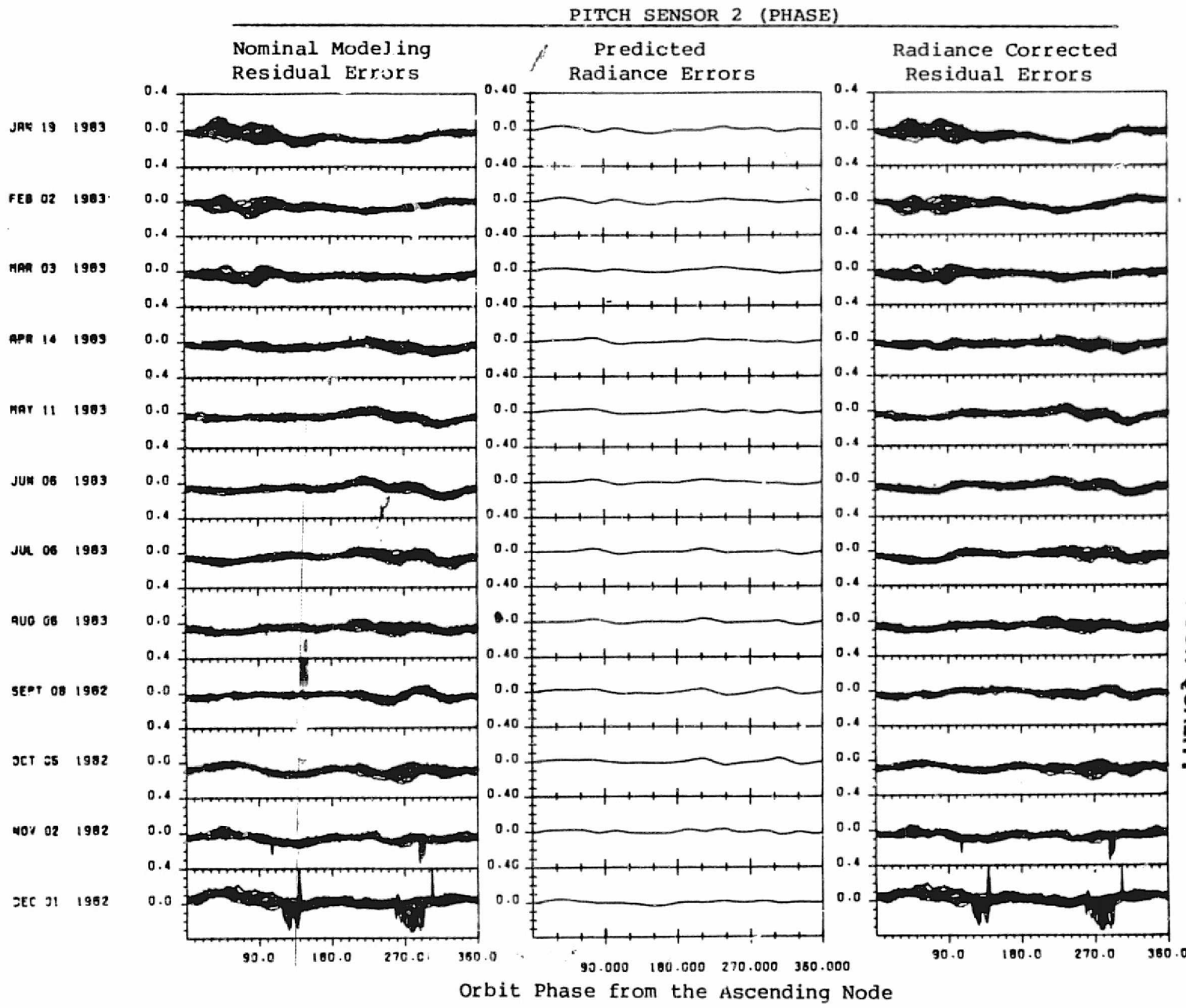

FIGURE 4-7. Residual Errors, Predicted Radiance Errors and Radiance Corrected Residual Errors for 12 Months (2 of 4, Pitch Sensor 2)

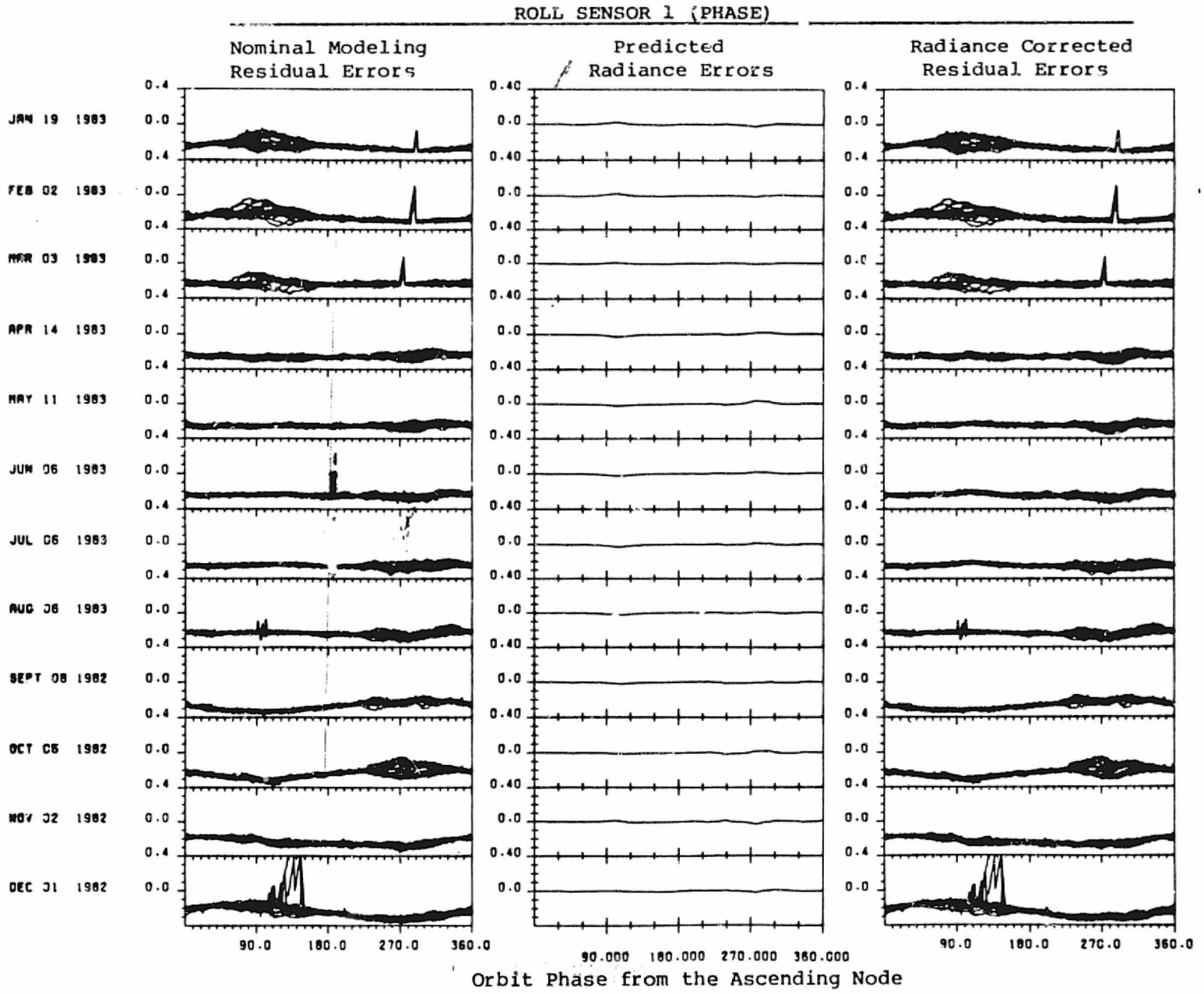

FIGURE 4-7. Residual Errors, Predicted Radiance Errors and Radiance Corrected Residual Errors for 12 Months (3 of 4, Roll Sensor 1)

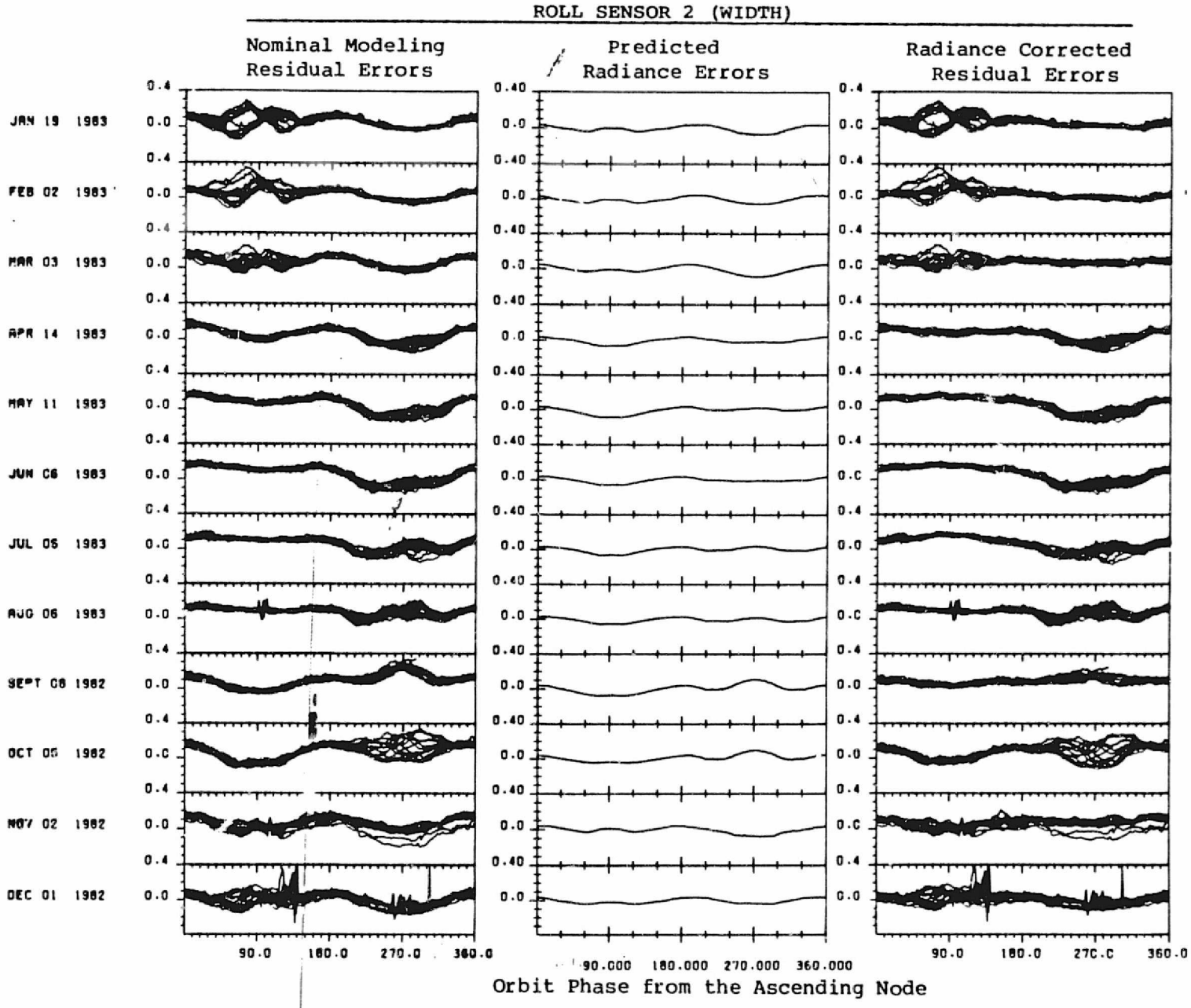

FIGURE 4-7.: Residual Errors, Predicted Radiance Errors and Radiance Corrected Residual Errors for 12 Months (4 of 4, Roll Sensor 2)

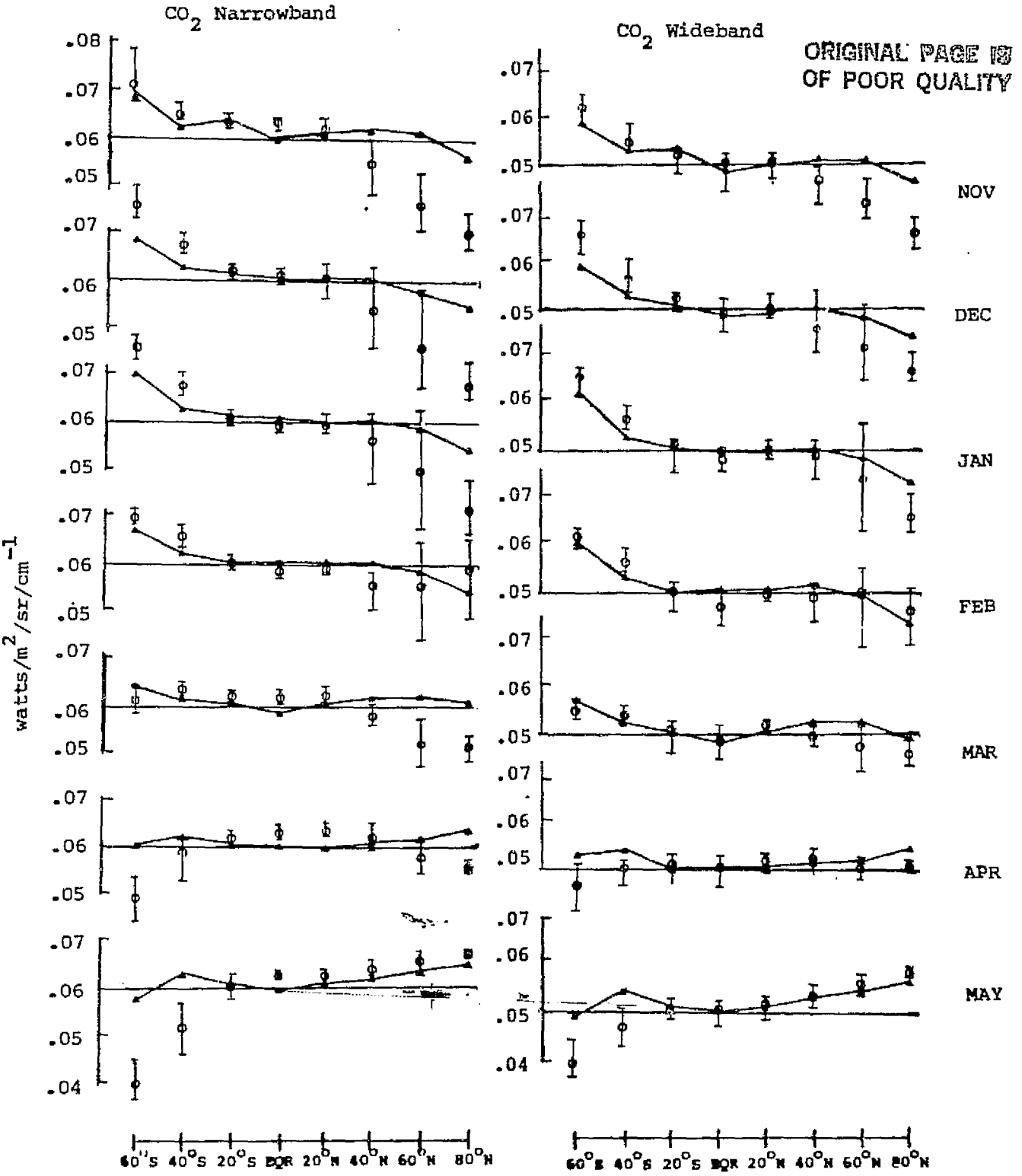

FIGURE 4-8. Radiance at 0 Kilometers Tangent Height Observed by LIMS (O) and Predicted by the HRDB (▲). Bars Indicate Minimum and Maximum LIMS Values.

The most severe underestimate of the systematic latitude dependent radiance gradient is found in the northern hemisphere in November and in the southern hemisphere in May. These are actually late fall months for the respective hemispheres and are the months for which the amplitude of the radiance effect is apparently most severely underestimated by the HRDB/SOES modeling for the Landsat-4 data. In the subsequent winter months in the northern hemisphere the HRDB-LIMS agreement improves as does the HRDB/SOES-Landsat-4 Data agreement, although the large spread that appears in the LIMS data and the Landsat-4 horizon measurements around the pole regions make the comparison less meaningful. (This polar radiance variability is discussed in Section 7.1.) Unfortunantely the LIMS data is not available through the southern hemisphere winter and early spring months when the large and rapid changes in the southern hemisphere radiance effects occur.

Further details of the HRDB model deficiencies are discussed in Reference 11. It is clear that this data base can be improved significantly.

Note that the HRDB does not model the longitude dependence of the Earth radiance. Thus the HRDB and SOES cannot model any orbit to orbit sensor measurement variations. As will be discussed further in Section 7.1, the longitude dependence of the Earth radiance is particularly strong in the winter polar regions.

4.5 UNMODELED ERROR SOURCES

The possibility that other systematic errors beside radiance effects are contributing to the residual errors needs to be given consideration. One large scale feature not predicted by the radiance modeling is particularly noteworthy in the residual errors. In the sensor 1 roll (phase) channel where very little radiance effects are

predicted, a strong orbit period pattern is present. This pattern seems to grow in amplitude from the early part of the mission and changes sign between October and December. It has the highest amplitude on December 1 and December 28 and lower amplitude on neighboring days and then disappears starting in March. This orbit period variation also shows up in the sensor 2 roll (width) channel in addition to the radiance effects in that channel. Recent data from September 14, 1983 does not show the same orbit period pattern indicated on September 8 and 22 of 1982, so therefore this does not appear to be a seasonal effect. Because the feature does not repeat itself, because its erratic amplitude, and because it shows up in both roll channels, the likely explanation for this effect is the early mission problems with the reference attitudes (see Section 2.2). This point will be illustrated further after the data fitting is performed in Section 5.3.

In addition to the possibility of reference attitude errors, the possibility of onboard ephemeris errors also must be considered. The ephemeris error which would be most likely to show up in scanner data would be an in-track orbit error or a timing bias. This type of error would be equivalent to a pitch bias in the reference attitudes and would probably be constant over a particular data span. Another ephemeris error which could cause some effect on the scanner measurements would be a radial distance error, and this would show up in both the Earth width channels. Radial distance errors which are large for ephemeris computation standards, 100 meters, would cause a small effect on the predicted Earth widths, about 0.0054 degrees, which corresponds to about 0.003 degrees of pitch or roll. The onboard ephemeris is updated each day for Landsat, so conceivably a significant change in the updated ephemeris could show up as a discontinuity in the residual pattern in the middle of the data span. However no discontinuities like that are found in the data. It is most likely that ephemeris errors are not a significant contribution

to the residual errors. The possibility of ephemeris errors is discussed further in view of the data fitting results in Section 5.3.

Several additional error sources have been considered briefly. Many possible error sources will cause constant biases in the pitch or roll measurements, and therefore can be lumped together as part of the constant bias removal for each channel. These errors include sensor calibration offsets, triggering height biases, Earth angular radius biases, voltage output biases, or circuit time delays. These errors should be constant over the whole mission.

An error in the slope of the calibration curves in each channel would introduce an Earth width or phase dependent biases. However the actual variations in the width and phase measurements are small because the attitude stays close to zero pitch/roll/yaw. Therefore the errors in the calibration curves slopes would have to be very large to show significant effects. Moreover, since the widths and phases vary at orbit frequency in virtually the same way for nearly all the data spans examined, even a large calibration curve slope error would show virtually the same effect in all the data spans. Fortunately, two data spans included periods with the spacecraft at a slightly non-nominal attitude while in acquisition mode (see Section 2.1). The observation that the residual errors at these non-nominal attitudes (up to one degree off zero roll) are consistent with the residuals observed in the precision Earth pointing mode gives some indication that large calibration curve slope errors are not present.

A temperature dependence of the measurements was considered a possibility. The most likely dependence expected was on the electronics temperatures, however practically no variation has been seen in the Earth sensor assembly housing temperatures that would test that possibility. A dependence on the bolometer temperature is not expected from the sensor design and none can be observed in flight data for the range that these temperatures vary, which is not a high

range. The sensor 1 bolometer temperature shows the widest temperature range and a distinctive orbit period variation pattern. This pattern has been virtually the same throughout the mission. This pattern cannot be seen in the residual errors, at least not above the level of the noise and variations introduced by other sources such as the radiance variations.

SECTION 5 - DATA FITTING RESULTS AND RESIDUAL STATISTICS

In order to provide convenient corrections to the systematic errors observed in the scanner data, fits to these errors are being made, and the seasonal dependence of the fit coefficients is being examined. This represents an empirical approach to correcting the systematic errors regardless of the error source, although the largest seasonal dependent source is presumed to be Earth radiance effects.

Section 5.1 describes the fitting procedure and defines the fit coefficients. Section 5.2 examines and parameterizes the seasonal dependence of the coefficients. An analysis of the error sources contributing to the seasonal dependence of the coefficients is given in Section 5.3. Finally, Section 5.4 discusses the residual error statistics for the data fitting and other measurement modeling options.

5.1 FITTING PROCEDURE AND FIT COEFFICIENTS

The purpose of the data fitting is to determine a set of calibration coefficients for each output channel (pitch and roll) of both Conical Scanners in order to correct the systematic errors in the data. This requires a simple expression which can be easily used by the OBC and can reasonably describe the major systematic errors in the data.

Second order finite Fourier series have been found useful to fit both the Earth oblateness and the major Earth radiance effects. The following expression conveniently separates the major error sources.

$$\begin{aligned} \text{pitch (or roll)} = \text{counts} * a_0 - a_1 \\ + b_1 (R - R_0) \\ + c_0 + c_1 \cos A + c_2 \cos 2A \\ + d_1 \sin A + d_2 \sin 2A \\ + e_0(t) + e_1(t) \cos A + e_2(t) \cos 2A \\ + f_1(t) \sin A + f_2(t) \sin 2A \end{aligned} \qquad (5\text{-}1)$$

where

counts = raw counts from the spacecraft telemetry
R = spacecraft distance from the Earth center
R_0 = reference orbit radius
A = orbit angle from the ascending node
t = time of year

and a_0, a_1, b_1, c's, d's, e's and f's are the calibration coefficients to be determined.

A total of four sets of coefficients are required, one set for each channel of each scanner. Among these coefficients, a_0 and a_1 provide the linear approximation which converts from the sensor measurement counts to the pitch or roll attitude, b_1 gives the correction due to spacecraft altitude variation, c_0 gives a constant bias correction, c_1, c_2, d_1, and d_2 model the Earth oblateness effect. The b_1 term was added to conveniently separate the spacecraft altitude dependent effect, although the orbit effects could have been added to the c_1, c_2, d_1, and d_2 terms because the Landsat-4 orbit does not vary greatly. Finally, e_0, e_1, e_2, f_1, and f_2 provide further corrections describing the horizon radiance effects and other possible systematic errors. Therefore a_0, a_1, b_1, c's and d's are constant throughout the year, while e's and f's are in general time dependent.

Twenty-eight data passes spanning from August 10, 1982 to September 14, 1983 were used in determining the calibration coefficients. Most of these data passes cover approximately 24 hours. Each data pass was fit through Equation 5-1 with a_0, a_1, b_1, c's and d's fixed at their nominal values. These nominal values are provided in Table 5-1. The nominal values for a_0 and a_1 were determined from the nominal calibration through the ground bench tests. The nominal values for b_1 were derived theoretically using a linear approximation under nominal conditions. The nominal value for c_0 was determined based on average constant biases for the nominal calibration parameters. The biases in

TABLE 5-1. Nominal Values for the Time Independent Calibration Coefficients

	SENSOR 1		SENSOR 2	
COEFFICIENTS	PITCH	ROLL	PITCH	ROLL
a_0	0.040	0.040	0.040	0.040
a_1	5.000	5.000	5.000	5.000
b_1*	-0.027	0.000	0.000	-0.027
c_0*	-0.140	-0.050	-0.250	-0.280
c_1	0.00029	0.01353	0.01371	-0.00001
c_2	0.22749	0.00007	0.00000	0.21828
d_1	-0.00692	-0.04446	0.00000	-0.05112
d_2	0.15365	-0.00003	0.15399	-0.00000

* Based on R_0 = 7088.14 km

the width channels are different from Table 3-1 because of the effects of the altitude correction. The nominal values for c_1, c_2, d_1, and d_2 were determined through a Fourier series fit to the modeled Earth oblateness effect. The coefficients e's and f's which resulted from the fit to the remaining errors are tabulated in Table F-1 in Appendix F. A sample plot of the fit to the altitude and oblateness corrected data and residual errors after the fitting is shown in Figure 5-1 for the October 20-21 data pass. Appendix G contains a complete set of plots of the residual errors after the second order Fourier series fits to the data for all of the data spans. It has been observed that the second order Fourier series do not completely remove all of the consistent systematic errors in the data. A higher order fit, such as fourth order, could fit some of the remaining systematic errors. This is particularly true for the rise in errors due to radiance effects around the south pole in September, where a higher order fit would fit the systematic error pattern better. The application of higher order fits to the systematic errors may be pursued in future analysis.

5.2 SEASONAL DEPENDENCE OF COEFFICIENTS

The resulting correction coefficients given in Table F-1 show some variations from one time of the year to another. This time dependence is shown in Figure 5-2. By examing the coefficients as a function of time, it was found that the coefficients generally seem to vary sinusoidally with a period of either a year or half a year. This implies that they probably can be modeled by Fourier series expansions to the second order. With this modeling, each coefficient given in Table F-1 was fit by the following equation.

$$c = A_0 + \sum_{n=1}^{2} A_n \cos\left(nt \frac{2\pi}{365}\right) + \sum_{n=1}^{2} B_n \sin\left(nt \frac{2\pi}{365}\right) \qquad (5\text{-}2)$$

where c is the coefficient to be modeled, t is the day of the year and A_0, A_n's and B_n's are the coefficient determined from the fit to the time dependence of c.

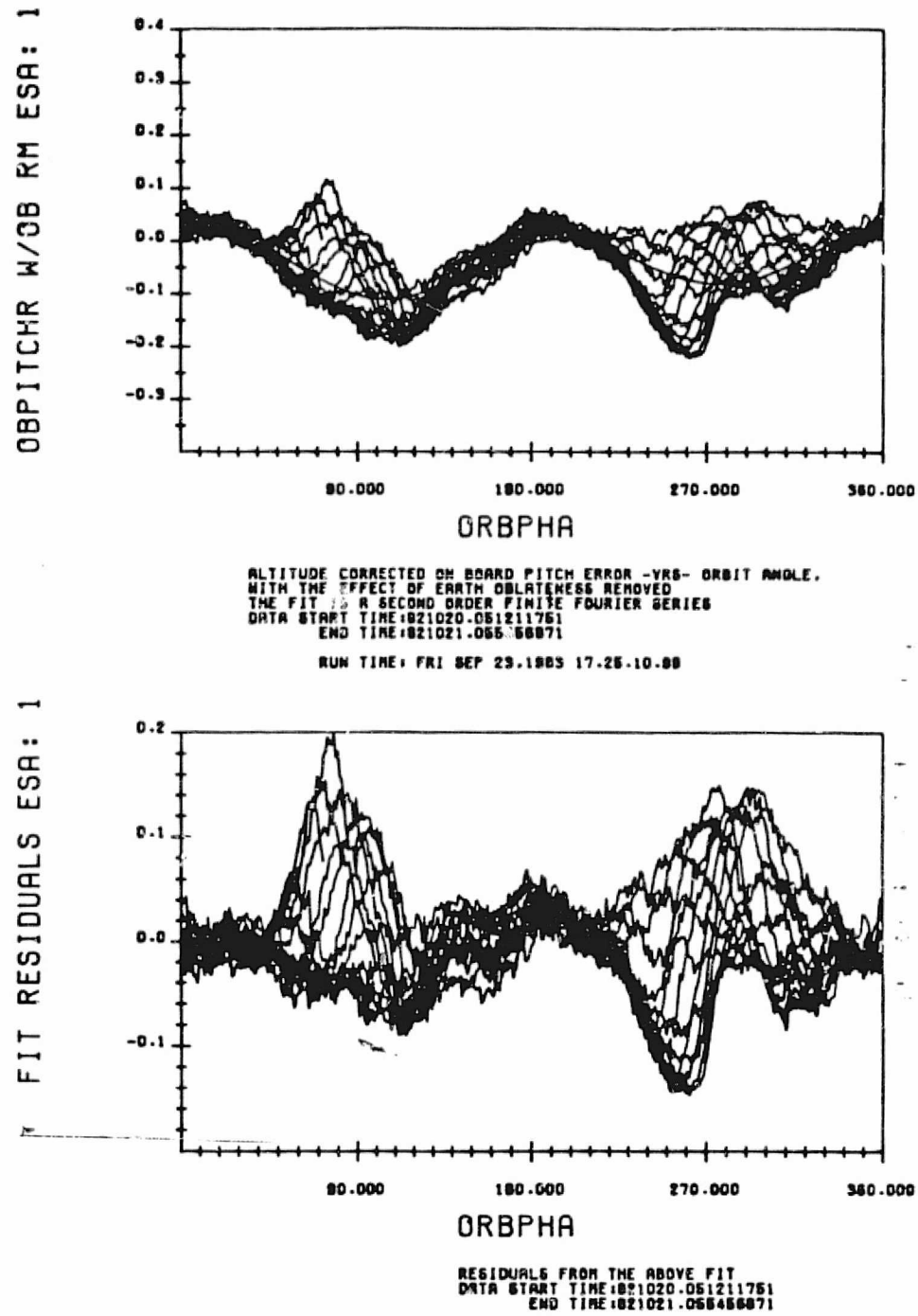

FIGURE 5-1. Second Order Fourier Series Fit to the Attitude, Orbit, and Oblateness Corrected Measurements and the Fit Residuals (1 of 4, Sensor 1 Pitch)

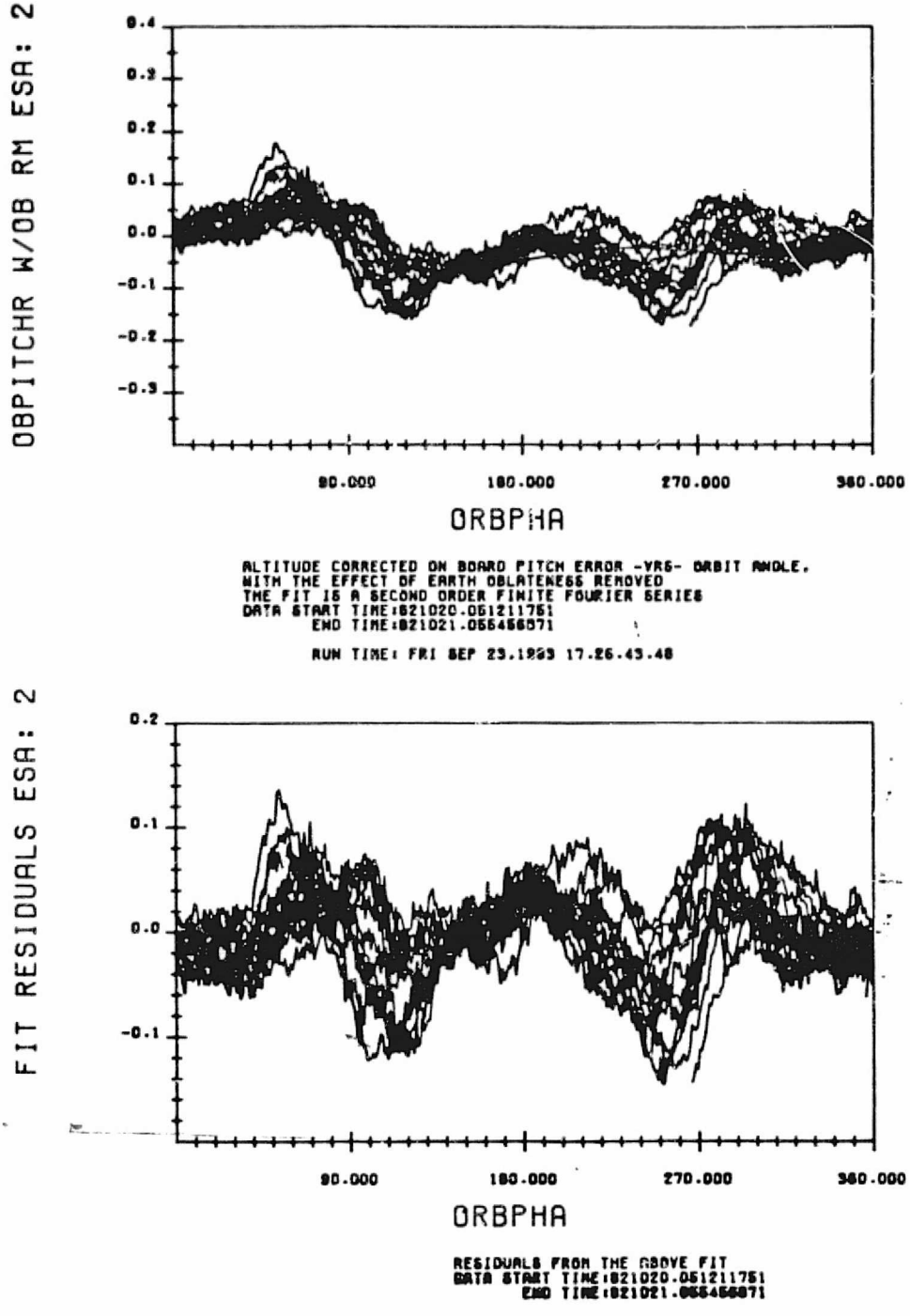

FIGURE 5-1. Second Order Fourier Series Fit to the Attitude, Orbit, and Oblateness Corrected Measurements and the Fit Residuals (2 of 4, Sensor 2 Pitch)

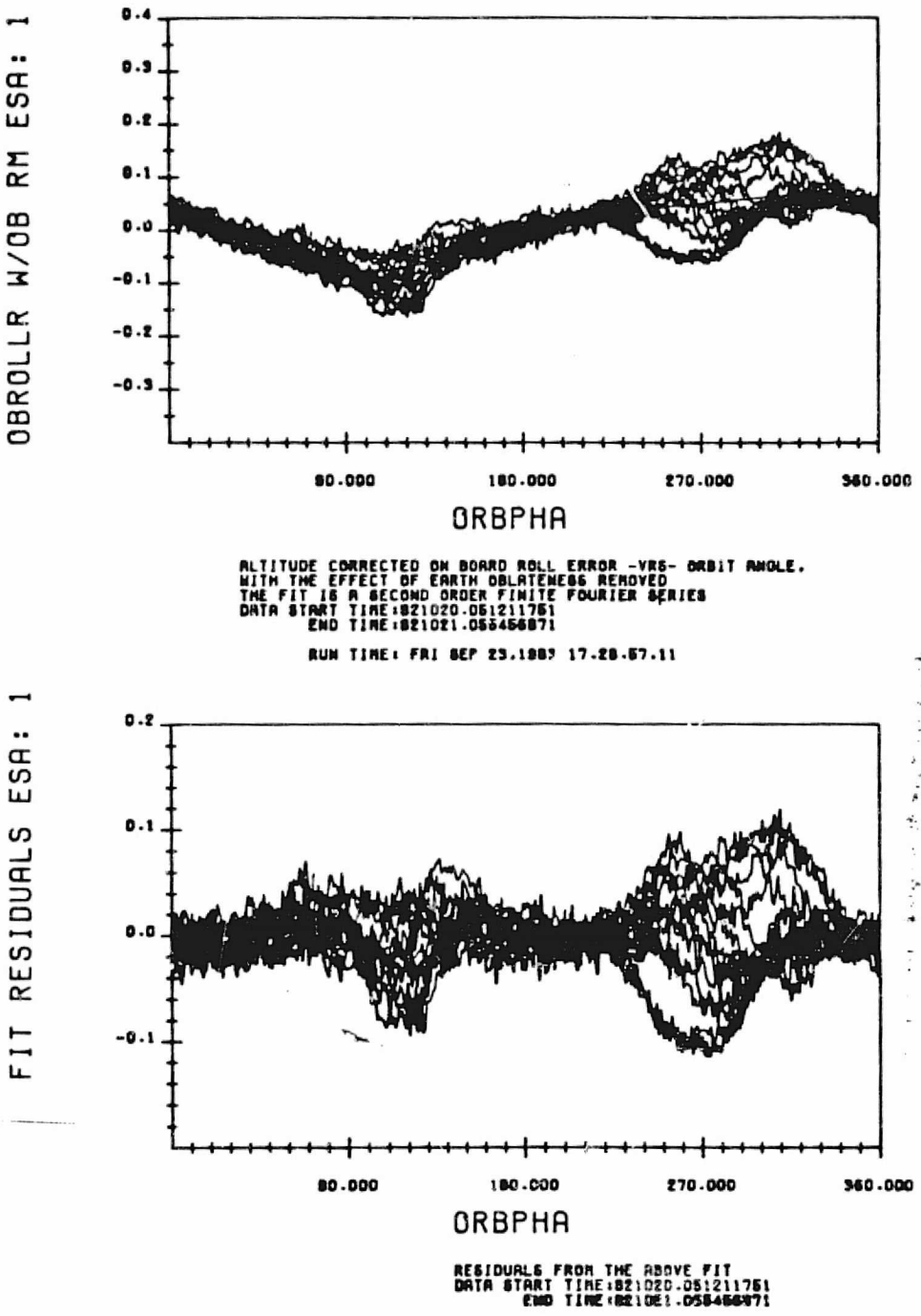

FIGURE 5-1. Second Order Fourier Series Fit to the Attitude, Orbit, and Oblateness Corrected Measurements and the Fit Residuals (3 of 4, Sensor 1 Roll)

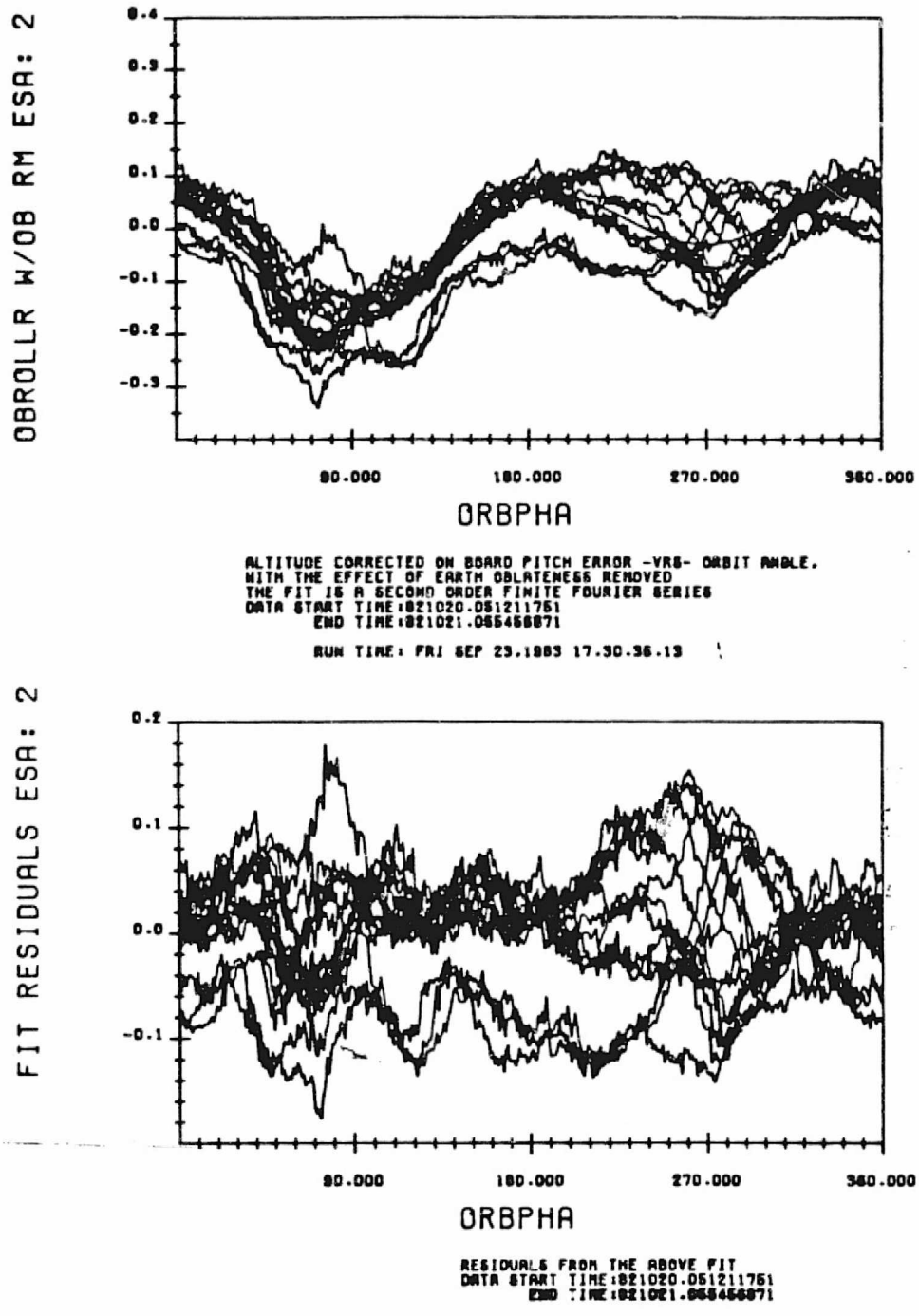

FIGURE 5-1. Second Order Fourier Series Fit to the Attitude, Orbit, and Oblateness Corrected Measurements and the Fit Residuals (4 of 4, Sensor 2 Roll)

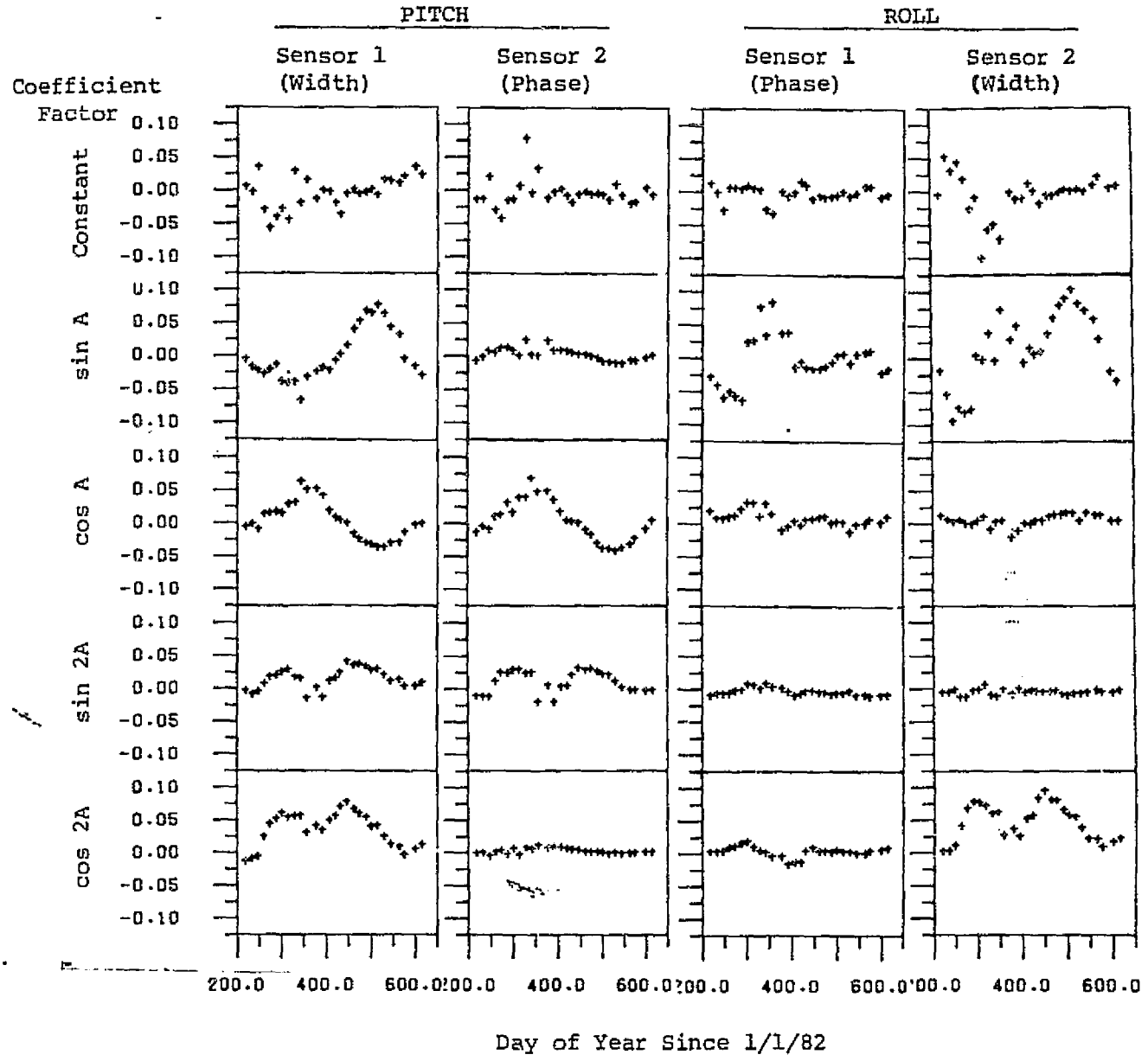

FIGURE 5-2. Time Dependence of Data Fitting Coefficients for 28 Data Spans

The fitting curves resulted from these fits are plotted in Figure 5-3 together with the correction coefficients. The coefficients A_0, A_n's, B_n's and the standard deviations corresponding to these fits are given in Table F-2 of Appendix F. Table F-3 of Appendix F then tabulates the correction coefficients e's and f's for the first day of each month throughout the year, using Equation (5-2).

The reliability and applicability of the results so obtained depend on the repeatibility of the time-dependent features in the data from one year to the next. Some of the time dependent characteristics are believed to be periodic in year, but certain features in the data seem to occur only in the early phase of the mission when problems with the reference attitudes occurred. This will be further discussed in the next subsection. This analysis for Landsat-4 may be continued to include data spans covering an entire year or longer after the time that the known reference attitude problems were eliminated (February 15, 1983). The additional period of time would be useful to separate the seasonal dependent features from perturbations due to other error sources and help demonstrate the accuracy and validity of the use of the coefficients for seasonal modeling.

5.3 ANALYSIS OF THE COEFFICIENTS VARIATIONS

This section discusses the interpretation of the seasonal variations in the data fit coefficients, particularly in light of the predicted radiance effects and the likelihood of errors contributed by early mission problems with the reference attitudes (Reference 9). The possibility of onboard ephemeris errors is also considered here. The ephemeris error which would be most likely to show up in scanner data would be an in-track orbit error or a timing bias. This type of error would be equivalent to a pitch bias in the reference attitudes that would probably be constant over a particular data span.

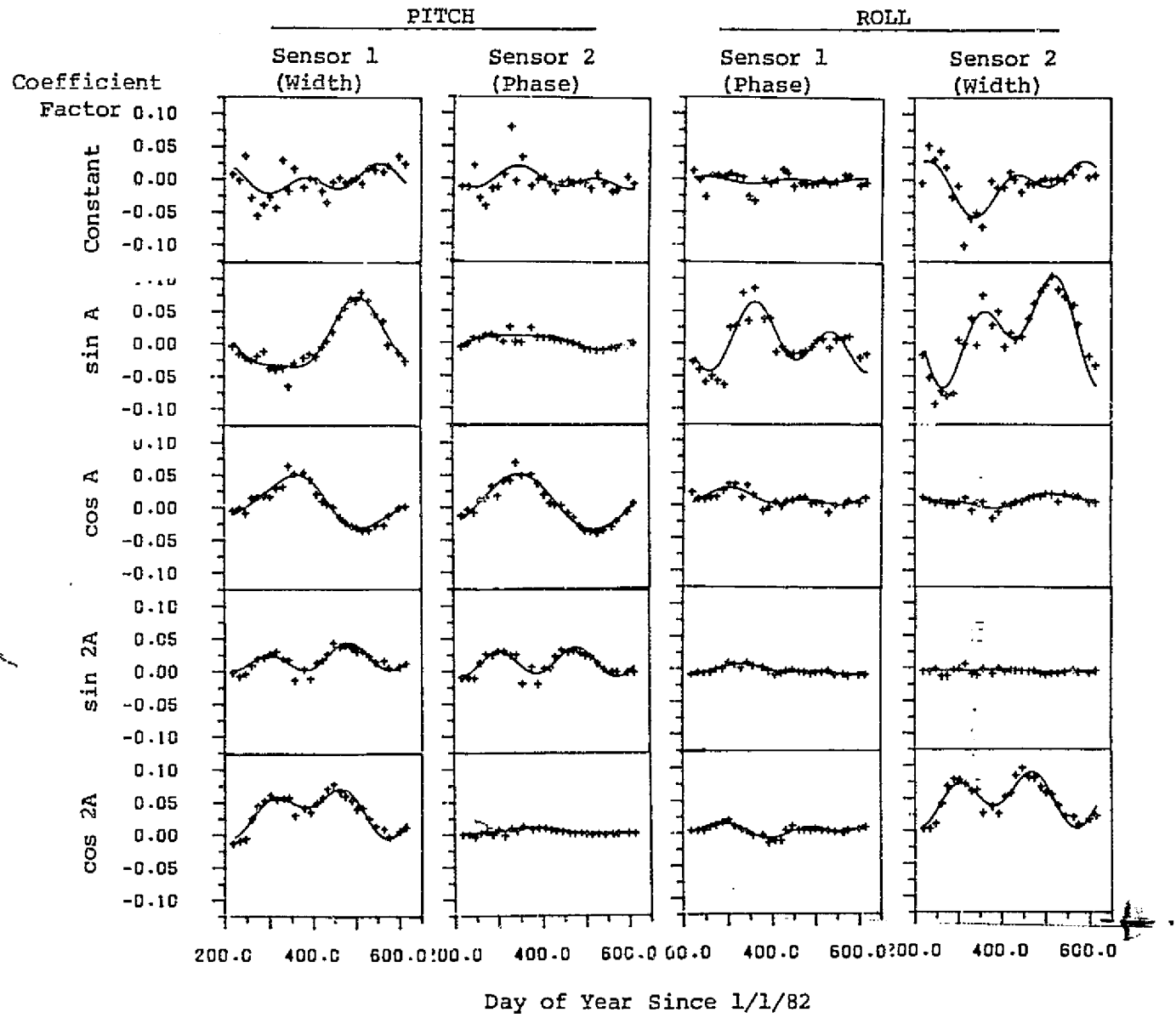

FIGURE 5-3. Time Dependence of Data Fitting Coefficients with Second Order Fourier Series Fit

In general the mounting geometry of the two Landsat-4 scanners helps to separate reference attitude related errror sources from sensor measurement related error sources because pitch and roll are each measured by the Earth width in one scanner and the Earth phase in the other. The width and phase measurements generally show different systematic effects due to radiance variations and other sensor or Earth related error sources. Notice for example the similar radiance effects predicted in the two Earth width channels (Figure 4-5) and the smaller effects in the phase channels. There are however differences in the effects predicted for the two width and the two phase channels due to the differences in the horizon crossing geometries, as discussed earlier in Section 4.

In order to better understand the predicted radiance effects as they relate to the data fitting coefficients, fits were made to predicted radiance effects in all the channels for all twelve months. The results are plotted in Figure 5-4 in the same format as the presentation of the flight data fitting coefficients to allow direct comparison with Figure 5-3. The y axis scale is expanded in Figure 5-4 over Figure 5-3 because the predicted coefficients are generally smaller than those observed.

The largest predicted coefficients are in the Earth width channels, dominated by the orbit period sin(A) and twice orbit period cos(2A) terms which cause effects that are symmetric about the pole crossings. The width channels also show some correlated variations in the constant term which is smaller in amplitude. These terms clearly can be expected from the plots of the radiance effects. What is more difficult to understand is that strong correlations are predicted in the fit coefficients terms cos(A) and sin(2A) for the two pitch channels, which constitute the Earth width measurement for sensor 1 and the Earth phase measurement for sensor 2. The actual predicted effects in these two channels is very different, because pitch for sensor 1 is dominated by the larger sin(A) and cos(2A) Earth width effects. The predicted fit coefficients for cos(A) and sin(2A) are

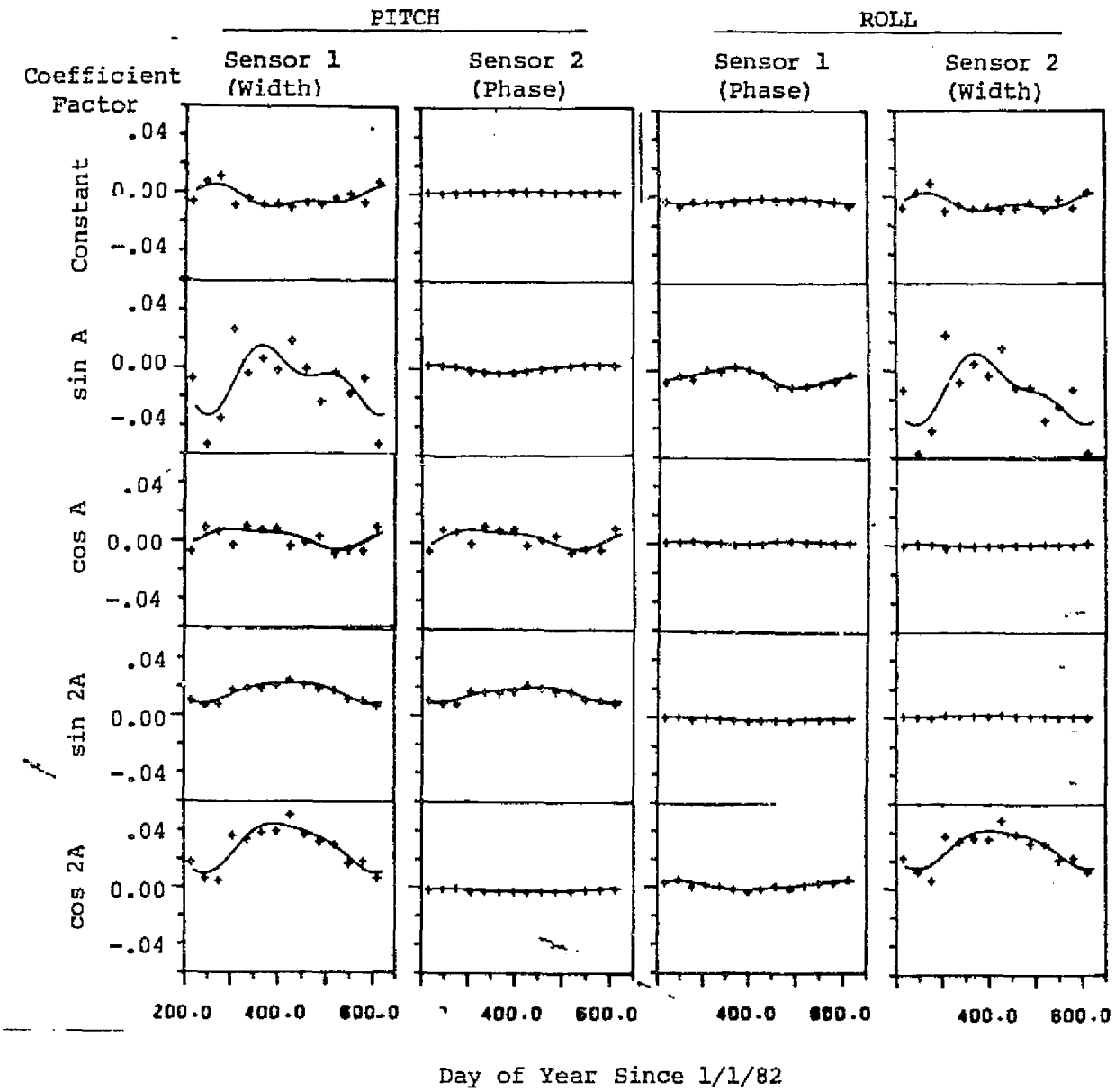

FIGURE 5-4. Time Dependence of Fit Coefficients to Predicted Radiance Effects with Second Order Fourier Series Fit

not high in amplitude, but nevertheless the correlation predicted in the two pitch channels is distinctive. Separate causes resulting from the different mounting geometries of the two sensors probably contribute to the appearance of these pitch coefficients. In sensor 1, the fact that both horizon crossings occur behind the subsatellite point (see Figure 1-5) apparently causes a phase lag in the Earth width effects around the orbit such that the maximum Earth width effects occur when the spacecraft is just past the pole (and the horizon crossings are near the pole). This orbit phase lag means that the dominant Earth width effects which are mainly symmetric about the pole and show up strongly in the sin(A) and cos(2A) coefficients, also show up somewhat in the -cos(A) and sin(2A) width coefficients. In sensor 2, the fact that the Earth-in horizon crossing is ahead while the Earth-out horizon crossing is behind the subsatellite point apparently causes the Earth phase measurement to effectively take a sort of numerical derivative of the Earth width history around the orbit (since the Earth width history indicates the average triggering height around the orbit while the Earth phase indicates the difference between the leading Earth-in and trailing Earth-out triggering heights). This effective differentiation, along with a sign reversal in the phase-to-pitch conversion, means that the dominant sin(A) and cos(2A) coefficients for Earth width effects also show up somewhat in the Earth phase channel in the -cos(A) and sin(2A) coefficents.

Analysis of the fit coefficients for the flight data and their comparison with those predicted by the horizon radiance effects modeling yields the following conclusions.

1. The orbit period sin(A) coefficients that are above the general trend in both the roll channels (November 2 through February 2) are probably due to reference attitude problems because this correlated error pattern is not predicted due to radiance effects, and it has an abrupt erratic pattern.

2. The sin(A) term seems to hit a peak around June of 1983 in both the Earth width channels. Although the fit coefficients are apparently corrupted by reference attitude problems in roll around December, if this problem is subtracted out by using the sensor 1 roll (phase) channel as a guide, it seems that both the width coefficients hit a minimum in December. It seems likely that this is an Earth radiance effect because the maximum in June and minimum in December correlate with the seasonal extremes in the polar CO_2 radiances indicated by the Fritz and Soules data (see Figure 4-2). This seasonal trend implies a tendency for lower triggering heights when the radiance is low in winter and higher triggering heights when the radiance is high in summer. Even though these seasonal extremes are not accurately predicted by the HRDB/SOES model, the strong correlation between the Earth width measurement channels in this coefficient is predicted.

3. The half orbit period cos(2A) term shows an effect in both the Earth width channels that is also very likely due to Earth radiance effects. It has a double peak functional form with the maximum corrections in November and April and minimum corrections in August. This term is like an additional Earth oblateness effect.

4. The cos(A) and sin(2A) terms show correlated effects in both of the pitch channels which could represent reference attitude problems but more likely represent a seasonal radiance effect that was underestimated by the HRDB/SOES modeling. The HRDB/SOES modeling does predict correlation in radiance effects in these two channels.

5. The constant term in roll for sensor 2 roll shows a lot of variation at the beginning of the mission which is apparently associated with that channel alone since it does not correlate with errors in the other channels. This anomoly is almost certainly associated with the previously noted larger than normal

orbit-to-orbit spread in the measurements in this channel. The larger than normal spread and the constant term variation both seem to disappear from the data starting in 1983.

6. The constant terms in pitch for both sensors show a lot of variation at the beginning of the mission. There is some tendency for the pitch errors in these two channels to correlate; i.e. the constant term moves up and down in both the pitch channels simultaneously. This correlation is not exact so there are probably other contributing effects, but this sort of correlation is not predicted by the radiance effects and so therefore probably represents an instability in the reference attitude or in-track orbit errors in the ephemeris. The radiance effect does predict a s all variation in constant term in width measurements.

5.4 COMPARATIVE ERROR STATISTICS

This section summarizes the residual error statistics for various models used in processing the Landsat-4 scanner measurements. This provides a quantitative comparison of the accuracies of the various models.

Standard deviation statistics were compiled for the five scanner measurement modeling options summarized below. All data processing included the 128-point averaging of the raw measurements to reduce the noise level.

1. Uncorrected Data: These are the raw pitch and roll angles, described in Section 2.4 and included in Appendix C, that are computed from a linear approximation without correction for oblateness or spacecraft altitude. The differences between these measurements and the reference attitudes were evaluated.

2. Oblate Earth Model: These measurement errors, discussed in Section 3.5 and included in Appendix D, include the corrections for the spacecraft altitude as well as the Earth oblateness effects.

3. HRDB/SOES Model: This modeling, discussed in Section 4.3 with residual errors plotted in Appendix E, includes the predicted Earth radiance effects from the Horizon Radiance Data Base and Sensor Optics and Electronics Simulator, as well as the Earth oblateness and spacecraft altitude effects.

4. Second Order Fit: Residuals, as plotted in Appendix G, were computed after fitting a second order Fourier series to the residual errors obtained in Option 2 above for all the data spans. This is virtually equivalent to the residuals from the data fitting described in Section 5.1 and to the residuals that would result from fits to the raw data, because the Earth oblateness and spacecraft altitude effects are accurately fit by a second order Fourier series.

5. Fit with Pole Removed: Because the "winter" hemisphere obviously has a much greater measurement errors, it has been discussed that an onboard algorithm for using horizon sensor data in the control law would choose not to use this polar region data. Therefore the residual errors from second order Fourier series fits were computed in which data from 90 degrees of true anomoly (one quarter orbit) around the noisest pole were eliminated. Based on visual inspection of the data plots, the "winter" hemisphere was defined as November through March in the Northern Hemisphere and April through October in the Southern Hemisphere.

Note that constant biases in any of these models is not important because the standard deviation statistic just shows the root-mean-square variation about the mean. Obviously other modeling or fitting or data flagging options could be considered. One logical model for

which statistics would be interesting would be based on the seasonal fits to the daily fit coefficients presented in Section 5.2. This model was not included because it would have required either a software update of the CSES or a large volume of hand entered coefficients in the necessary data production runs for which time was not available. However, there are reasons to believe that the results of this modeling would not differ greatly from the Second Order Fit standard deviations (model 4) because the seasonal fits generally match the daily fit coefficients closely (see Figure 5-3).

Figure 5-5 plots the standard deviations in pitch and roll for all of the data spans for the above modeling options. The standard deviations are listed in Table F-4 of Appendix F. One special note needs to be made about several outlier points. The few outlier points that show up particularly in the fit residuals were determined to be caused by the spurious attitude and ephemeris telemetry that had not been flagged (a single bad point out of about 6,000 was able to cause this by not being rejected or clipped to a small value). These points occur in the ninth data span (December 1, 1982) and the fourteenth data span (February 17, 1983), and should be ignored. Also, the statistics for the last four data spans for the HRDB/SOES model were obtained incorrectly due to a data processing error and were therefore eliminated from the data plots. The interpretation of these statistics is discussed qualitatively as follows.

The uncorrected data shows the greatest errors in the Earth width channels and the least in the Earth phase for sensor 2, as expected based on the oblateness and altitude effects illustrated in the raw data plots for the various channels. Improvement in all the channels is achieved as soon as the Earth oblateness modeling is added. The HRDB/SOES modeling shows some improvements over the Oblate Earth Model primarily in the Earth width channel standard deviations, but the improvements are not consistent. In the oblate Earth and HRDB/SOES models, one can clearly see in the sensor 1 roll channel the effects of the orbit period reference attitude problems in roll and the date

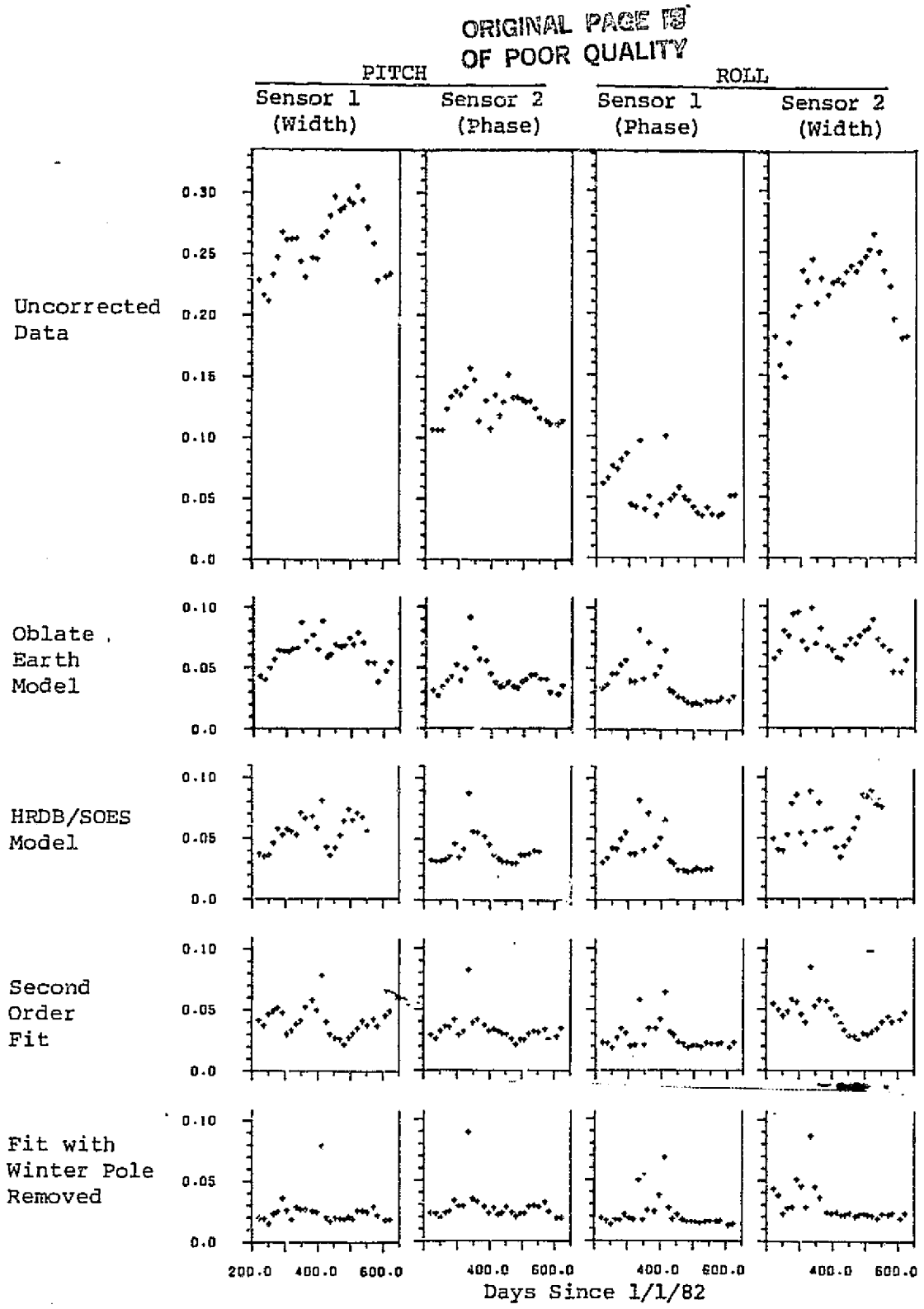

FIGURE 5-5. Pitch and Roll Standard Deviation Statistics for all Data Spans Processed Five Different Ways

of their elimination. The Second Order Fit shows notably lower standard deviations than the Oblate Earth and HRDB/SOES models. The influence of the reference attitude problems are mostly removed from these residuals because the attitude errors occur smoothly at orbit frequency and, are therefore taken out by the fitting. The effect of inaccuracies in the predicted radiance effects of orbit and half orbit periods are also removed. The fit with pole removed shows the lowest standard deviations, being on the order of 0.02 degrees in all the channels. This removes the contribution of the noisy pole data in the residual statistics. In this last fit, one can see most clearly the effects of the larger variation in the sensor 2 roll data for the early mission period. Sun and moon interference seem to have only a very slight influence on the residual statistics.

Table 5-2 provides the average residual errors standard deviations for each of the modeling options. These numbers may be interpreted as one sigma attitude accuracies for the 128-point averaged data processed with the specified modeling options and constant biases removed.

TABLE 5-2. Average Residual Error Standard Deviations for Five Modeling Options

	PITCH		ROLL	
	Sensor 1	Sensor 2	Sensor 1	Sensor 2
Uncorrected	.260	.127	.054	.217
Oblate Earth	.063	.043	.038	.071
HRDB/SOES	.055	.040	.038	.061
2nd Order Fit	.042	.034	.028	.045
Fit w/o Pole	.025	.028	.022	.030

SECTION 6 - INTERFERENCE AND ANOMOLIES

Data anomolies, or glitches, are names for temporary excursions from the normal pattern of measurements. This section discusses the glitches that have been determined to be due to Sun and Moon interferences, and briefly describes several unexplained temporary anomolies that were identified by careful review of all of the data spans. Another type of data anomoly can result from telemetry dropout or telemetry noise resulting in spurious or bad data. Usually any bad data values will stand out clearly since they are far away from the neighboring data values. Occasionally our data plots show spikes that are due to bad data points.

6.1 SUN INTERFERENCE

For the nominal Landsat orbit/sun/attitude geometry, the sensor 1 scan cone intersects the sun twice each orbit, however during one of these intersections, the sun is shadowed by the Earth, and during the other intersection the sun effects are usually eliminated by the blanking circuit. The Earth Sensor Electronics suppress the bolometer signal for 122 degrees of rotation centered on the sky side of the scan (this is described in Reference 2). As it turns out, the variations in the sun position relative to the orbit plane allows the sun to get just outside the blanking region for a period in January through March, and sun interference effects in the scanner measurements are seen at these times.

Figure 6-1 shows the sun elevation from the orbit plane as a function of time through the year for the Landsat-4 sun-synchronous orbit. The sun angle varies between 27 to 39 degrees above the orbit plane. The main drivers of this variation are the north-south motion of the sun relative to the equatorial plane and the eccentricity of the Earth's orbit. It is mainly due to the more rapid right ascension rate for the sun during the Earth's perigee relative to the nearly constant

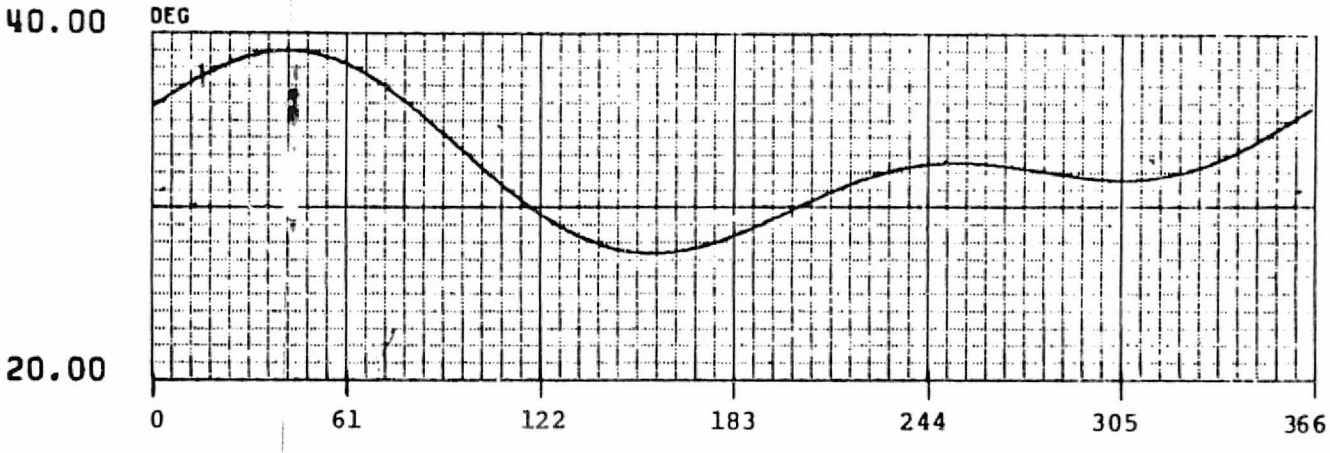

FIGURE 6-1. Sun Elevation Above the Orbit Plane as a Function of Day of Year for Landsat-4 Orbit (Adapted from Reference 21)

right ascension rate of the Landsat-4 orbit precession that the sun reaches the highest elevation above the orbit plane in February.

Figure 6-2 shows the geometry of the sensor 1 scan cone and blanking region, the Earth, and the sun path in the spacecraft reference frame. Since the spacecraft is nominally always Earth pointing (with the z-axis at the Earth, the x-axis in the velocity direction, and the negative y-axis pointing toward orbit normal), inertial vectors describe circles about the spacecraft y-axis as the spacecraft goes around the orbit. Therefore the sun follows the approximately circular path shown in Figure 6-2 which normally takes it past the blanked section of the scan cone and past the scan cone again when behind the Earth. Only when the sun gets closest to orbit normal does it get outside the blanked section of the scan cone.

Sun interference in scanner 1 was observed in four days acquired for this report; January 19, February 2, February 17, and March 3. Figure 6-3 shows the residual errors on these data spans, along with sample days preceding and following. The sun angle from orbit normal is listed on Figure 6-3 for each of the days. Based on the geometry illustrated in Figure 6-2 the sun gets outside the blanking region when within 52.7 degrees of orbit normal (37.3 degrees above the orbit plane). The four days covered show how the interference effect grew and than receded in amplitude as would be expected with the sun angle changes. The phase in the orbit where the effect occurred shifted gradually as the sun moved northward and backward in phase from the ascending node within the orbit plane.

It is noteworthy that the sun just misses the blanking region to cause interference in sensor 1. If the blanking region had been made just about 5° wider on this side of the scan, the sun interference apparently could have been avoided. The performance of the sensor indicates that the sun interference effects are being successfully eliminated when the sun is just inside the leading edge of the blanked

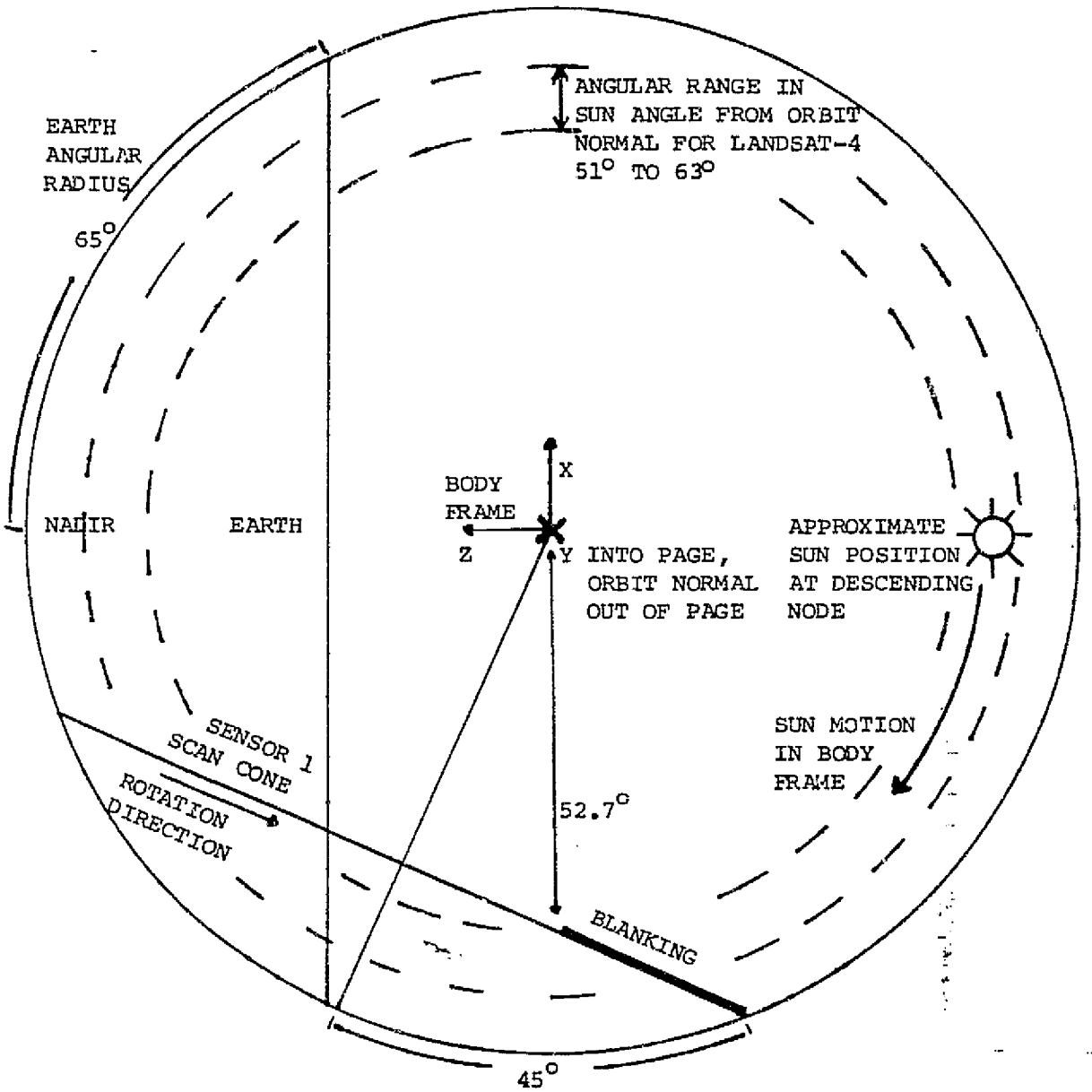

FIGURE 6-2. Sun Position and Sensor 1 Scan Cone Geometry for Landsat-4

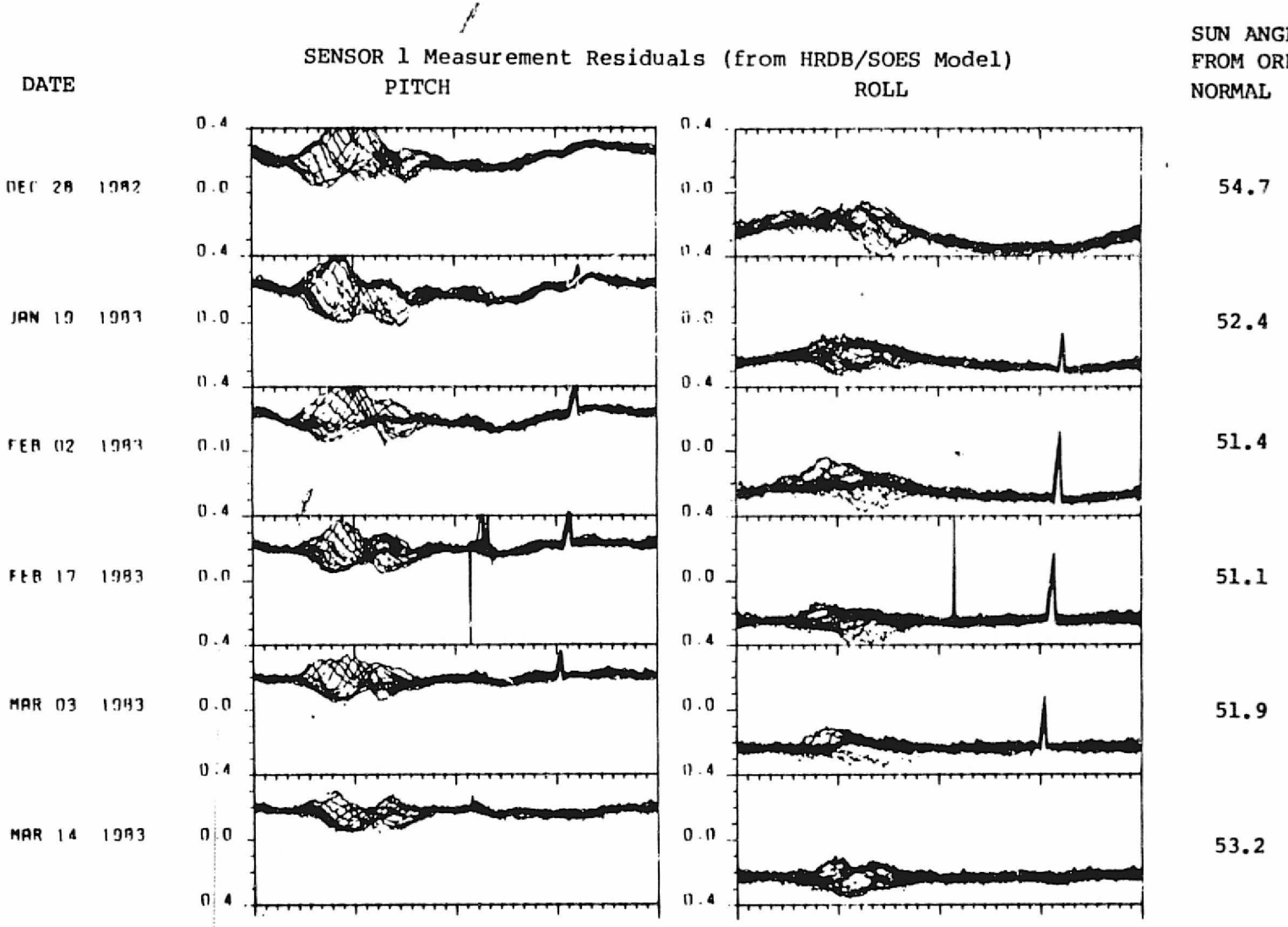

FIGURE 6-3. Sensor 1 Residual Errors for 6 Dates Illustrating Sun Interference Appearance for Various Sun Angles from Orbit Normal

part of the scan cone. It is important to note that the sun interference is occurring on the leading edge of the blanked region of scan; this gives the bolometer the remainder of the blanking region to recover from the sun effects. The blanking would probably not be as effective close to the trailing edge of the blanking region, because the bolometer would not recover completely before the electronics continues to process its signal.

6.2 MOON INTERFERENCE

The presence of the moon outside the blanked region of the scan cone has been observed to cause interference in both scanners on Landsat-4. For any given orbit the moon, like the sun, follows a circular path about the spacecraft y-axis. However, the moon moves over a much greater variety of positions relative to the orbit plane than does the sun, and therefore enters both scan cones at a greater variety of positions.

Figure 6-2, which was used to illustrate the sun path through the sensor 1 scan cone, also illustrates the geometry for the moon entering the scan cone. Note that the moon can enter the scan cone when below the orbit plane as well as above it, in which case it enters the scan cone just before the Earth-in crossing. At 45 degrees above or below the orbit plane (45 to 135 degrees from orbit normal) the moon will move in a path that takes it tangent to the scan cone. At these positions the moon will stay in the scan cone for the longest period of time. Note that just within 45 degrees of the orbit plane the moon will pass through the scan cone twice, passing inside and then outside the scan cone a short time apart. This only happens over a short range of angles, because when the moon position moves within about 43.7 degrees of the orbit plane the second moon crossing of the scan cone gets eclipsed by the Earth. When the moon position gets within 37.3 degrees of the orbit plane the first moon crossing of the sensor 1 scan cone gets within the blanking region.

The geometry for moon interference in the sensor 2 scan cone is illustrated in Figure 6-4. With the moon at angles between 125.8 and 141.8 degrees of orbit normal, the moon will pass through the unblanked, uneclipsed region of the scan cone twice each orbit. Below 125.8 degrees from the scan cone the moon intersections with the scan cone are eclipsed by the Earth, while above 141.8 degrees the moon enters the blanked regions of the scan cone.

The ranges of angles from orbit normal where the moon will enter the two scan cones are summarized in Table 6-1. Also indicated is the number of times that the moon passes the unblanked uneclipsed scan cone at those angles. Table 6-2 summarizes the angle of the moon from orbit normal for the days, among the available data spans, when moon interference has been noted. The moon angle is given at the start of the day for a pair of days to indicate the direction that the moon is moving relative to the orbit plane. The key features of the moon interference are explained by the time history of the moon position on the days where the interference is found.

Figure 6-5 shows a serial stacked plot of data from December 1, 1982, when glitches due to moon interference can be seen in both scanners. The glitches can be seen to move slowly in orbit position throughout the day. The interference in scanner 1 disappears after 23:00 hours when the Moon moves past 135 degrees below from orbit normal. Also the Moon interference in scanner 1 lasts longest just before it disappears. It seems that the second potential Moon hit in Scanner 1 is eclipsed by the Earth for the early part of the day, but does appear just before the last Moon hit at about 23:00. The sharpest spikes in both sensors occur when the moon is near the horizon crossing position.

The moon interference can be seen in both scanners on July 26 as well. On the November 2 and March 29 data spans the moon interference

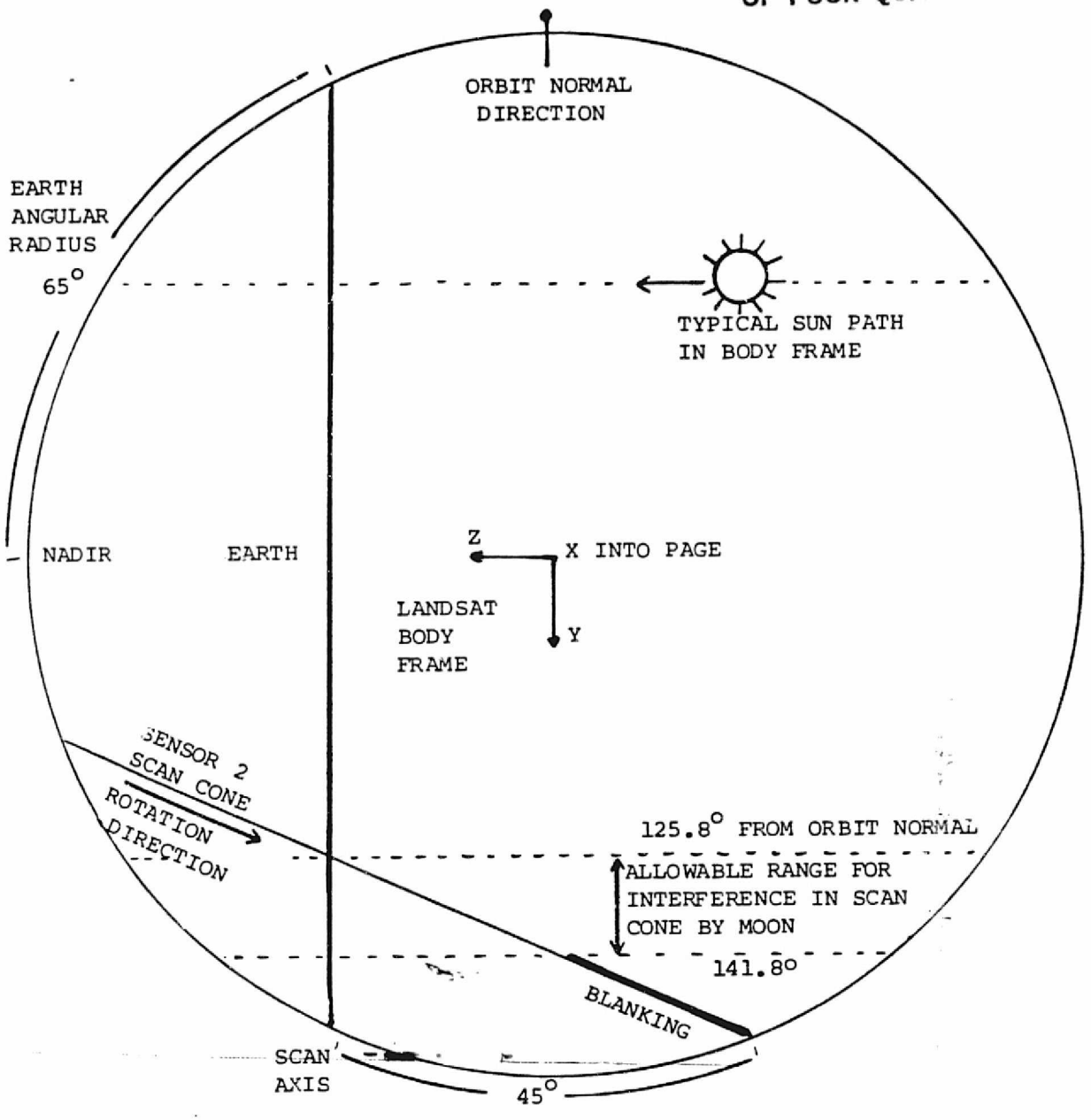

FIGURE 6-4. Sensor 2 Scan Cone Geometry Indicating Allowable Range for Interference in Scan Cone by Moon

TABLE 6-1. Ranges from Orbit Normal that can Intersect Scan Cone Outside Blanking Region and Earth for Landsat-4 at Nominal Attitude

	FROM (Degrees)	TO (Degrees)	Number of Times Position Will Intersect Scan Cone During Orbit
Sensor 1	45.0	46.3	2
	46.3	52.7	1
	127.3	133.7	1
	133.7	135.0	2
Sensor 2	125.8	141.8	2

TABLE 6-2. Moon Angle from Orbit Normal on Dates with Moon Interference

DATE	MOON ANGLE (AT 0 HOUR GMT)	PERCENT ILLUMINATION
11/3	141	97
11/4	152	92
12/1	123	100
12/2	136	99
3/30	140	98
3/31	148	94
7/26	130	99
7/27	141	96
9/14	33	49
9/15	44	59

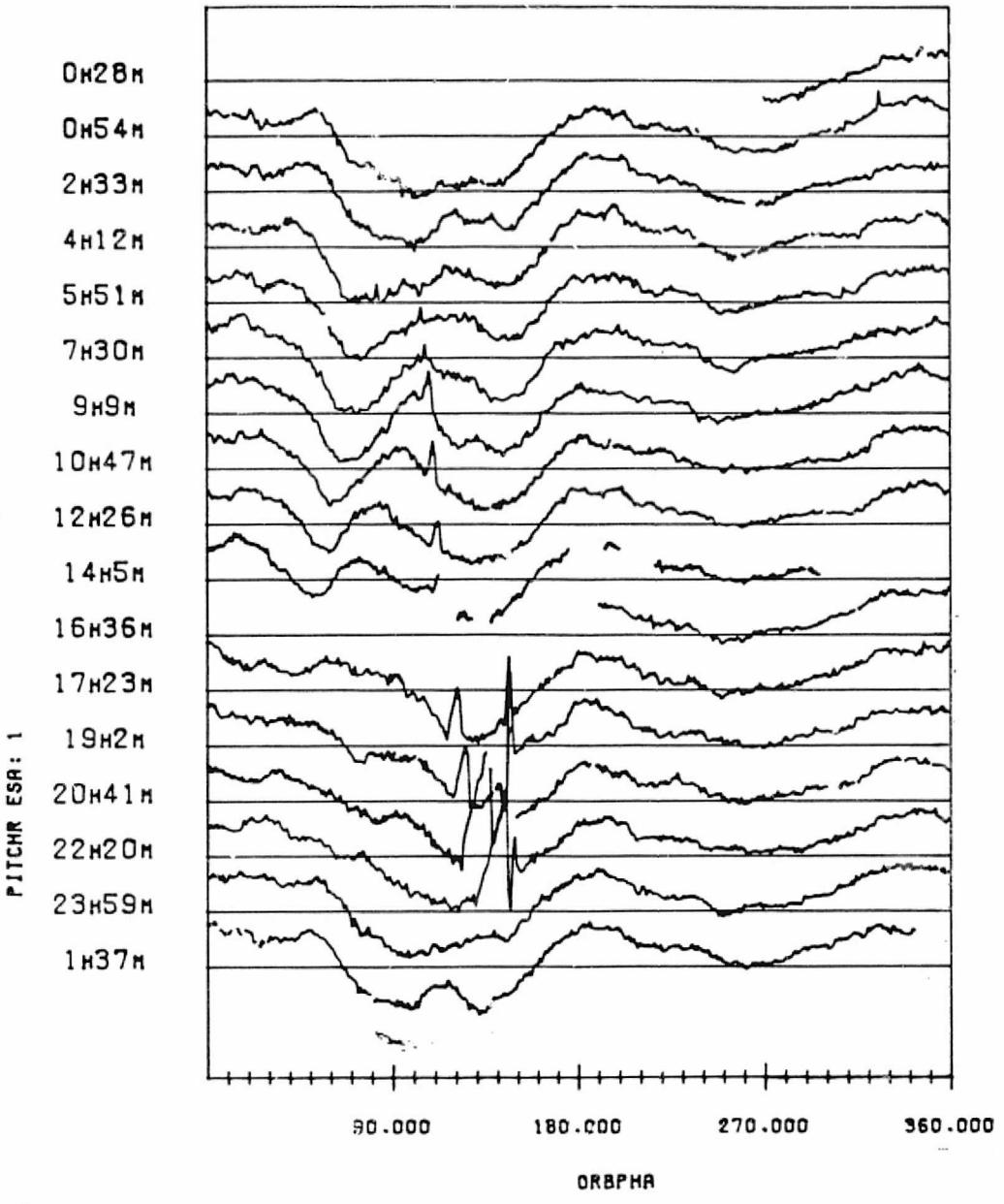

FIGURE 6-5. Serial Stacked Plot of Data on December 1, 1982 (1 of 4, Sensor 1 Pitch)

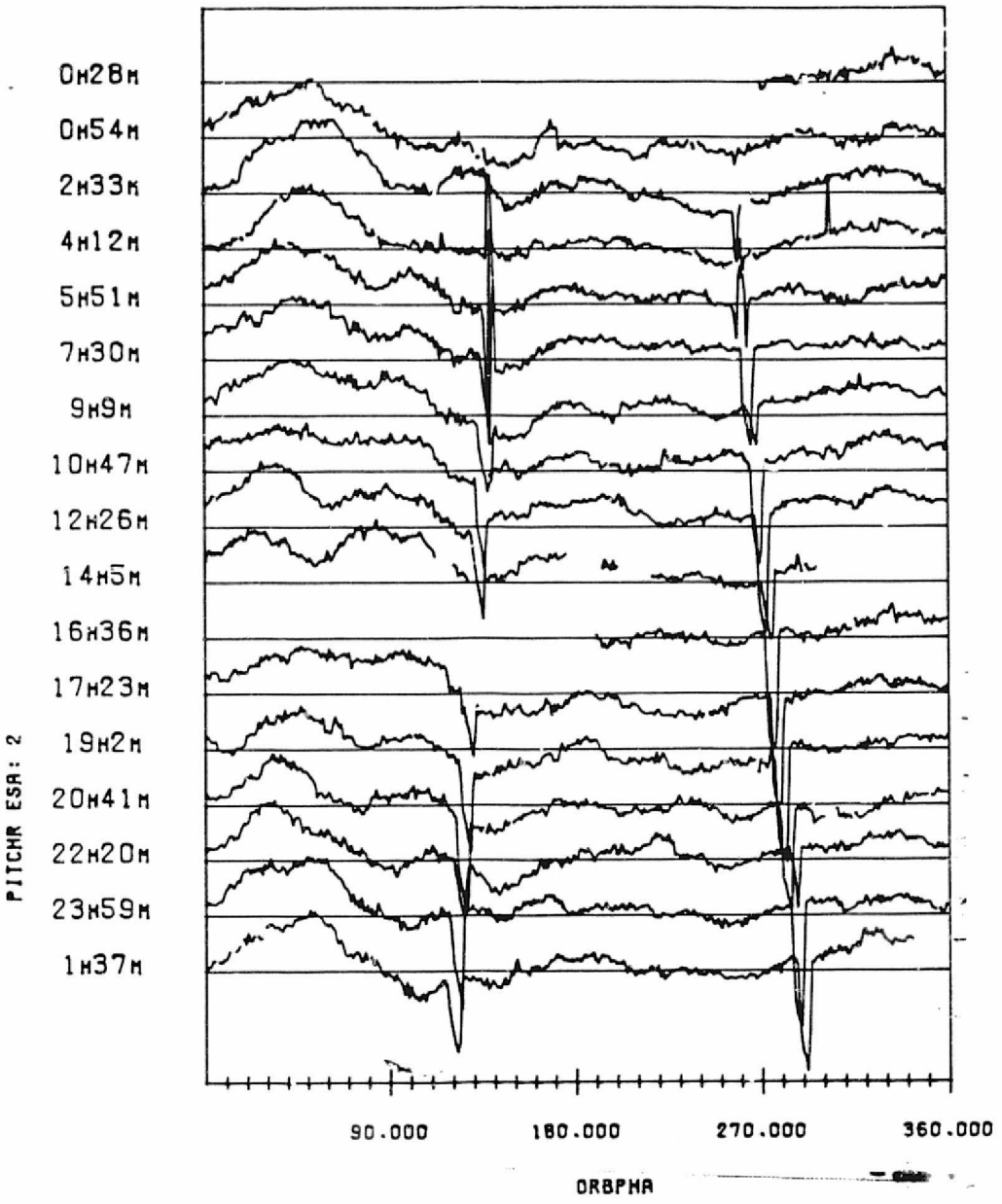

FIGURE 6-5. Serial Stacked Plot of Data on December 1, 1982 (2 of 4, Sensor 2 Pitch)

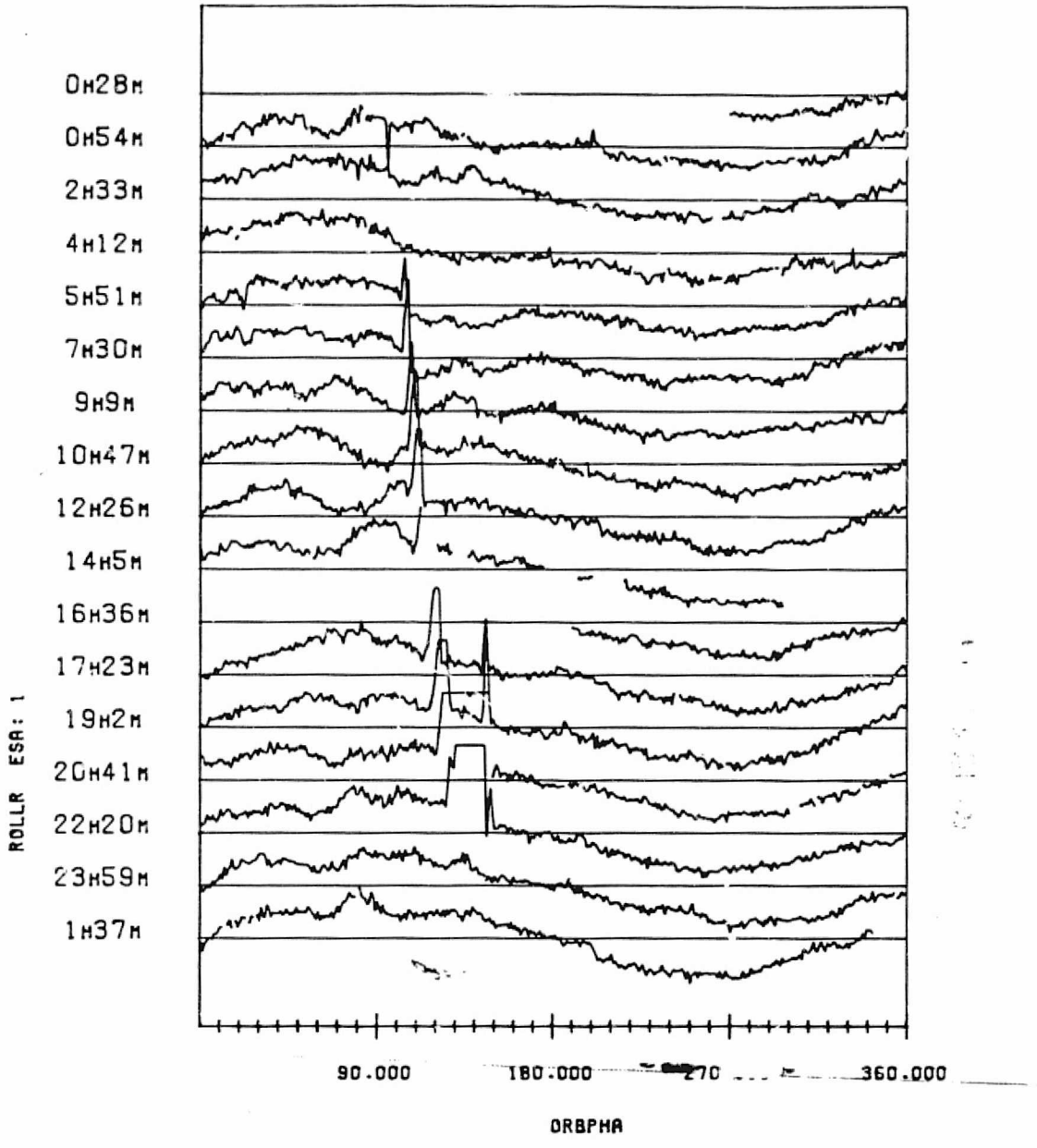

FIGURE 6-5. Serial Stacked Plot of Data on December 1, 1982 (3 of 4, Sensor 1 Roll)

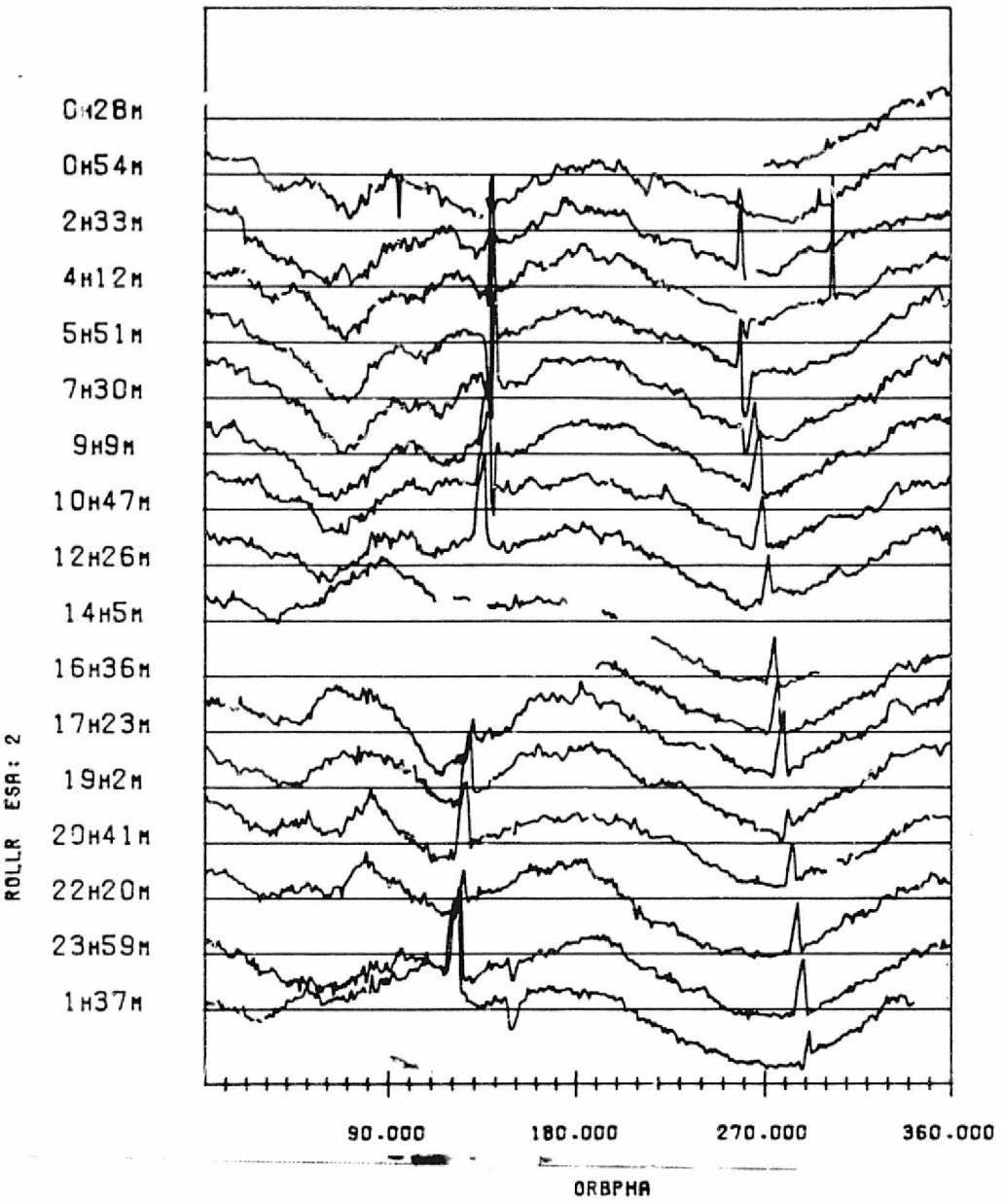

FIGURE 6-5. Serial Stacked Plot of Data on December 1, 1982 (4 of 4, Sensor 2 Roll)

appears only in sensor 2 for the beginning of the data span before the moon moves more than 142 degrees from orbit normal and into the blanked regions of the scan cone.

All but one of the moon interference periods occur when the phase of the moon is near full. However one interference period shows up in sensor 1 when the moon is just past first quarter. The interference effect appears smaller in amplitude on that day, and is found when the moon is close to the Earth-out horizon crossing.

6.3 OTHER ANOMOLIES

Several additional anomolies have been noted which are unexplained at the present time. These are described briefly below. Their effects can be noted in the appendix plots.

1. On the February 17th, 1983 data span there are two short periods of correlated noiselike spikes in both of the scanner pitch measurement channels. These occur on 2/17 from 05:20 to 05:28 and on 2/18 from 04:25 to 04:30. Since the errors correlate in the two pitch channels, it is possible that this indicates a problem in the reference attitudes, although no anomolies in the reference attitude data are seen in these times. This anomoly can be seen clearly in the appendix plots of the scanner data for February 17.

2. In the March 14, 1983 data span, periods of spikelike noise are seen in both pitch channels. The spikes occur around the same orbit position but the largest spikes appear at different times of the day for the two pitch channels. Figure 6-6 shows a serial stacked plot of the pitch residual errors for this span, illustrating the anomolies.

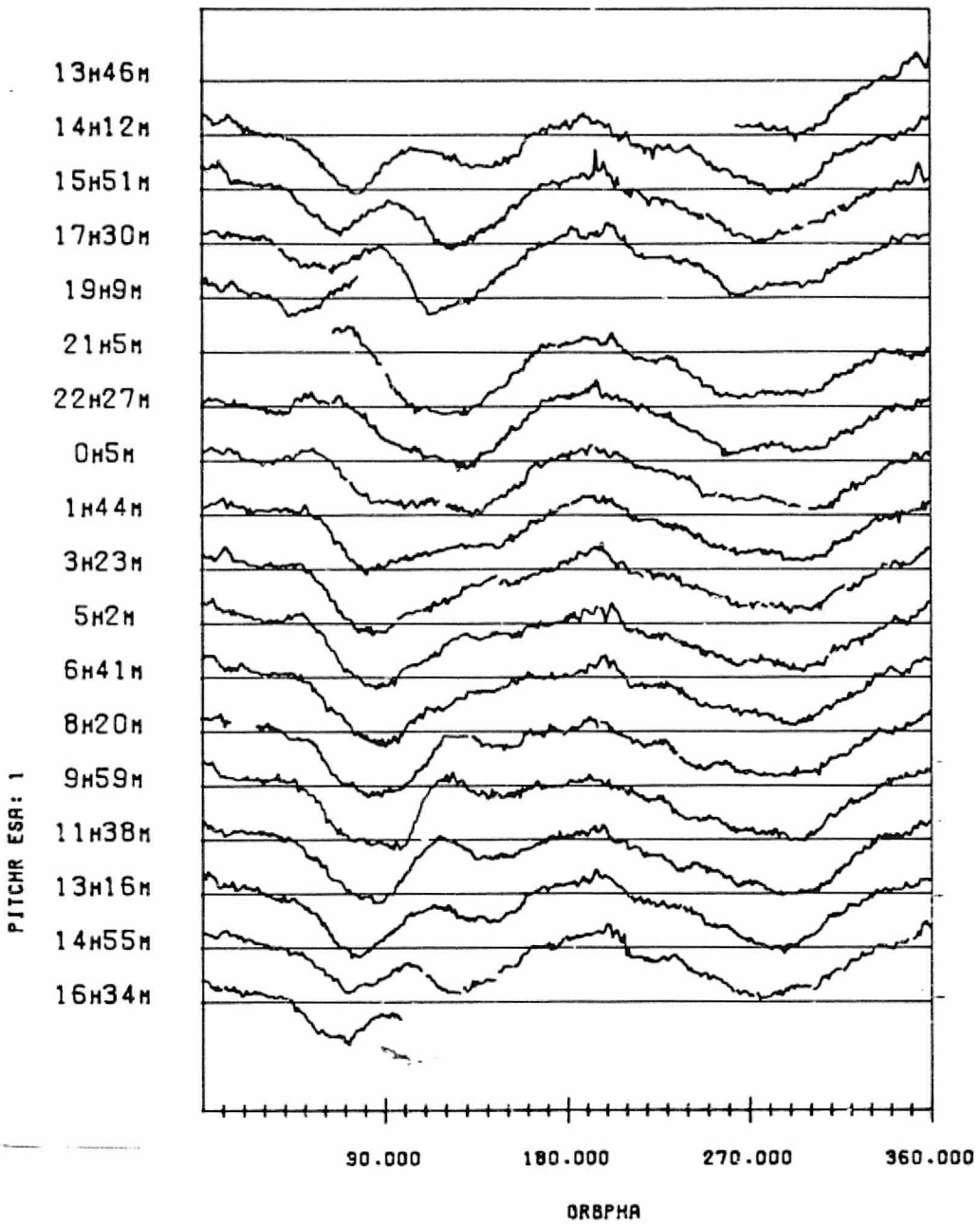

FIGURE 6-6. Pitch Residual Errorsfrom Oblate Earth Model for Consecutive Orbits on March 14, 1983 Data Span (1 of 2, Sensor 1 Pitch)

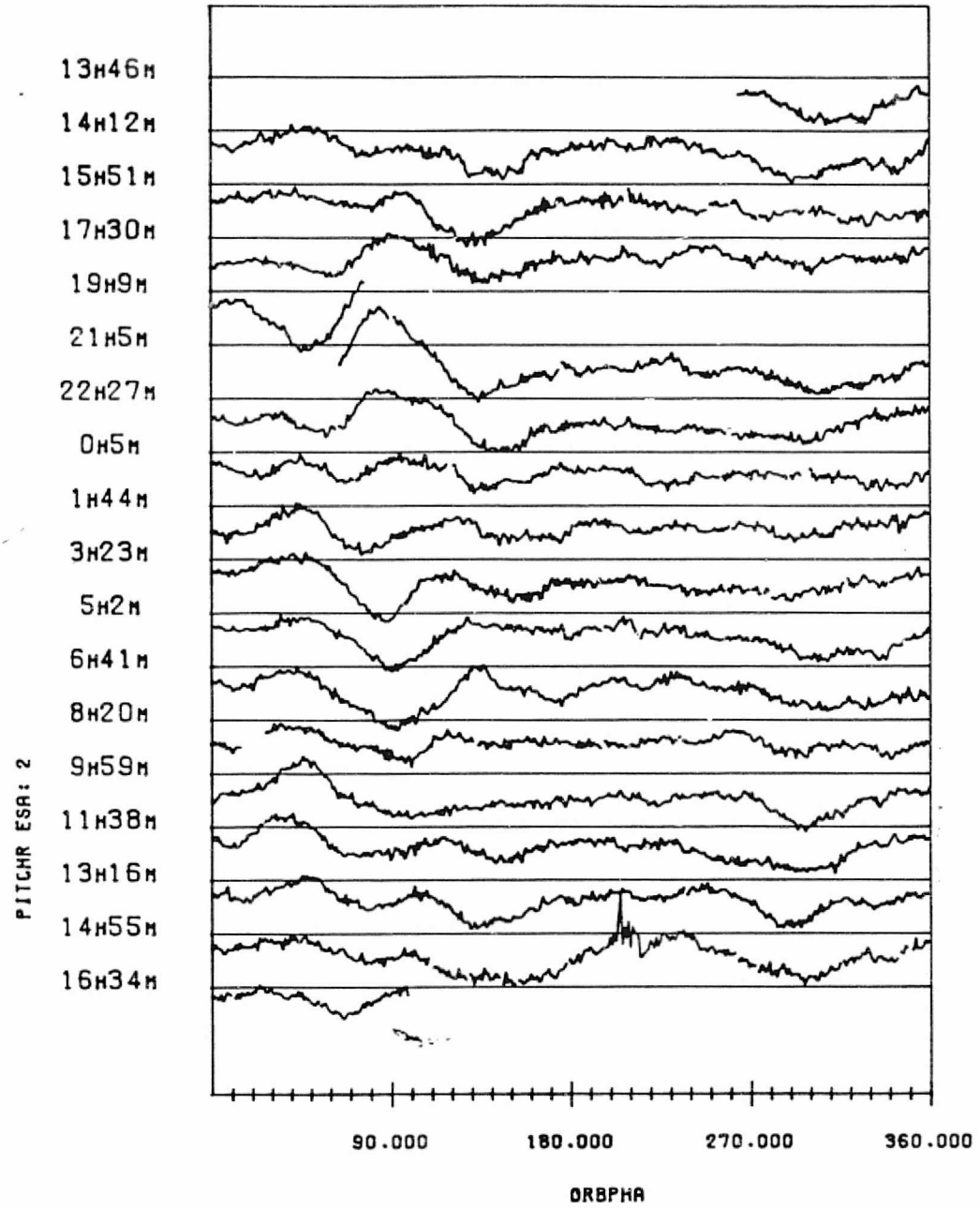

FIGURE 6-6. Pitch Residual Errors from Oblate Earth Model for Consecutive Orbits on March 14, 1983 Data Span (2 of 2, Sensor 2 Pitch)

3. Near the end of the April 14 data span, a period of about 40 minutes of anomolously high noise is seen in both pitch channels. This is illustrated in Figure 6-7. The spikes show some correlations between the two pitch channels.

4. In the August 6 and 7 data span, two periods of excursions take place in the scanner residuals. The excursion are 0.1 to 0.2 degrees in the roll residuals and smaller in the pitch residuals. Excursions take place in the reference attitudes at the same time of about the same amplitude. The presence of the residuals excursions probably indicates that the reference attitudes do not track the spacecraft motion as indicated by the scanners. Therefore this is almost certainly a period where the reference attitude accuracy was temporarily lost for some reason. Figure 6-8 shows the residual errors for this day.

5. Also illustrated in Figure 6-8 is another curious feature in the residual errors that appears barely distinguishable above the noise level. It is a very small amplitude spike in the roll residual that occurs every orbit at about 38 degrees of the anomoly from the ascending node. This slight spike correlates precisely with the temporary attitude excursion that occurs when the spacecraft leaves the Earth's shadow and the solar panels reorient toward the sun. The attitude motion is shown in Appendix A and the effect of this attitude motion on the raw scanner measurements is clearly illustrated in Appendix C. The plots in Appendix D indicate that the attitude motion effects were not perfectly removed from the residual errors in all the data spans, particularly for the shadow exit. Several errors may contribute to this error, including the response time of the scanner output to rapid changes, uncertainties in the reference attitudes for the excursions, and small timing differences between the reference attitude flight software times and the averaged scanner data times that may become significant when the

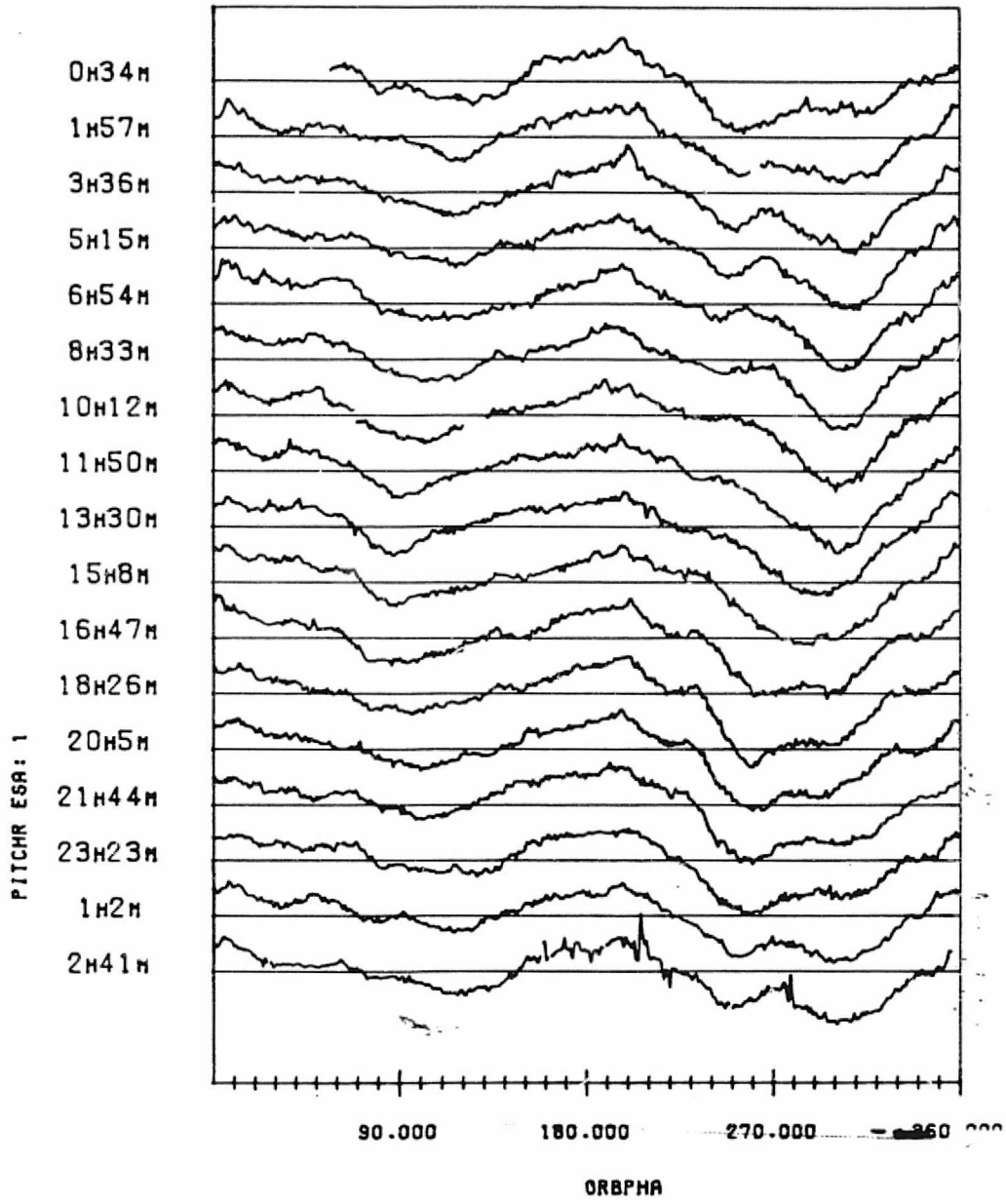

FIGURE 6-7. Pitch Residual Errors from Oblate Earth Model for Consecutive Orbits on April 14, 1983 Data Span (1 of 2, Sensor 1 Pitch)

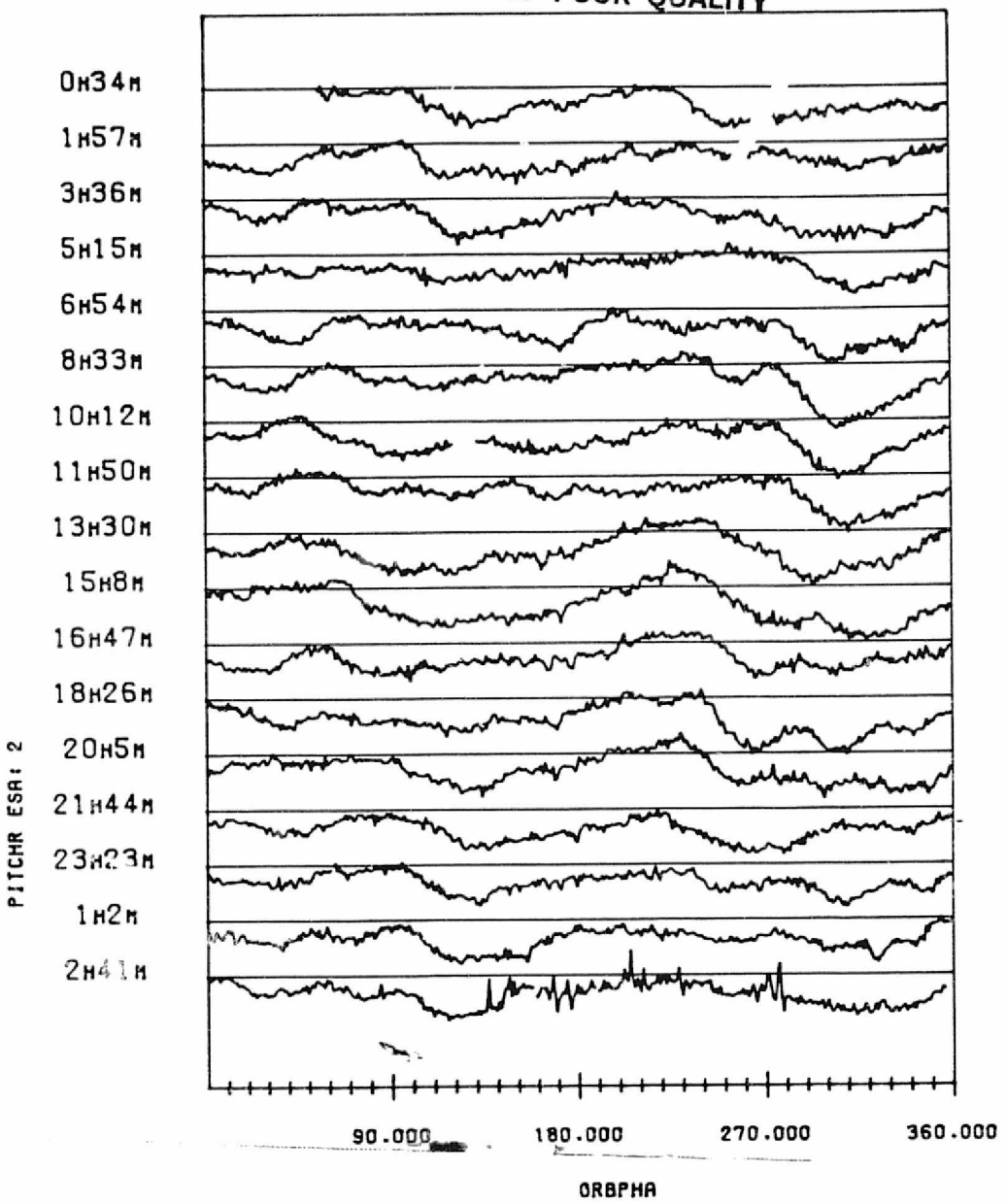

FIGURE 6-7. Pitch Residual Errors from Oblate Earth Model for Consecutive Orbits on April 14, 1983 Data Span (2 of 2, Sensor 2 Pitch)

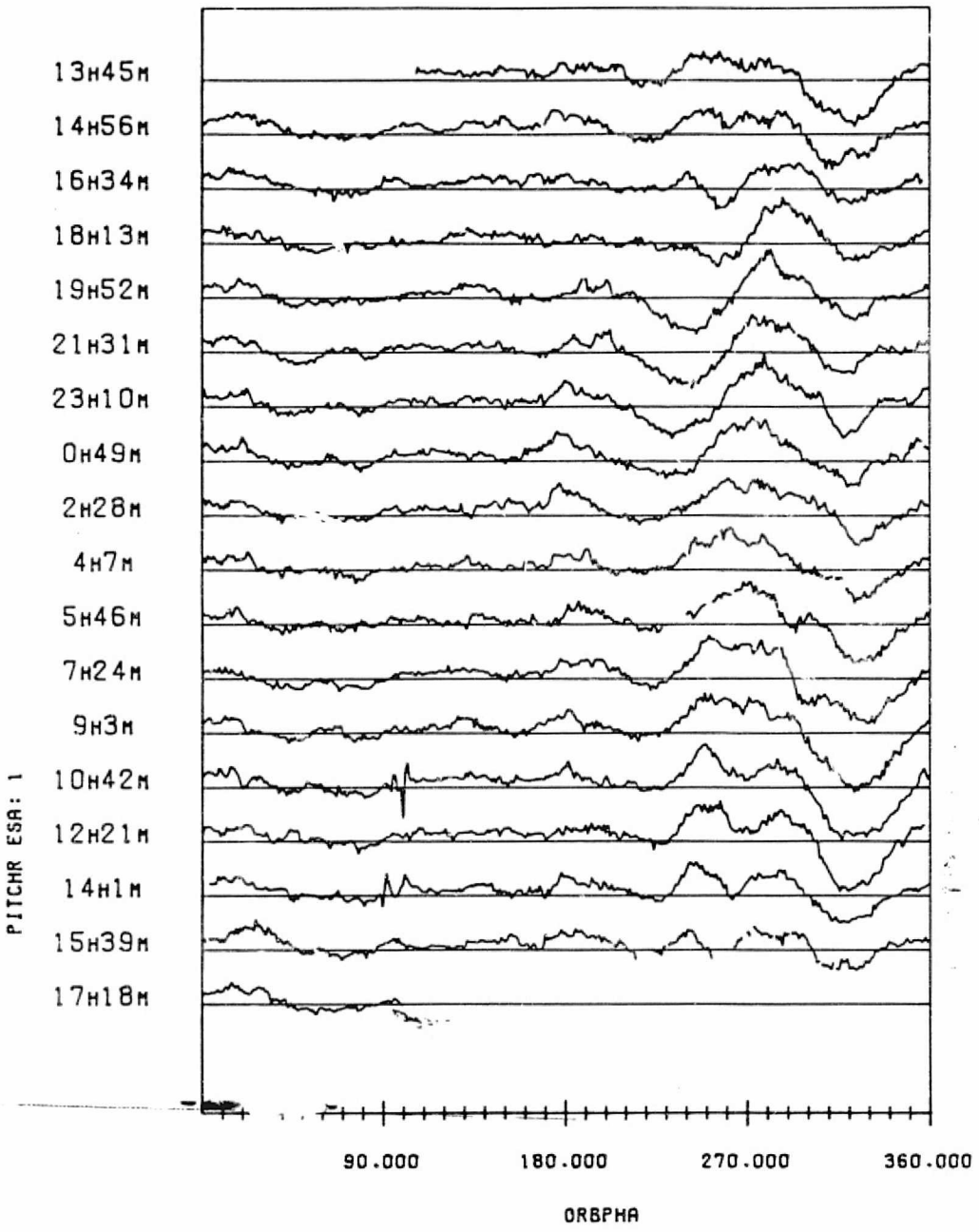

FIGURE 6-8. Residual Errors from the Oblate Earth Model for Consecutive Orbits on August 6, 1983 Data Span (1 of 4, Sensor 1 Pitch)

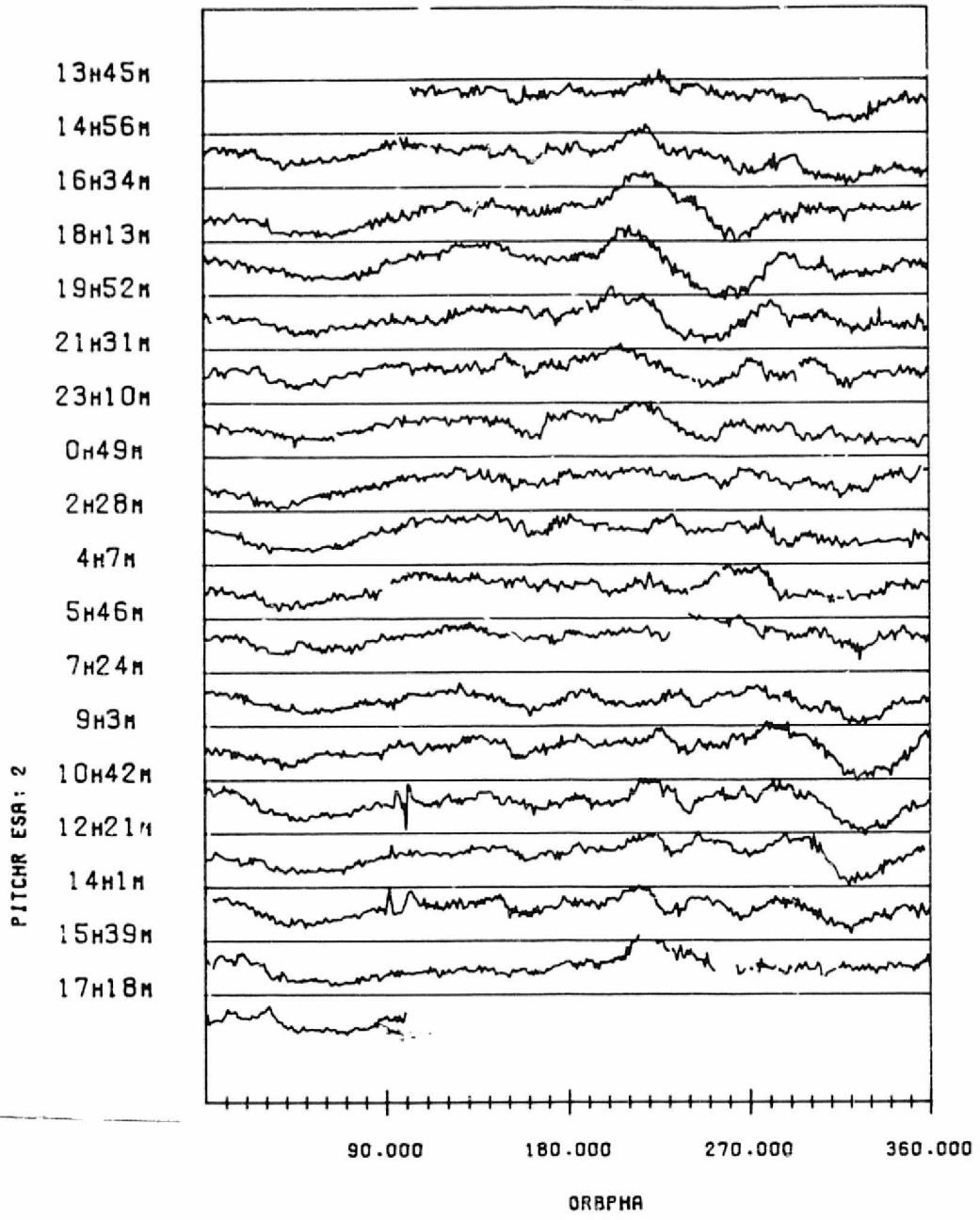

FIGURE 6-8. Residual Errors from the Oblate Earth Model for Consecutive Orbits on August 6, 1983 Data Span (2 of 4, Sensor 2 Pitch)

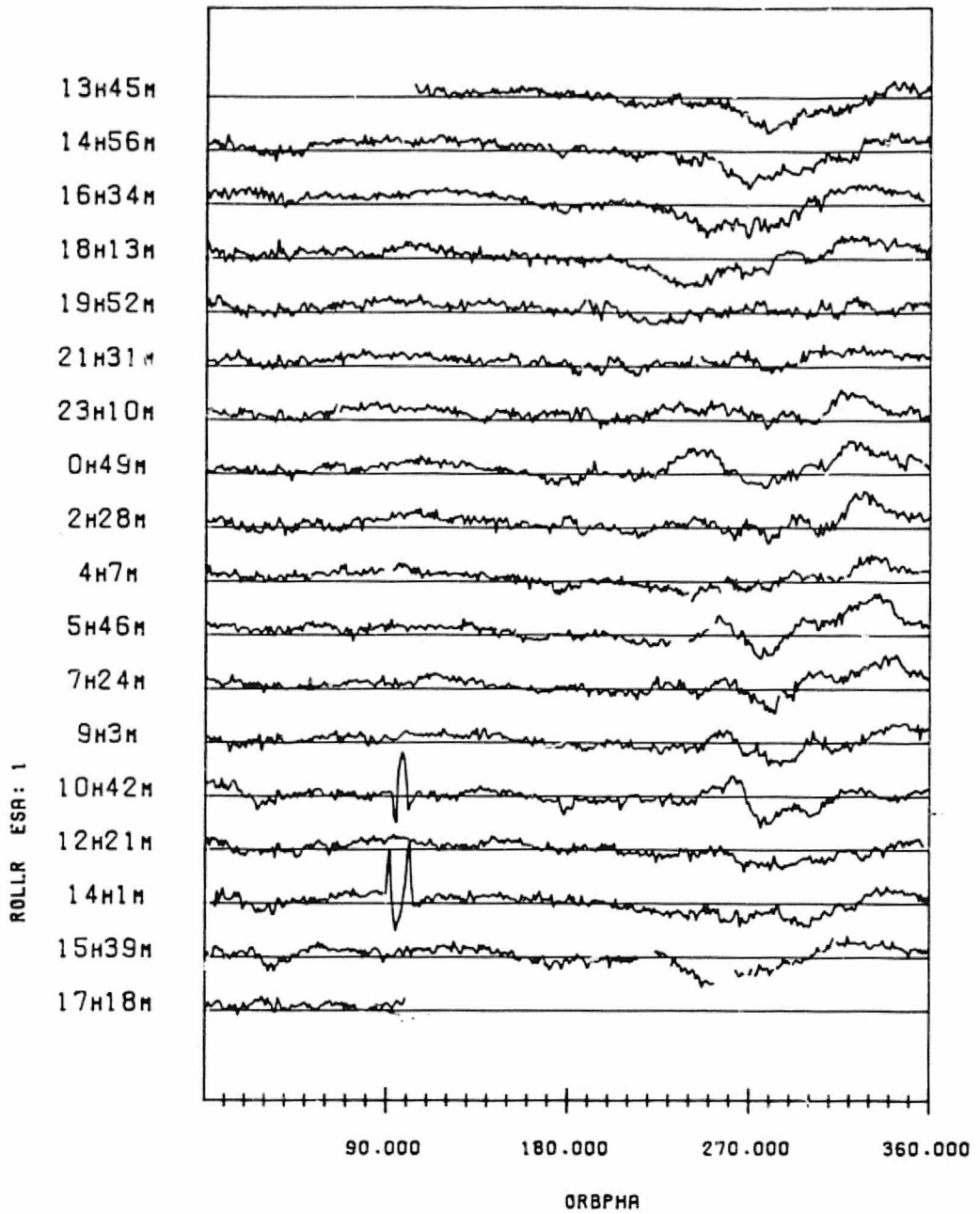

FIGURE 6-8. Residual Errors from the Oblate Earth Model for Consecutive Orbits on August 6, 1983 Data Span (3 of 4, Sensor 1 Roll)

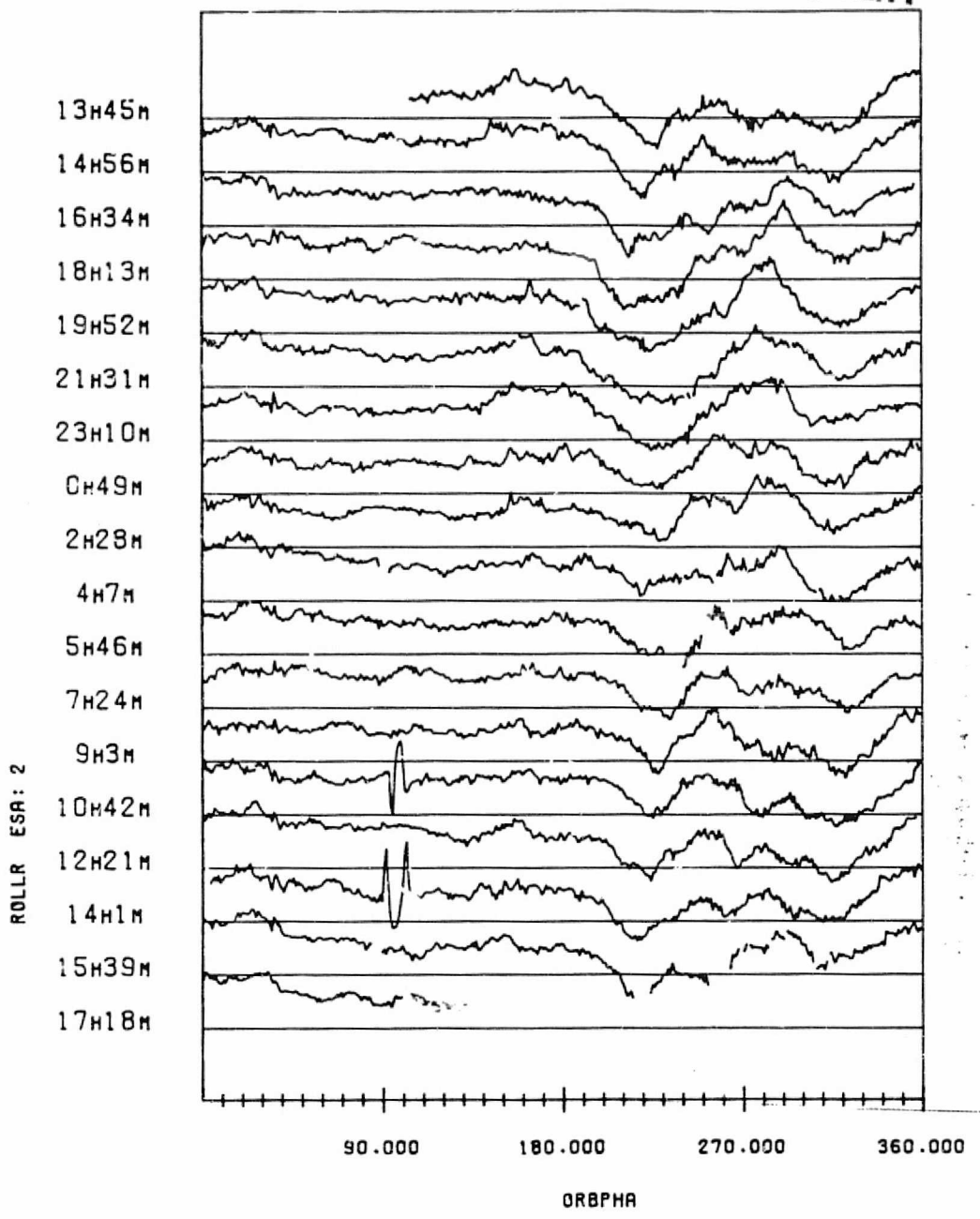

FIGURE 6-8. Residual Errors from the Oblate Earth Model for Consecutive Orbits on August 6, 1983 Data Span (4 of 4, Sensor 2 Roll)

attitude motion is rapid. This error is not considered a significant source of concern.

6. One additional anomoly that spans long periods of time has been noted already in this report; the sensor 2 roll measurement residuals show an unusually large spread from orbit to orbit in August, November, and December 1982 data. This can be seen in the residual error plots shown in Appendices C, D, E, and G. The reason for this is not known, and this feature has not been seen in 1983 data processed so far.

SECTION 7 - POLAR RADIANCE VARIATION AND CLOUD EFFECTS

This section discusses the radiance effects on the scanner measurements that may be considered random in the sense that the variations are hard to predict and are inconsistent from one orbit to the next. Section 4.1 provided general background about the Earth radiance. Section 7.1 provides more details about the Earth radiance variability, particularly in the winter polar regions where that variability is quite large. The winter polar radiance variability turns out to be mostly a longitude dependence of the Earth radiance. Section 7.2 discusses the effects on the horizon measurements in the winter polar regions. Section 7.3 analyzes the effects of cold clouds on the Landsat-4 horizon scanner measurements. The effects of cold clouds on the Landsat-4 scanner appear significantly smaller than the effects on scanners in previous missions.

7.1 RADIANCE VARIABILITY AND LONGITUDE DEPENDENCE

Figure 7-1 shows the peak-to-peak spread in the CO_2 Narrowband limb radiance for latitudes between 60 South and 80 North for one date in each of the seven months that LIMS data was available. This data clearly demonstrates the larger variability of the radiances in the winter polar region in the northern hemisphere. Moveover there is more variation at 60° North than at 80° North for these winter months. This is probably partly the result of the 60 degree latitude circle spanning a greater geographic distance. The southern hemisphere shows slightly higher spreads in the radiance at the beginning and end of the LIMS data spans (November and May) indicating that the radiance spread in the southern latitudes may increase in the winter as well.

Figure 7-2 shows the longitude dependence of the peak CO_2 limb radiance measured by LIMS at 60° North latitude on one date each month. For the months where a large spread in the radiance is present there is a general pattern such that one side of the Earth is brighter

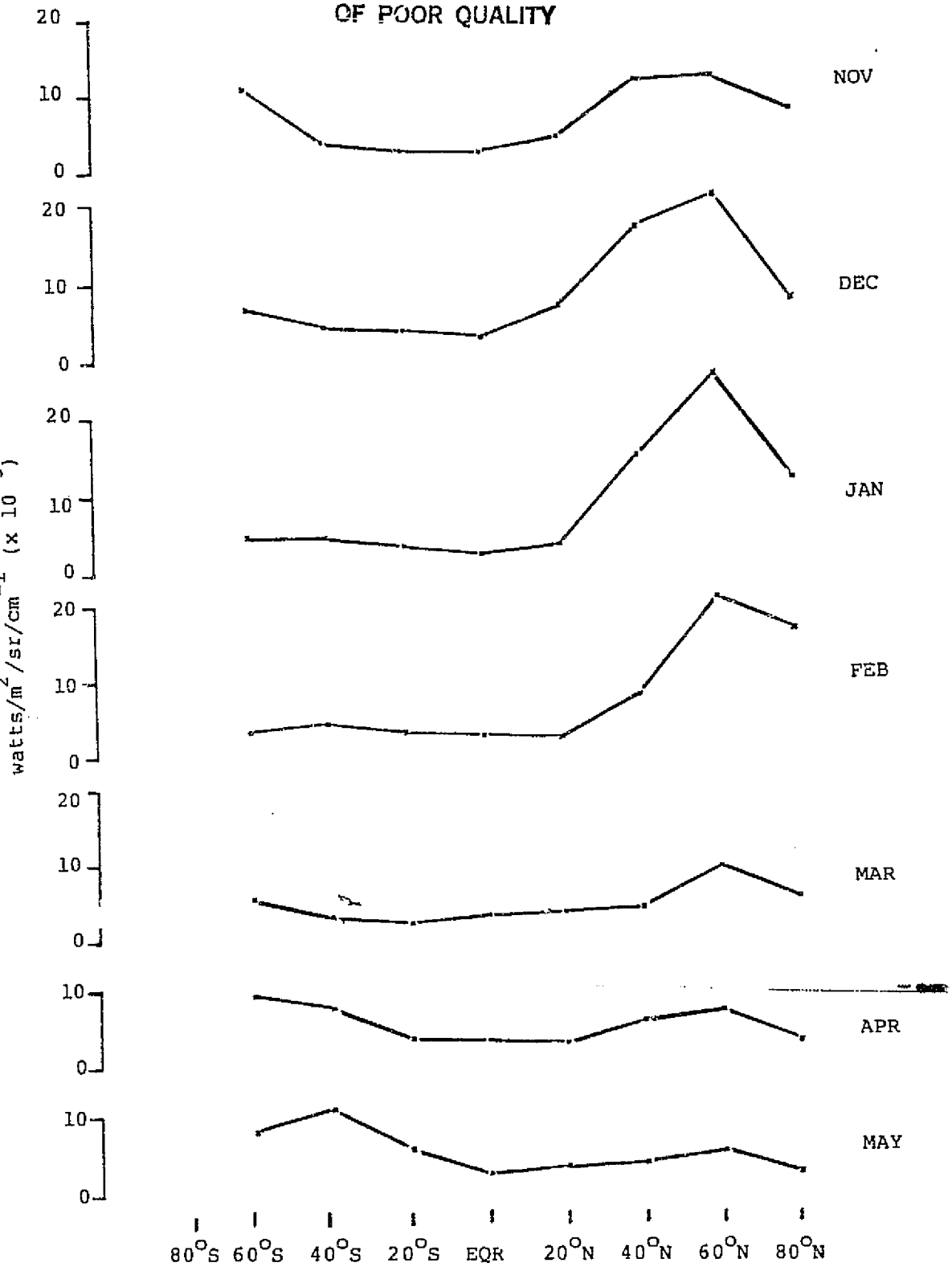

FIGURE 7-1. Peak-to-Peak 0 Kilometer Radiance as a Function of Latitude (CO_2N)

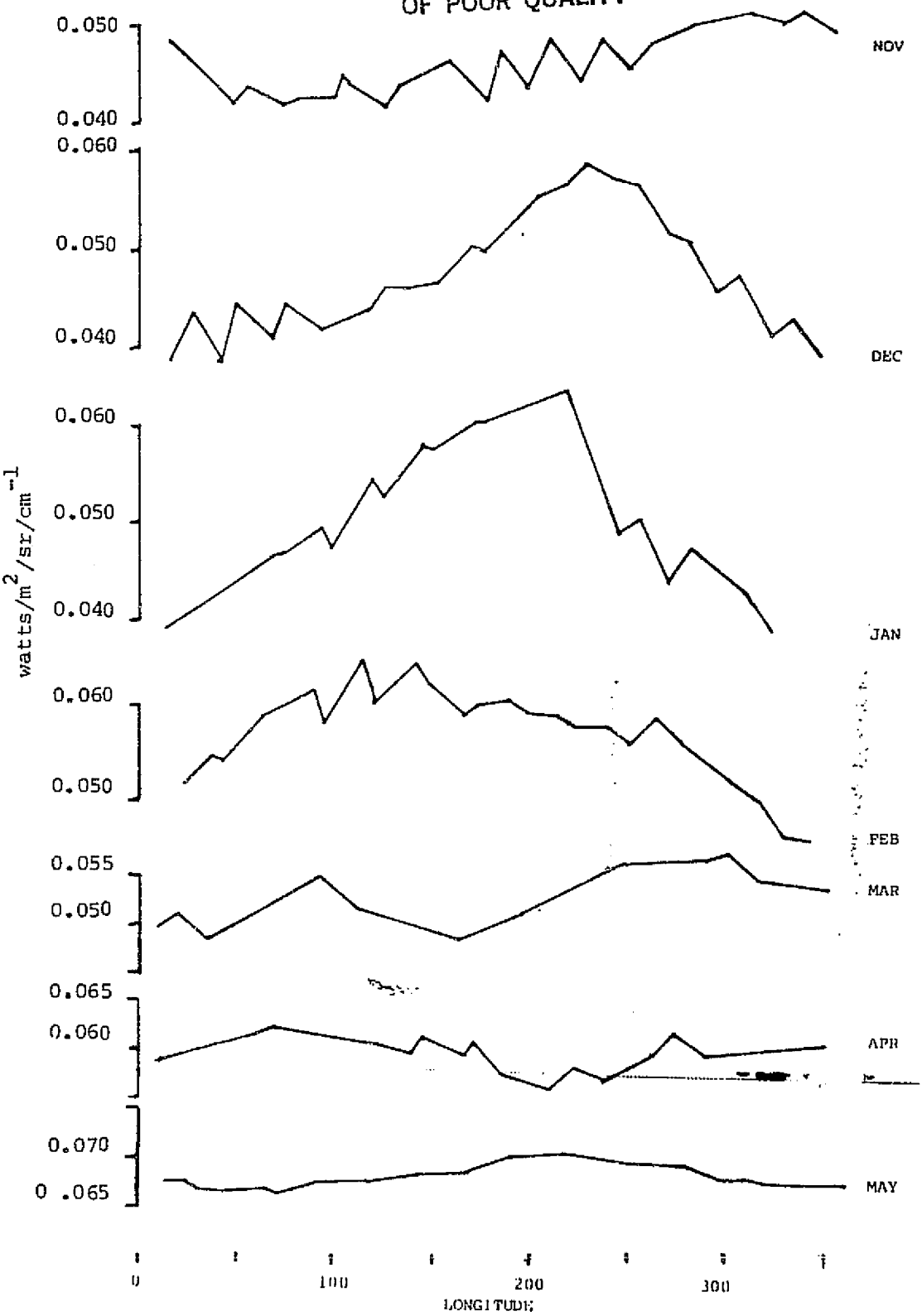

FIGURE 7-2. Peak LIMS Narrow CO_2 Band Radiance versus Longitude at $60^{\circ}N$

than the other. Examination of this longitude dependence for all the days with LIMS data available (about 4 days per month) confirms this general pattern. The peak brightness tends to stay in the west longitudes (though not exclusive). Perhaps this tendency indicates some systematic component to the polar radiance patterns but these variations are probably indicative of large scale variable "weather" patterns in the upper atmosphere.

Examination of the individual profile shapes around 60° North for a sample day with the strong longitude dependence indicating another interesting observation about the profile variability. Profiles observed at nearly the same geographic position showed significantly different shapes when viewed on the northbound and southbound sides of the orbit. The northbound and southbound passes view the same longitude from different directions on day and night sides of the orbit, so this seems to indicate azimuthal viewing direction or diurnal dependence of the limb profiles.

7.2 WINTER POLAR RADIANCE VARIABILITY EFFECTS ON TRIGGERING HEIGHTS

As noted earlier, there is a strong longitude dependence of the Earth radiance in the Winter polar regions, and this longitude dependence is the likely cause of the large orbit-to-orbit variations in the scanner measurements made over those regions. This section analyzes the horizon scanner measurements in the polar regions in more detail in order to confirm that longitude dependent radiance patterns rotating with the Earth are the cause of the orbit-to-orbit variations. There is evidence from the way that polar radiance variations influence each of the four horizon crossings separately that it is not just the geographic location of the horizon that influences the measurement, but also the azimuthal direction that the Earth limb is scanned.

The qualifier "winter" for the polar region discussion is used loosely here to indicate those days where there is a large spread in the

orbit-to-orbit scanner measurements over the northern or southern polar region part of orbit. The northern hemisphere demonstrates this large spread starting in mid-November and continuing through mid-March which spans the winter season. However the southern hemisphere only shows a slightly higher than usual orbit-to-orbit spread throughout its winter months of June, July, and August, and then shows a large spread mainly only in October. Therefore, in the southern hemisphere the large spread really occurs in mid-spring during which time the southern hemisphere seems to undergo a rather rapid transition in the pattern of systematic radiance effects. It seems that the southern hemisphere must maintain much more symmetry in the radiance pattern around the pole in the winter months, and this symmetry breaks down in spring. The hemispheric differences in the radiance effects probably result from climatological differences due to the different distributions of land mass.

To analyze the radiance effects on the horizon crossings it is useful to convert the Earth width and phase measurements to Earth-in and Earth-out horizon triggering heights in kilometers. This conversion must make use of the reference attitude, orbit, and Earth oblateness modeling. The conversion is computed in the Data Plotting and Fitting Utility by taking the difference between the observed triggering rotation angles and the predicted triggering angles which are based on a fixed height above the oblate Earth and multiplying by the partial of the Earth half-width with respect to triggering height (which is practically constant at 0.027 degrees per kilometer for the Landsat flight geometry), and finally adding back the nominal predicted triggering height (40 kilometers).

Figure 7-3 shows a serial stacked format plot of the horizon triggering heights as a function of orbit phase angle from the ascending node for 12 consecutive orbits on February 2, 1983, when there is large orbit-to-orbit variation in the northern hemisphere

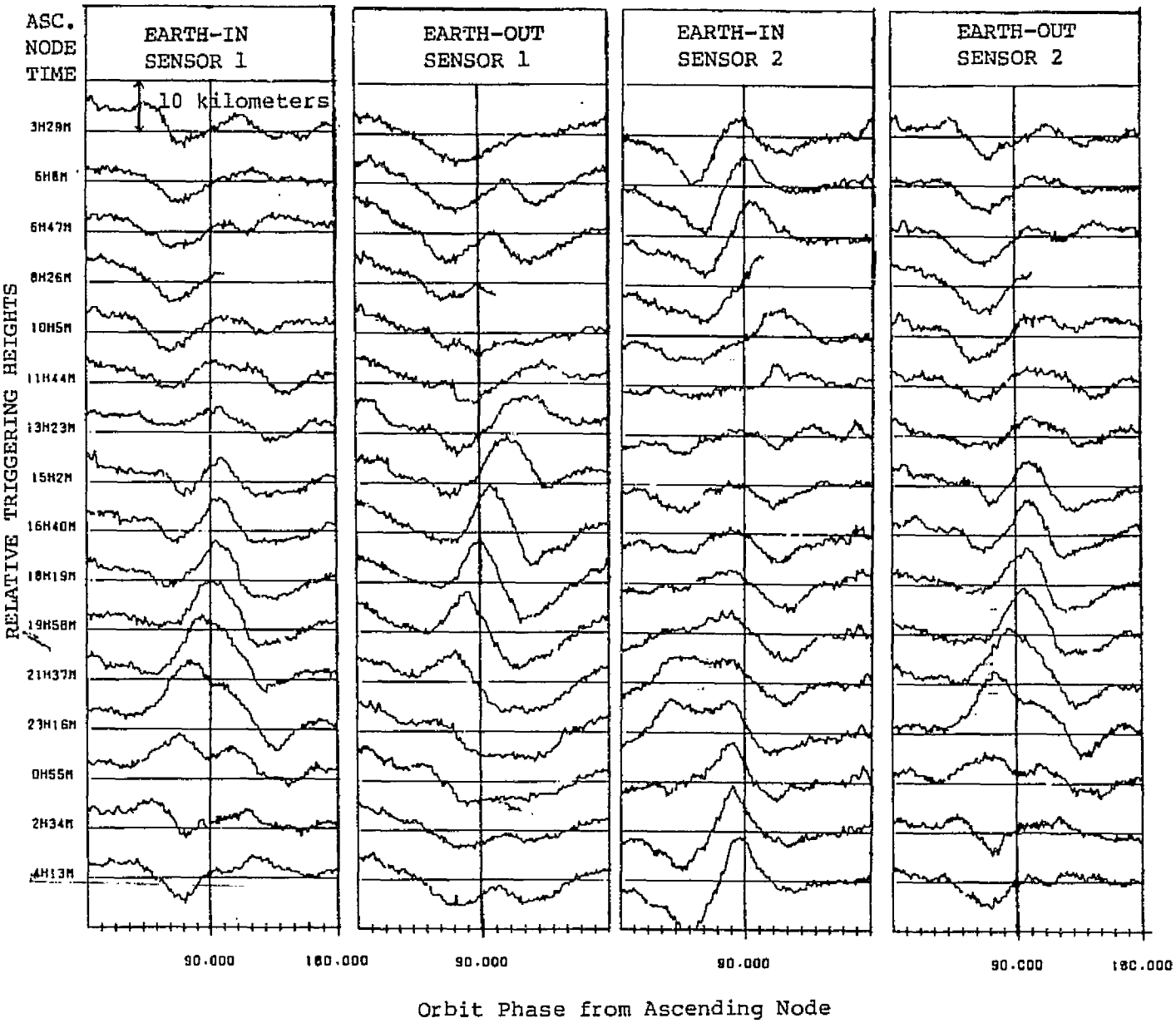

FIGURE 7-3. Horizon Triggering Heights in the Northern Hemisphere for Consecutive Orbits on February 2, 1983

measurements. There are two important observations that stand out from these plots.

First of all there is obviously a very strong correlation in the polar effects on the sensor 1 Earth-in crossing and the sensor 2 Earth-out crossing. These are the two horizon crossings that view nearly the same direction as indicated in Figure 1-5.

Second of all there is not the correlation that would be expected if certain triggering heights could be directly associated with geographic location on the Earth. Most important, the Earth-in for scanner 2 crosses the same geographic positions as the Earth-out for scanner 2, just about ten minutes earlier in the spacecraft orbit. Therefore one might expect the Earth-in scanner 2 triggering heights to show the same pattern as Earth-out scanner 2 with a slight phase lag in the spacecraft orbit phase from the ascending node. However, one can see that there is a very different pattern in the polar effect on the sensor 2 in and out crossings for the same orbits. In fact it is an entirely different part of the day that the peak polar effects are found on the Earth-in and Earth-out crossings.

An explanation for the patterns in the various horizon crossings suggested by the close correlation between sensor 1 Earth-in and sensor 2 Earth-out. This explanation is that the triggering heights are associated strongly with the direction in which the horizon is viewed or possibly with the gradient in the Earth radiance along the direction that the scanner moves into the Earth. The sensor electronics response is such that about seven degrees of scanner rotation is important in shaping the output pulse at any given time. Moreover the geographic range covered by the scanner by moving just a few degrees into the horizon is rather large, as indicated in Figure 1-5.

In support of this explanation, note that sensor 1 Earth-out and sensor 2 Earth-in, which are looking in opposite directions, show their maximum effects due to radiance effects about 12 hours apart in the day. Also consistent with this explanation is the observation that these two horizon crossings show the opposite sequence of high-to-low (or low-to-high) triggering heights when passing the pole in opposite directions.

The trends in each horizon crossing as a function of orbit on consecutive orbits make sense in terms of the rotation of the Earth. For example the place in each orbit where the maximum or minimum error in the sensor 1 Earth-out heights occurs a little earlier each orbit so that the feature starts out just after the pole crossing and gradually moves in front of the pole crossing before it disappears.

More analysis of the triggering height variations around the pole will be needed to fully understand the effects of the radiance patterns on the sensor measurements.

7.3 COLD CLOUD EFFECTS

The effects of cold clouds on the scanner horizon was observed in the Seasat and Magsat missions (Reference 16). Therefore, a search was made of the Landsat-4 scanner data to see if cold clouds were effecting the measurements.

For Seasat and Magsat, specific signatures (correlated error patterns in measurements) of clouds were predicted and observed based on the scanner mounting and flight geometry. The cloud signatures that may be expected for Landsat were discussed in Reference 2 and are shown in Figure 7-4. The most striking effect that should be seen might be from an isolated cloud on the right of the scanner ground track. This cloud would get in the right scanner Earth-in crossing, and then the tail scanner Earth-in and the right scanner Earth-out nearly

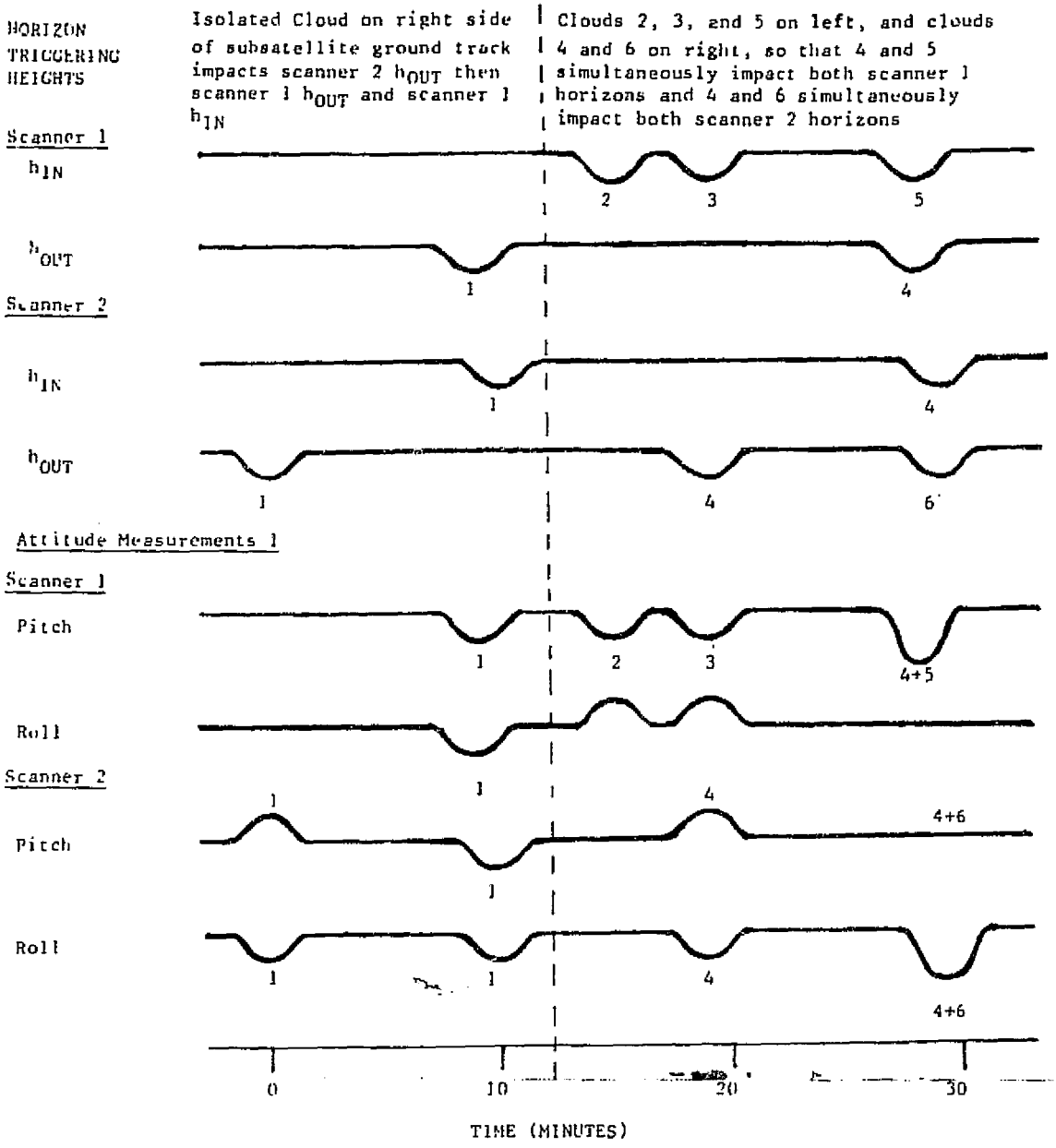

FIGURE 7-4. Landsat-4 Cold Cloud Signatures

simultaneously. A reduction in the triggering height is assumed in the cloud signature which is diagramed, but it was not certain what the cloud effect would be. One procedure to identify a cloud effect then is to search the data for a sequence of bumps having this pattern. However a search of the Landsat-4 data does not readily yield any such patterns. Moreover it hardly yields any outstanding bumps at all that are above the level of the noise. The largest effect is the large scale polar one that cannot be associated with a particular cloud. Both the Seasat and Magsat missions showed much more obvious bumps or excursions in the scanner measurements that could much more readily be associated with clouds.

The basic materials required to analyze correlations between the noise and cloud effects are data plots, cloud coverage photographs, and an indication of the horizon crossing positions in latitude and longitude. These materials are included in Appendix G for June 6, 1983 data.

A careful review of the horizon crossing paths and cloud system crossings was made and no consistent correlations could be made between cloud crossings and bumps in the triggering heights in any of the channels.

SECTION 8 - NOISE ANALYSIS

8.1 NOISE CHARACTERISTICS AND DISTRIBUTIONS

Figure 8-1 shows every observation in pitch and roll plotted for a one minute data span. Single observations are indicated by plus symbols. These plots demonstrate the noise and quantization in the telemetry data. Each integer count in the telemetry represents 0.04 degrees change in pitch and roll. One observation arrives every 0.128 seconds. The noise amplitude is higher in the Earth phase measurements than in the Earth width measurements. The scatter in the phase channels (sensor 2 pitch and sensor 1 roll) spans about 8 to 12 counts peak to peak, while the scatter in the width channels (sensor 1 pitch and sensor 2 roll) spans 3 to 5 counts.

The scatter is not a simple uniform or Gaussian distribution. This can be seen particularly for the Earth phase (roll) in scanner 1 where a large number of counts fall at a certain level below the main concentration. Also in this channel's sample plot it is seen that no observations are made at a certain count value in the middle of the noise range. Since this would not be expected from chance, the existence of a quantization level which is unrealizable may be indicated.

A sample plot of the measurement noise for a 20 minute data span is shown in Figure 8-2.

In these plots a particularly interesting phenomenon can be observed in the scanner 2 phase measurement. The readings do not fall below certain count values when the mean measurement is just above these values. This pattern has been found consistently in all of the data spans. The reasons for this phenomenon are unknown. It may be related to the behavior of the analog-to-digital sampling process in the presence of the high level of noise.

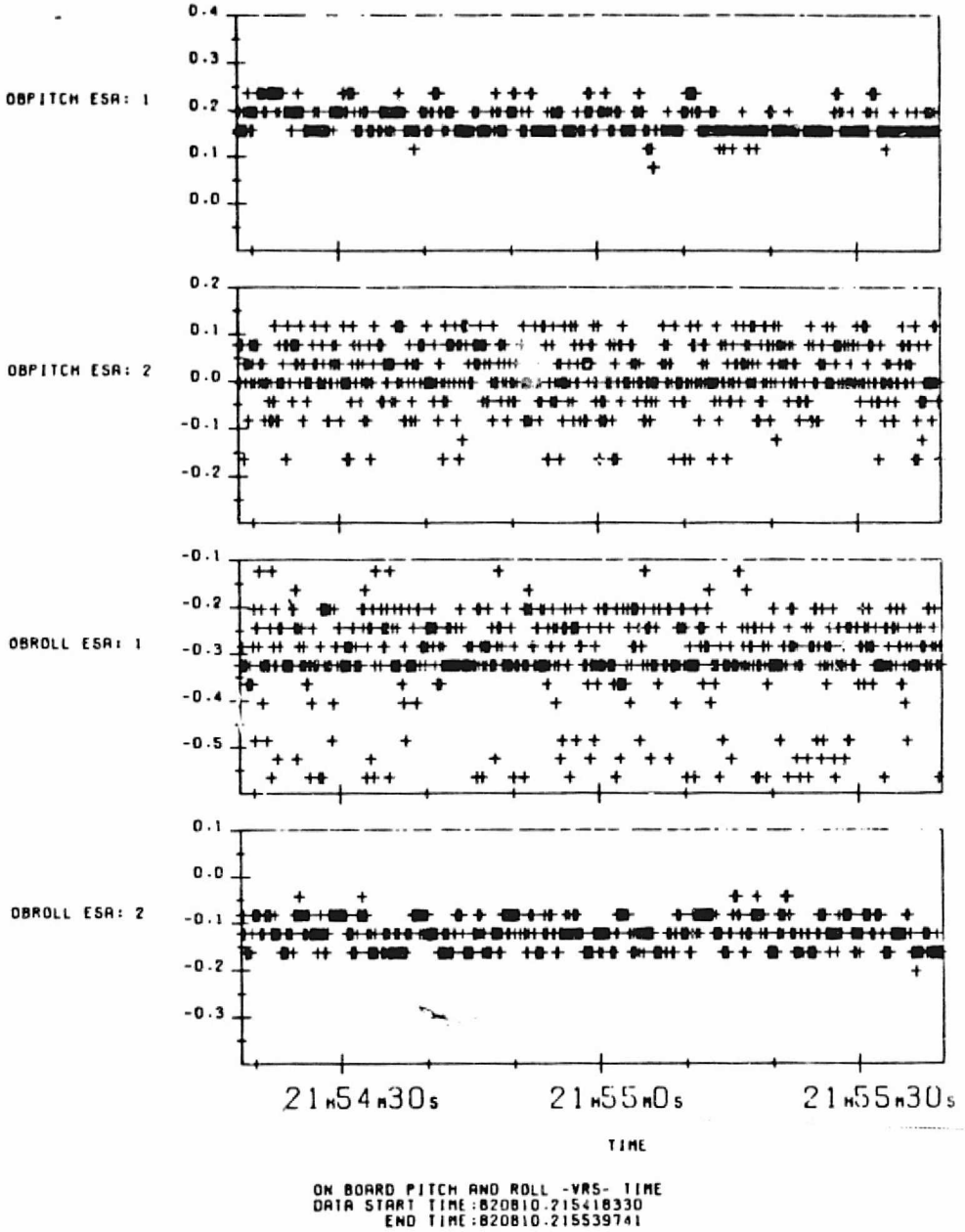

FIGURE 8-1. Scanner Measurements, Every Observation for One Minute

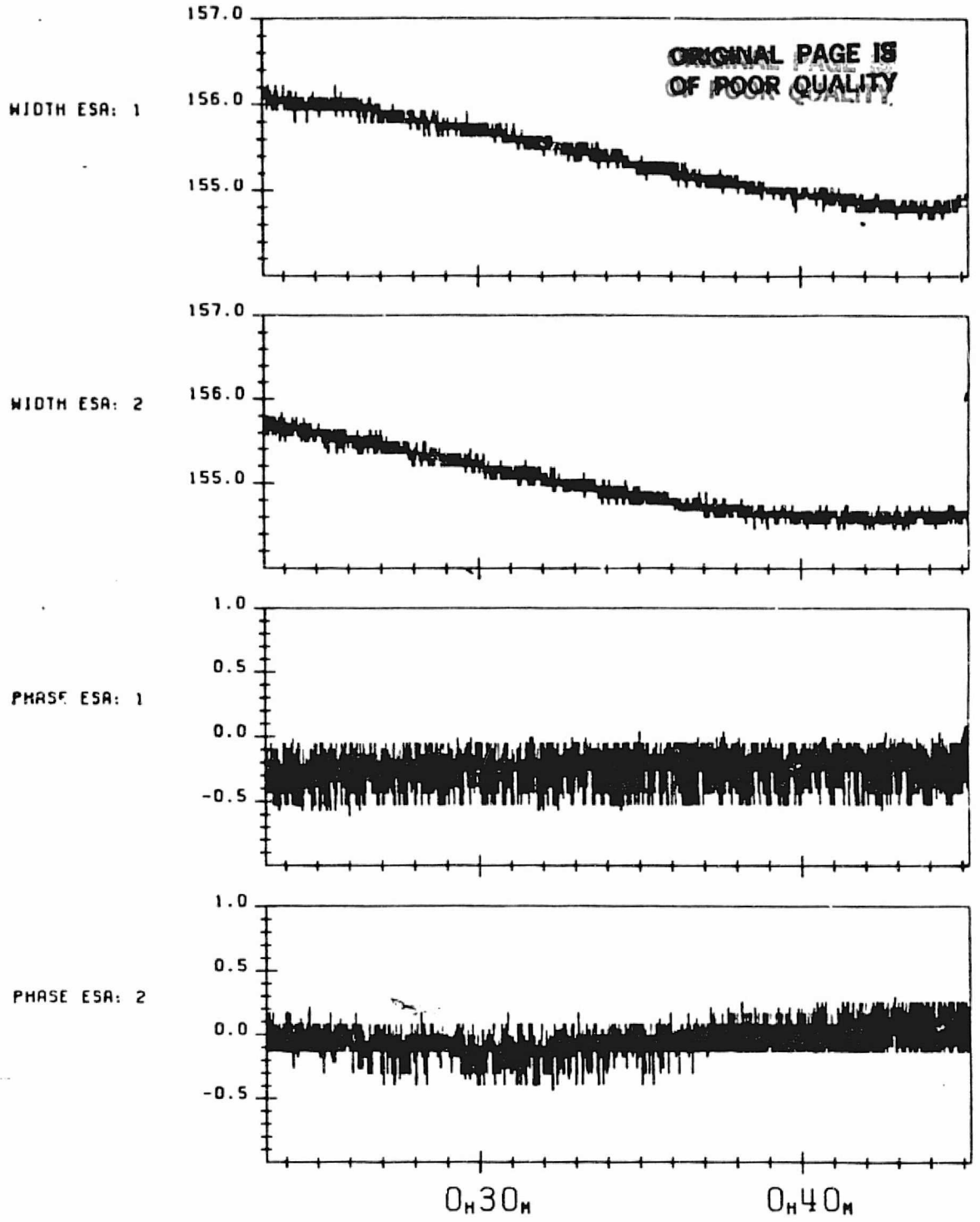

FIGURE 8-2. Plots of the Earth Width and Phase Measurement for a 20 Minute Data Span

There is an obvious high frequency observation-to-observation noise in the scanner measurements, especially in the Earth phase. This noise was not expected based on the scanner design. The scanner electronics have an analog sample and hold circuit (implemented with operational amplifiers) in the output buffer for each channel clamping the output voltage at a constant value for the duration of the spin period, which is 0.5 seconds. Since telemetry samples are made every 0.128 seconds, the telemetered data should show the same reading for four consecutive samples. In addition a two pole Butterworth Filter is applied to the output channels to further smooth the output signal. This filter has a 3 db cutoff at 0.5 hertz.

An explanation for this high frequency noise was offered by personnel at Ithaco, Inc. and General Electric Company based on testing of the scanners for the Landsat-D prime mission (References 17 and 18). It was determined that there was some contamination of the output signals by some capacitative coupling with the DC power supply, which incorporates a 10,000 Hertz signal. Apparently the Remote Interface Unit, which samples many voltage channels on board the spacecraft sequentially by multiplexing, responds fast enough to pick up some of this signal. The strip chart recorder used for ground measurement of the noise did not have this high a frequency response and therefore failed to detect this contamination. The Earth phase measurements were more affected by this problem than the Earth width measurements. A simple fix has been implemented for Landsat-D prime; a capacitor was added to the output line to serve as a low pass filter.

8.2 NOISE AMPLITUDES

Table 8-1 summarizes the standard deviations in the pitch and roll angle measurements. These values represent average values computed from several sample data spans.

TABLE 8-1. Summary of Landsat-4 Conical Scanner Noise Amplitudes In Flight Data

	ROLL	PITCH
SCANNER 1	rms .083 p-p .46 (H channel, Earth Phase)	rms .029 p-p .12 (E channel, Earth Width)
SCANNER 2	rms .031 p-p .14 (E channel, Earth Width	rms .070 p-p .36 (H-channel, Earth Phase)

NOTES: Units are degrees for noise amplitudes.

rms noise is based on standard deviations in 30 sample major frames of data (128 observations per major frame)

p-p noise is the average peak to peak range in 30 sample major frames of data.

It is noteworthy to compare the ground measurement of the scanner noise with the in-flight observations. Ground measurements of the scanner noise were made by the scanner manufacturer Ithaco, Inc. (Reference 19). These noise estimates were based on strip chart measurements of the scanner voltage outputs. Figure 8-3 shows sample outputs from the ground tests. Table 8-2 shows a comparison of the peak to peak noise estimated from the ground measurements and the flight data.

The peak to peak noise in the H (phase) channel outputs is 4 to 7 times higher in the flight data than in the ground measurements. The flight noise in the E (width) channels is only 20 or 30 percent higher than the ground measurements.

Table 8-3 shows the standard deviations in the Earth width and phase measurements after several N-point averages are applied. These numbers represent the residual statistics from the data spans which were plotted in Figure 2-7. For pure white noise, one would expect the standard deviations of the N-point averaged data to be reduced by $1/\sqrt{N}$. One can note from Table 8-3 that the standard deviations in the Earth widths are reduced less rapidly than that rate while the standard deviations in Earth phase are reduced at nearly that rate.

8.3 POWER SPECTRUM

This section describes the power spectral density estimates which were computed for each of the scanner outputs. The following steps outline the procedure taken for obtaining the Power Spectrum estimates.

1. A data span of 8192 points (17.5 minutes of data) was selected that was free from data gaps, attitude motion, and data anomolies.

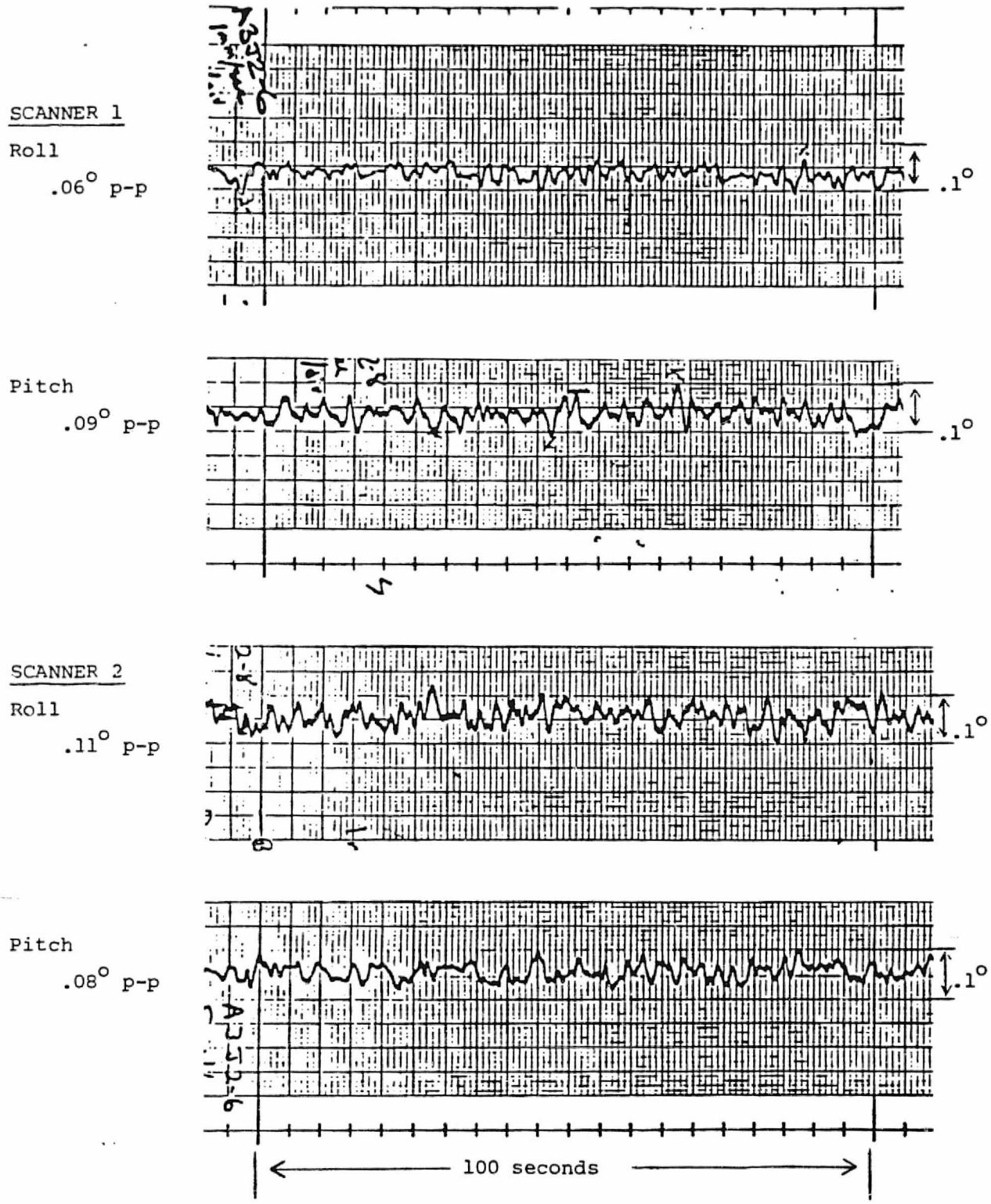

FIGURE 8-3. Ground Measurements of the Landsat-4 Horizon Scanner Noise Amplitudes (adapted from Reference 19)

TABLE 8-2. Comparison of Peak to Peak Noise in Ground Testing and Flight Data

CHANNEL TYPE	SCANNER NUMBER	MEASUREMENT ANGLE	PEAK-TO-PEAK NOISE IN DEGREES	
			GROUND TEST	FLIGHT DATA
E (Width)	1	Pitch	.09	.12
	2	Roll	.11	.14
H (Phase)	1	Roll	.06	.46
	2	Pitch	.08	.36

TABLE 8-3. Standard Deviations for N-Point Averaged Data

Number of Points Averaged	Width		Phase	
	Scanner 1	Scanner 2	Scanner 1	Scanner 2
1	.0577	.0617	.0886	.0829
8	.0437	.0481	.0356	.0354
32	.0267	.0309	.0177	.0182
128	.0176	.0217	.0073	.0101

2. Each channel was fit with a fifth order polynomial. The fit was used to remove the general trend over the time span which would be due to systematic variations.

3. The autocorrelation function, or mean lagged product, was computed for the time series with the polynomial fit subtracted out. The function is computed for lags up to 781 samples or 100 seconds.

4. A Hanning window was applied to the autocorrelation function. This smoothes the spectral estimates.

5. A discrete Fourier transform was applied to the autocorrelation function to obtain estimates of the power spectral density at the frequencies 0.0, 0.005, 0.01, 0.015, ..., 3.901, 3.906 hertz.

The above procedure was repeated for several independent data spans to confirm that the power spectrum result do not vary significantly for different data spans. The results for several data spans are included in Appendix F of Reference 3.

Figure 8-4 shows the residual time series (polynomial subtracted out) in all channels for a sample data span measured on February 17, 1983. The telemetry quantization levels are clearly visible in these plots; their c[illegible]ature is due to the trend removal by the polynomial. The Earth widths were decreasing in this interval while the Earth phases were nearly constant.

Figure 8-5 shows the autocorrelation function, or mean lagged product, for these intervals. The unit lag is the telemetry sample period (0.128 seconds). The function is computed for lags up to 781 samples which is 100 seconds. The most conspicuous feature evident in these plots is the marked difference in signature between the Earth width and Earth phase autocorrelation functions. The low amplitude high

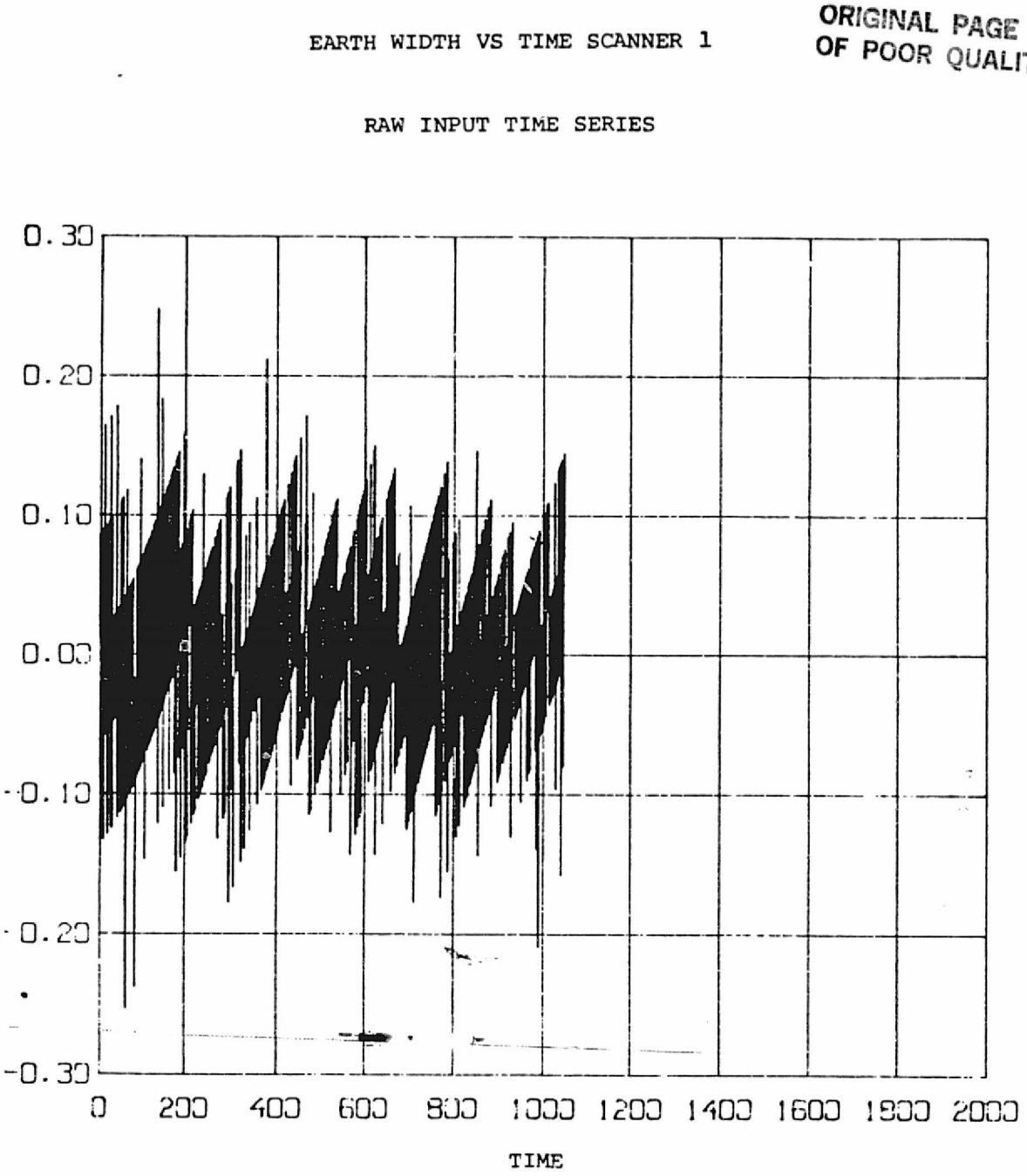

FIGURE 8-4. Scanner Measurement Noise with Polynomial Fit Removed (1 of 4, Earth Width Scanner 1)

EARTH WIDTH VS TIME SCANNER 2

RAW INPUT TIME SERIES

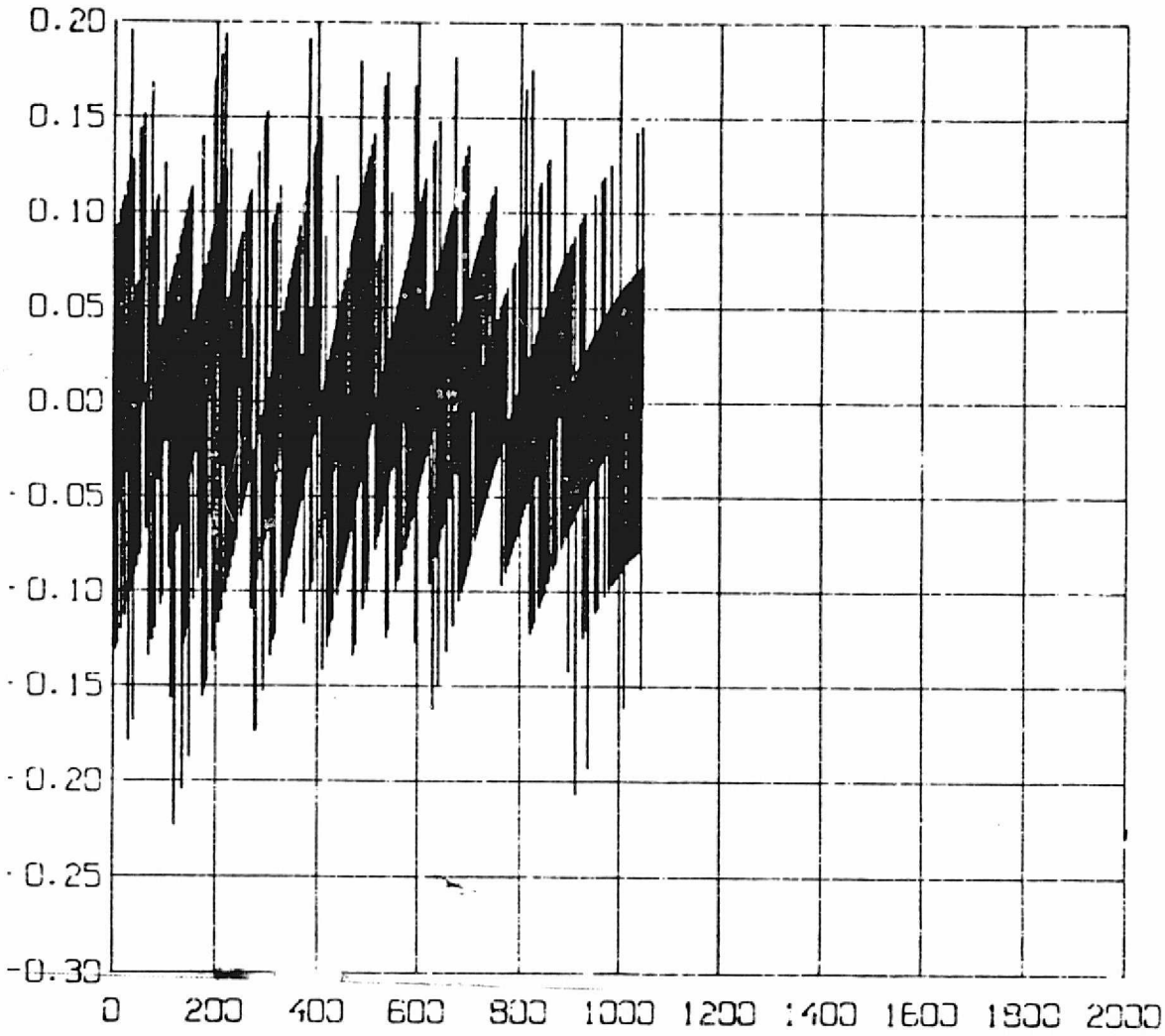

FIGURE 8-4. Scanner Measurement Noise with Polynomial Fit Removed (2 of 4, Earth Width Scanner 2)

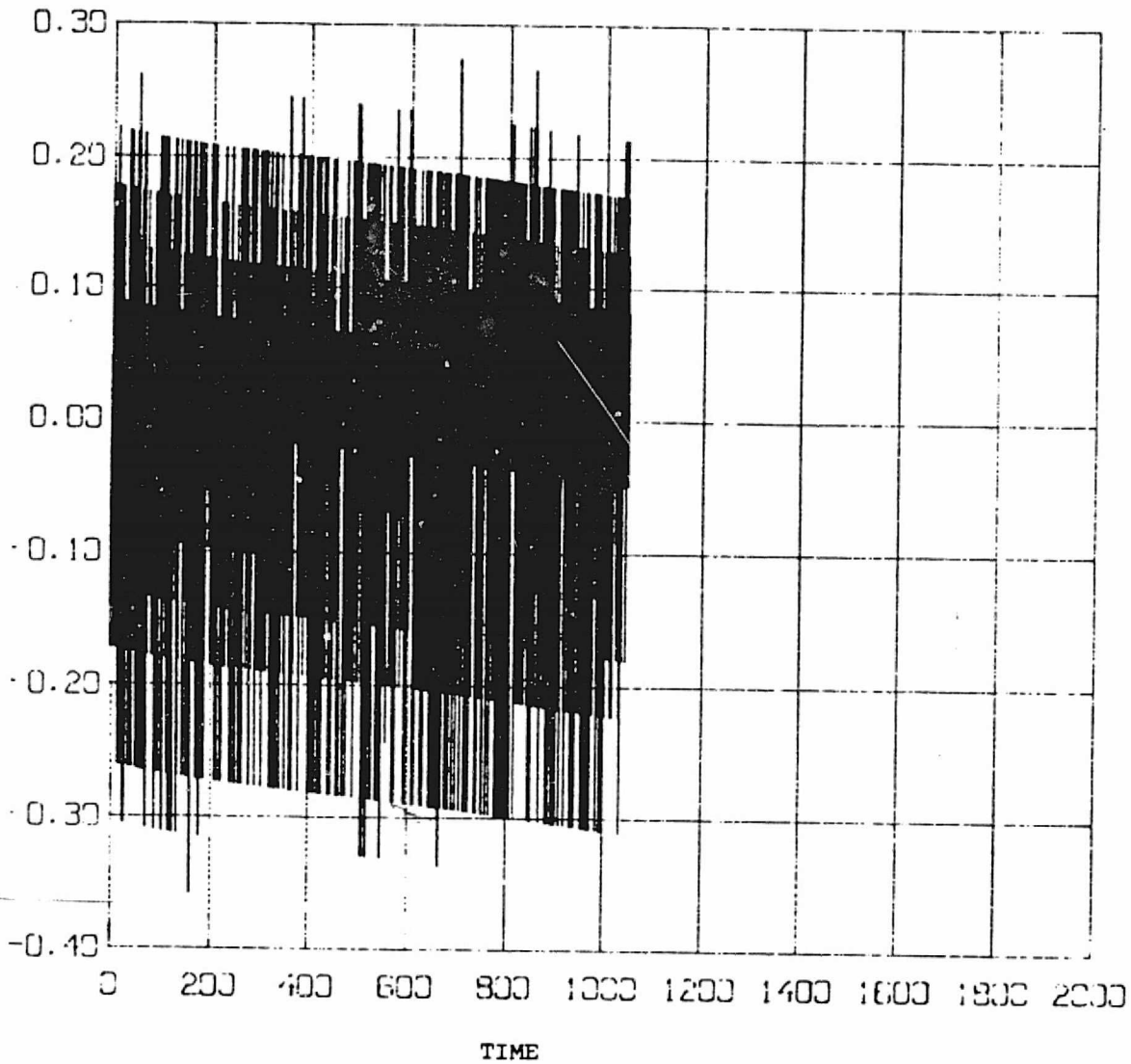

FIGURE 8-4. Scanner Measurement Noise with Polynomial Fit Removed (3 of 4, Earth Phase Scanner 1)

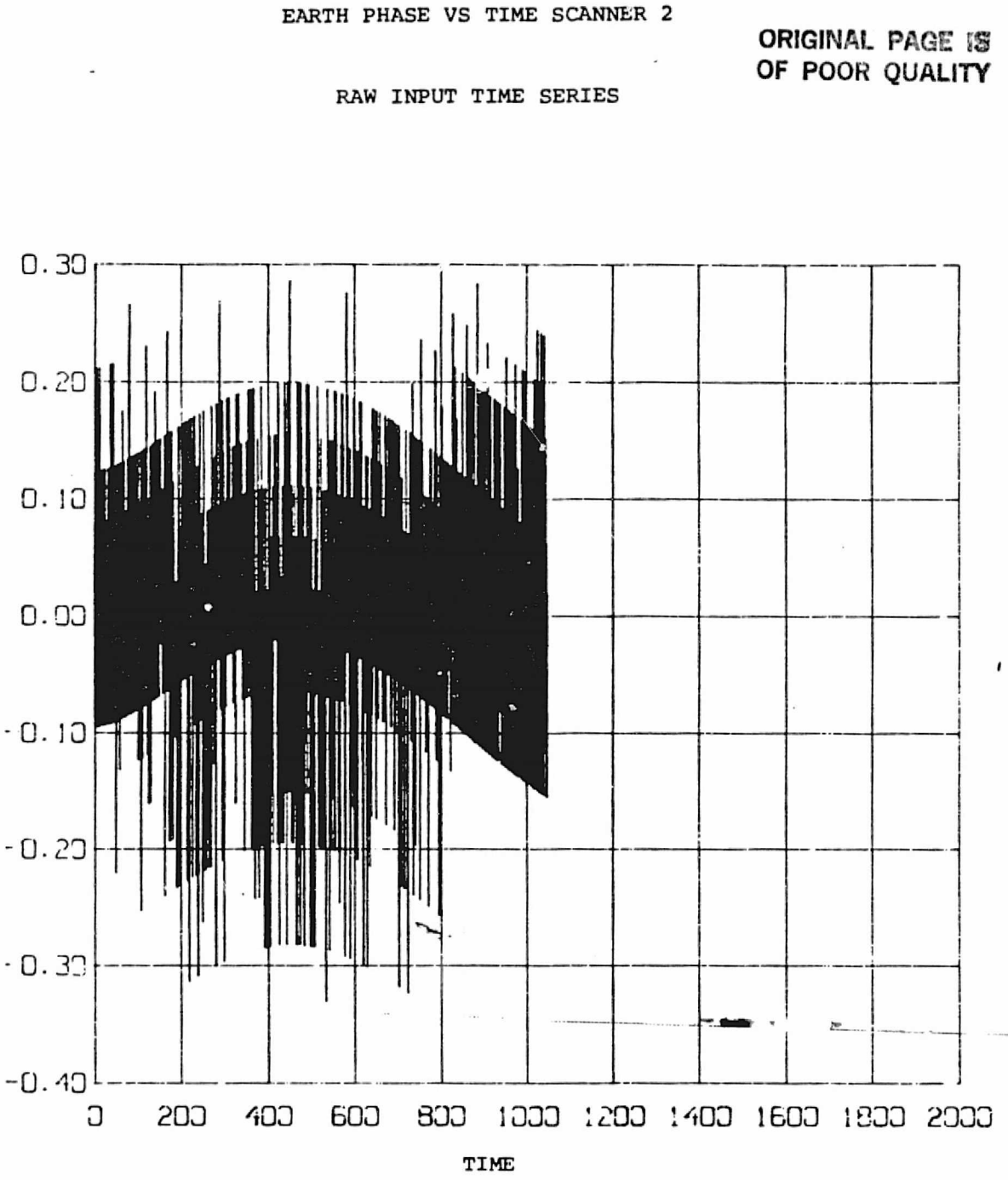

FIGURE 8-4. Scanner Measurement Noise with Polynomial Fit Removed (4 of 4, Earth Phase Scanner 2)

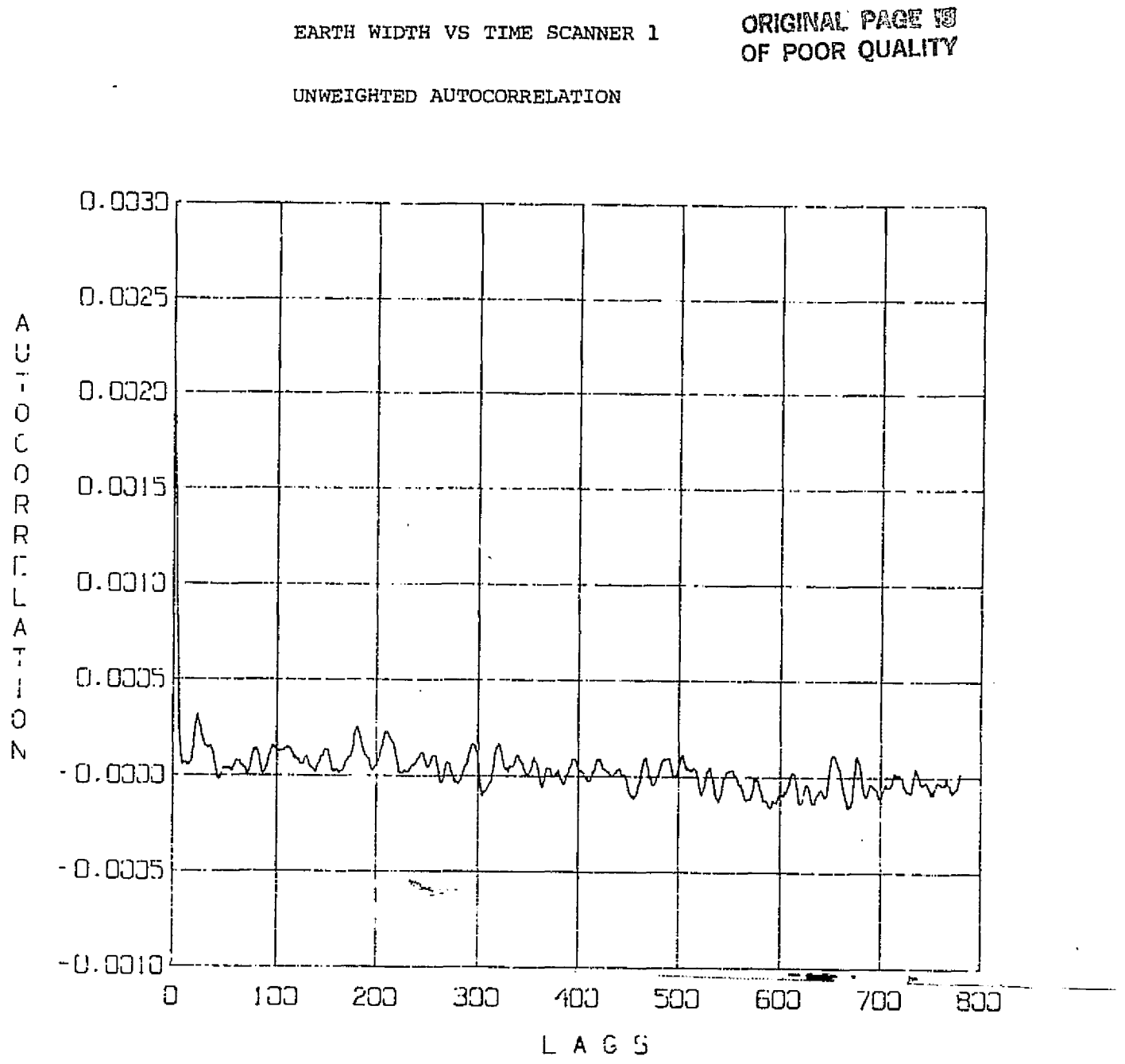

FIGURE 8-5. Autocorrelation Function for Scanner Measurement Noise (1 of 4, Earth Width Scanner 1)

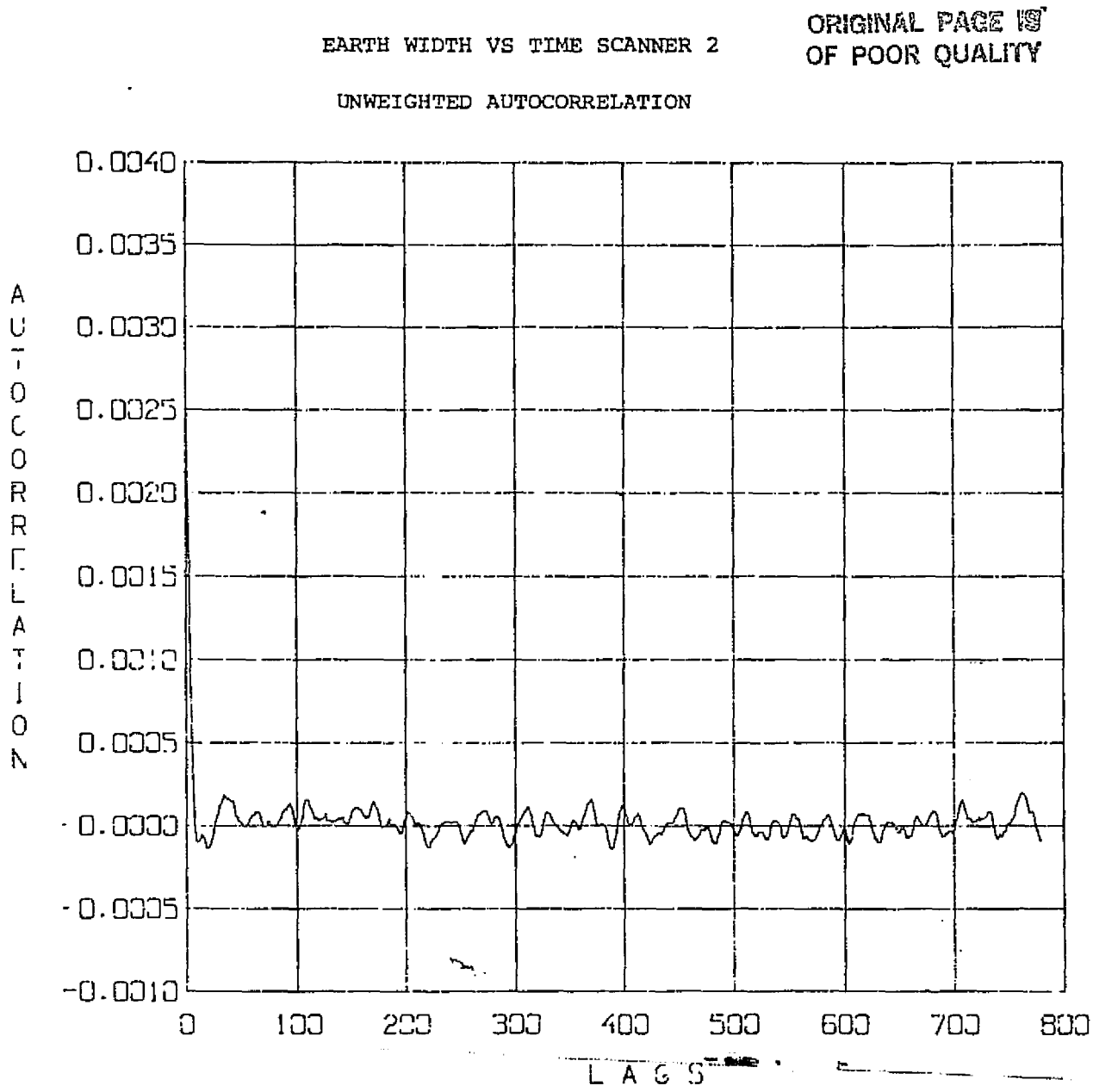

FIGURE 8-5. Autocorrelation Function for Scanner Measurement Noise (2 of 4, Earth Width Scanner 2)

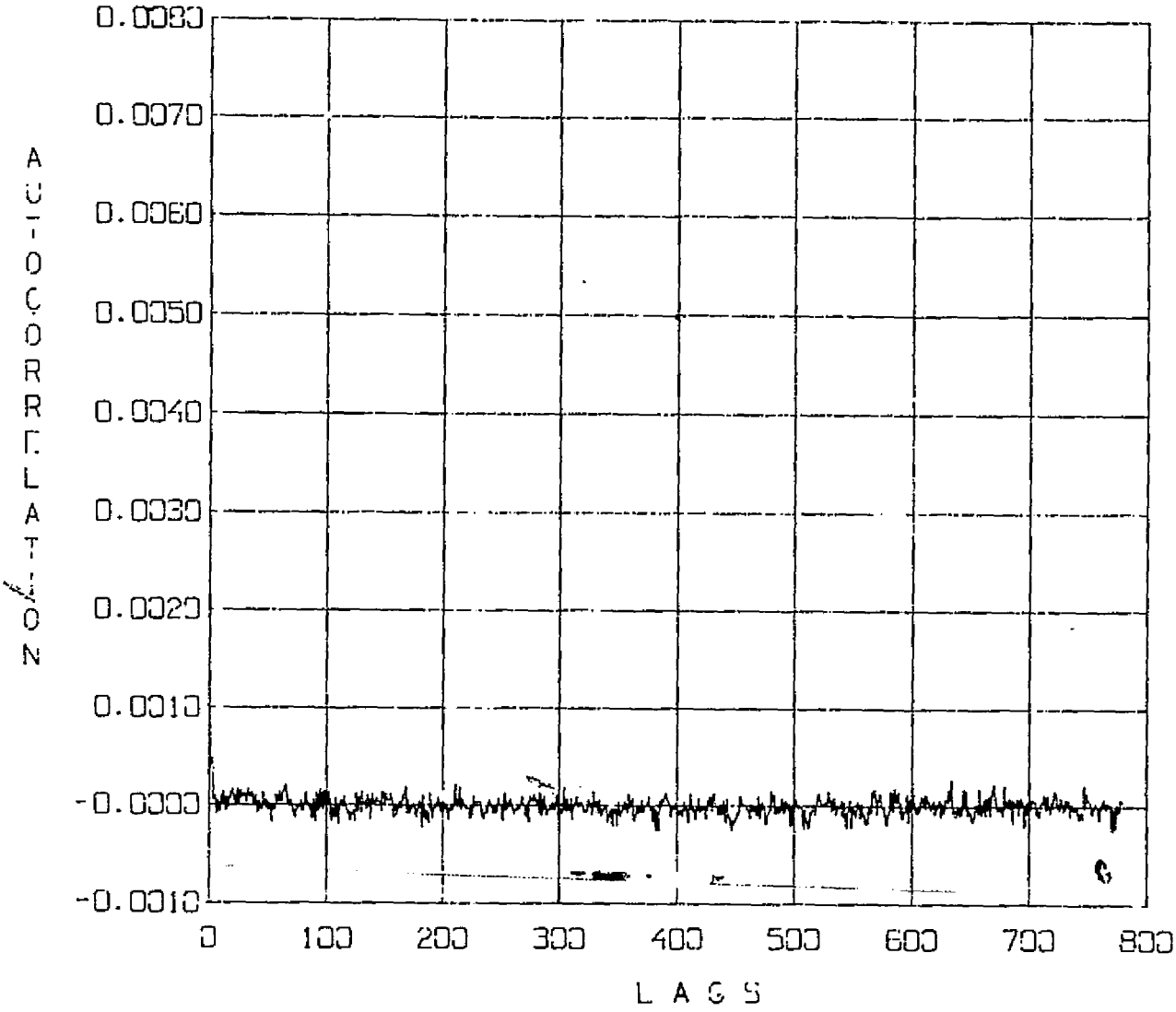

FIGURE 8-5. Autocorrelation Function for Scanner Measurement Noise (3 of 4, Earth Phase Scanner 1)

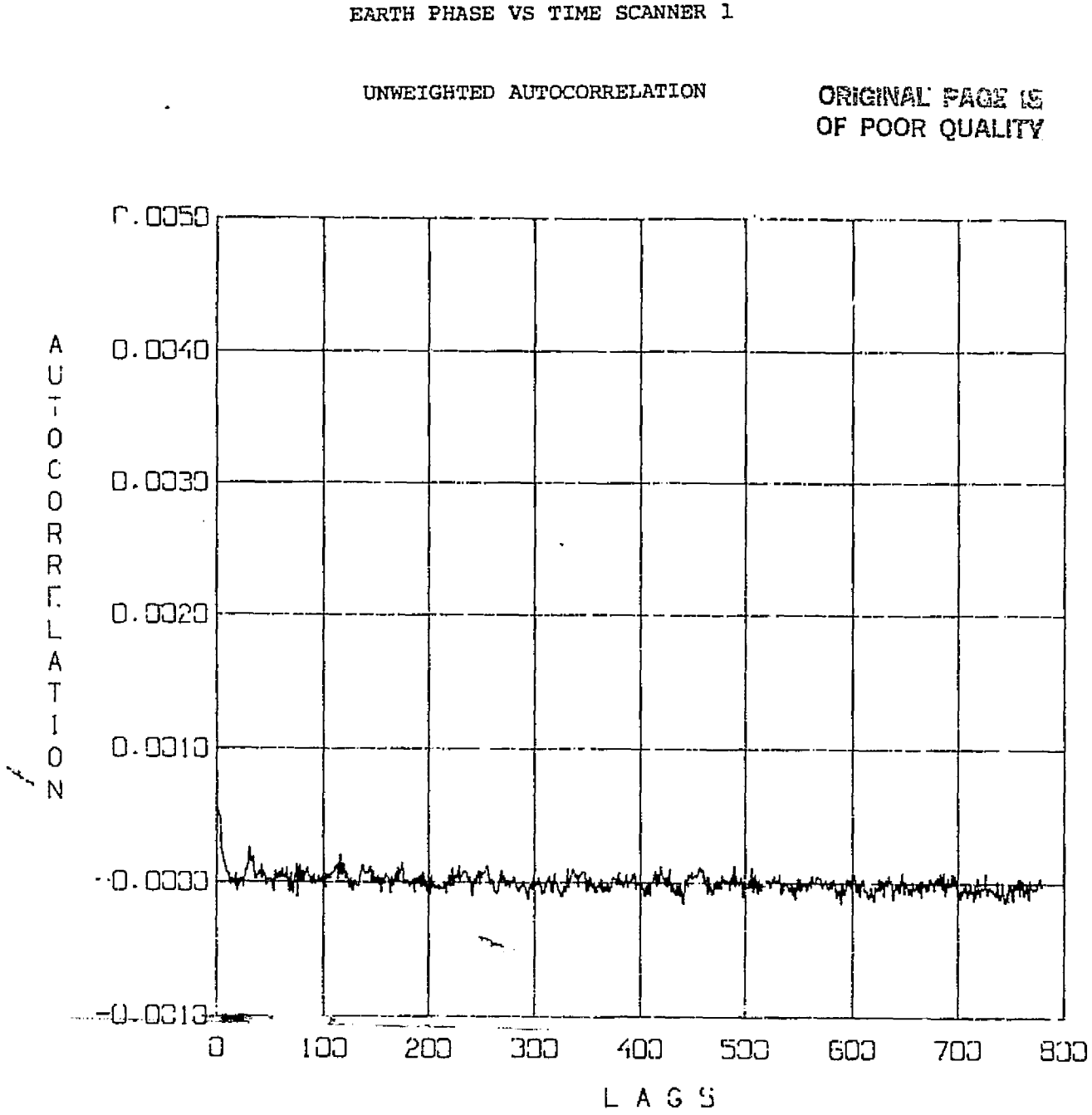

FIGURE 8-5. Autocorrelation Function for Scanner Measurement Noise (4 of 4, Earth Phase Scanner 2)

frequency nature of the Earth phase autocorrelation function indicates that these channels are highly uncorrelated with themselves. The width channel autocorrelation functions reveal that these measurements contain coherent harmonic content. Correlation peaks with separations on the order of 30 lags are quite evident. Conspiciously absent are correlation peaks with separations of much less than 30 lags (3.84 sec. wavelength). Thirty lag correlation peaks correspond to harmonic content on the order of 0.25 hertz. This content can be clearly seen in the power spectrum estimates.

The Power spectrum plots for this data are shown in Figure 8-6. The power spectral estimates are in units of squared magnitude per hertz and are plotted against hertz along the abscissa. As suggested by the autocorrelation functions, the Earth width channels are quite free of harmonic content at wavelengths higher than 1.0 hertz. Possible spectral peaks are found at the lowest resolvable frequencies and around 0.25 hertz but these are barely above the level of the noise in the spectral estimates. From 0.25 hertz to 0.75 hertz there is a gradual fall-off in power with negligible power found at frequencies higher than about 1.0 hertz.

This same distribution is possibly embedded in the Earth phase power spectral estimates, however there is a large amount of white noise superimposed on this signature across all frequencies.

The Earth phase power spectrum characteristics probably result from the high frequency signal which is contaminating the Earth phase measurements (see Section 8.2). If in fact a 10 KHZ signal is being superimposed on the Earth phase measuresments then the 0.128 second sampling frequency employed by the electronics would obtain a highly aliased sample of this signal. Such a highly aliased signal would, to a high degree of probability, have a white-noise-like spectrum. The Earth width spectra, on the other hand, show less high frequency

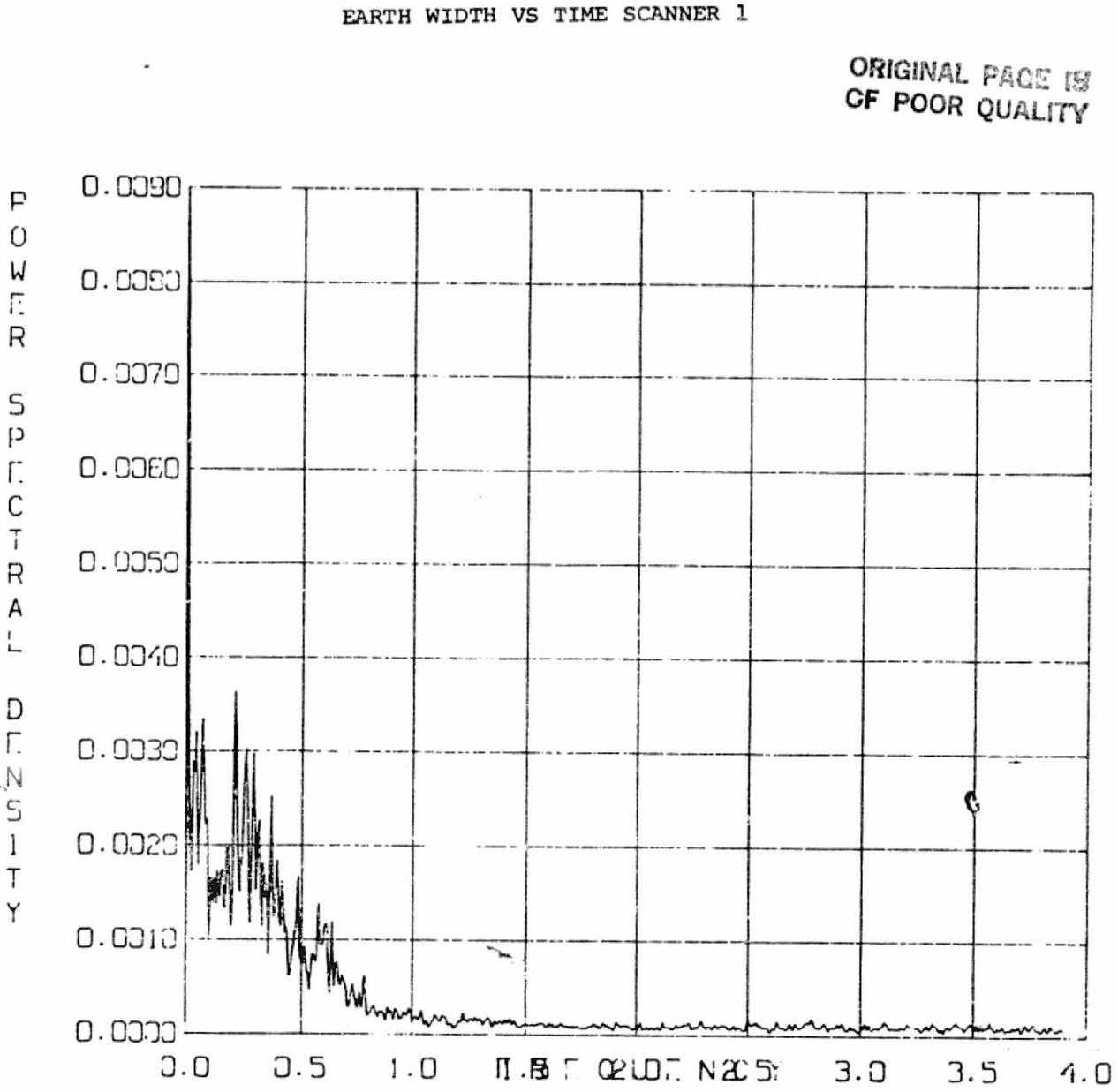

FIGURE 8-6. Power Spectrums of the Scanner Measurement Noise (1 of 4, Earth Width Scanner 1)

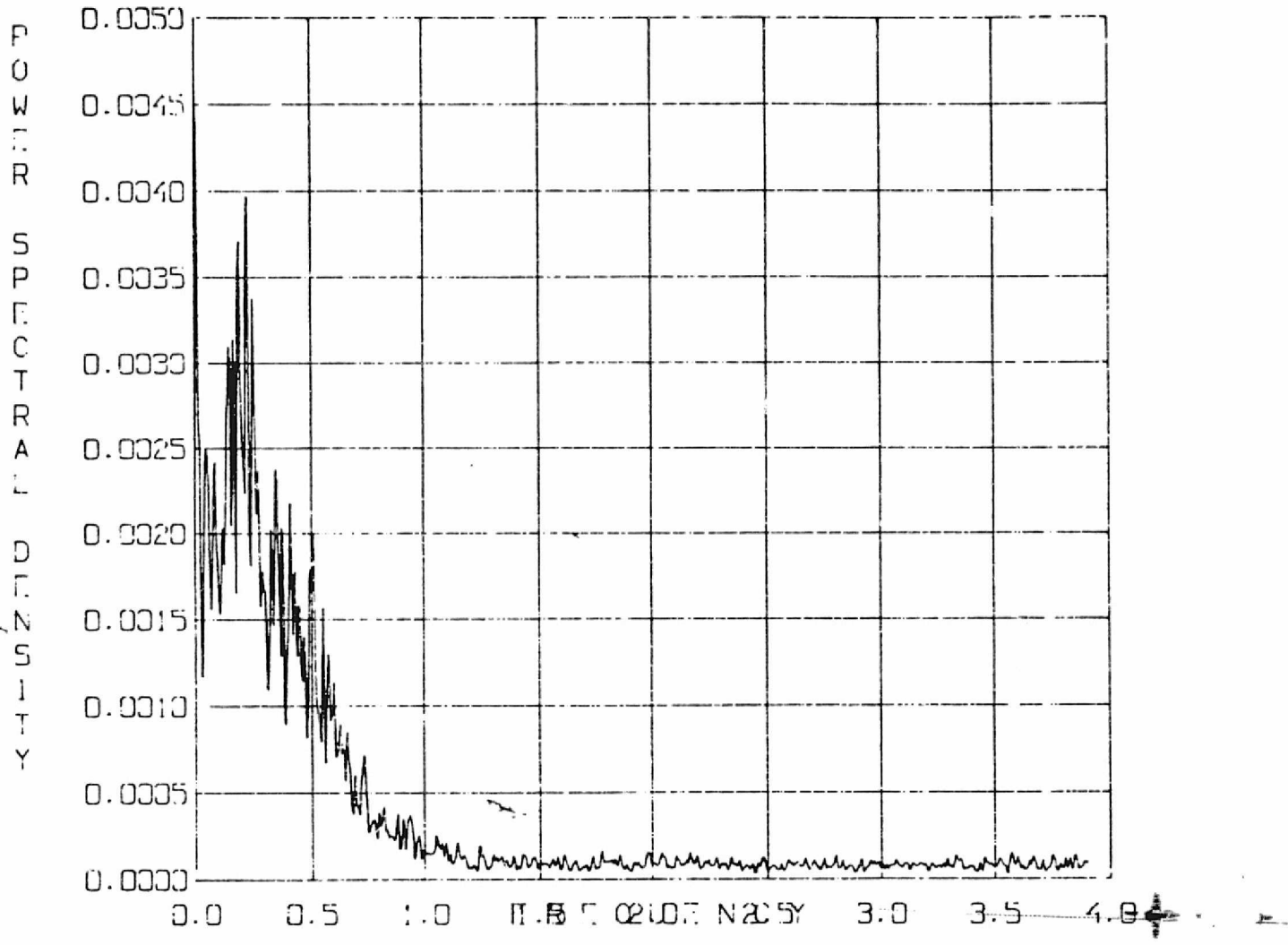

FIGURE 8-6. Power Spectrums of the Scanner Measurement Noise (2 of 4, Earth Width Scanner 2)

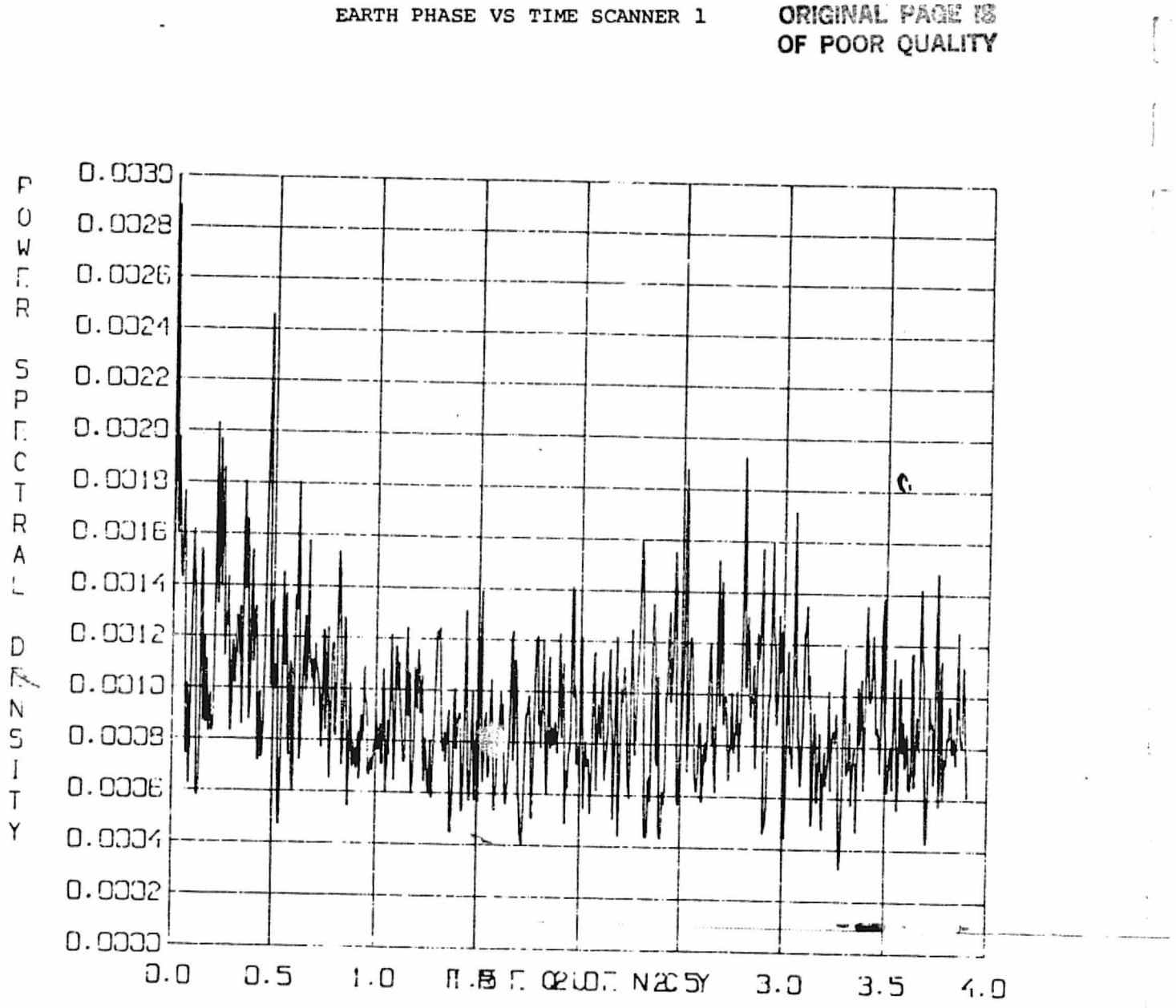

FIGURE 8-6. Power Spectrums of the Scanner Measurement Noise (3 of 4, Earth Phase Scanner 1)

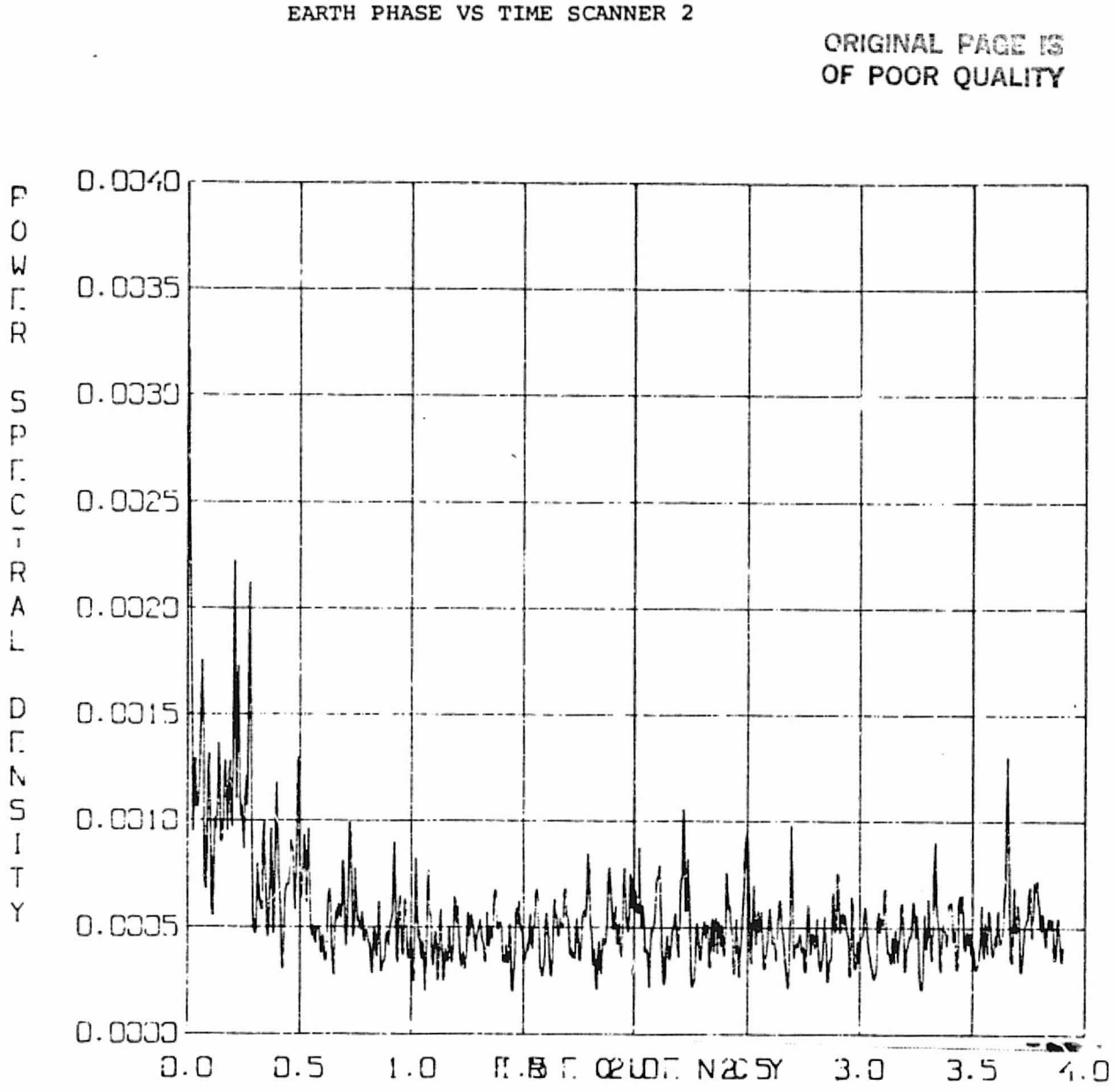

FIGURE 8-6. Power Spectrums of the Scanner Measurement Noise (4 of 4, Earth Phase Scanner 2)

contamination and may indicate that the low pass filtering employed by the electronics is working.

SECTION 9 - FULL ORBIT AVERAGES

This section discusses the variability of averages taken over full orbit data spans of the pitch and roll residual measurement errors. The full orbit averages demonstrate the long term stability of the sensor measurements. In general, the orbit period systematic effects will average out over the orbits and the remaining variability of the full orbit averages represents a very low frequency noise. The variation of full orbit average as a function of orbit within a day and as a function of day of year is examined. These results are extracted from Reference 20.

9.1 DAILY VARIATION OF FULL ORBIT AVERAGES

Figures 9-1 through 9-4 show full orbit average pitch and roll residuals as a function of orbit on four dates for which complete successive orbits are well represented over a period of 24 hours. The vertical scale is in degrees and horizontal lines indicate mean full orbit average for each 24 hour segement. From these figures, there appears to be no evidence of systematic variation of full orbit average pitch or roll residuals over the course of one day.

The variation of the full orbit averages from orbit to orbit is larger than one would expect if the only error source were simply white noise, i.e., independent random errors from one observation to the next. The expected standard deviations of averaged white noise is given by the standard deviation of the raw observations divided by the square root of the number of observations. Section 5.4 indicates standard deviations of the 128 point averaged data of about 0.02°. The yields estimates of about 0.001° for the standard deviation of the orbit averages if the 128 point averaged observations were corrupted by white noise alone. The actual standard deviations of the averaged orbits is more on the order of 0.01 degrees, indicating that lower frequency error sources are contributing to the variation of the orbit averages.

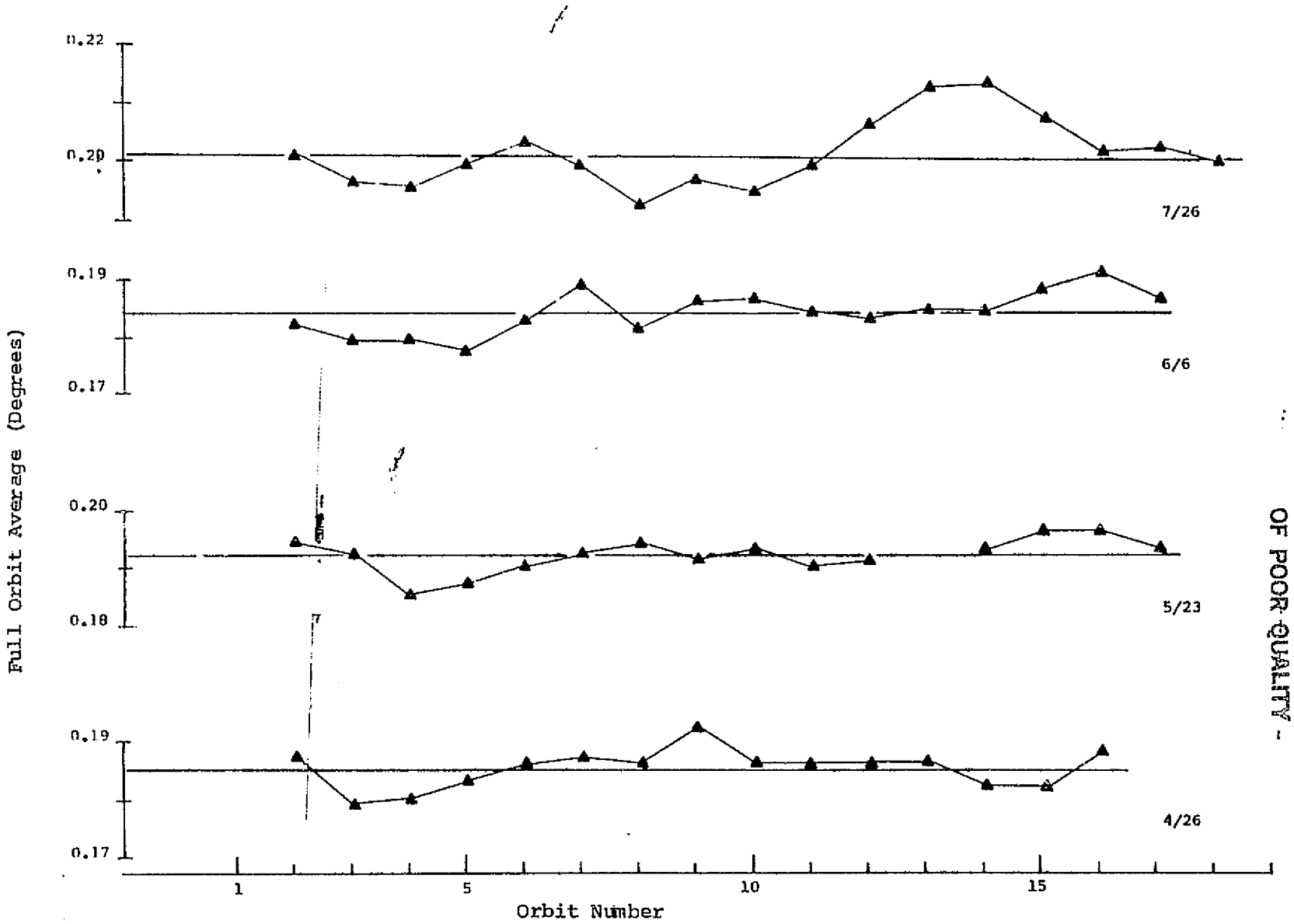

FIGURE 9-1. Orbit to Orbit Variation of Full Orbit Averages for Sensor 1 Pitch Residual on Four Sample Days in 1983.

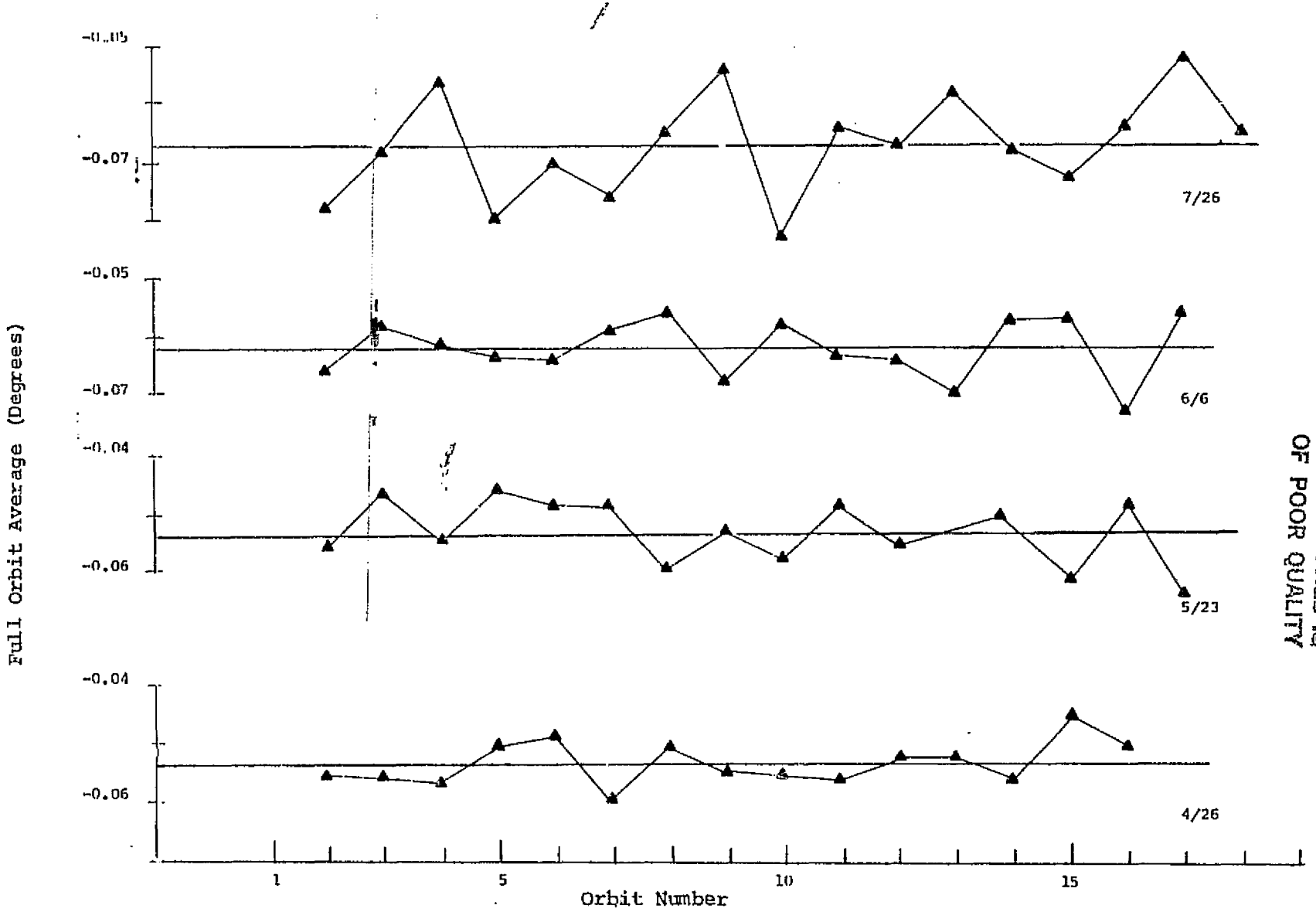

FIGURE 9-2. Orbit to Orbit Variation of Full Orbit Averages for Sensor 2 Pitch Residual on Four Sample Days in 1983.

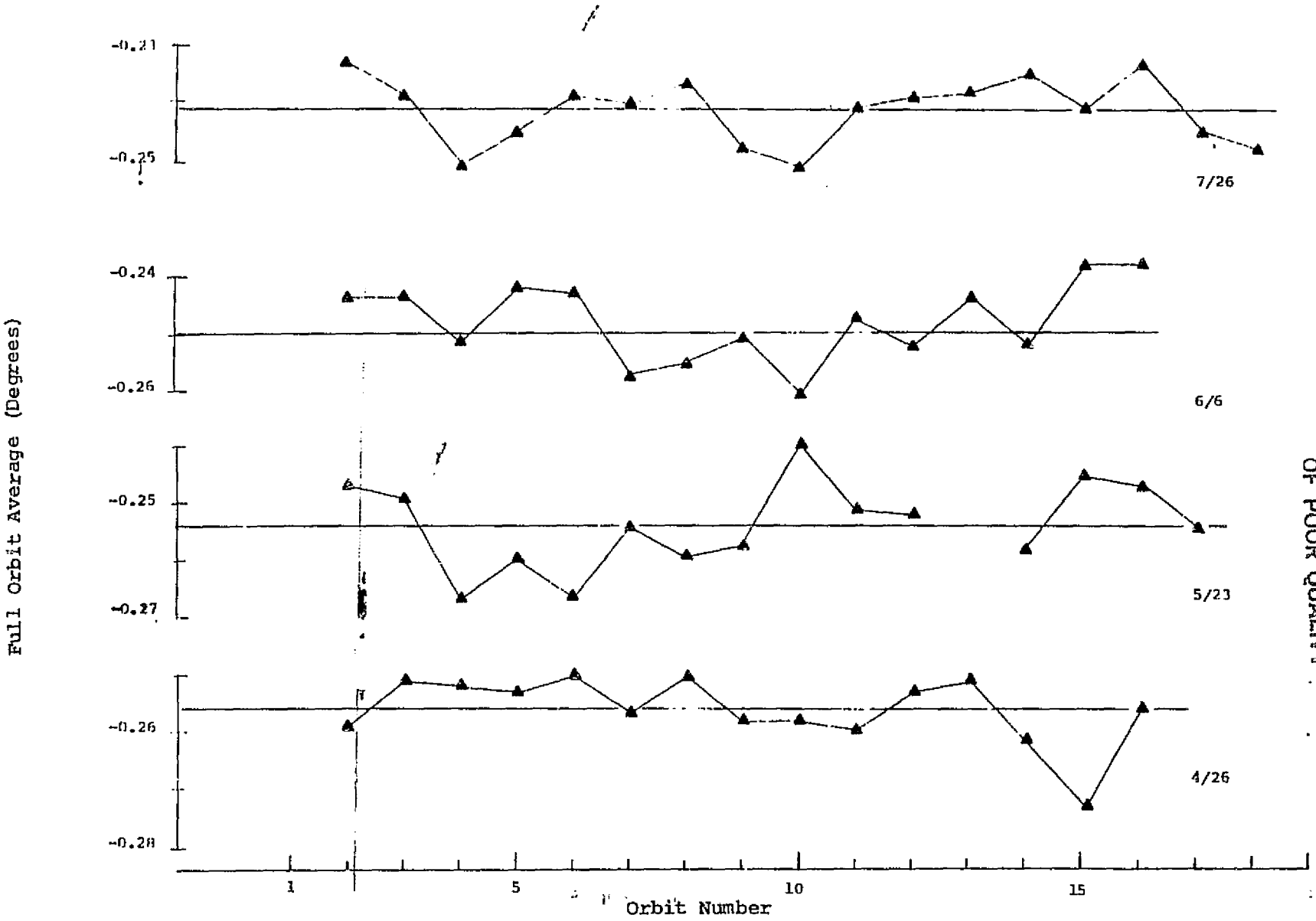

FIGURE 9-3. Orbit to Orbit Variation of Full Orbit Averages for Sensor 1 Roll Residual on Four Sample Days in 1983.

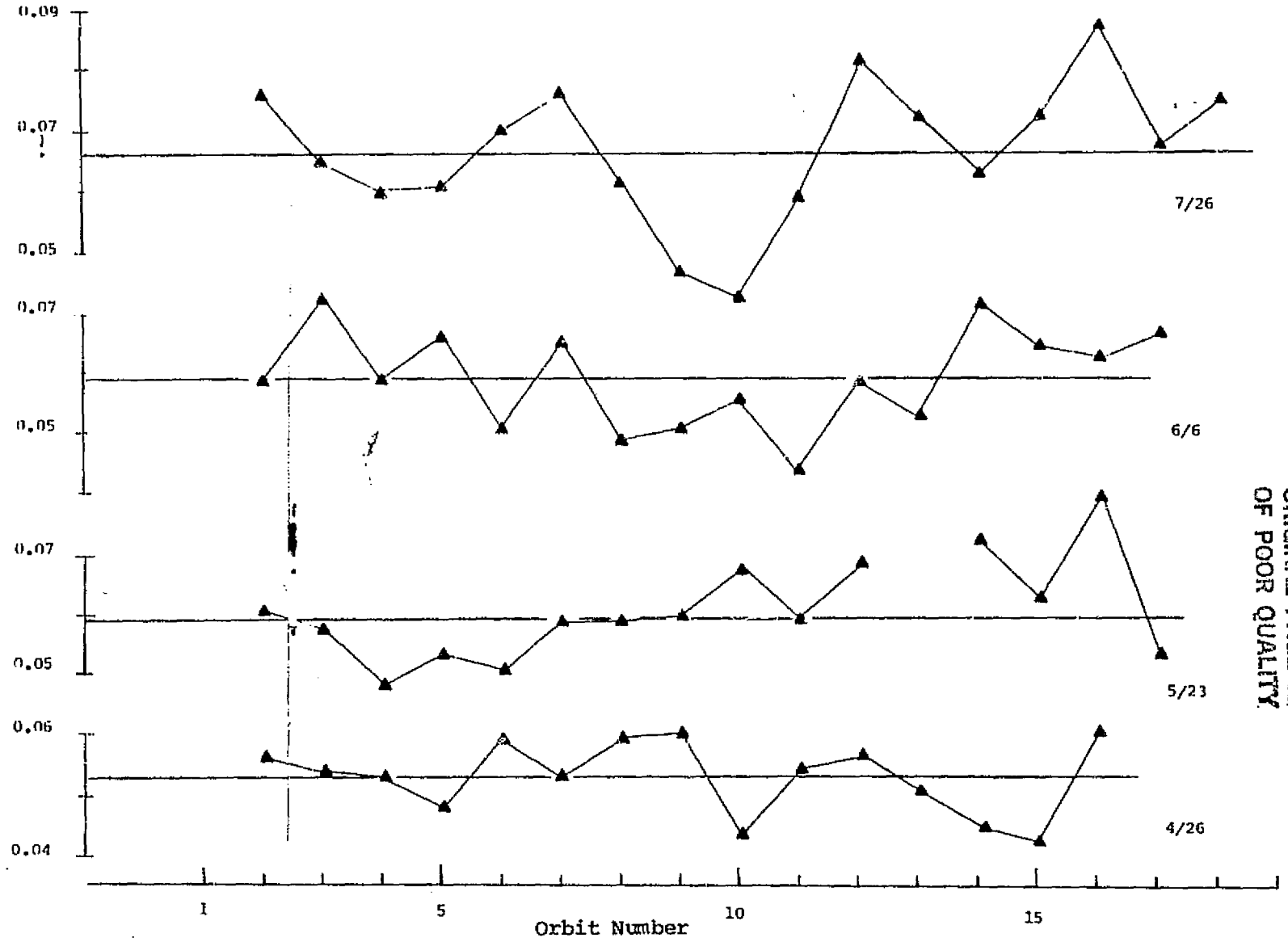

FIGURE 9-4. Orbit to Orbit Variation of Full Orbit Averages for Sensor 2 Roll Residual on Four Sample Days in 1983.

9.2 VARIATION OF FULL ORBIT AVERAGES OVER THE YEAR

The variation of mean, peak-to-peak and standard deviation of full orbit average pitch and roll residual as a function of day of year is shown graphically in Figures 9-5 through 9-7, respectively. Horizontal lines indicate overall mean values.

The mean orbit averages naturally show an annual variation similar to the constant terms in the fitting results in Section 5. The full orbit averages of both pitch and roll residual show only sight variation over the months January through July 1983 (Figure 9-5). However, with the exception of sensor 1 roll residual, the full orbit average residuals exhibit significant variation over the months September through December. There is some evidence of a correlation between the orbit averages in the two pitch channels, particularly in the 1982 data. This could indicate that the orbit average variability is due to instability in the reference attitudes for pitch, or an in-track orbit error as discussed in Section 5.3.

The most significant feature in the daily variability of the orbit averages is the rather large peak-to-peak and standard deviations of the orbit averages found in the 1982 days in the sensor 2 roll measurement. This cannot be a problem with the reference attitudes because it does not show up in the sensor 1 roll measurement. This orbit to orbit variability shows up clearly in the data plots, and was noted earlier in Section 3. The reason for this variability, and its disappearance in 1983 days is not known.

In general, the peak-to-peak and standard deviation, like the orbit averages themselves, show more variability in the early part of the mission.

Table 9-1 provides a comparison of the averages values of mean full orbit averages, peak-to-peak and standard deviation for all 23 segments, for the 1982 segments only and for the 1983 segments only.

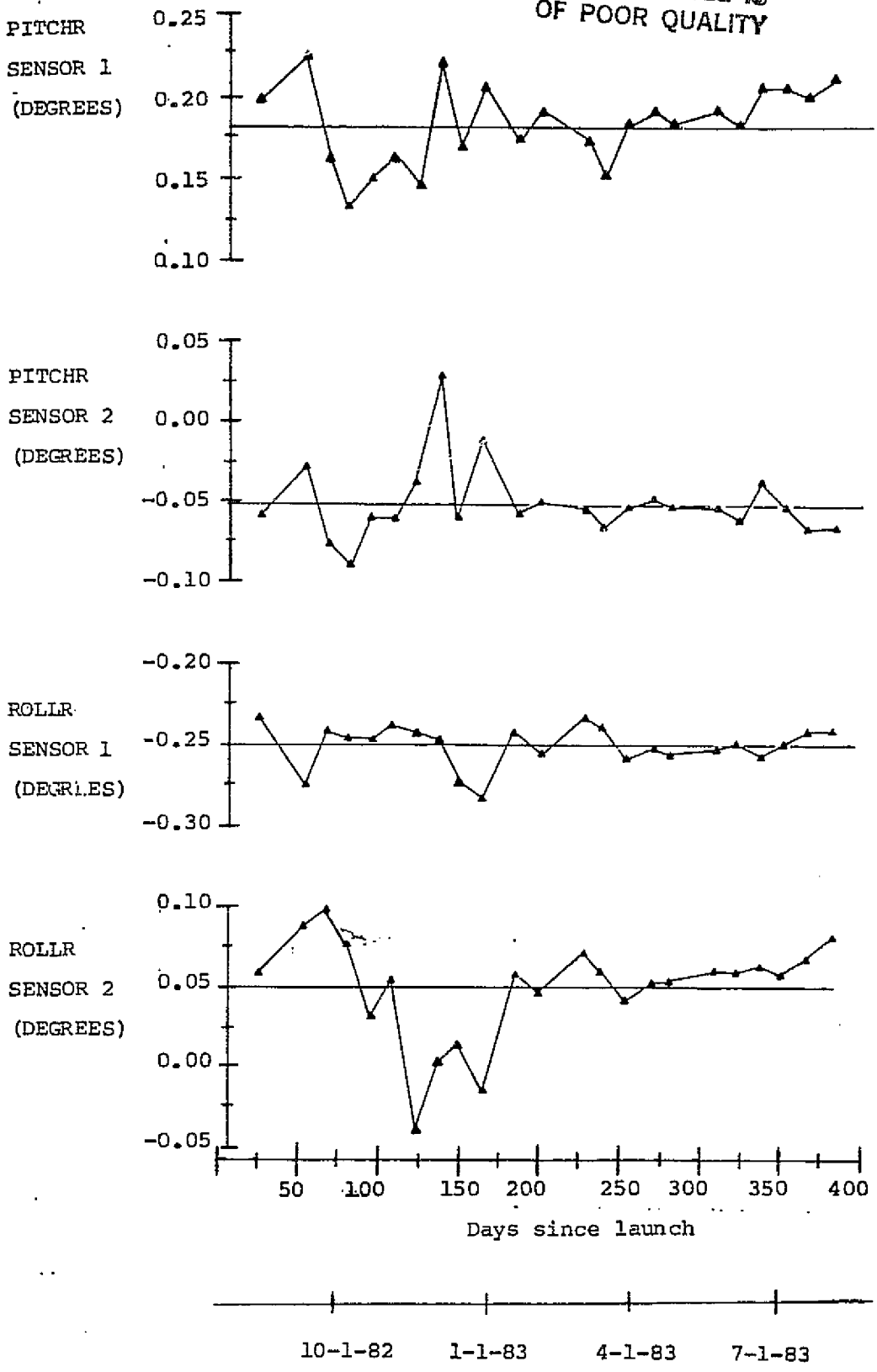

FIGURE 9-5. Mean Full Orbit Averages Versus Days Since Launch

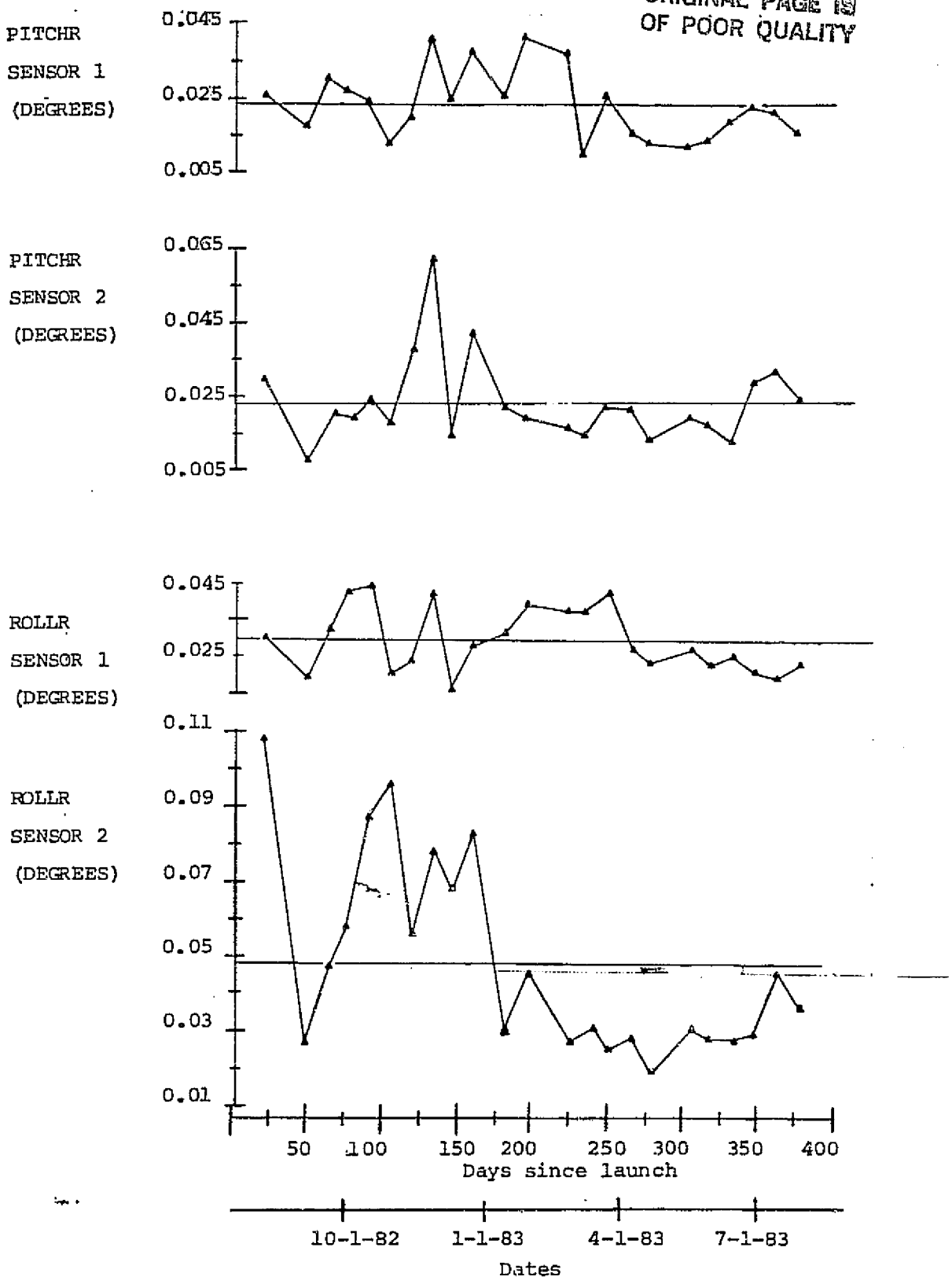

FIGURE 9-6. Peak-to-Peak Variation in Orbit Averages Versus Days Since Launch

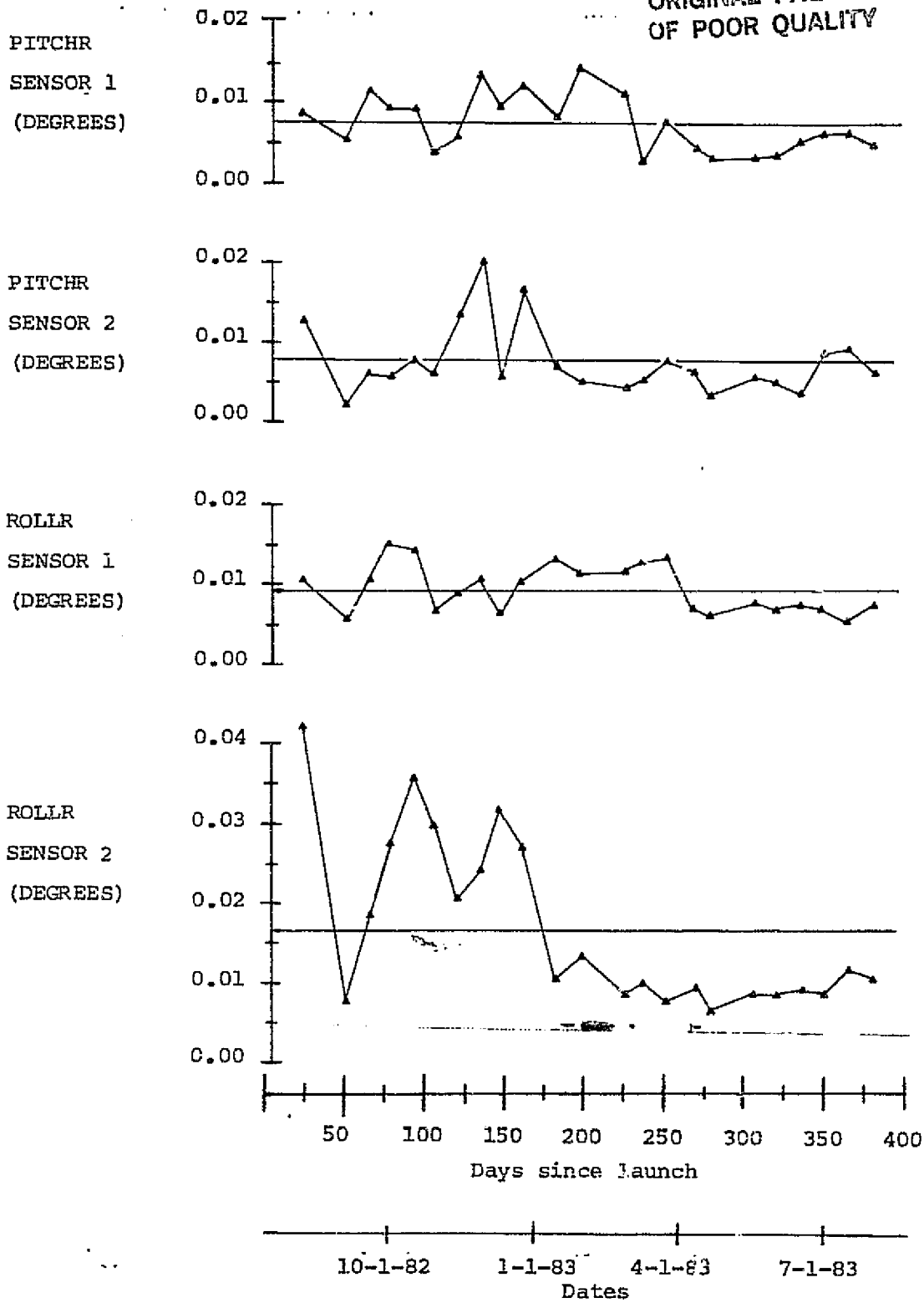

FIGURE 9-7. Standard Deviation of Orbit Averages Versus Days Since Launch.

TABLE 9-1. Average Mean, Average Peak-to-Peak and Average Standard Deviation of Full Orbit Average Pitch and Roll Residual for All Days, 1982 Days Only, and 1983 Days Only

DATA	PITCHR: 1			PITCHR: 2			ROLLR: 1			ROLLR: 2		
	Mean	p-p	σ	Mean	p-p	σ	Mean	p-p	σ	Mean	p-p	σ
ALL	.1836	.0229	.0074	-.0517	.0233	.0098	-.2503	.0292	.0094	.0493	.0484	.0168
1982	.1778	.0261	.0089	-.0458	.0273	.0077	-.2528	.0298	.0100	.0366	.0710	.0264
1983	.1888	.0205	.0063	-.0562	.0203	.0060	-.2484	.0288	.0090	.0590	.0310	.0093

SECTION 10 - CONCLUSIONS AND RECOMMENDATIONS

Conclusions that can be made based on the current analysis of the Landsat-4 Conical Scanner flight data are summarized below grouped by category.

Systematic Errors

- Earth oblateness and spacecraft altitude variations are the dominant error sources in the raw horizon scanner measurements, but these effects can be removed by the appropriate modeling. After these effects are removed, the principal remaining errors seem to be due to Earth radiance variations.

- Systematic orbit period errors in the reference attitude roll angles on the order of 0.05 degrees in amplitude seem to be indicated by the horizon scanner data, after careful examination of the residual errors. The Landsat-4 mounting geometry in which the two scanners are mounted on different axes helped to distinguish the attitude and orbit dependent error sources from the sensor dependent error sources.

- The Earth phase measurements are more accurate than the Earth width measurements because the horizon radiance effects are generally on a large geographic scale so that they raise or lower both Earth-in and Earth-out horizon triggering heights the same way. The sensor 1 Earth phase measurement has the least impact from Earth oblateness and seasonal systematic horizon radiance effects because both horizons cross the Earth at nearly the same latitudes.

Earth Radiance Effects

- The regions of greatest variation in the horizon scanner measurements seem to be associated with the longitude dependent variability in the stratosphere in the winter polar region.

- Predictions of the effects due to seasonal systematic latitude dependent horizon radiance variations show general agreement with the flight data, although the predicted magnitudes of the errors are mostly too low.

- Cold clouds do not appear to be a major error source as in past missions.

Interference Effects and Anomolies

- Interference effects from the sun and moon have been identified. The blanking circuit operates successfully to eliminate the interference for parts of the scan cone.

- A larger than normal variation in the sensor 2 Earth width errors early in the mission remains unexplained.

- A few small short duration anomolies in the scanner measurements have been identified and are currently unexplained.

Noise Characteristics

- Noise averaging is necessary to reduce the point-to-point measurement noise.

- The noise distribution shows some unusual currently unexplained characteristics with certain count values less likely to occur in the phase channels.

- The phase channels have a high frequency noise due to contamination from the power supply signal.

- The measurements show higher noise power at lower frequencies.

- The full orbit averages are generally stable to about 0.01 degrees.

Sensor Accuracy

The achievable attitude accuracy in general depends on the accuracy of the systematic error removal, on the amplitude and frequency characteristics of the measurement noise, and on the noise filtering which is applied in the attitude determination procedure. The following bullets summarizes the approximate 3 sigma attitude accuracies based on the modeling options discussed in Section 5.4. These accuracies apply specifically for 128-point averaging of the raw measurements for noise reduction. With the systematic errors accurately removed (as in the data fitting results with the poles removed) the attitude accuracies may be further improved by the additional filtering of the noise (such as would be inherent in an onboard Kalman filter using gyro data in combination with the scanner data). However, for the modeling options that do not adequately remove the seasonal or other systematic effects, the errors are generally dominated by the systematic effects and not the noise, so additional noise filtering is not useful. Note that additional noise filtering is also not useful in removing the large errors (up to 0.4 degrees peak to peak) around the winter polar regions.

- The accuracies of the uncorrected measurements with constant biases removed are in the order of 0.7 degrees for the Earth width channels, 0.3 degrees for the sensor 2 Earth phase channel, and less than 0.2 degrees for the sensor 1 Earth phase channel.

- After the Earth oblateness and spacecraft altitude, effects are modeled, the sensor accuracies are in the order of 0.20 degrees in the Earth width channels and 0.12 degrees in the Earth phase channels.

- Removing the systematic horizon radiance effects using the HRDB/SOES model improves the sensor accuracies by about 13% for the Earth width channels and produces negligible effects to the Earth phase channels.

- Applying the seasonal dependent second order Fourier series correction coefficients to the data further improves the sensor accuracies to the order of 0.13 degrees for the Earth width channels and 0.09 degrees for the Earth phase channels.

- With the winter polar region data removed, the sensor accuracy is in the order of 0.08 degrees for all channels. This primarily indicates the noise in the 128-point average data.

There are obviously many areas of the flight performance that can receive further analysis. Nevertheless the analysis to date already indicates a great deal about the sensor performance, and demonstrates the value of reviewing a large volume of data across selected days and across all seasons. The analysis of the Landsat-4 mission data provides basic data on the flight performance of this sensor which can be used for future mission planning.

Further analysis is recommended in the following areas.

- Continue the evaluation of the seasonal effects with additional data, first, to cover an entire year after the reference attitude problems were resolved and second to cover additional time to evaluate the consistency of the radiance effects from year to year.

- Extend the data fitting results to higher order and analyze the improvements that are achievable.

- Further analyze the measurement variations in the winter polar region to better understand and possibly model the sensor response to the polar radiance variations.

- Work on an improved HRDB which can more accurately describe the radiance effects observed in the Landsat-4 data.

- Analyze the scanner ground calibration and alignment procedures to evaluate the possible error sources.

- Further analyze the unusual noise characteristics by obtaining a histogram of the noise distribution and investigate possible explanations for these characteristics.

- Perform similar studies on the horizon scanners to be flown on future missions to further understand the performance and modeling of this type of sensor.

APPENDIX A - REFERENCE ATTITUDES AND SPACECRAFT ALTITUDE

Figure A-1 through A-28 provides plots of the reference attitude and the spacecraft altitude for all the data spans processed for this report. These plots show the pitch, roll, and yaw attitude in degrees as a function of orbit phase from the ascending node for several orbits overlayed. The attitude is computed by the Onboard Computer (OBC) and downlinked as a quaternion. Orbit ephemeris data is also provided by the OBC. The altitude in kilometers is computed by taking the difference between the spacecraft position vector magnitude and the Earth equatorial radius of 6378.14 kilometers.

Excursions in the attitudes twice per orbit are caused by movements of the solar arrays. The following anomolies are noted:

- The spacecraft was in Earth acquisition mode at the beginning of the data spans on 9/22/82 and 7/26/83 and the reference attitudes are mostly off the plot scale for these periods.

- Two spikes in the reference attitude on 12/1/82 and one spike in the attitude and ephemeris on 2/17/83 are due to spurious telemetry data.

- Two temporary excursions where the reference attitudes appear bad occurred on 8/7/83.

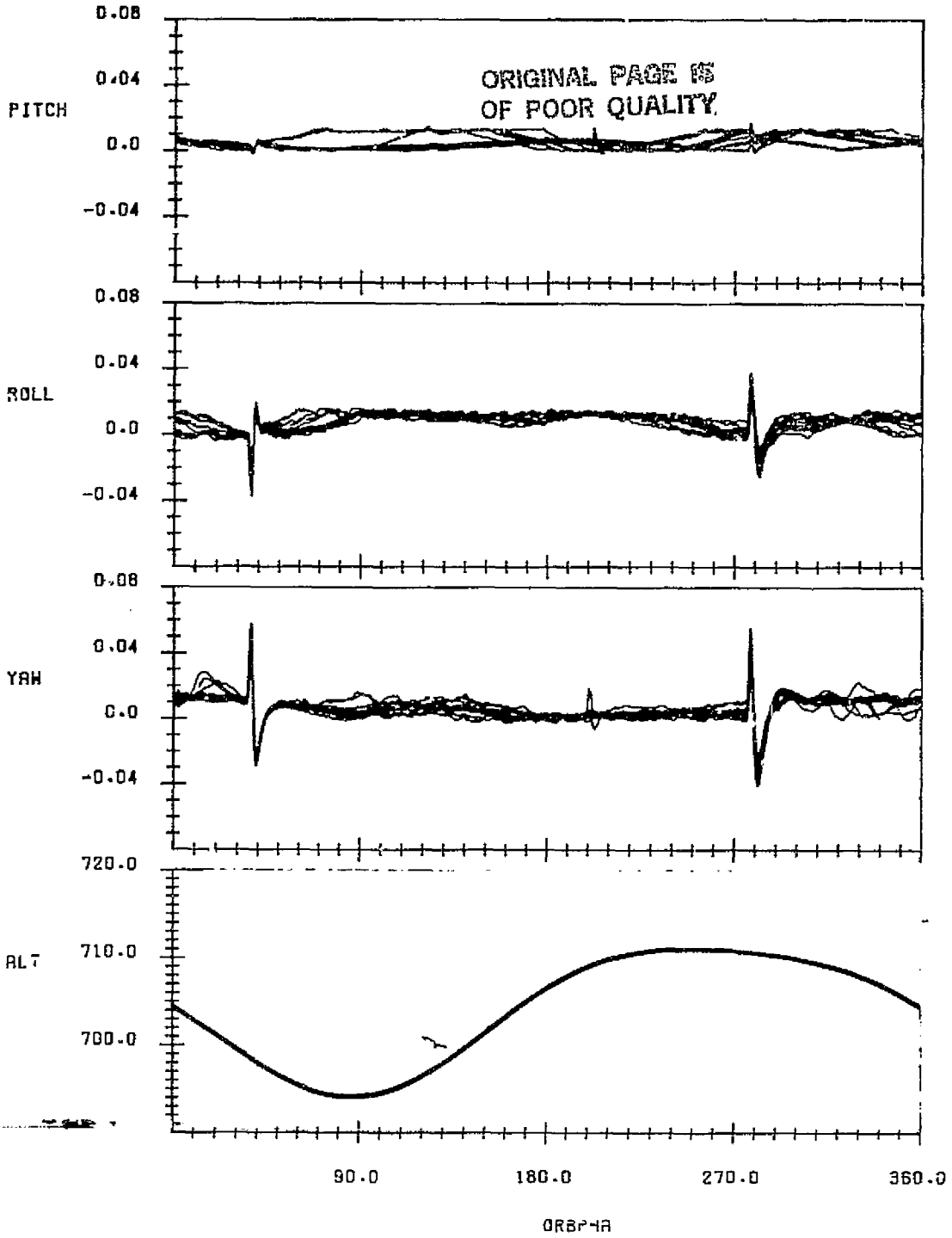

LANDSAT-4 ONBOARD COMPUTER(OBC) REFERENCE ATTITUDE(DEGREES)
AND SPACECRAFT ALTITUDE(KILOMETERS) ABOVE 6378.14 KM RADIUS
VERSUS ORBIT PHASE FROM THE ASCENDING NODE WITH CONSECUTIVE
ORBITS OVERLAID
DATA START TIME:820810.215426522
END TIME:820811.203329690

FIGURE A-1. Reference Attitude and Altitude for Data Span on August 10-11, 1982

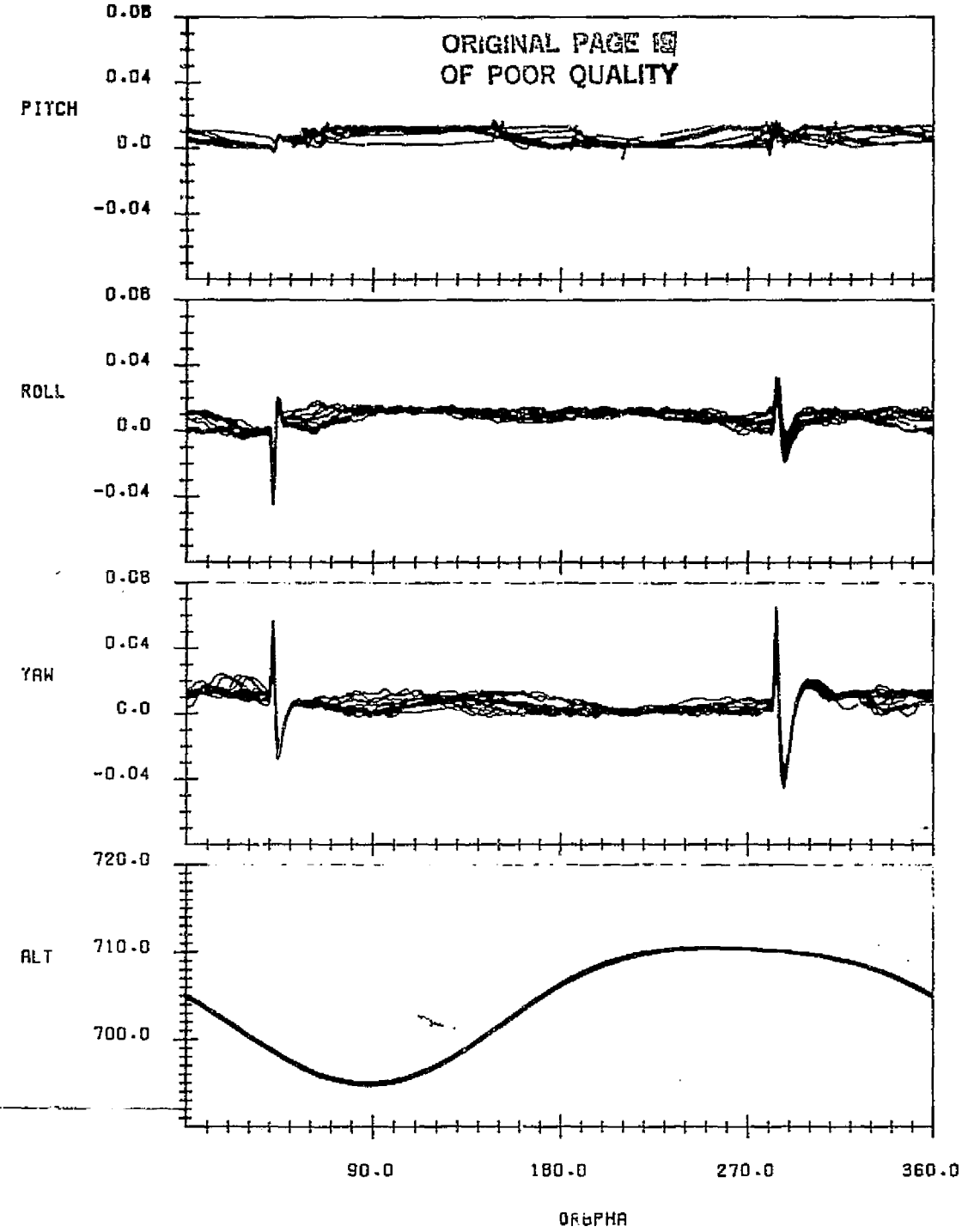

LANDSAT-4 ONBOARD COMPUTER(OBC) REFERENCE ATTITUDE(DEGREES) AND SPACECRAFT ALTITUDE(KILOMETERS) ABOVE 6378.14 KM RADIUS VERSUS ORBIT PHASE FROM THE ASCENDING NODE WITH CONSECUTIVE ORBITS OVERLAID
DATA START TIME:820825.010606091
END TIME:820826.032214554

FIGURE A-2. Reference Attitude and Altitude for Data Span on August 26-26, 1982

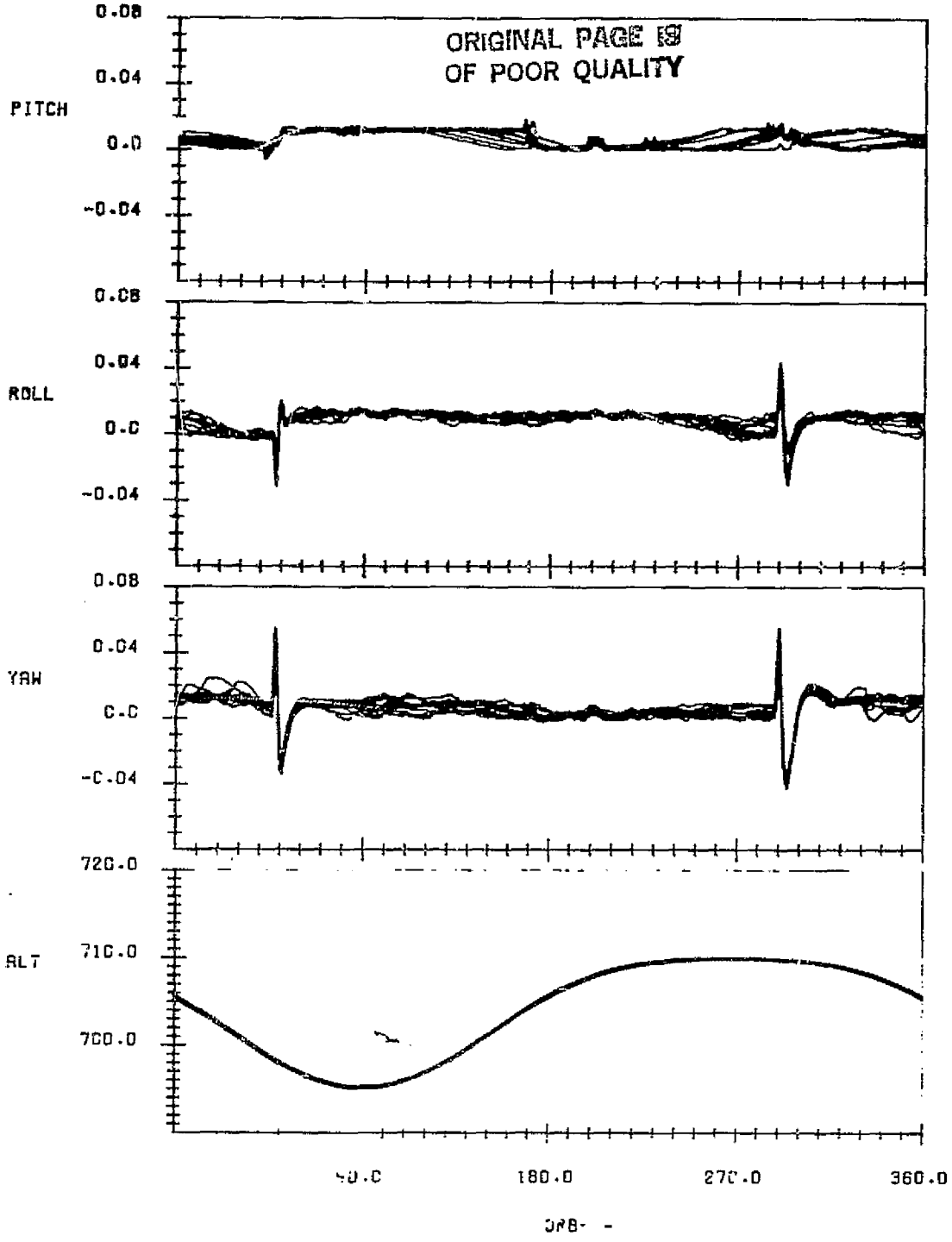

LANDSAT-4 ONBOARD COMPUTER(OBC) REFERENCE ATTITUDE(DEGREES)
AND SPACECRAFT ALTITUDE(KILOMETERS) ABOVE 6378.14 KM RADIUS
VERSUS ORBIT PHASE FROM THE ASCENDING NODE WITH CONSECUTIVE
ORBITS OVERLAID
DATA START TIME:820908.043319559
END TIME:820909.051848519

FIGURE A-3. Reference Attitude and Altitude for Data Span on September 8-9, 1982

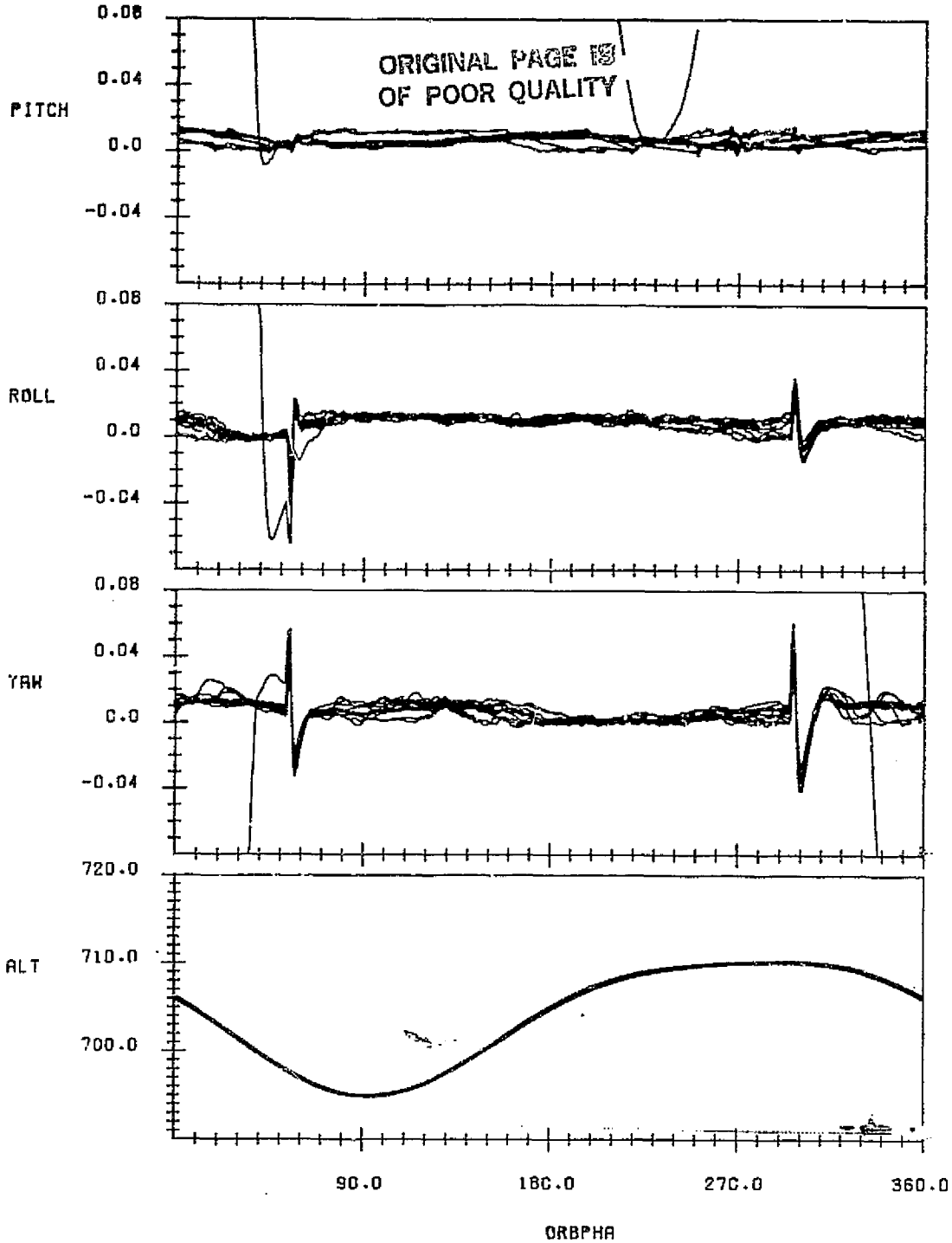

LANDSAT-4 ONBOARD COMPUTER(OBC) REFERENCE ATTITUDE(DEGREES)
AND SPACECRAFT ALTITUDE(KILOMETERS) ABOVE 6378.14 KM RADIUS
VERSUS ORBIT PHASE FROM THE ASCENDING NODE WITH CONSECUTIVE
ORBITS OVERLAID
DATA START TIME:820922.003327683
END TIME:820923.020043395

FIGURE A-4. Reference Attitude and Altitude for Data Span on September 22-23, 1982

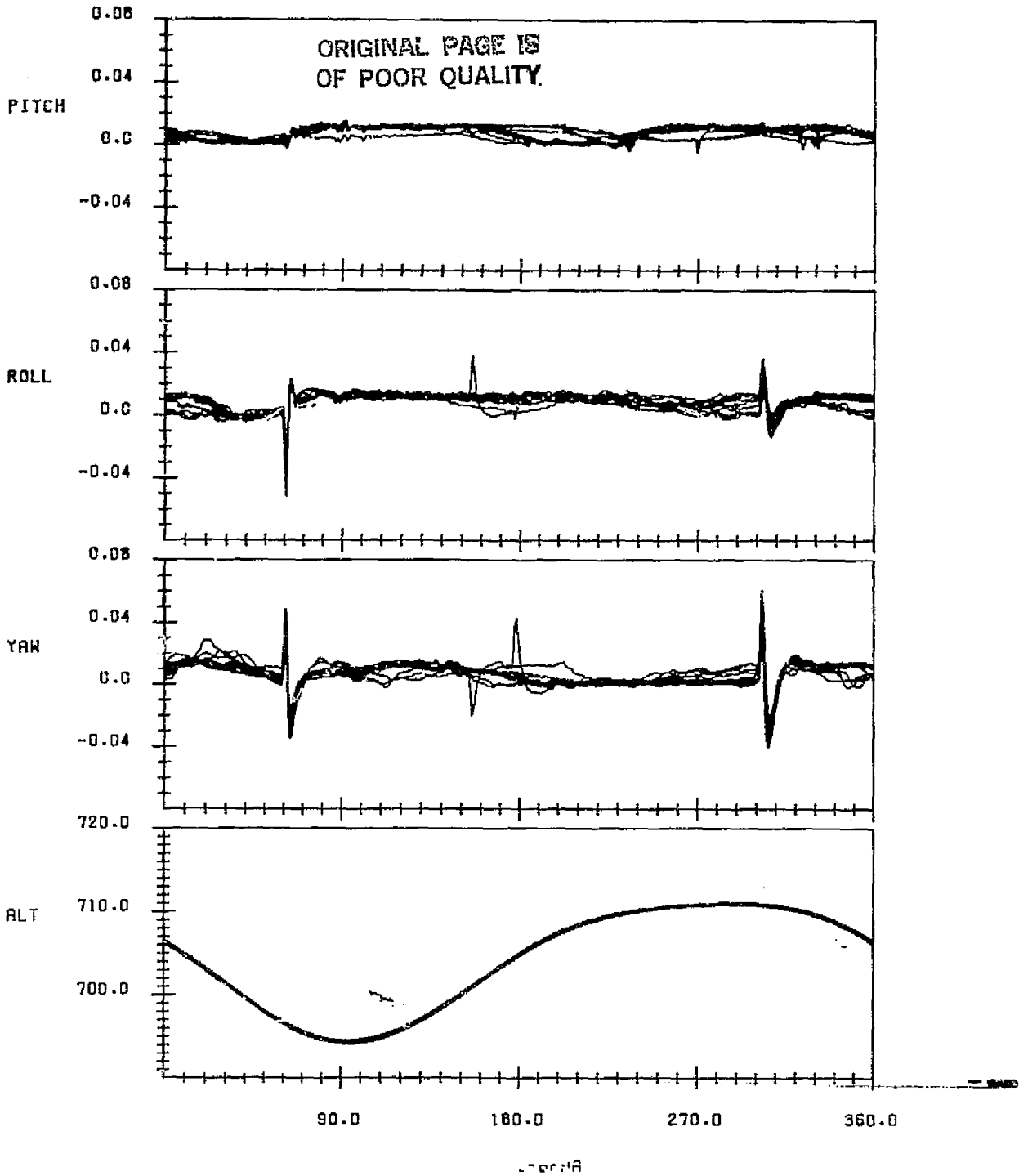

LANDSAT-4 ONBOARD COMPUTER(OBC) REFERENCE ATTITUDE(DEGREES) AND SPACECRAFT ALTITUDE(KILOMETERS) ABOVE 6378.14 KM RADIUS VERSUS ORBIT PHASE FROM THE ASCENDING NODE WITH CONSECUTIVE ORBITS OVERLAID
DATA START TIME:821005.153123435
END TIME:821006.164427194

FIGURE A-5. Reference Attitude and Altitude for Data Span on October 5-6, 1982

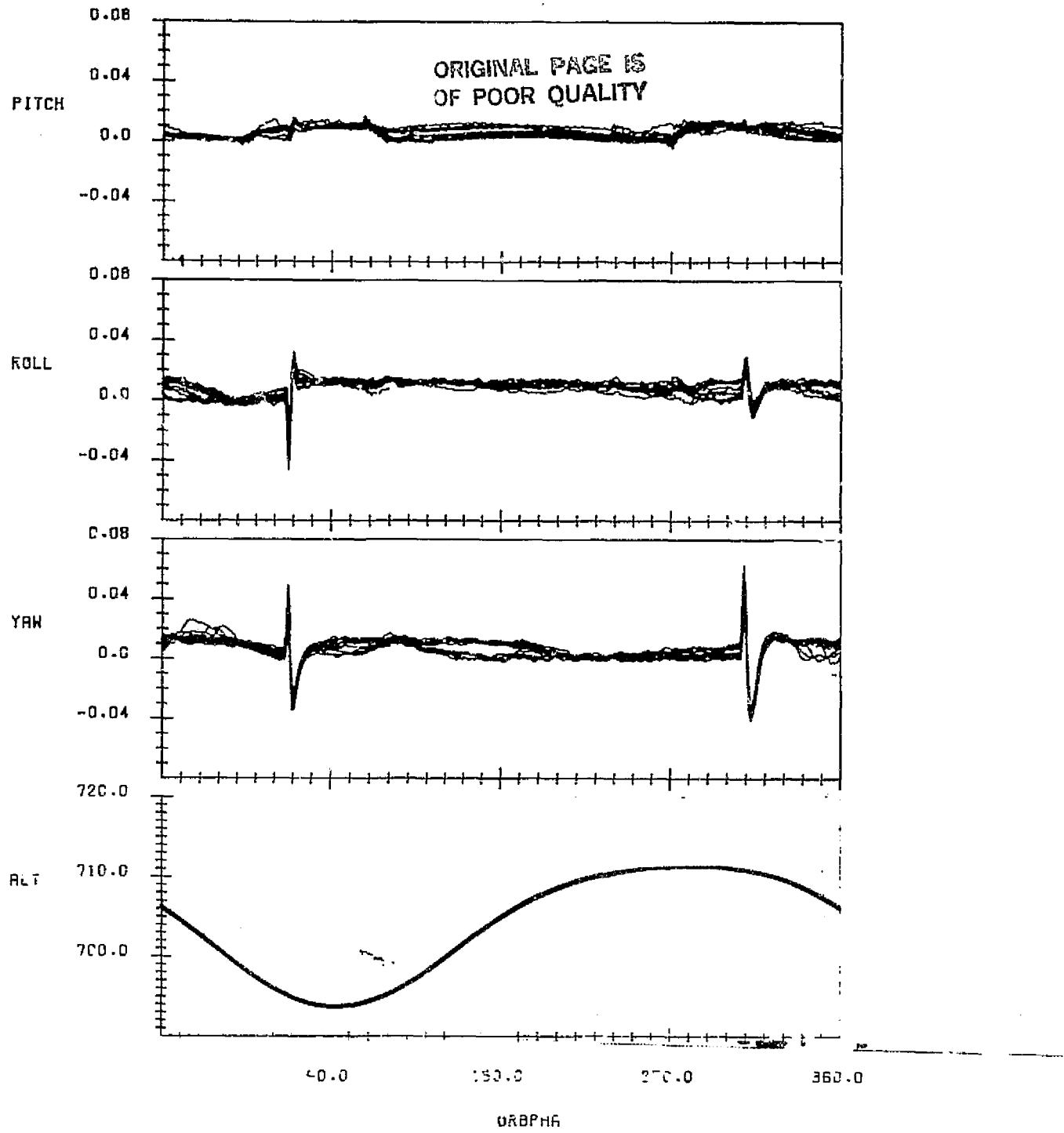

LANDSAT-4 ONBOARD COMPUTER(OBC) REFERENCE ATTITUDE(DEGREES) AND SPACECRAFT ALTITUDE(KILOMETERS) ABOVE 6378.14 KM RADIUS VERSUS ORBIT PHASE FROM THE ASCENDING NODE WITH CONSECUTIVE ORBITS OVERLAID
DATA START TIME:821020.051211751
END TIME:821021.055456871

FIGURE A-6. Reference Attitude and Altitude for Data Span on October 20-21, 1982

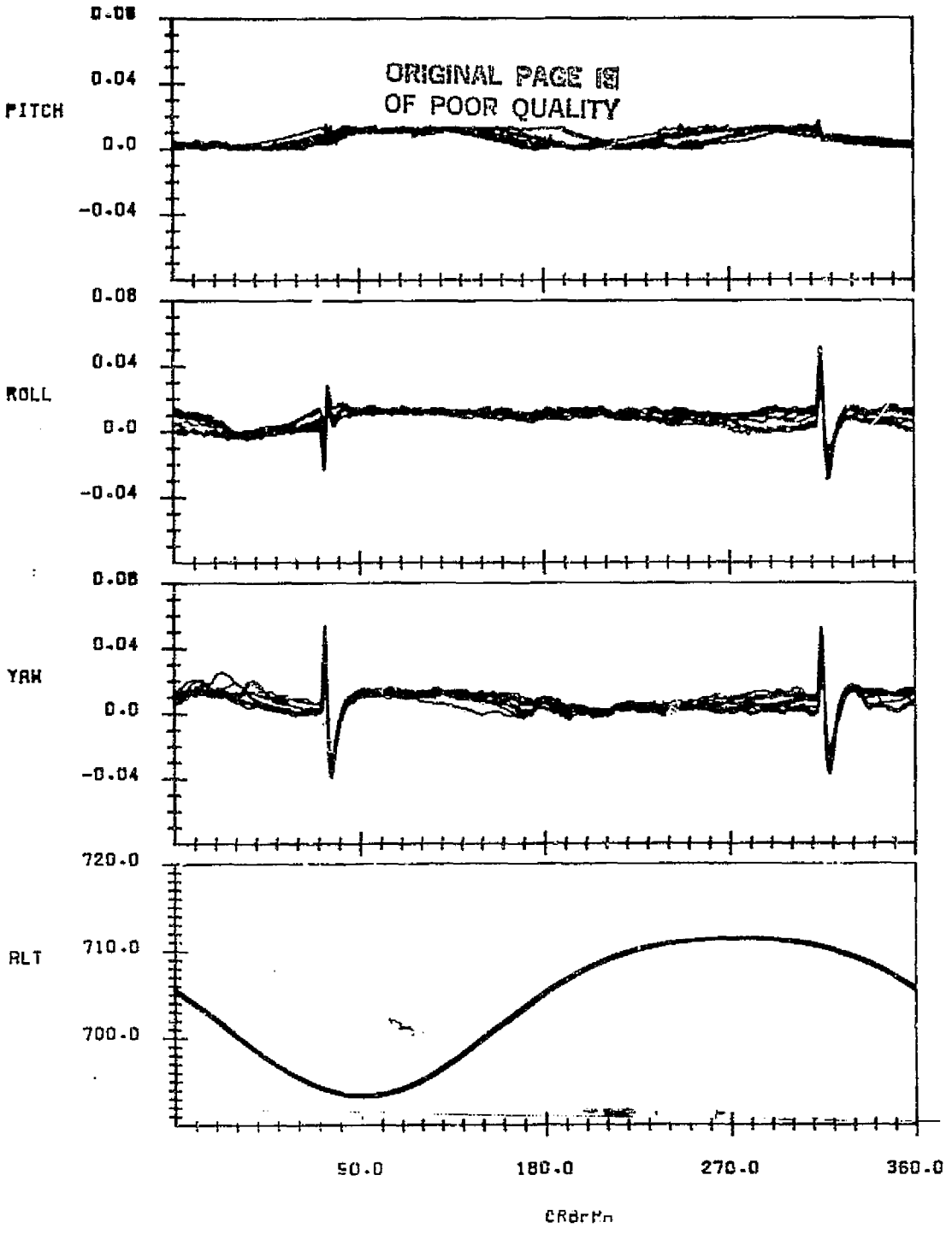

FIGURE A-7. Reference Attitude and Altitude for Data Span on November 2-3, 1982

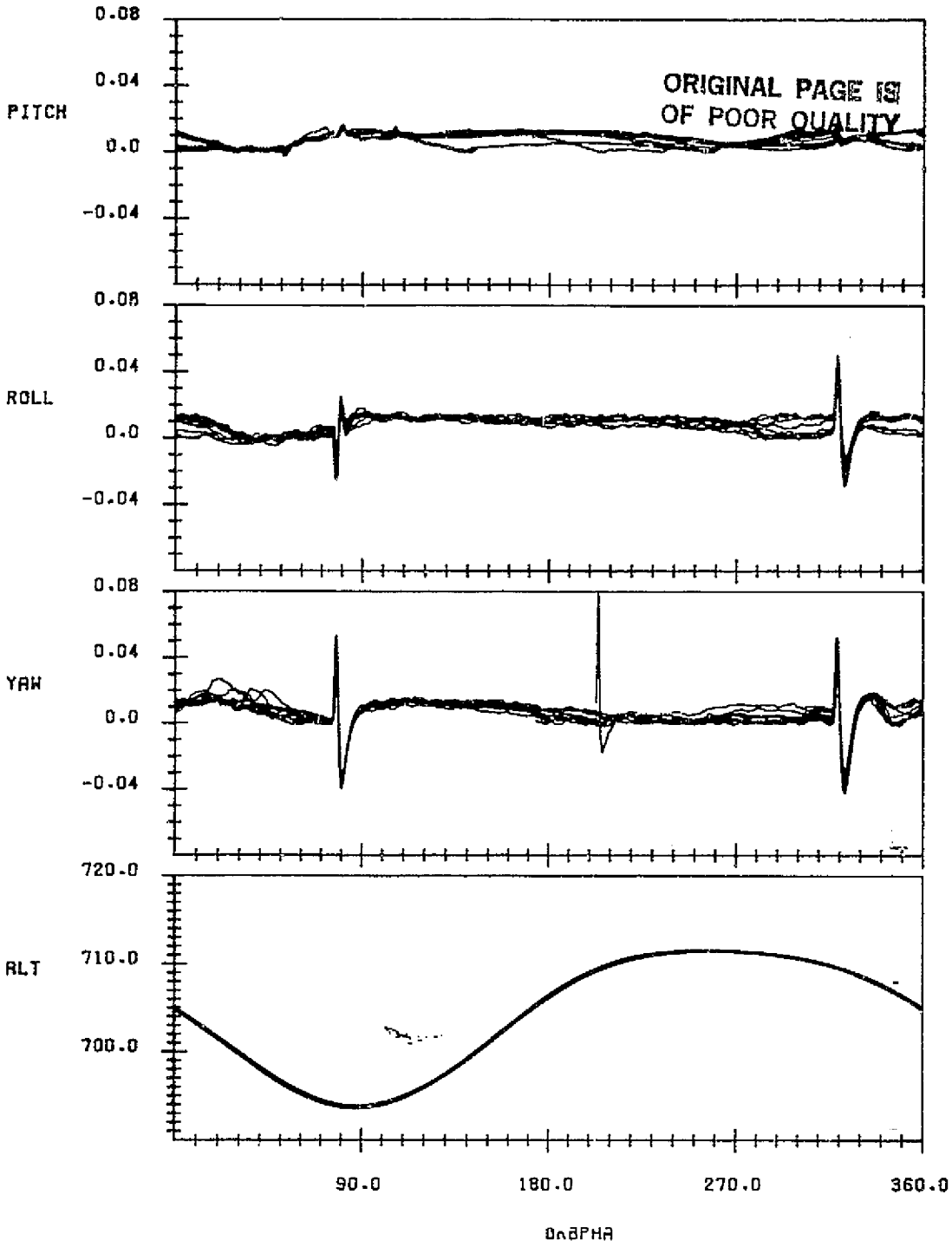

LANDSAT-4 ONBOARD COMPUTER(OBC) REFERENCE ATTITUDE(DEGREES) AND SPACECRAFT ALTITUDE(KILOMETERS) ABOVE 6378.14 KM RADIUS VERSUS ORBIT PHASE FROM THE ASCENDING NODE WITH CONSECUTIVE ORBITS OVERLAID
DATA START TIME:821116.063354045
END TIME:821116.232203818

FIGURE A-8. Reference Attitude and Altitude for Data Span on November 16, 1982

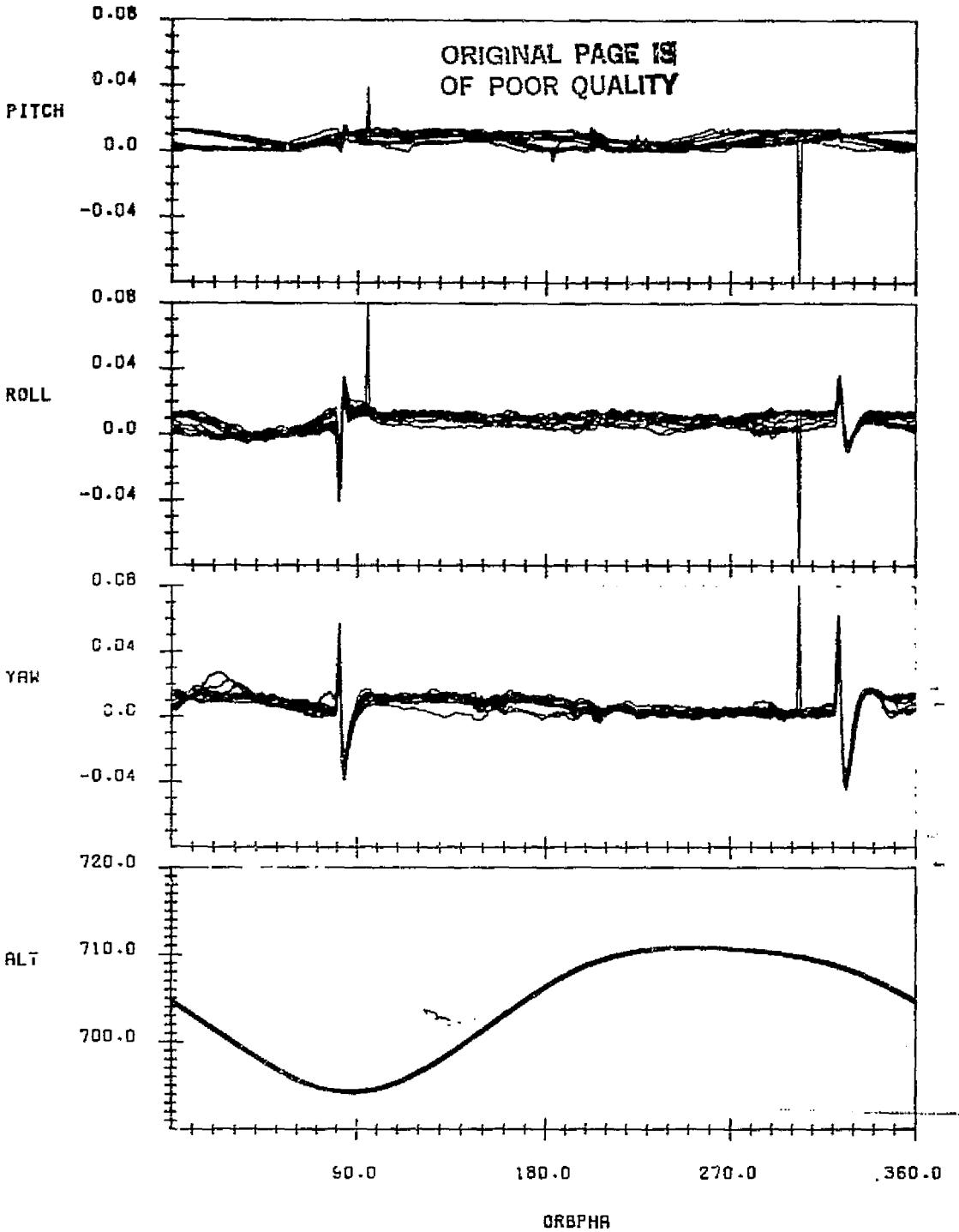

LANDSAT-4 ONBOARD COMPUTER(OBC) REFERENCE ATTITUDE(DEGREES) AND SPACECRAFT ALTITUDE(KILOMETERS) ABOVE 6378.14 KM RADIUS VERSUS ORBIT PHASE FROM THE ASCENDING NODE WITH CONSECUTIVE ORBITS OVERLAID
DATA START TIME:821201.002856720
END TIME:821202.031150860

FIGURE A-9. Reference Attitude and Altitude for Data Span on December 1-2, 1982

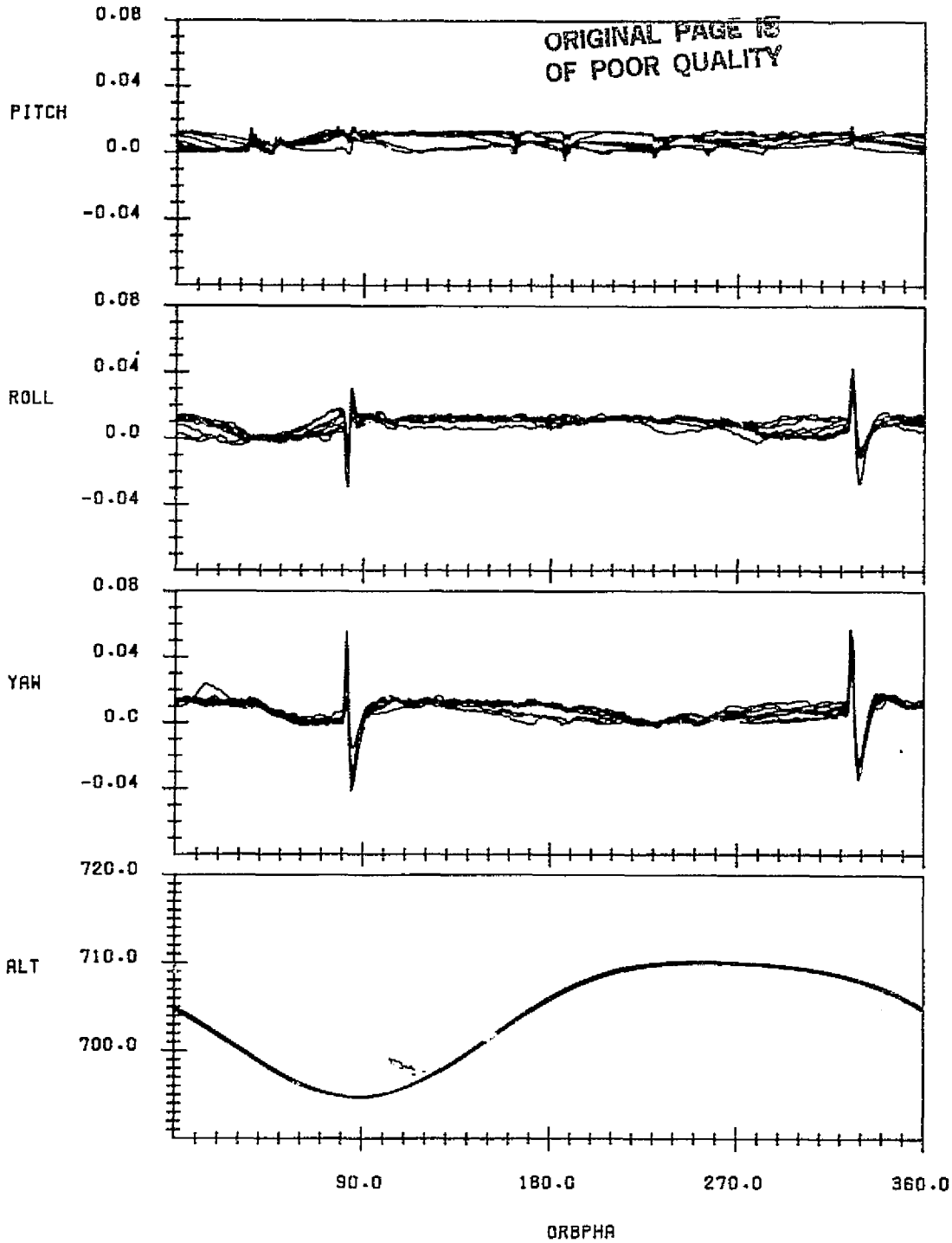

LANDSAT-4 ONBOARD COMPUTER(OBC) REFERENCE ATTITUDE(DEGREES) AND SPACECRAFT ALTITUDE(KILOMETERS) ABOVE 6378.14 KM RADIUS VERSUS ORBIT PHASE FROM THE ASCENDING NODE WITH CONSECUTIVE ORBITS OVERLAID
DATA START TIME:821214.122607064
END TIME:821215.143809812

FIGURE A-10. Reference Attitude and Altitude for Data Span on December 14-15, 1982

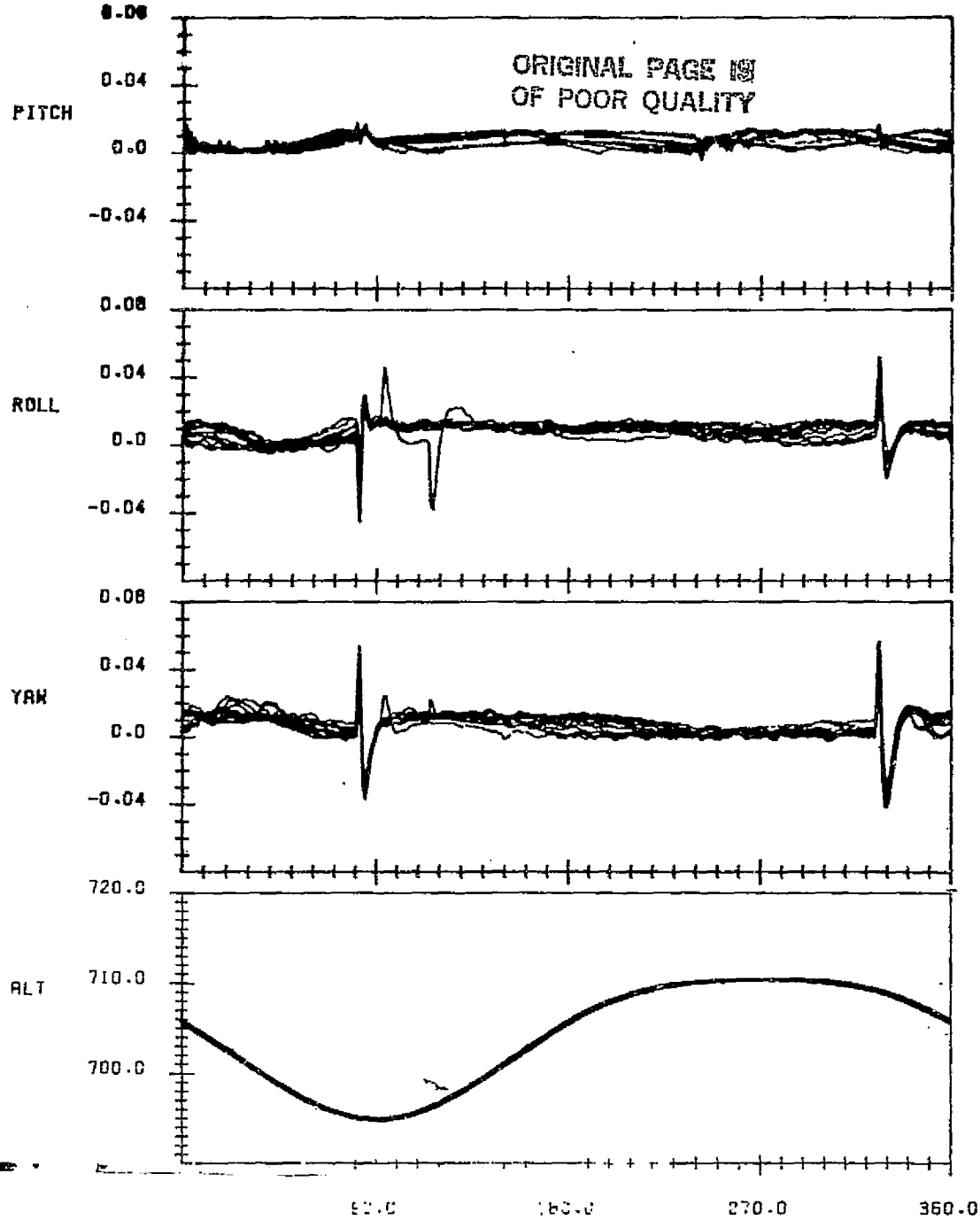

LANDSAT-4 ONBOARD COMPUTER(OBC) REFERENCE ATTITUDE(DEGREES) AND SPACECRAFT ALTITUDE(KILOMETERS) ABOVE 6376.14 KM RADIUS VERSUS ORBIT PHASE FROM THE ASCENDING NODE WITH CONSECUTIVE ORBITS OVERLAID
DATA START TIME:821228.053240460
END TIME:821229.061420139

FIGURE A-11. Reference Attitude and Altitude for Data Span on December 28-29, 1982

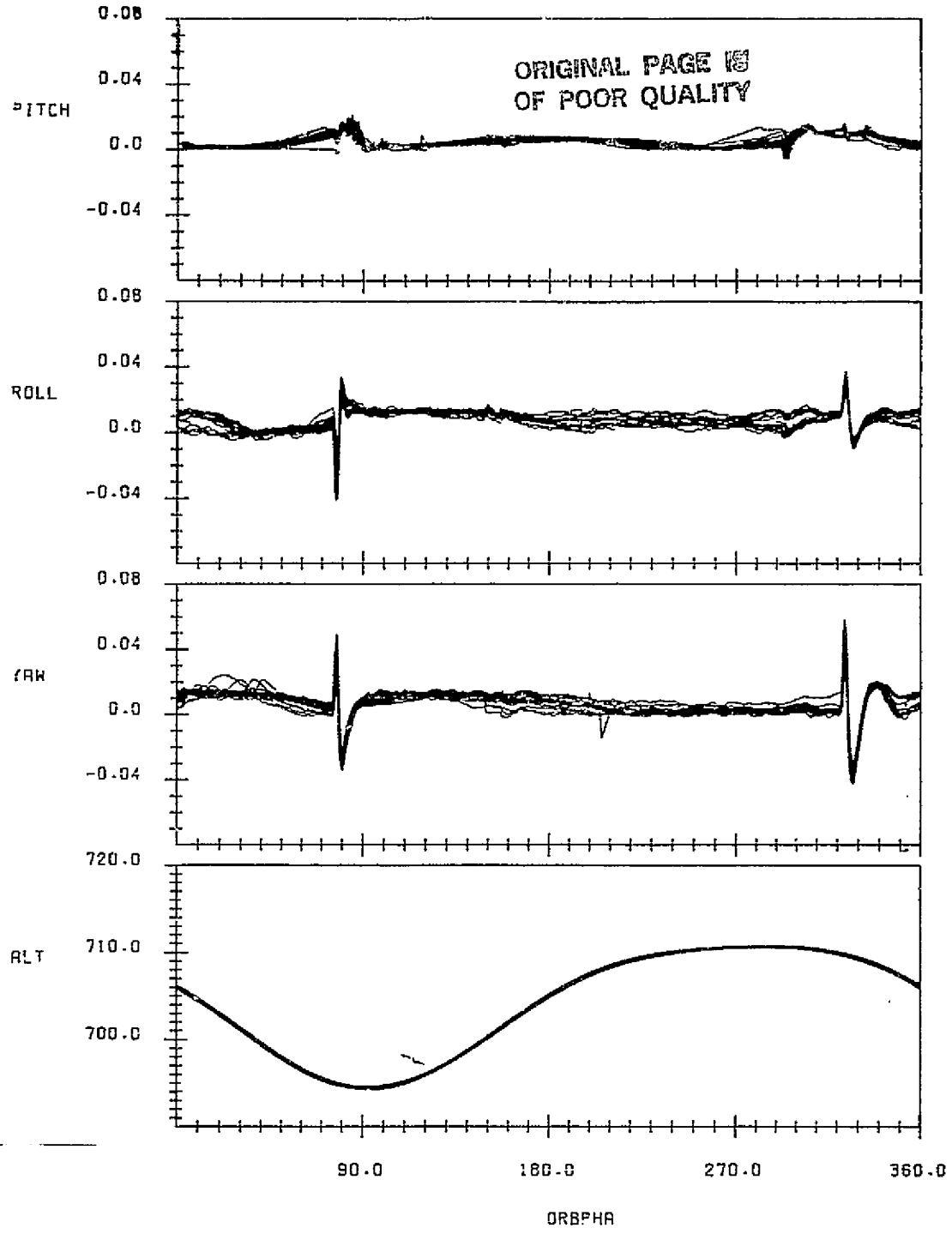

LANDSAT-4 ONBOARD COMPUTER(OBC) REFERENCE ATTITUDE(DEGREES) AND SPACECRAFT ALTITUDE(KILOMETERS) ABOVE 6378.14 KM RADIUS VERSUS ORBIT PHASE FROM THE ASCENDING NODE WITH CONSECUTIVE ORBITS OVERLAID
DATA START TIME:830119.063608627
END TIME:830120.120626114

FIGURE A-12. Reference Attitude and Altitude for Data Span on January 19-20, 1983

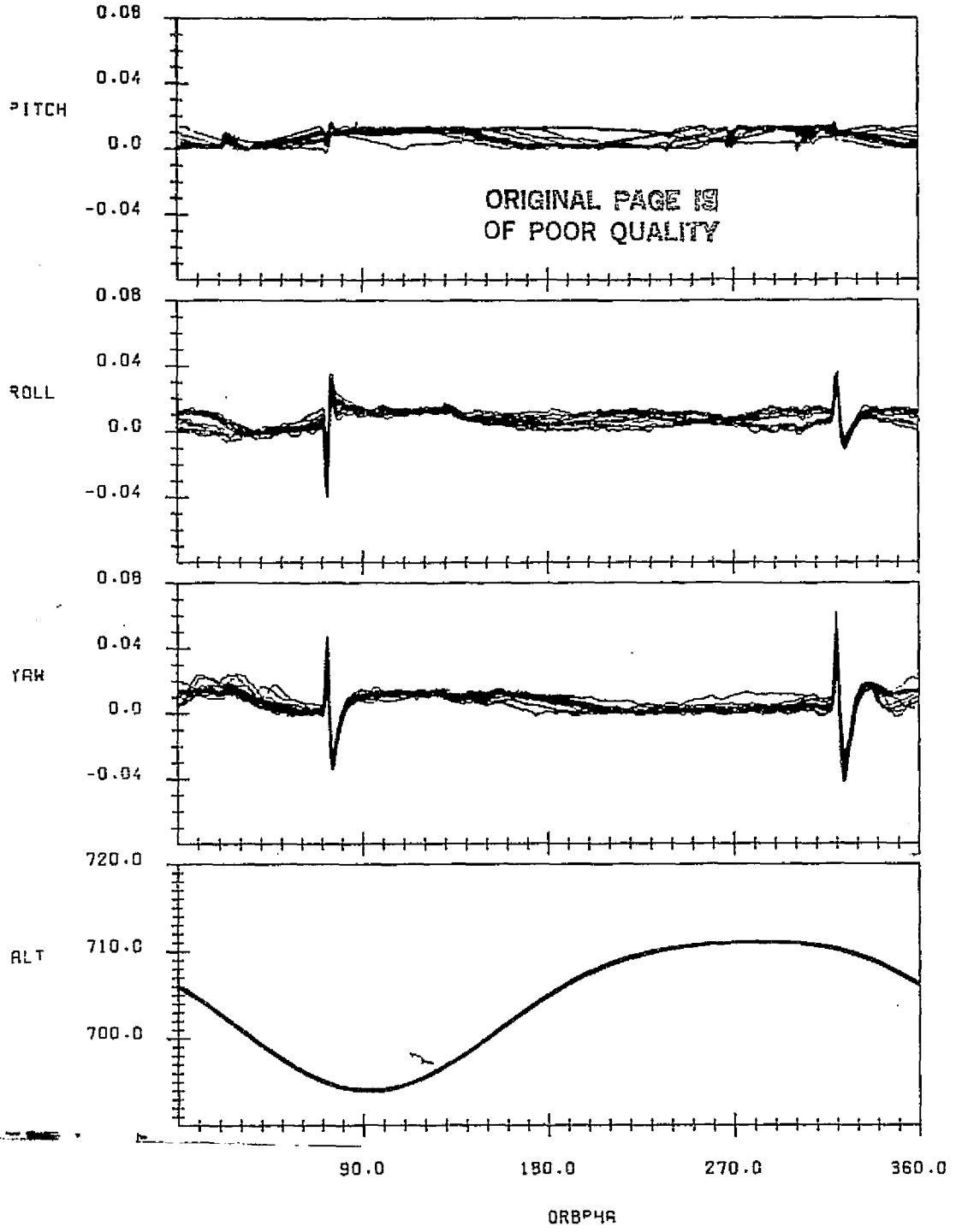

LANDSAT-4 ONBOARD COMPUTER(OBC) REFERENCE ATTITUDE(DEGREES)
AND SPACECRAFT ALTITUDE(KILOMETERS) ABOVE 6378.14 KM RADIUS
VERSUS ORBIT PHASE FROM THE ASCENDING NODE WITH CONSECUTIVE
ORBITS OVERLAID
DATA START TIME:830202.032425071
END TIME:830203.054950590

FIGURE A-13. Reference Attitude and Altitude for Data Span on February 2-3, 1983

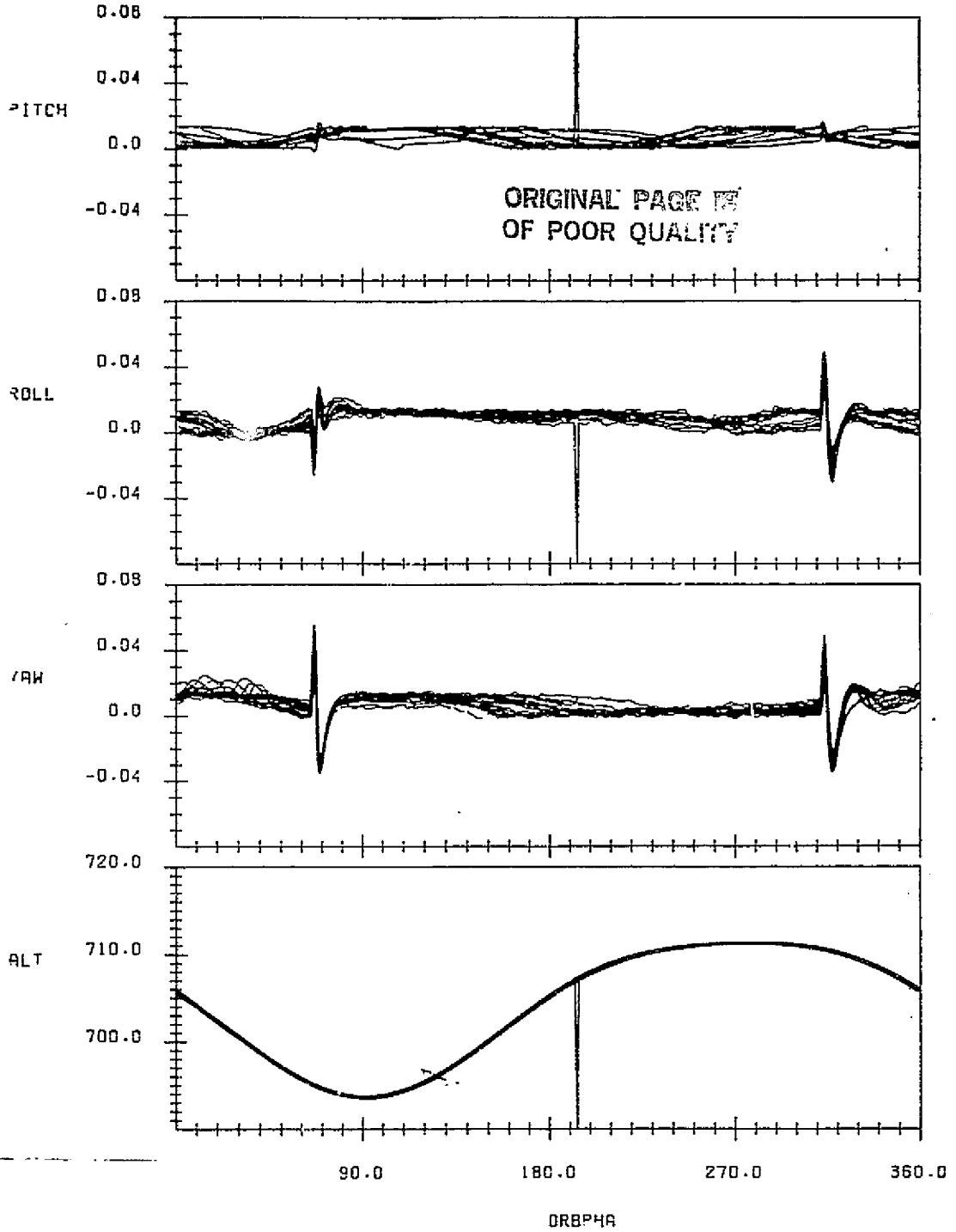

LANDSAT-4 ONBOARD COMPUTER(OBC) REFERENCE ATTITUDE(DEGREES) AND SPACECRAFT ALTITUDE(KILOMETERS) ABOVE 6378.14 KM RADIUS VERSUS ORBIT PHASE FROM THE ASCENDING NODE WITH CONSECUTIVE ORBITS OVERLAID
DATA START TIME:830217.000122618
END TIME:830218.065513594

FIGURE A-14. Reference Attitude and Altitude for Data Span on February 17-18, 1983

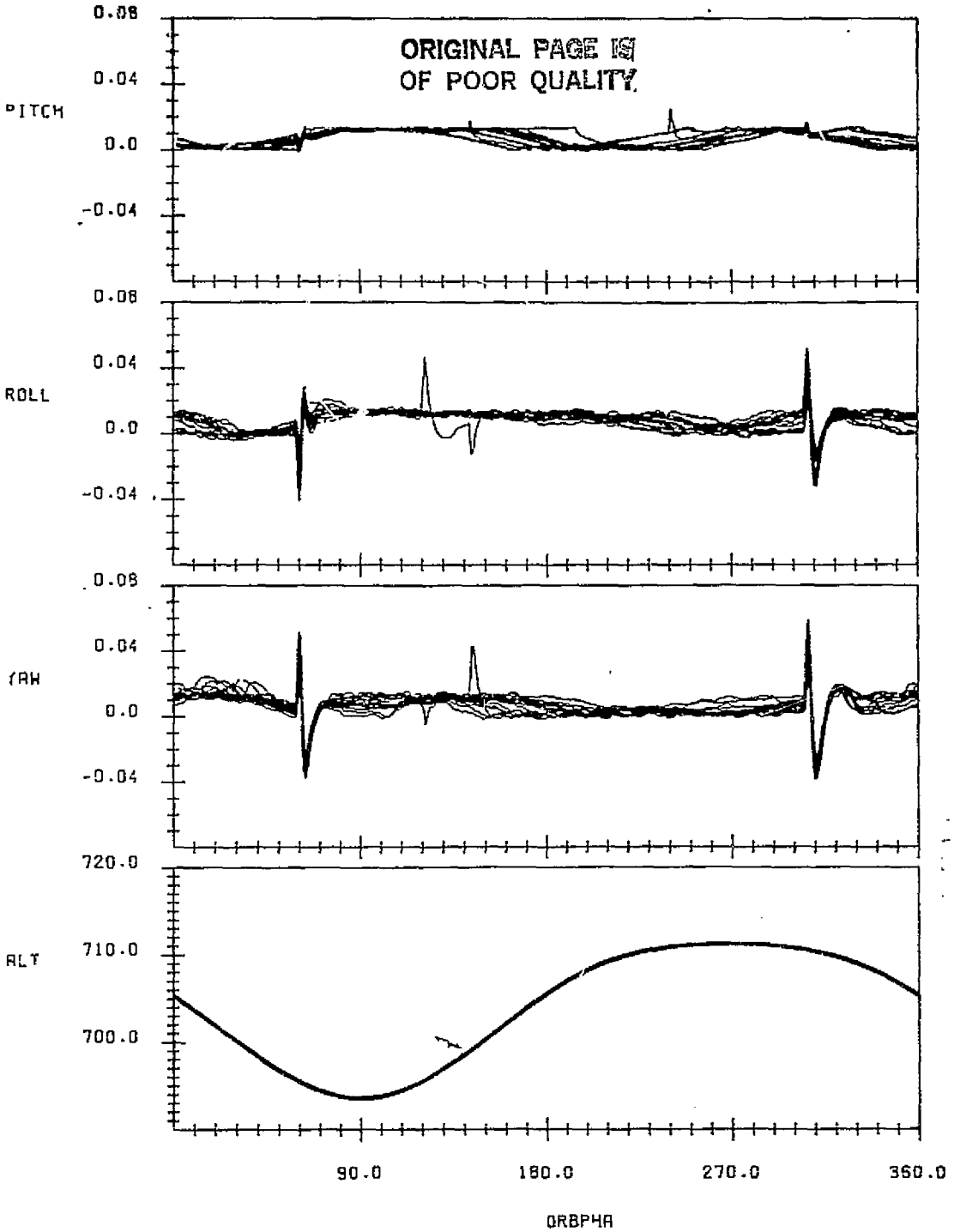

LANDSAT-4 ONBOARD COMPUTER(OBC) REFERENCE ATTITUDE(DEGREES) AND SPACECRAFT ALTITUDE(KILOMETERS) ABOVE 6378.14 KM RADIUS VERSUS ORBIT PHASE FROM THE ASCENDING NODE WITH CONSECUTIVE ORBITS OVERLAID
DATA START TIME:830303.025744694
END TIME:830304.034257270

FIGURE A-15. Reference Attitude and Altitude for Data Span on March 3-4, 1983

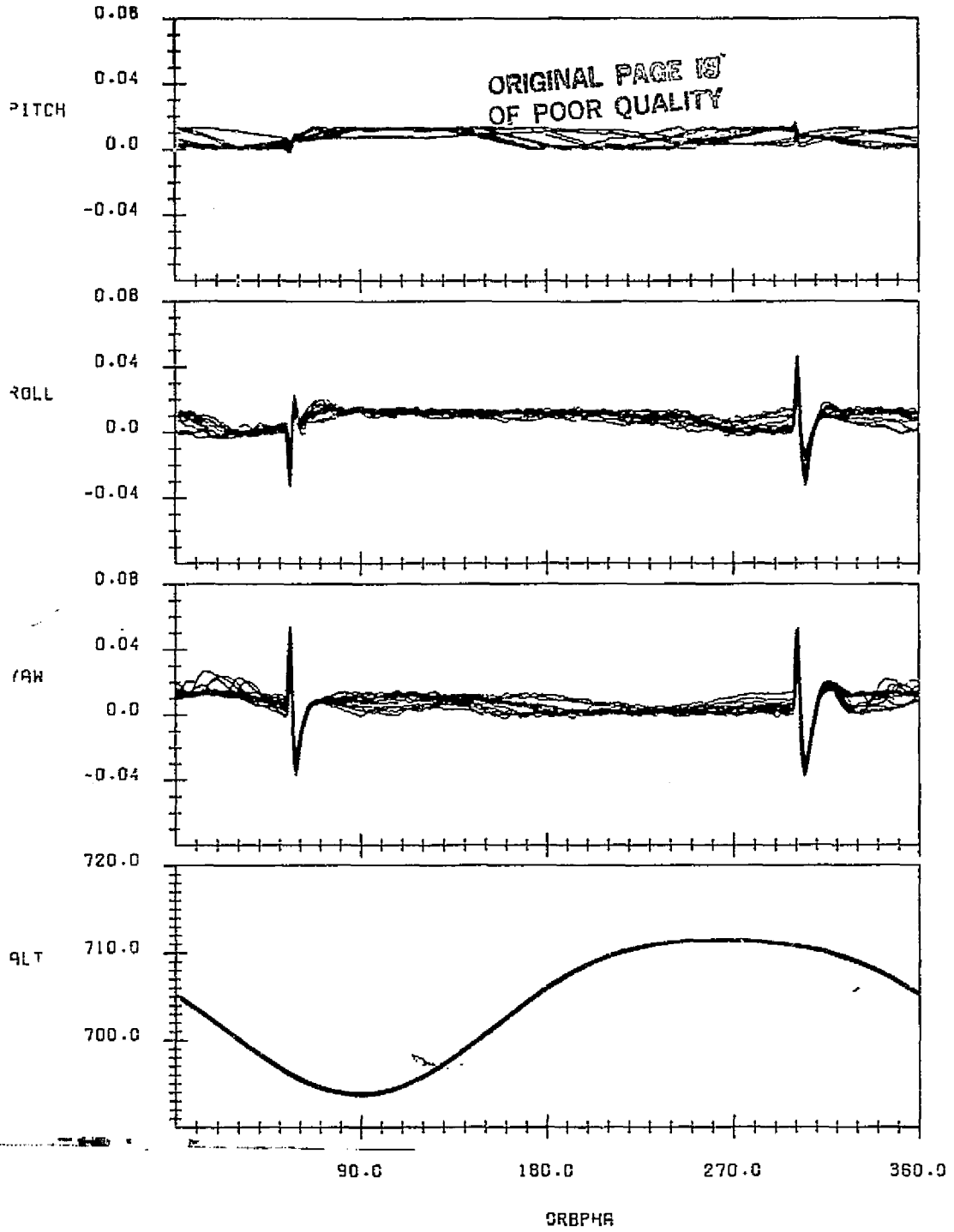

LANDSAT-4 ONBOARD COMPUTER(OBC) REFERENCE ATTITUDE(DEGREES) AND SPACECRAFT ALTITUDE(KILOMETERS) ABOVE 6378.14 KM RADIUS VERSUS ORBIT PHASE FROM THE ASCENDING NODE WITH CONSECUTIVE ORBITS OVERLAID
DATA START TIME:830314.134603442
END TIME:830315.170127218

FIGURE A-16. Reference Attitude and Altitude for Data Span on March 14-15, 1983

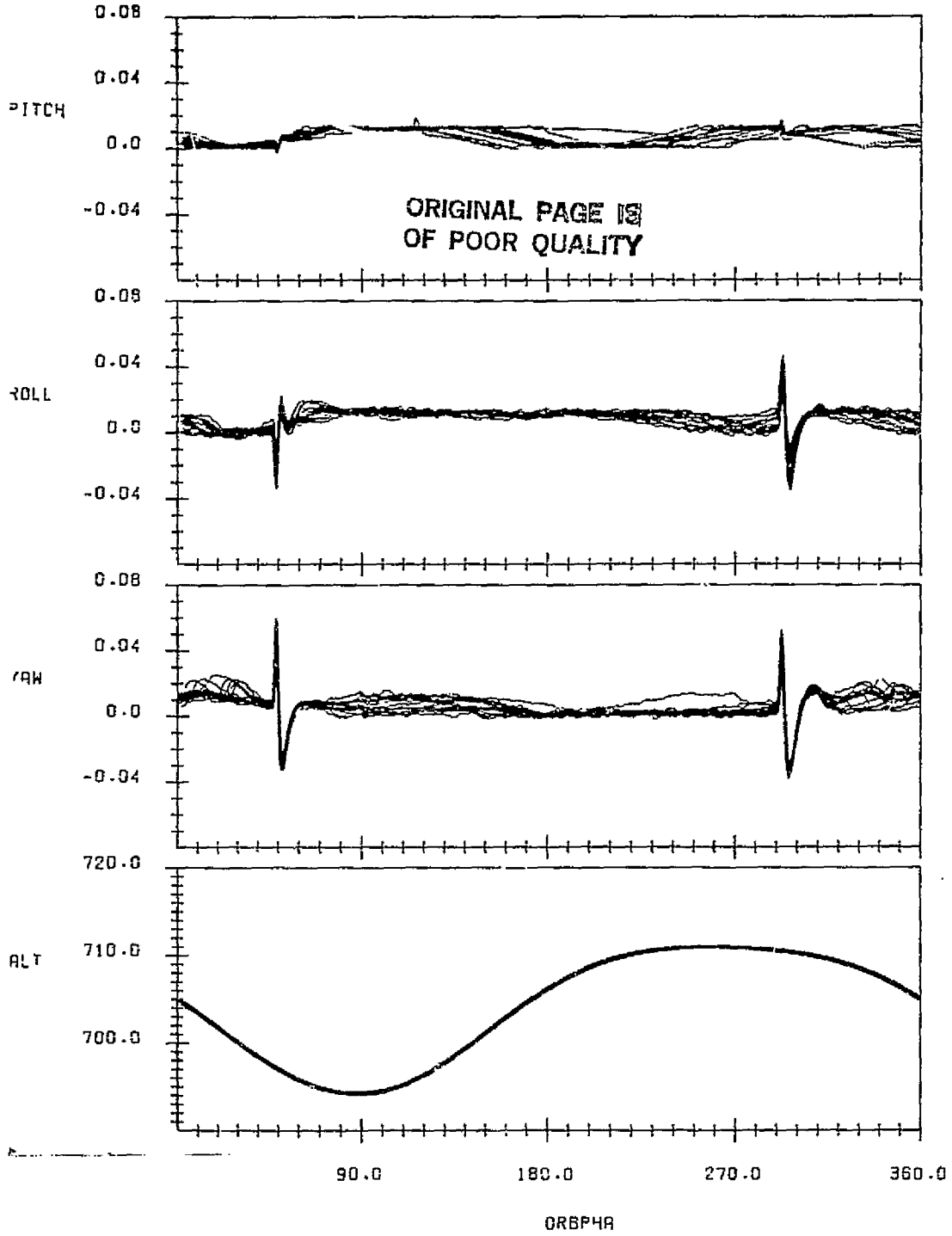

LANDSAT-4 ONBOARD COMPUTER(OBC) REFERENCE ATTITUDE(DEGREES) AND SPACECRAFT ALTITUDE(KILOMETERS) ABOVE 6378.14 KM RADIUS VERSUS ORBIT PHASE FROM THE ASCENDING NODE WITH CONSECUTIVE ORBITS OVERLAID
DATA START TIME:830329.236506990
END TIME:830331.003946798

FIGURE A-17. Reference Attitude and Altitude for Data Span on March 29-31, 1983

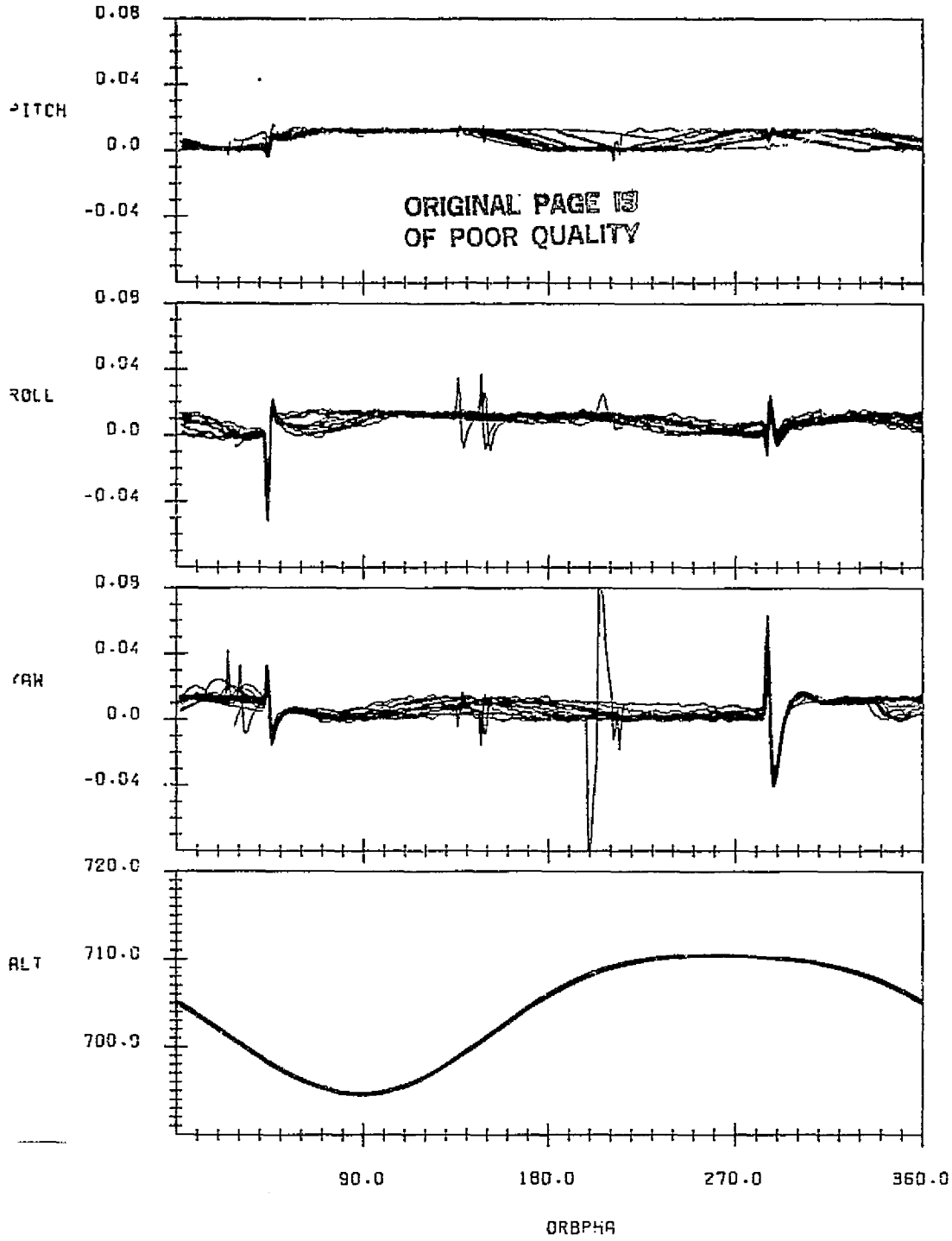

LANDSAT-4 ONBOARD COMPUTER(OBC) REFERENCE ATTITUDE(DEGREES) AND SPACECRAFT ALTITUDE(KILOMETERS) ABOVE 6378.14 KM RADIUS VERSUS ORBIT PHASE FROM THE ASCENDING NODE WITH CONSECUTIVE ORBITS OVERLAID
DATA START TIME:830414.003417145
END TIME:830415.041837625

FIGURE A-18. Reference Attitude and Altitude for Data Span on April 14-15, 1983

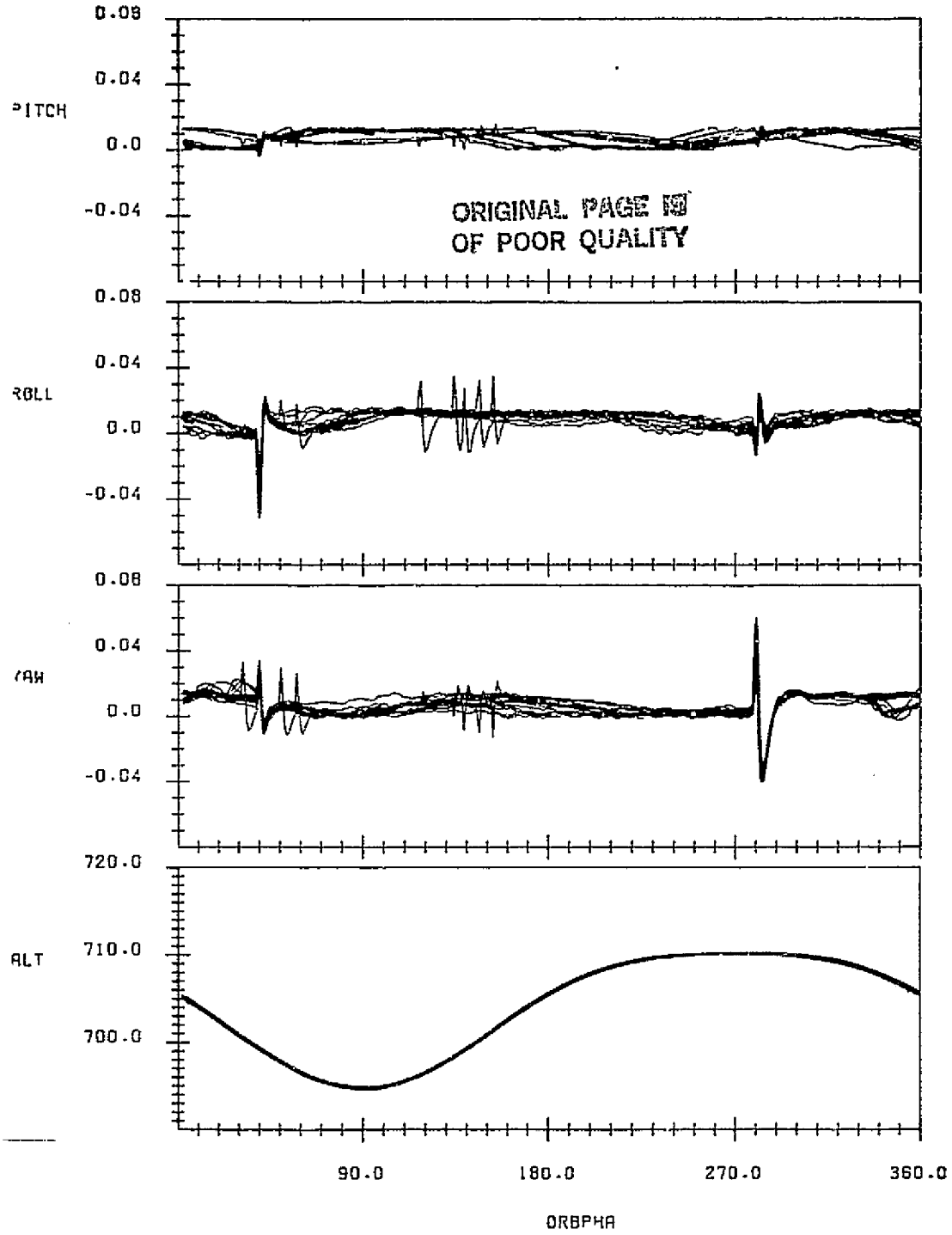

LANDSAT-4 ONBOARD COMPUTER(OBC) REFERENCE ATTITUDE(DEGREES) AND SPACECRAFT ALTITUDE(KILOMETERS) ABOVE 6378.14 KM RADIUS VERSUS ORBIT PHASE FROM THE ASCENDING NODE WITH CONSECUTIVE ORBITS OVERLAID
DATA START TIME:830426.0204:9829
END TIME:830427.0307009981

FIGURE A-19. Reference Attitude and Altitude for Data Span on April 26-27, 1983

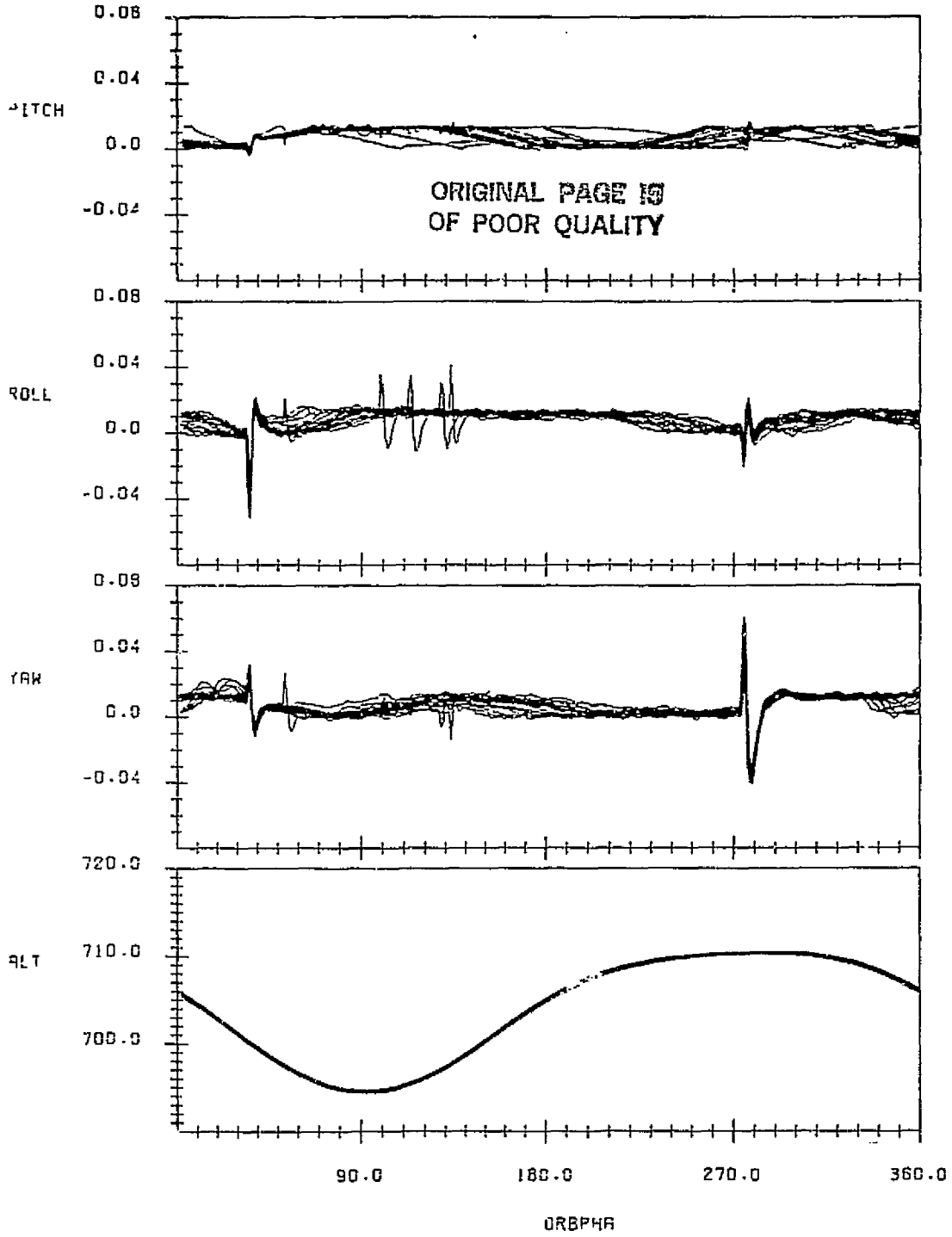

LANDSAT-4 ONBOARD COMPUTER(OBC) REFERENCE ATTITUDE(DEGREES)
AND SPACECRAFT ALTITUDE(KILOMETERS) ABOVE 6378.14 KM RADIUS
VERSUS ORBIT PHASE FROM THE ASCENDING NODE WITH CONSECUTIVE
ORBITS OVERLAID
DATA START TIME:83051 1.001602608
END TIME:830512.022204864

FIGURE A-20. Reference Attitude and Altitude for Data Span on May 11-12, 1983

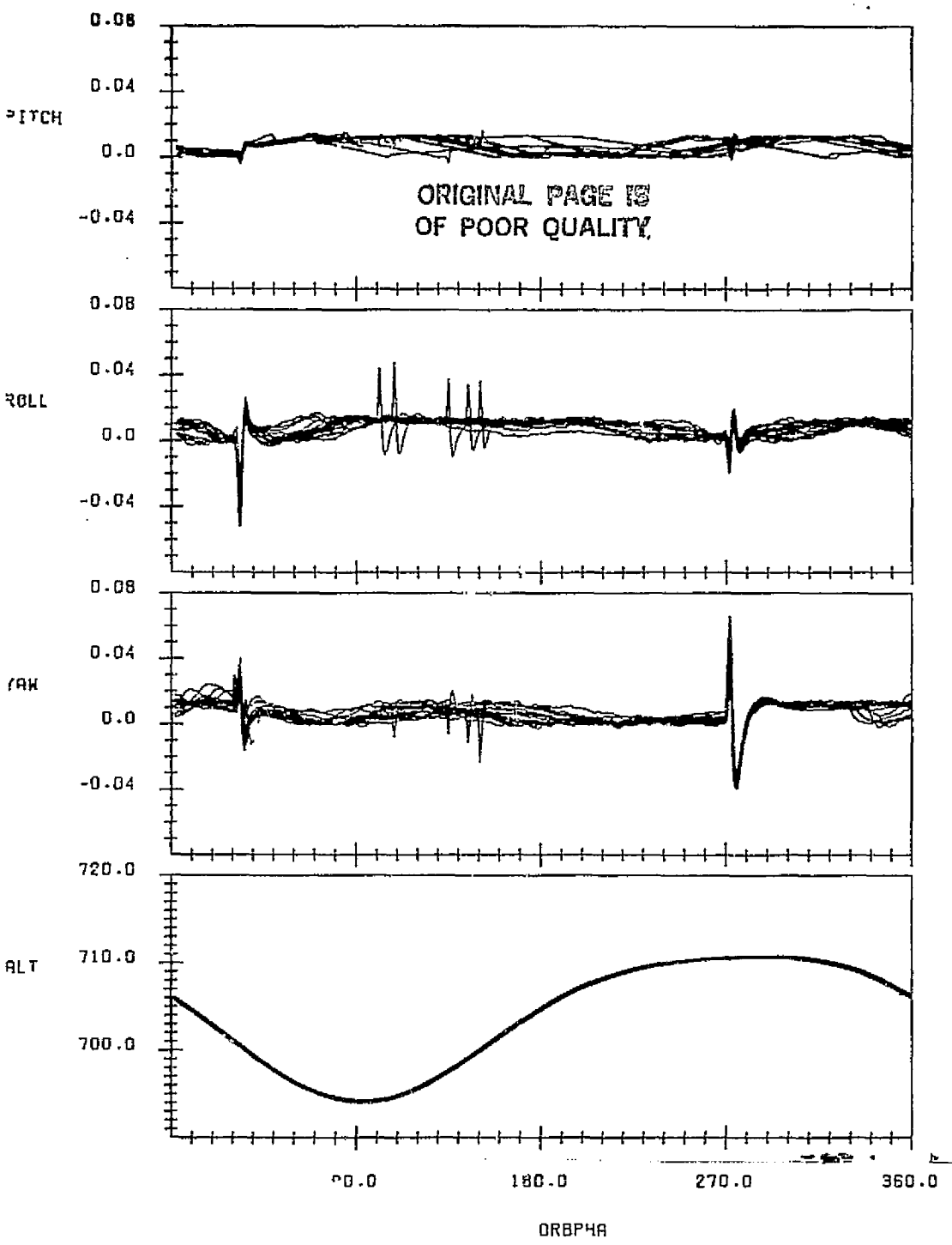

LANDSAT-4 ONBOARD COMPUTER(OBC) REFERENCE ATTITUDE(DEGREES)
AND SPACECRAFT ALTITUDE(KILOMETERS) ABOVE 6378.14 KM RADIUS
VERSUS ORBIT PHASE FROM THE ASCENDING NODE WITH CONSECUTIVE
ORBITS OVERLAID
DATA START TIME:830523.004000365
END TIME:830524.042404476

FIGURE A-21. Reference Attitude and Altitude for Data Span on May 23-24, 1983

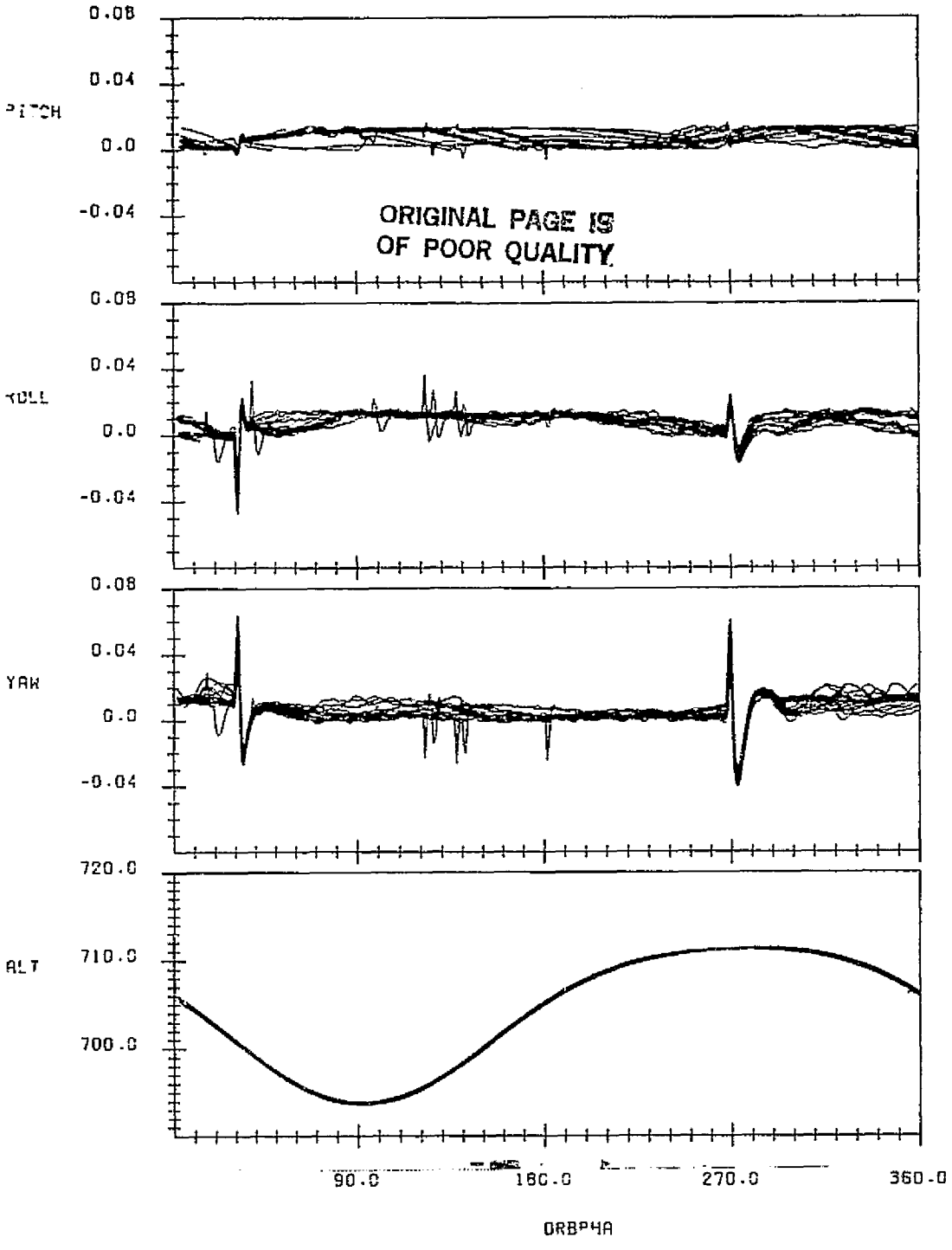

LANDSAT-4 ONBOARD COMPUTER(OBC) REFERENCE ATTITUDE(DEGREES) AND SPACECRAFT ALTITUDE(KILOMETERS) ABOVE 6378.14 KM RADIUS VERSUS ORBIT PHASE FROM THE ASCENDING NODE WITH CONSECUTIVE ORBITS OVERLAID
DATA START TIME:830506.002351736
END TIME:830607.025956216

FIGURE A-22. Reference Attitude and Altitude for Data Span on June 6-7, 1983

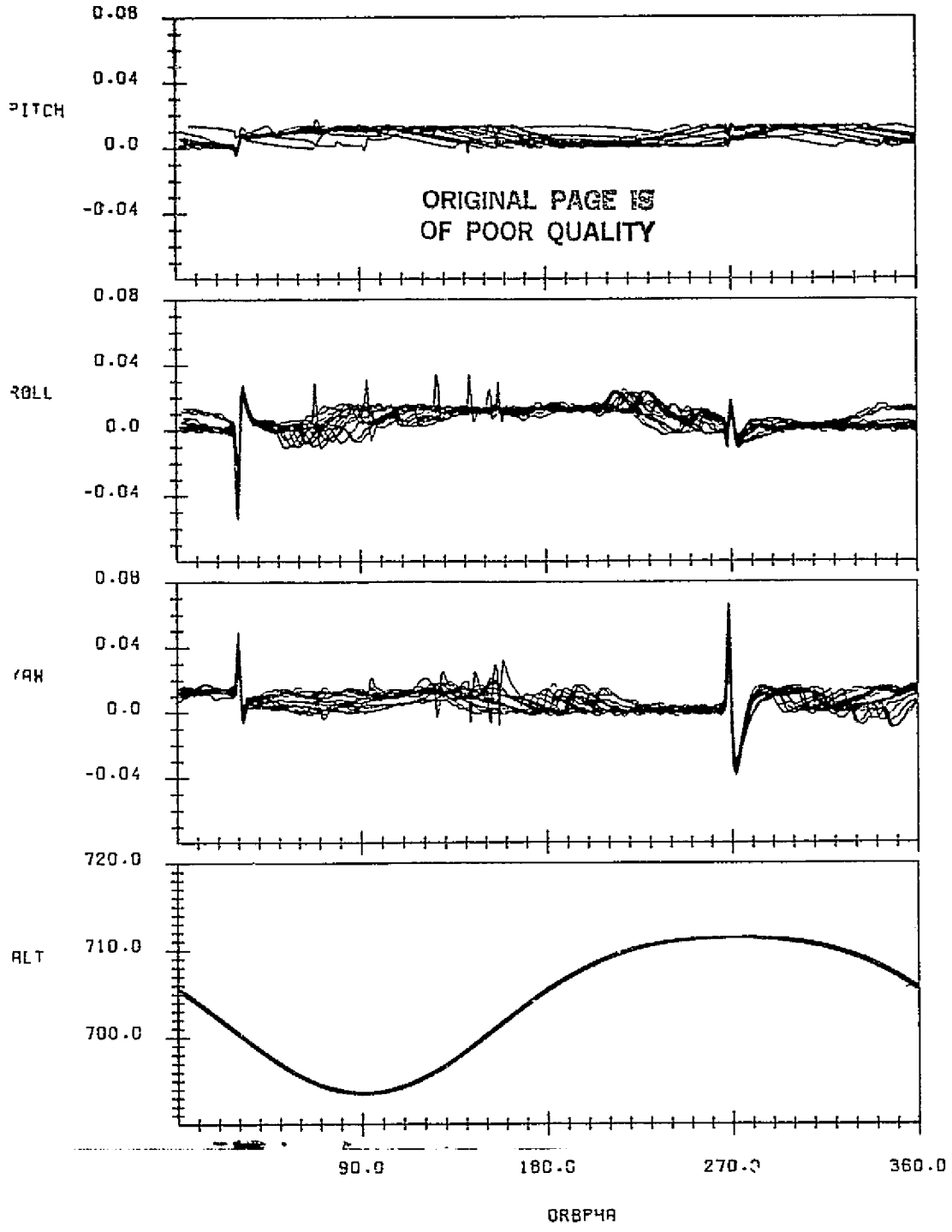

LANDSAT-4 ONBOARD COMPUTER(OBC) REFERENCE ATTITUDE(DEGREES) AND SPACECRAFT ALTITUDE(KILOMETERS) ABOVE 6378.14 KM RADIUS VERSUS ORBIT PHASE FROM THE ASCENDING NODE WITH CONSECUTIVE ORBITS OVERLAID
DATA START TIME:830621.225929155
END TIME:830623.012243587

FIGURE A-23. Reference Attitude and Altitude for Data Span on June 21-23, 1983

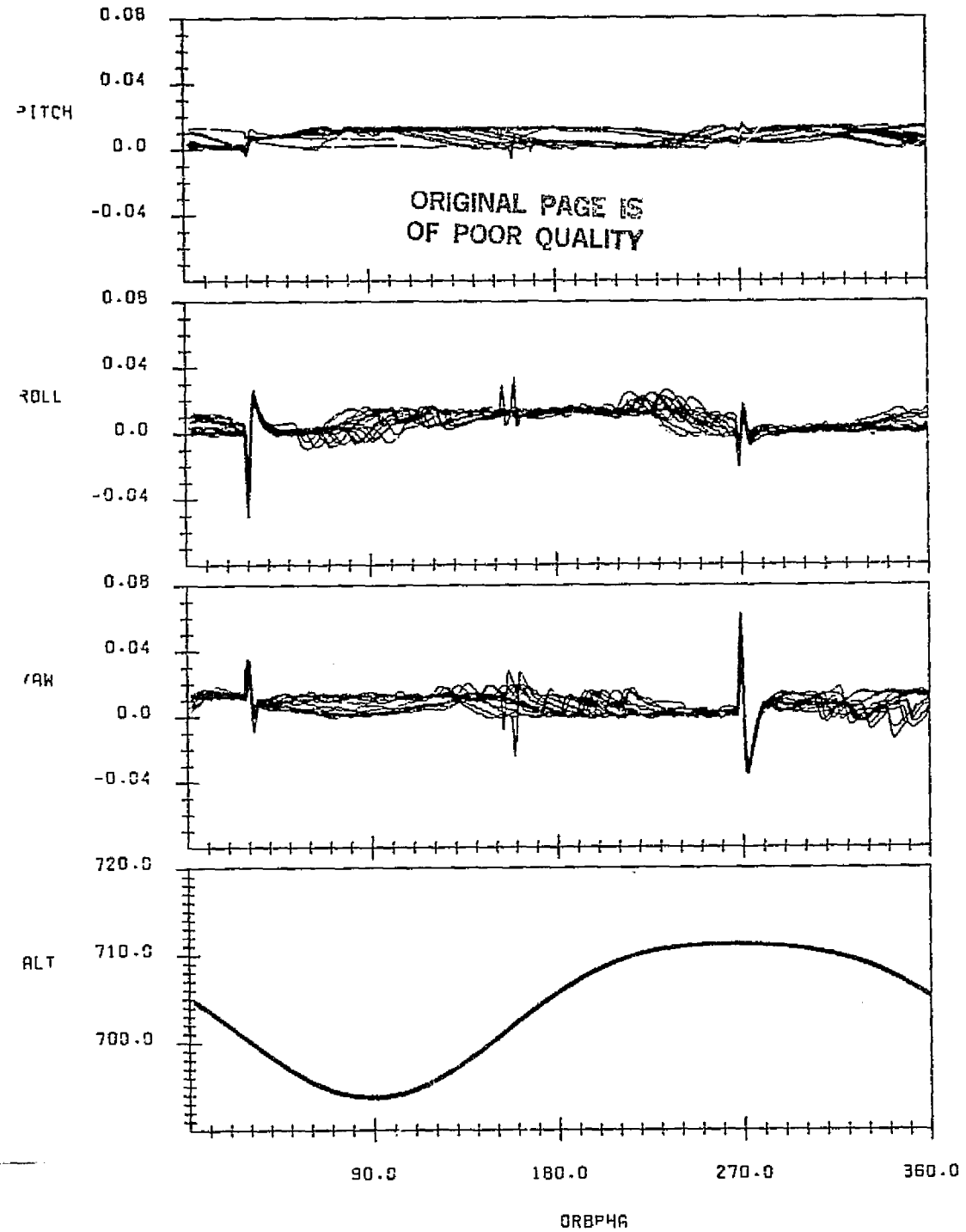

LANDSAT-4 ONBOARD COMPUTER(OBC) REFERENCE ATTITUDE(DEGREES) AND SPACECRAFT ALTITUDE(KILOMETERS) ABOVE 6378.14 KM RADIUS VERSUS ORBIT PHASE FROM THE ASCENDING NODE WITH CONSECUTIVE ORBITS OVERLAID
DATA START TIME:830706.154825062
END TIME:830707.182940635

FIGURE A-24. Reference Attitude and Altitude for Data Span on July 6-7, 1983

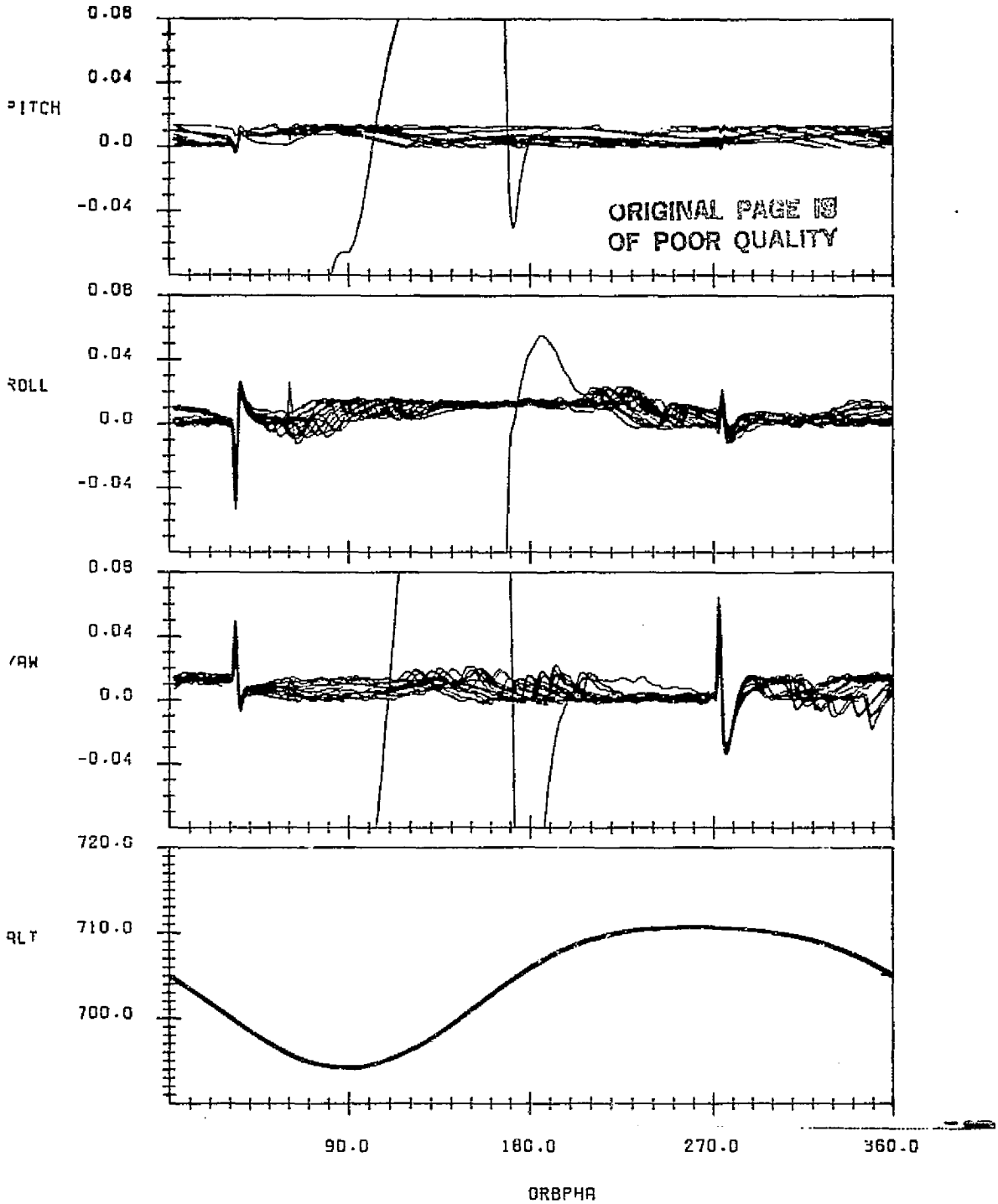

LANDSAT-4 ONBOARD COMPUTER(OBC) REFERENCE ATTITUDE(DEGREES) AND SPACECRAFT ALTITUDE(KILOMETERS) ABOVE 6378.14 KM RADIUS VERSUS ORBIT PHASE FROM THE ASCENDING NODE WITH CONSECUTIVE ORBITS OVERLAID
DATA START TIME:830726.00401&064
END TIME:830727.061244608

FIGURE A-25. Reference Attitude and Altitude for Data Span on July 26-27, 1983

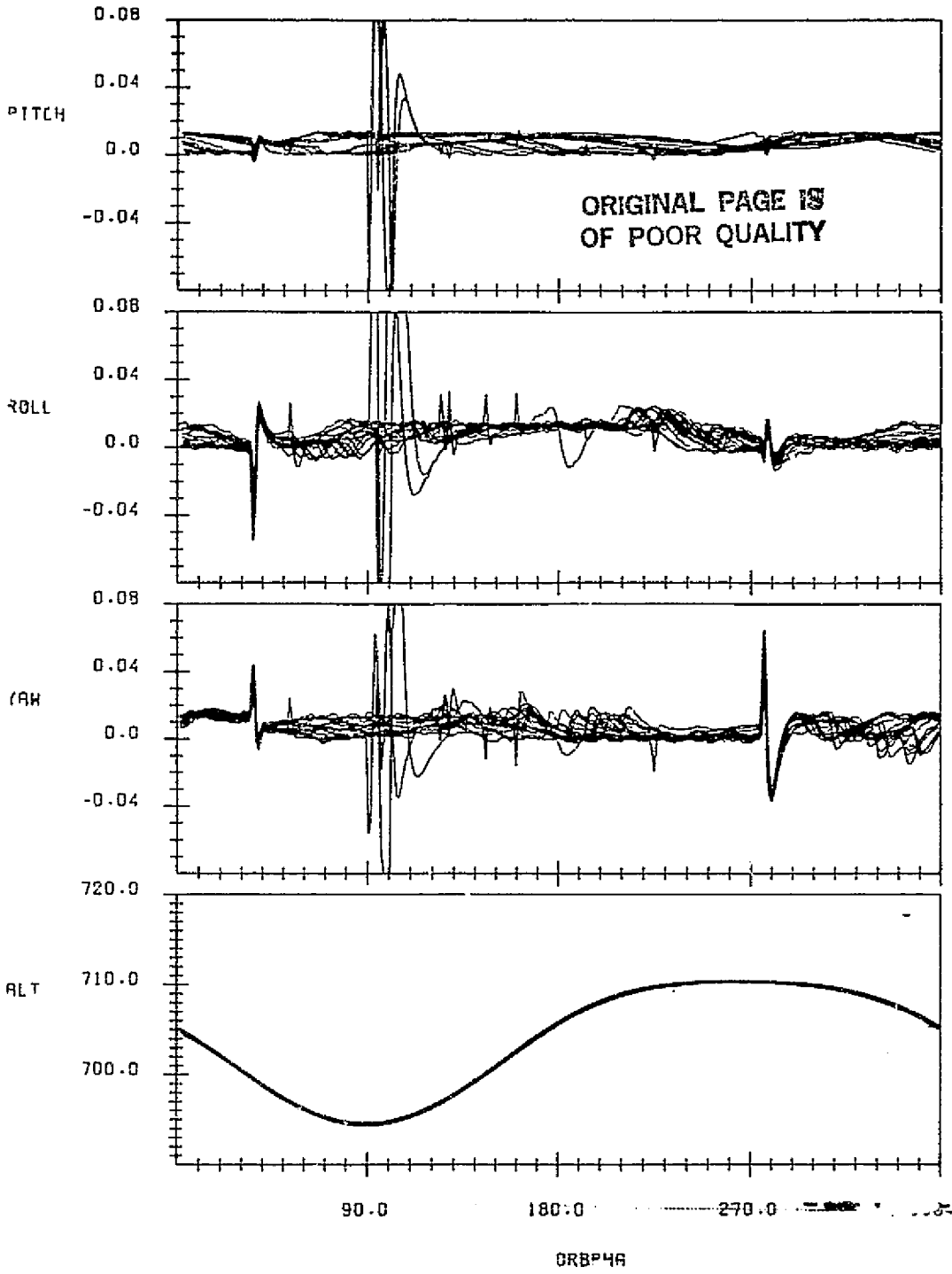

LANDSAT-4 ONBOARD COMPUTER(OBC) REFERENCE ATTITUDE(DEGREES) AND SPACECRAFT ALTITUDE(KILOMETERS) ABOVE 6378.14 KM RADIUS VERSUS ORBIT PHASE FROM THE ASCENDING NODE WITH CONSECUTIVE ORBITS OVERLAID
DATA START TIME:830806.134523196
END TIME:830807.174517564

FIGURE A-26. Reference Attitude and Altitude for Data Span on August 6-7, 1983

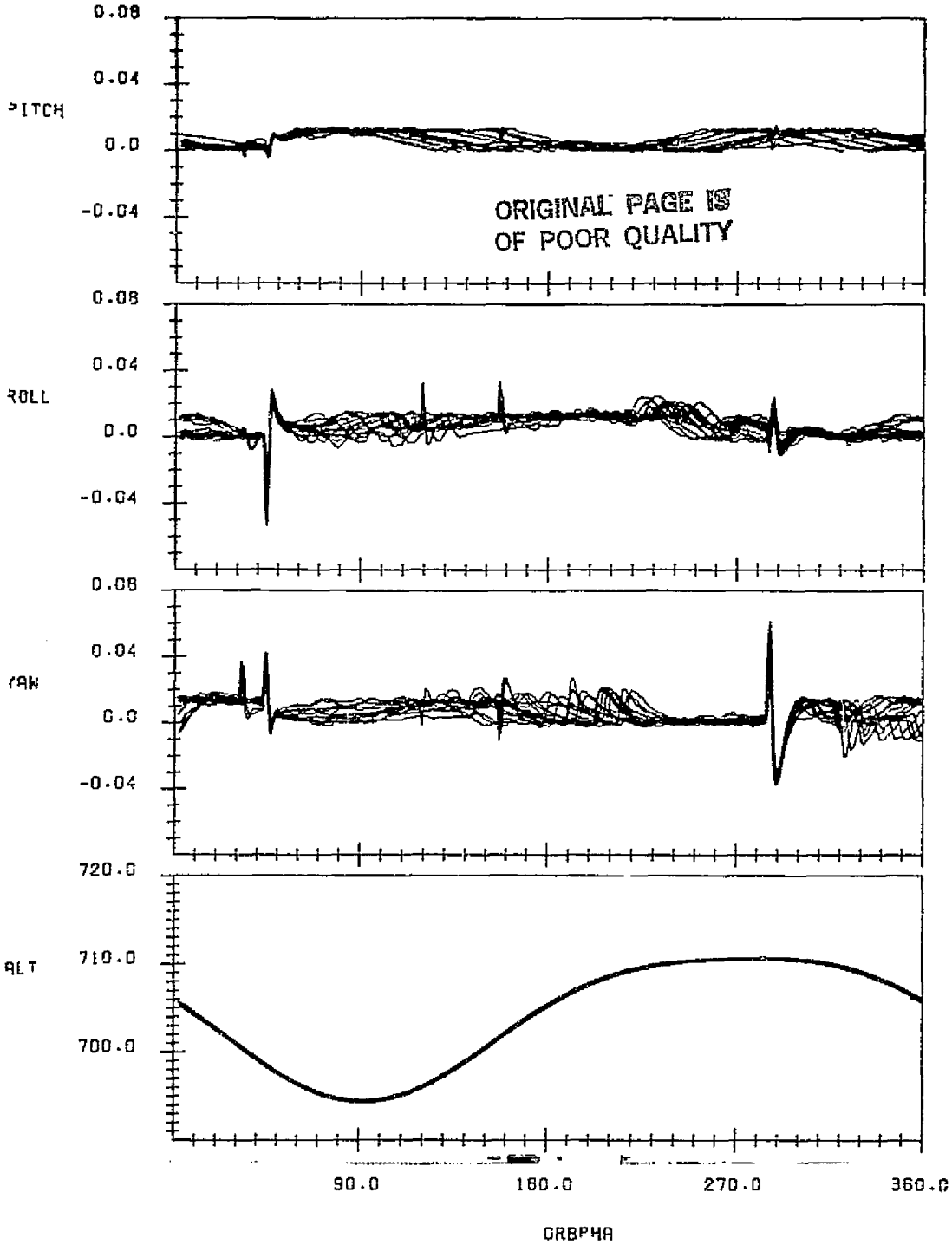

LANDSAT-4 ONBOARD COMPUTER(OBC) REFERENCE ATTITUDE(DEGREES) AND SPACECRAFT ALTITUDE(KILOMETERS) ABOVE 6378.14 KM RADIUS VERSUS ORBIT PHASE FROM THE ASCENDING NODE WITH CONSECUTIVE ORBITS OVERLAID
DATA START TIME:830831.001456628
END TIME:830901.041150787

FIGURE A-27. Reference Attitude and Altitude for Data Span on August 31 - September 1, 1983

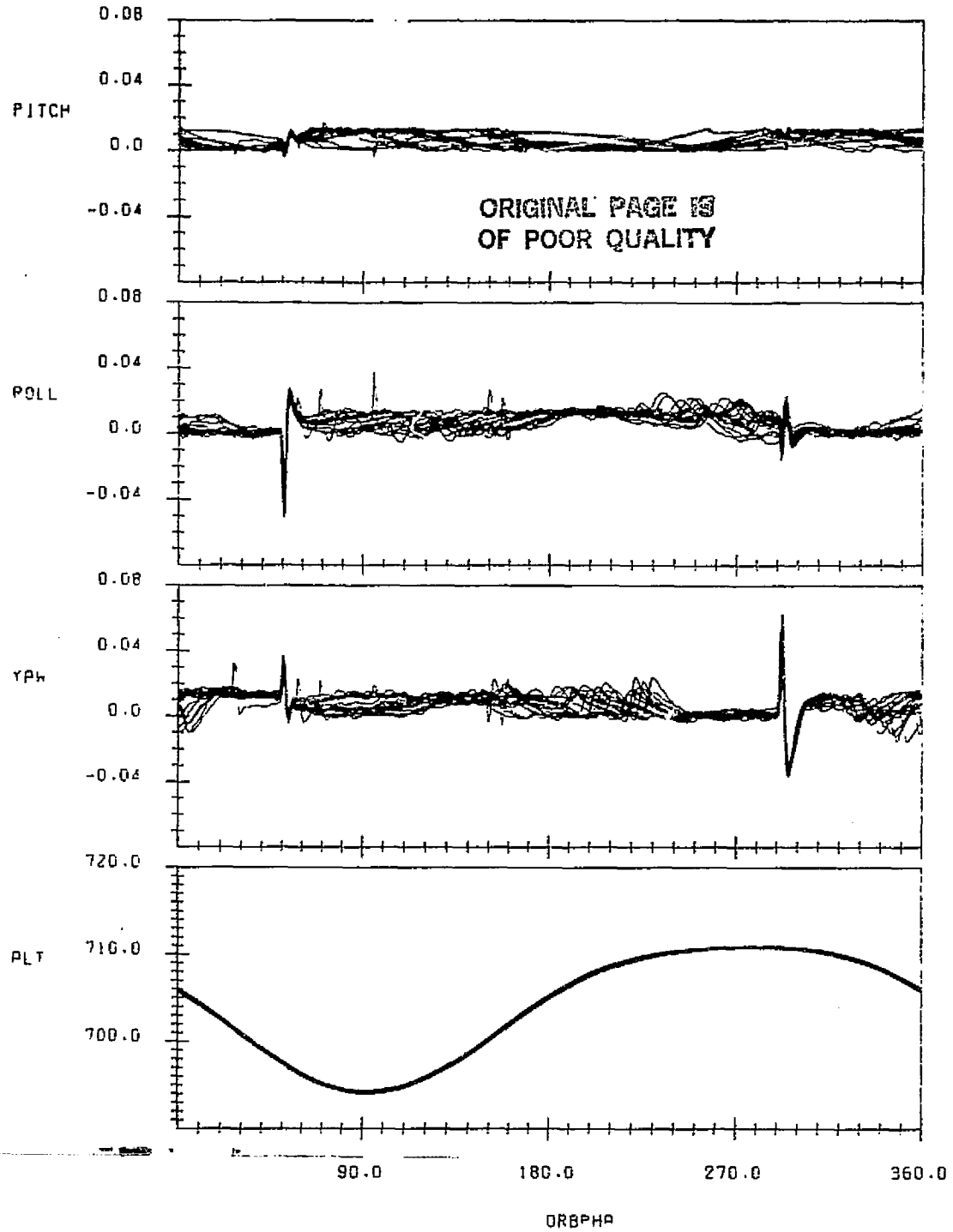

LANDSAT-4 ONBOARD COMPUTER(OBC) REFERENCE ATTITUDE(DEGREES) AND SPACECRAFT ALTITUDE(KILOMETERS) ABOVE 6378.14 KM RADIUS VERSUS ORBIT PHASE FROM THE ASCENDING NODE WITH CONSECUTIVE ORBITS OVERLAID
DATA START TIME:83091 4.002744703
END TIME:83091 5.055956878

FIGURE A-28. Reference Attitude and Altitude for Data Span on September 14-15, 1983

APPENDIX B - SCANNER TEMPERATURES

Figures B-1 through B-28 provide plots of the bolometer and sensor assembly housing temperatures for all the data spans processed for this report. The plots show the temperatures in degrees centigrade as a function of orbit phase from the ascending node for several orbits overlayed.

A spike in the bolometer 1 temperature on December 1 is due to a spurious telemetry reading.

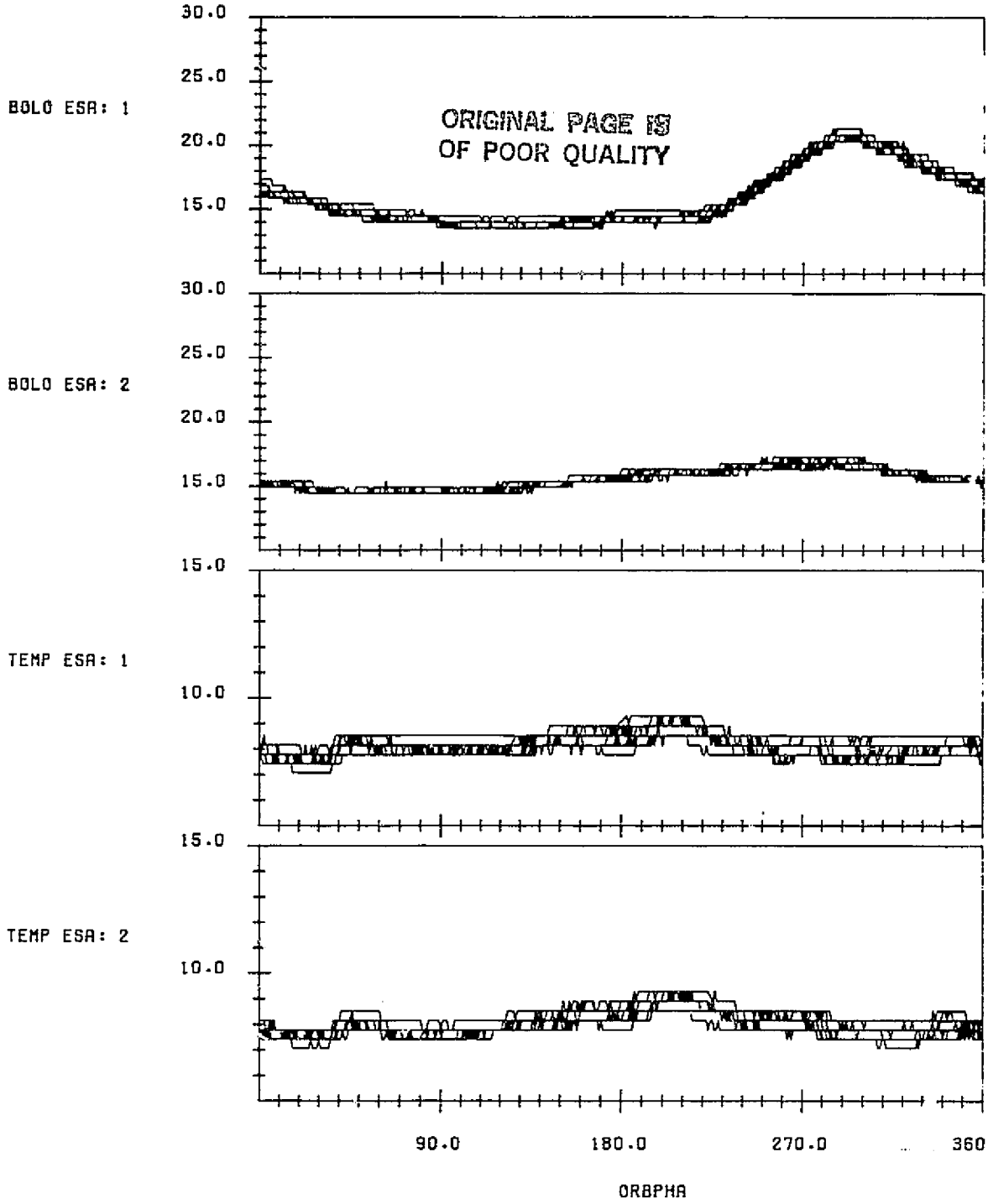

LANDSAT-4 CONICAL SCANNER BOLOMETER TEMPERATURE AND EARTH SENSOR ASSEMBLY HOUSING TEMPERATURE(DEGREES CELSIUS) VERSUS ORBIT PHASE FROM THE ASCENDING NODE WITH CONSECUTIVE ORBITS OVERLAID
DATA START TIME:820810.215426522
END TIME:820811.203329690

FIGURE B-1. Scanner Temperatures for Data Span on August 10-11, 1982

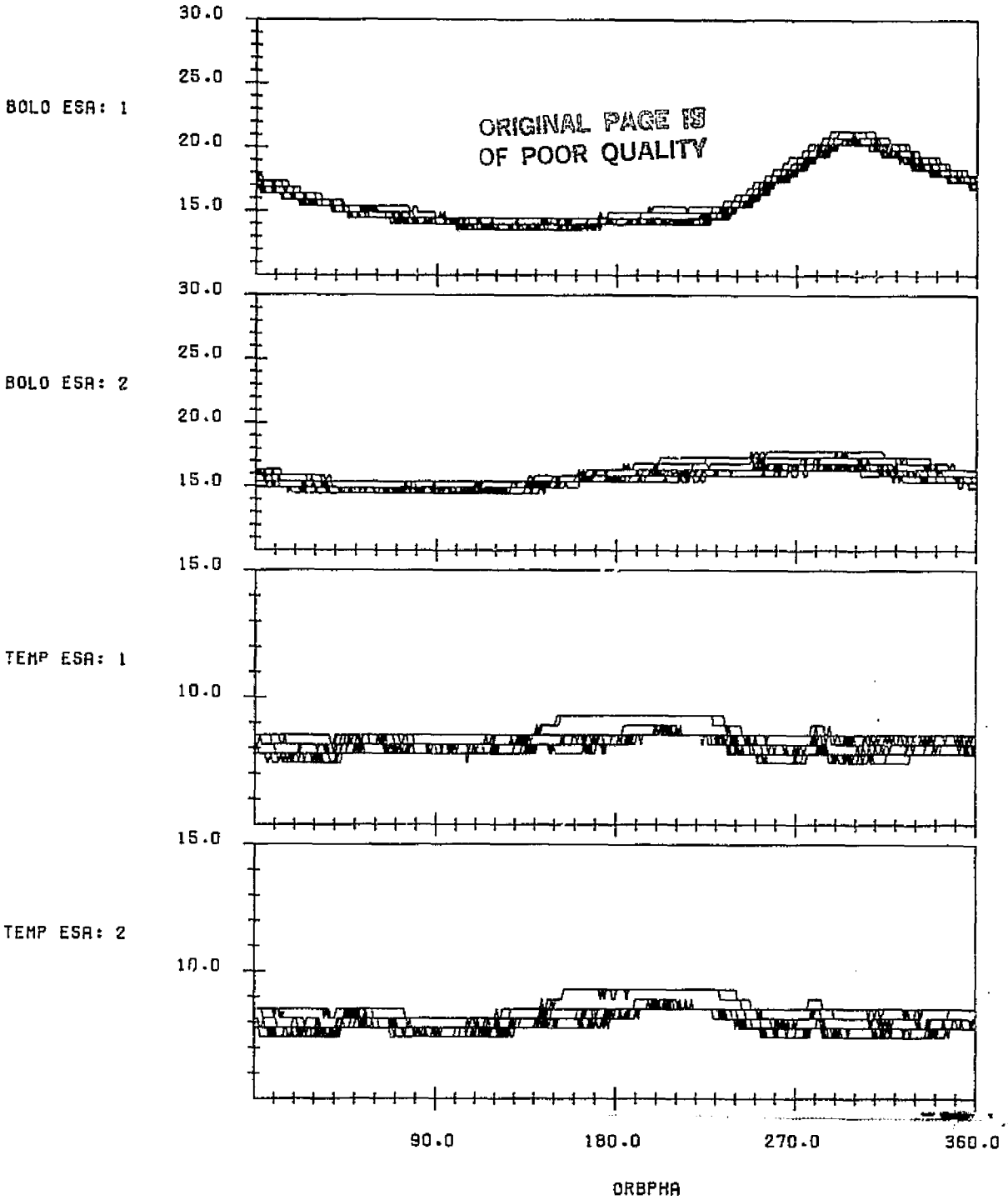

LANDSAT-4 CONICAL SCANNER BOLOMETER TEMPERATURE AND EARTH SENSOR ASSEMBLY HOUSING TEMPERATURE(DEGREES CELSIUS) VERSUS ORBIT PHASE FROM THE ASCENDING NODE WITH CONSECUTIVE ORBITS OVERLAID
DATA START TIME:820825.010606091
END TIME:820826.032214554

FIGURE B-2. Scanner Temperatures for Data Span on August 25-26, 1982

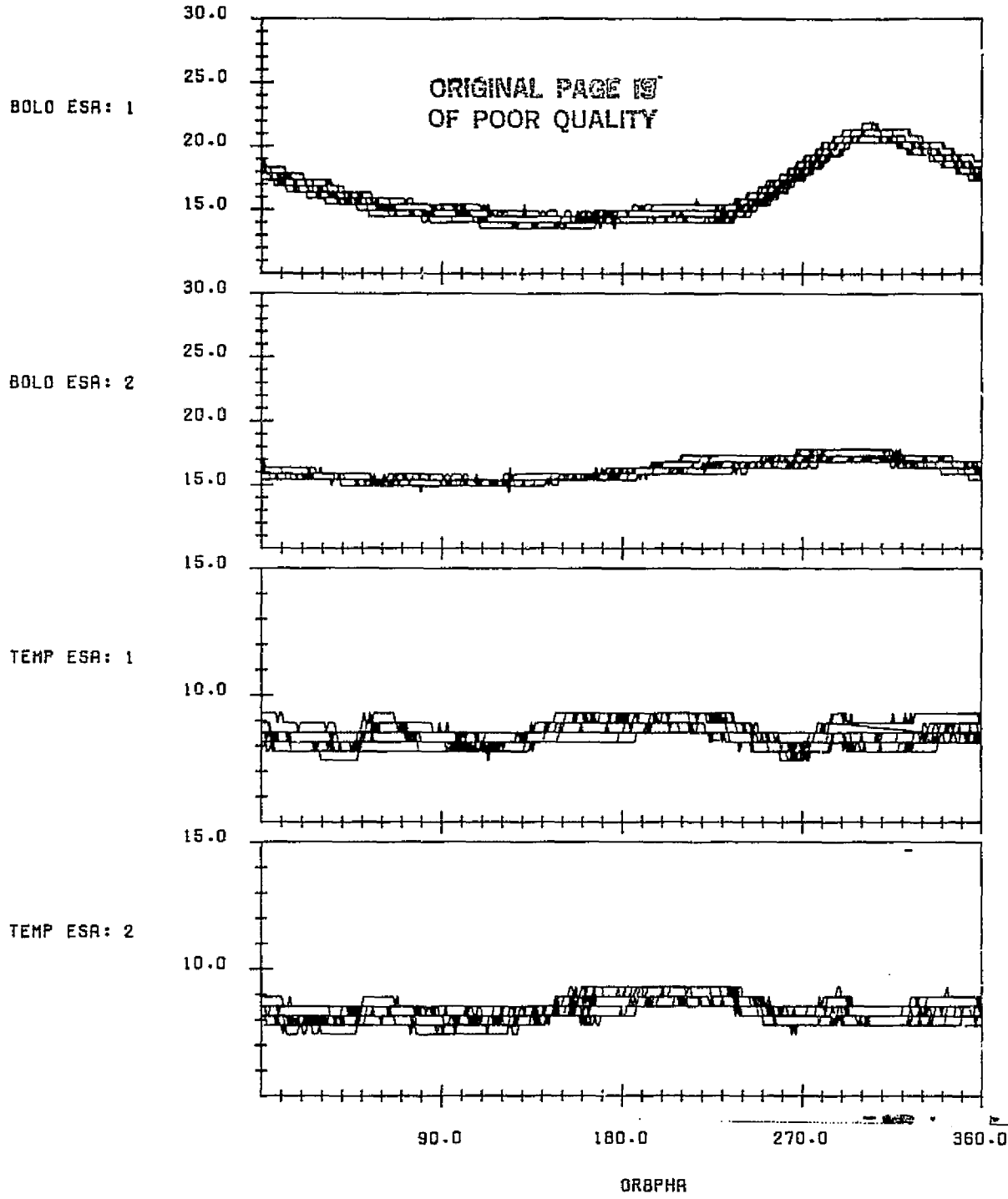

FIGURE B-3. Scanner Temperatures for Data Span on September 8-9, 1982

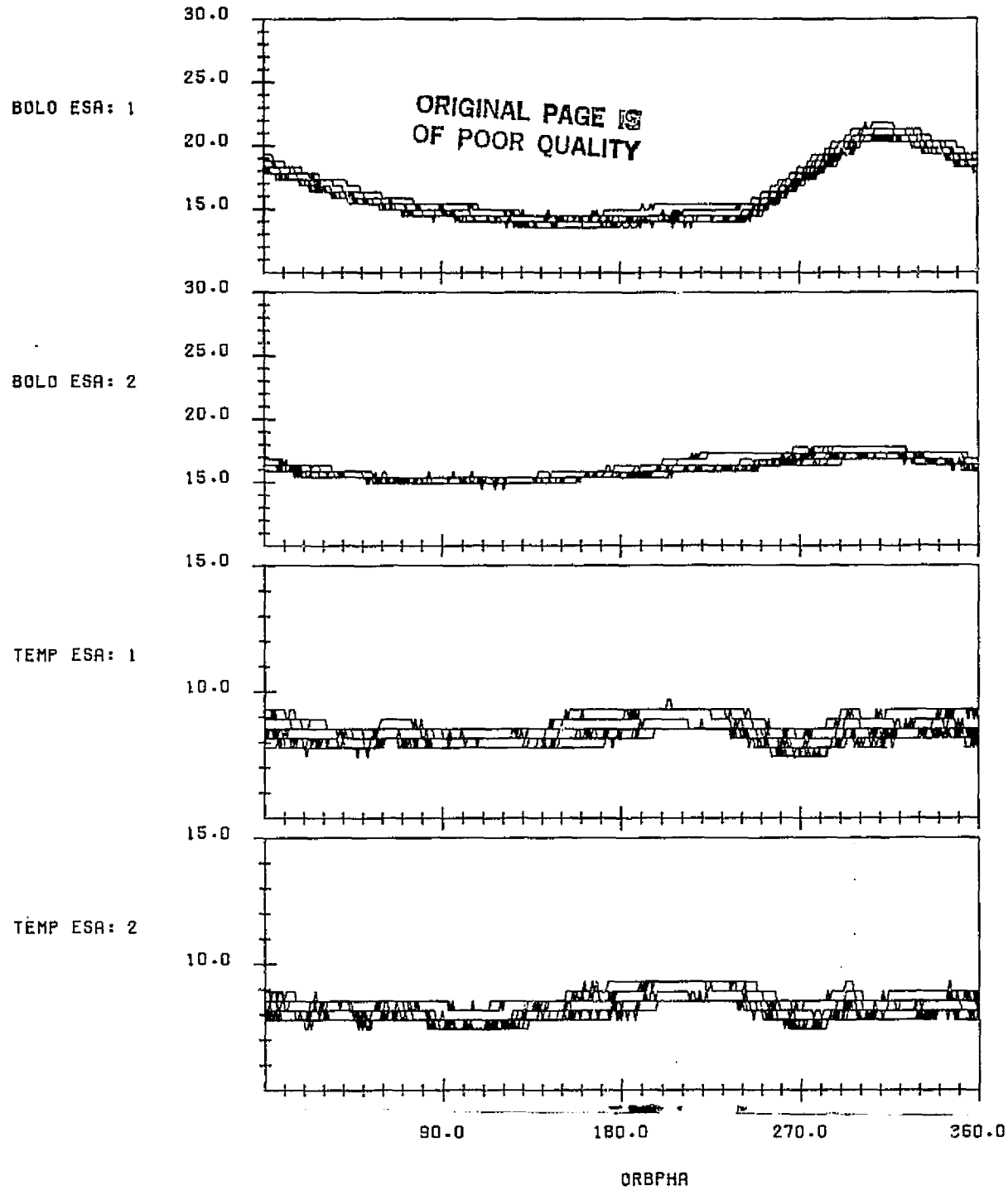

FIGURE B-4. Scanner Temperatures for Data Span on September 22-23, 1982

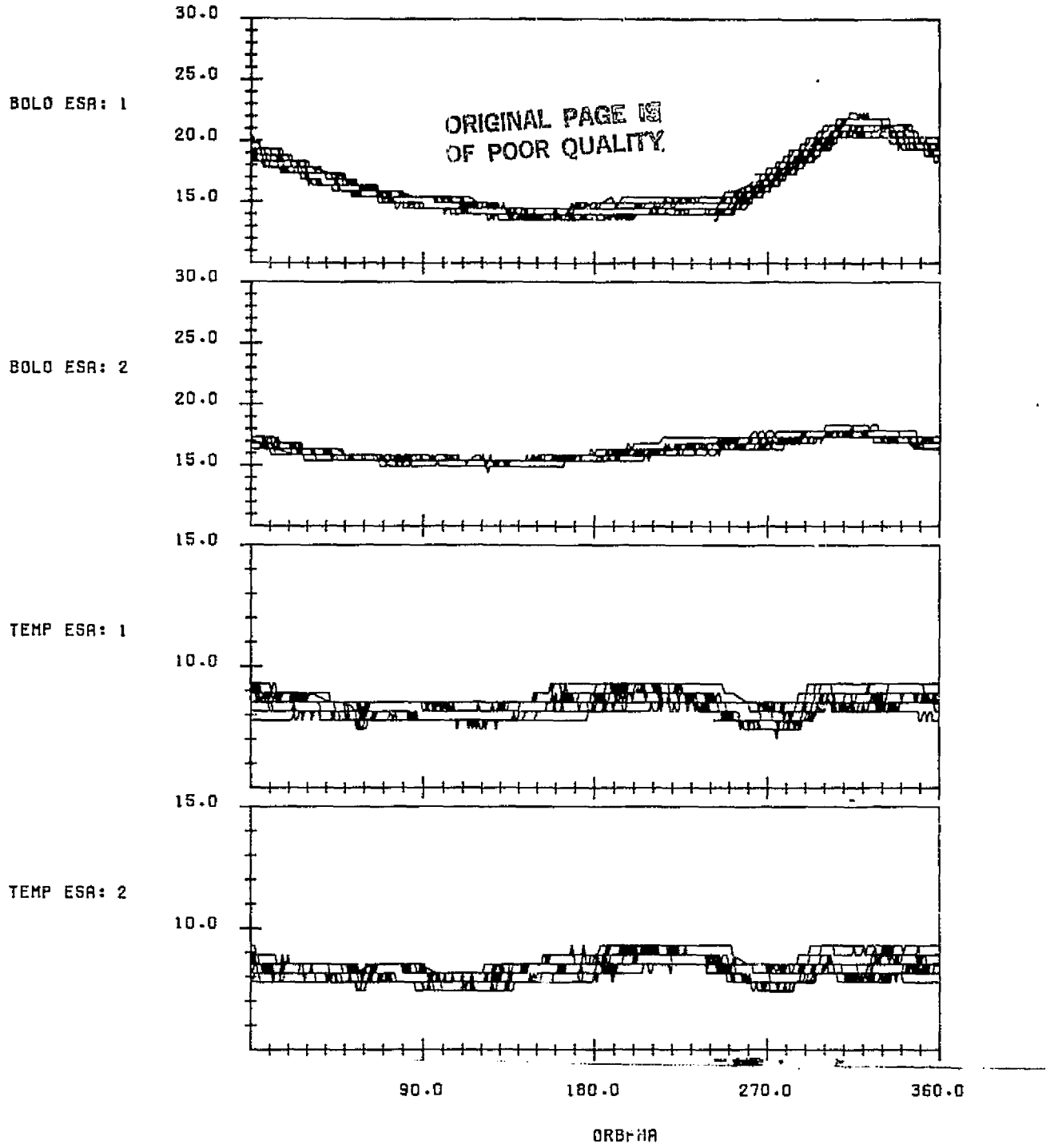

LANDSRT-4 CONICAL SCANNER BOLOMETER TEMPERATURE AND EARTH SENSOR ASSEMBLY HOUSING TEMPERATURE(DEGREES CELSIUS) VERSUS ORBIT PHASE FROM THE ASCENDING NODE WITH CONSECUTIVE ORBITS OVERLAID
DATA START TIME:821005.153123435
END TIME:821006.164427194

FIGURE B-5. Scanner Temperatures for Data Span on October 5-6, 1982

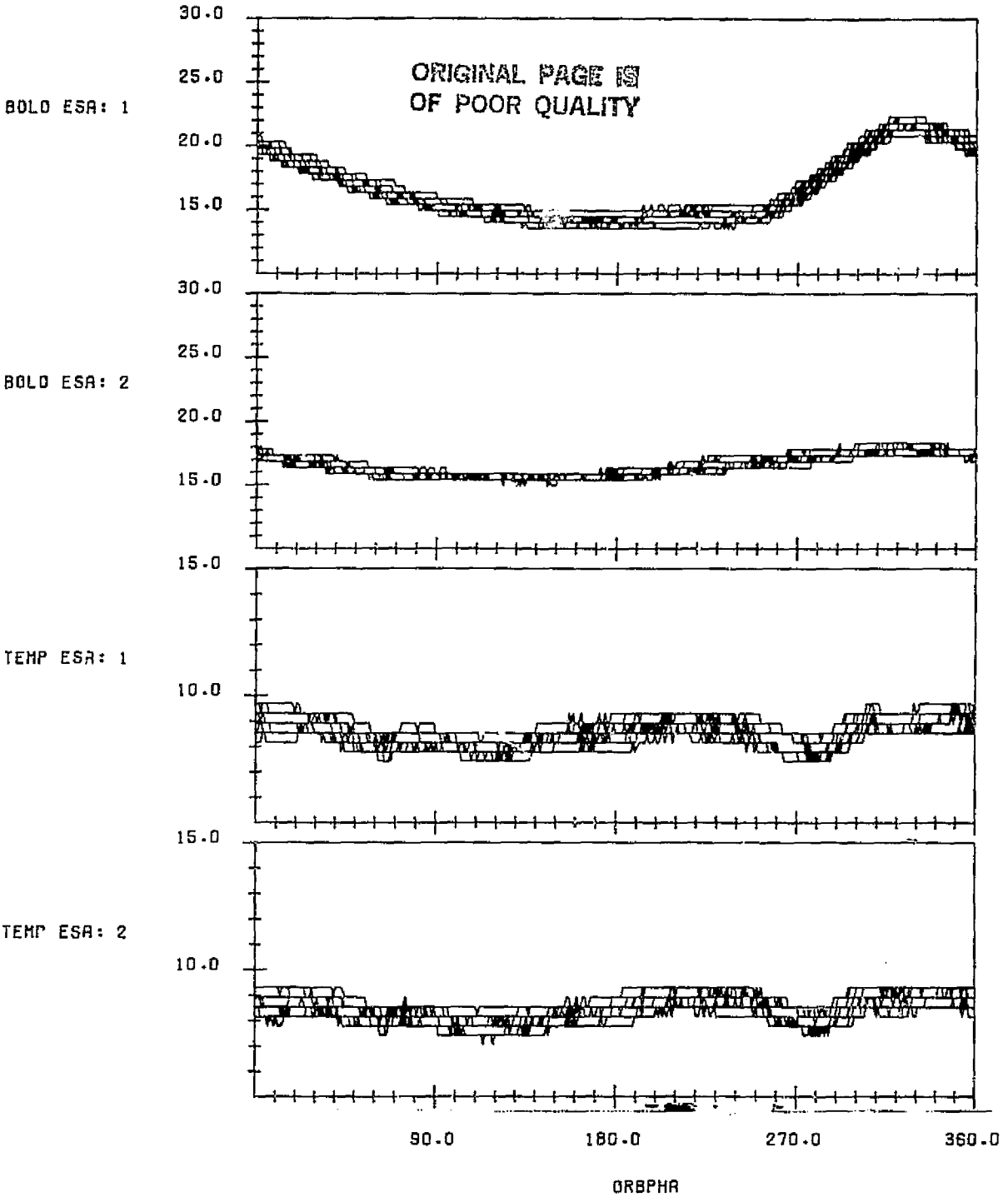

LANDSAT-4 CONICAL SCANNER BOLOMETER TEMPERATURE AND EARTH SENSOR ASSEMBLY HOUSING TEMPERATURE(DEGREES CELSIUS) VERSUS ORBIT PHASE FROM THE ASCENDING NODE WITH CONSECUTIVE ORBITS OVERLAID
DATA START TIME:821020.051211751
END TIME:821021.055456871

FIGURE B-6. Scanner Temperatures for Data Span on October 20-21, 1982

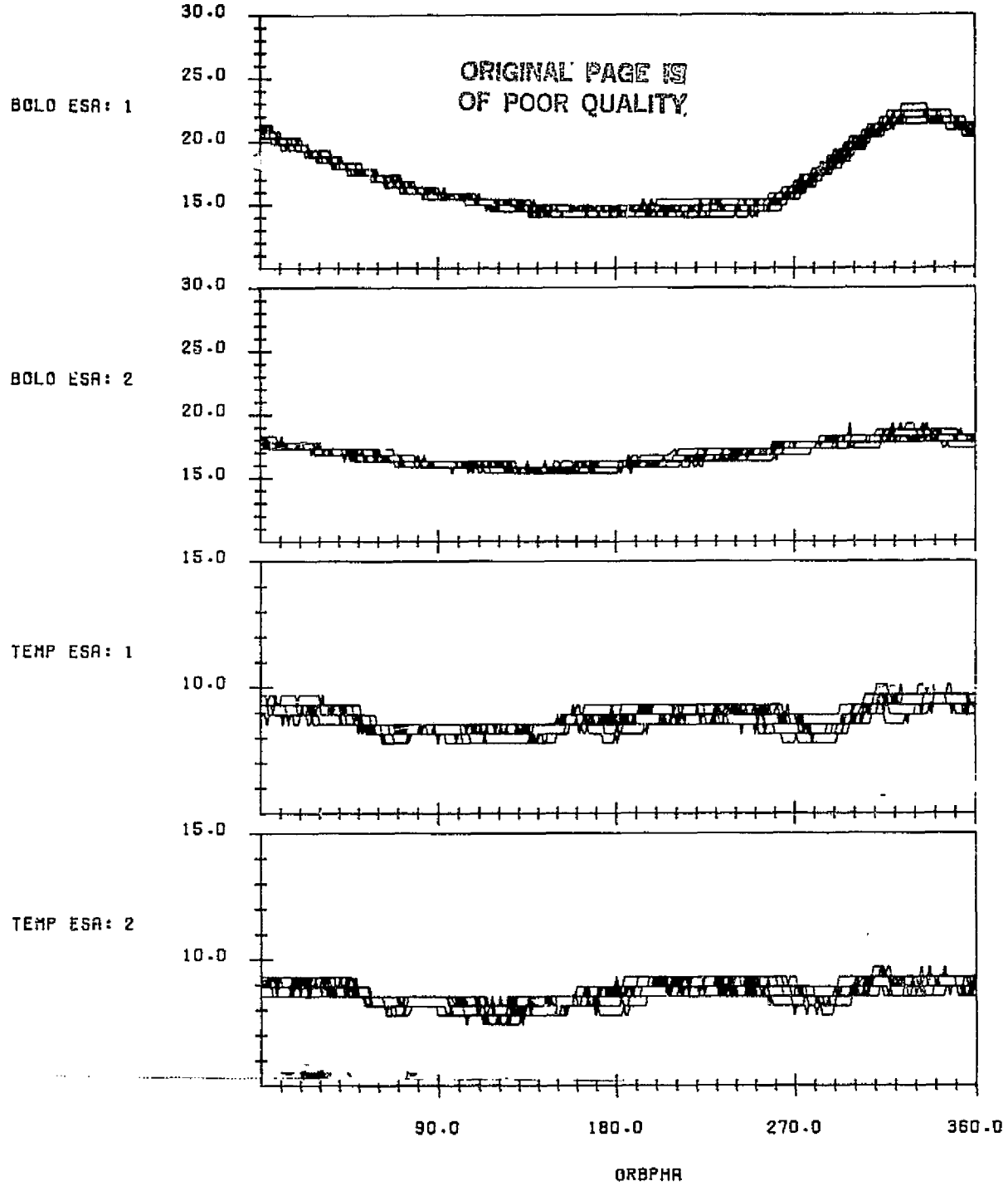

LANDSAT-4 CONICAL SCANNER BOLOMETER TEMPERATURE AND EARTH SENSOR ASSEMBLY HOUSING TEMPERATURE(DEGREES CELSIUS) VERSUS ORBIT PHASE FROM THE ASCENDING NODE WITH CONSECUTIVE ORBITS OVERLAID
DATA START TIME:821102.230736644
END TIME:821103.220936128

FIGURE B-7. Scanner Temperatures for Data Span on November 11-12, 1982

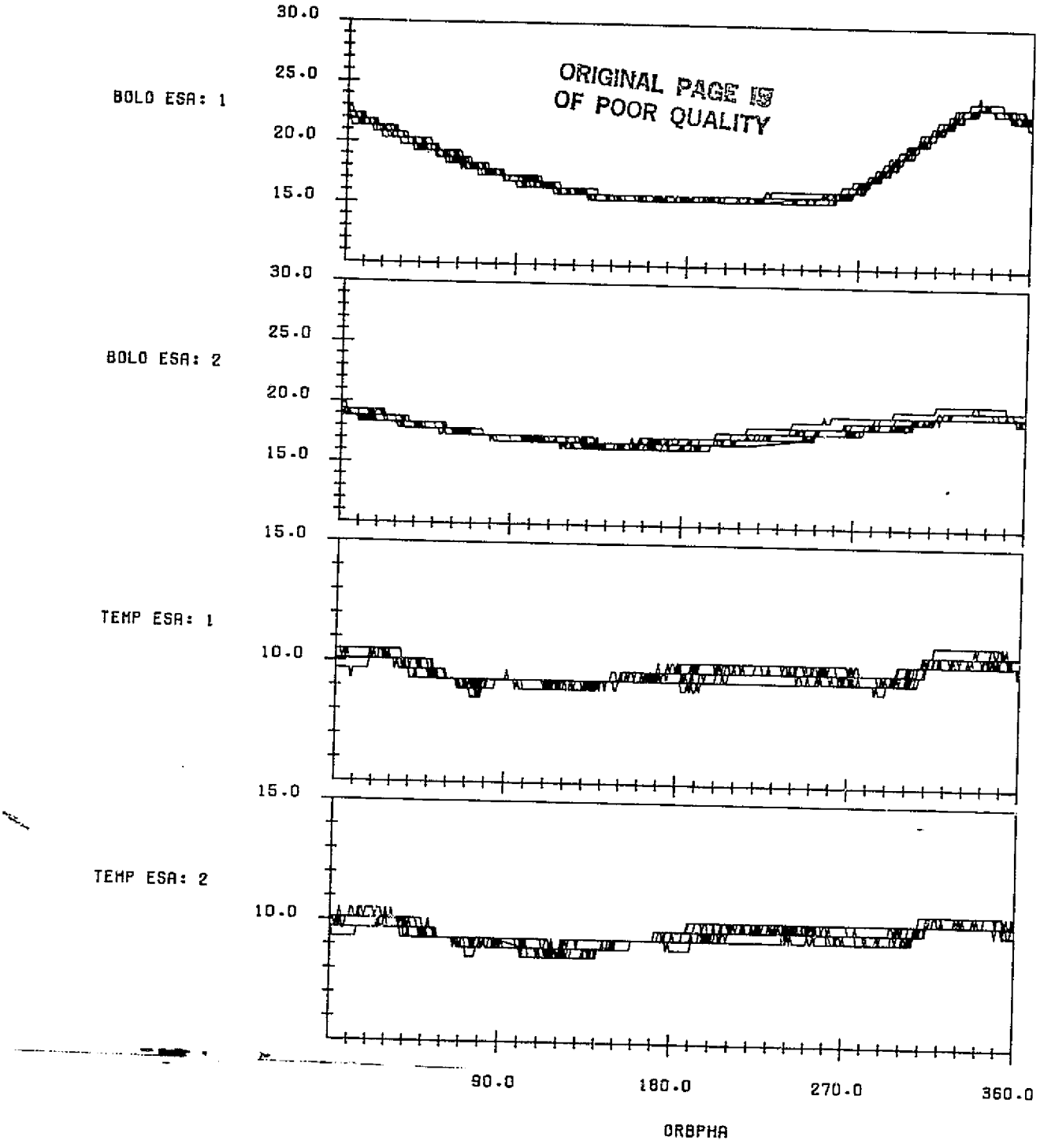

LANDSAT-4 CONICAL SCANNER BOLOMETER TEMPERATURE AND EARTH SENSOR ASSEMBLY HOUSING TEMPERATURE(DEGREES CELSIUS) VERSUS ORBIT PHASE FROM THE ASCENDING NODE WITH CONSECUTIVE ORBITS OVERLAID
DATA START TIME:821116.063354045
END TIME:821116.232203818

FIGURE B-8. Scanner Temperatures for Data Span on November 16, 1982

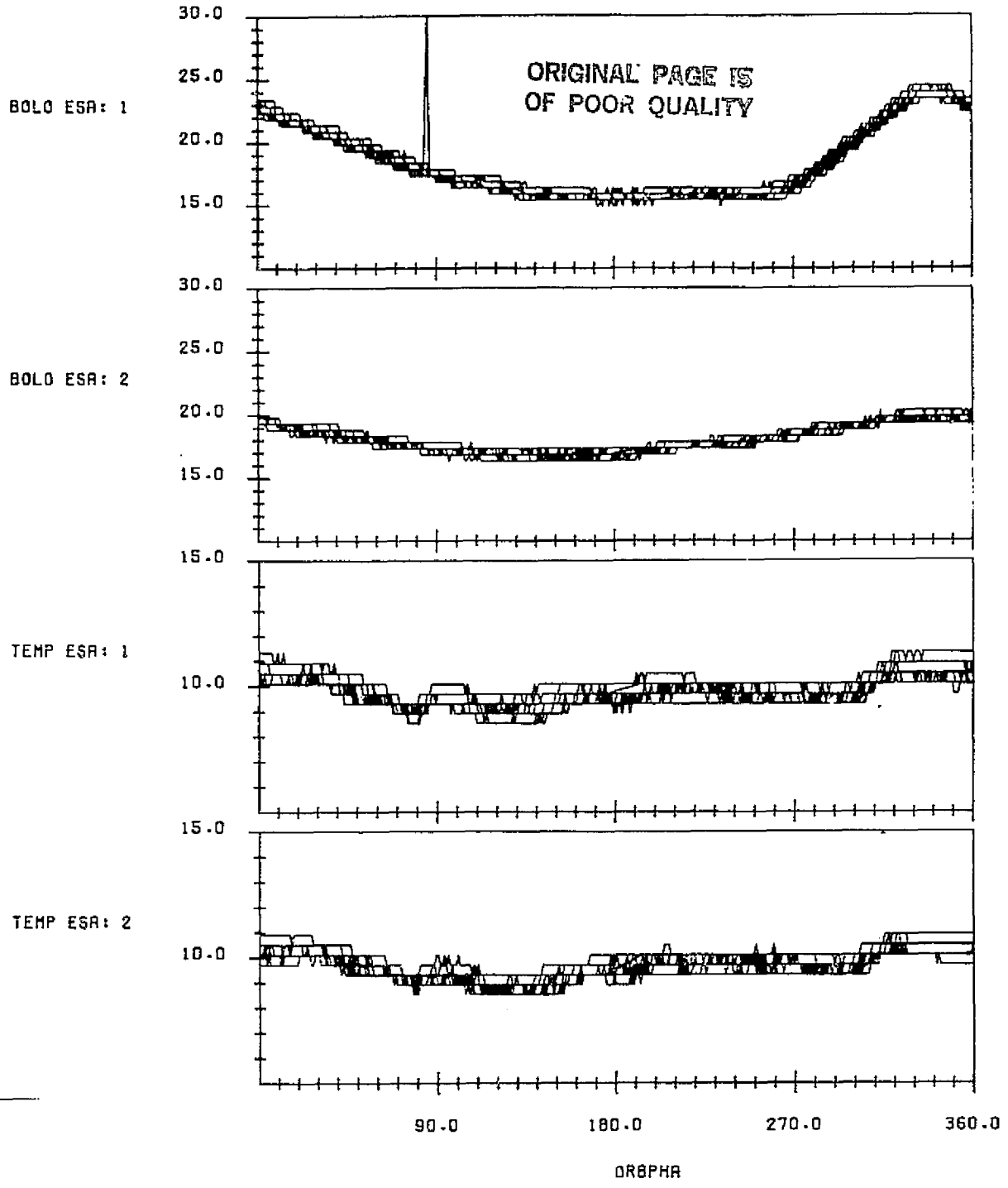

LANDSAT-4 CONICAL SCANNER BOLOMETER TEMPERATURE AND EARTH SENSOR ASSEMBLY HOUSING TEMPERATURE(DEGREES CELSIUS) VERSUS ORBIT PHASE FROM THE ASCENDING NODE WITH CONSECUTIVE ORBITS OVERLAID
DATA START TIME:821201.002856720
END TIME:821202.031150860

FIGURE B-9. Scanner Temperatures for Data Span on December 1-2, 1982

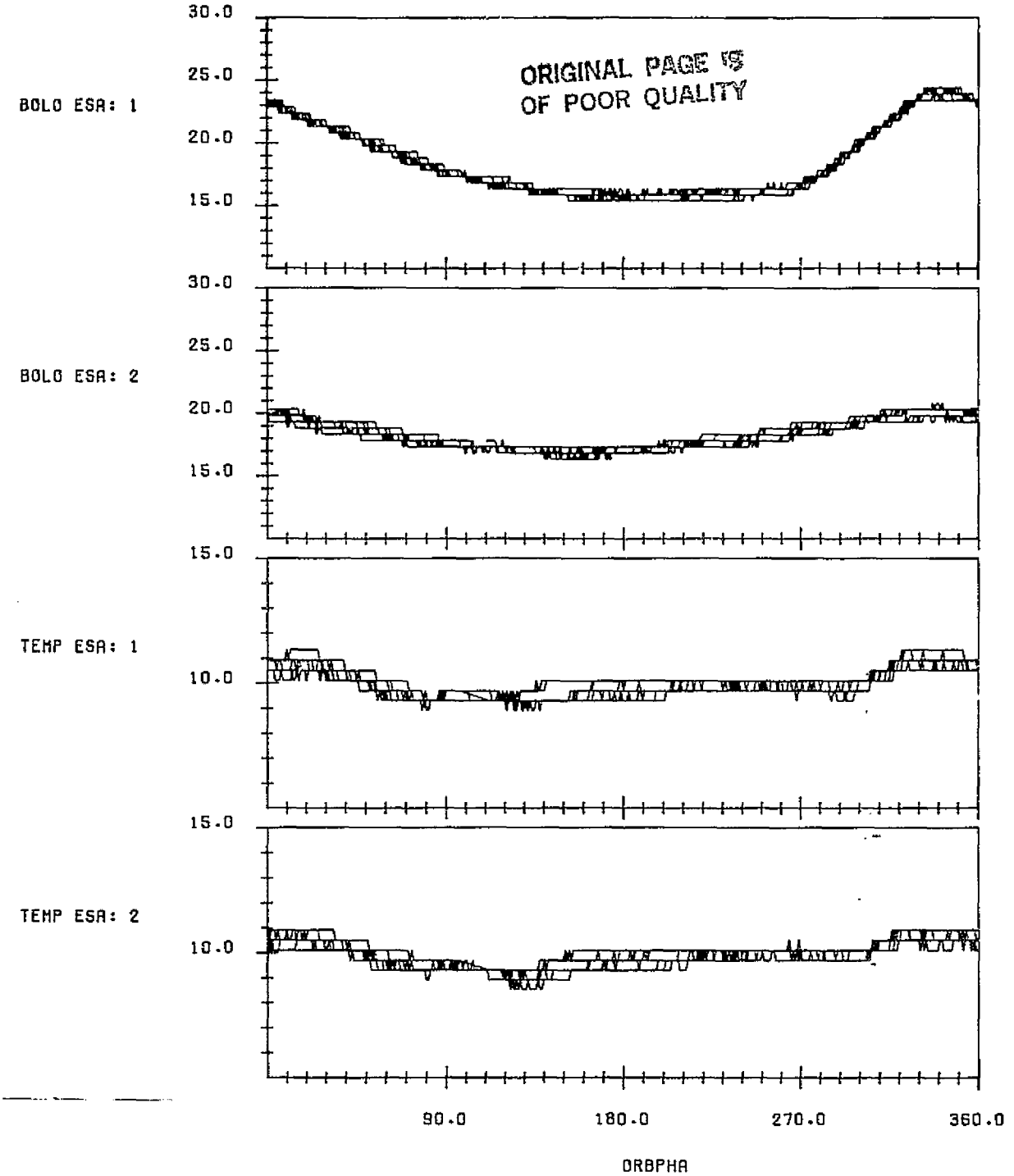

LANDSAT-4 CONICAL SCANNER BOLOMETER TEMPERATURE AND EARTH SENSOR ASSEMBLY HOUSING TEMPERATURE(DEGREES CELSIUS) VERSUS ORBIT PHASE FROM THE ASCENDING NODE WITH CONSECUTIVE ORBITS OVERLAID
DATA START TIME:821214.122607064
END TIME:821215.143809812

FIGURE B-10. Scanner Temperatures for Data Span on December 14-15, 1982

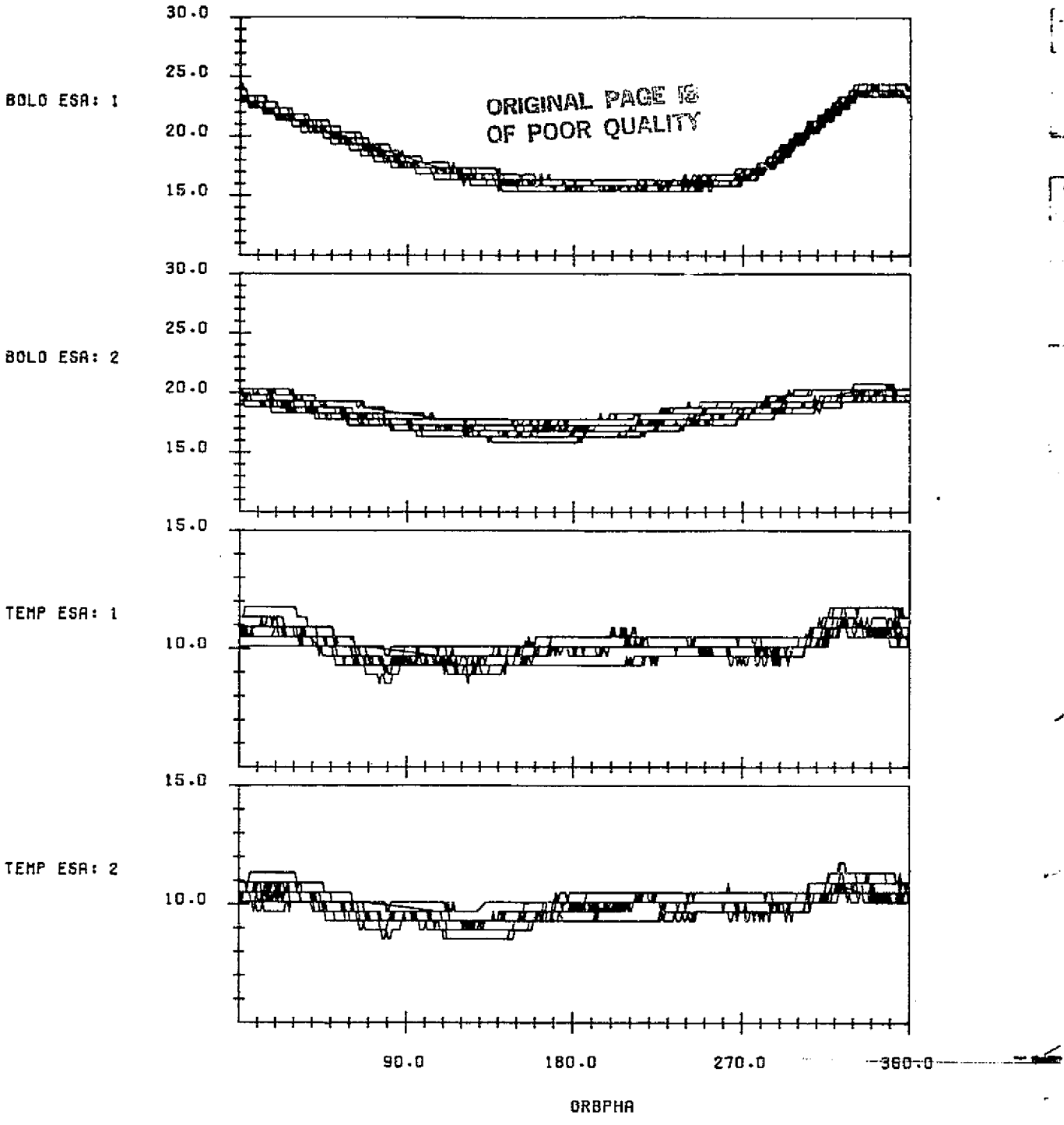

FIGURE B-11. Scanner Temperatures for Data Span on December 28-29, 1982

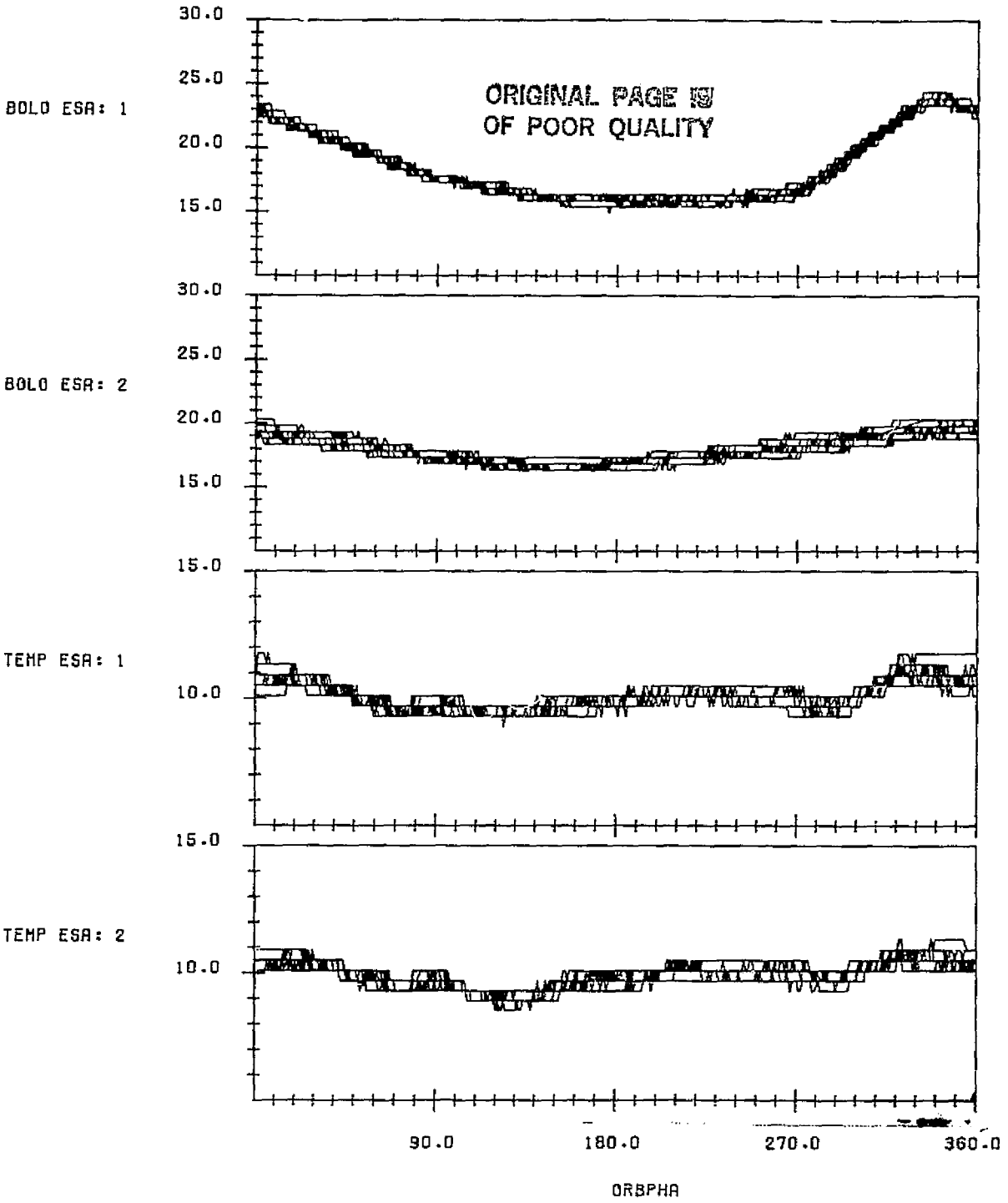

LANDSAT-4 CONICAL SCANNER BOLOMETER TEMPERATURE AND EARTH SENSOR ASSEMBLY HOUSING TEMPERATURE(DEGREES CELSIUS) VERSUS ORBIT PHASE FROM THE ASCENDING NODE WITH CONSECUTIVE ORBITS OVERLAID
DATA START TIME:830119.063608627
END TIME:830120.120626114

FIGURE B-12. Scanner Temperatures for Data Span on January 19-20, 1983

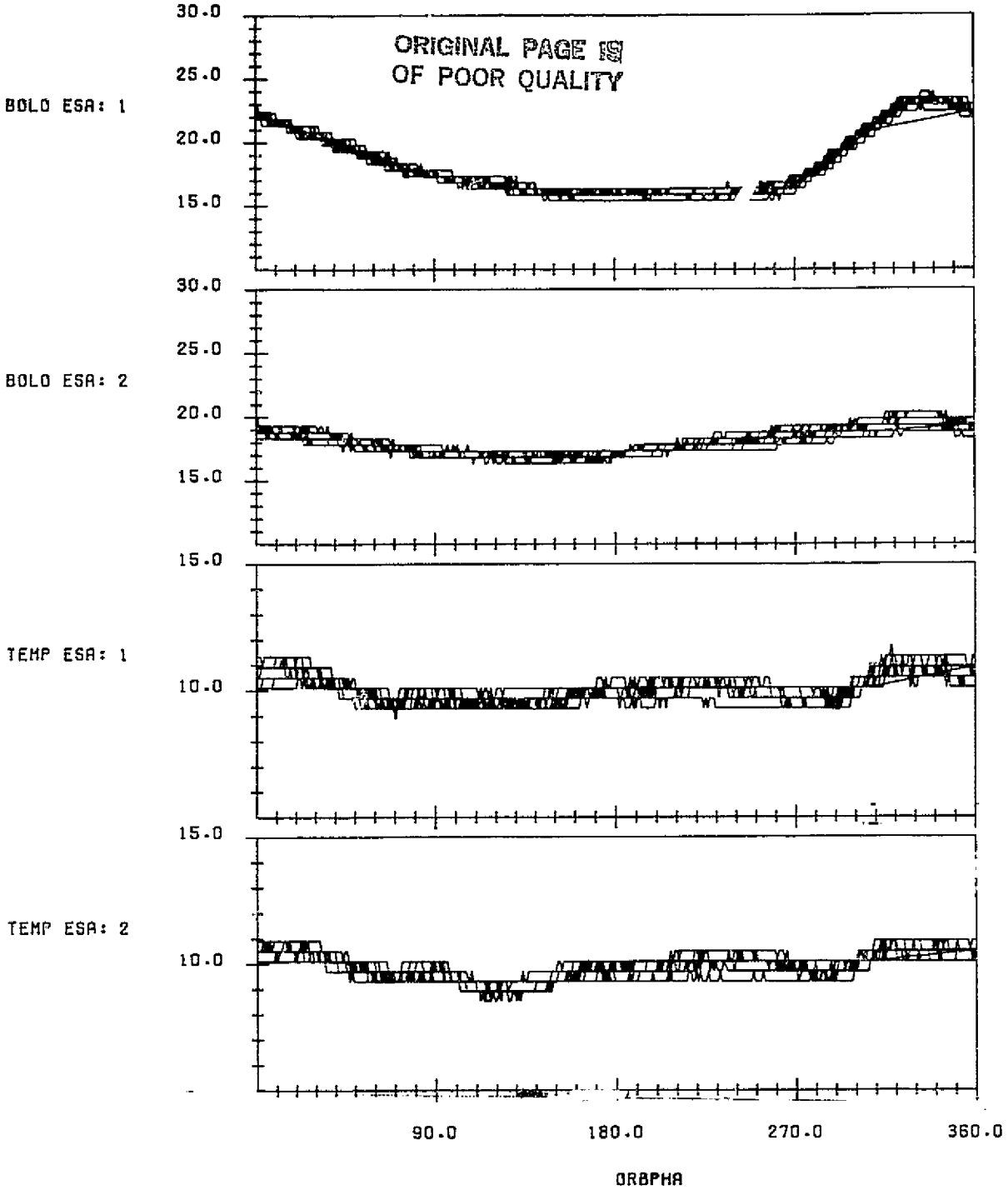

FIGURE B-13. Scanner Temperatures for Data Span on February 2-3, 1983

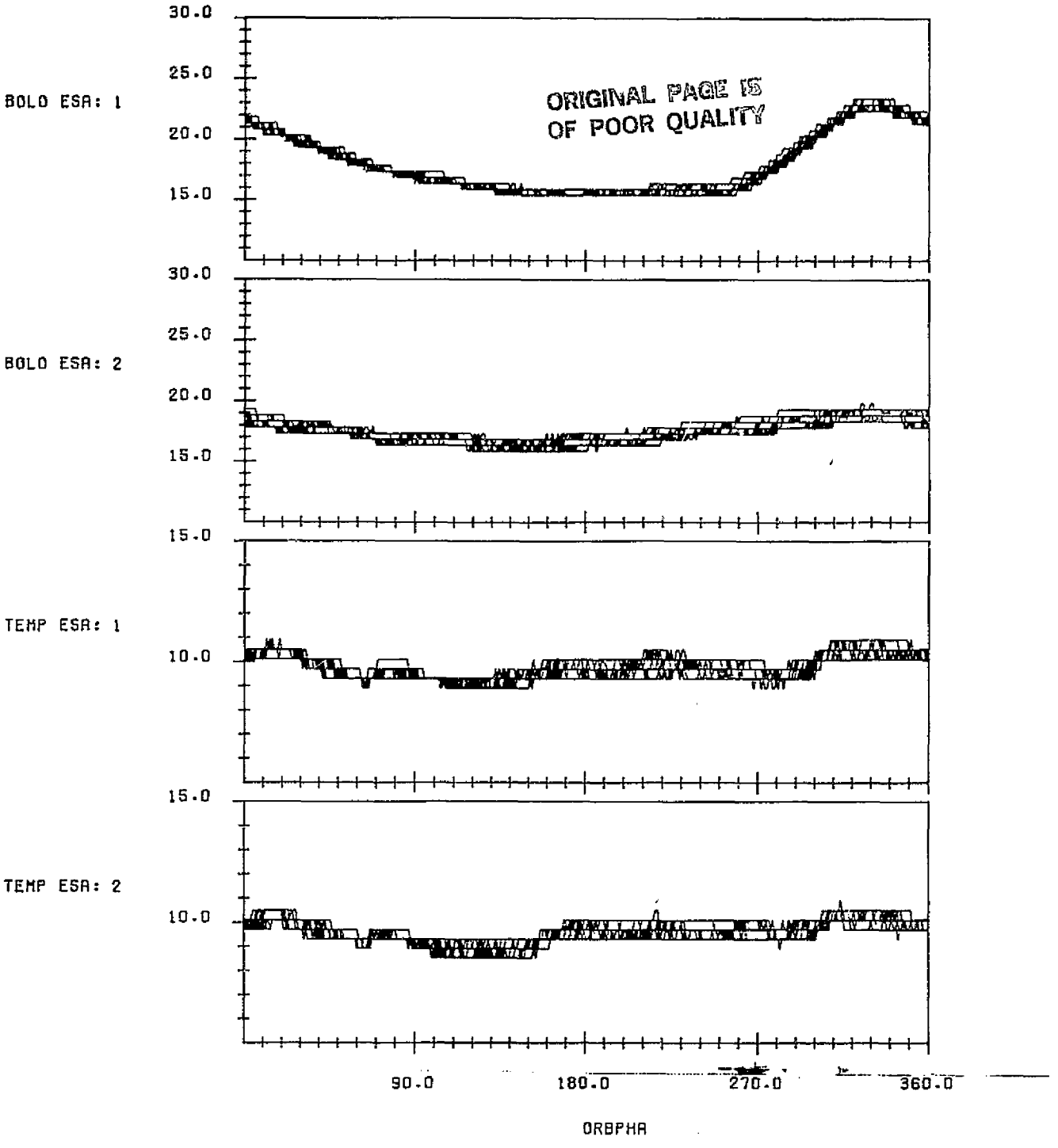

LANDSAT-4 CONICAL SCANNER BOLOMETER TEMPERATURE AND EARTH SENSOR ASSEMBLY HOUSING TEMPERATURE(DEGREES CELSIUS) VERSUS ORBIT PHASE FROM THE ASCENDING NODE WITH CONSECUTIVE ORBITS OVERLAID
DATA START TIME:830217.000122618
END TIME:830218.065513594

FIGURE B-14. Scanner Temperatures for Data Span on February 17018, 1983

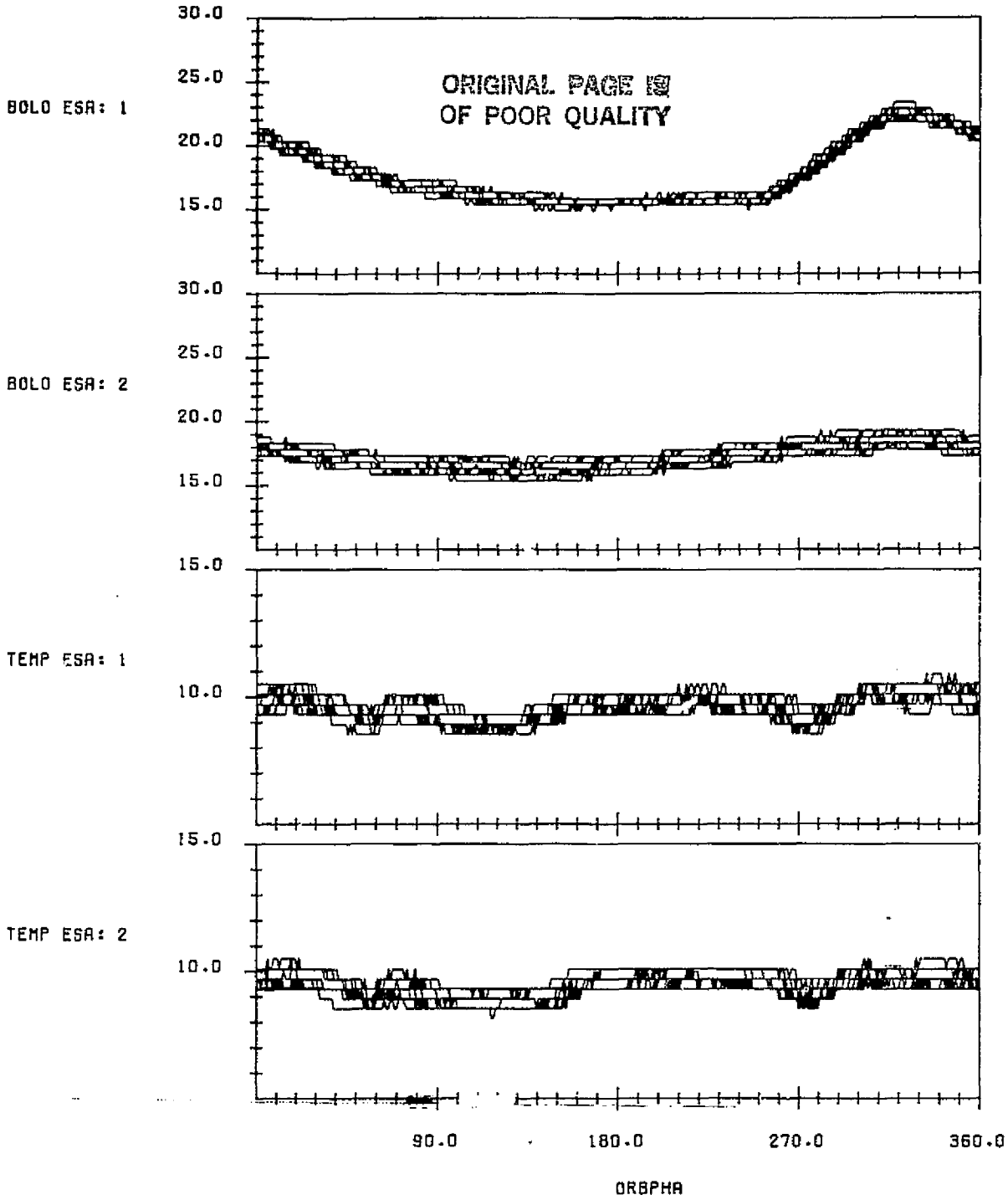

LANDSAT-4 CONICAL SCANNER BOLOMETER TEMPERATURE AND EARTH SENSOR ASSEMBLY HOUSING TEMPERATURE(DEGREES CELSIUS) VERSUS ORBIT PHASE FROM THE ASCENDING NODE WITH CONSECUTIVE ORBITS OVERLAID
DATA START TIME:830303.025744694
END TIME:830304.034257270

FIGURE B-15. Scanner Temperatures for Data Span on March 3-4, 1983

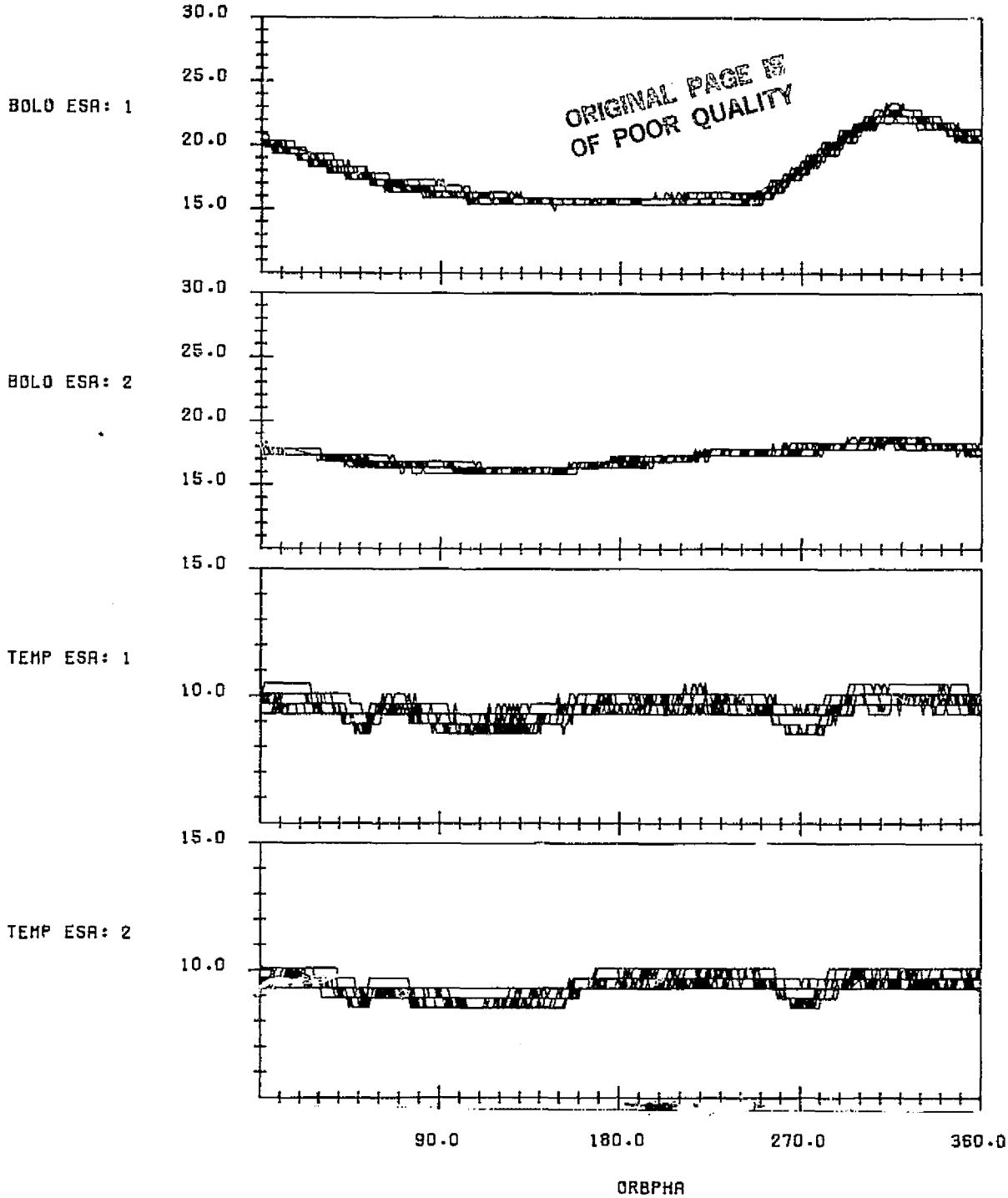

LANDSAT-4 CONICAL SCANNER BOLOMETER TEMPERATURE AND EARTH SENSOR ASSEMBLY HOUSING TEMPERATURE(DEGREES CELSIUS) VERSUS ORBIT PHASE FROM THE ASCENDING NODE WITH CONSECUTIVE ORBITS OVERLAID
DATA START TIME:830314.134603442
END TIME:830315.170127218

FIGURE B-16. Scanner Temperatures for Data Span on March 14-15, 1983

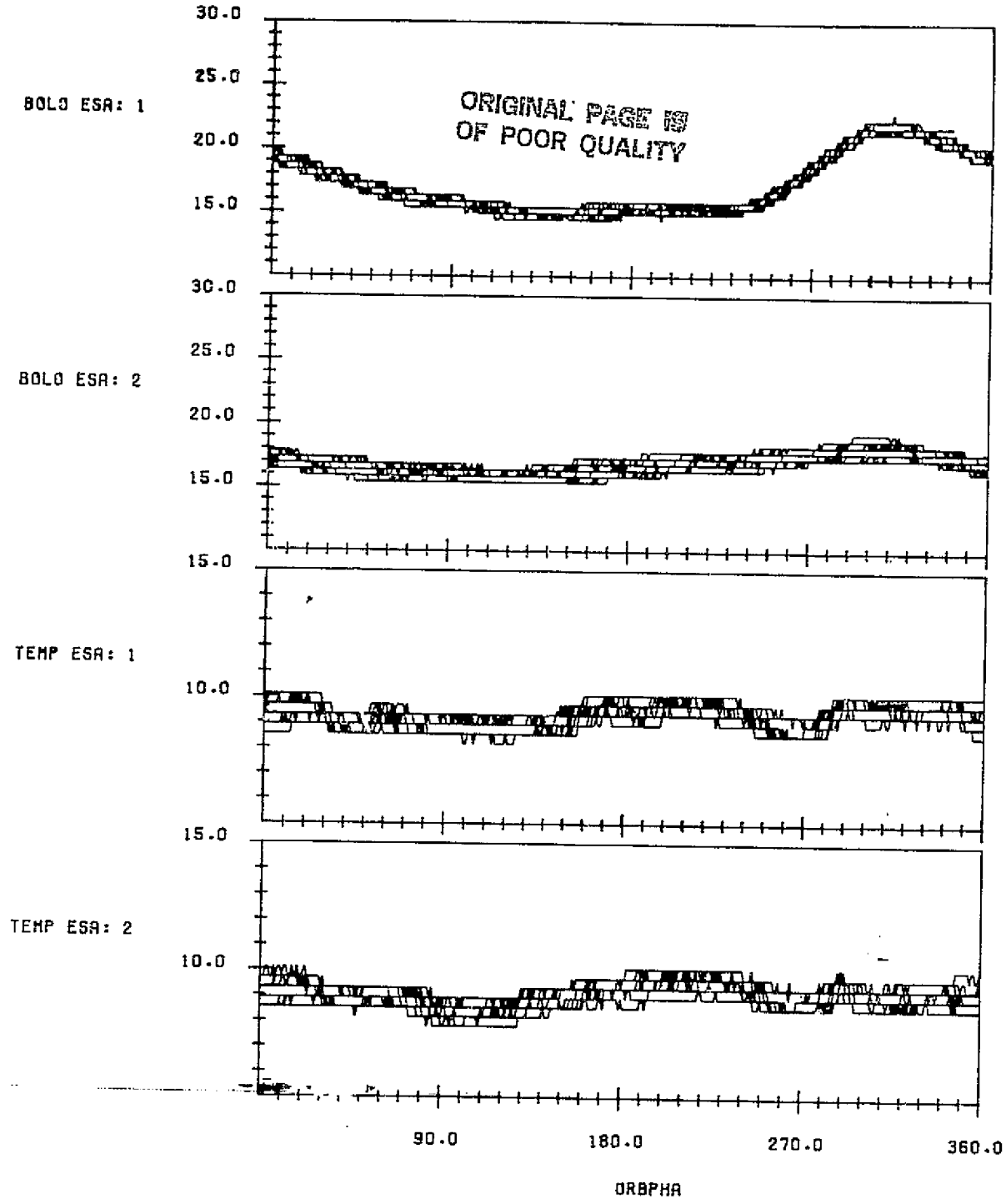

LANDSAT-4 CONICAL SCANNER BOLOMETER TEMPERATURE AND EARTH SENSOR ASSEMBLY HOUSING TEMPERATURE(DEGREES CELSIUS) VERSUS ORBIT PHASE FROM THE ASCENDING NODE WITH CONSECUTIVE ORBITS OVERLAID
DATA START TIME:830329.235506990
END TIME:830331.003946798

FIGURE B-17. Scanner Temperatures for Data Span on March 29-31, 1983

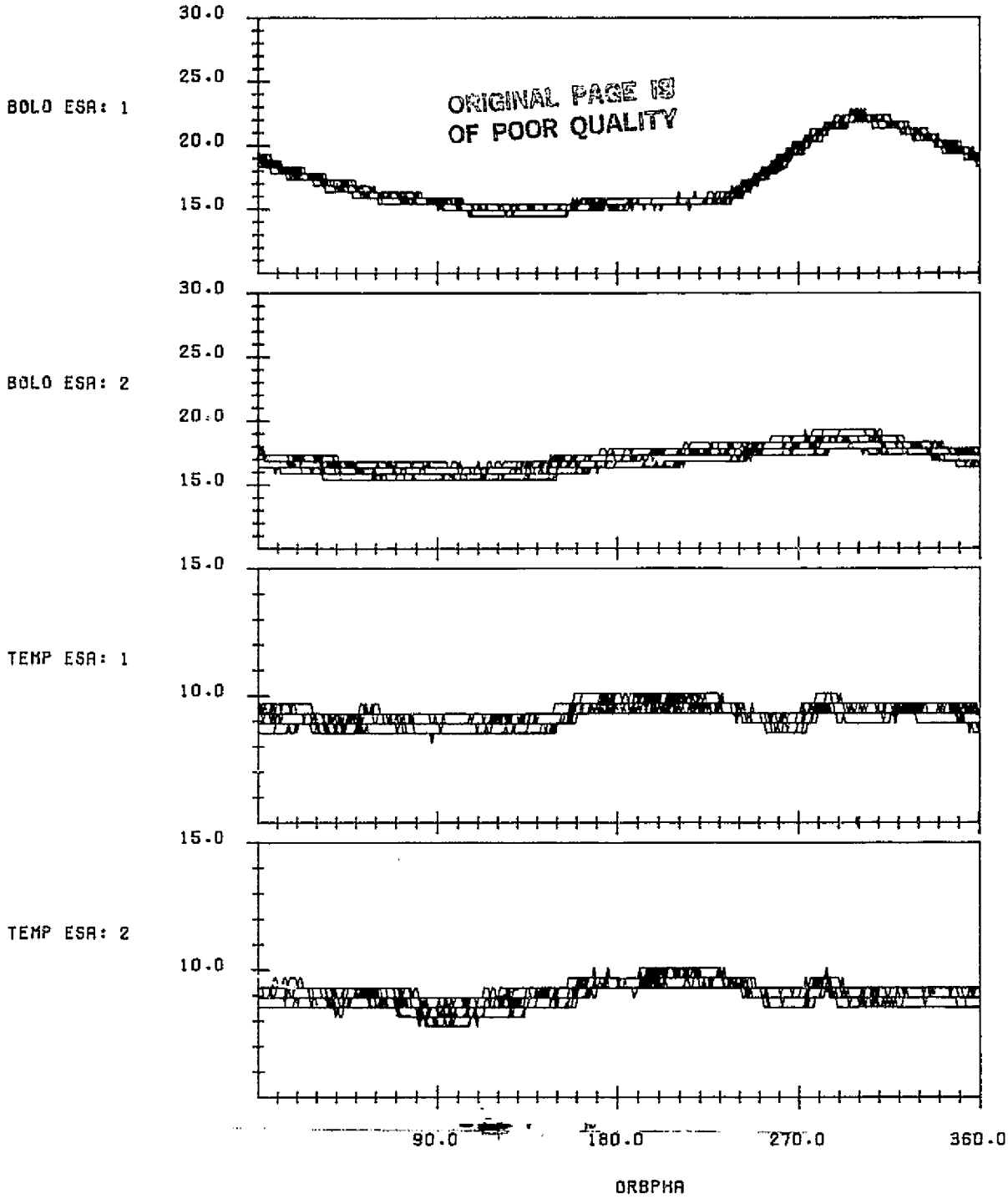

LANDSAT-4 CONICAL SCANNER BOLOMETER TEMPERATURE AND EARTH SENSOR ASSEMBLY HOUSING TEMPERATURE(DEGREES CELSIUS) VERSUS ORBIT PHASE FROM THE ASCENDING NODE WITH CONSECUTIVE ORBITS OVERLAID
DATA START TIME:830414.003417145
END TIME:830415.041837625

FIGURE B-18. Scanner Temperatures for Data Span on April 14-15, 1983

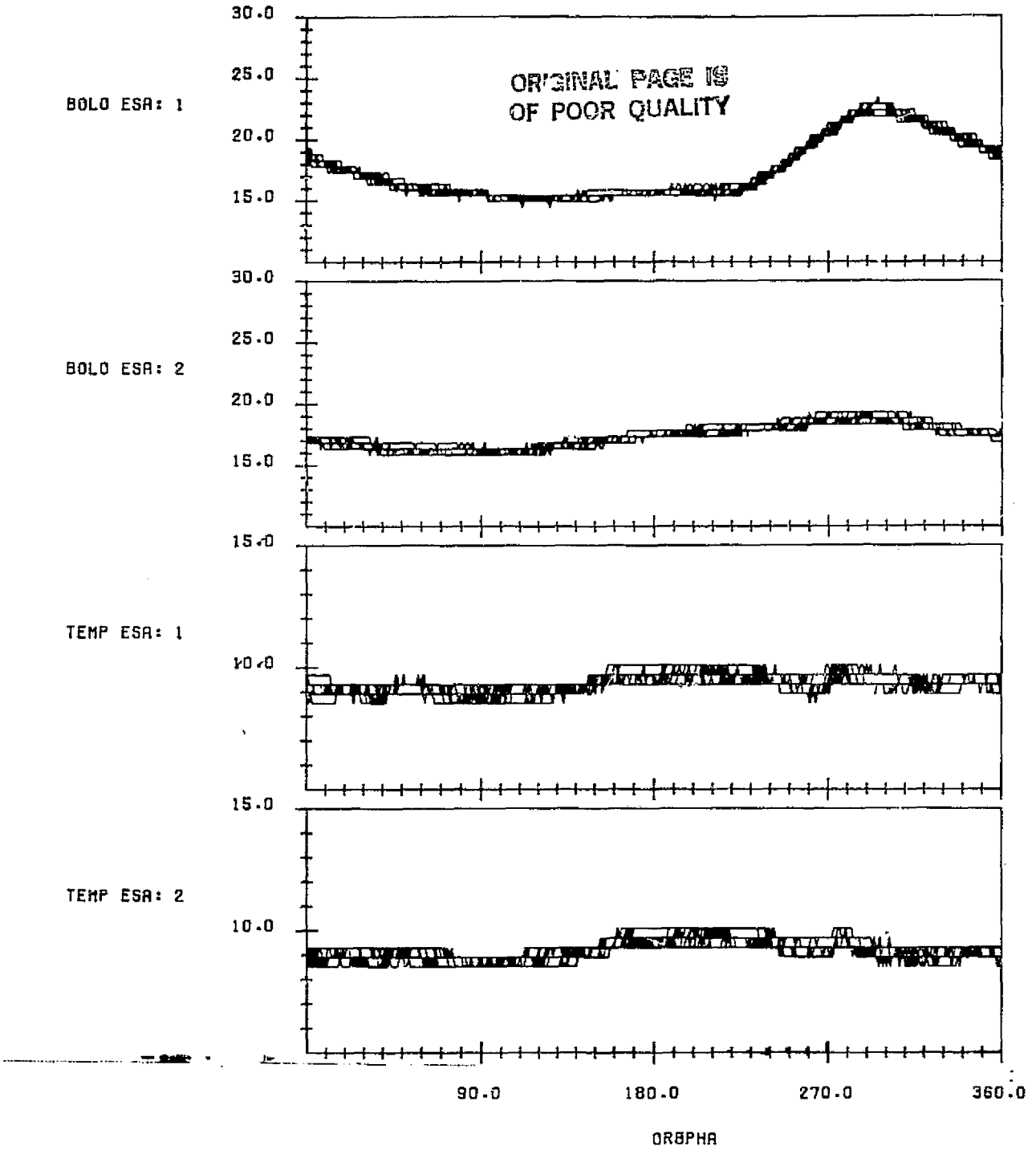

LANDSAT-4 CONICAL SCANNER BOLOMETER TEMPERATURE AND EARTH SENSOR ASSEMBLY HOUSING TEMPERATURE(DEGREES CELSIUS) VERSUS ORBIT PHASE FROM THE ASCENDING NODE WITH CONSECUTIVE ORBITS OVERLAID
DATA START TIME:830426.020419629
END TIME:830427.030700961

FIGURE B-19. Scanner Temperatures for Data Span on April 26-27, 1983

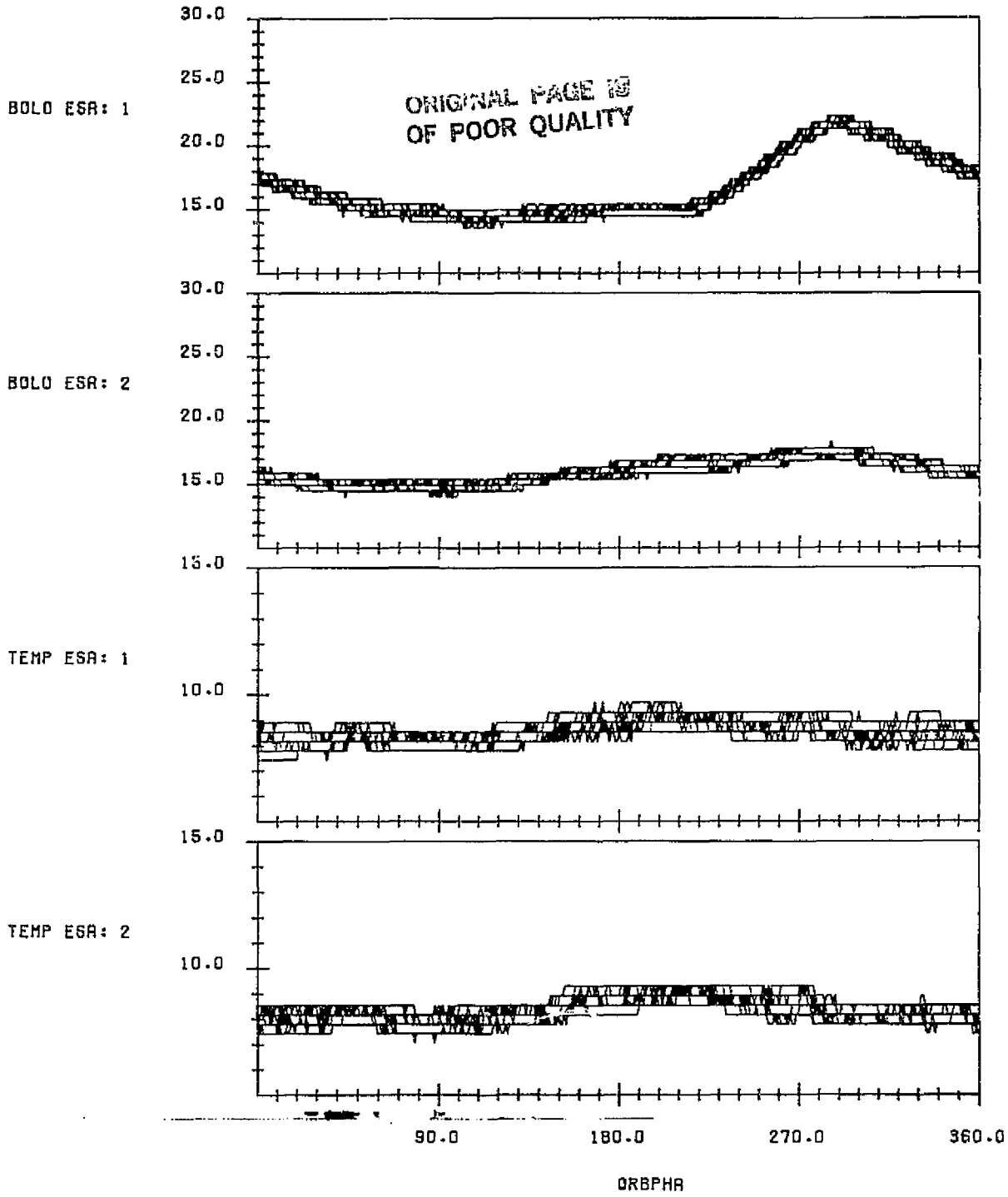

LANDSAT-4 CONICAL SCANNER BOLOMETER TEMPERATURE AND EARTH SENSOR ASSEMBLY HOUSING TEMPERATURE(DEGREES CELSIUS) VERSUS ORBIT PHASE FROM THE ASCENDING NODE WITH CONSECUTIVE ORBITS OVERLAID
DATA START TIME:830511.001602609
END TIME:830512.022204864

FIGURE B-20. Scanner Temperatures for Data Span on May 11-12, 1983

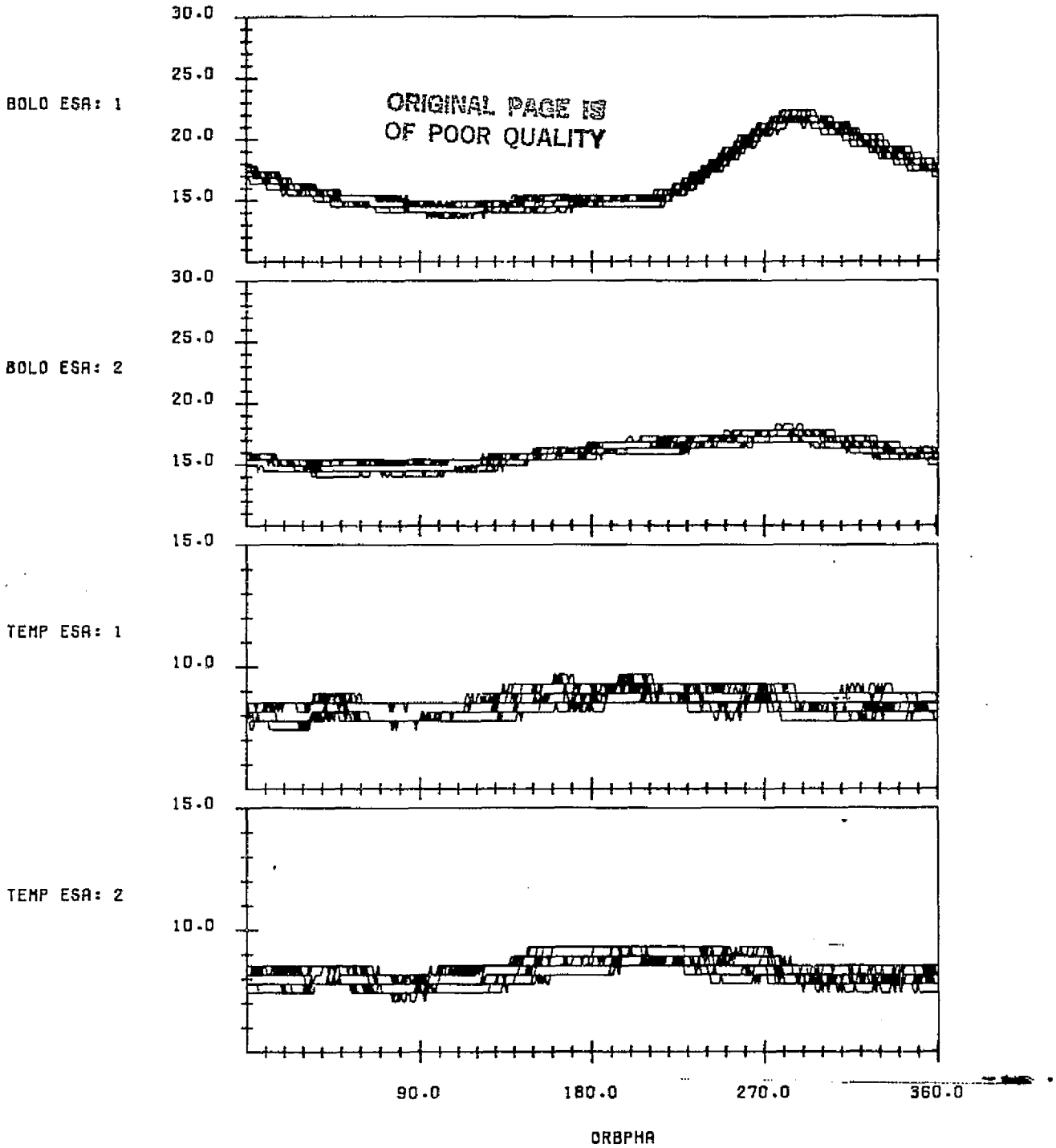

LANDSAT-4 CONICAL SCANNER BOLOMETER TEMPERATURE AND EARTH SENSOR ASSEMBLY HOUSING TEMPERATURE(DEGREES CELSIUS) VERSUS ORBIT PHASE FROM THE ASCENDING NODE WITH CONSECUTIVE ORBITS OVERLAID
DATA START TIME:830523.004000365
END TIME:830524.042404476

FIGURE B-21. Scanner Temperatures for Data Span on May 23-24, 1983

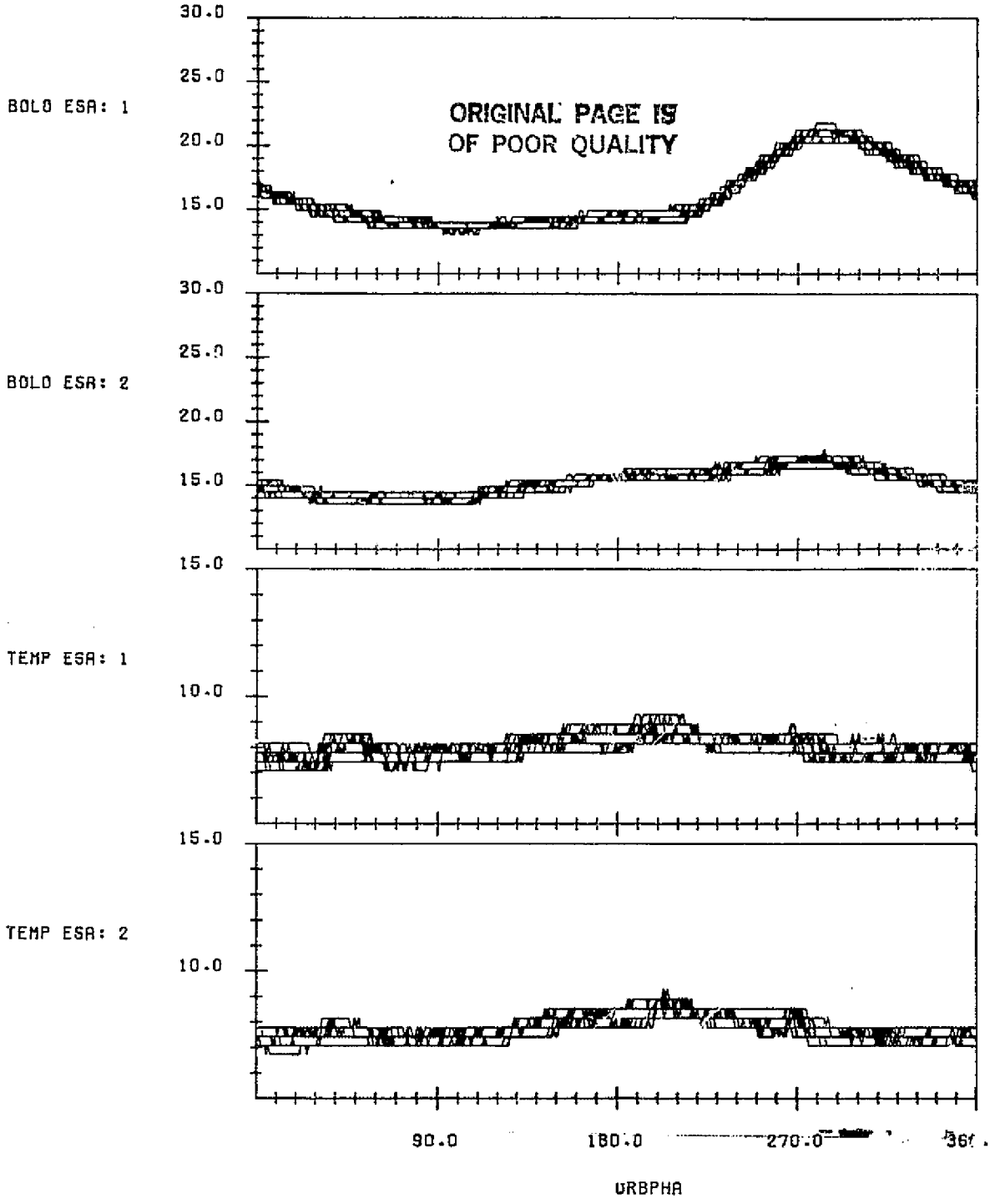

LANDSAT-4 CONICAL SCANNER BOLOMETER TEMPERATURE AND EARTH SENSOR ASSEMBLY HOUSING TEMPERATURE(DEGREES CELSIUS) VERSUS ORBIT PHASE FROM THE ASCENDING NODE WITH CONSECUTIVE ORBITS OVERLAID
DATA START TIME:830606.002351736
END TIME:830607.025956216

FIGURE B-22. Scanner Temperatures for Data Span on June 6-7, 1983

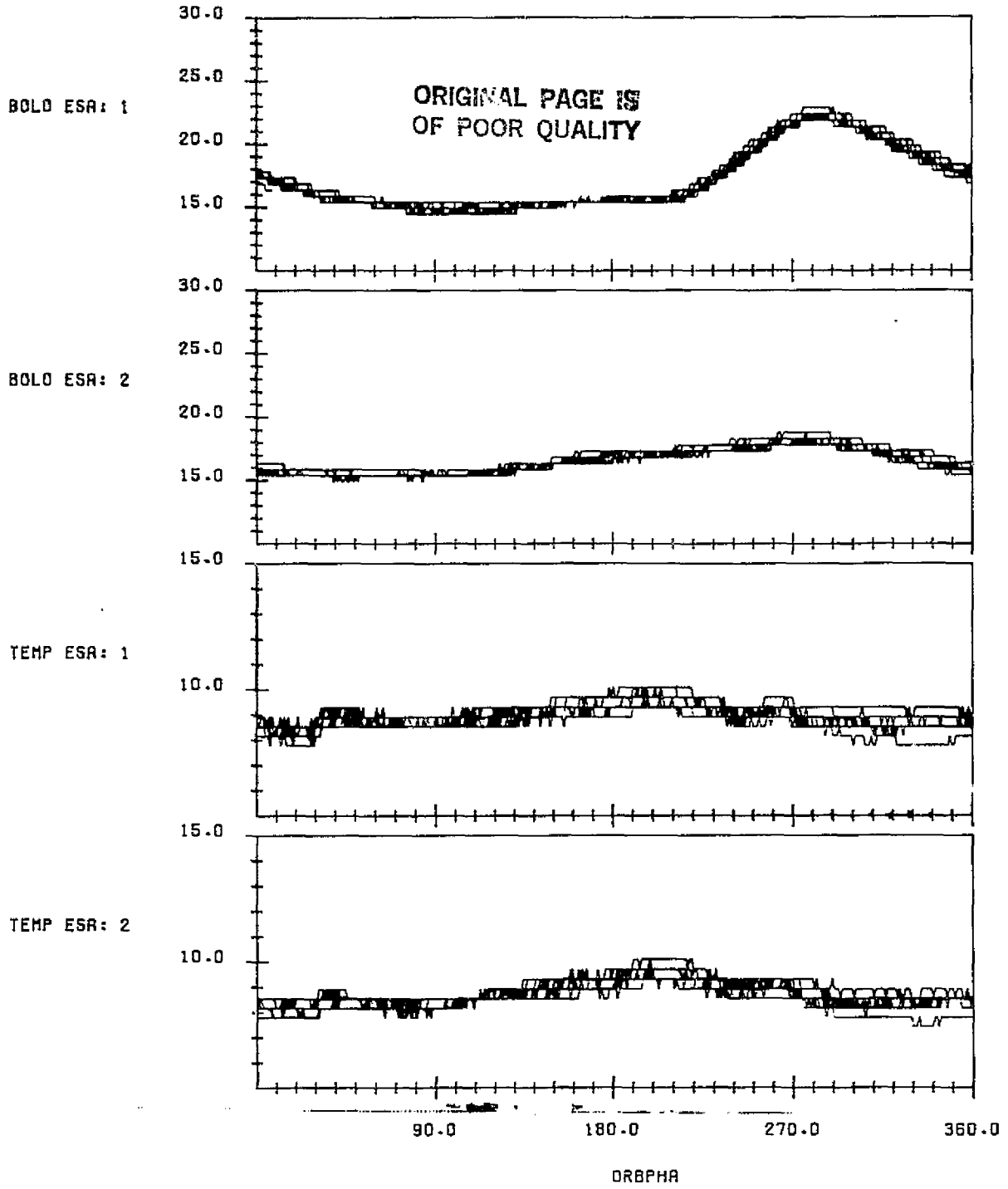

LANDSAT-4 CONICAL SCANNER BOLOMETER TEMPERATURE AND EARTH SENSOR ASSEMBLY HOUSING TEMPERATURE(DEGREES CELSIUS) VERSUS ORBIT PHASE FROM THE ASCENDING NODE WITH CONSECUTIVE ORBITS OVERLAID
DATA START TIME:830621.225929155
END TIME:830623.012243587

FIGURE B-23. Scanner Temperatures for Data Span on June 21-23, 1983

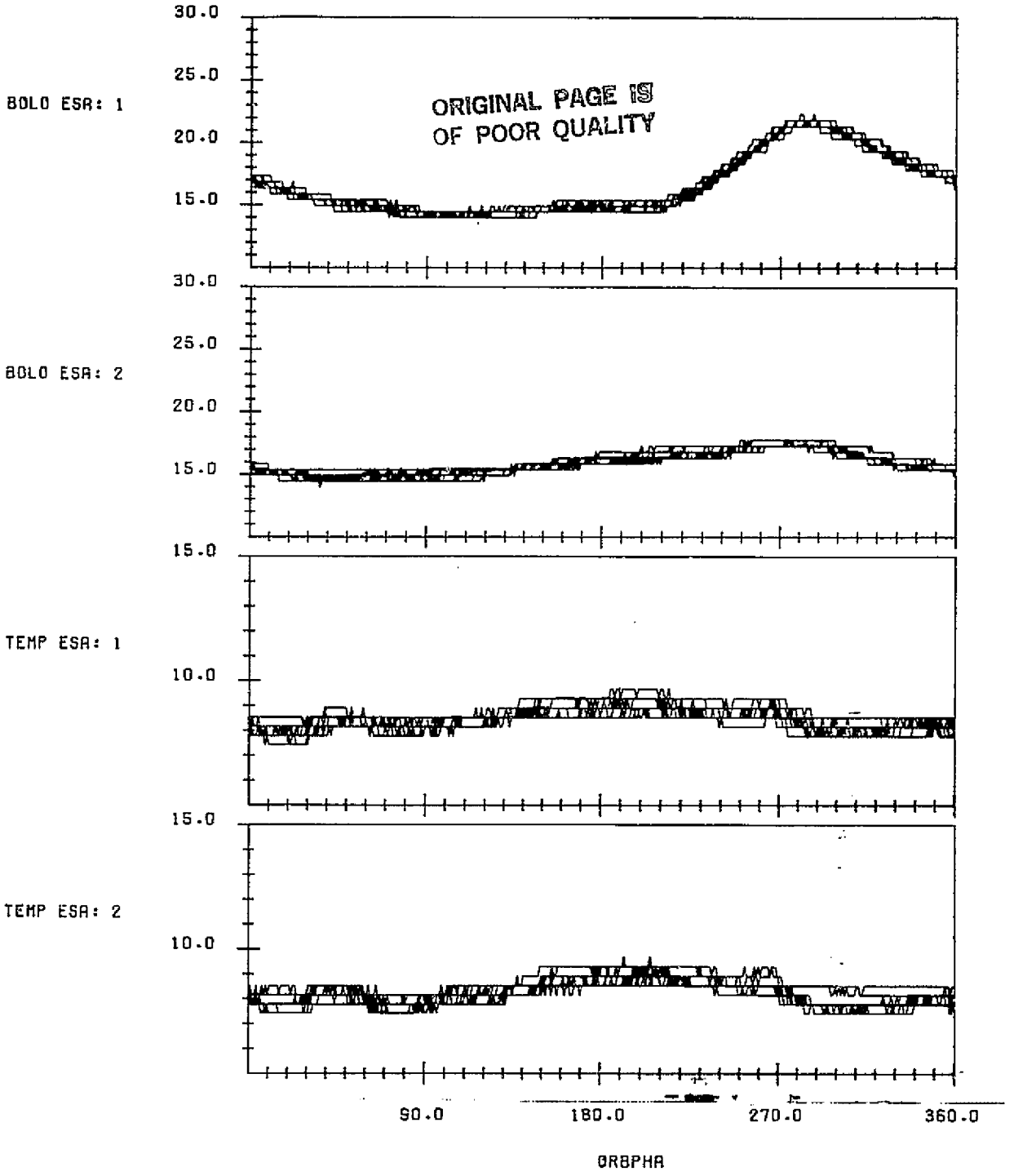

LANDSAT-4 CONICAL SCANNER BOLOMETER TEMPERATURE AND EARTH SENSOR ASSEMBLY HOUSING TEMPERATURE(DEGREES CELSIUS) VERSUS ORBIT PHASE FROM THE ASCENDING NODE WITH CONSECUTIVE ORBITS OVERLAID
DATA START TIME:830706.154825062
END TIME:830707.182940838

FIGURE B-24. Scanner Temperatures for Data Span on July 6-7, 1983

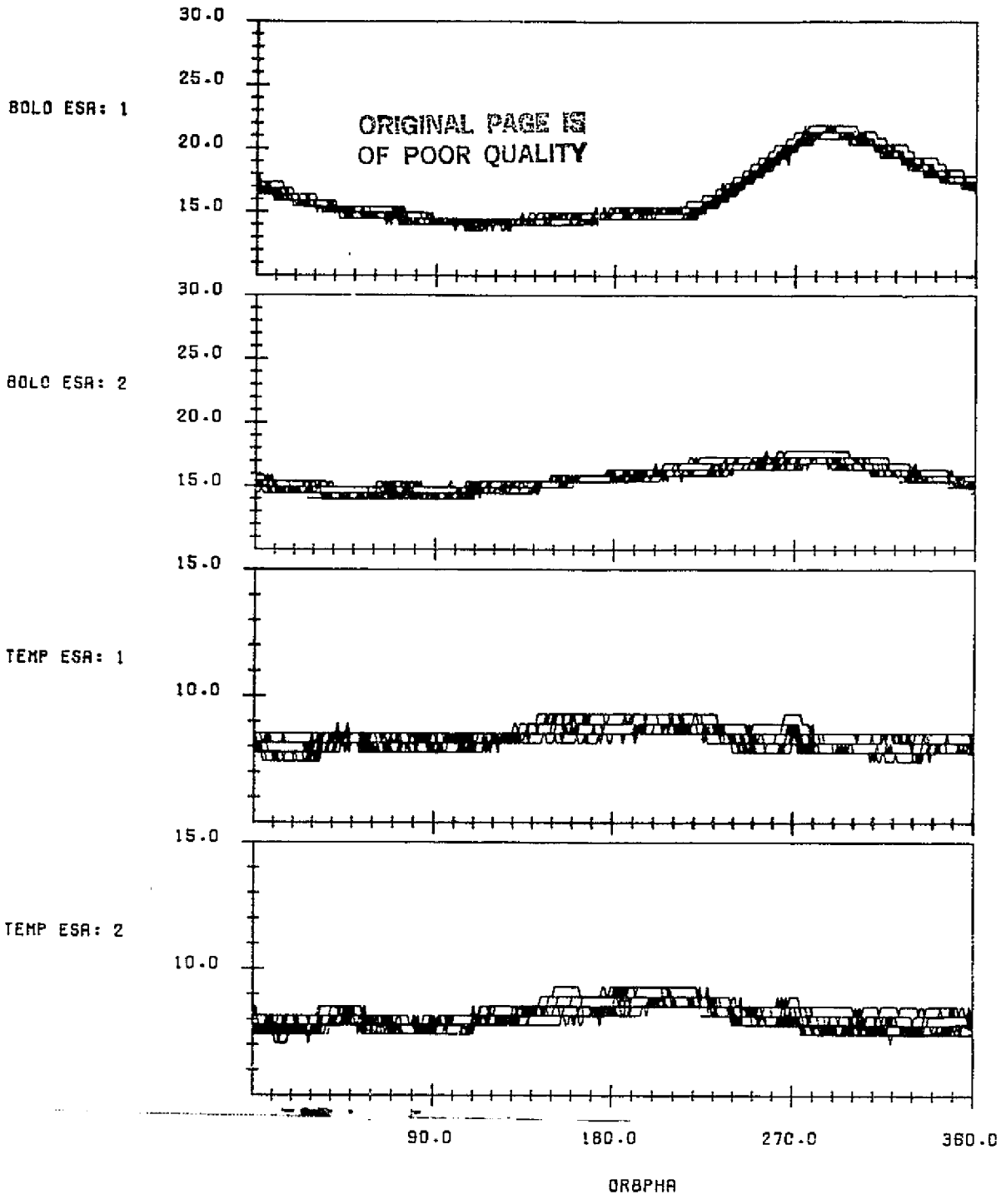

LANDSAT-4 CONICAL SCANNER BOLOMETER TEMPERATURE AND EARTH SENSOR ASSEMBLY HOUSING TEMPERATURE(DEGREES CELSIUS) VERSUS ORBIT PHASE FROM THE ASCENDING NODE WITH CONSECUTIVE ORBITS OVERLAID
DATA START TIME:830726.004016064
END TIME:830727.061244608

FIGURE B-25. Scanner Temperatures for Data Span on July 26-27, 1983

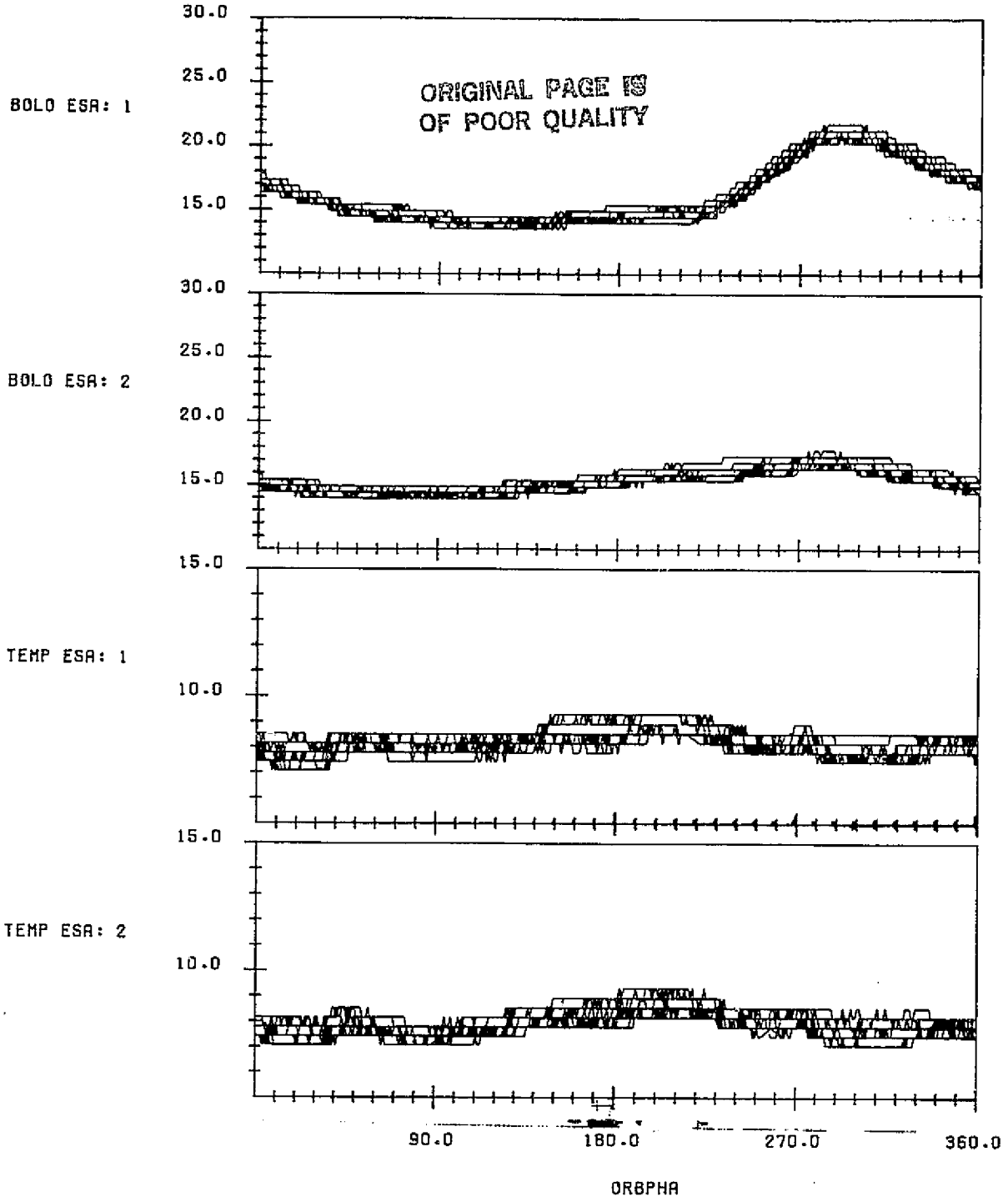

LANDSAT-4 CONICAL SCANNER BOLOMETER TEMPERATURE AND EARTH SENSOR ASSEMBLY HOUSING TEMPERATURE(DEGREES CELSIUS) VERSUS ORBIT PHASE FROM THE ASCENDING NODE WITH CONSECUTIVE ORBITS OVERLAID
DATA START TIME:830806.134523196
END TIME:830807.174517564

FIGURE B-26. Scanner Temperatures for Data Span on August 6-7, 1983

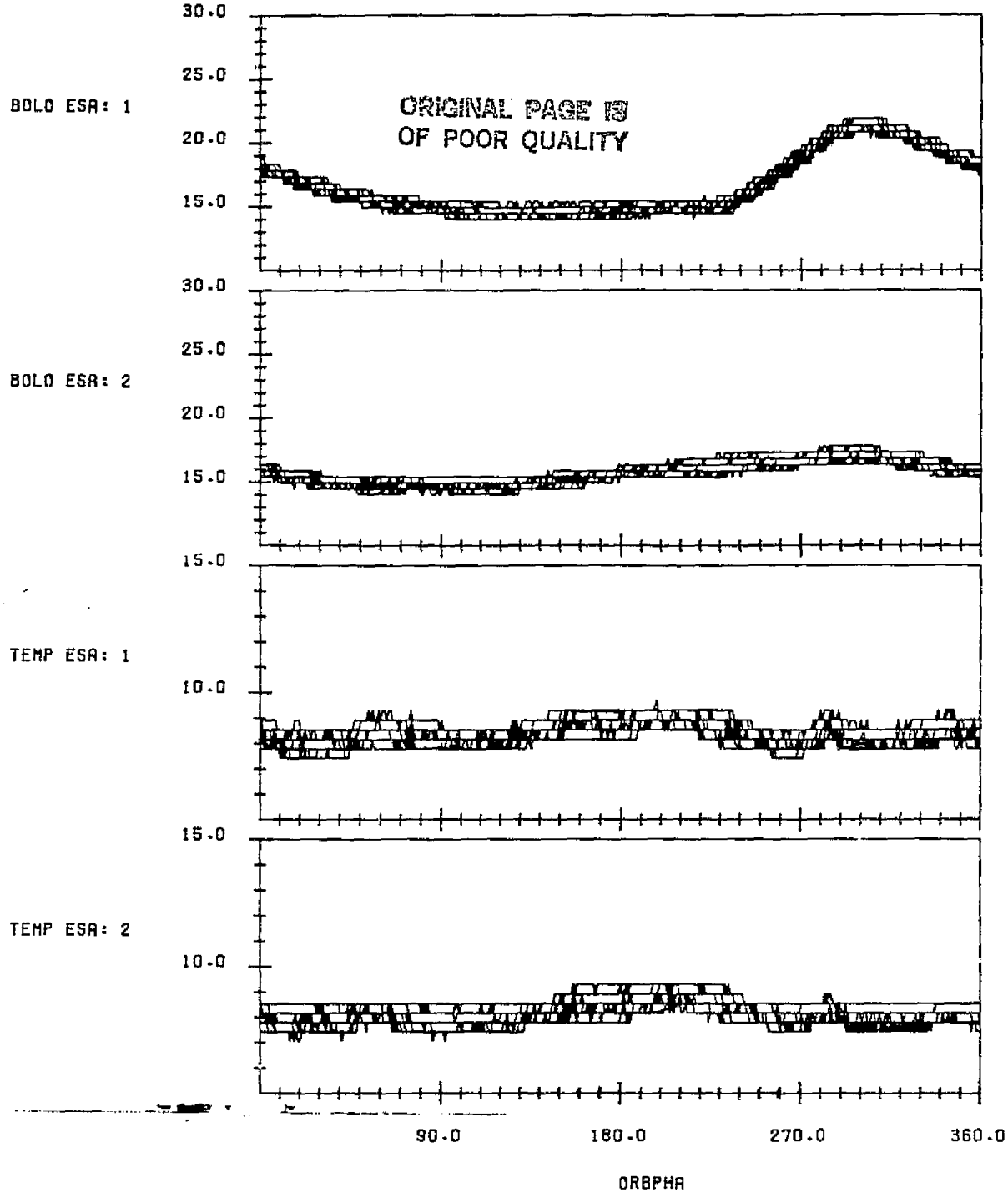

LANDSAT-4 CONICAL SCANNER BOLOMETER TEMPERATURE AND EARTH SENSOR ASSEMBLY HOUSING TEMPERATURE(DEGREES CELSIUS) VERSUS ORBIT PHASE FROM THE ASCENDING NODE WITH CONSECUTIVE ORBITS OVERLAID
DATA START TIME:830831.001456628
END TIME:830901.041150787

FIGURE B-27. Scanner Temperatures for Data Span on August 31 - September 1, 1983

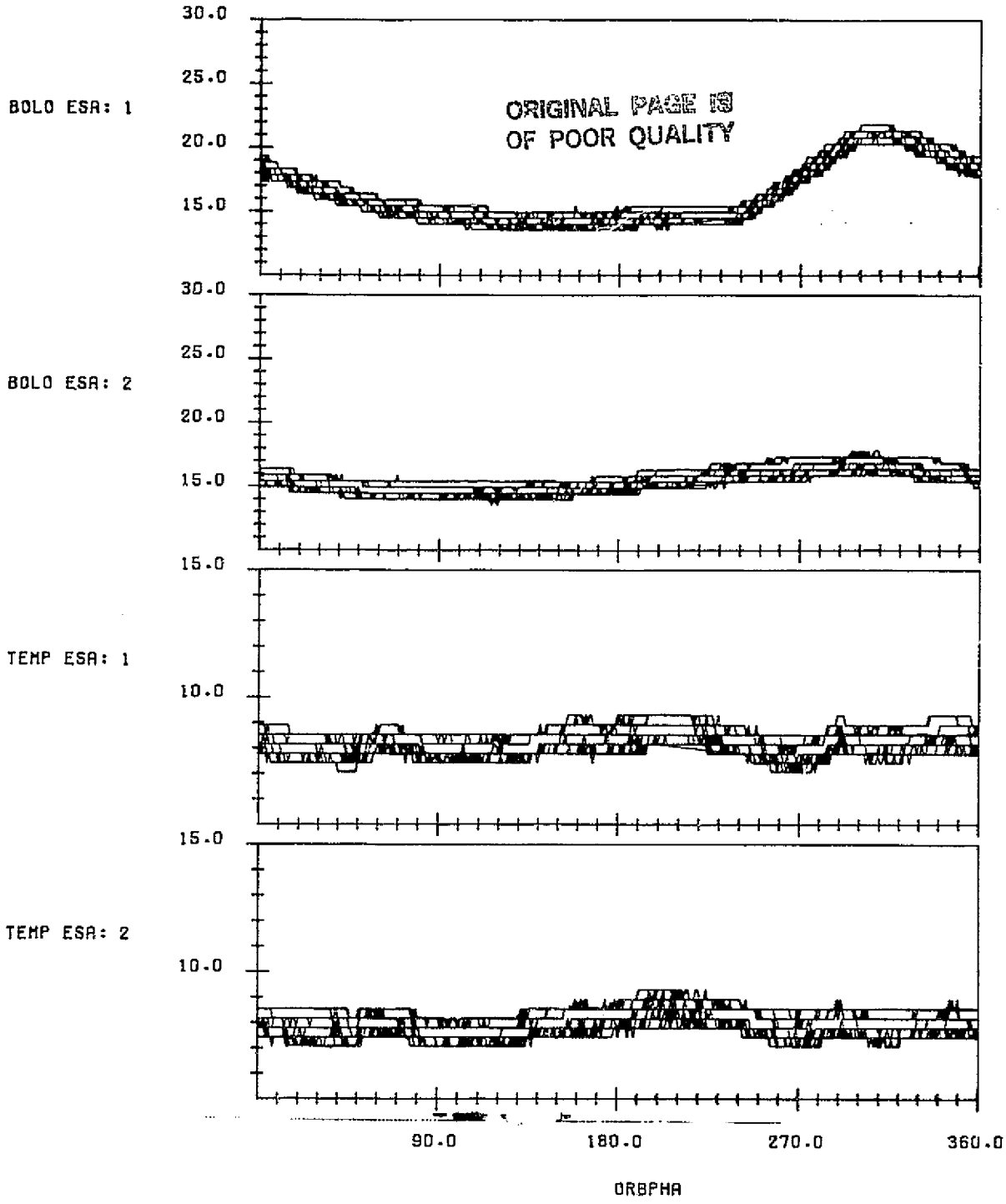

FIGURE B-28. Scanner Temperatures for Data Span on September 14-15, 1983

APPENDIX C - UNCORRECTED PITCH AND ROLL MEASUREMENTS

Figures C-1 through C-28 provide plots of the scanner uncorrected on board pitch and roll measurements for all the data spans processed for this report. The data is plotted as a function of orbit phase from the ascending node for several orbits overlayed. The on board pitch and roll are computed in degrees from the nominal calibrations, without corrections for the effects of Earth oblateness and orbit eccentricity. These are the measurements effectively used for the Safehold Mode. Averaging of each major frame of data, 128 points, was performed to reduce the noise.

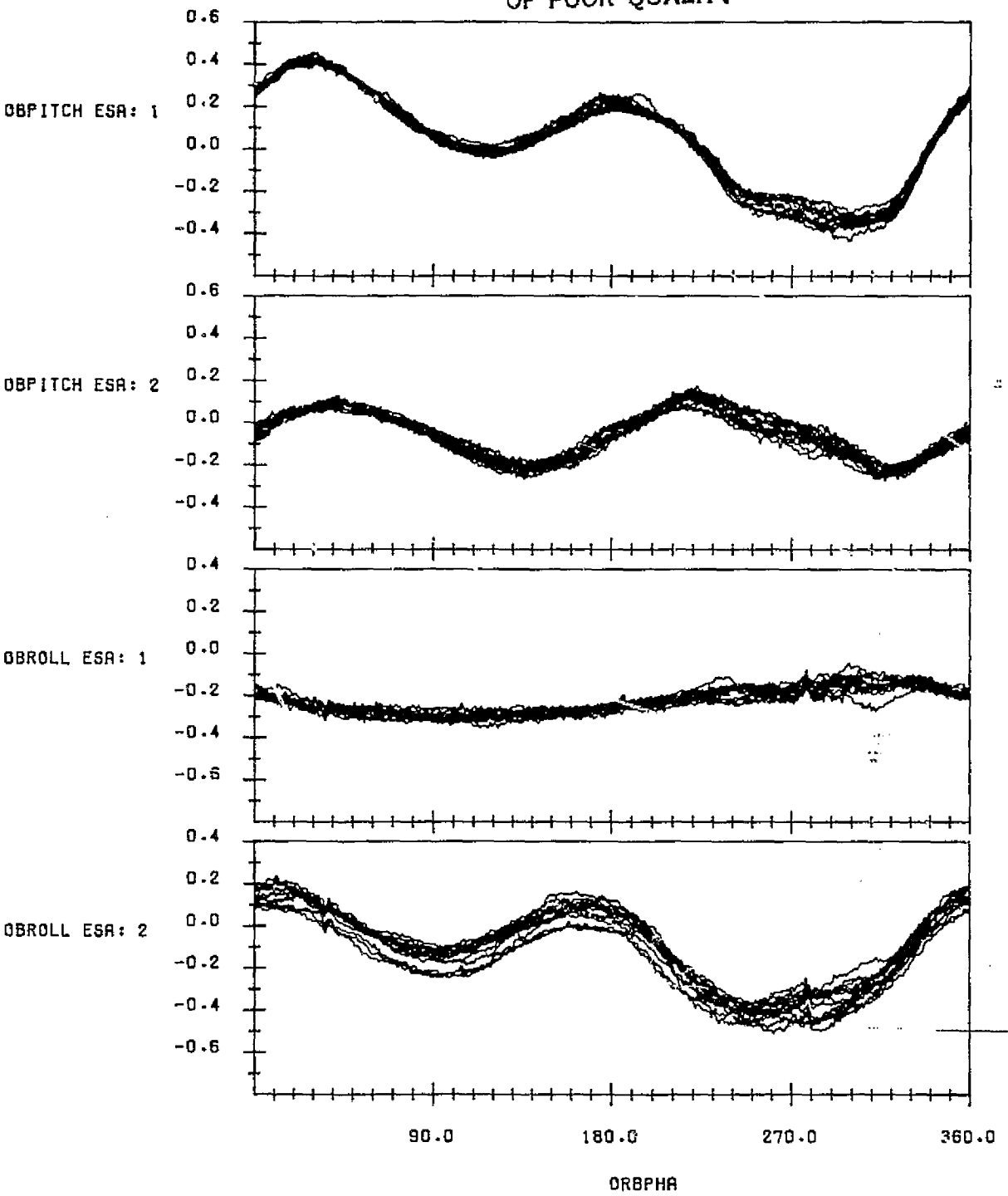

LANDSAT-4 SCANNER UNCORRECTED PITCH AND ROLL MEASUREMENTS (DEGREES) USING NOMINAL CALIBRATION VERSUS ORBIT PHASE FROM THE ASCENDING NODE WITH CONSECUTIVE ORBITS OVERLAID
DATA START TIME:820810.215426522
END TIME:820811.203329690

FIGURE C-1. Uncorrected Scanner Pitch and Roll Measurements for Data Span on August 10-11, 1982

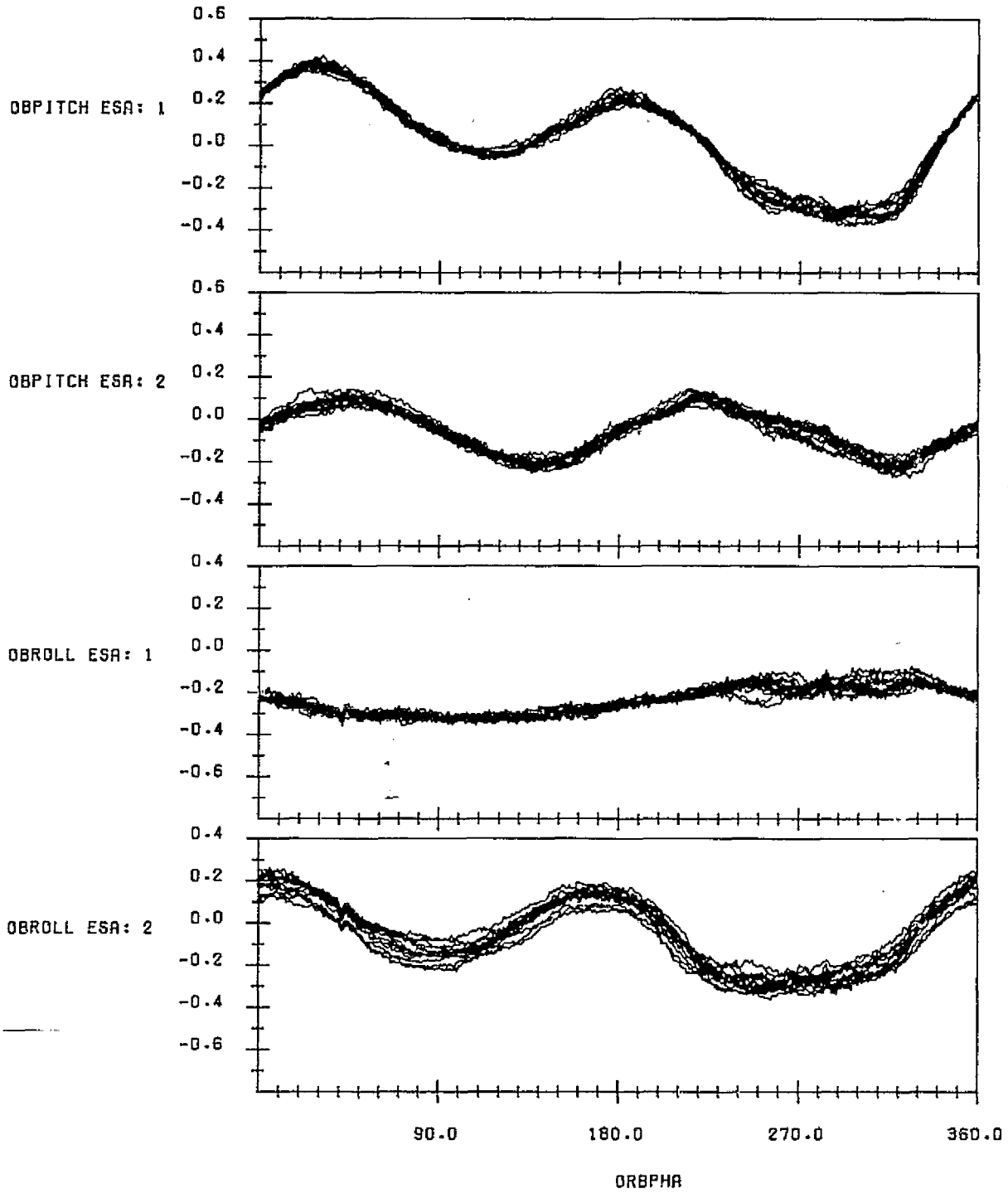

LANDSAT-4 SCANNER UNCORRECTED PITCH AND ROLL MEASUREMENTS (DEGREES) USING NOMINAL CALIBRATION VERSUS ORBIT PHASE FROM THE ASCENDING NODE WITH CONSECUTIVE ORBITS OVERLAID
DATA START TIME:820825.01060609
END TIME:820826.032214554

FIGURE C-2. Uncorrected Scanner Pitch and Roll Measurements for Data Span on August 25-26, 1982

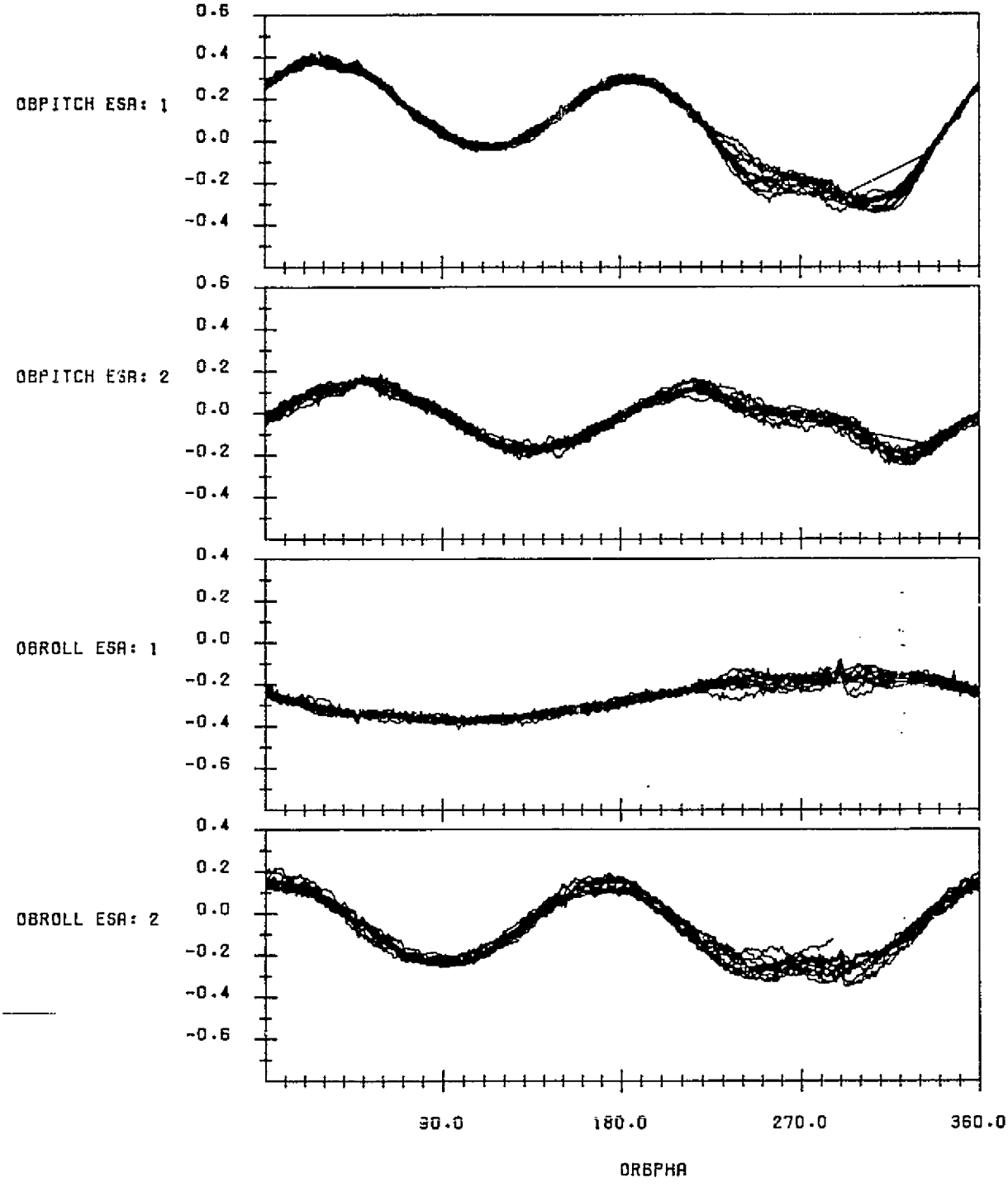

LANDSAT-4 SCANNER UNCORRECTED PITCH AND ROLL MEASUREMENTS
(DEGREES) USING NOMINAL CALIBRATION VERSUS ORBIT PHASE FROM
THE ASCENDING NODE WITH CONSECUTIVE ORBITS OVERLAID
DATA START TIME:820908.043319559
END TIME:820909.051848519

FIGURE C-3. Uncorrected Scanner Pitch and Roll Measurements for Data Span on September 8-9, 1982

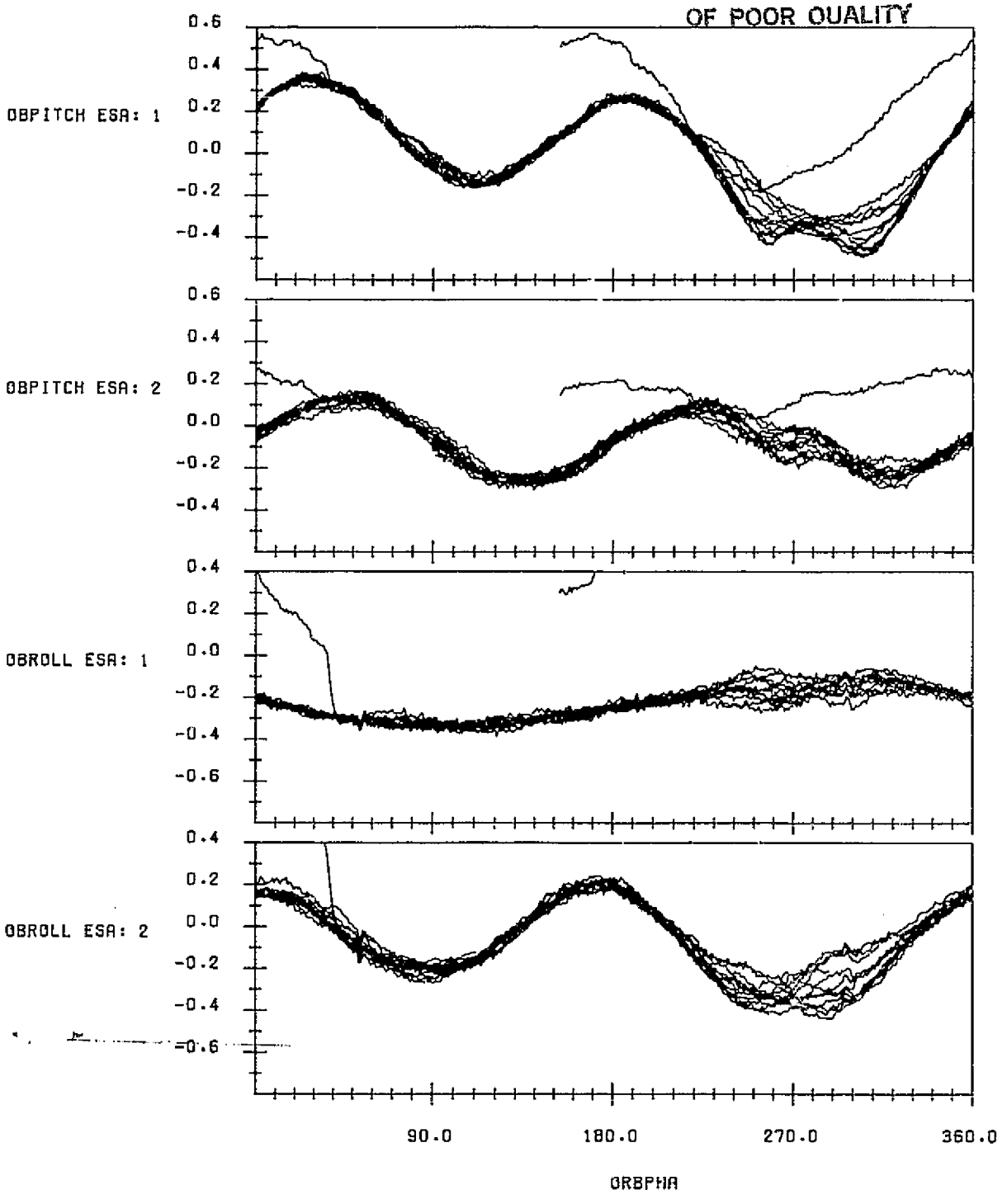

FIGURE C-4. Uncorrected Scanner Pitch and Roll Measurements for Data Span on September 22-23, 1982

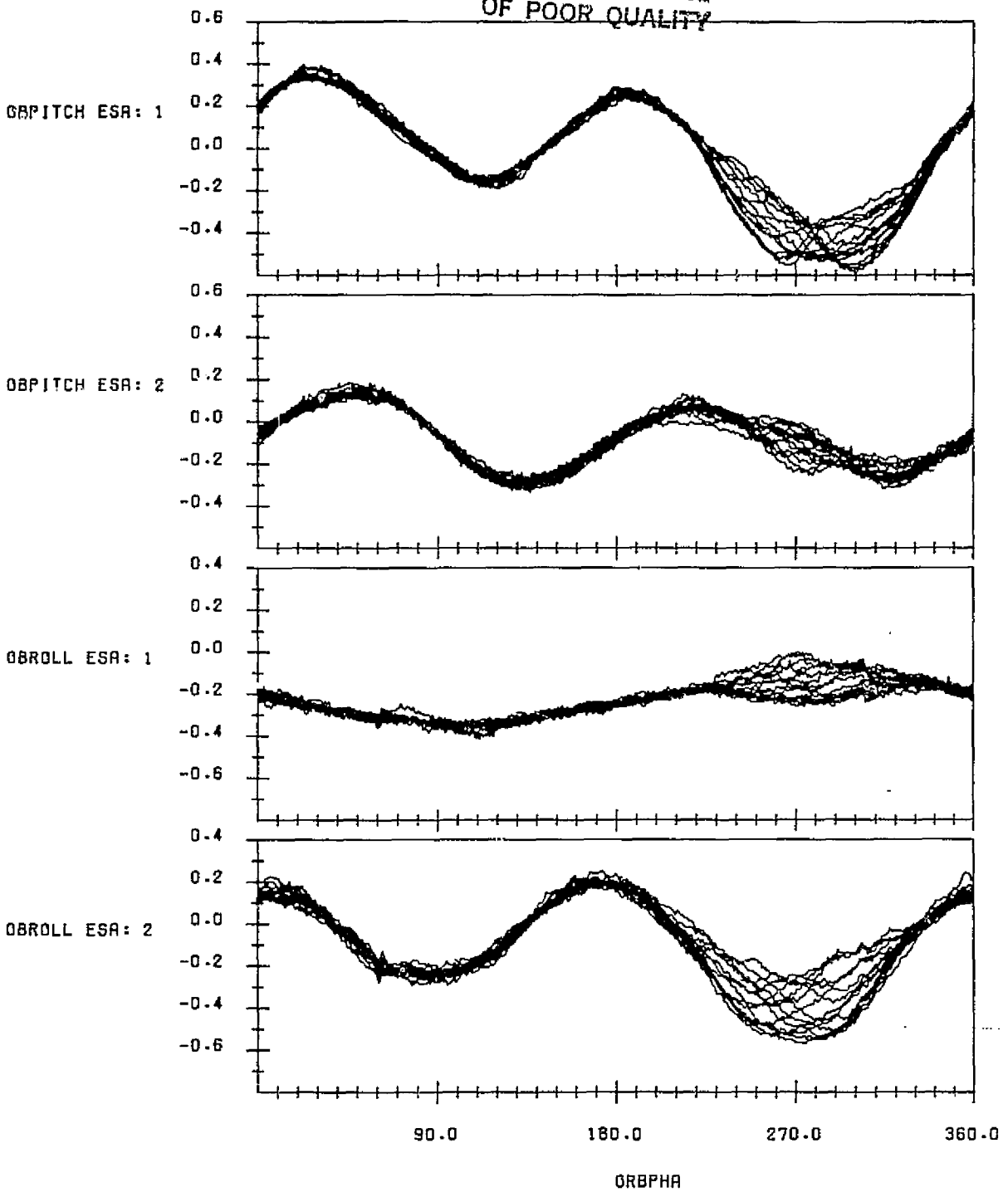

LANDSAT-4 SCANNER UNCORRECTED PITCH AND ROLL MEASUREMENTS (DEGREES) USING NOMINAL CALIBRATION VERSUS ORBIT PHASE FROM THE ASCENDING NODE WITH CONSECUTIVE ORBITS OVERLAID
DATA START TIME:821005.153123435
END TIME:821006.164427194

FIGURE C-5. Uncorrected Scanner Pitch and Roll Measurements for Data Span on October 5-6, 1982

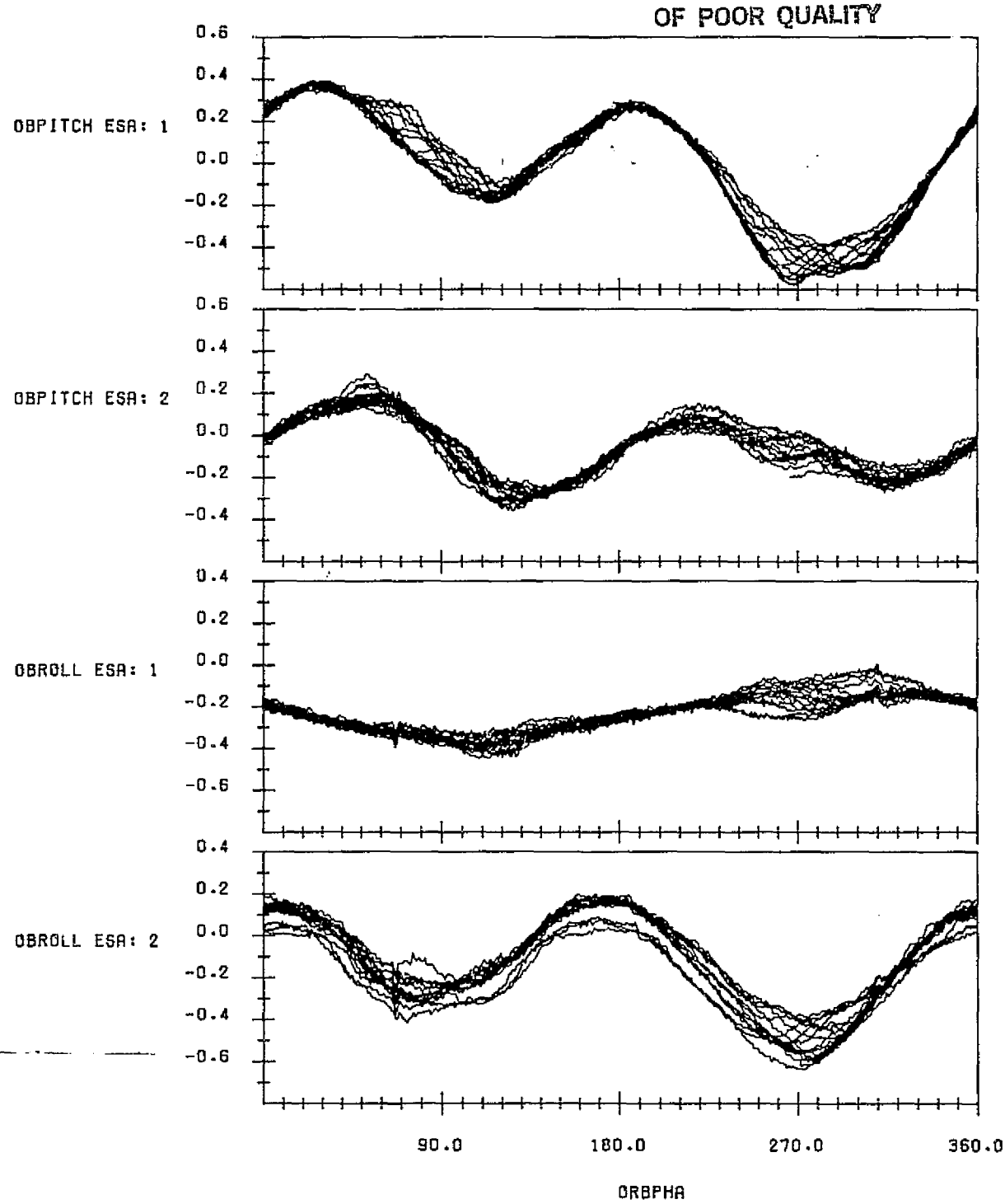

FIGURE C-6. Uncorrected Scanner Pitch and Roll Measurements for Data Span on October 20-21, 1982

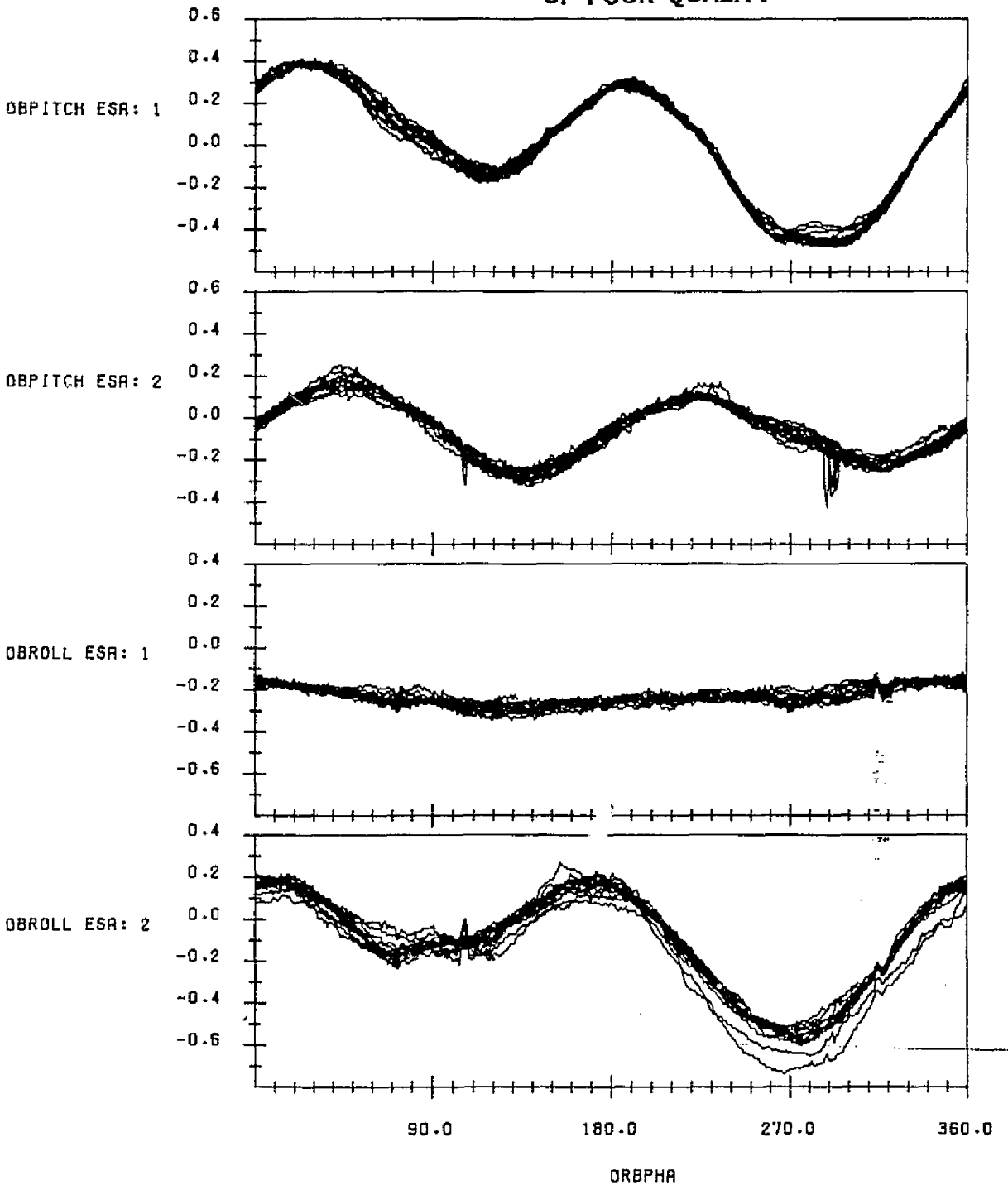

FIGURE C-7. Uncorrected Scanner Pitch and Roll Measurements for Data Span on November 2-3, 1982

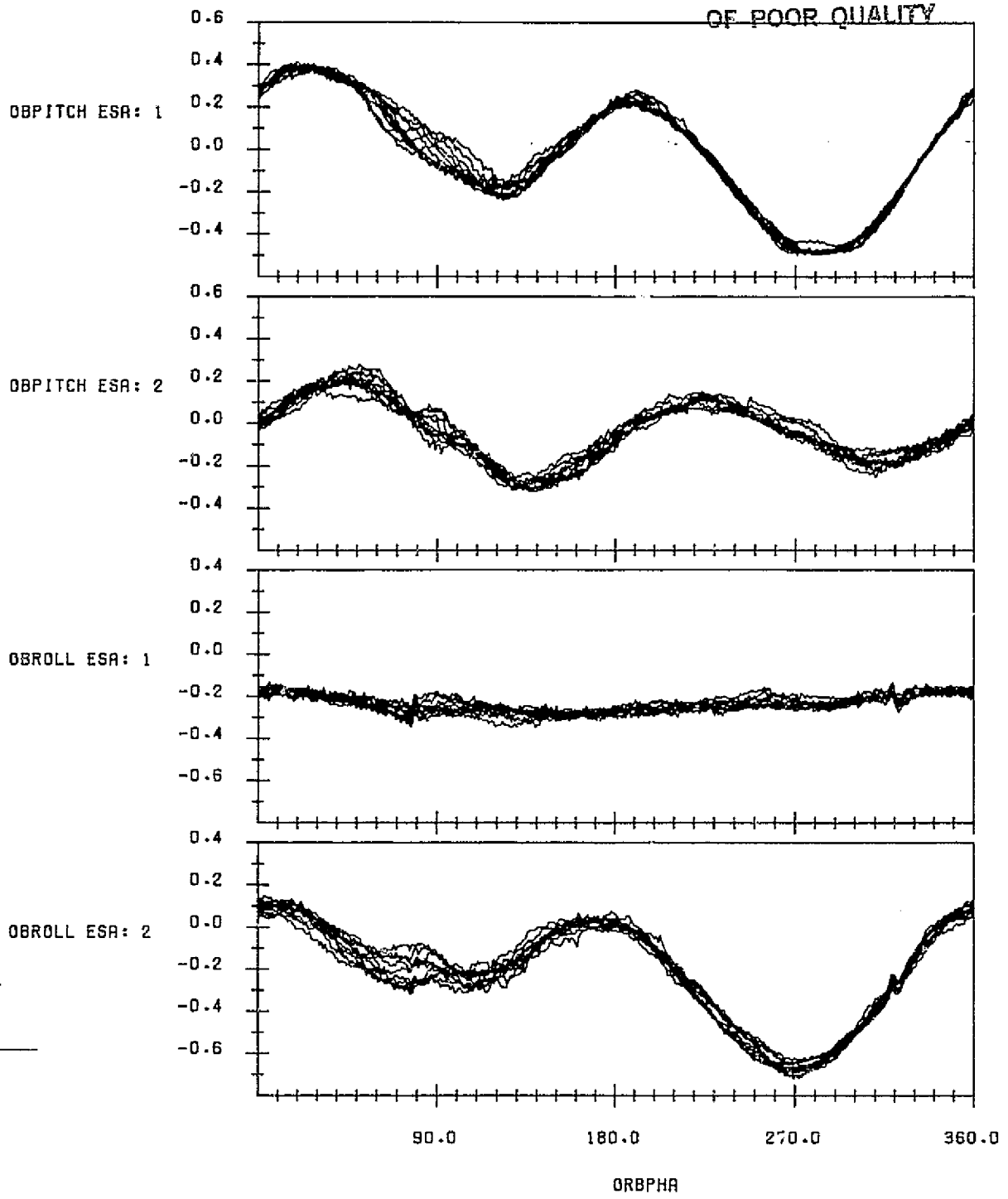

FIGURE C-8. Uncorrected Scanner Pitch and Roll Measurements for Data Span on November 16, 1982

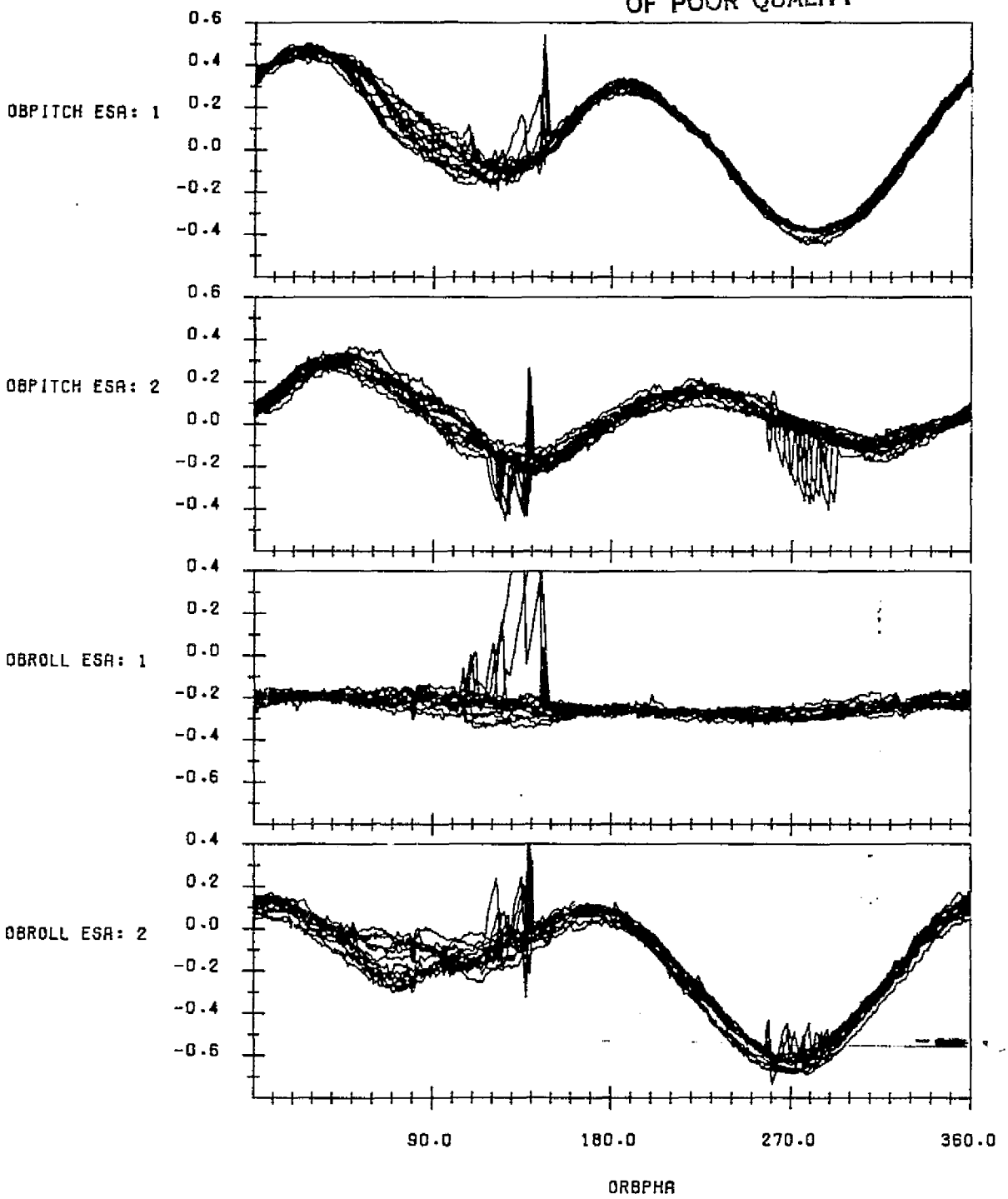

LANDSAT-4 SCANNER UNCORRECTED PITCH AND ROLL MEASUREMENTS (DEGREES) USING NOMINAL CALIBRATION VERSUS ORBIT PHASE FROM THE ASCENDING NODE WITH CONSECUTIVE ORBITS OVERLAID
DATA START TIME:821201.002856720
END TIME:821202.031150860

FIGURE C-9. Uncorrected Scanner Pitch and Roll Measurements for Data Span on December 1-2, 1982

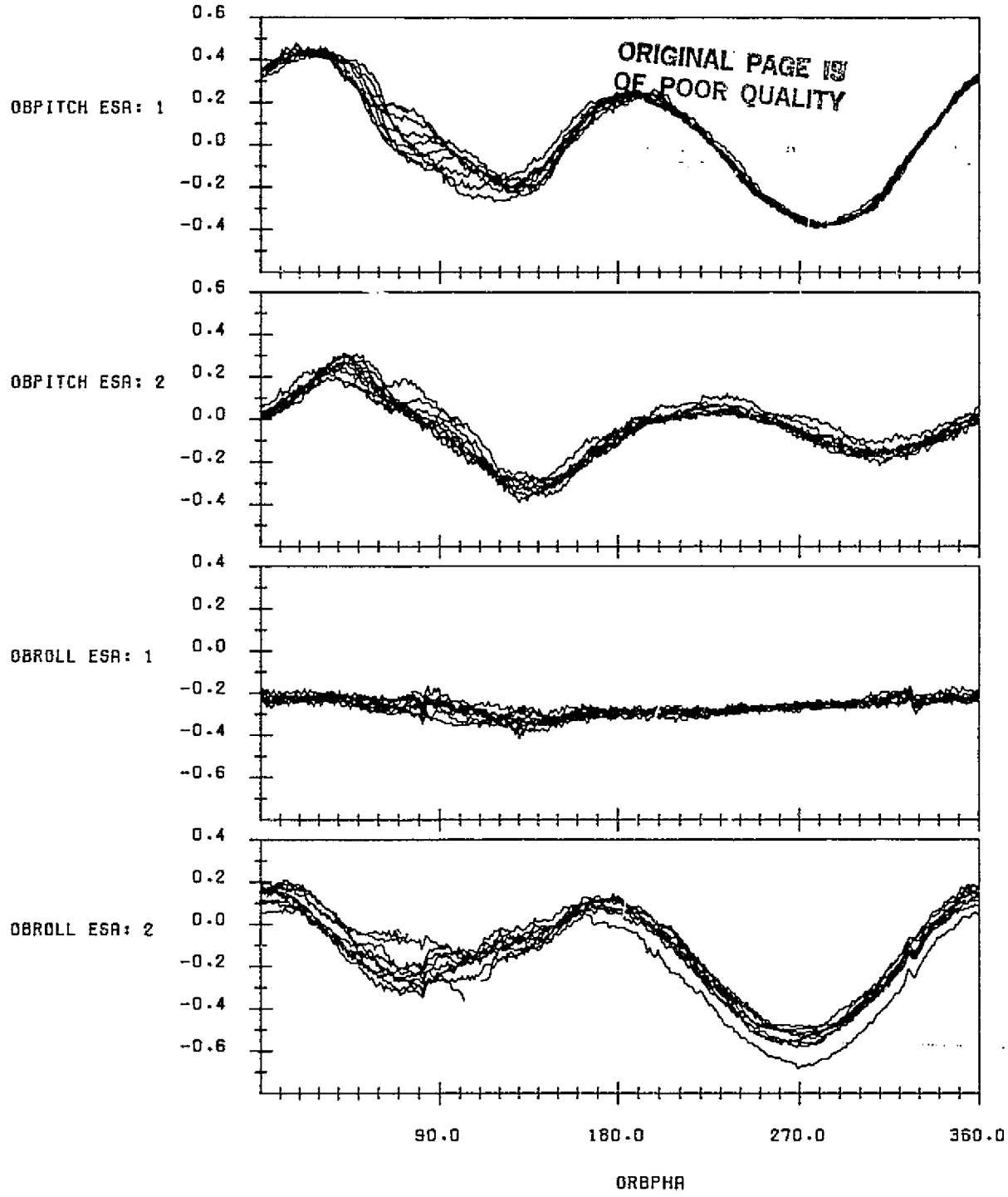

LANDSAT-4 SCANNER UNCORRECTED PITCH AND ROLL MEASUREMENTS (DEGREES) USING NOMINAL CALIBRATION VERSUS ORBIT PHASE FROM THE ASCENDING NODE WITH CONSECUTIVE ORBITS OVERLAID
DATA START TIME:821214.122607064
END TIME:821215.143809812

FIGURE C-10. Uncorrected Scanner Pitch and Roll Measurements for Data Span on December 14-15, 1982

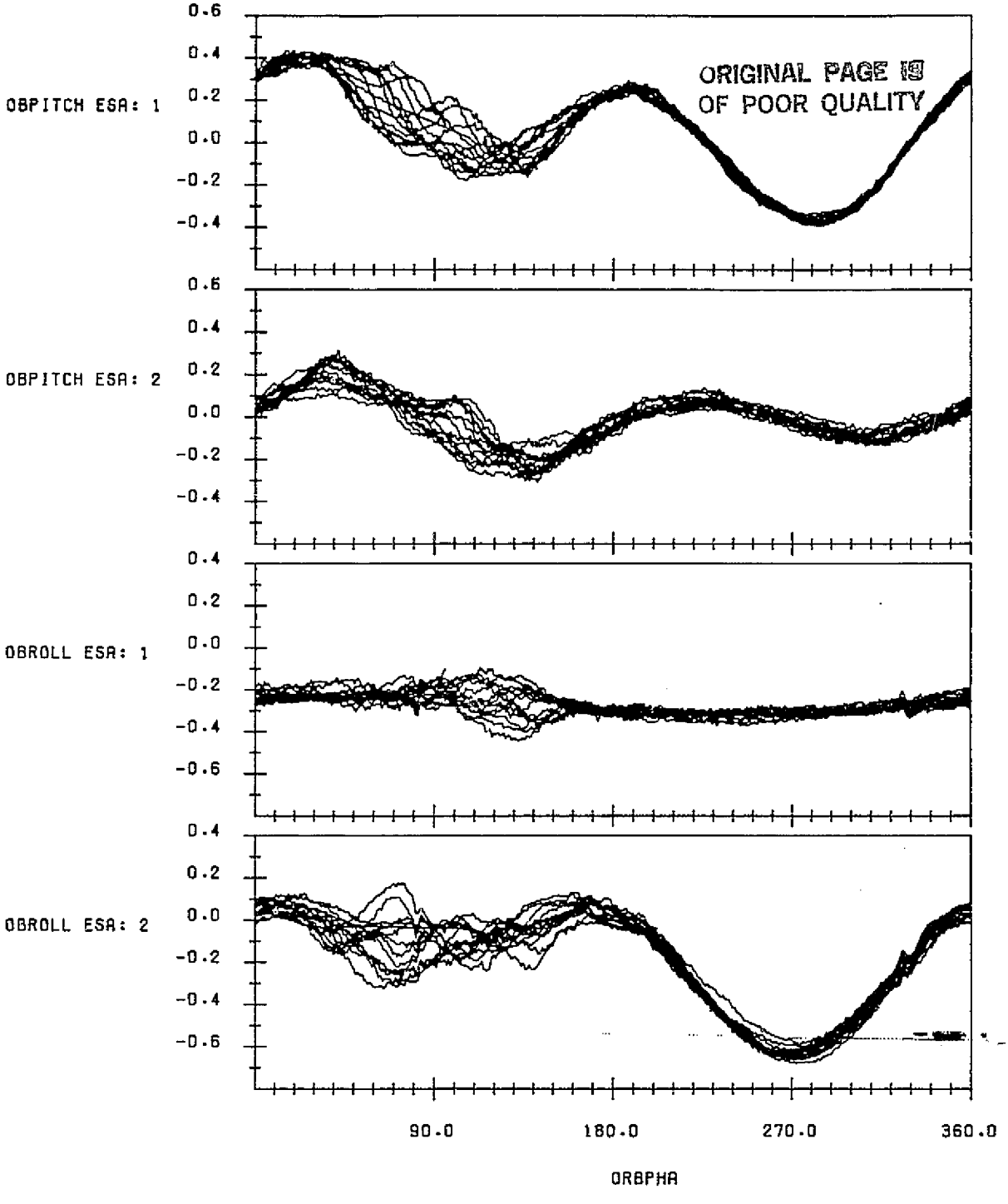

FIGURE C-11. Uncorrected Scanner Pitch and Roll Measurements for Data Span on December 28-29, 1982

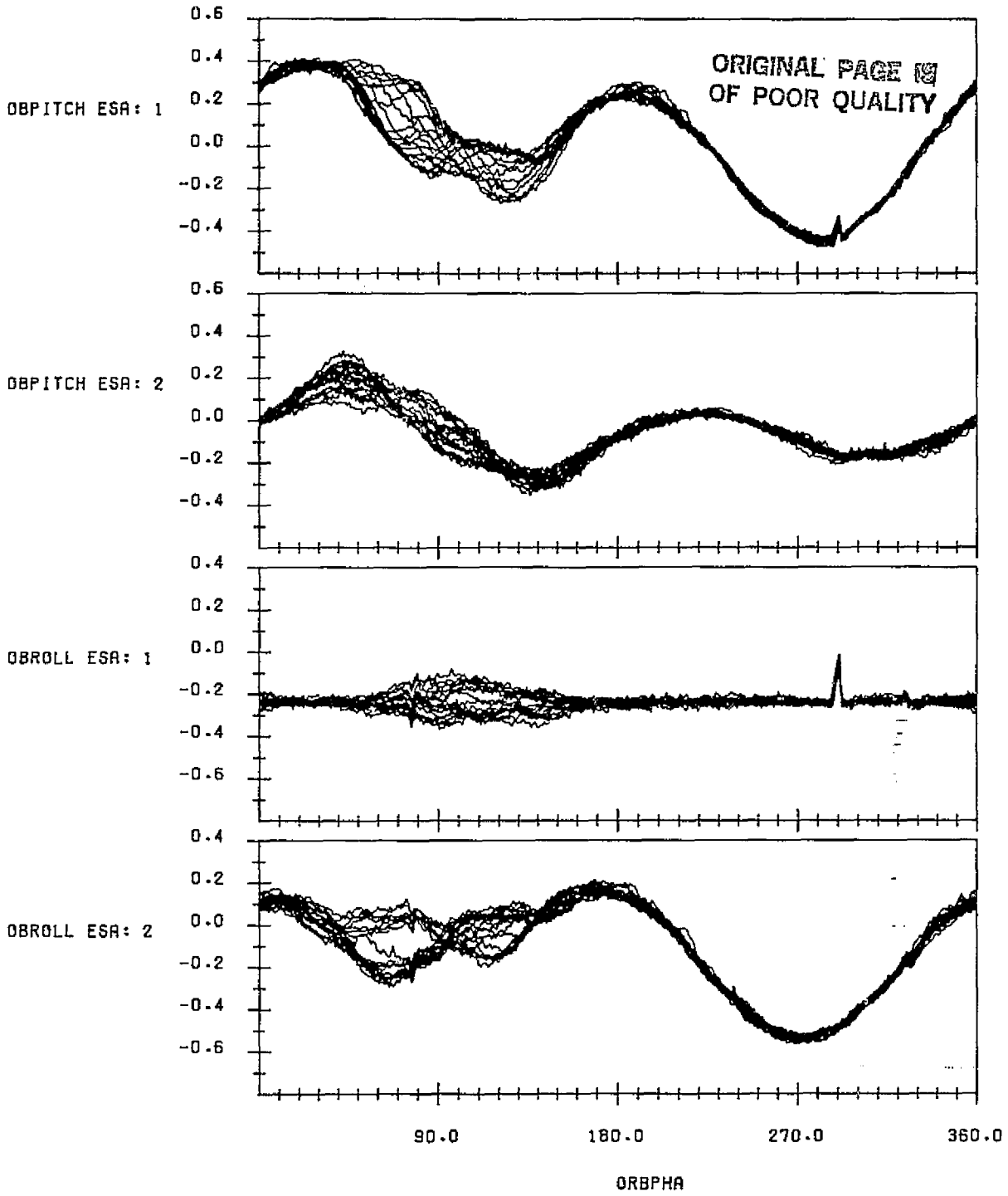

FIGURE C-12. Uncorrected Scanner Pitch and Roll Measurements for Data Span on January 19-20, 1983

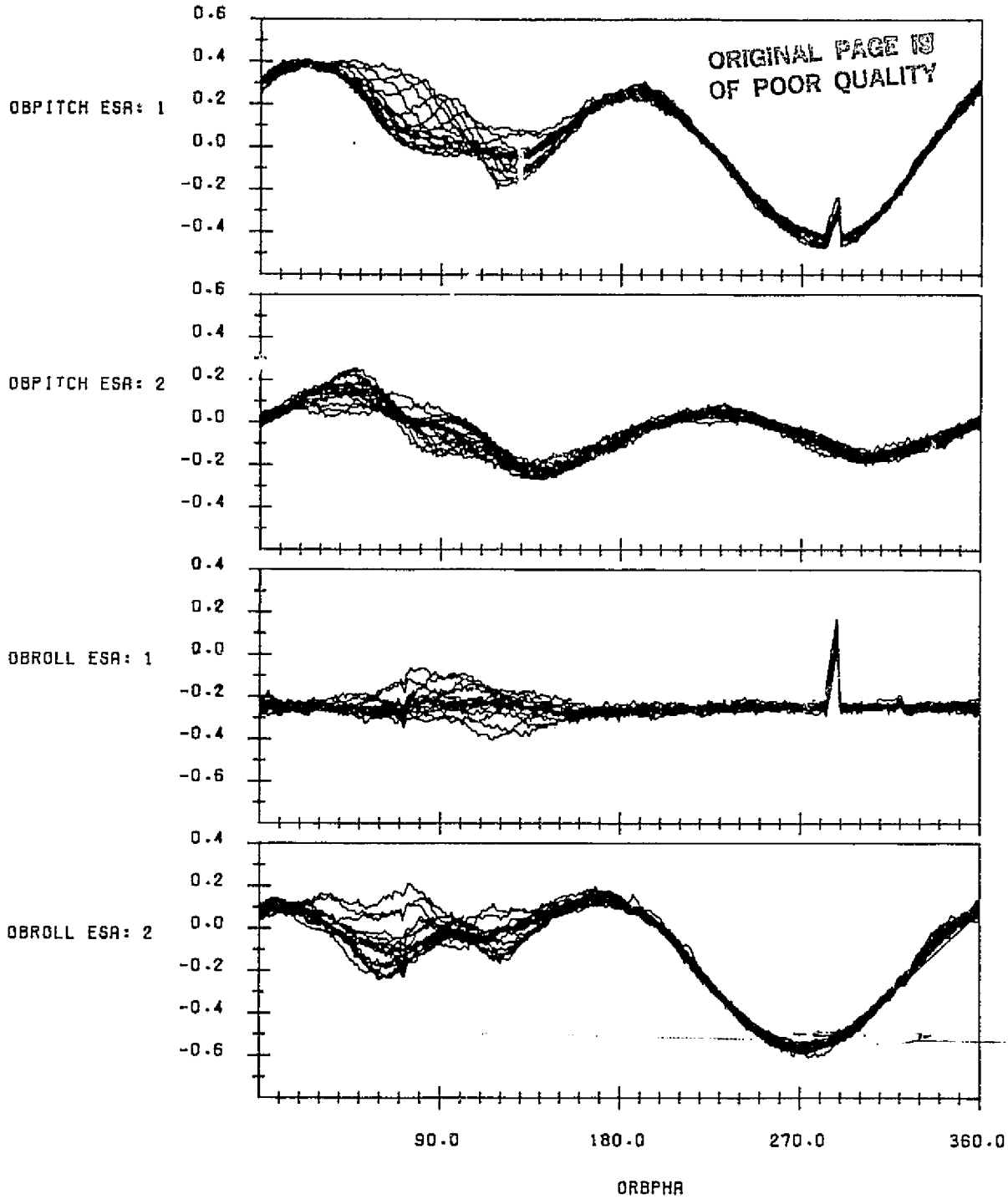

FIGURE C-13. Uncorrected Scanner Pitch and Roll Measurements for Data Span on February 2-3, 1983

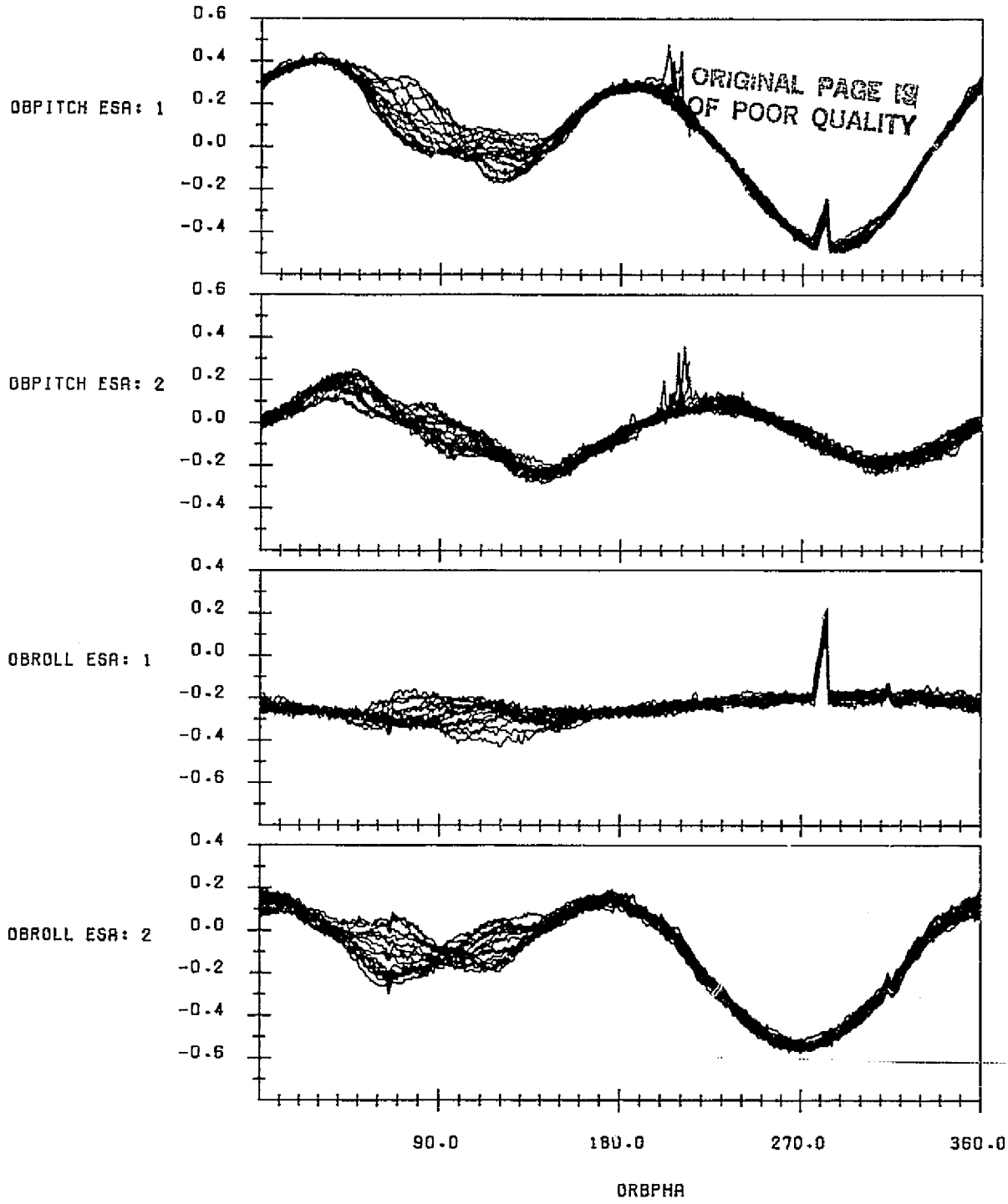

LANDSAT-4 SCANNER UNCORRECTED PITCH AND ROLL MEASUREMENTS (DEGREES) USING NOMINAL CALIBRATION VERSUS ORBIT PHASE FROM THE ASCENDING NODE WITH CONSECUTIVE ORBITS OVERLAID
DATA START TIME:830217.000122618
END TIME:830218.065513594

FIGURE C-14. Uncorrected Scanner Pitch and Roll Measurements for Data Span on February 17-18, 1983

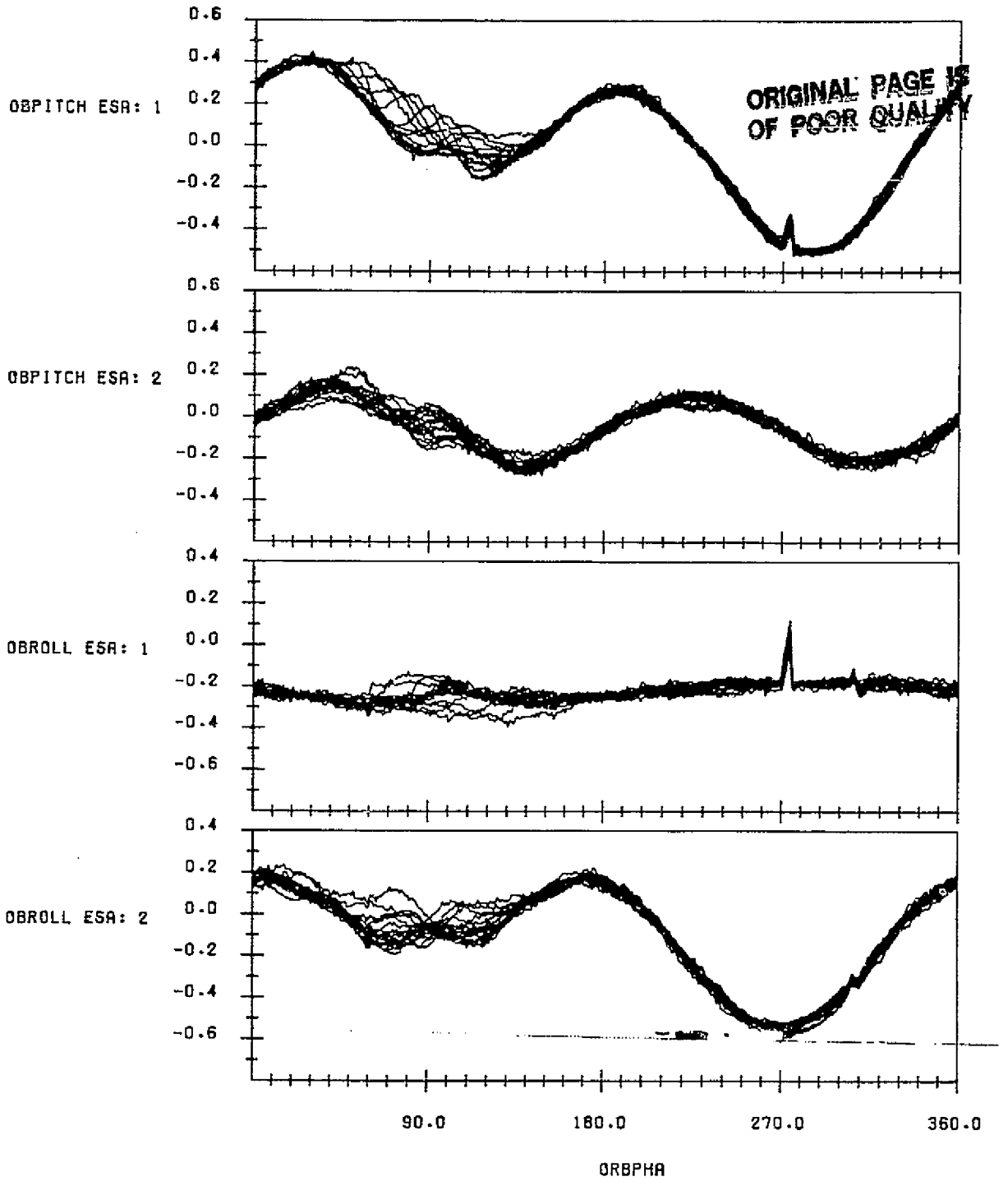

LANDSAT-4 SCANNER UNCORRECTED PITCH AND ROLL MEASUREMENTS (DEGREES) USING NOMINAL CALIBRATION VERSUS ORBIT PHASE FROM THE ASCENDING NODE WITH CONSECUTIVE ORBITS OVERLAID
DATA START TIME:830303.025744694
END TIME:830304.034257270

FIGURE C-15. Uncorrected Scanner Pitch and Roll Measurements for Data Span on March 3-4, 1983

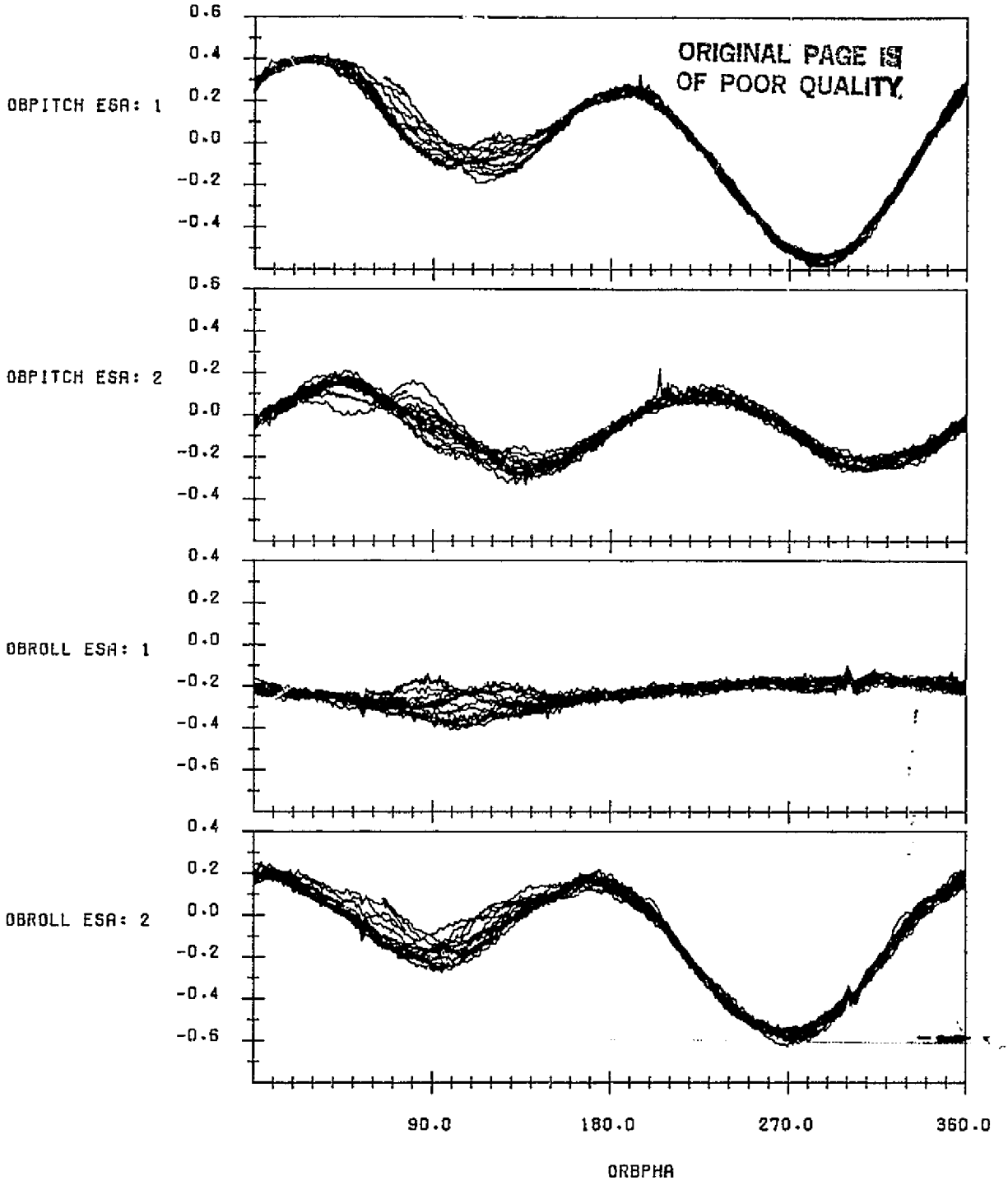

FIGURE C-16. Uncorrected Scanner Pitch and Roll Measurements for Data Span on March 14-15, 1983

ORIGINAL PAGE IS
OF POOR QUALITY

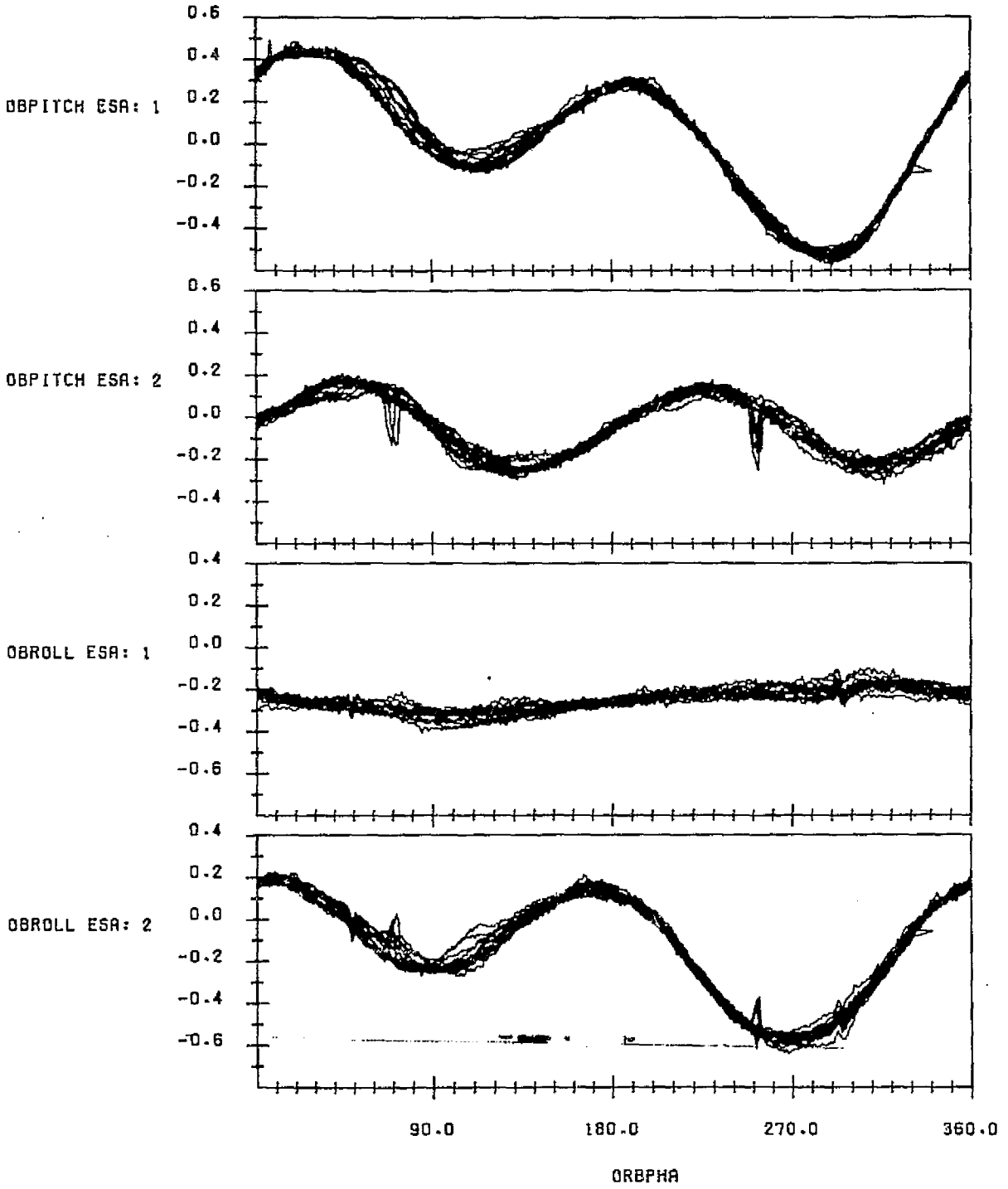

LANDSAT-4 SCANNER UNCORRECTED PITCH AND ROLL MEASUREMENTS (DEGREES) USING NOMINAL CALIBRATION VERSUS ORBIT PHASE FROM THE ASCENDING NODE WITH CONSECUTIVE ORBITS OVERLAID
DATA START TIME:830329.235506990
END TIME:830331.003946798

FIGURE C-17. Uncorrected Scanner Pitch and Roll Measurements for Data Span on March 29-31, 1983

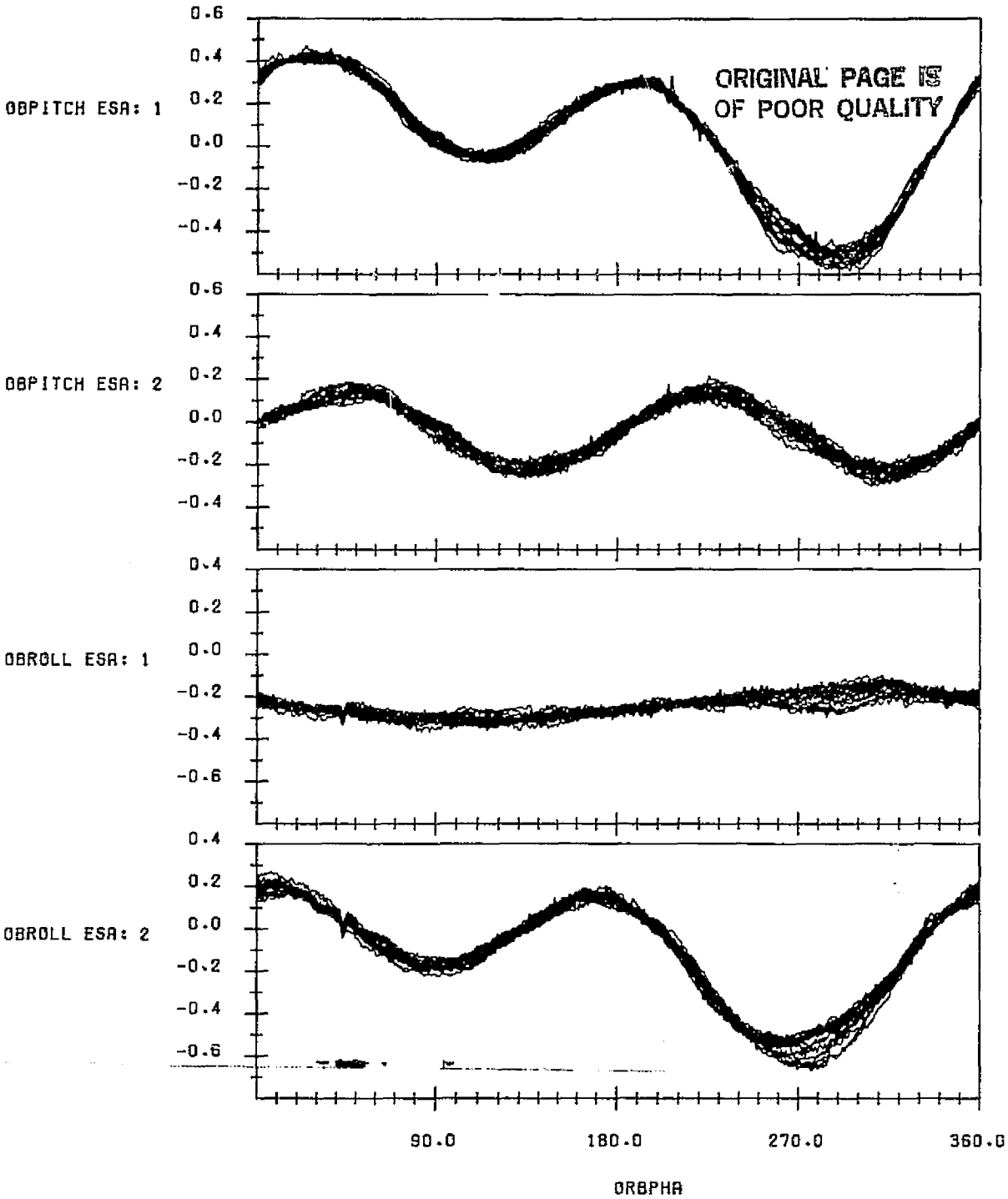

LANDSAT-4 SCANNER UNCORRECTED PITCH AND ROLL MEASUREMENTS (DEGREES) USING NOMINAL CALIBRATION VERSUS ORBIT PHASE FROM THE ASCENDING NODE WITH CONSECUTIVE ORBITS OVERLAID
DATA START TIME:830414.003417145
END TIME:830415.041837625

FIGURE C-18. Uncorrected Scanner Pitch and Roll Measurements for Data Span on April 14-15, 1983

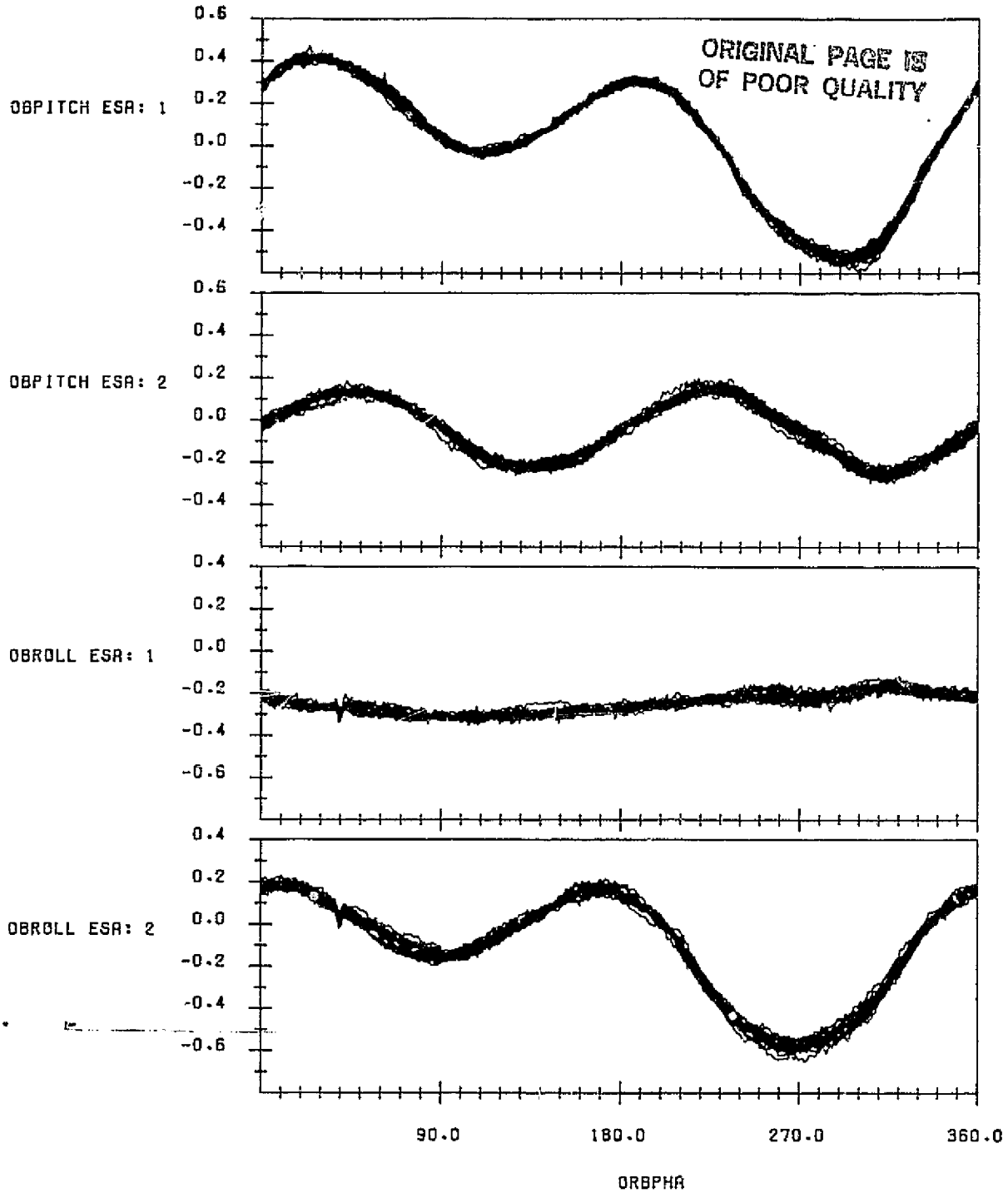

FIGURE C-19. Uncorrected Scanner Pitch and Roll Measurements for Data Span on April 26-27, 1983

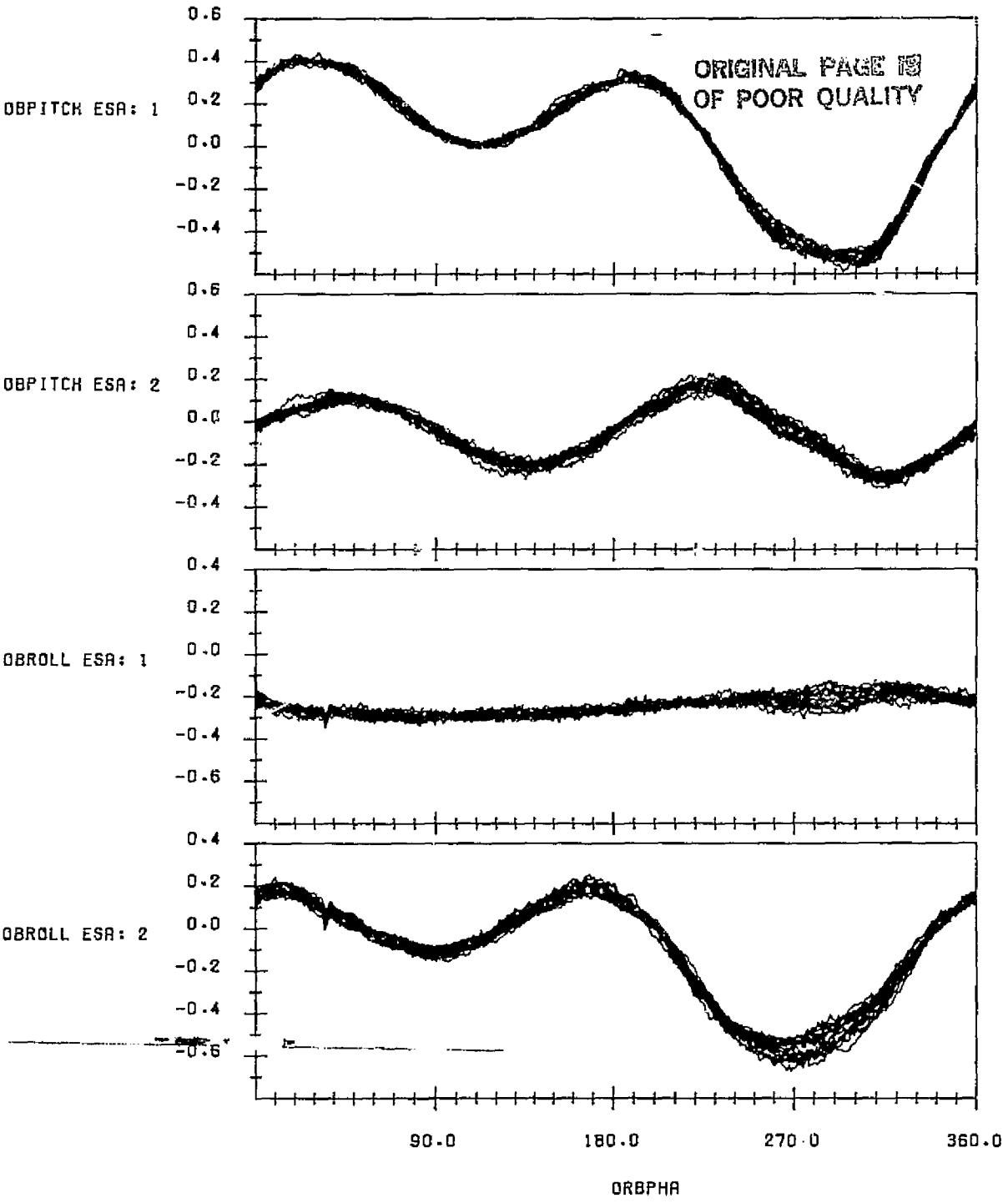

FIGURE C-20. Uncorrected Scanner Pitch and Roll Measurements for Data Span on May 11-12, 1983

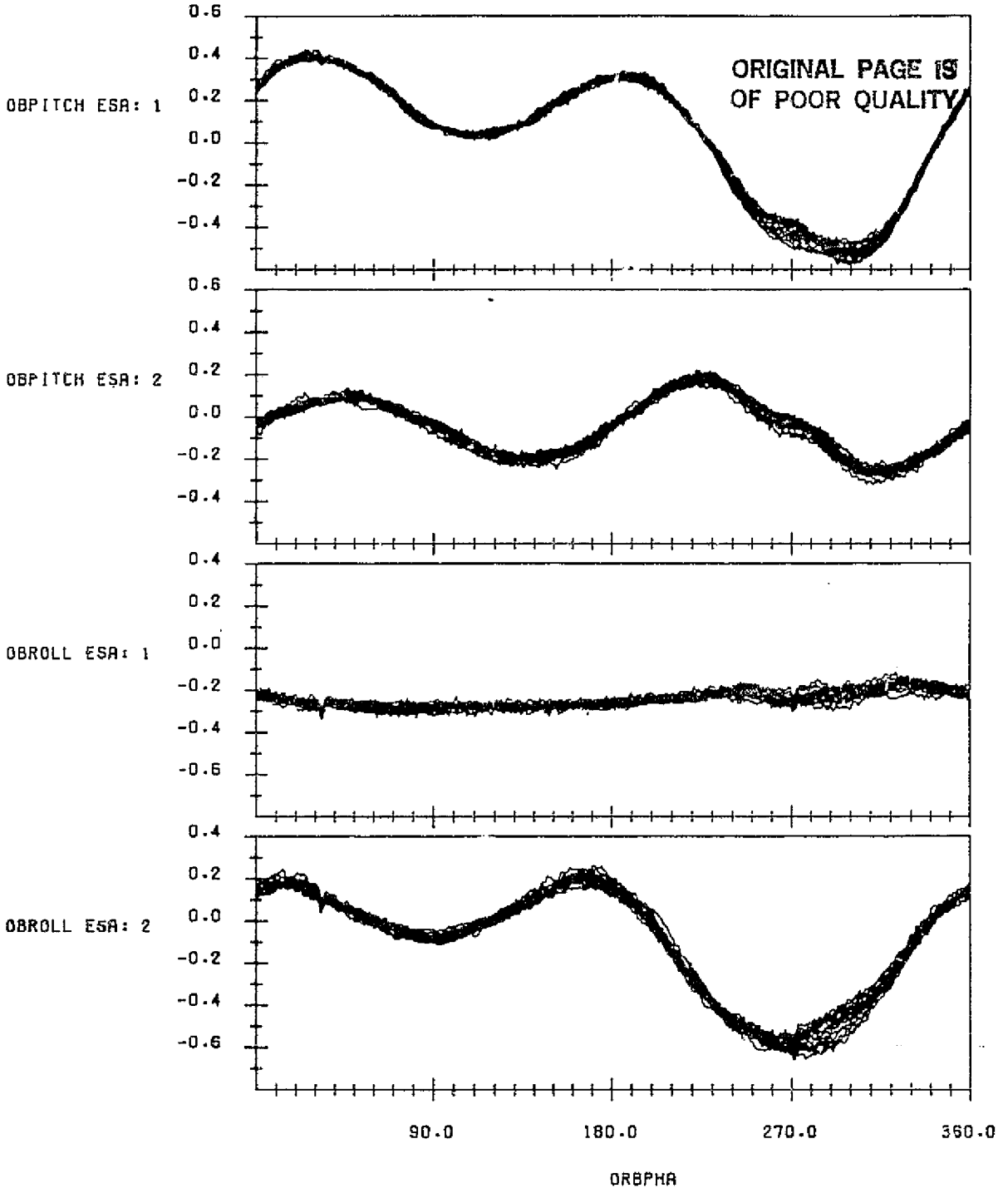

FIGURE C-21. Uncorrected Scanner Pitch and Roll Measurements for Data Span on May 23-24, 1983

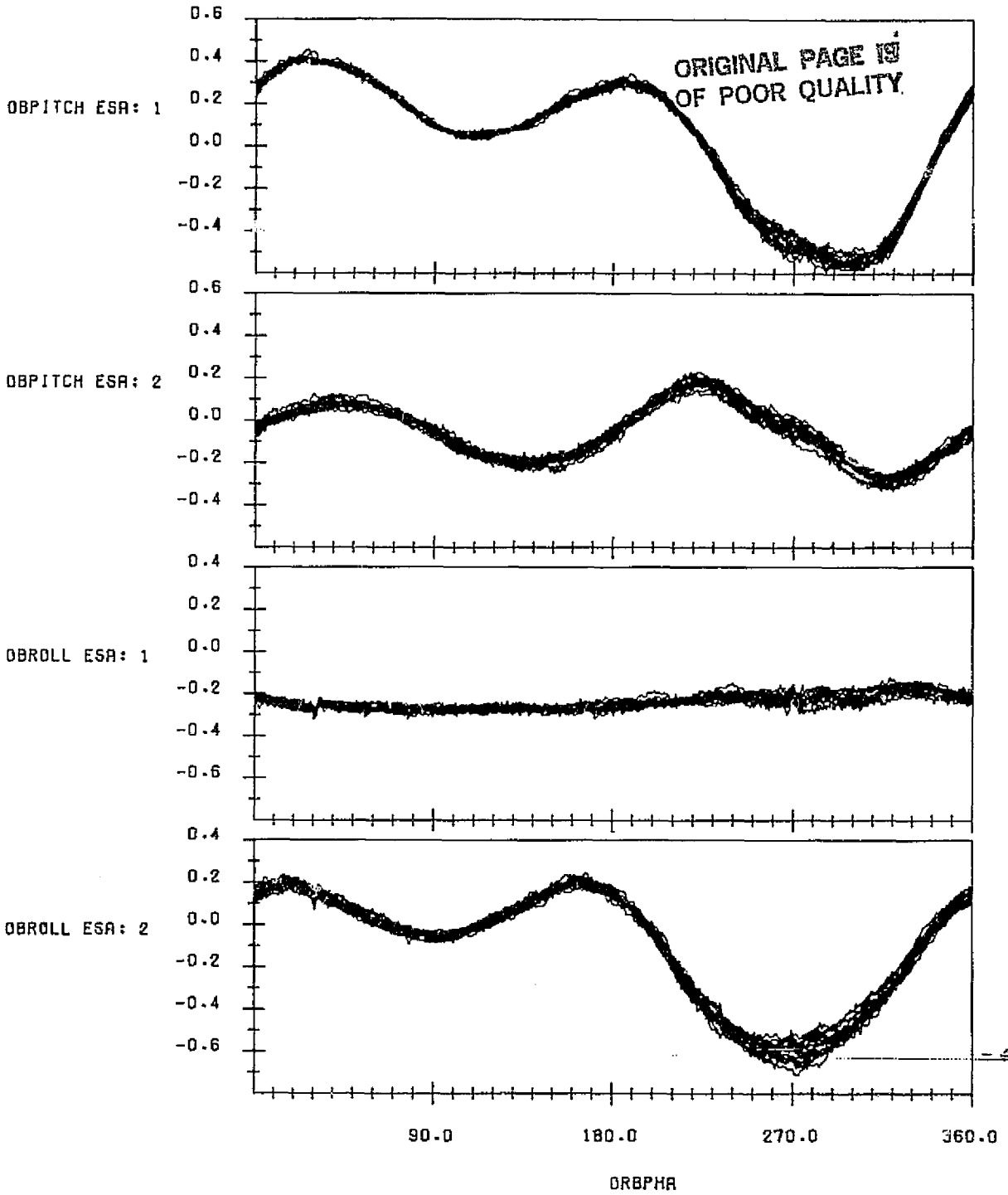

FIGURE C-22. Uncorrected Scanner Pitch and Roll Measurements for Data Span on June 6-7, 1983

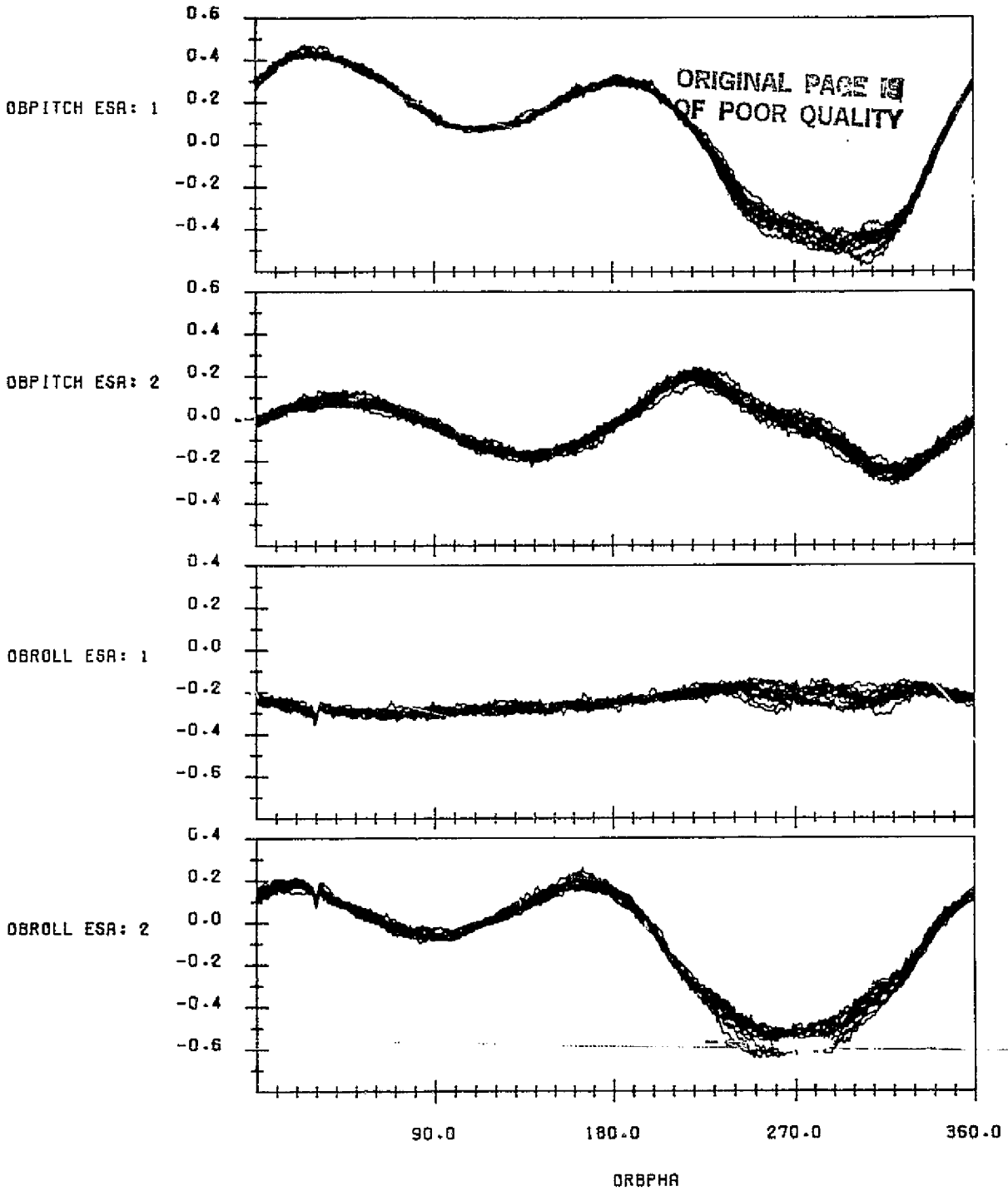

LANDSAT-4 SCANNER UNCORRECTED PITCH AND ROLL MEASUREMENTS (DEGREES) USING NOMINAL CALIBRATION VERSUS ORBIT PHASE FROM THE ASCENDING NODE WITH CONSECUTIVE ORBITS OVERLAID
DATA START TIME:830621.225929155
END TIME:830623.012243587

FIGURE C-23. Uncorrected Scanner Pitch and Roll Measurements for Data Span on June 21-23, 1983

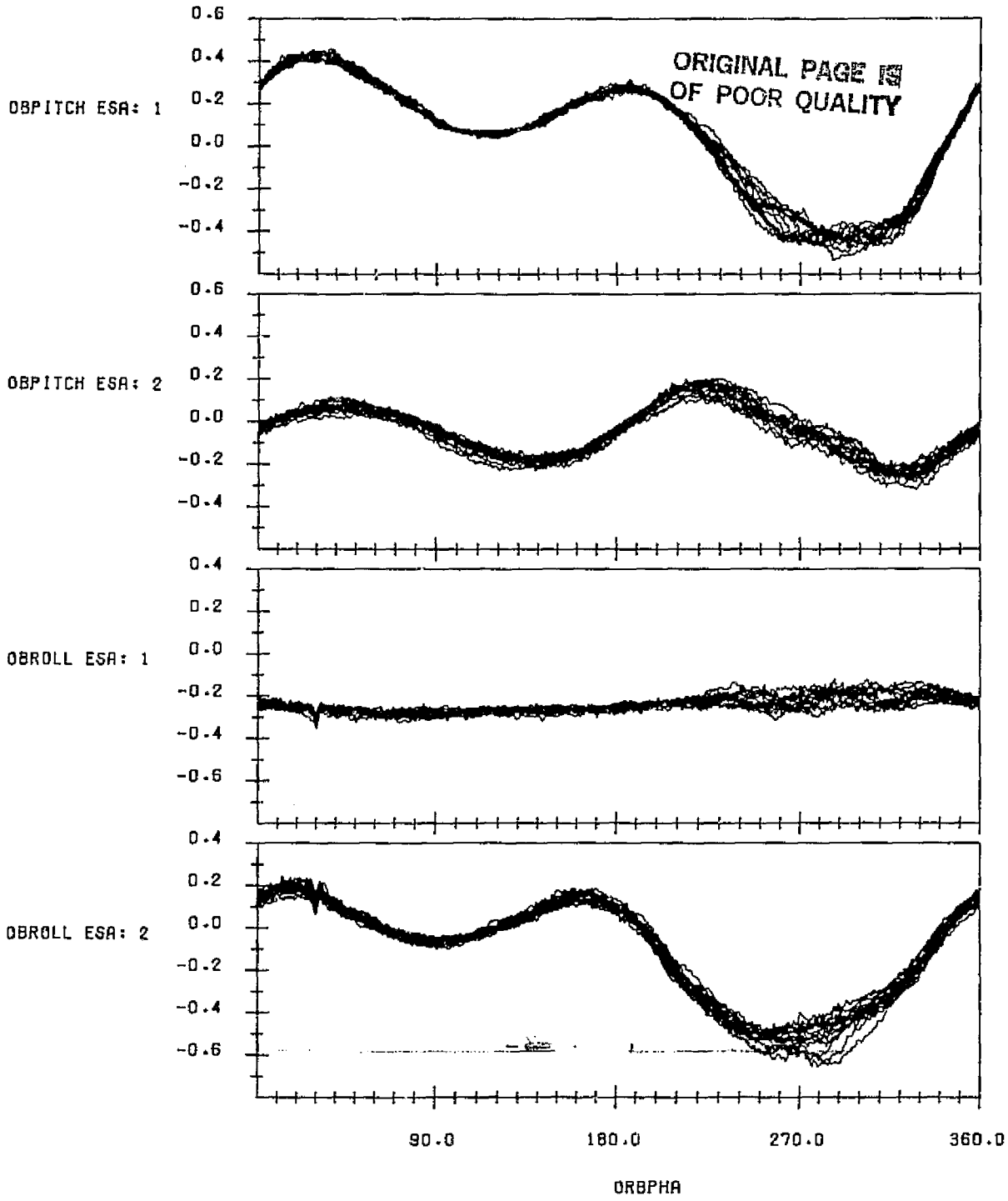

LANDSAT-4 SCANNER UNCORRECTED PITCH AND ROLL MEASUREMENTS
(DEGREES) USING NOMINAL CALIBRATION VERSUS ORBIT PHASE FROM
THE ASCENDING NODE WITH CONSECUTIVE ORBITS OVERLAID
DATA START TIME:830706.154825062
END TIME:830707.182940838

FIGURE C-24. Uncorrected Scanner Pitch and Roll Measurements for Data Span on July 6-7, 1983

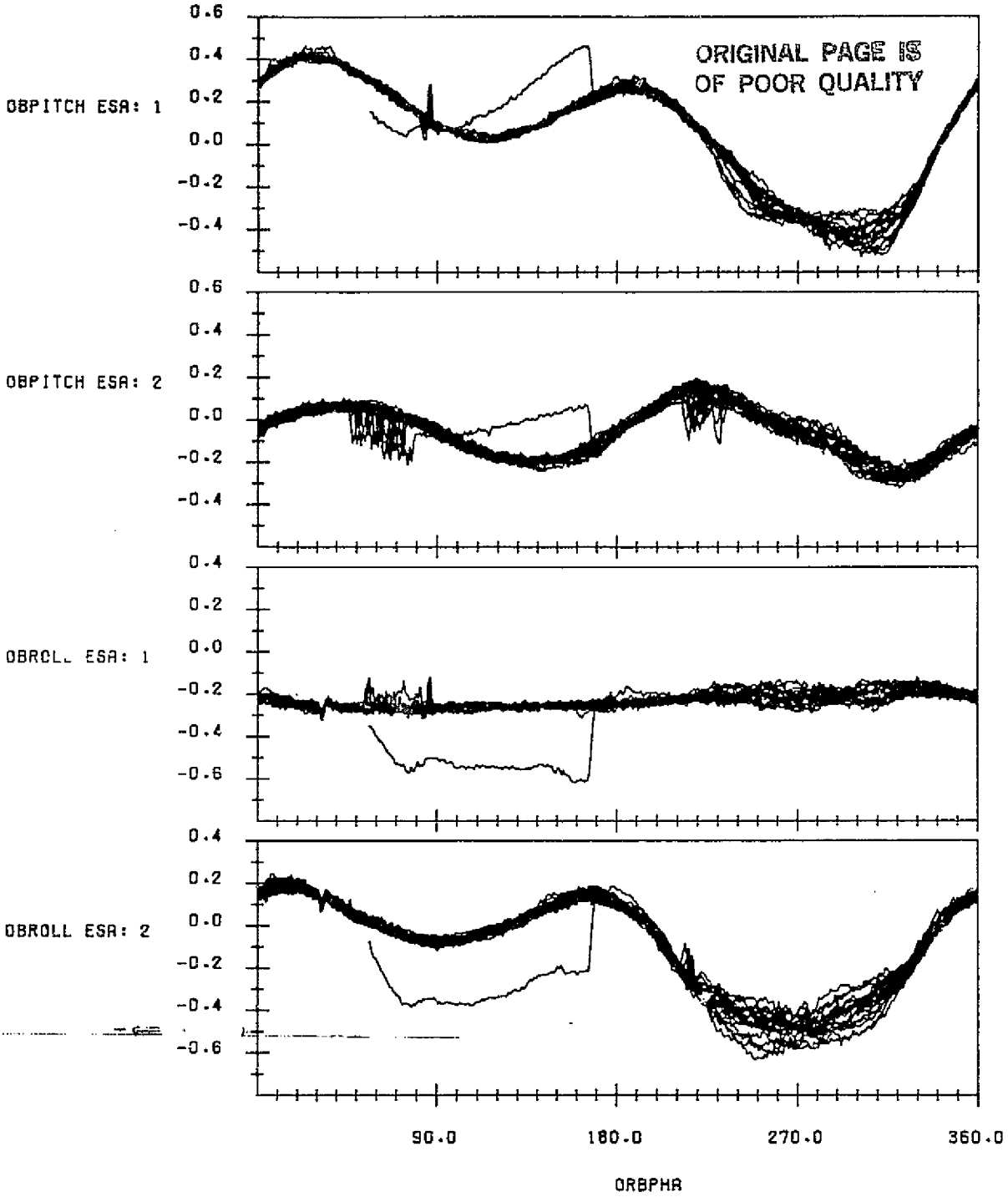

LANDSAT-4 SCANNER UNCORRECTED PITCH AND ROLL MEASUREMENTS
(DEGREES) USING NOMINAL CALIBRATION VERSUS ORBIT PHASE FROM
THE ASCENDING NODE WITH CONSECUTIVE ORBITS OVERLAID
DATA START TIME:830726.004016064
END TIME:830727.061244608

FIGURE C-25. Uncorrected Scanner Pitch and Roll Measurements on Data Span on July 26-27, 1983

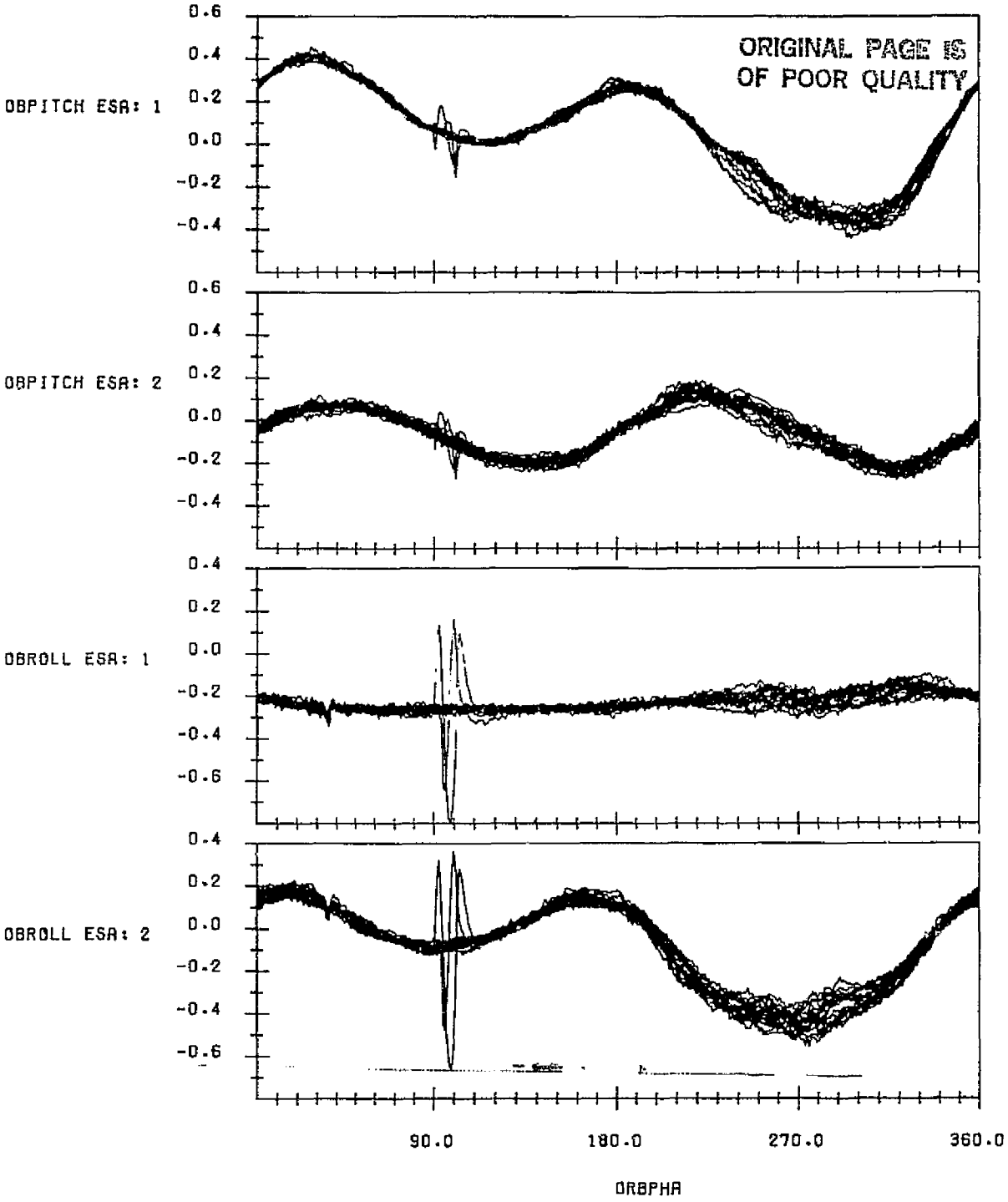

FIGURE C-26. Uncorrected Scanner Pitch and Roll Measurements for Data Span on August 6-7, 1983

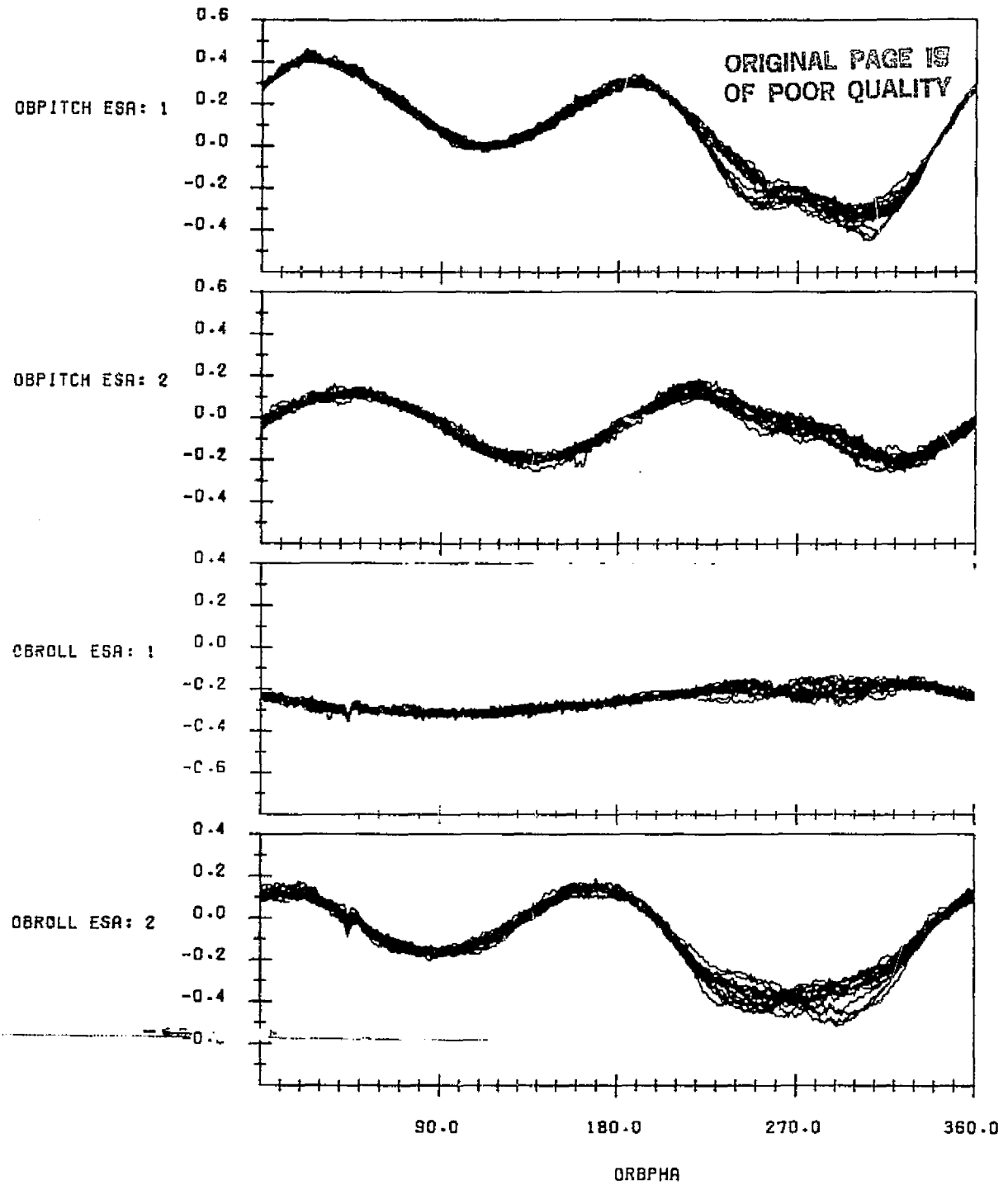

LANDSAT-4 SCANNER UNCORRECTED PITCH AND ROLL MEASUREMENTS
(DEGREES) USING NOMINAL CALIBRATION VERSUS ORBIT PHASE FROM
THE ASCENDING NODE WITH CONSECUTIVE ORBITS OVERLAID
DATA START TIME:830831.001456628
END TIME:830901.041150787

FIGURE C-27. Uncorrected Scanner Pitch and Roll Measurements for Data Span on August 31 - September 1, 1983

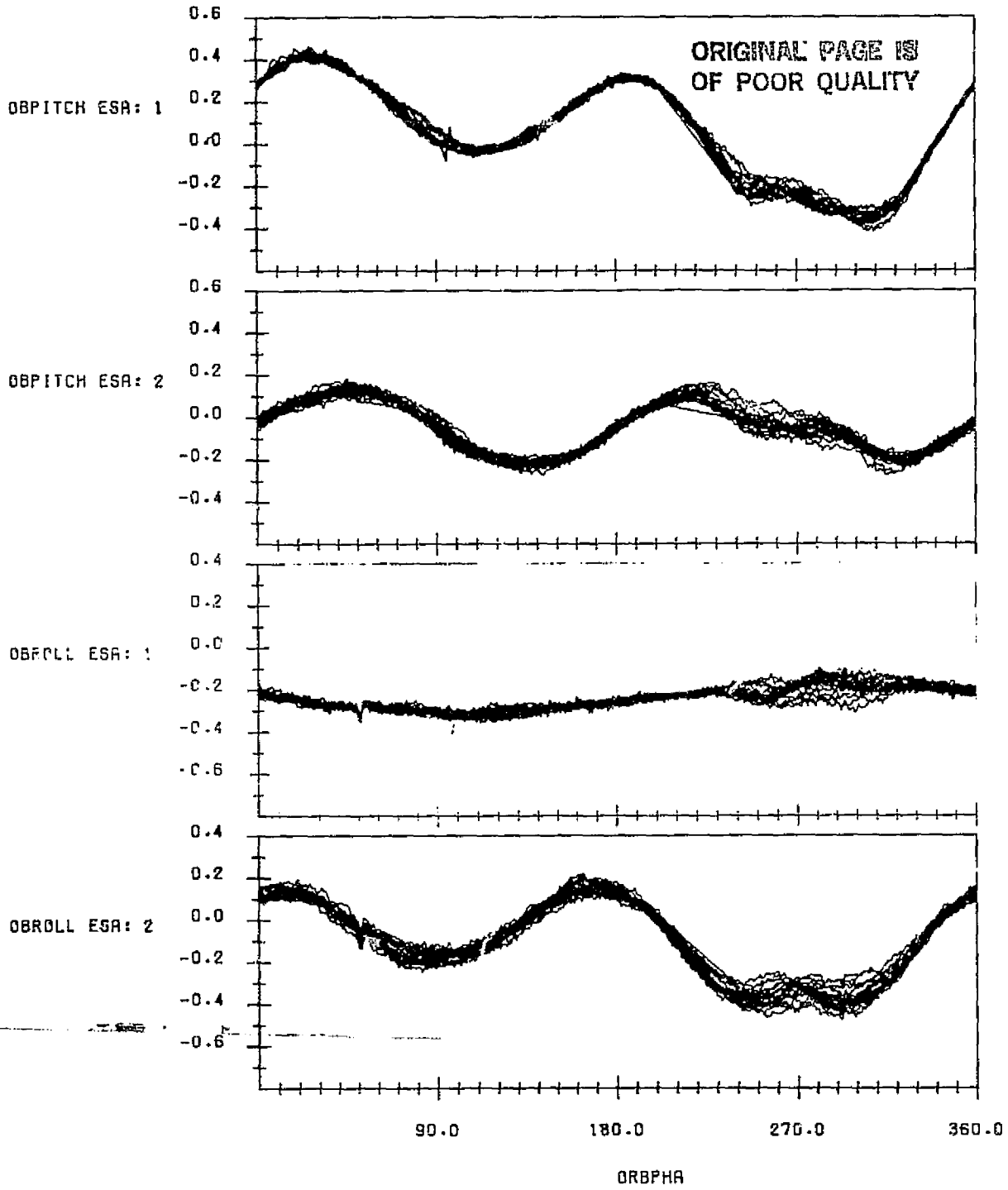

LANDSAT-4 SCANNER UNCORRECTED PITCH AND ROLL MEASUREMENTS
(DEGREES) USING NOMINAL CALIBRATION VERSUS ORBIT PHASE FROM
THE ASCENDING NODE WITH CONSECUTIVE ORBITS OVERLAID
DATA START TIME:830914.002744703
END TIME:830915.055956878

FIGURE C-28. Uncorrected Scanner Pitch and Roll Measurements for Data Span on September 14-15, 1983

APPENDIX D - RESIDUAL ERRORS FROM OBLATE EARTH MODEL

Figures D-1 through D-28 provides plots of the residual errors from the nominal oblate Earth model for all the data spans processed for this report. The model is based on the flight data differences from the predicted sensor measurements using the nominal sensor calibration, the reference attitude and orbit provided by the OBC, a 40 kilometer horizon triggering height above the standard oblate Earth, and constant bias adjustments for each channel. The constant biases removed are as follows:

Pitch	Sensor 1	0.19
Pitch	Sensor 2	-0.05
Roll	Sensor 1	-0.25
Roll	Sensor 2	0.06

The residual in degrees are plotted as a function of orbit phase from the ascending node for several orbits overlayed.

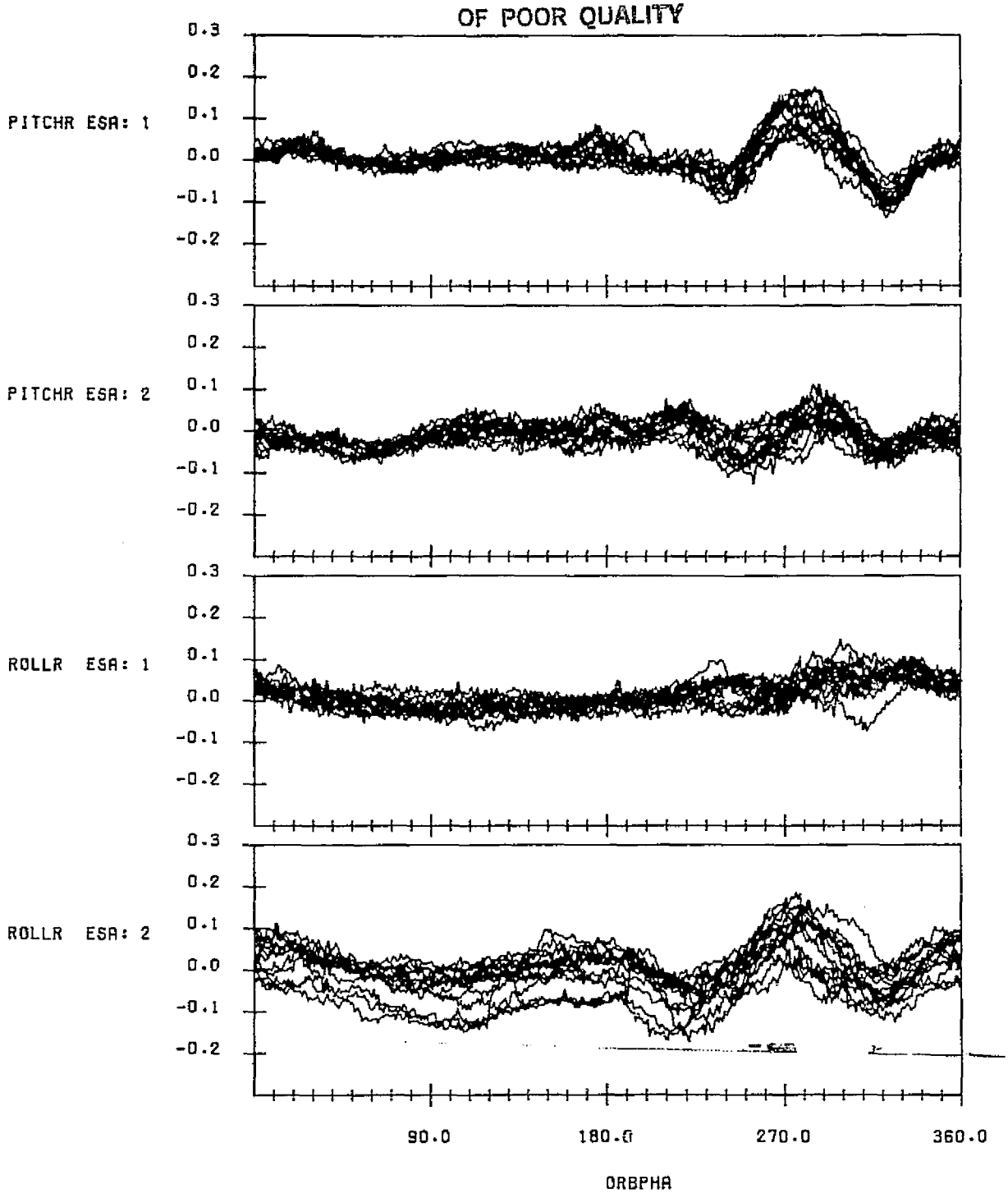

FIGURE D-1. Residual Errors from Oblate Earth Model for Data Span on August 10-11, 1982

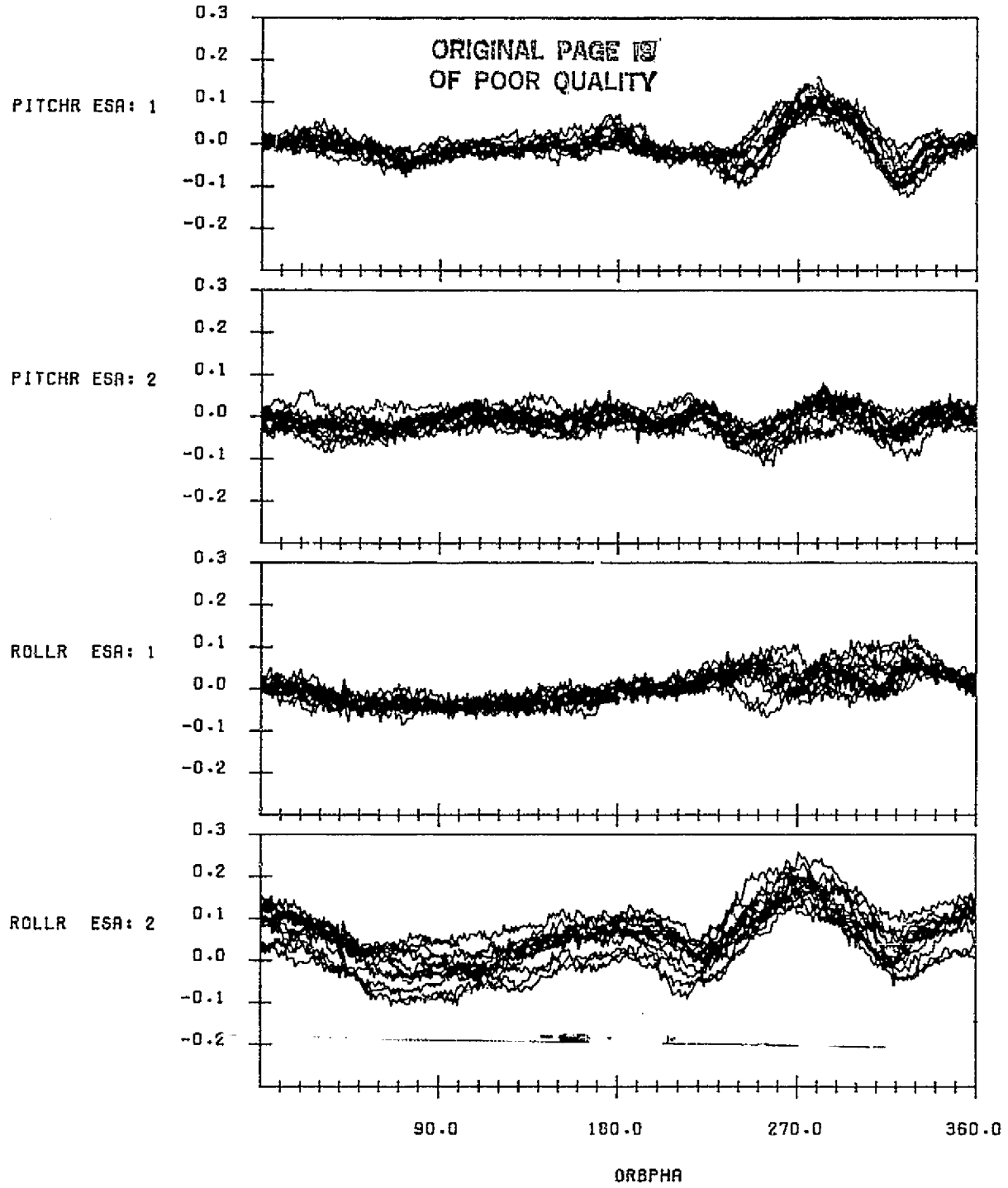

FIGURE D-2. Residual Errors from Oblate Earth Model for Data Span on August 25-26, 1982

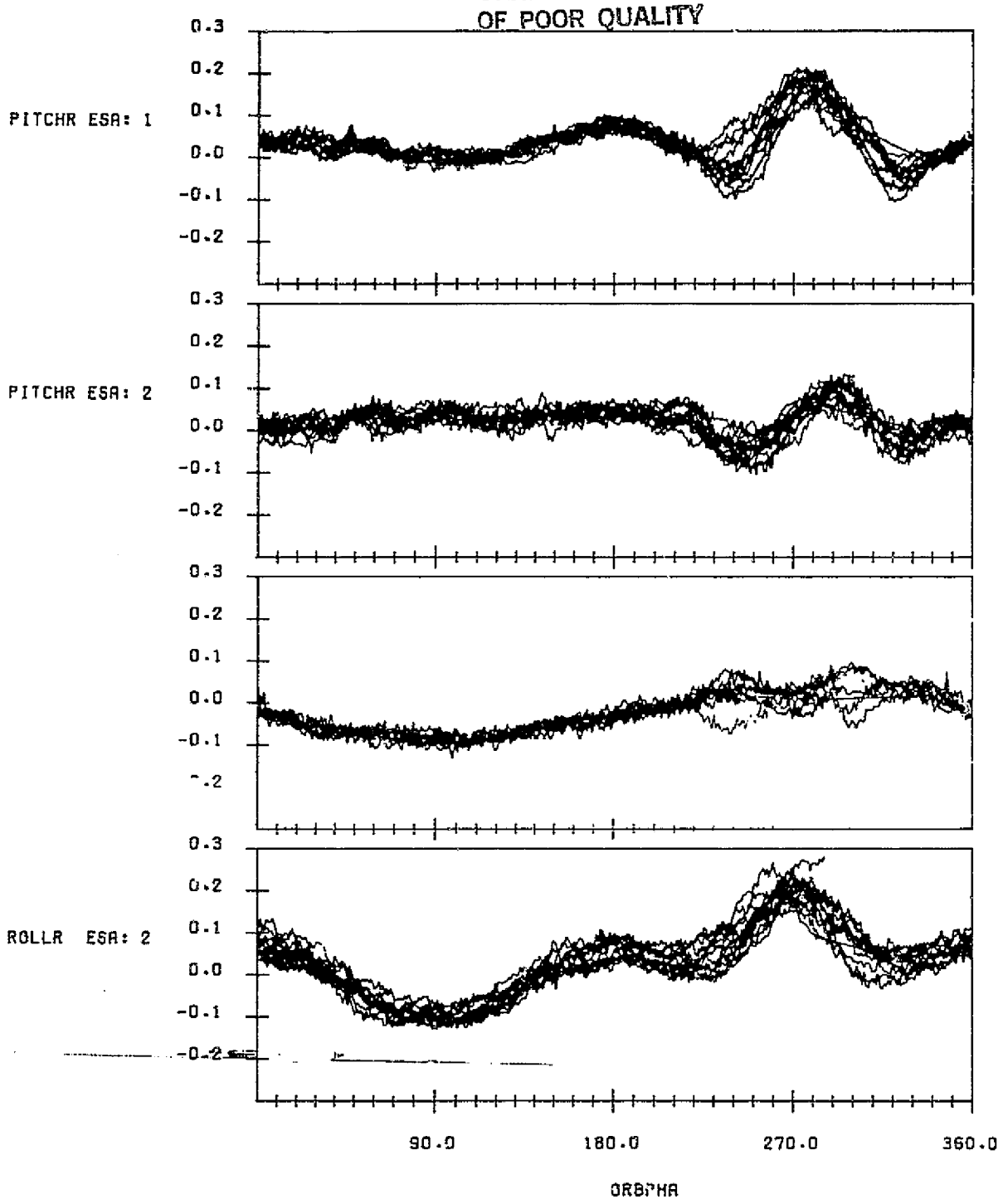

SCANNER RESIDUAL ERRORS IN DEGREES FOR NOMINAL CALIBRATION
WITH EARTH OBLATENESS, 08C ORBIT AND 08F REFERENCE ATTITUDE
EFFECTS MODELLED AND CONSTANT BIASES REMOVED
DATA START TIME:820908.043319559
END TIME:820909.051848519

FIGURE D-3. Residual Errors from Oblate Earth Model for Data Span on September 8-9, 1982

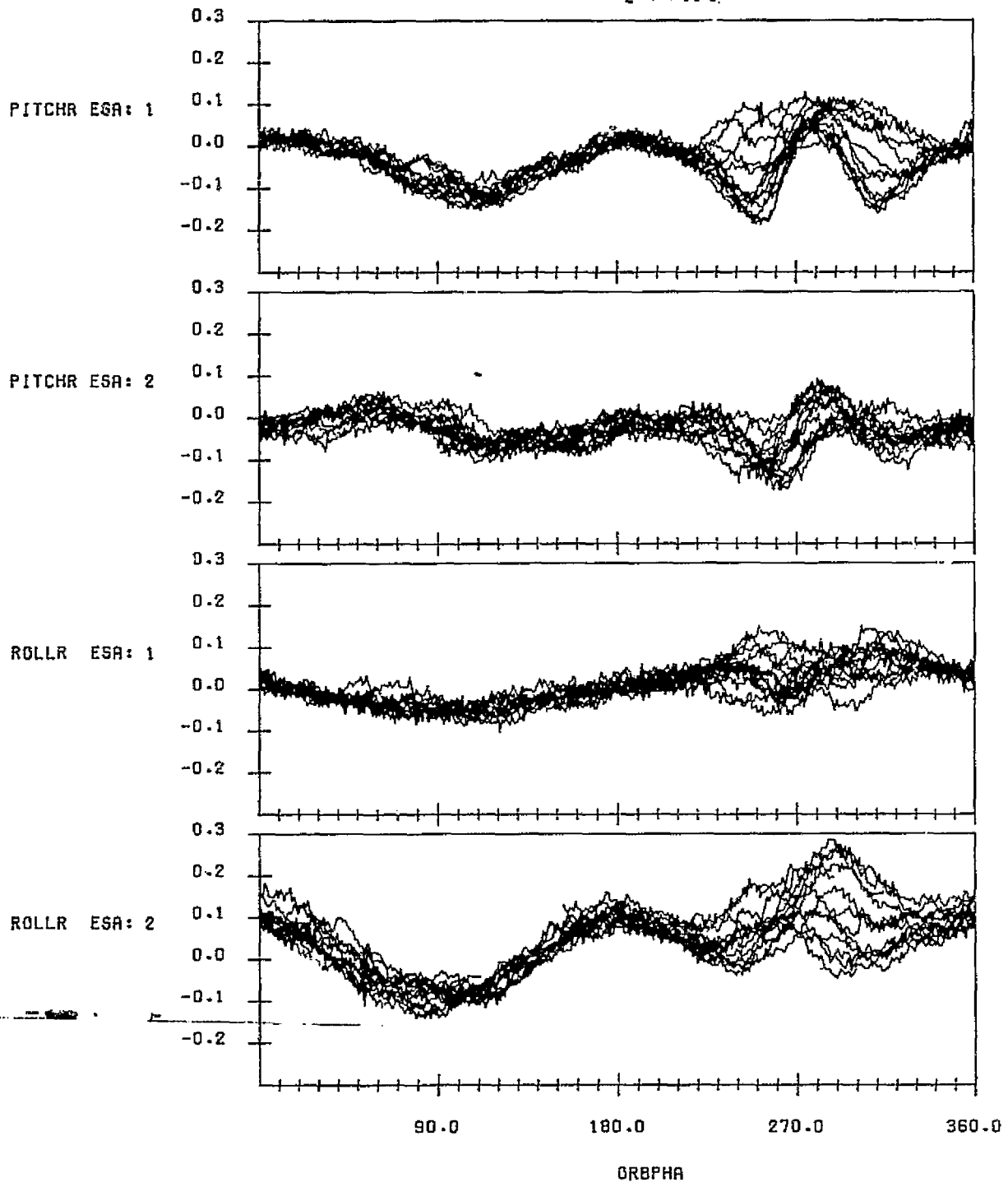

FIGURE D-4. Residual Errors from Oblate Earth Model for Data Span on September 22-23, 1982

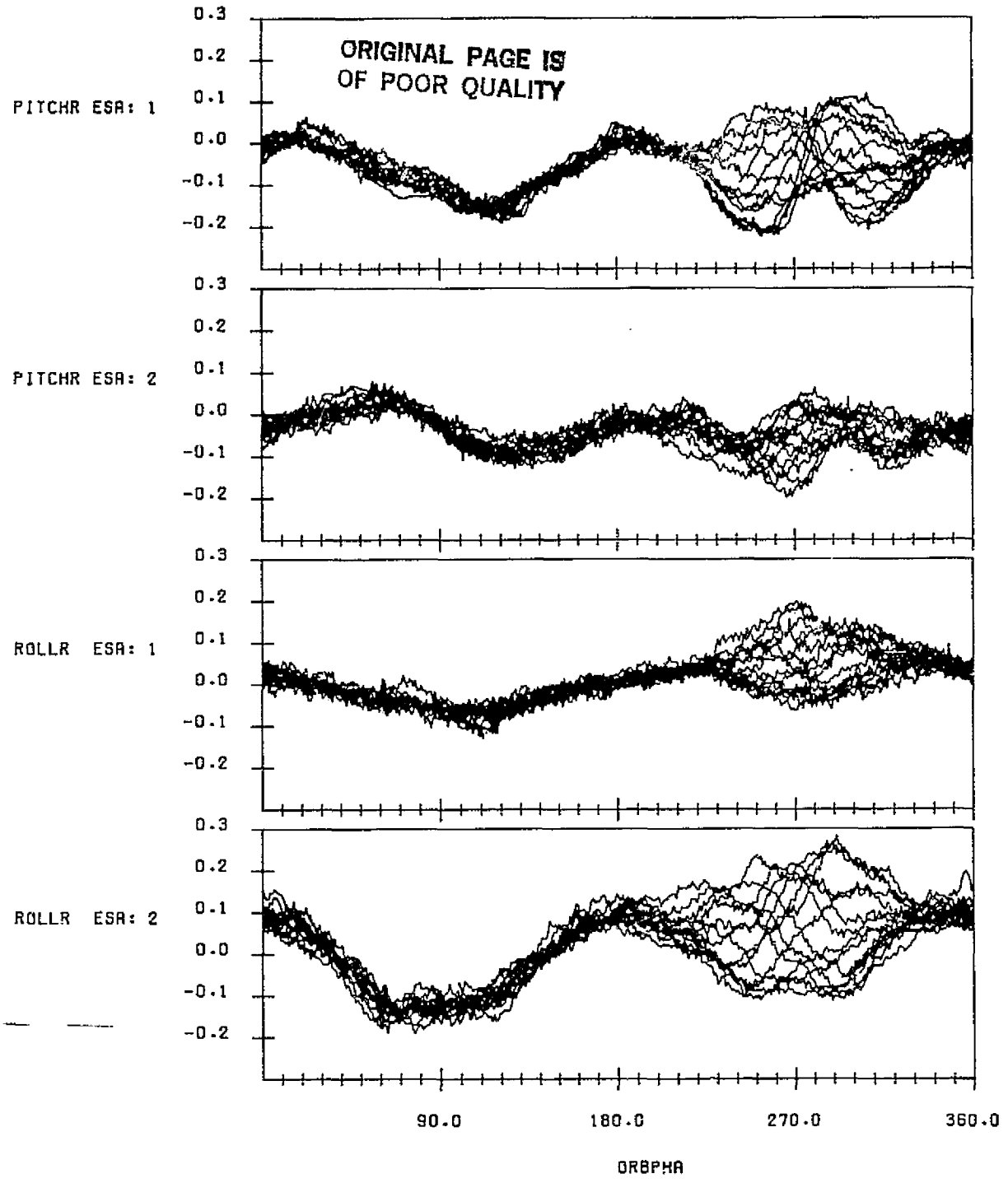

SCANNER RESIDUAL ERRORS IN DEGREES FOR NOMINAL CALIBRATION
WITH EARTH OBLATENESS, OBC ORBIT AND OBC REFERENCE ATTITUDE
EFFECTS MODELLED AND CONSTANT BIASES REMOVED
DATA START TIME:821005.153123435
END TIME:821006.164427194

FIGURE D-5. Residual Errors from Oblate Earth Model for Data Span on October 5-6, 1982

C-4

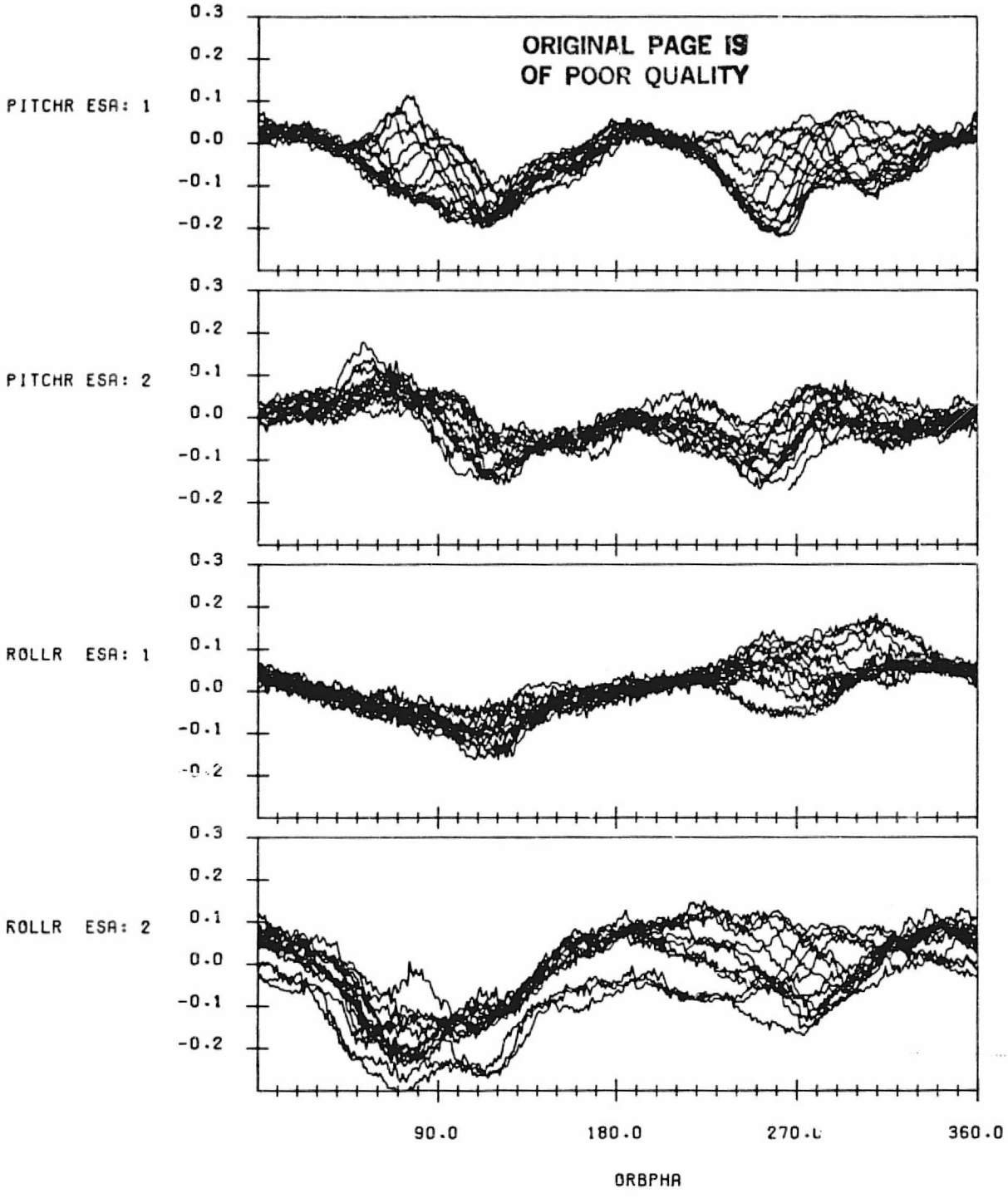

FIGURE D-6. Residual Errors from Oblate Earth Model for Data Span on October 20-21, 1982

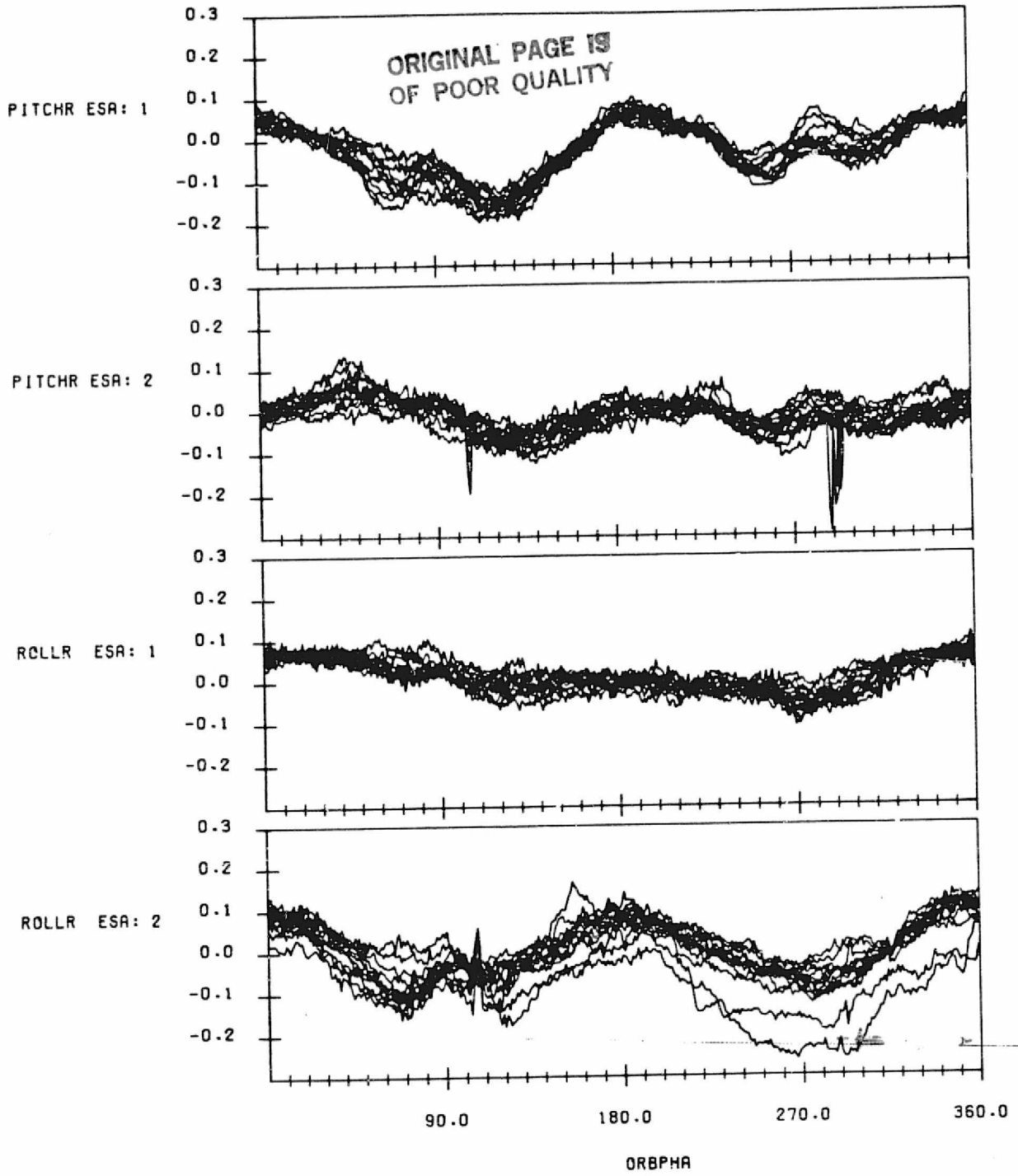

FIGURE D-7. Residual Errors from Oblate Earth Model for Data Span on November 2-3, 1982

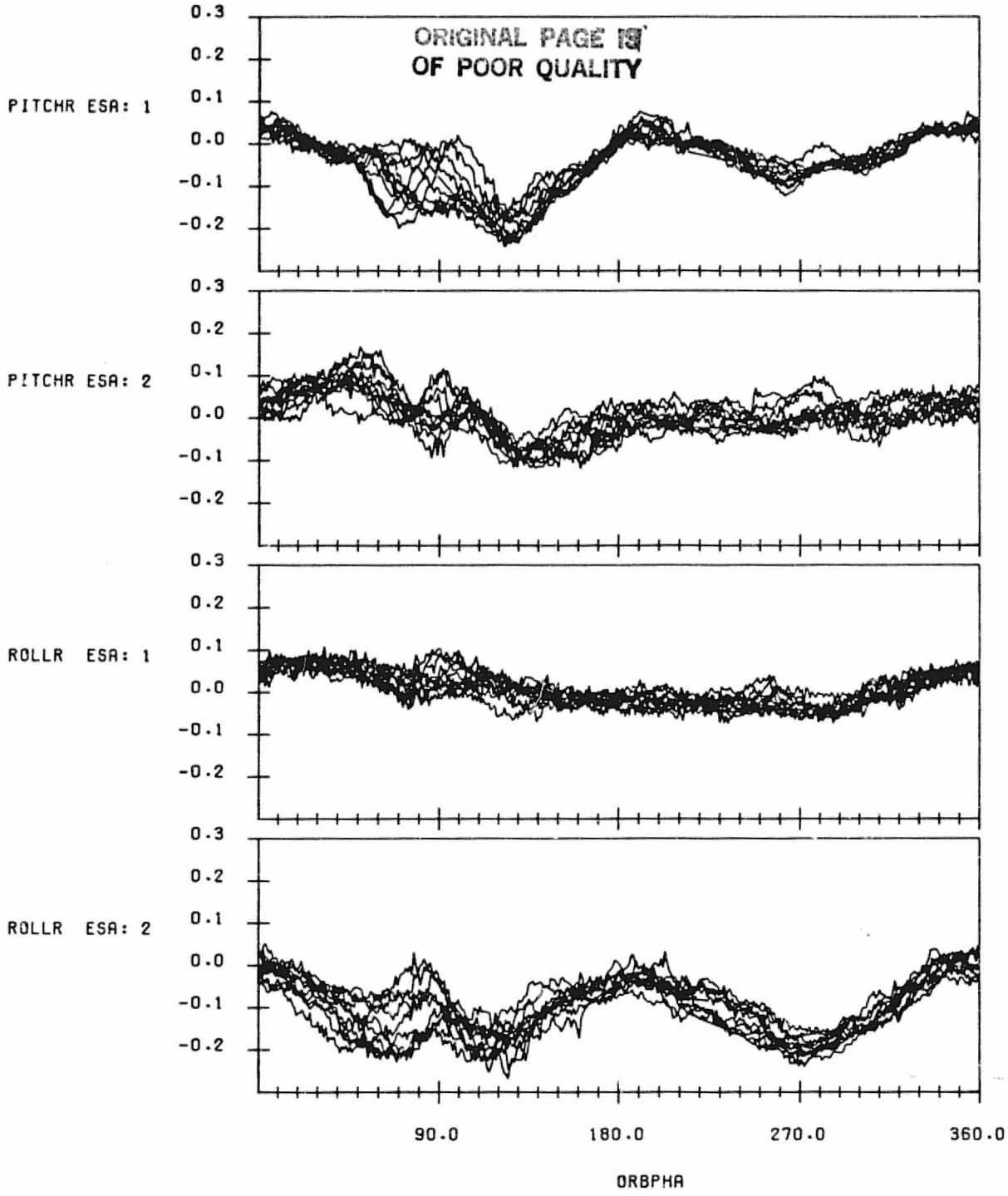

FIGURE D-8. Residual Errors from Oblate Earth Model for Data Span on November 16, 1982

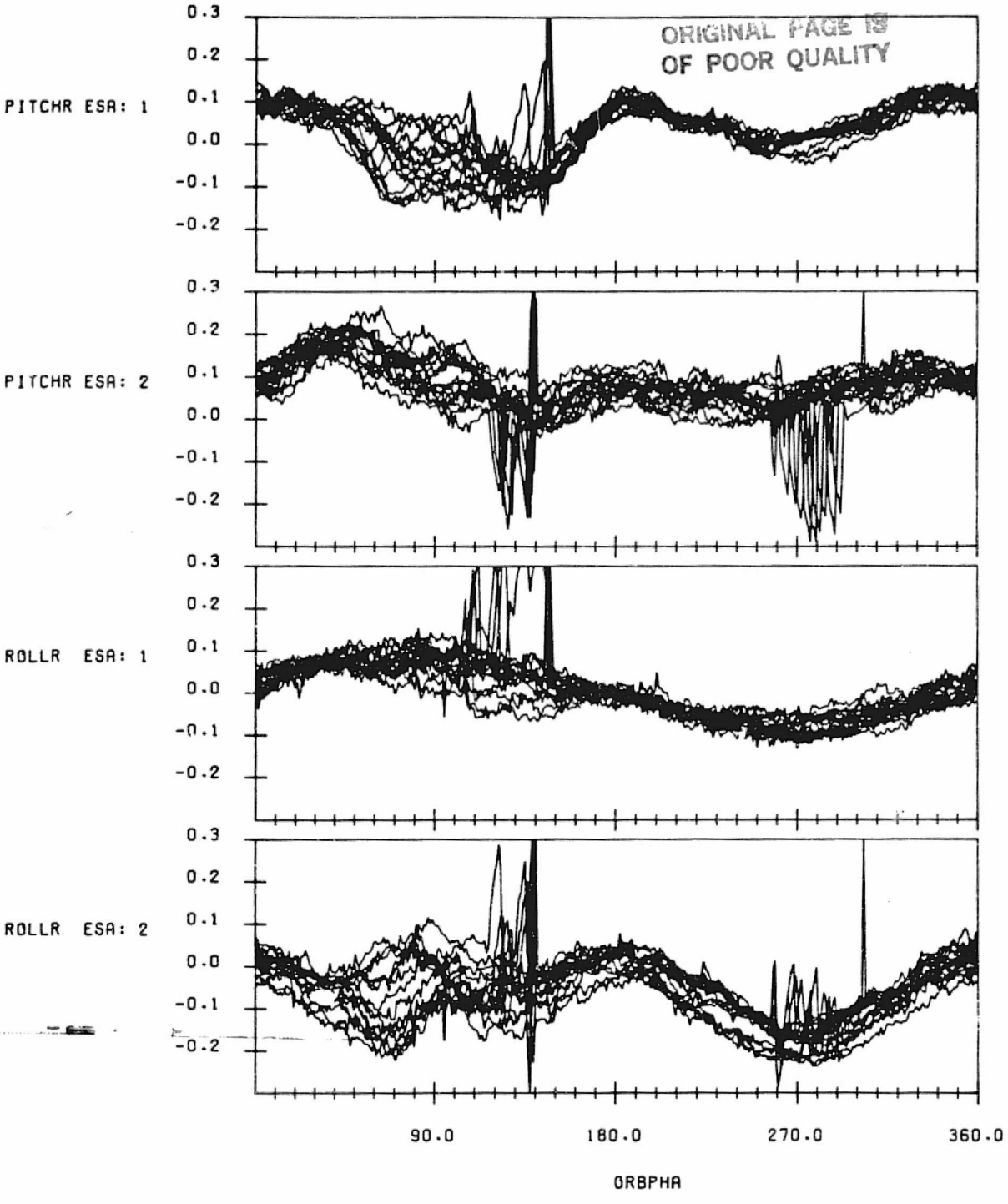

FIGURE D-9. Residual Errors from Oblate Earth Model for Data Span on December 1-2, 1982

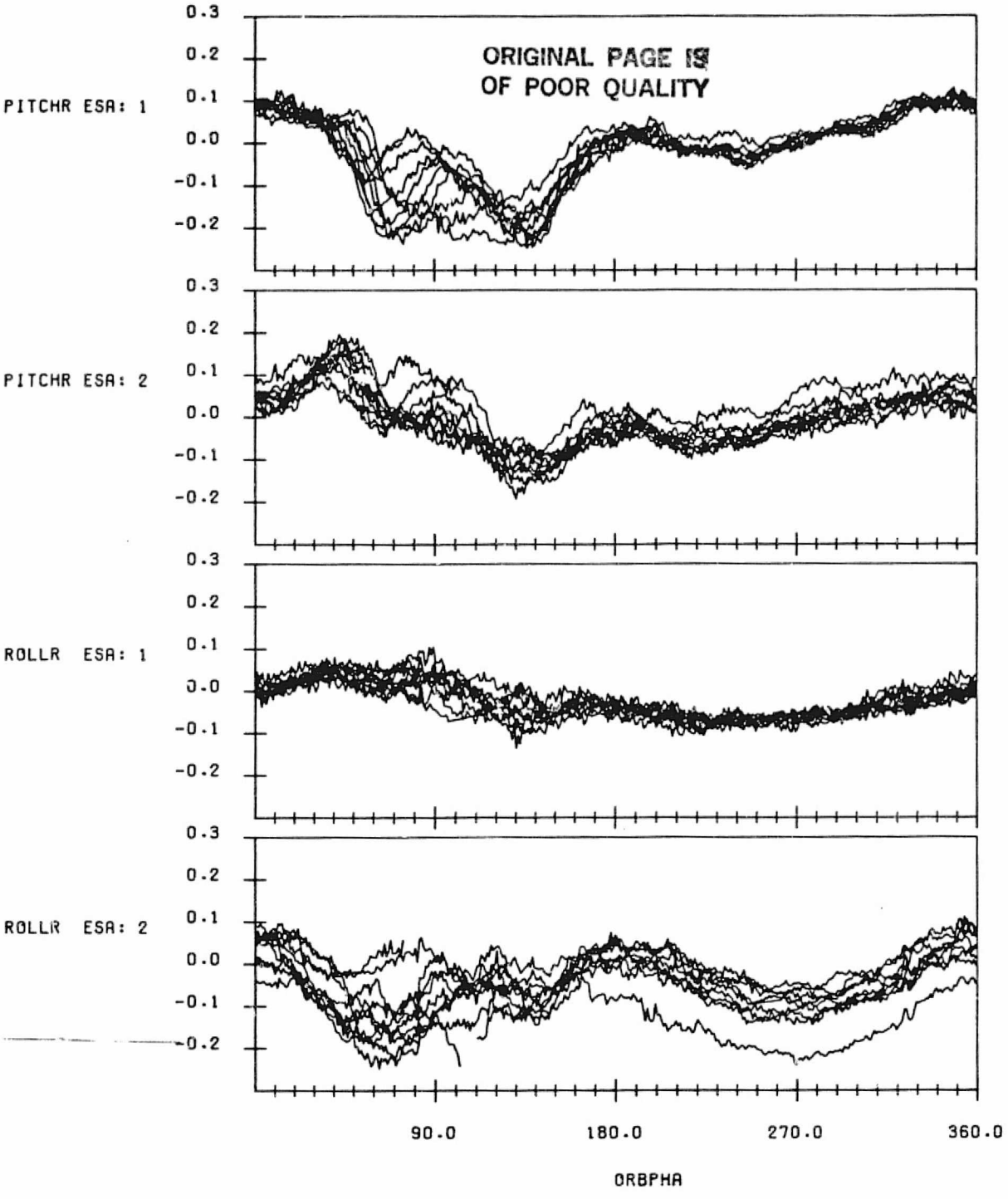

FIGURE D-10. Residual Errors from Oblate Earth Model for Data Span on December 14-15, 1982

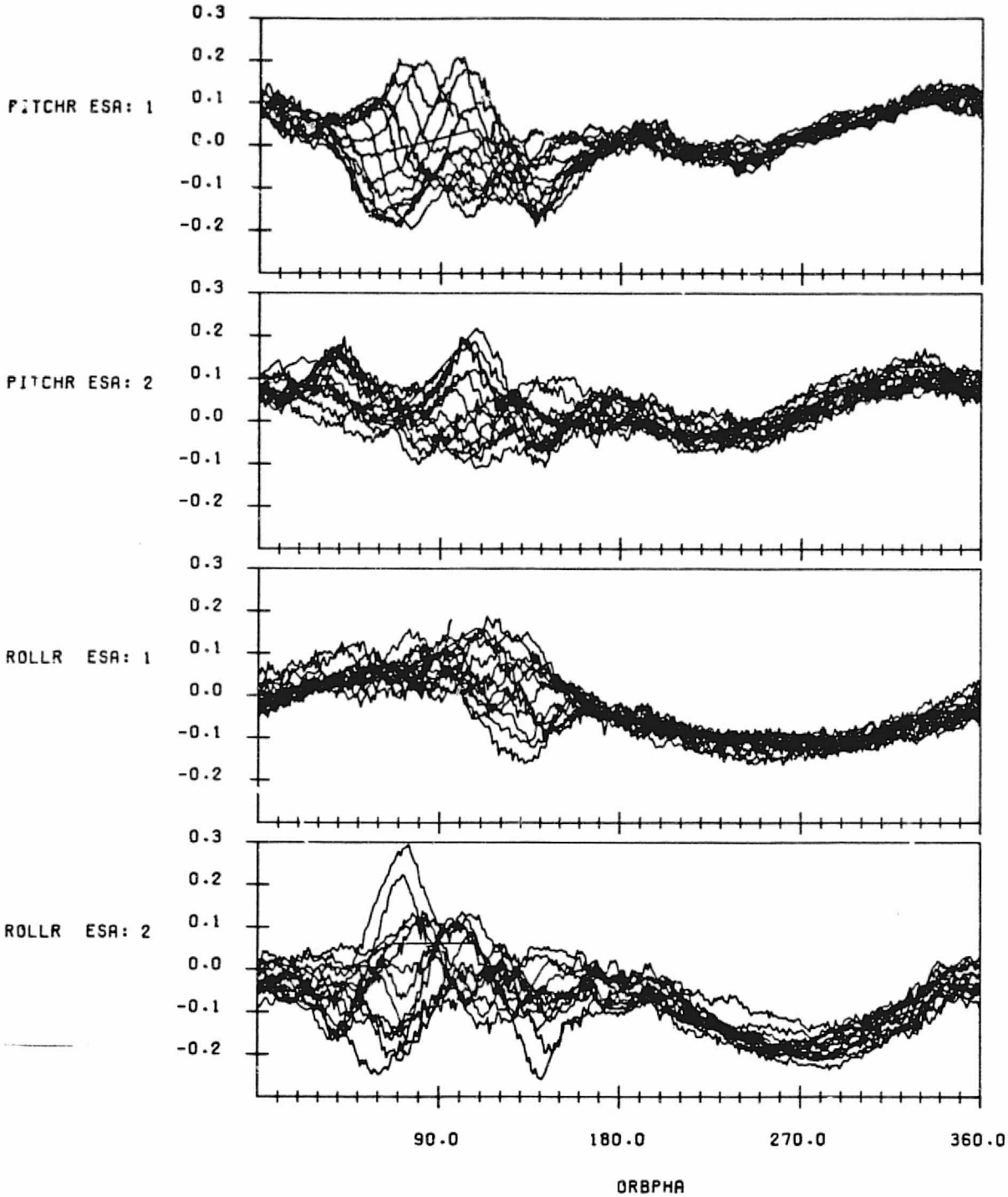

FIGURE D-11. Residual Errors from Oblate Earth Model for Data Span on December 28-29, 1982

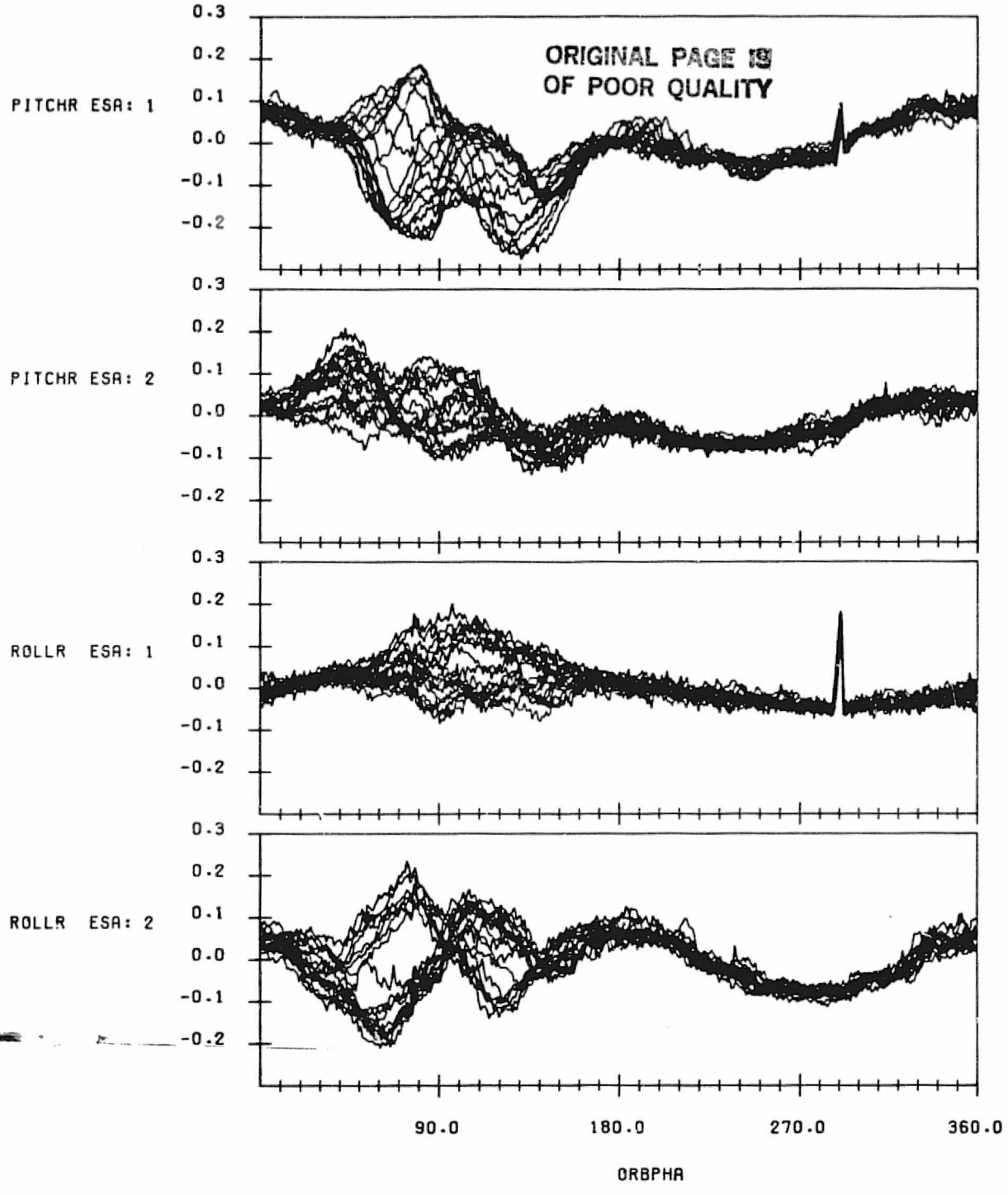

SCANNER RESIDUAL ERRORS IN DEGREES FOR NOMINAL CALIBRATION
WITH EARTH OBLATENESS, OBC ORBIT AND OBC REFERENCE ATTITUDE
EFFECTS MODELLED AND CONSTANT BIASES REMOVED
DATA START TIME:830119.063608627
END TIME:830120.120626114

FIGURE D-12. Residual Errors from Oblate Earth Model for Data Span on January 19-20, 1983

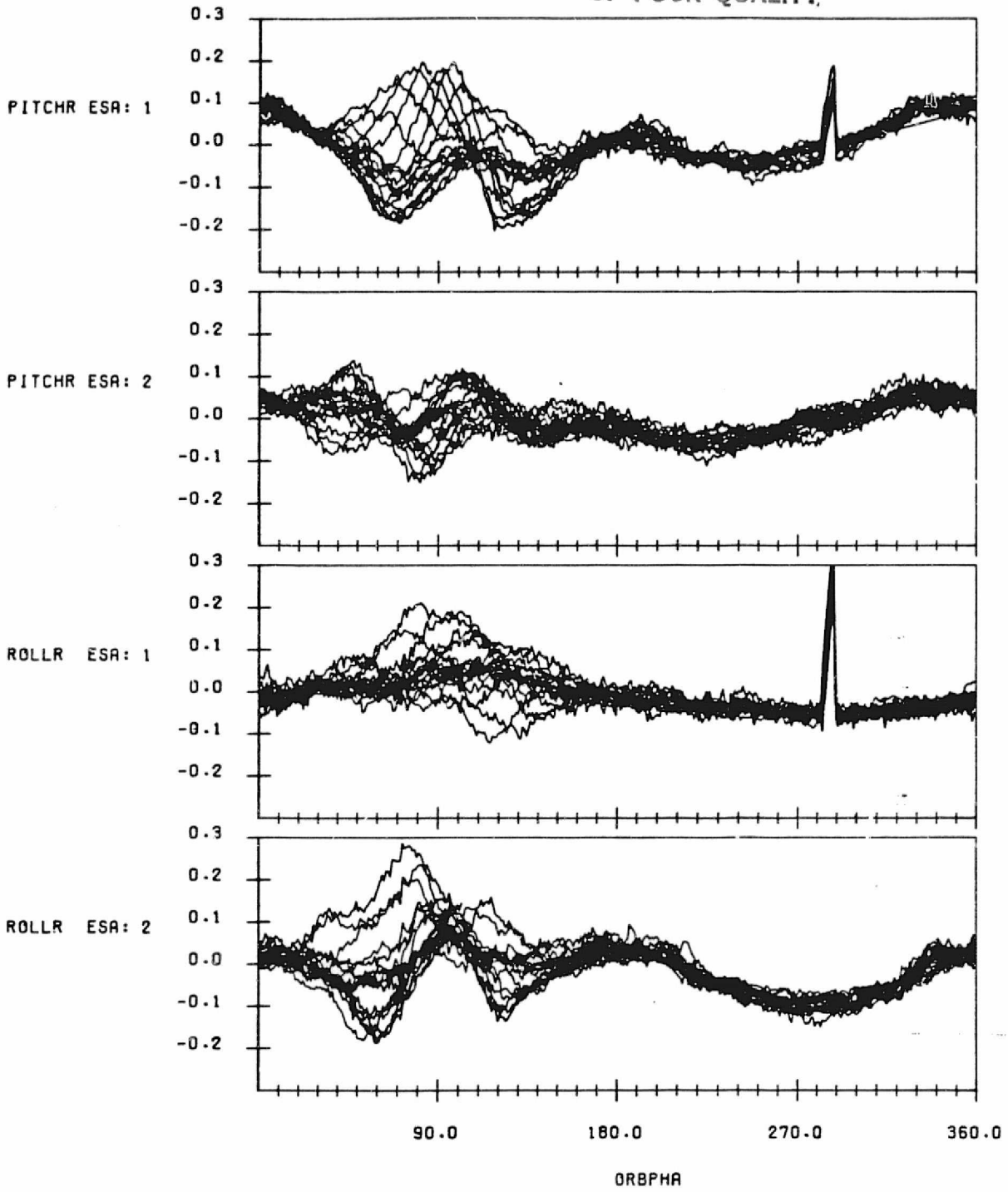

FIGURE D-13. Residual Errors from Oblate Earth Model for Data Span on February 2-3, 1983

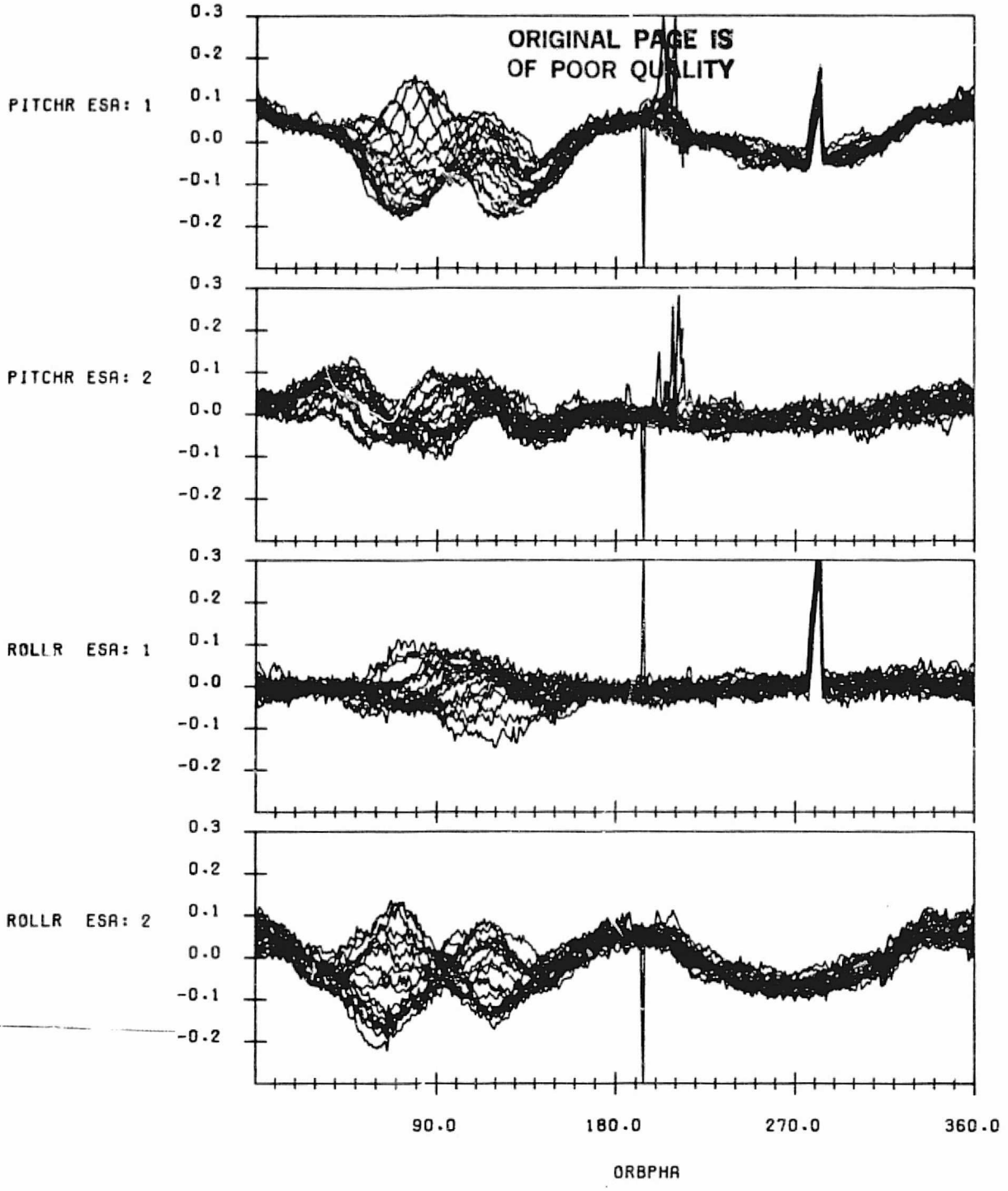

FIGURE D-14. Residual Errors from Oblate Earth Model for Data Span on February 17-18, 1983

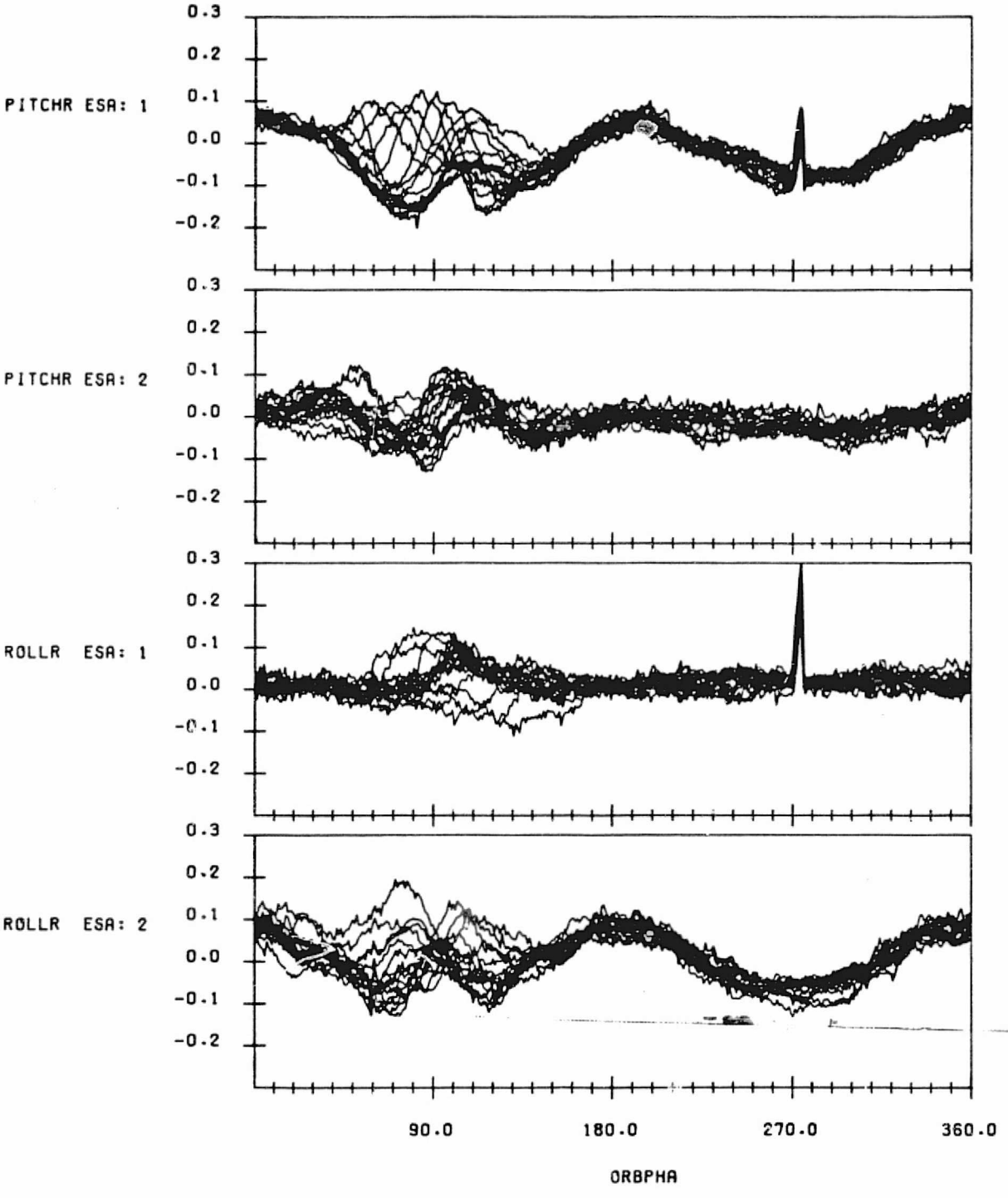

FIGURE D-15. Residual Errors from Oblate Earth Model for Data Span on March 3-4, 1983

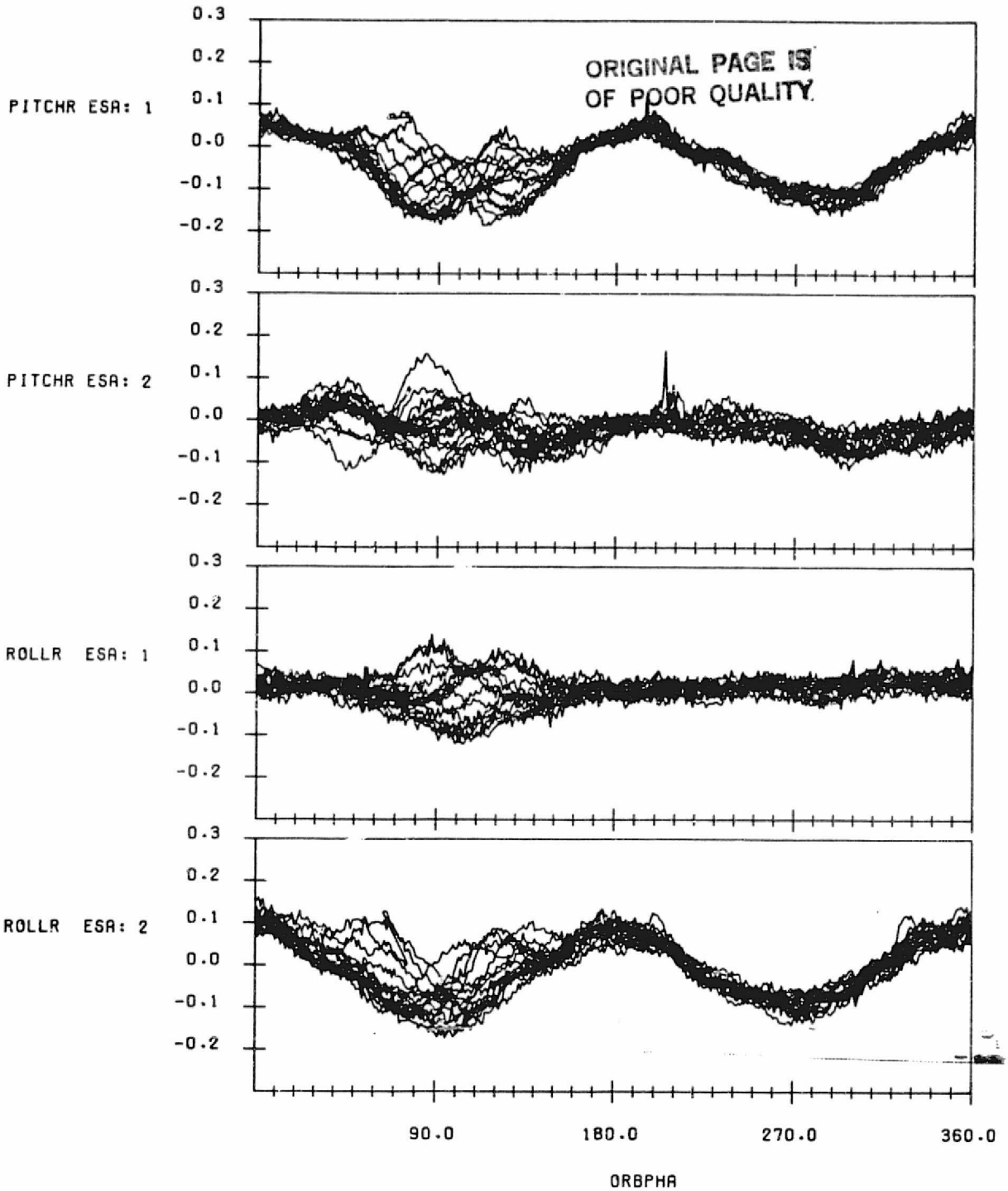

FIGURE D-16. Residual Errors from Oblate Earth Model for Data Span on March 14-15, 1983

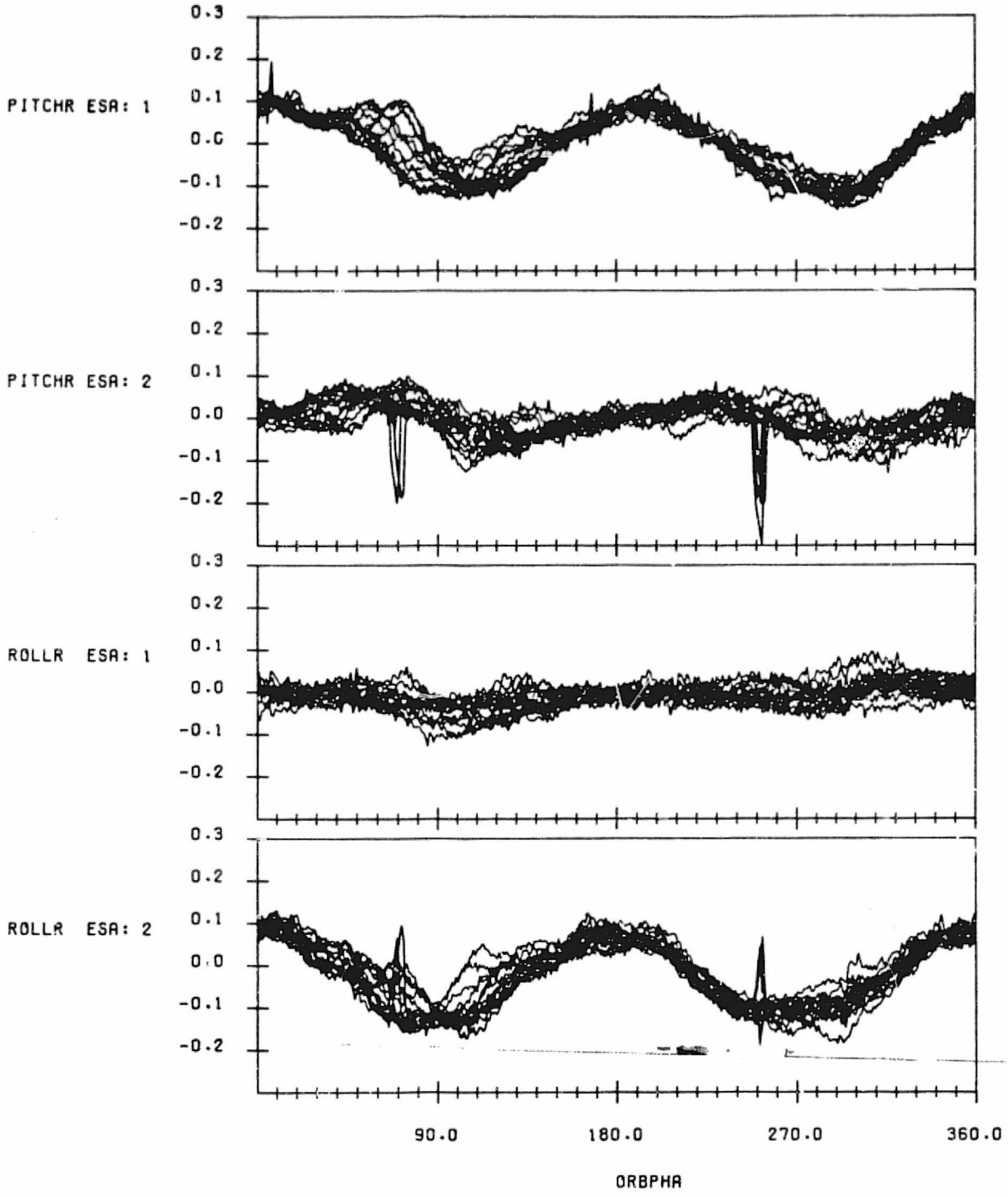

FIGURE D-17. Residual Errors from Oblate Earth Model for Data Span on March 29-31, 1983

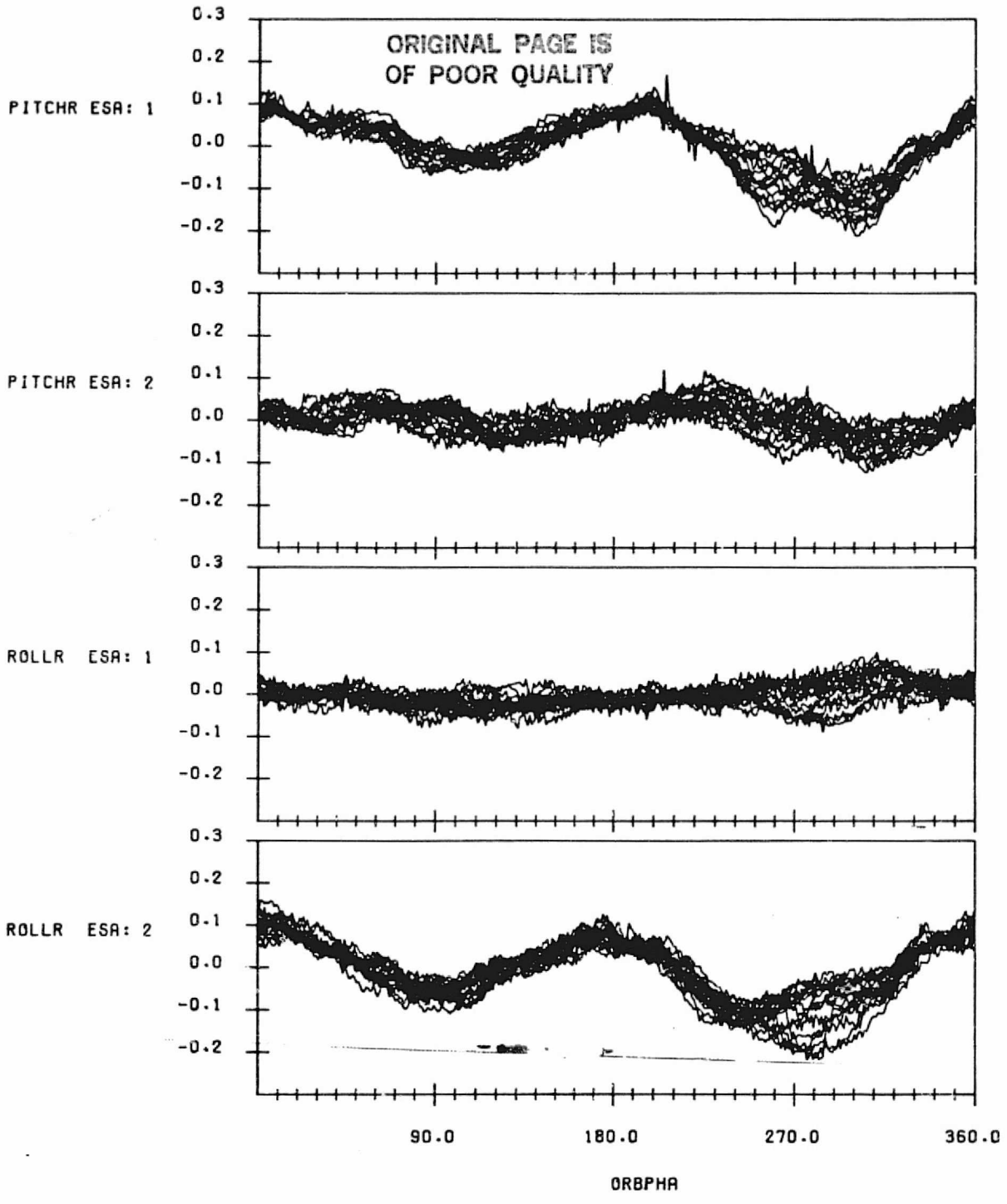

FIGURE D-18. Residual Errors from Oblate Earth Model for Data Span on April 14-15, 1983

ORIGINAL PAGE IS
OF POOR QUALITY

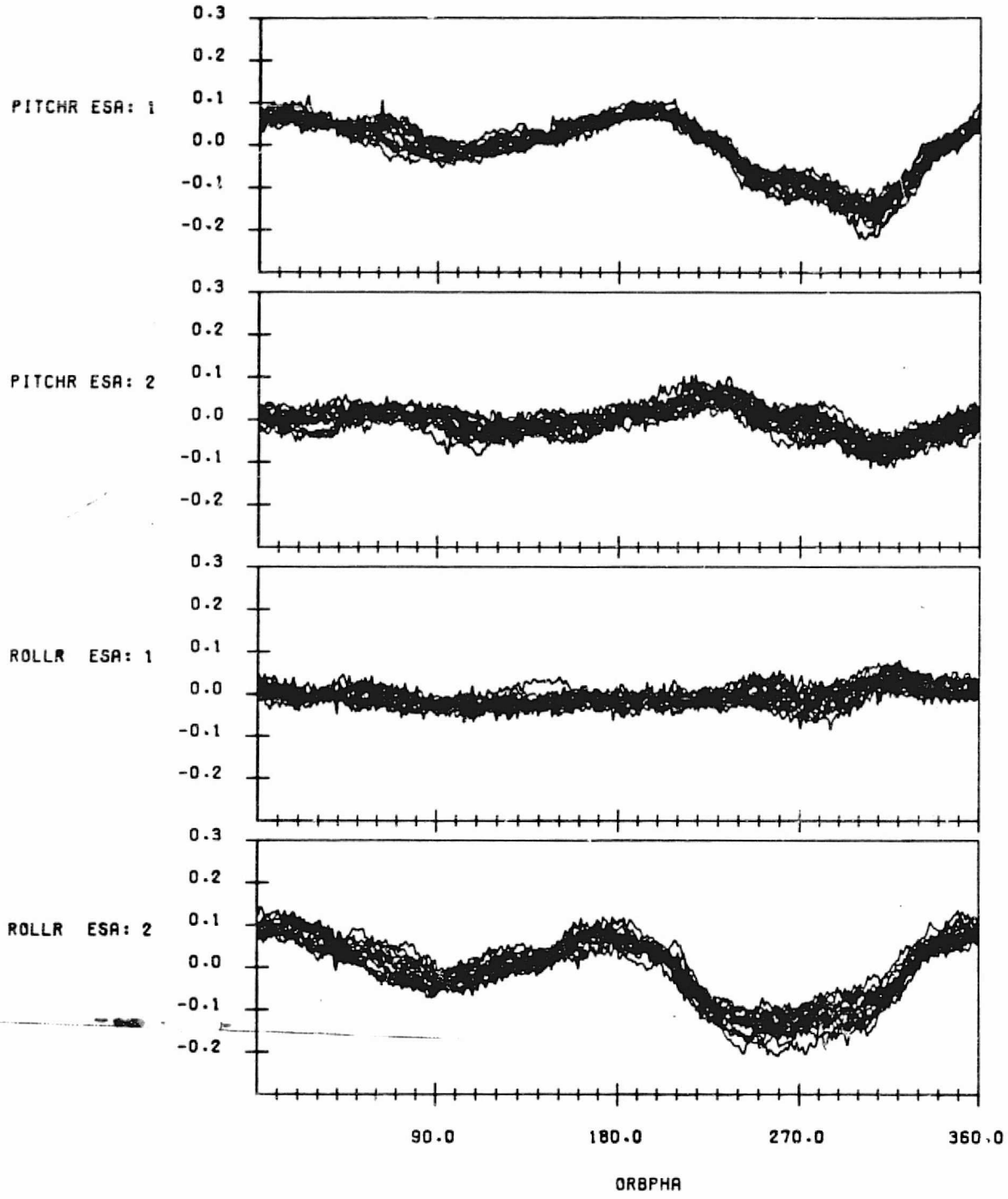

FIGURE D-19. Residual Errors from Oblate Earth Model for Data Span on April 26-27, 1983

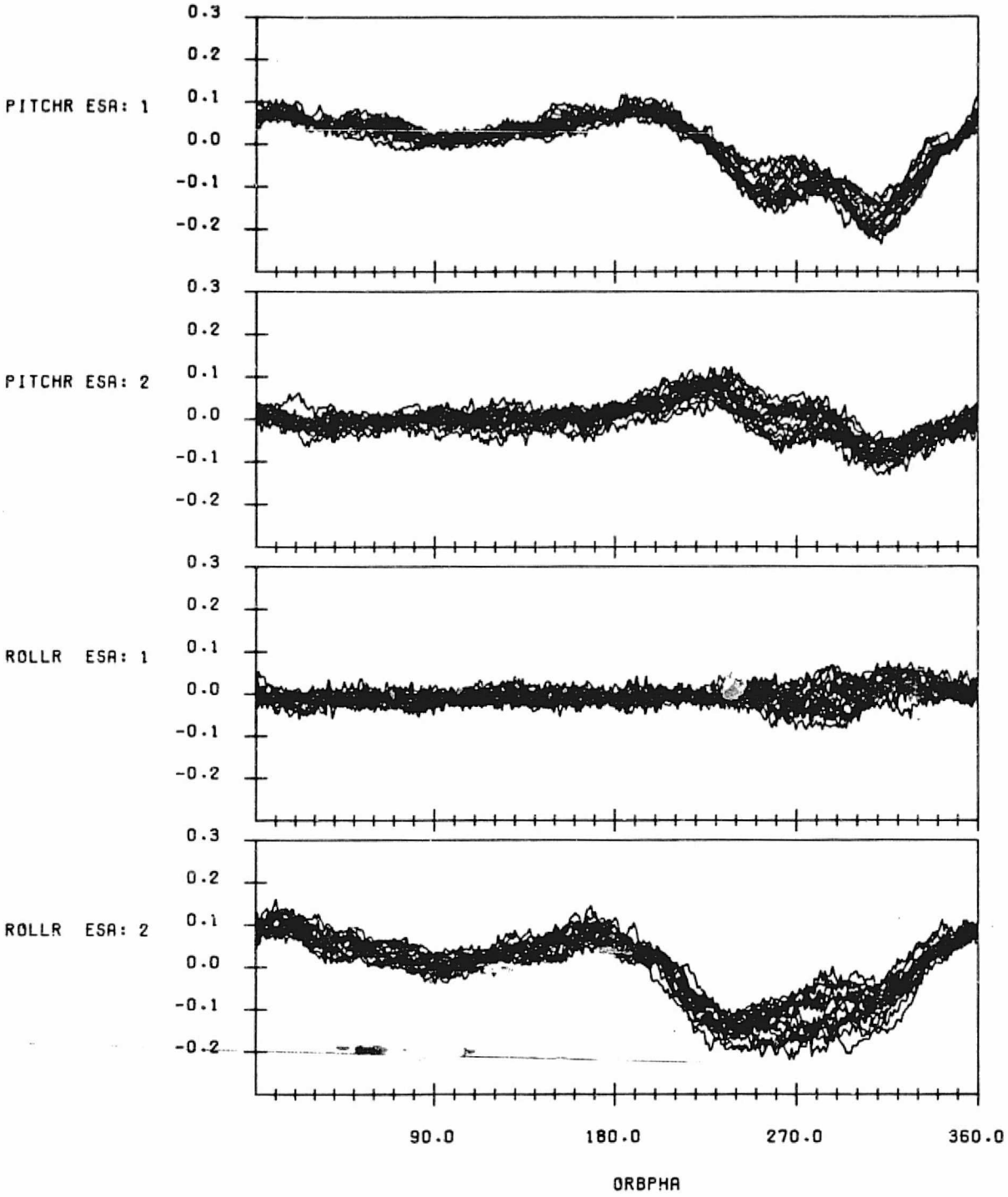

FIGURE D-20. Residual Errors from Oblate Earth Model for Data Span on May 11-12, 1983

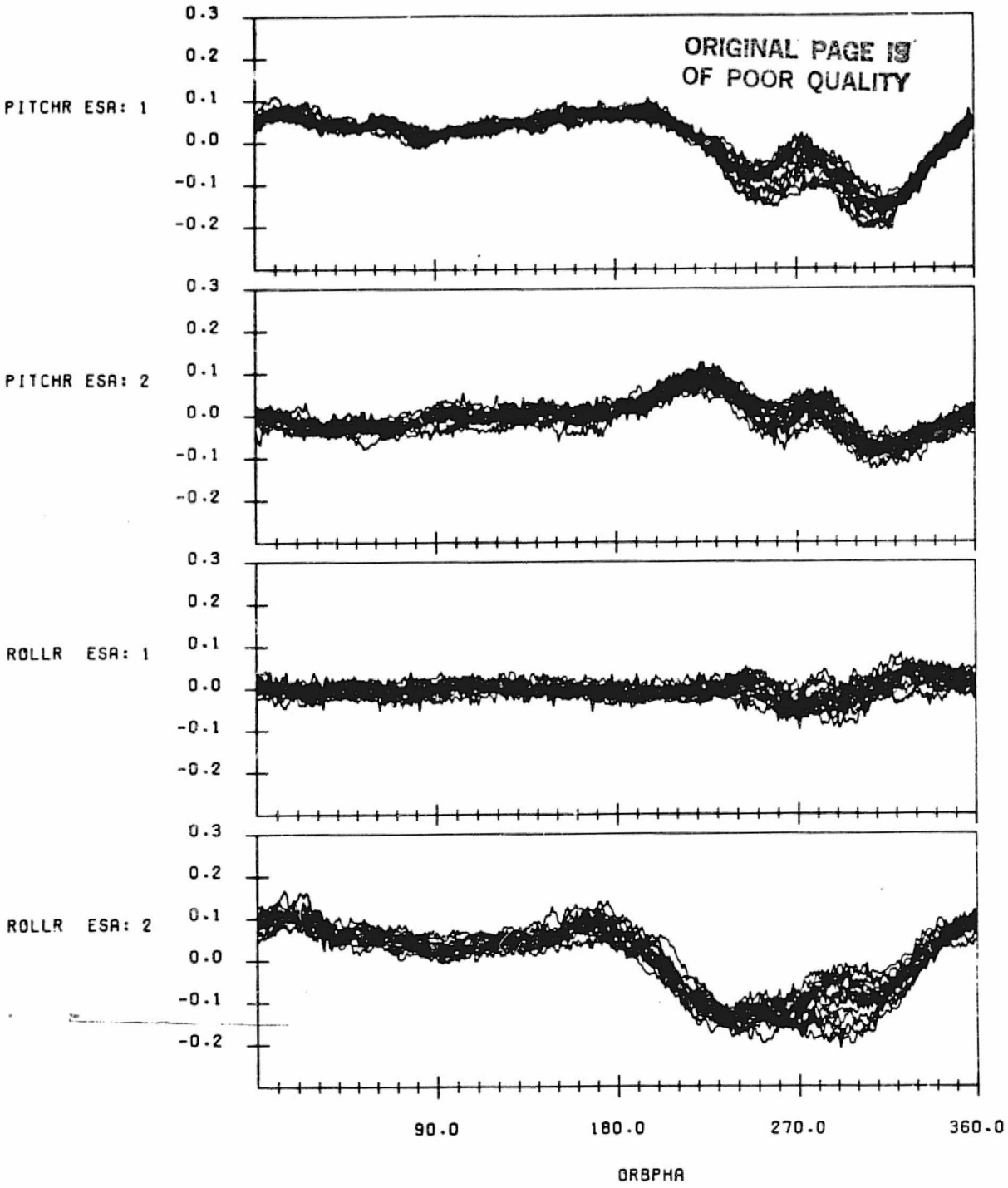

FIGURE D-21. Residual Errors from Oblate Earth Model for Data Span on May 23-24, 1983

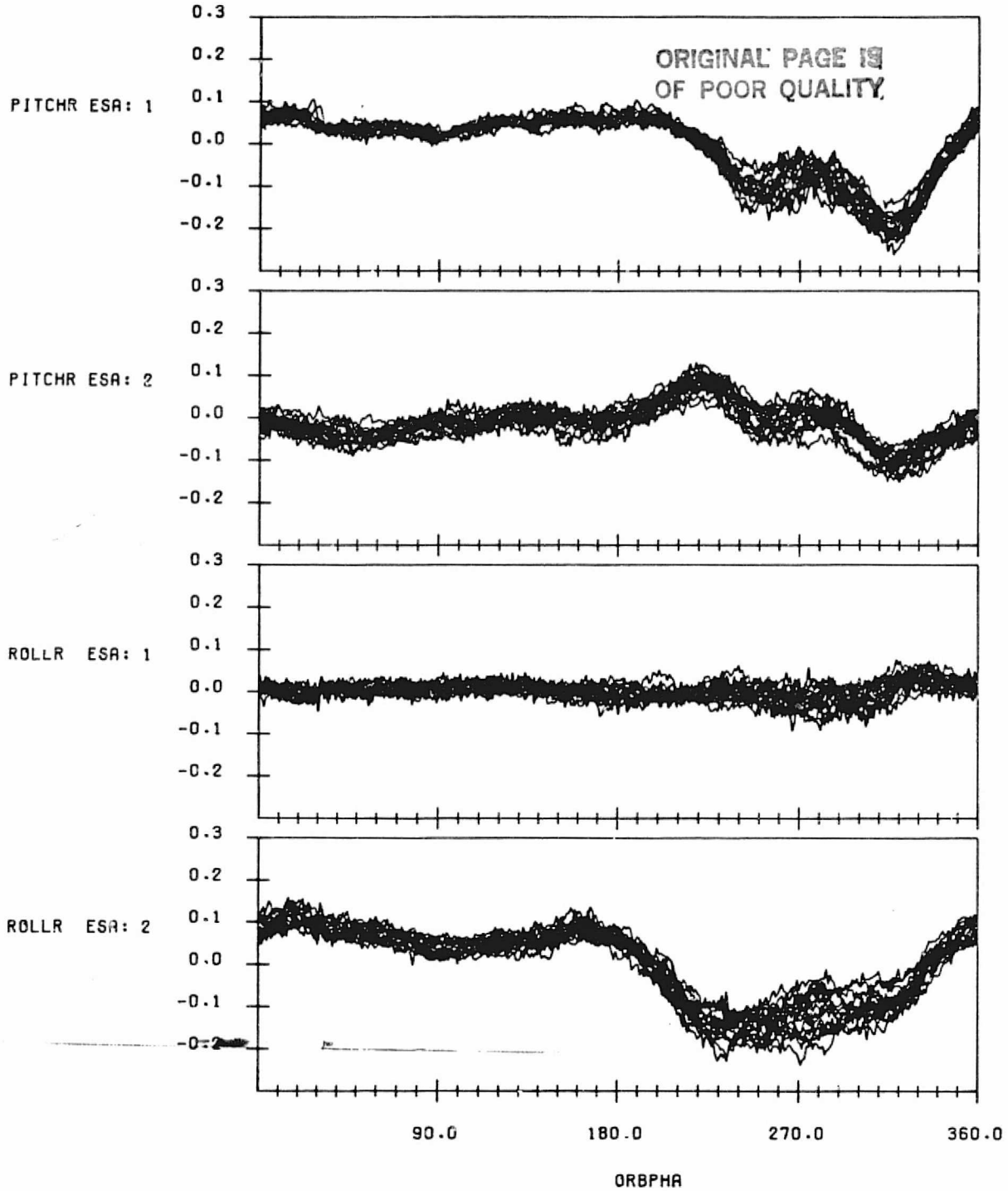

FIGURE D-22. Residual Errors from Oblate Earth Model for Data Span on June 6-7, 1983

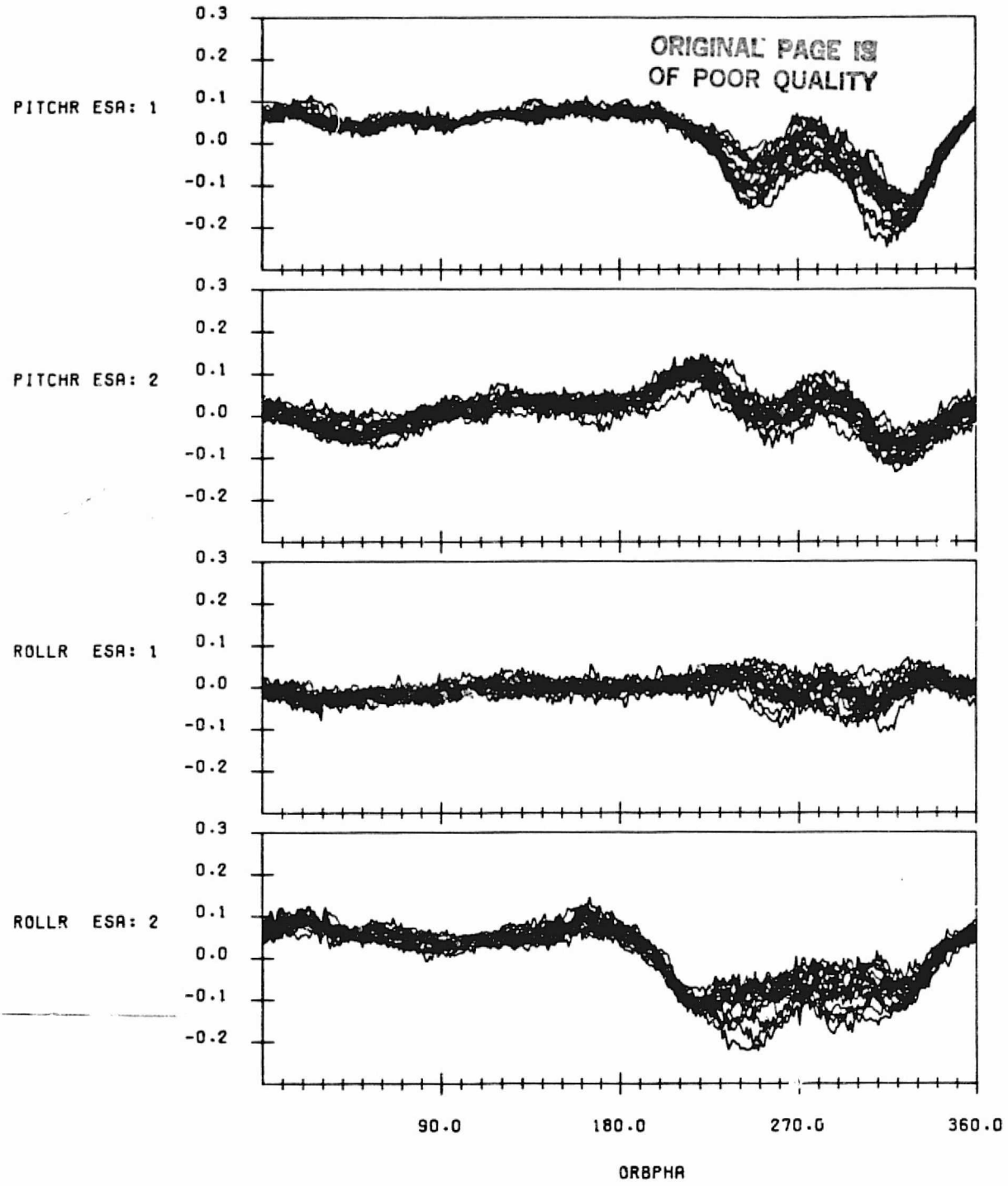

FIGURE D-23. Residual Errors from Oblate Earth Model for Data Span on June 21-23, 1983

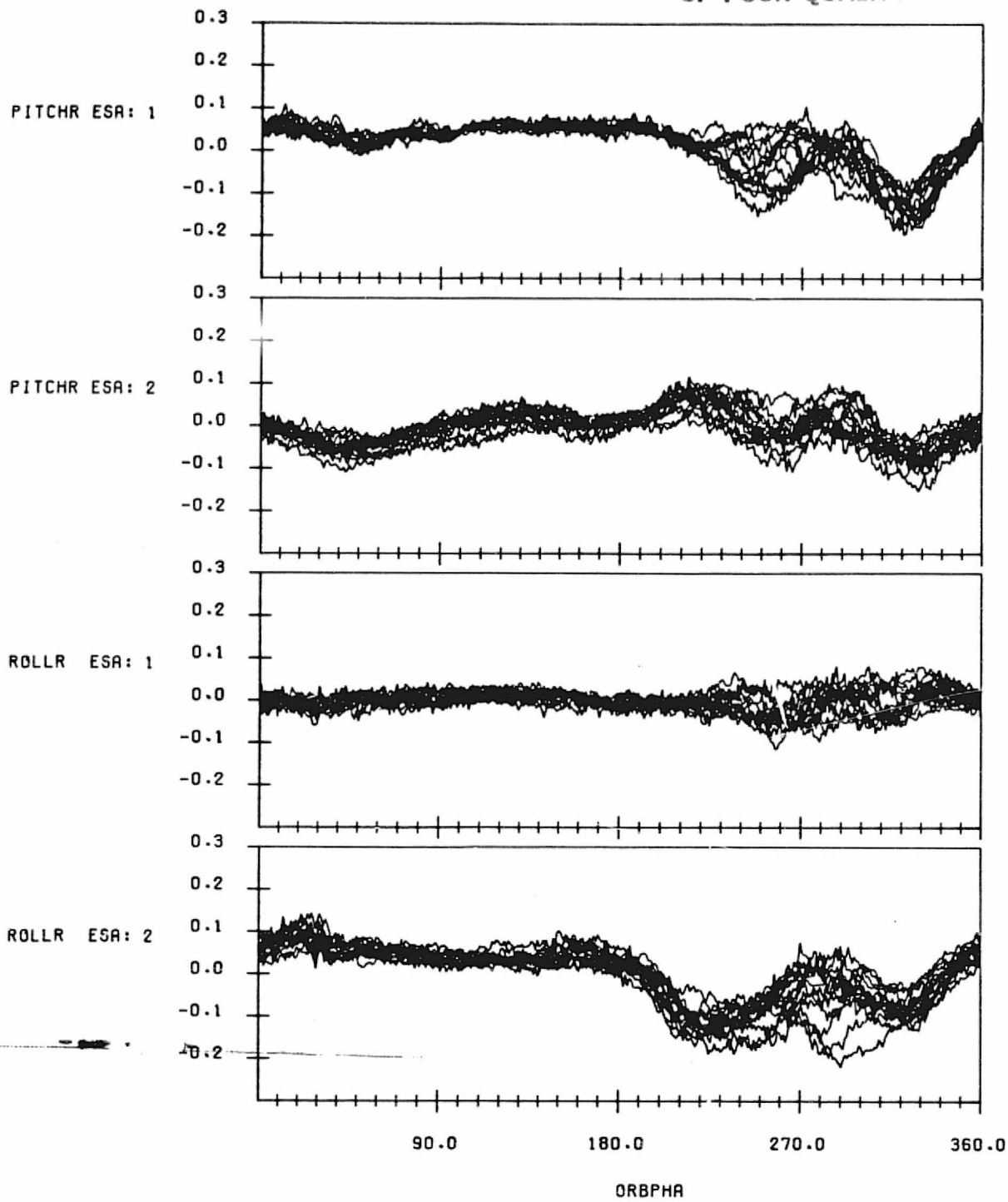

FIGURE D-24. Residual Errors from Oblate Earth Model for Data Span on July 6-7, 1983

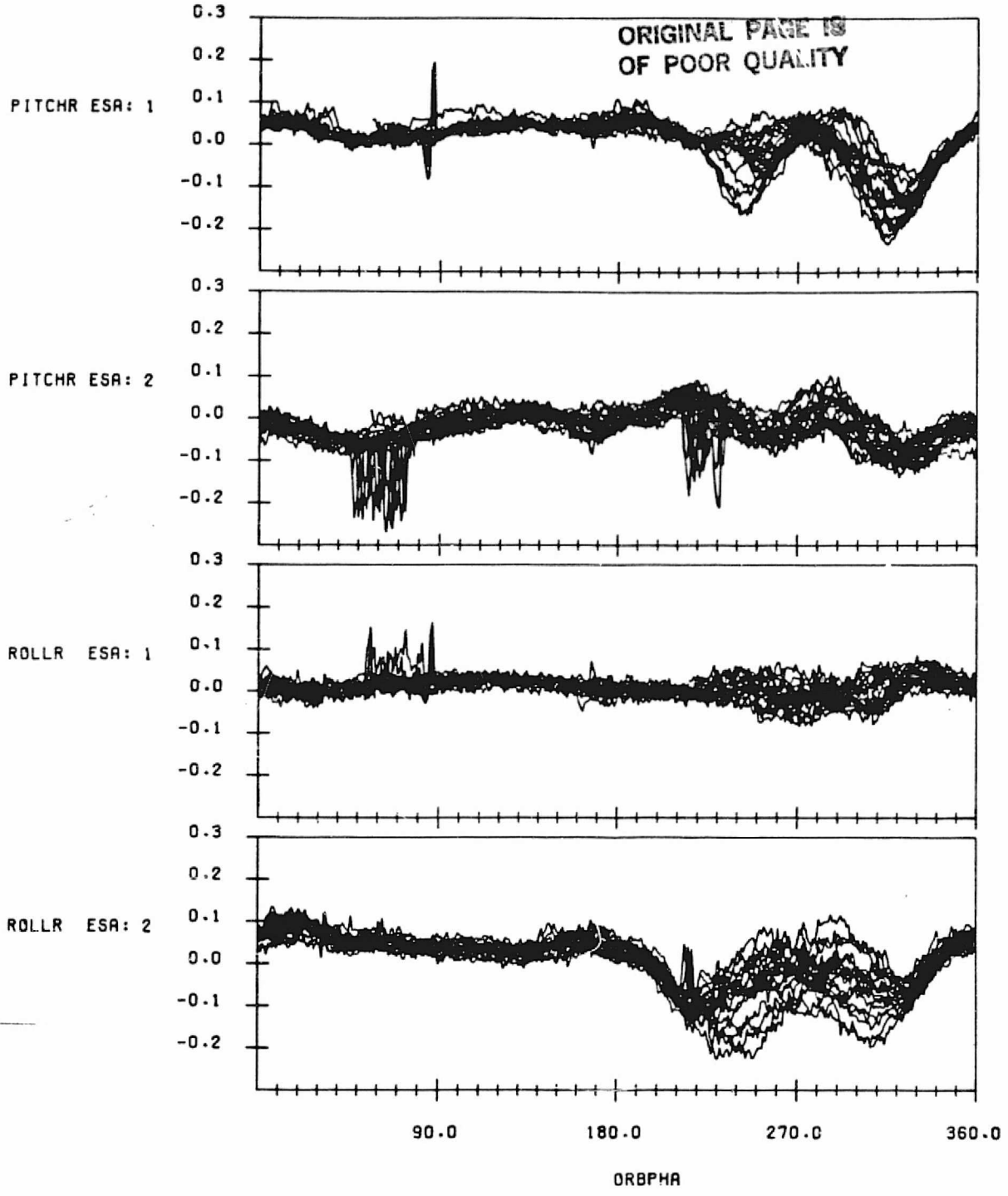

FIGURE D-25. Residual Errors from Oblate Earth Model for Data Span on July 26-27, 1983

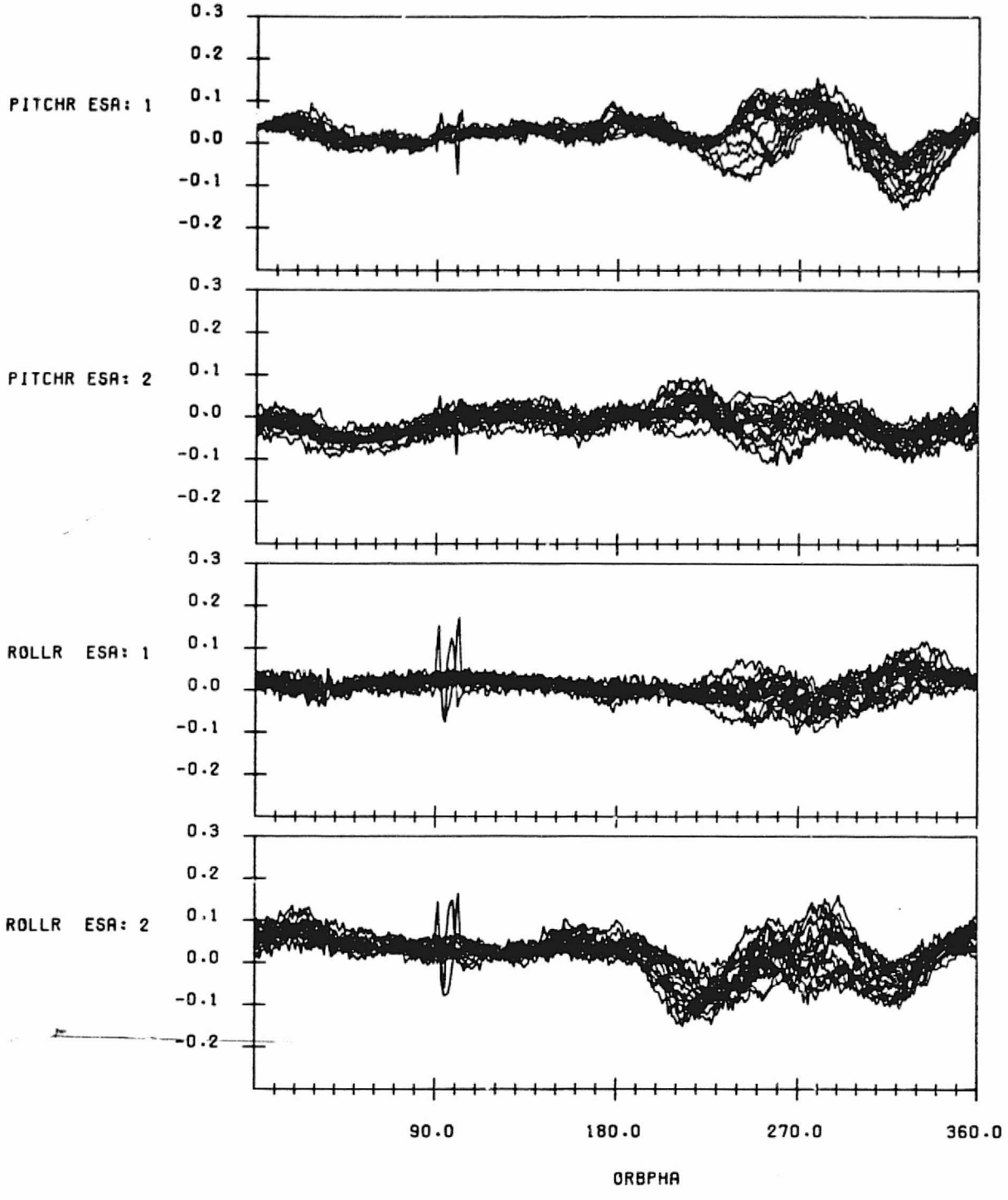

FIGURE D-26. Residual Errors from Oblate Earth Model for Data Span on August 6-7, 1983

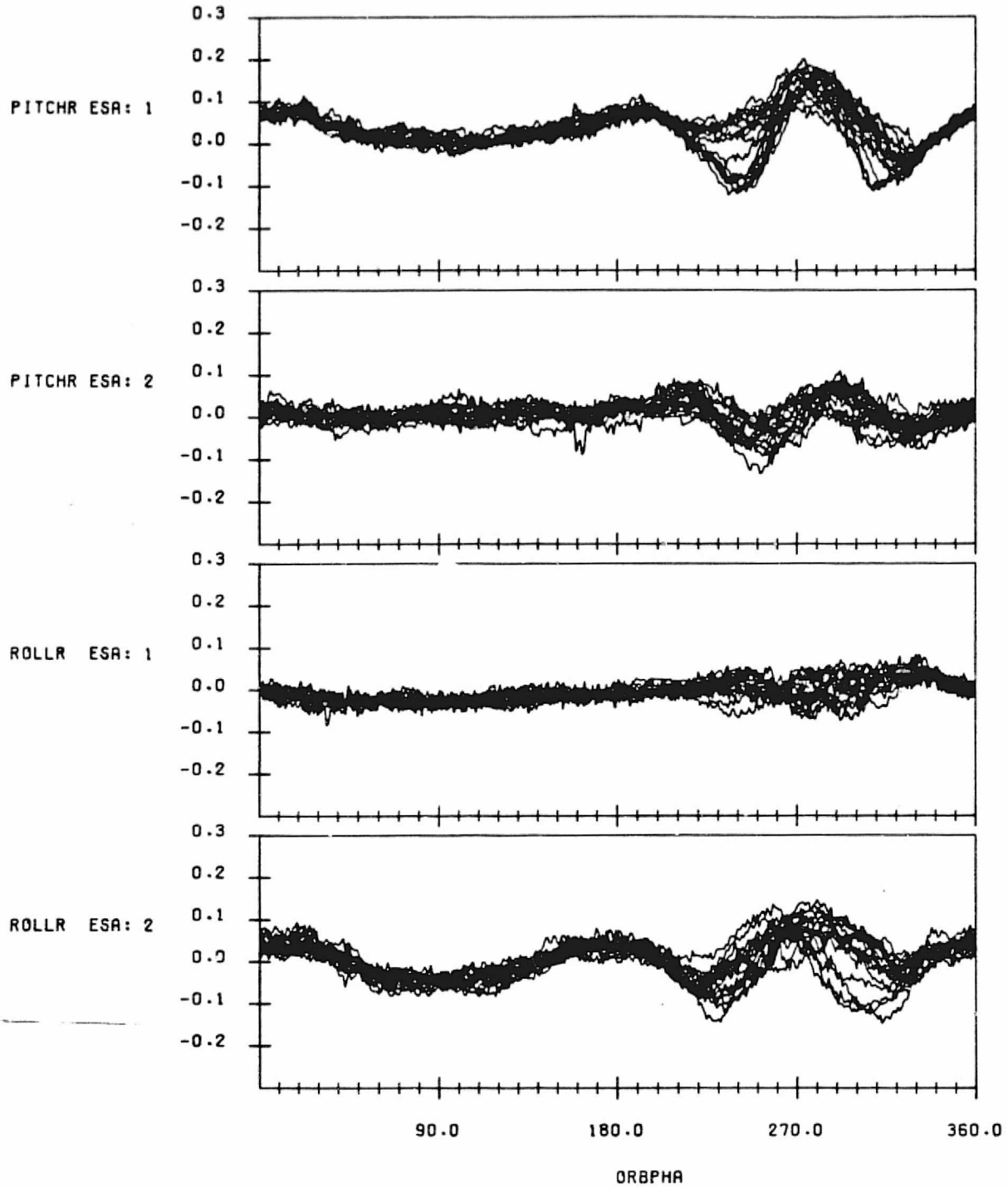

SCANNER RESIDUAL ERRORS IN DEGREES FOR NOMINAL CALIBRATION
WITH EARTH OBLATENESS, OBC ORBIT AND OBC REFERENCE ATTITUDE
EFFECTS MODELLED AND CONSTANT BIASES REMOVED
DATA START TIME:830831.001456628
END TIME:830901.041150787

FIGURE D-27. Residual Errors from Oblate Earth Model for Data Span on August 31 - September 1, 1983

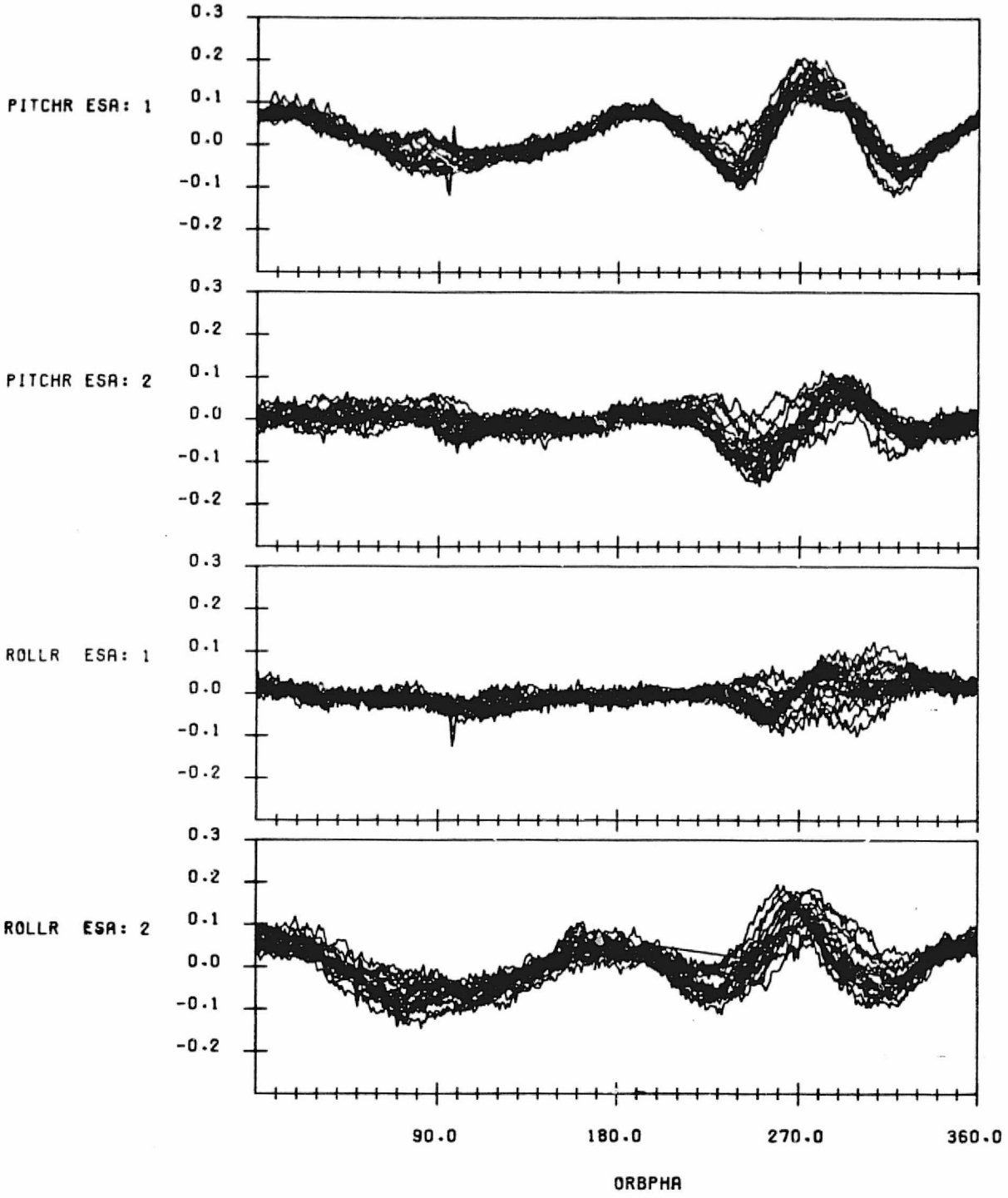

FIGURE D-28. Residual Errors from Oblate Earth Model for Data Span on September 14-15, 1983

APPENDIX E - RESIDUAL ERRORS FROM HRDB/SOES MODEL

Figures E-1 through E-28 provides plots of the residual errors from the HRDB/SOES model for all the data spans processed for this report. This model uses the nominal Oblate Earth Model with constant biases removed (Appendix D) and applies corrections due to the horizon triggering height variations predicted by the Horizon Radiance Data Base (HRDB) and the Sensor Optics and Electronics Simulator (SOES).

The residual in degrees are plotted as a function of orbit phase from the ascending node for several orbits overlayed.

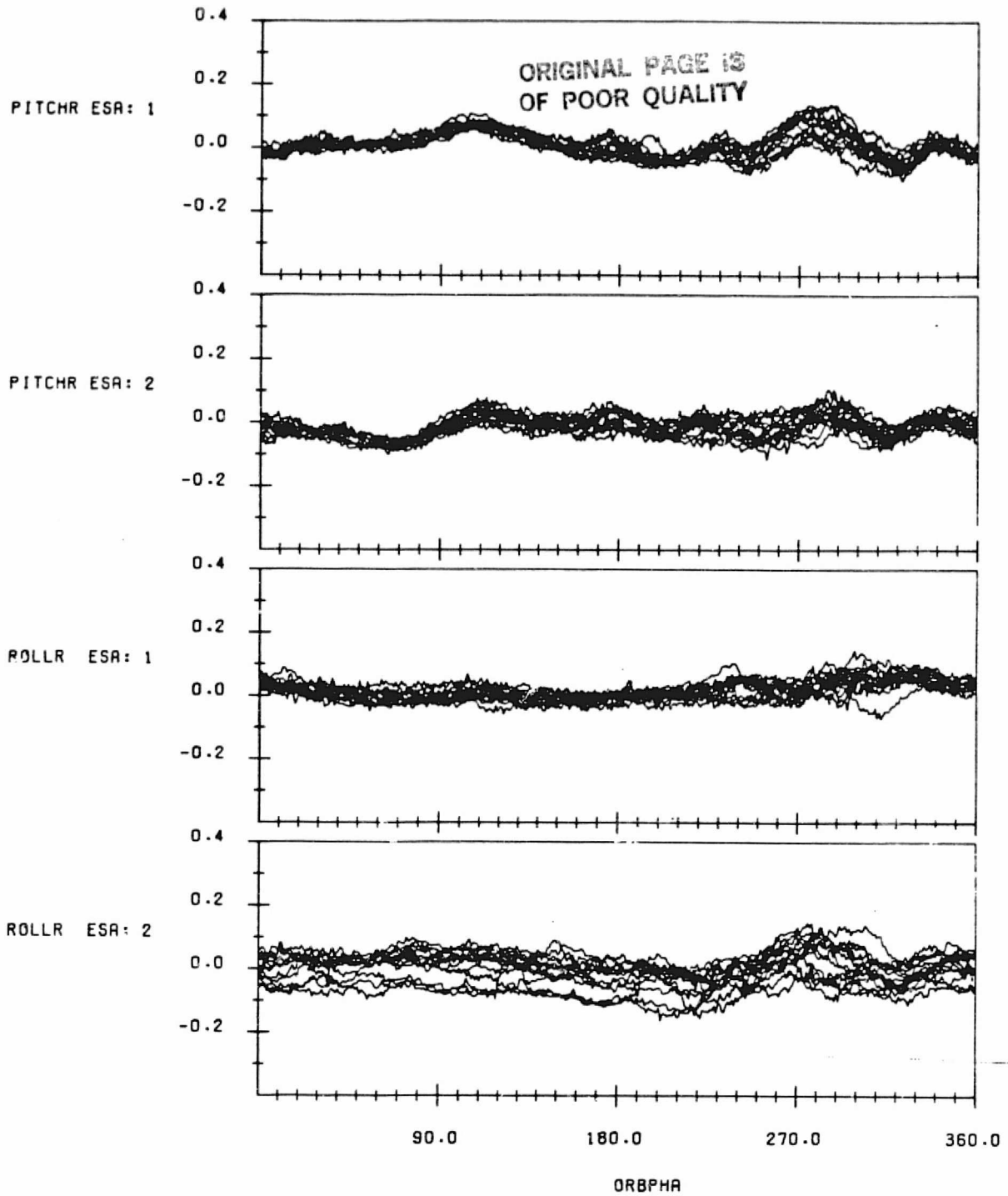

FIGURE E-1. Residual Errors from HRDB/SOES Model for Data Span on August 10-11, 1982

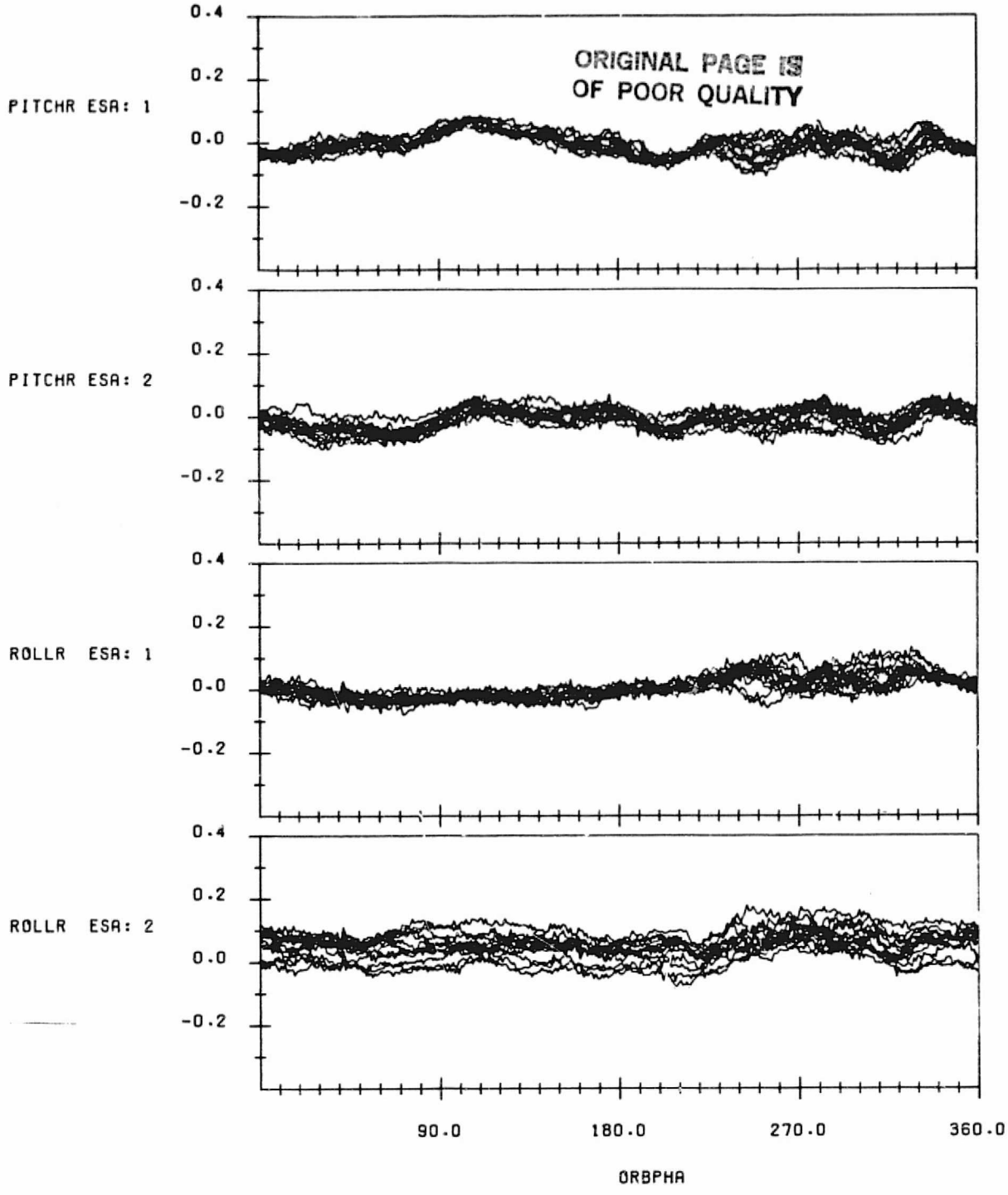

SCANNER RESIDUAL ERRORS IN DEGREES WITH THE HRDB/SOES PREDICTED
RADIANCE EFFECTS REMOVED ALONG WITH NOMINAL OBLATENESS.
ORBIT AND ATTITUDE EFFECTS AND CONSTANT BIASES.
DATA START TIME:820825.010606091
END TIME:820826.032214554

FIGURE E-2. Residual Errors from HRDB/SOES Model for Data Span on August 25-26, 1982

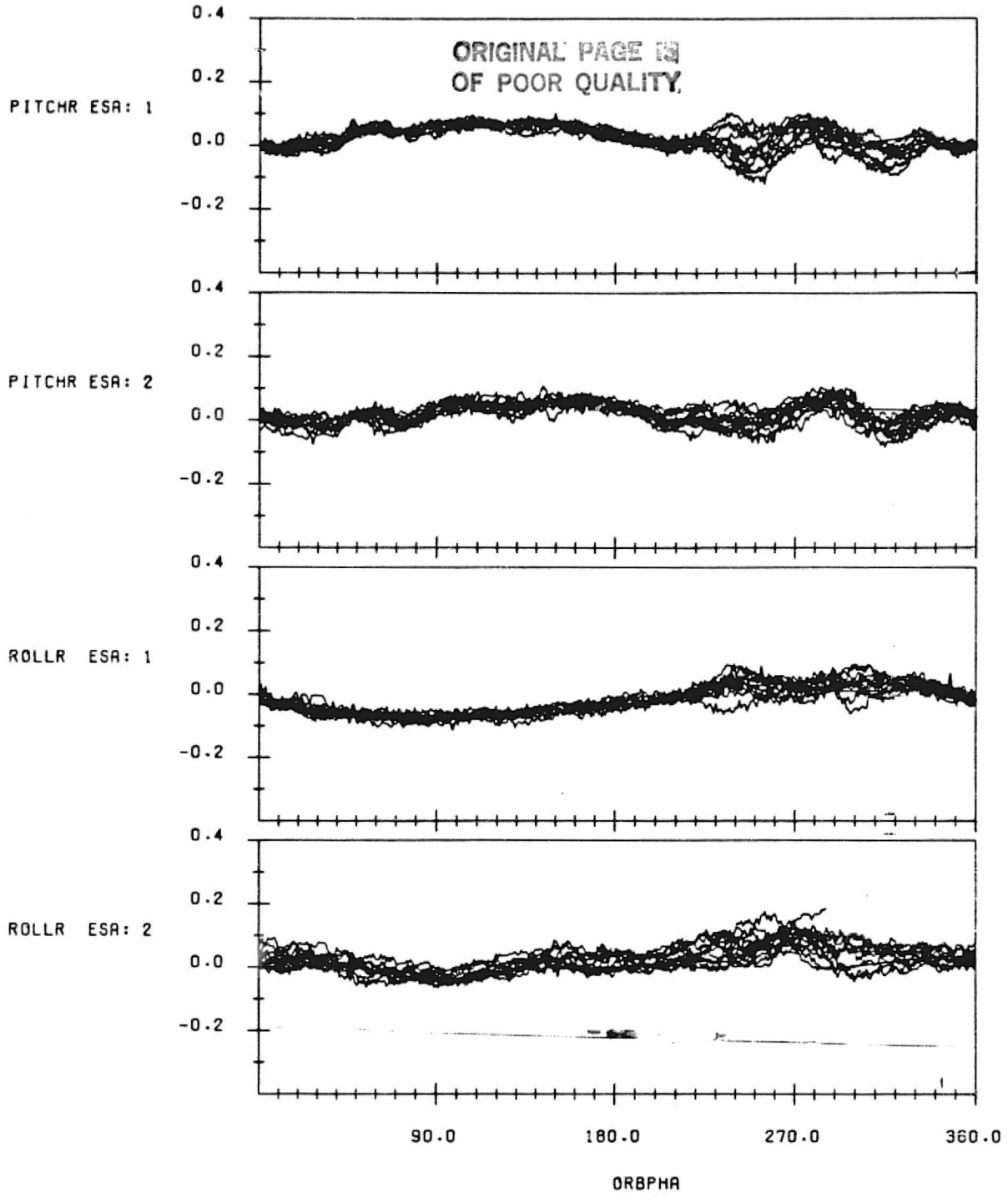

SCANNER RESIDUAL ERRORS IN DEGREES WITH THE HRDB/SOES PREDICTED
RADIANCE EFFECTS REMOVED ALONG WITH NOMINAL OBLATENESS.
ORBIT AND ATTITUDE EFFECTS AND CONSTANT BIASES.
DATA START TIME:820908.043319559
END TIME:820909.051848519

FIGURE E-3. Residual Errors from HRDB/SOES Model for Data Span on September 8-9, 1982

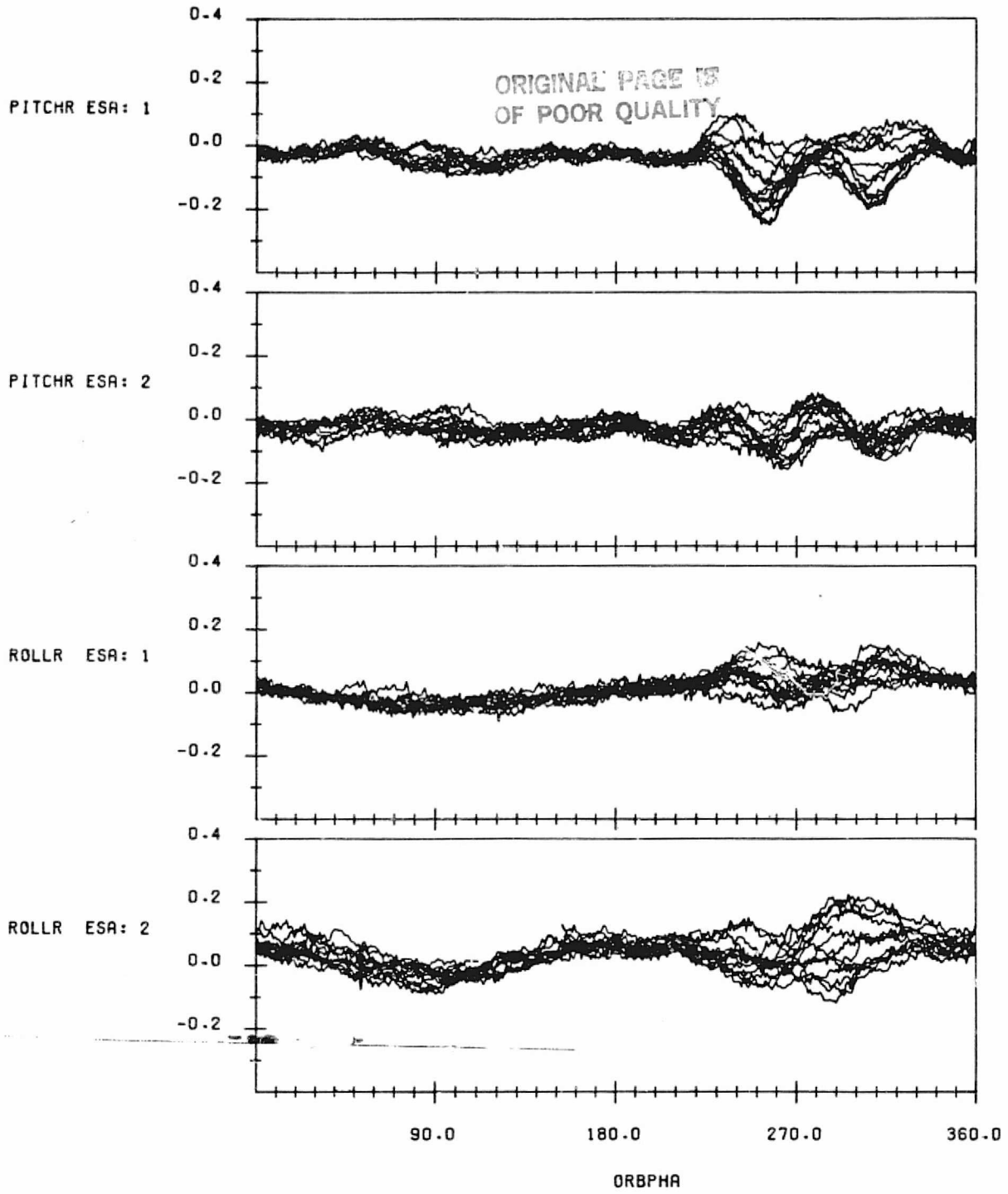

FIGURE E-4. Residual Errors from HRDB/SOES Model for Data Span on September 22-23, 1982

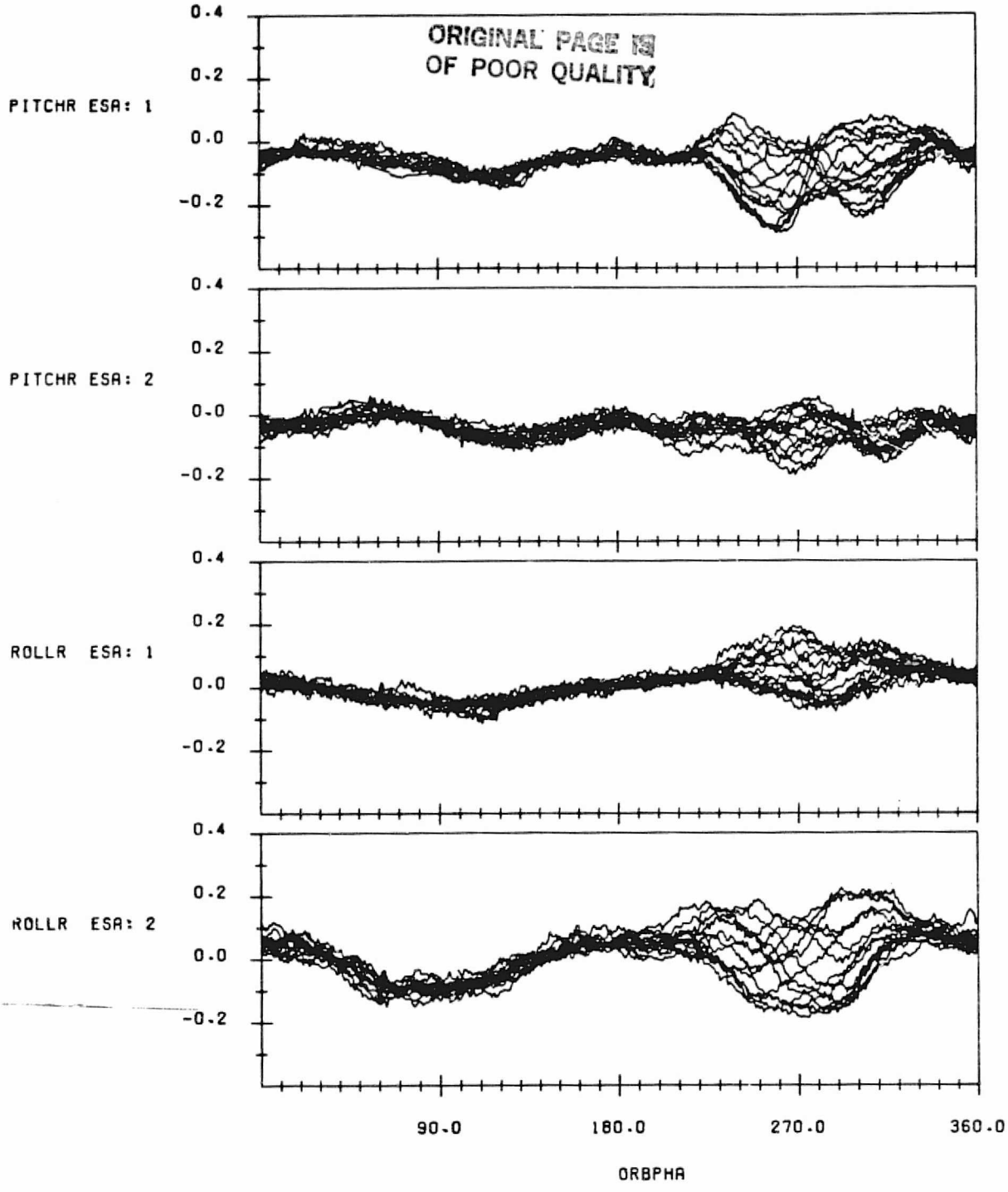

FIGURE E-5. Residual Errors from HRDB/SOES Model for Data Span on October 5-6, 1982

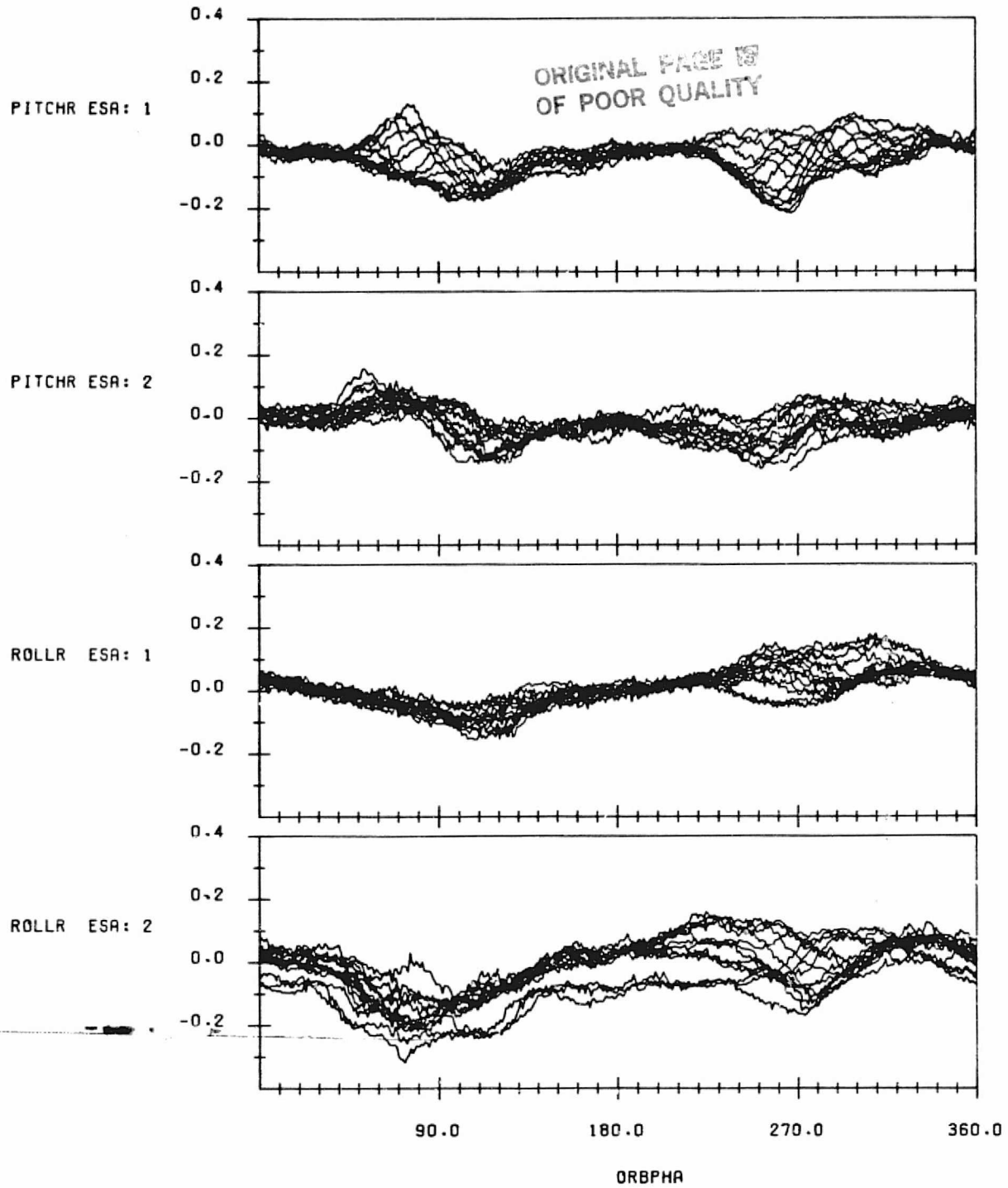

FIGURE E-6. Residual Errors from HRDB/SOES Model for Data Span on October 20-21, 1982

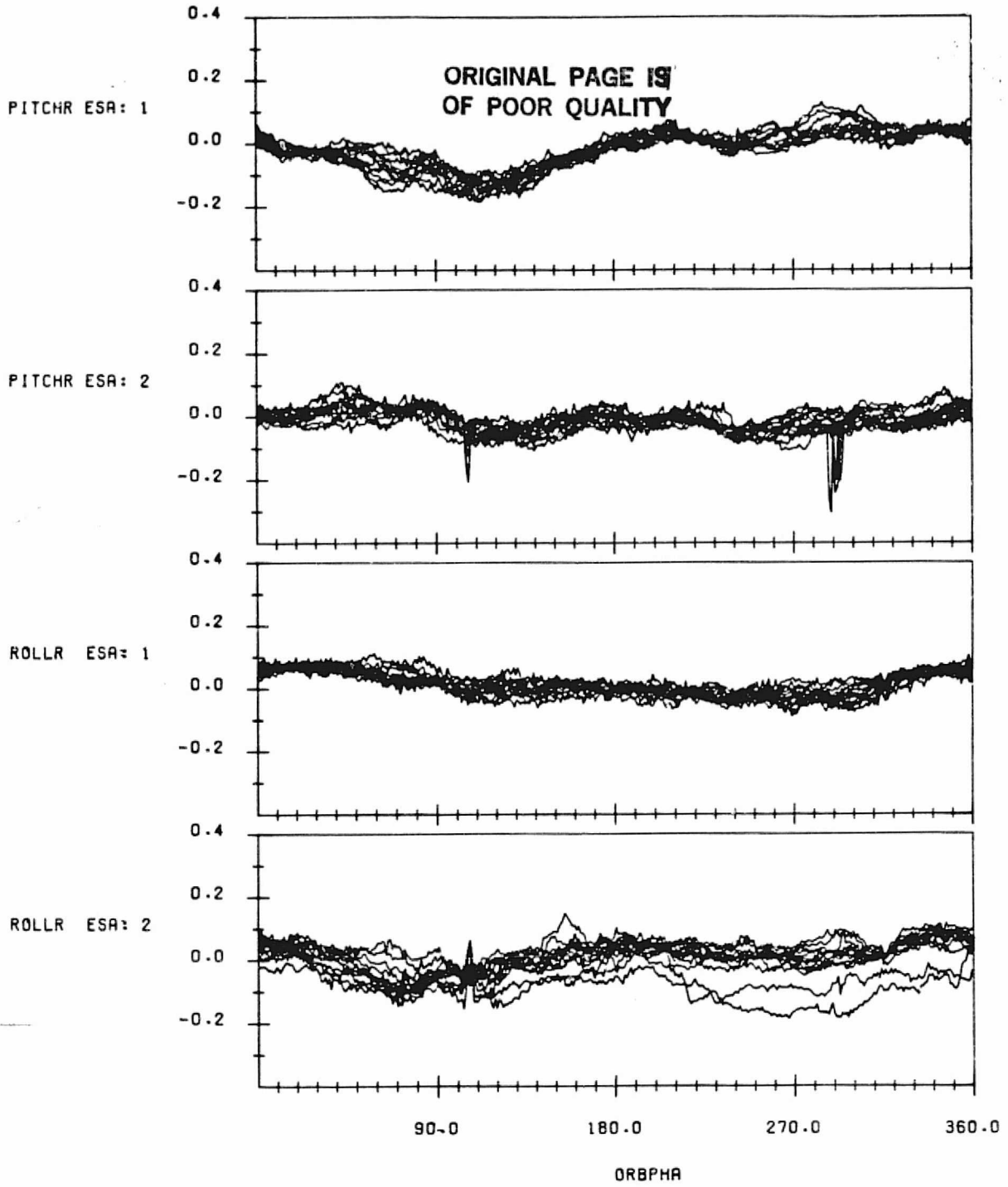

FIGURE E-7. Residual Errors from HRDB/SOES Model for Data Span on November 2-3, 1982

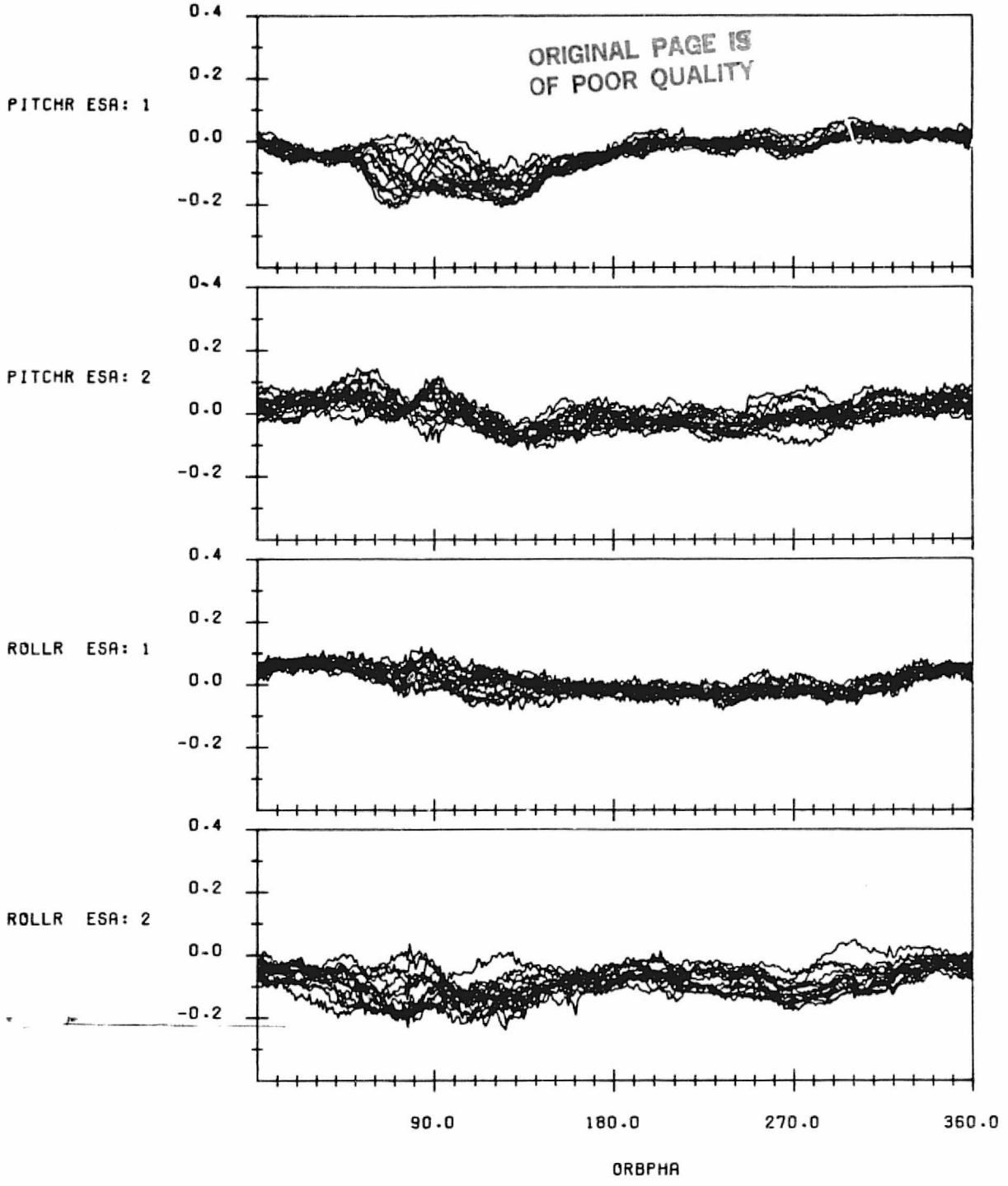

FIGURE E-8. Residual Errors from HRDB/SOES Model for Data Span on November 16-17, 1982

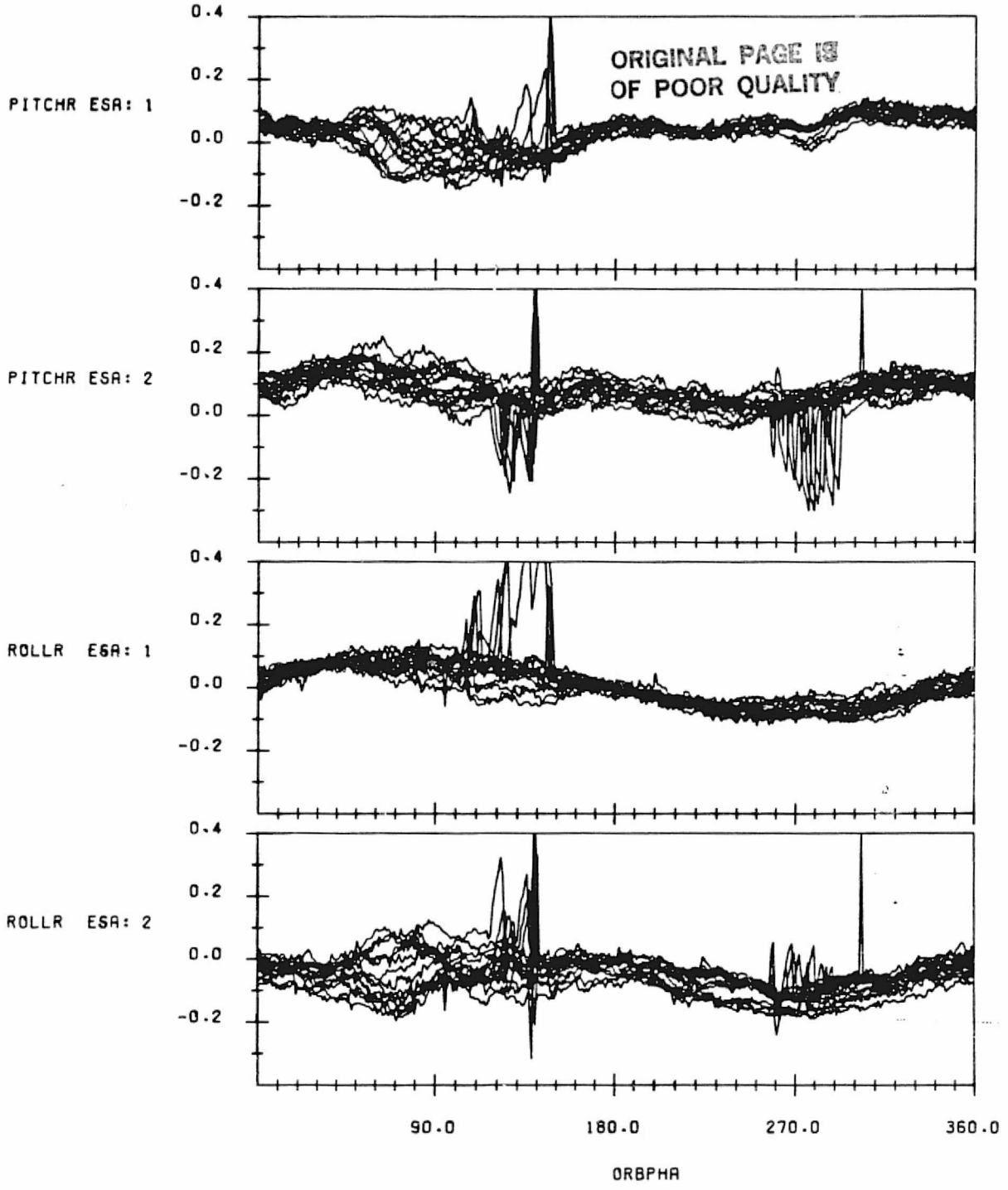

SCANNER RESIDUAL ERRORS IN DEGREES WITH THE HRDB/SOES PREDICTED
RADIANCE EFFECTS REMOVED ALONG WITH NOMINAL OBLATENESS,
ORBIT AND ATTITUDE EFFECTS AND CONSTANT BIASES.
DATA START TIME:821201.002856720
END TIME:821202.031150860

FIGURE E-9. Residual Errors from HRDB/SOES Model for Data Span on December 1-2, 1982

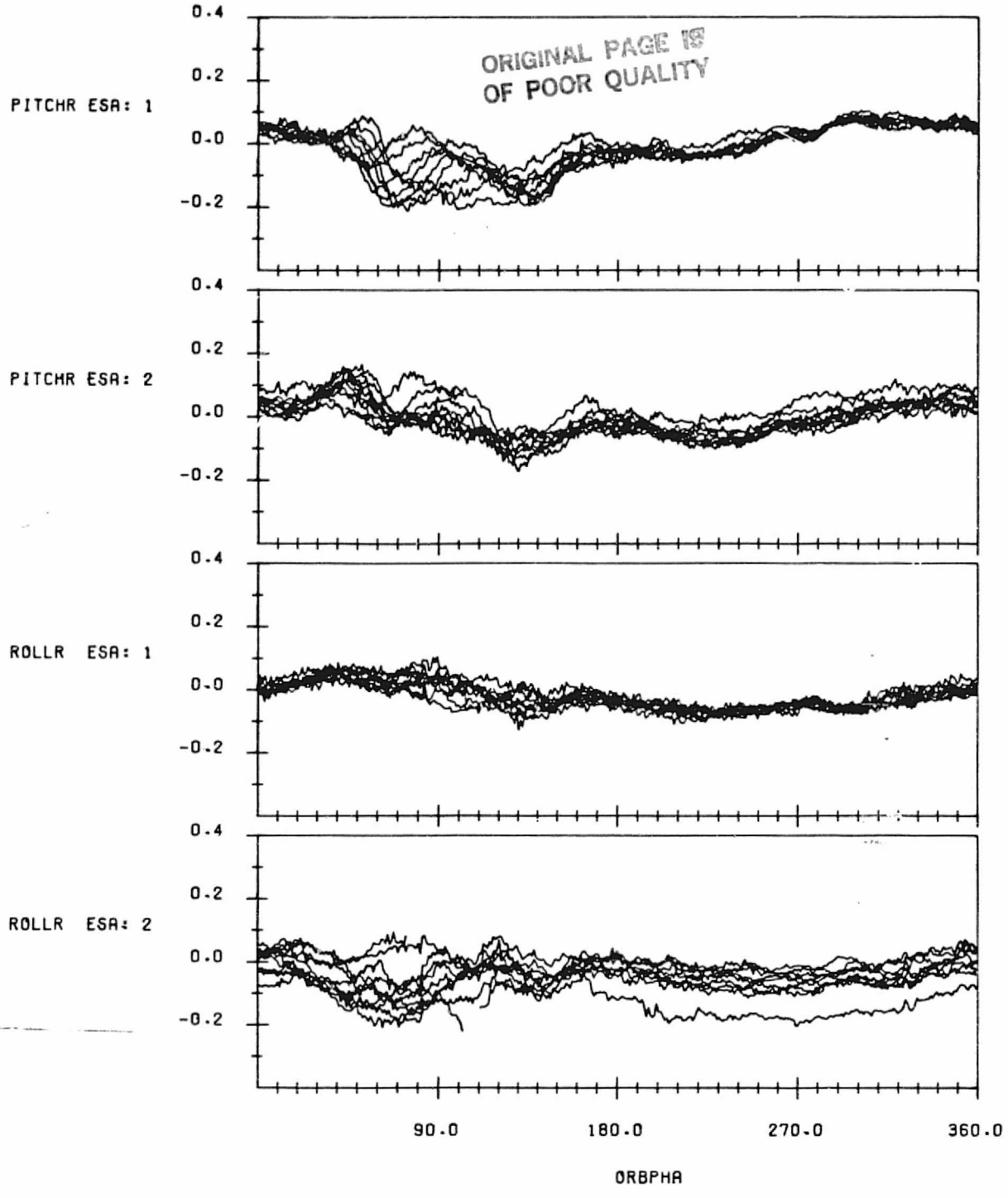

SCANNER RESIDUAL ERRORS IN DEGREES WITH THE HRDB/SOES PREDICTED
RADIANCE EFFECTS REMOVED ALONG WITH NOMINAL OBLATENESS,
ORBIT AND ATTITUDE EFFECTS AND CONSTANT BIASES.
DATA START TIME:821214.122607064
END TIME:821215.143809812

FIGURE E-10. Residual Errors from HRDB/SOES Model for Data Span on December 14-15, 1982

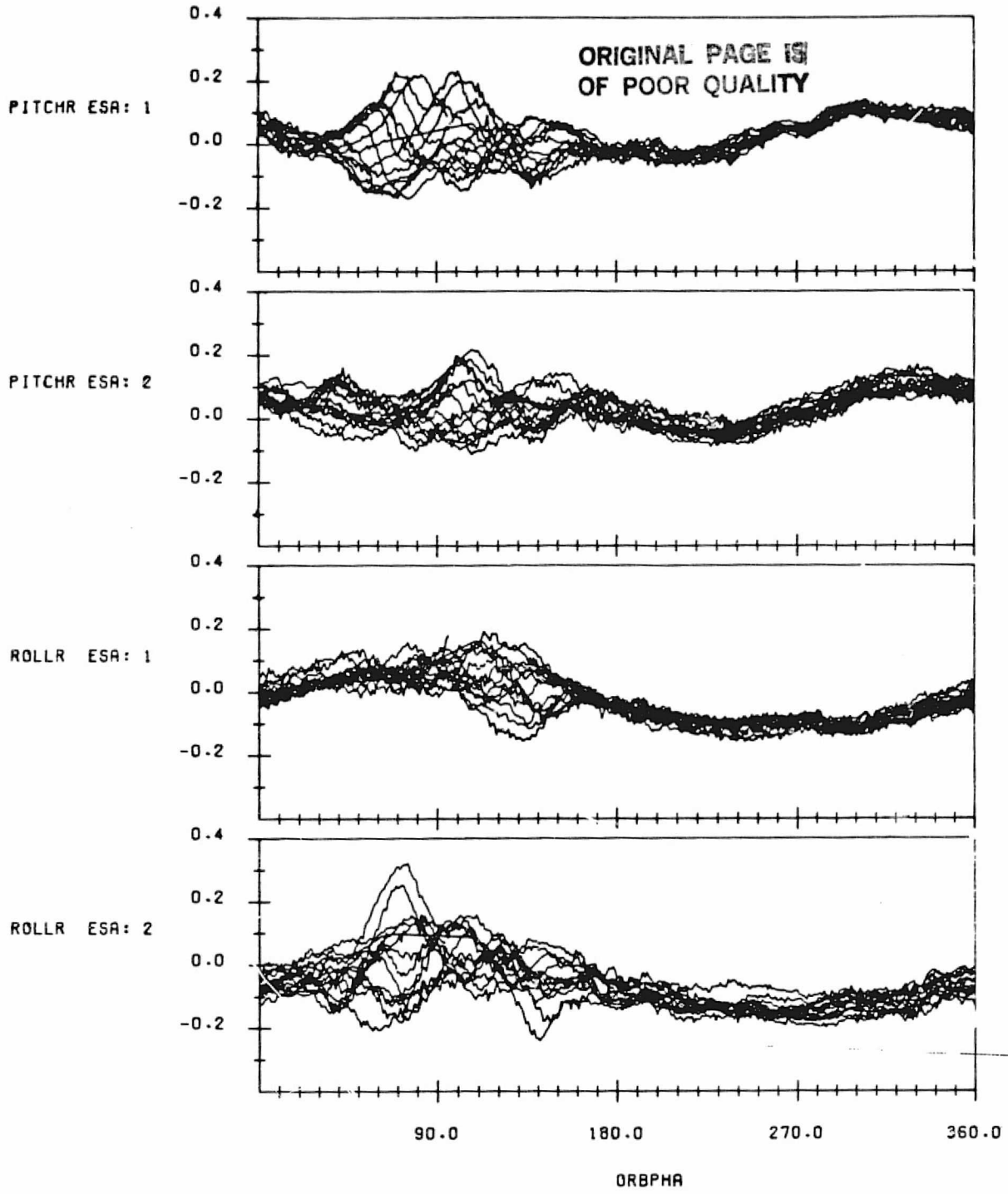

SCANNER RESIDUAL ERRORS IN DEGREES WITH THE HRDB/SOES PREDICTED
RADIANCE EFFECTS REMOVED ALONG WITH NOMINAL OBLATENESS.
ORBIT AND ATTITUDE EFFECTS AND CONSTANT BIASES.
DATA START TIME:821228.053240480
END TIME:821229.061420139

FIGURE E-11. Residual Errors from HRDB/SOES Model for Data Span on December 28-29, 1982

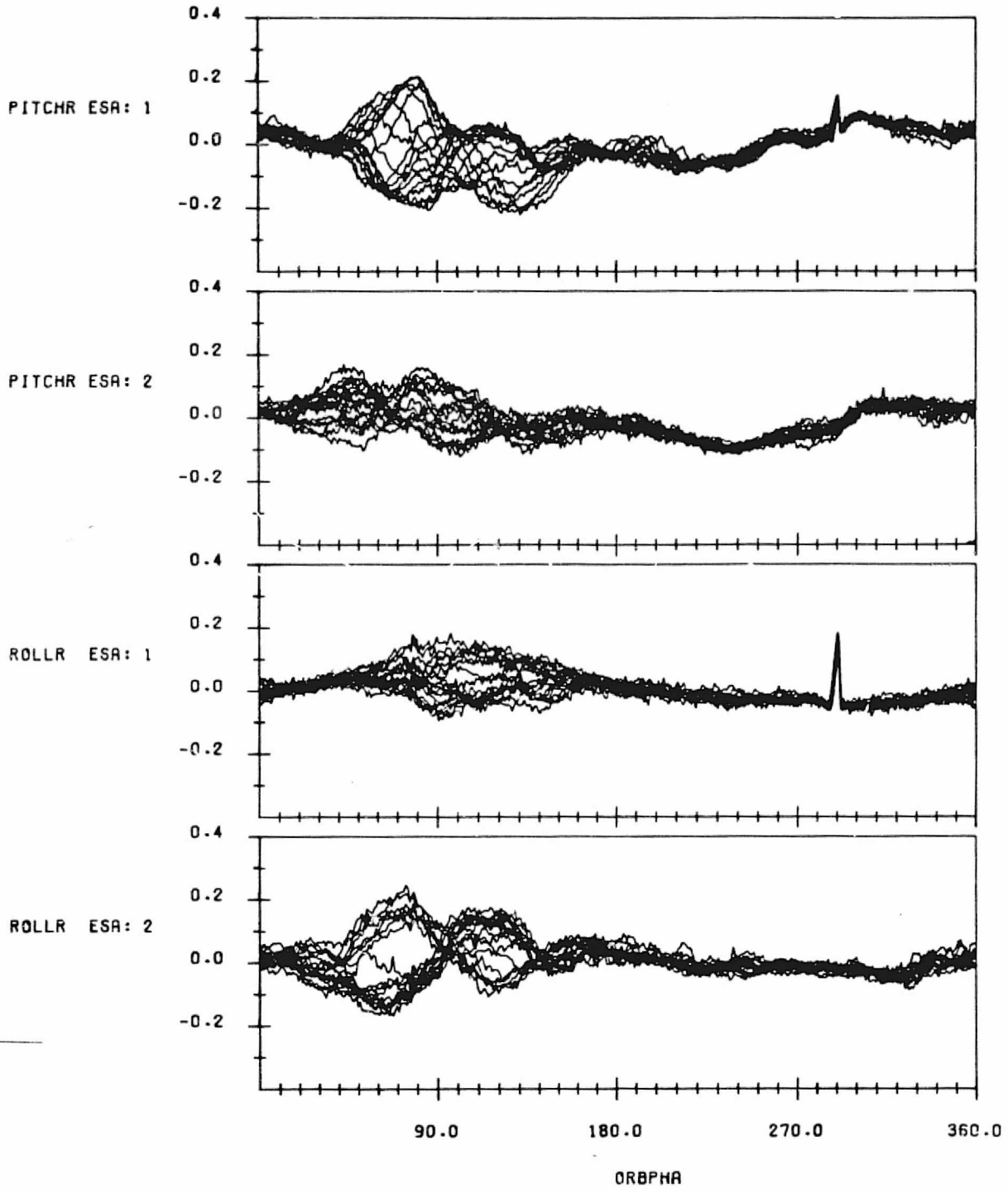

FIGURE E-12. Residual Errors from HRDB/SOES Model for Data Span on January 19-20, 1983

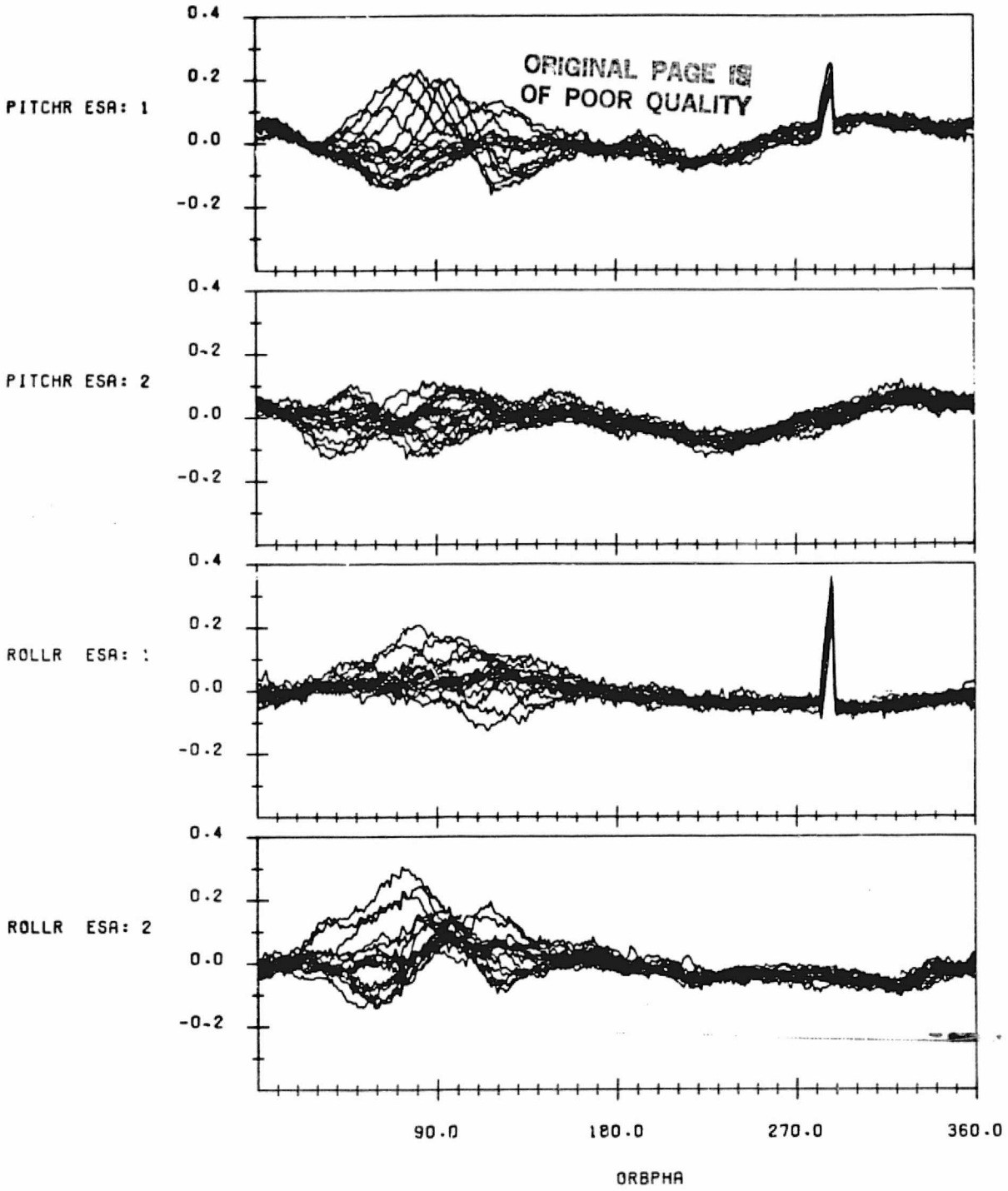

SCANNER RESIDUAL ERRORS IN DEGREES WITH THE HRDB/SOES PREDICTED
RADIANCE EFFECTS REMOVED ALONG WITH NOMINAL OBLATENESS,
ORBIT AND ATTITUDE EFFECTS AND CONSTANT BIASES.
DATA START TIME:830202.032425071
END TIME:830203.054950590

FIGURE E-13. Residual Errors from HRDB/SOES Model for Data Span on February 2-3, 1983

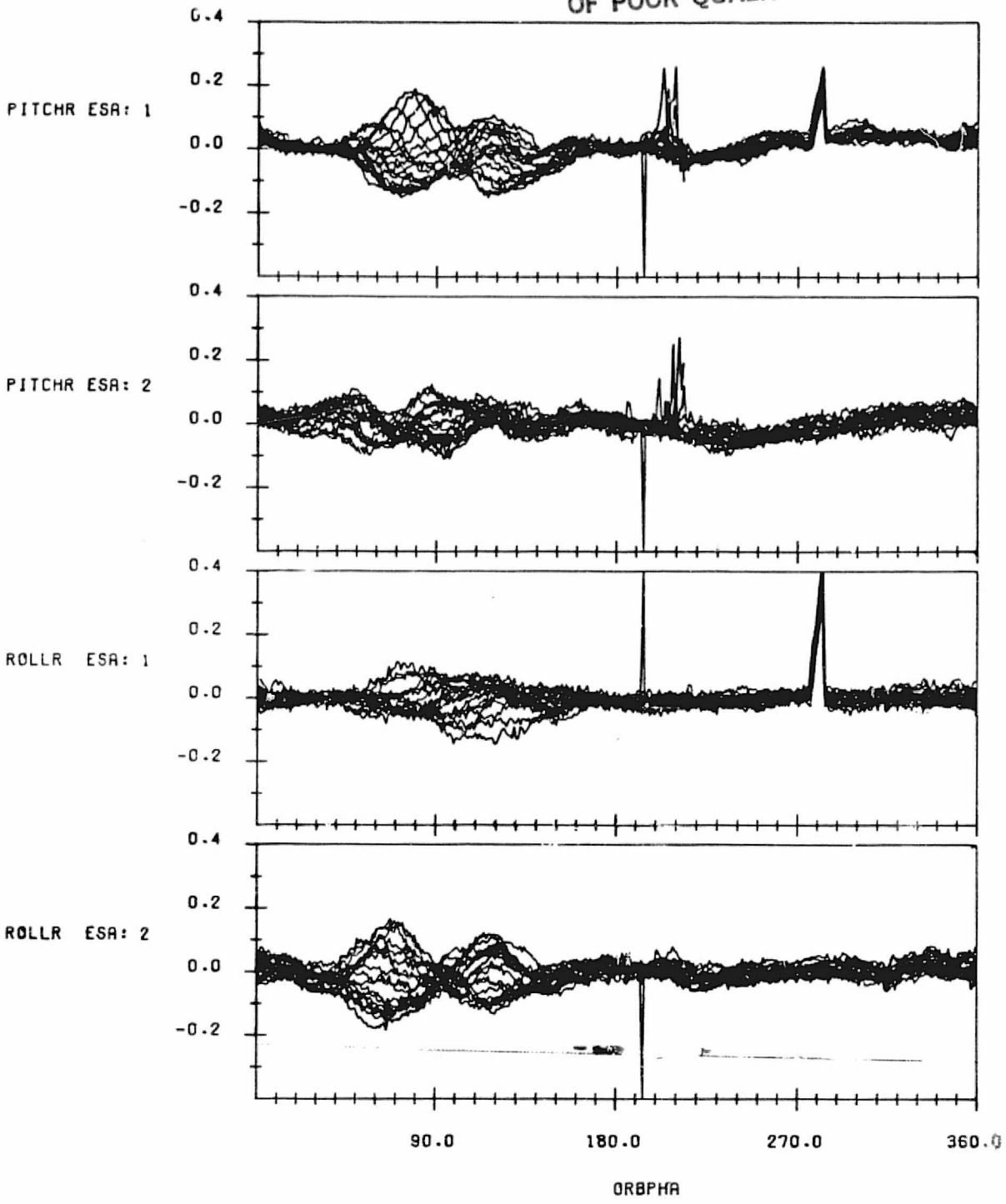

SCANNER RESIDUAL ERRORS IN DEGREES WITH THE HRDB/SOES PREDICTED
RADIANCE EFFECTS REMOVED ALONG WITH NOMINAL OBLATENESS,
ORBIT AND ATTITUDE EFFECTS AND CONSTANT BIASES.
DATA START TIME:830217.000122618
END TIME:830218.065513594

FIGURE E-14. Residual Errors from HRDB/SOES Model for Data Span on February 17-18, 1983

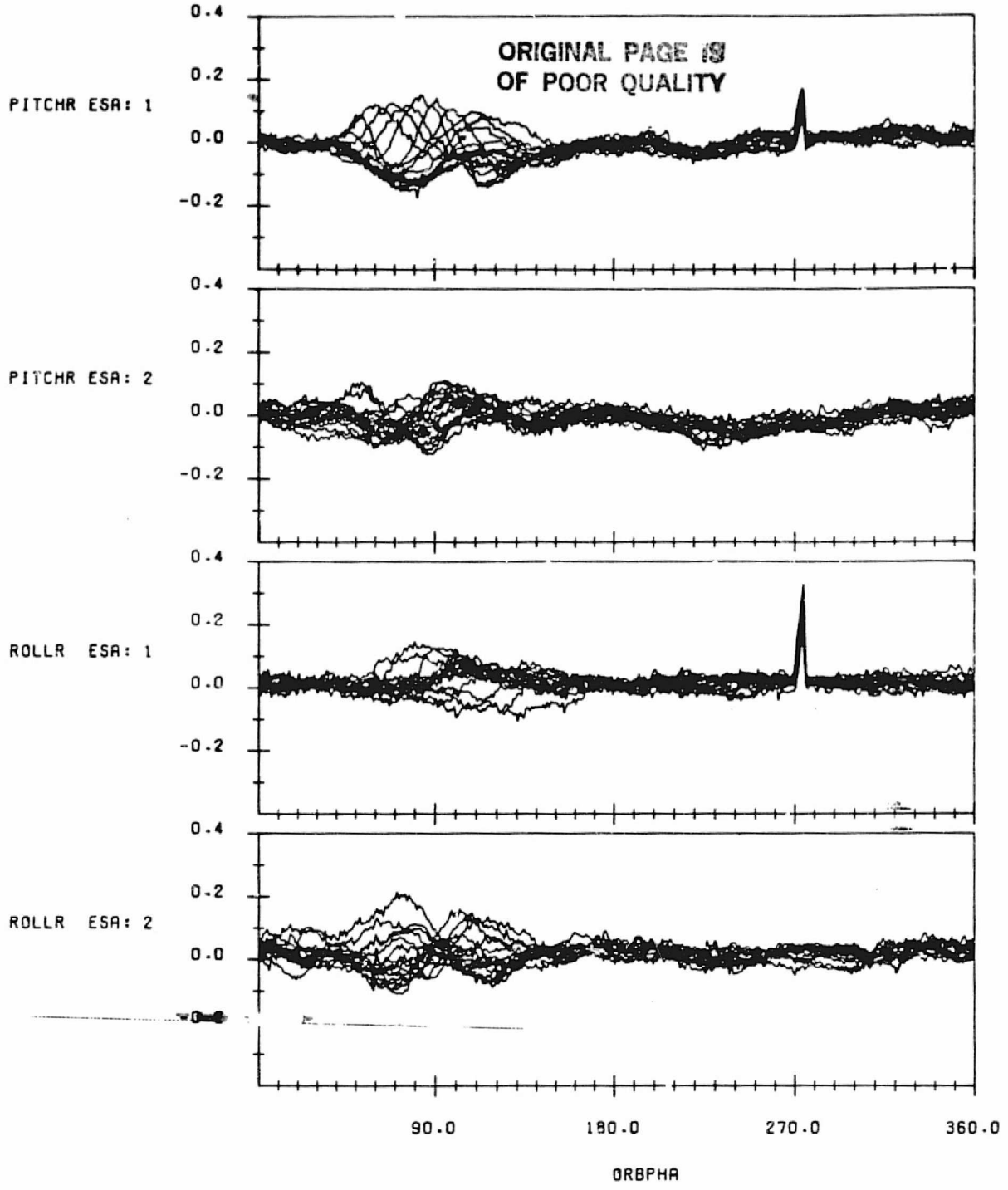

SCANNER RESIDUAL ERRORS IN DEGREES WITH THE HRDB/SOES PREDICTED
RADIANCE EFFECTS REMOVED ALONG WITH NOMINAL OBLATENESS,
ORBIT AND ATTITUDE EFFECTS AND CONSTANT BIASES.
DATA START TIME:830303.025744694
END TIME:830304.034257270

FIGURE E-15. Residual Errors from HRDB/SOES Model for Data Span on March 3-4, 1983

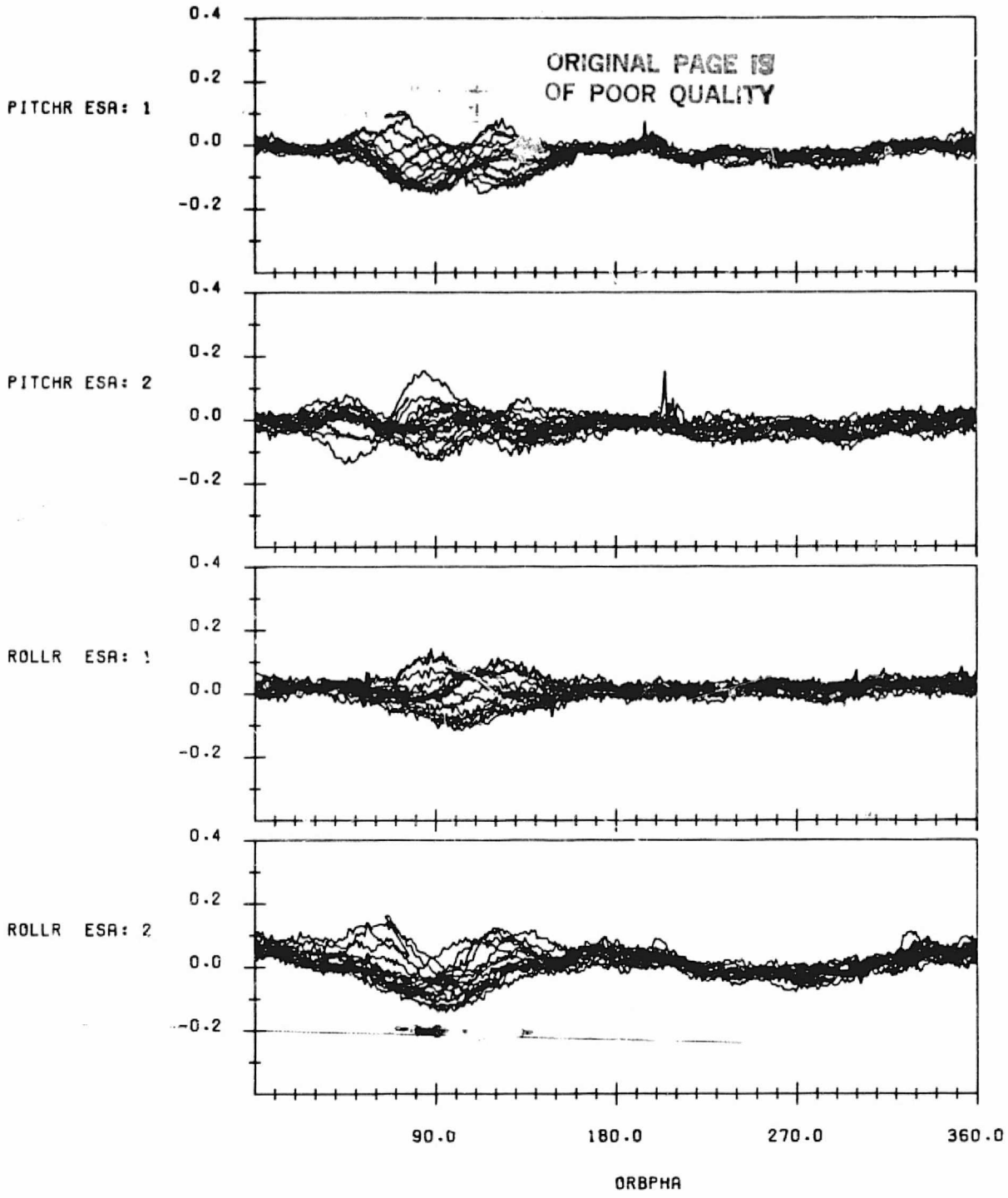

SCANNER RESIDUAL ERRORS IN DEGREES WITH THE HRDB/SOES PREDICTED
RADIANCE EFFECTS REMOVED ALONG WITH NOMINAL OBLATENESS,
ORBIT AND ATTITUDE EFFECTS AND CONSTANT BIASES.
DATA START TIME:830314.134603442
END TIME:830315.170127218

FIGURE E-16. Residual Errors from HRDB/SOES Model for Data Span on March 14-15, 1983

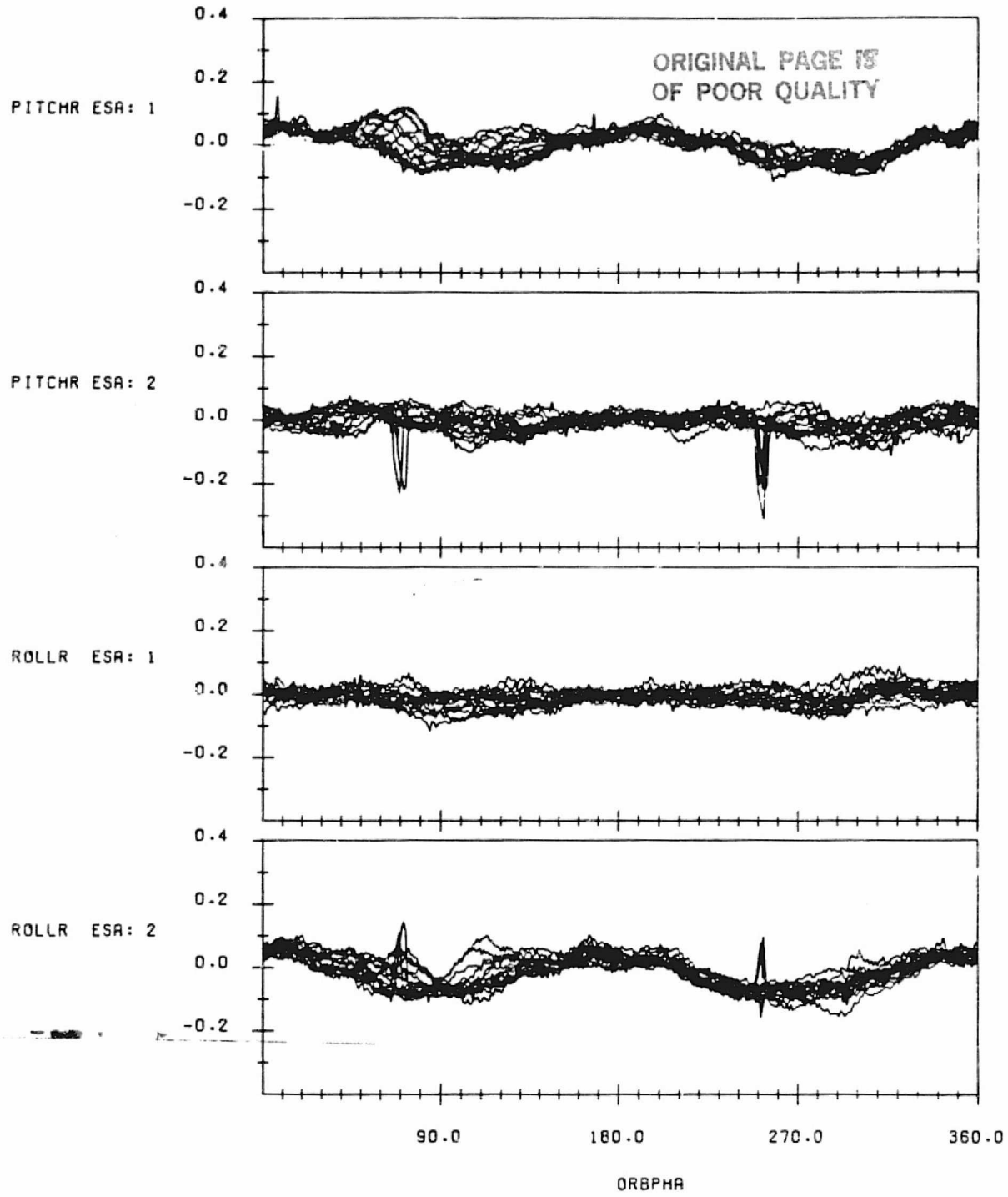

SCANNER RESIDUAL ERROR, IN DEGREES WITH THE HRDB/SOES PREDICTED
RADIANCE EFFECTS REMOVED ALONG WITH NOMINAL OBLATENESS.
ORBIT AND ATTITUDE EFFECTS AND CONSTANT BIASES.
DATA START TIME:830329.235506990
END TIME:830331.003946798

FIGURE E-17. Residual Errors from HRDB/SOES Model for Data Span on March 29-31, 1983

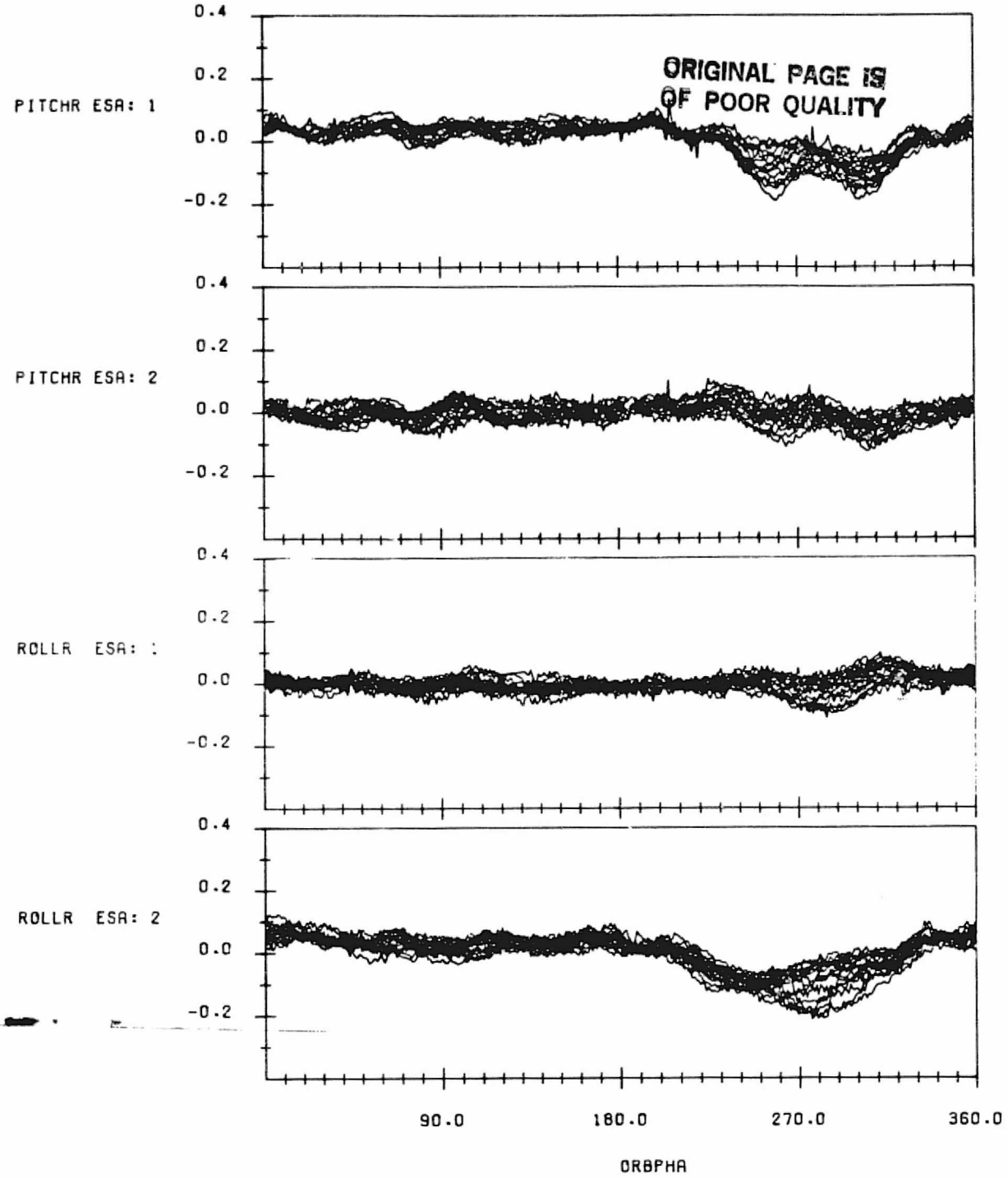

SCANNER RESIDUAL ERRORS IN DEGREES WITH THE HRDB/SOES PREDICTED
RADIANCE EFFECTS REMOVED ALONG WITH NOMINAL OBLATENESS,
ORBIT AND ATTITUDE EFFECTS AND CONSTANT BIASES.
DATA START TIME:830414.003417145
END TIME:830415.041837625

FIGURE E-18. Residual Errors from HRDB/SOES Model for Data Span on April 14-15, 1983

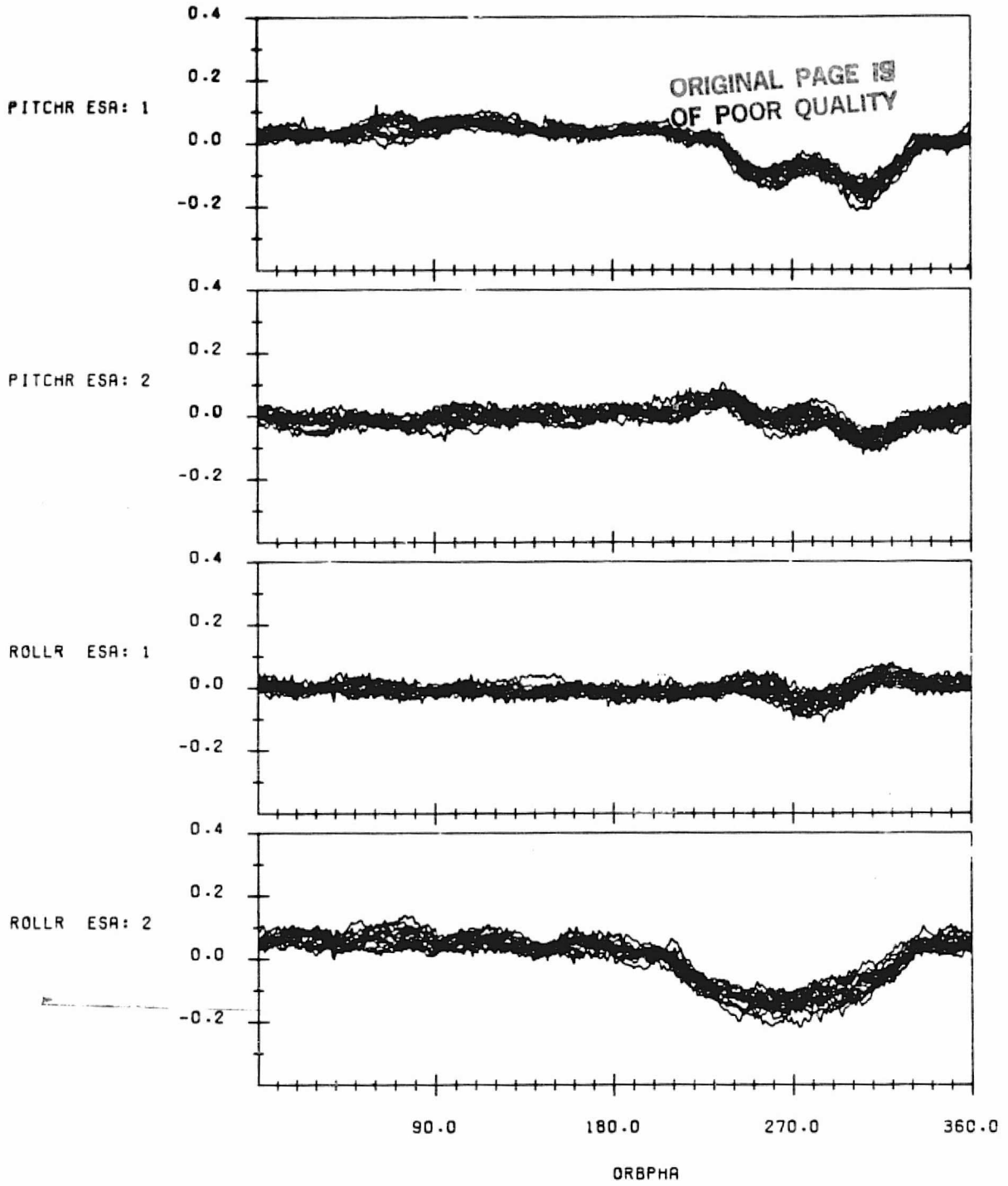

SCANNER RESIDUAL ERRORS IN DEGREES WITH THE HRDB/SOES PREDICTED
RADIANCE EFFECTS REMOVED ALONG WITH NOMINAL OBLATENESS.
ORBIT AND ATTITUDE EFFECTS AND CONSTANT BIASES.
DATA START TIME:830426.020419829
END TIME:830427.030700981

FIGURE E-19. Residual Errors from HRDB/SOES Model for Data Span on April 26-27, 1983

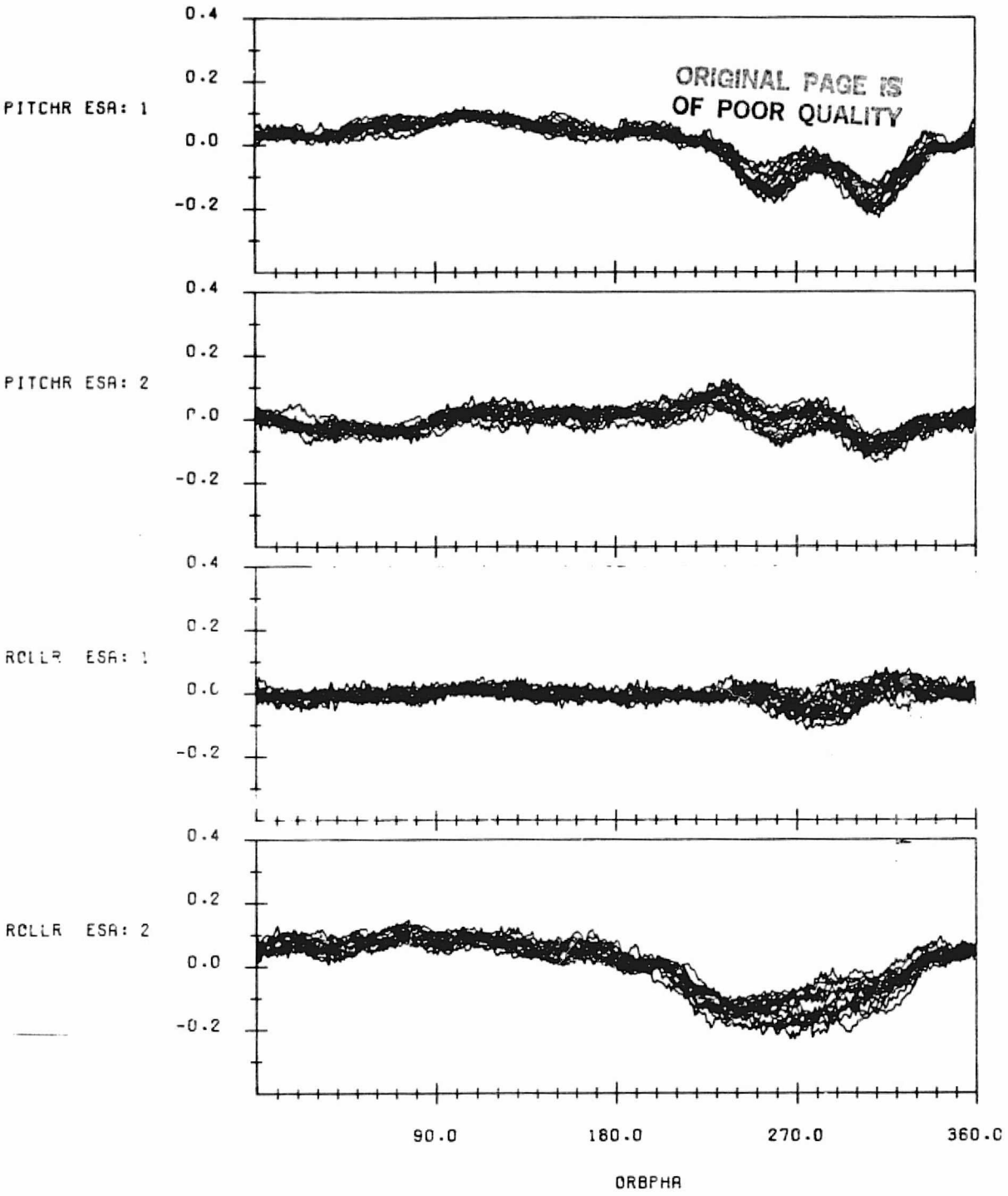

SCANNER RESIDUAL ERRORS IN DEGREES WITH THE HRDB/SOES PREDICTED
RADIANCE EFFECTS REMOVED ALONG WITH NOMINAL OBLATENESS,
ORBIT AND ATTITUDE EFFECTS AND CONSTANT BIASES.
DATA START TIME:830511.001602609
END TIME:830512.022204864

FIGURE E-20. Residual Errors from HRDB/SOES Model for Data Span on May 11-12, 1983

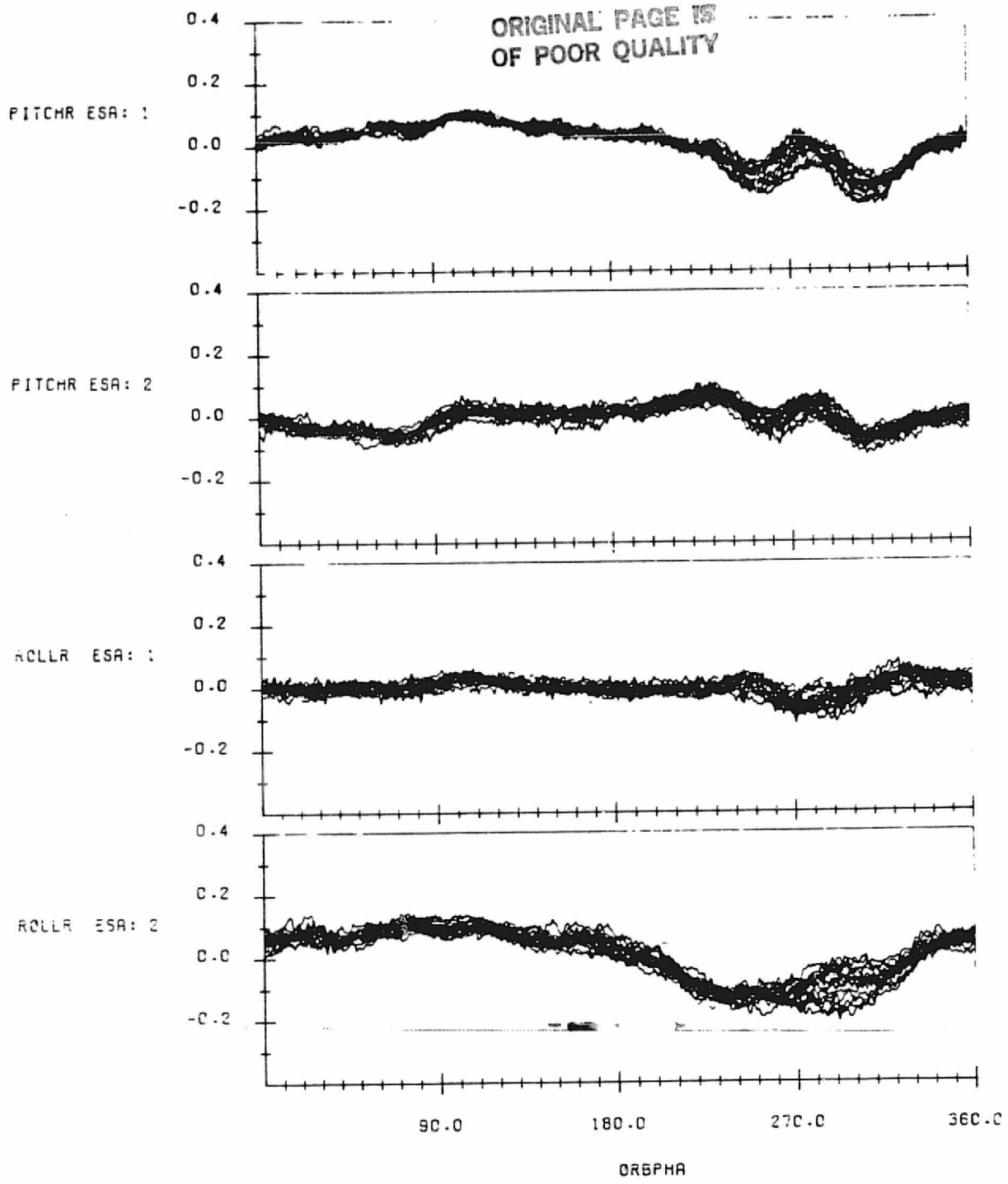

SCANNER RESIDUAL ERRORS IN DEGREES WITH THE HRDB/SOES PREDICTED
RADIANCE EFFECTS REMOVED ALONG WITH NOMINAL OBLATENESS,
ORBIT AND ATTITUDE EFFECTS AND CONSTANT BIASES.
DATA START TIME:830523.004000365
END TIME:830524.042404476

FIGURE E-21. Residual Errors from HRDB/SOES Model for Data Span on May 23-24, 1983

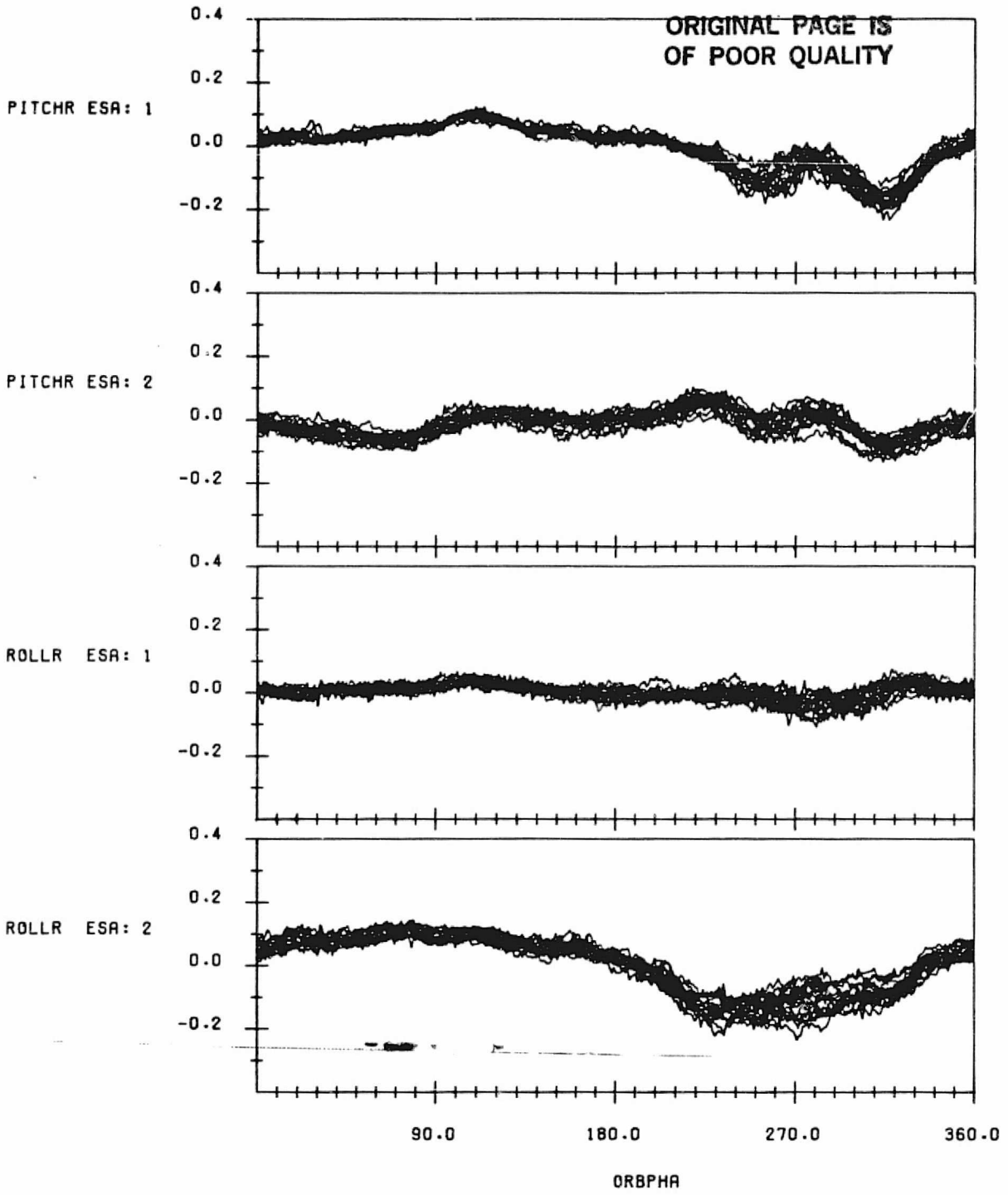

FIGURE E-22. Residual Errors from HRDB/SOES Model for Data Span on June 6-7, 1983

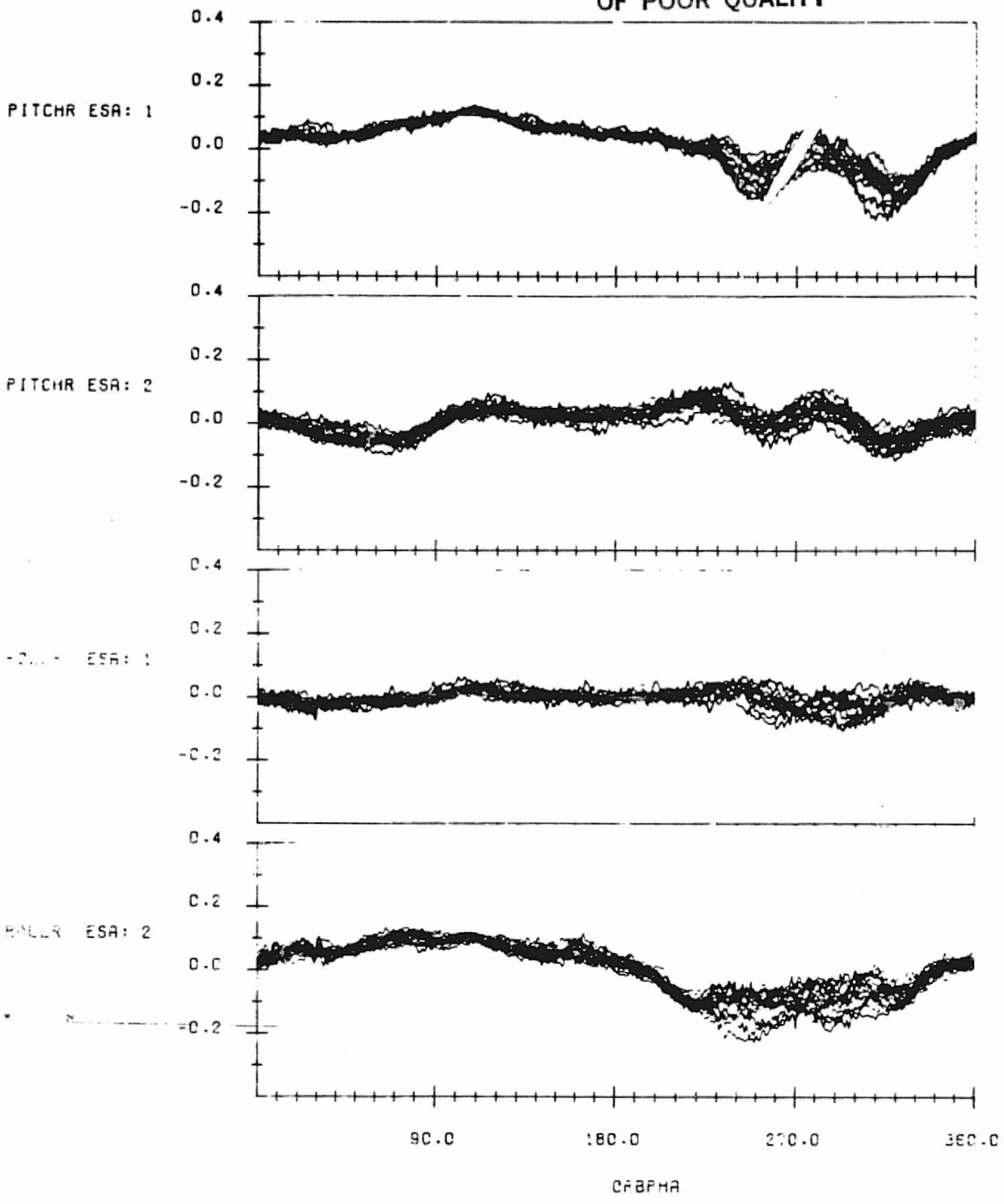

SCANNER RESIDUAL ERRORS IN DEGREES WITH THE HRDB/SOES PREDICTED
RADIANCE EFFECTS REMOVED ALONG WITH NOMINAL OBLATENESS,
ORBIT AND ATTITUDE EFFECTS AND CONSTANT BIASES.
DATA START TIME:830621.225929155
END TIME:830623.012243587

FIGURE E-23. Residual Errors from HRDB/SOES Model for Data Span on June 21-23, 1983

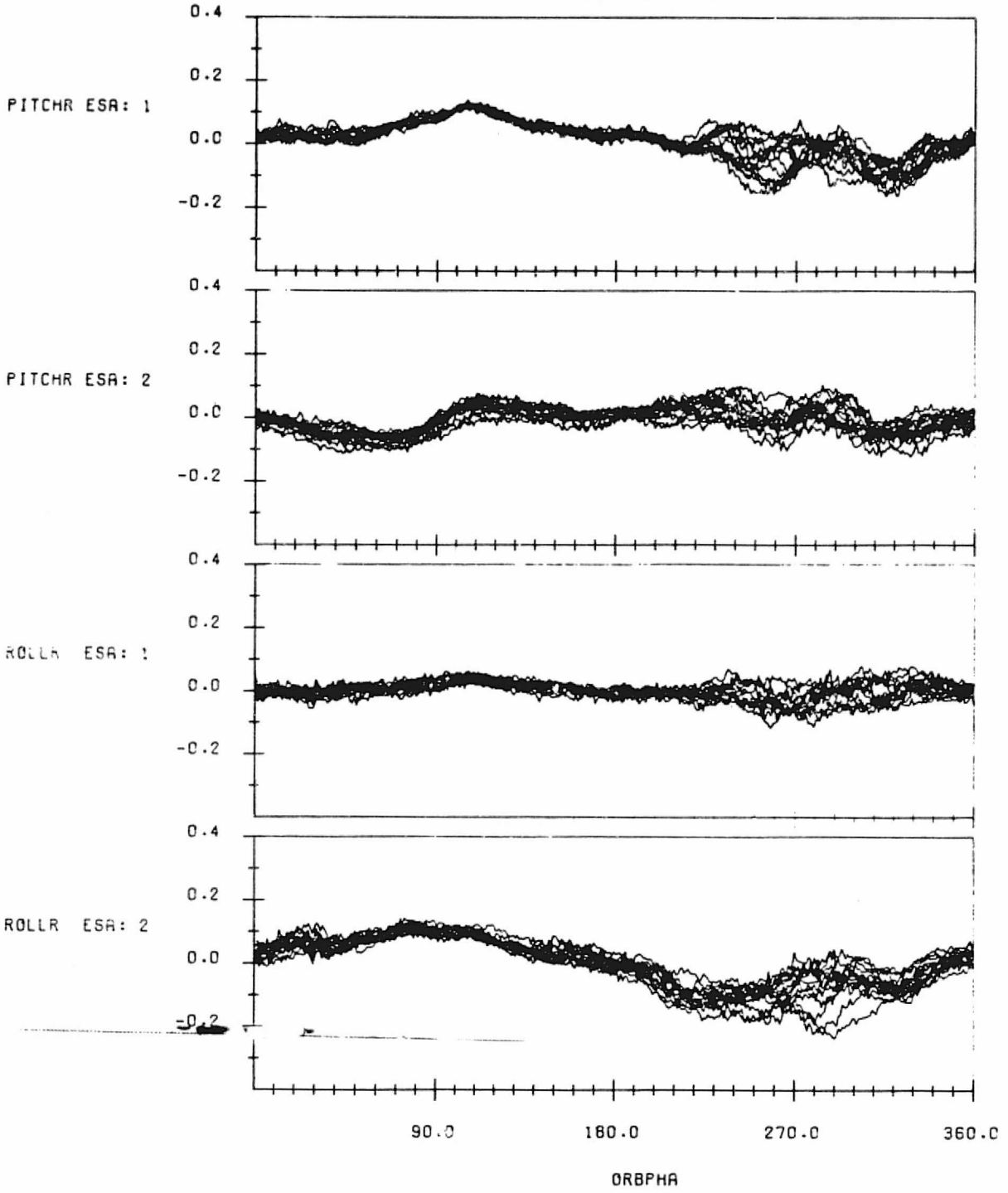

SCANNER RESIDUAL ERRORS IN DEGREES WITH THE HRDB/SOES PREDICTED
RADIANCE EFFECTS REMOVED ALONG WITH NOMINAL OBLATENESS,
ORBIT AND ATTITUDE EFFECTS AND CONSTANT BIASES.
DATA START TIME:830706.154825062
END TIME:830707.182940838

FIGURE E-24. Residual Errors from HRDB/SOES Model for Data Span on July 6-7, 1983

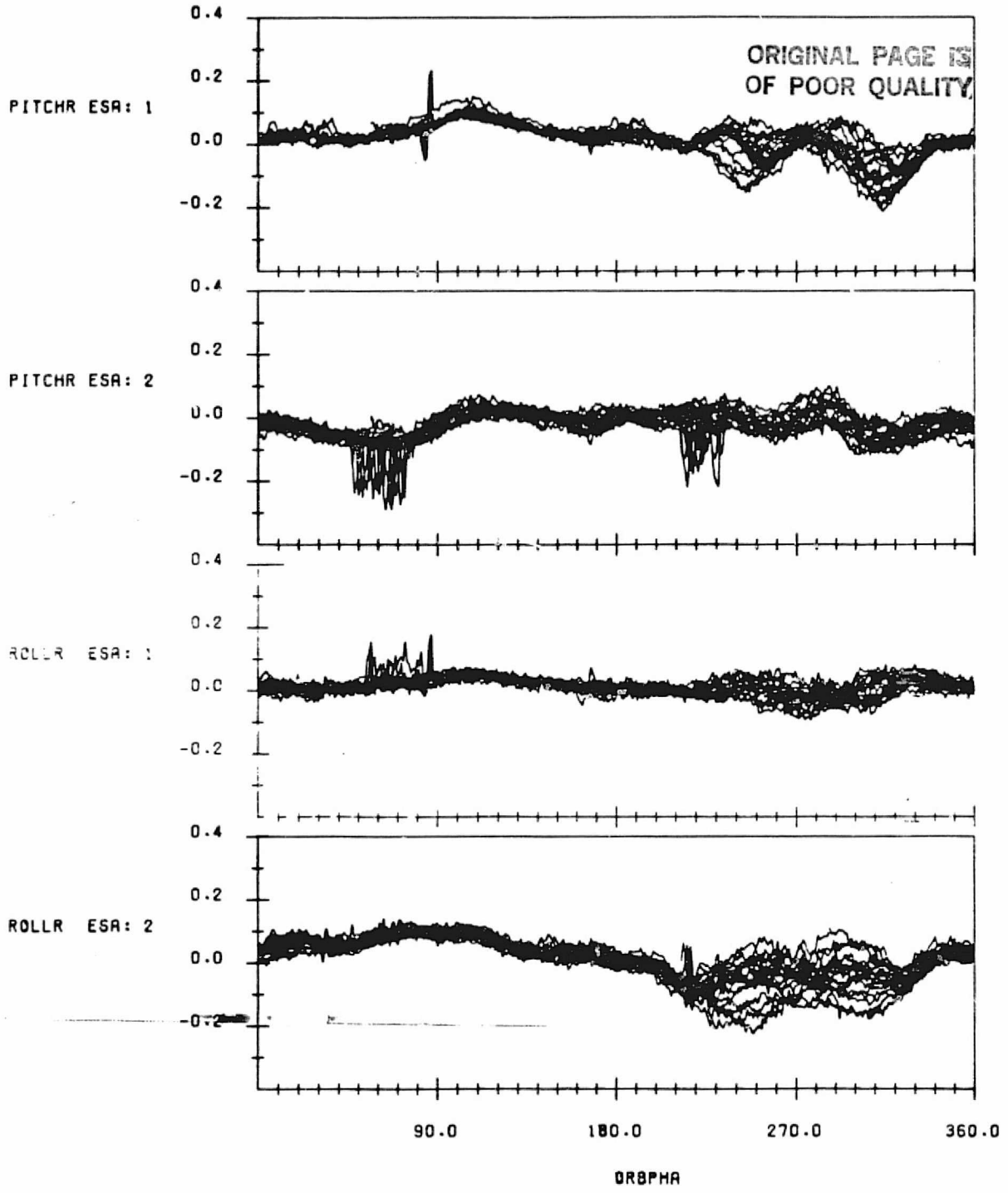

FIGURE E-25. Residual Errors from HRDB/SOES Model for Data Span on July 26-27, 1983

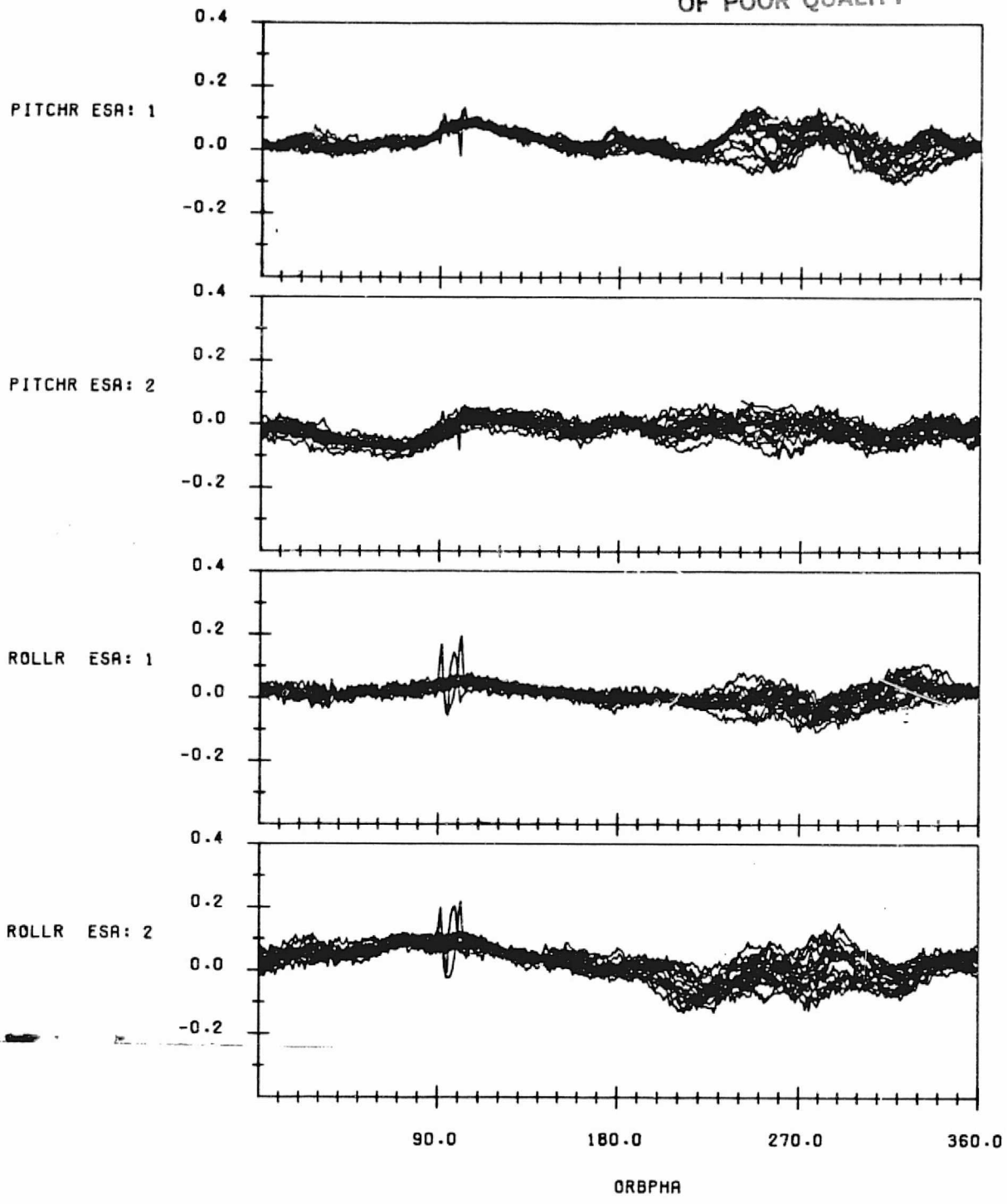

FIGURE E-26. Residual Errors from HRDB/SOES Model for Data Span on August 6-7, 1983

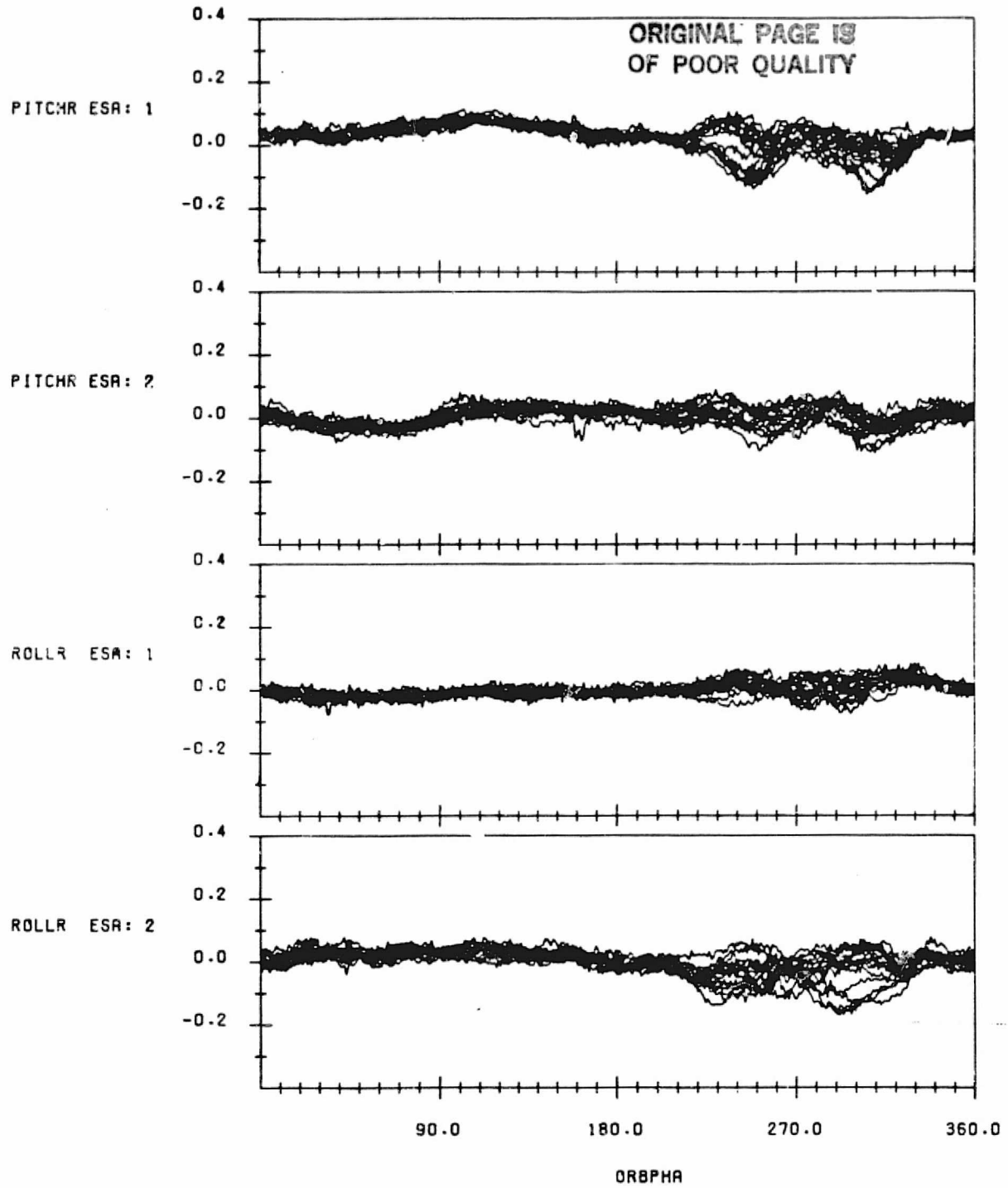

FIGURE E-27. Residual Errors from HRDB/SOES Model for Data Span on August 31 - September 1, 1983

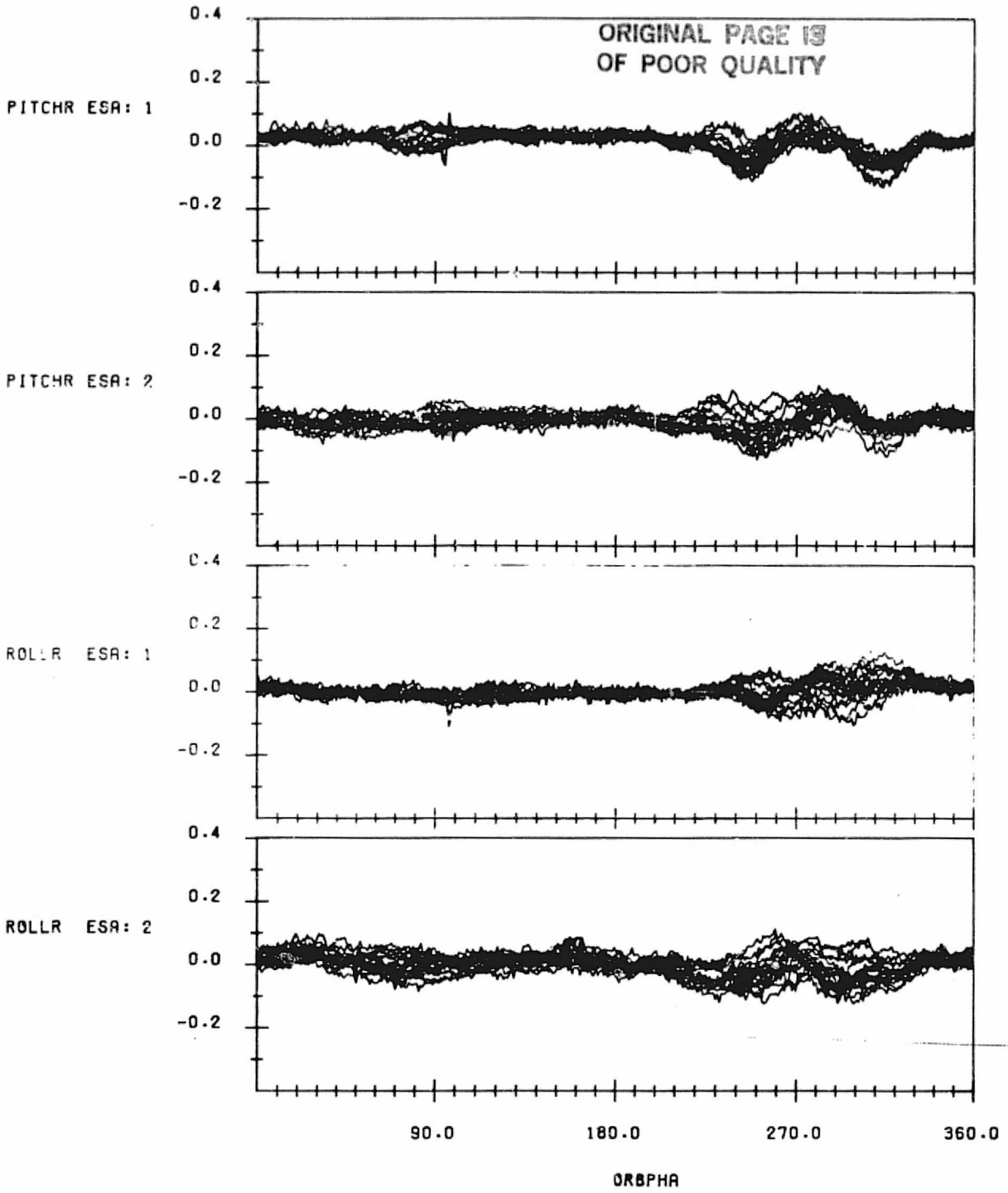

FIGURE E-28. Residual Errors from HRDB/SOES Model for Data Span on September 14-15, 1983

APPENDIX F - DATA FITTING COEFFICIENTS

This appendix provides tables of the coefficients resulting from various data fittings described in Section 5. Table F-1 gives the coefficients resulting from the second order finite Fourier series fits to each of the 28 data spans for all four measurement channels. Table F-2 gives the fit coefficients resulting from the seasonal dependence of the coefficients in Table F-1. Table F-3 gives the fit coefficients that result from evaluating the seasonal dependence fits at the beginning of each month. Table F-4 provides the residual error standard deviation statistics for various data modeling options. In Table F-4 the HRDB/SOES model statistics on the last four dates were obtained incorrectly and should be ignored. Also note that the statistics for the last 4 models on December 1, 1983, and on February 17, 1983 are corrupted by bad reference attitude points which were not flagged in the data processing.

TABLE F-1. Data Fitting Coefficients (1 of 4, Pitch Sensor 1)

DATA PASS	START DATE	DAY OF YEAR	CONSTANT	SIN A	COS A	SIN 2A	COS 2A
10	82 08 10	222	0.00868	-0.00264	-0.00404	-0.00071	-0.01177
20	82 08 25	237	-0.00059	-0.01458	0.00036	-0.00692	-0.00811
30	82 09 08	251	0.03668	-0.01997	-0.00785	-0.00301	-0.00447
40	82 09 22	265	-0.02725	-0.02504	0.01551	0.00959	0.02651
50	82 10 05	278	-0.05441	-0.01840	0.01721	0.02026	0.04564
60	82 10 20	293	-0.03828	-0.01109	0.01872	0.02180	0.05309
70	82 11 02	306	-0.02631	-0.03649	0.01649	0.02745	0.06248
80	82 11 16	320	-0.04269	-0.03862	0.02962	0.03102	0.05611
90	82 12 01	335	0.03030	-0.03650	0.03220	0.02038	0.05732
00	82 12 14	348	-0.01679	-0.06419	0.06435	0.01791	0.05822
10	82 12 28	362	0.01724	-0.02935	0.05233	-0.01261	0.03142
20	83 01 19	019	-0.01150	-0.02111	0.05372	0.00397	0.04264
30	83 02 02	033	0.00228	-0.01505	0.04385	-0.01071	0.03596
40	83 02 17	048	-0.00012	-0.01903	0.02060	0.01381	0.05026
50	83 03 03	062	-0.01727	-0.00452	0.01003	0.01757	0.05823
60	83 03 14	073	-0.03407	0.00494	0.00567	0.02660	0.07221
70	83 03 29	088	-0.00321	0.01896	0.00112	0.04397	0.07931
80	83 04 14	104	0.00339	0.04334	-0.01426	0.03787	0.06801
90	83 04 26	116	-0.00362	0.05612	-0.02163	0.04059	0.06093
00	83 05 11	131	-0.00062	0.07078	-0.02731	0.03691	0.05485
10	83 95 23	143	0.00327	0.06776	-0.03037	0.03074	0.04124
20	83 06 06	157	-0.00482	0.08050	-0.03466	0.03205	0.04248
30	83 06 22	173	0.01809	0.06705	-0.03440	0.02357	0.02658
40	83 07 06	187	0.01610	0.04701	-0.02766	0.01453	0.01455
50	83 07 26	207	0.01306	0.03615	-0.02698	0.01639	0.01061
60	83 08 06	218	0.02266	-0.00073	-0.01215	0.00574	-0.00216
70	83 08 31	243	0.03718	-0.01201	-0.00031	0.00674	0.00662
80	83 09 14	257	0.02560	-0.02523	0.00157	0.01199	0.01344

TABLE F-1. Data Fitting Coefficients (2 of 4, Pitch Sensor 2)

DATA PASS	START DATE	DAY OF YEAR	CONSTANT	SIN A	COS A	SIN 2A	COS 2A
01	82 08 10	222	-0.01104	-0.00532	-0.01158	-0.00874	0.00128
02	82 08 25	237	-0.01077	0.00013	-0.00287	-0.00921	0.00194
03	82 09 08	251	0.02205	0.00952	-0.00729	-0.00980	-0.00293
04	82 09 22	265	-0.02785	0.00745	0.01206	0.01391	0.00334
05	82 10 05	278	-0.03976	0.01383	0.01528	0.02703	0.00539
06	82 10 20	293	-0.01331	0.01499	0.03321	0.02579	0.00010
07	82 11 02	306	-0.01162	0.00993	0.01780	0.03125	0.00839
08	82 11 16	320	0.00809	0.00296	0.04103	0.03137	-0.00135
09	82 12 01	335	0.08060	0.02630	0.04160	0.02588	0.00986
10	82 12 14	348	-0.00157	0.00362	0.06967	0.02611	0.00683
11	82 12 28	362	0.03480	0.00193	0.04945	-0.01800	0.01313
12	83 01 19	019	-0.00905	0.02495	0.05117	0.00738	0.00890
13	83 02 02	033	-0.00035	0.01019	0.03711	-0.01855	0.01090
14	83 02 17	048	0.00401	0.01027	0.01929	0.00476	0.01033
15	83 03 03	062	-0.00602	0.00977	0.00640	0.00573	0.00852
16	83 03 14	073	-0.01621	0.00725	0.00508	0.02298	0.00684
17	83 03 29	088	-0.00371	0.00496	0.00281	0.03356	0.00583
18	83 04 14	104	0.00024	0.00435	-0.00849	0.03083	0.00336
19	83 04 26	116	-0.00373	0.00216	-0.01581	0.03260	0.00276
20	83 05 11	131	-0.00152	-0.00024	-0.02820	0.02886	0.00298
21	83 95 23	143	-0.00398	-0.00672	-0.03612	0.02430	0.00201
22	83 06 06	157	-0.01196	-0.00742	-0.03715	0.02351	0.00063
23	83 06 22	173	0.01093	-0.00857	-0.03967	0.01347	0.00198
24	83 07 06	187	-0.00480	-0.00893	-0.03571	0.00395	0.00040
25	83 07 26	207	-0.01666	-0.00423	-0.03043	0.00016	0.00093
26	83 08 06	218	-0.01473	-0.00514	-0.02122	-0.00039	0.00195
27	83 08 31	243	0.00620	-0.00067	-0.00646	-0.00089	0.00273
28	83 09 14	257	-0.00414	0.00305	0.00626	-0.00032	0.00257

TABLE F-1. Data Fitting Coefficients (3 of 4, Roll Sensor 1)

DATA PASS	START DATE	DAY OF YEAR	CONSTANT	SIN A	COS A	SIN 2A	COS 2A
01	82 08 10	222	0.01393	-0.02655	0.02066	-0.00792	0.00513
02	82 08 25	237	0.00008	-0.03942	0.01056	-0.00458	0.00500
03	82 09 08	251	-0.02580	-0.05836	0.00955	-0.00529	0.00522
04	82 09 22	265	0.00767	-0.04916	0.01221	-0.00524	0.01031
05	82 10 05	278	0.00770	-0.05625	0.01373	0.00006	0.01296
06	82 10 20	293	0.00548	-0.06237	0.02327	0.00089	0.01728
07	82 11 02	306	0.01038	0.02628	0.03413	0.01026	0.02065
08	82 11 16	320	0.00673	0.02852	0.03381	0.00776	0.01175
09	82 12 01	335	0.00445	0.07925	0.01262	0.00214	0.00652
10	82 12 14	348	-0.02492	0.03647	0.03246	0.01086	0.00365
11	82 12 28	362	-0.03152	0.08655	0.01728	0.00530	-0.00251
12	83 01 19	019	0.00222	0.03973	-0.00722	0.00331	-0.00248
13	83 02 02	033	-0.00468	0.04035	-0.00220	-0.00235	-0.01443
14	83 02 17	048	0.00020	-0.01157	0.00686	-0.00803	-0.01111
15	83 03 03	062	0.01697	-0.00340	-0.00015	-0.00554	-0.01149
16	83 03 14	073	0.01108	-0.01168	0.00832	-0.00174	0.00518
17	83 03 29	088	-0.00902	-0.01396	0.00958	-0.00021	0.01097
18	83 04 14	104	-0.00408	-0.01329	0.01308	-0.00305	0.00524
19	83 04 26	116	-0.00617	-0.01013	0.01389	-0.00370	0.00550
20	83 05 11	131	-0.00527	-0.00388	0.00388	-0.00598	0.00405
21	83 95 23	143	-0.00397	0.00625	0.00587	-0.00409	0.00759
22	83 06 06	157	0.00194	0.00844	0.00486	-0.00413	0.00414
23	83 06 22	173	-0.00449	-0.00493	-0.00929	-0.00085	0.00428
24	83 07 06	187	-0.00068	0.00821	0.00145	-0.00805	0.00253
25	83 07 26	207	0.00956	0.01143	0.00265	-0.00646	0.00133
26	83 08 06	218	0.00857	0.01311	0.00917	-0.00894	0.00543
27	83 08 31	243	-0.00632	-0.01926	0.00513	-0.00753	0.00652
28	83 09 14	257	-0.00245	-0.01383	0.01324	-0.00712	0.00938

TABLE F-1. Data Fitting Coefficients (4 of 4, Roll Sensor 2)

DATA PASS	START DATE	DAY OF YEAR	CONSTANT	SIN A	COS A	SIN 2A	COS 2A
01	82 08 10	222	-0.00384	-0.01694	0.01348	-0.00337	0.00427
02	82 08 25	237	0.05350	-0.05157	0.00914	-0.00332	0.00457
03	82 09 08	251	0.03218	-0.09181	0.00516	0.00062	0.01260
04	82 09 22	265	0.04514	-0.07249	0.00834	-0.01098	0.04307
05	82 10 05	278	0.02022	-0.07962	0.00323	-0.01097	0.07001
06	82 10 20	293	-0.02445	-0.07556	0.00179	-0.00090	0.08054
07	82 11 02	306	-0.00805	0.00615	0.00645	0.00025	0.07918
08	82 11 16	320	-0.09898	-0.00007	0.01245	0.00760	0.07362
09	82 12 01	335	-0.05666	0.03948	-0.00660	-0.00696	0.06264
10	82 12 14	348	-0.04884	-0.00170	0.00564	-0.00935	0.06428
11	82 12 28	362	-0.07023	0.07530	0.00691	0.00108	0.02843
12	83 01 19	019	-0.00028	0.02938	-0.01872	-0.00653	0.03880
13	83 02 02	033	-0.01070	0.05047	-0.00898	0.00226	0.02744
14	83 02 17	048	-0.00985	-0.00453	0.00342	-0.00367	0.05358
15	83 03 03	062	0.01274	0.01694	0.00122	-0.00031	0.05841
16	83 03 14	073	0.00163	0.00753	0.00667	-0.00156	0.08575
17	83 03 29	088	-0.01761	0.01157	0.00756	-0.00216	0.09736
18	83 04 14	104	-0.00530	0.03879	0.01353	-0.00244	0.08295
19	83 04 26	116	-0.00514	0.06257	0.01592	-0.00130	0.08247
20	83 05 11	131	-0.00102	0.08119	0.01593	-0.00567	0.06825
21	83 95 23	14	0.00331	0.09142	0.01945	-0.00752	0.05992
22	83 06 06	15	0.00130	0.10522	0.01886	-0.00518	0.05706
23	83 06 22	173	0.00421	0.08445	0.00719	-0.00512	0.04032
24	83 07 06	187	0.00070	0.07408	0.01880	-0.00319	0.02406
25	83 07 26	207	0.00957	0.06072	0.01636	0.00014	0.02282
26	83 08 06	218	0.02229	0.03106	0.01554	-0.00277	0.01077
27	83 08 31	243	0.00561	-0.01847	0.00666	-0.00419	0.01905
28	83 09 14	257	0.00827	-0.03267	0.00627	-0.00098	0.02436

TABLE F-2. Fourier Series Fits to the Time Dependencies of Correction Coefficients (1 to 4, Sensor 1 Pitch)

	A_0	A_1	A_2	B_1	B_2	STDV
e_0	-.00202	-.01228	.01215	.00015	.00953	.01949
e_1	.00652	.03826	.00504	-.00884	.00527	.00684
f_1	.00462	-.04403	.00357	.02973	-.01408	.00957
e_2	.03991	.01764	-.01137	.01806	-.01771	.00819
f_2	.01773	-.00506	-.00820	.00862	-.01399	.00724

TABLE F-2. Fourier Series Fits to the Time Dependencies of Correction Coefficients (2 of 4, Sensor 2 Pitch)

	A_0	A_1	A_2	B_1	B_2	STDV
e_0	-.00007	.00935	.01004	-.00069	-.00520	.01863
e_1	.00615	.04183	.00197	-.01016	.00073	.00706
f_1	.00448	.01017	-.00338	-.00124	.00039	.00524
e_2	.00465	.00432	.00092	.00166	.00108	.00227
f_2	.01320	.00013	-.00888	.00436	-.01734	.00819

TABLE F-2. Fourier Series Fits to the Time Dependencies of Correction Coefficients (3 of 4, Sensor 1 Roll)

	A_0	A_1	A_2	B_1	B_2	STDV
e_0	-.00134	-.00227	-.00327	-.00060	.00182	.01113
e_1	.01056	.00531	-.00354	-.00715	-.00650	.00726
f_1	.00464	.02355	.03607	.00685	-.00769	.01869
e_2	.00406	-.00252	-.00451	-.00563	-.00635	.00361
f_2	-.00165	.00525	.00121	-.00156	-.00383	-.00263

TABLE E-2. Fourier Series Fits to Time Dependencies of Correction Coefficients (4 of 4, Sensor 2 Roll)

	A_0	A_1	A_2	B_1	B_2	STDV
e_0	-.00876	.02568	-.01478	.00046	.01926	.01910
e_1	.00729	-.00953	-.00056	.00079	-.00365	.00533
f_1	.02226	-.01990	.04650	.04351	-.01991	.01993
e_2	.05110	.01143	-.01798	.01497	-.02324	.01016
f_2	-.00306	.00098	-.00013	.00026	.00065	.00398

TABLE F-3. Correction Coefficients at the Beginning of Each Month (1 of 4, Sensor 1 Pitch)

Month	e_0	e_1	f_1	e_2	f_2
1	-.00182	.04984	-.04043	.04589	.00414
2	.00159	.04147	-.03290	.04346	.00174
3	-.00557	.02078	-.01111	.05427	.01412
4	-.01399	-.00715	.02585	.06926	.03441
5	-.01033	-.02706	.05767	.06805	.04394
6	.00646	-.03308	.06699	.04340	.03449
7	.02224	-.02687	.04810	.01136	.01491
8	.02284	-.01508	.01276	-.00543	.00157
9	.00569	-.00264	-.01822	.00630	.00501
10	-.01445	.01044	-.03337	.03345	.01741
11	-.02260	.02668	-.03740	.05442	.02394
12	-.01445	.04177	-.03898	.05594	.01729

TABLE F-3. Correction Coefficients at the Beginning of Each Month (2 of 4, Sensor 2 Pitch)

Month	e_0	e_1	f_1	e_2	f_2
1	.01912	.04979	.01126	.00995	.00393
2	.00744	.03802	.01132	.01058	-.00389
3	-.00522	.01856	.01057	.00880	.00597
4	-.01080	-.00579	.00667	.00542	.02629
5	-.00603	-.02485	-.00016	.00258	.03637
6	.00010	-.03479	-.00696	.00126	.02590
7	.00070	-.03381	-.00909	.00125	.00453
8	-.00733	-.02334	-.00504	.00147	-.00856
9	-.01371	-.00589	.00267	.00153	-.00086
10	-.00933	.01451	.00914	.00208	.01787
11	.00512	.03473	.01202	.00405	.02900
12	.01773	.04764	.01189	.00702	.02200

TABLE F-3. Correction Coefficients at the Beginning of Each Month (3 of 4, Sensor 1 Roll)

Month	e_0	e_1	f_1	e_2	f_2
1	-.00683	.01198	.06409	-.00328	-.00494
2	-.00344	.00394	.03774	-.00874	-.00264
3	.00014	.00310	-.00131	-.00551	.00364
4	.00134	.00692	-.02454	.00287	-.00511
5	-.00061	.00912	-.01311	.00816	-.00185
6	-.00288	.00626	.01231	.00668	.00531
7	-.00238	.00176	.01735	.00213	-.00277
8	.00088	.00215	-.00790	.00131	-.00381
9	.00355	.01048	-.03819	.00712	-.00437
10	.00250	.02133	-.03811	.01424	-.00802
11	-.00204	.02682	.00046	.01533	-.00430
12	-.00616	.02275	.04557	.00814	-.00269

TABLE F-3. Correction Coefficients at the Beginning of Each Month (4 of 4, Sensor 2 Roll)

Month	e_0	e_1	f_1	e_2	f_2
1	-.05325	.01720	.09737	.02991	-.00429
2	-.04317	.01794	.08279	.07961	-.00415
3	-.00249	.00590	-.04449	.07076	-.00329
4	.00605	.00782	-.06181	.03365	-.00312
5	.02676	-.00344	.02557	.04228	-.00153
6	.00002	-.00242	.04839	.04640	-.00230
7	-.05158	.01873	.09630	.06836	-.00435
8	-.00809	.01206	.03470	.08926	-.00316
9	.02821	.00060	.00909	.05971	-.00174
10	-.02458	.01209	.03050	.00471	-.00359
11	-.05555	.01790	.10226	.03806	-.00436
12	-.04953	.01858	.09292	.07195	-.00430

TABLE F-4. Residual Error Standard Deviation Statistics (1 of 4, Pitch Sensor 1)

DATA PASS	START DATE	DAY OF YEAR	UNCORRECTED	OBLATE EARTH	HRDB/SOES	2ND-ORDER FIT	FIT W/O POLE
01	82 08 10	222	0.22892	0.04329	0.037657	0.04194	0.020192
02	82 08 25	237	0.21679	0.04058	0.035133	0.03763	0.019549
03	82 09 08	251	0.21218	0.05017	0.036546	0.04688	0.015391
04	82 09 22	265	0.23368	0.05708	0.046625	0.04968	0.023220
05	82 10 05	278	0.24784	0.06488	0.058170	0.05220	0.025499
06	82 10 20	293	0.26828	0.06403	0.053139	0.04815	0.036275
07	82 11 02	306	0.26207	0.06323	0.057590	0.03083	0.026436
08	82 11 16	320	0.26307	0.06566	0.055995	0.03372	0.018997
09	82 12 01	335	0.26341	0.06655	0.053239	0.03882	0.029069
10	82 12 14	348	0.24458	0.08778	0.071126	0.04170	0.027318
11	82 12 28	362	0.23178	0.07209	0.066650	0.05306	0.027416
12	83 01 19	019	0.24763	0.07709	0.068177	0.05874	0.025836
13	83 02 02	033	0.24637	0.06523	0.058743	0.05023	0.024810
14	83 02 17	048	0.26497	0.08877	0.081147	0.07895	0.079552
15	83 03 03	062	0.26886	0.05882	0.043073	0.04081	0.020782
16	83 03 14	073	0.28221	0.06144	0.036000	0.03087	0.017513
17	83 03 29	088	0.29763	0.06961	0.042217	0.02781	0.020369
18	83 04 14	104	0.28668	0.06714	0.052452	0.02651	0.019910
19	83 04 26	116	0.28928	0.06867	0.064299	0.02237	0.019199
20	83 05 11	131	0.29516	0.07470	0.074015	0.02812	0.021480
21	83 95 23	143	0.29234	0.06960	0.064799	0.03148	0.019302
22	83 06 06	157	0.30609	0.07921	0.070763	0.03552	0.026257
23	83 06 22	173	0.29515	0.07114	0.067338	0.04174	0.026607
24	83 07 06	187	0.27261	0.05488	0.056123	0.03832	0.025146
25	83 07 26	207	0.25957	0.05431	0.054337	0.04326	0.029605
26	83 08 06	218	0.22918	0.03888	0.038880	0.03756	0.022400
27	83 08 31	243	0.23241	0.04755	0.047554	0.04616	0.018701
28	83 09 14	257	0.23476	0.05459	0.054588	0.04975	0.018974

TABLE F-4. Residual Error Standard Deviation Statistics (2 of 4, Pitch Sensor 2)

DATA PASS	START DATE	DAY OF YEAR	UNCORRECTED	OBLATE EARTH	HRDB/SOES	2ND-ORDER FIT	FIT W/O POLE
01	82 08 10	222	0.10699	0.03144	0.033278	0.02953	0.023420
02	82 08 25	237	0.10667	0.02731	0.032088	0.02636	0.022984
03	82 09 08	251	0.10670	0.03439	0.032292	0.03253	0.019458
04	82 09 22	265	0.12407	0.03931	0.033550	0.03659	0.023537
05	82 10 05	278	0.13406	0.04287	0.036380	0.03553	0.024925
06	82 10 20	293	0.13858	0.05244	0.046592	0.04179	0.033473
07	82 11 02	306	0.13581	0.03967	0.035430	0.02933	0.028942
08	82 11 16	320	0.14166	0.04924	0.042167	0.03230	0.029036
09	82 12 01	335	0.15718	0.09142	0.088280	0.08266	0.089816
10	82 12 14	348	0.14781	0.06653	0.056718	0.03931	0.035035
11	82 12 28	362	0.11403	0.05726	0.056215	0.04211	0.032792
12	83 01 19	019	0.13091	0.05578	0.052870	0.03758	0.028608
13	83 02 02	033	0.10783	0.04516	0.046258	0.03268	0.023168
14	83 02 17	048	0.13572	0.03840	0.037513	0.03440	0.027753
15	83 03 03	062	0.11865	0.03454	0.034811	0.03279	0.022126
16	83 03 14	073	0.12979	0.03577	0.032245	0.03088	0.023553
17	83 03 29	088	0.15218	0.03864	0.031936	0.03012	0.028188
18	83 04 14	104	0.13352	0.03493	0.030728	0.02644	0.023672
19	83 04 26	116	0.13396	0.03379	0.030987	0.02190	0.020494
20	83 05 11	131	0.13234	0.03871	0.037768	0.02609	0.022816
21	83 05 23	143	0.12991	0.04041	0.037699	0.02589	0.023078
22	83 06 06	157	0.13056	0.04384	0.038535	0.03043	0.028660
23	83 06 22	173	0.12450	0.04458	0.041455	0.03266	0.029681
24	83 07 06	187	0.11689	0.04123	0.040577	0.03186	0.028527
25	83 07 26	207	0.11488	0.04066	0.040626	0.03428	0.032314
26	83 08 06	218	0.11199	0.03039	0.030385	0.02616	0.024484
27	83 08 31	243	0.11185	0.02872	0.028715	0.02829	0.019359
28	83 09 14	257	0.11483	0.03560	0.035604	0.03521	0.019403

TABLE F-4. Residual Error Standard Deviation Statistics (3 of 4, Roll Sensor 1)

DATA PASS	START DATE	DAY OF YEAR	UNCORRECTED	OBLATE EARTH	HRDB/SOES	2ND-ORDER FIT	FIT W/O POLE
01	82 08 10	222	0.061569	0.03406	0.031223	0.02326	0.019176
02	82 08 25	237	0.066218	0.03709	0.034887	0.02286	0.016979
03	82 09 08	251	0.076231	0.04564	0.043374	0.01903	0.013938
04	82 09 22	265	0.073526	0.04622	0.042523	0.02720	0.017907
05	82 10 05	278	0.081332	0.05331	0.050561	0.03467	0.017485
06	82 10 20	293	0.086415	0.05744	0.056154	0.03099	0.022293
07	82 11 02	306	0.044731	0.04019	0.038413	0.02053	0.019460
08	82 11 16	320	0.042704	0.03967	0.038616	0.02146	0.018039
09	82 12 01	335	0.096832	0.08270	0.082539	0.05813	0.050552
10	82 12 14	348	0.040452	0.04201	0.041684	0.02152	0.017743
11	82 12 28	362	0.051029	0.07174	0.071892	0.03484	0.025656
12	83 01 19	019	0.035400	0.04526	0.044866	0.03484	0.024652
13	83 02 02	033	0.044421	0.05223	0.051462	0.04238	0.037963
14	83 02 17	048	0.100660	0.06561	0.065602	0.06430	0.069315
15	83 03 03	062	0.048428	0.03342	0.032993	0.03209	0.027599
16	83 03 14	073	0.051953	0.03129	0.030416	0.02933	0.018452
17	83 03 29	088	0.058534	0.02749	0.025393	0.02361	0.022112
18	83 04 14	104	0.050527	0.02631	0.025147	0.02235	0.017858
19	83 04 26	116	0.047606	0.02321	0.023762	0.01912	0.016541
20	83 05 11	131	0.042246	0.02170	0.024173	0.02072	0.016294
21	83 05 23	143	0.037465	0.02285	0.027184	0.02115	0.016248
22	83 06 06	157	0.035049	0.02154	0.025223	0.01975	0.015354
23	83 06 22	173	0.041945	0.02443	0.025582	0.02309	0.016469
24	83 07 06	187	0.036144	0.02396	0.026600	0.02248	0.017023
25	83 07 26	207	0.034488	0.02411	0.024122	0.02221	0.016824
26	83 08 06	218	0.036615	0.02677	0.026772	0.02312	0.016924
27	83 08 31	243	0.051261	0.02475	0.024745	0.01901	0.013332
28	83 09 14	257	0.051839	0.02822	0.028222	0.02325	0.014736

TABLE F-4. Residual Error Standard Deviation Statistics (4 of 4, Roll Sensor 2)

DATA PASS	START DATE	DAY OF YEAR	UNCORRECTED	OBLATE EARTH	HRDB/SOES	2ND-ORDER FIT	FIT W/O POLE
01	82 08 10	222	0.18180	0.05760	0.049947	0.05503	0.043690
02	82 08 25	237	0.15837	0.06343	0.041179	0.05014	0.038211
03	82 09 08	251	0.14876	0.08039	0.040560	0.04498	0.023076
04	82 09 22	265	0.17659	0.07626	0.053361	0.04881	0.027827
05	82 10 05	278	0.19816	0.09425	0.079001	0.05872	0.028544
06	82 10 20	293	0.20644	0.09572	0.086068	0.05638	0.051591
07	82 11 02	306	0.23540	0.07194	0.054837	0.04651	0.046097
08	82 11 16	320	0.22669	0.06523	0.045860	0.03990	0.028434
09	82 12 01	335	0.24475	0.09917	0.089027	0.08533	0.087204
10	82 12 14	348	0.20887	0.06935	0.055826	0.05327	0.045015
11	82 12 28	362	0.22903	0.08233	0.079636	0.05826	0.036387
12	83 01 19	019	0.21532	0.06717	0.057268	0.05726	0.023867
13	83 02 02	033	0.22544	0.06464	0.058409	0.05114	0.023225
14	83 02 17	048	0.22773	0.05819	0.042809	0.04521	0.024296
15	83 03 03	062	0.22460	0.05662	0.034950	0.03876	0.022054
16	83 03 14	073	0.23417	0.06832	0.044087	0.03347	0.022146
17	83 03 29	088	0.23899	0.07384	0.049557	0.02877	0.023856
18	83 04 14	104	0.23465	0.06936	0.058679	0.02835	0.020869
19	83 04 26	116	0.24192	0.07605	0.067416	0.02537	0.022434
20	83 05 11	131	0.24672	0.07999	0.085892	0.03113	0.023425
21	83 05 23	143	0.25230	0.08225	0.084829	0.02996	0.022297
22	83 06 06	157	0.26529	0.08970	0.089699	0.03225	0.021557
23	83 06 22	173	0.25044	0.07335	0.078129	0.03475	0.019407
24	83 07 06	187	0.23510	0.06795	0.076309	0.04000	0.023037
25	83 07 26	207	0.22224	0.06398	0.063398	0.04450	0.022337
26	83 08 06	218	0.19552	0.04675	0.046753	0.04020	0.023785
27	83 08 31	243	0.17989	0.04633	0.046326	0.04192	0.019238
28	83 09 14	257	0.18132	0.05619	0.056190	0.04778	0.023571

APPENDIX G - RESIDUAL ERRORS FROM SECOND ORDER FIT

Figures G-1 through G-28 provides plots of the residual errors from second order Fourier series fits to all the data spans processed for this report. The fits are made to the errors from the Nominal Oblate Earth model.

The fits residuals in degrees are plotted as a function of orbit phase from the ascending node for several orbits overlayed.

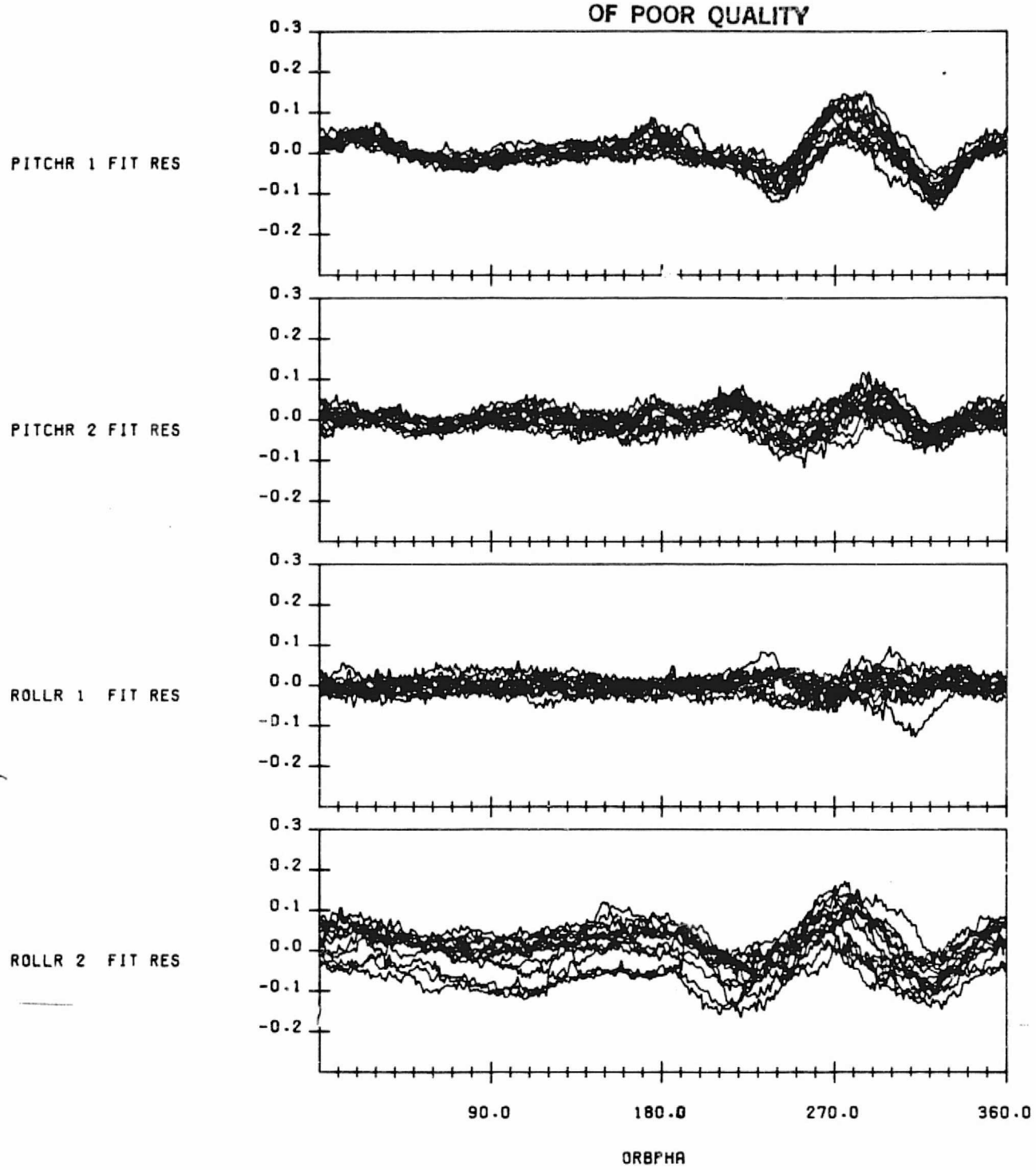

FIGURE G-1. Residual Errors from Second Order Fourier Series Fit Data Span on August 10-11, 1982

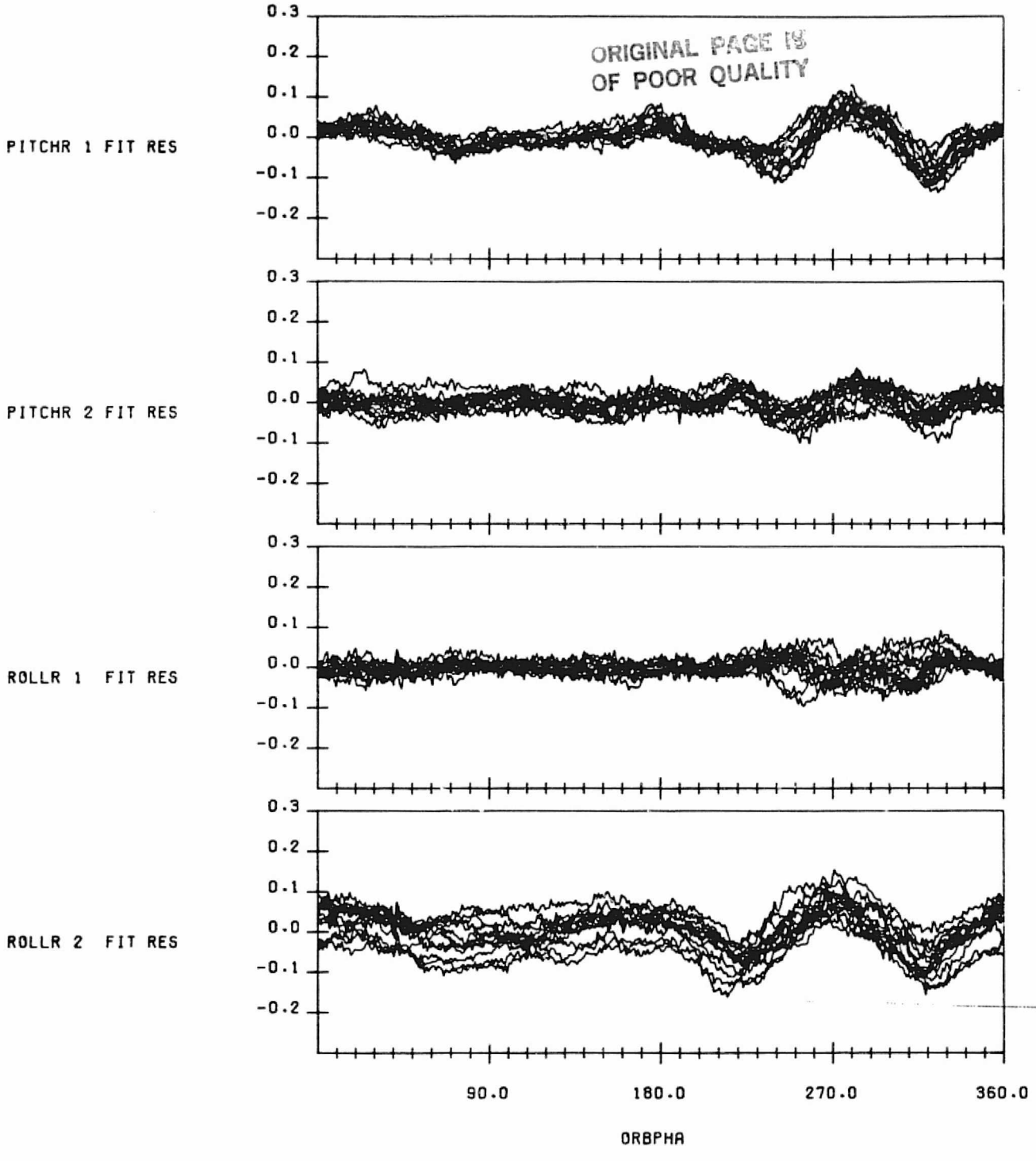

FIGURE G-2. Residual Errors from Second Order Fourier Series Fit to Data Span on August 25-26, 1982

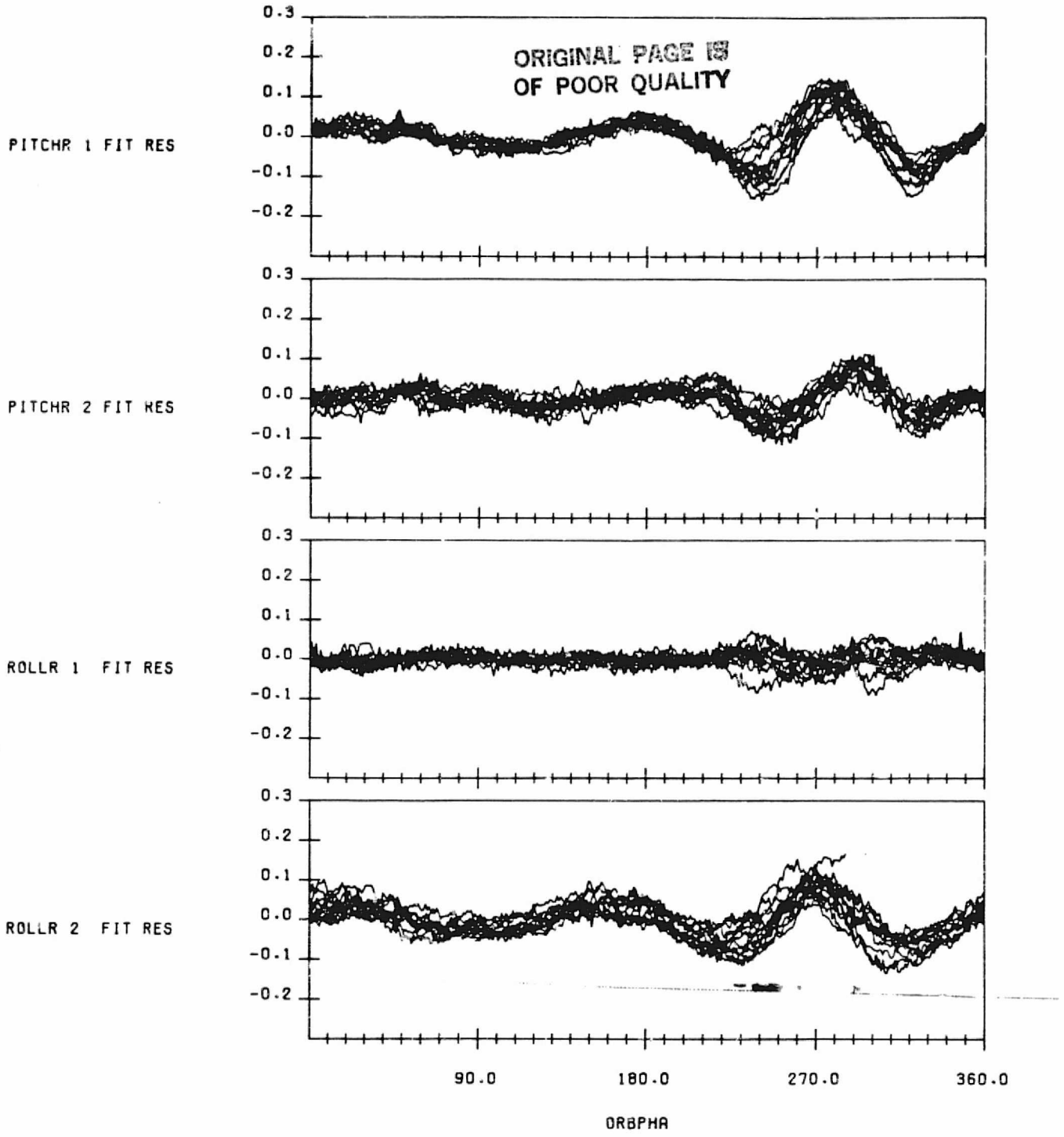

FIGURE G-3. Residual Errors from Second Order Fourier Series Fit to Data Span on September 8-9, 1982

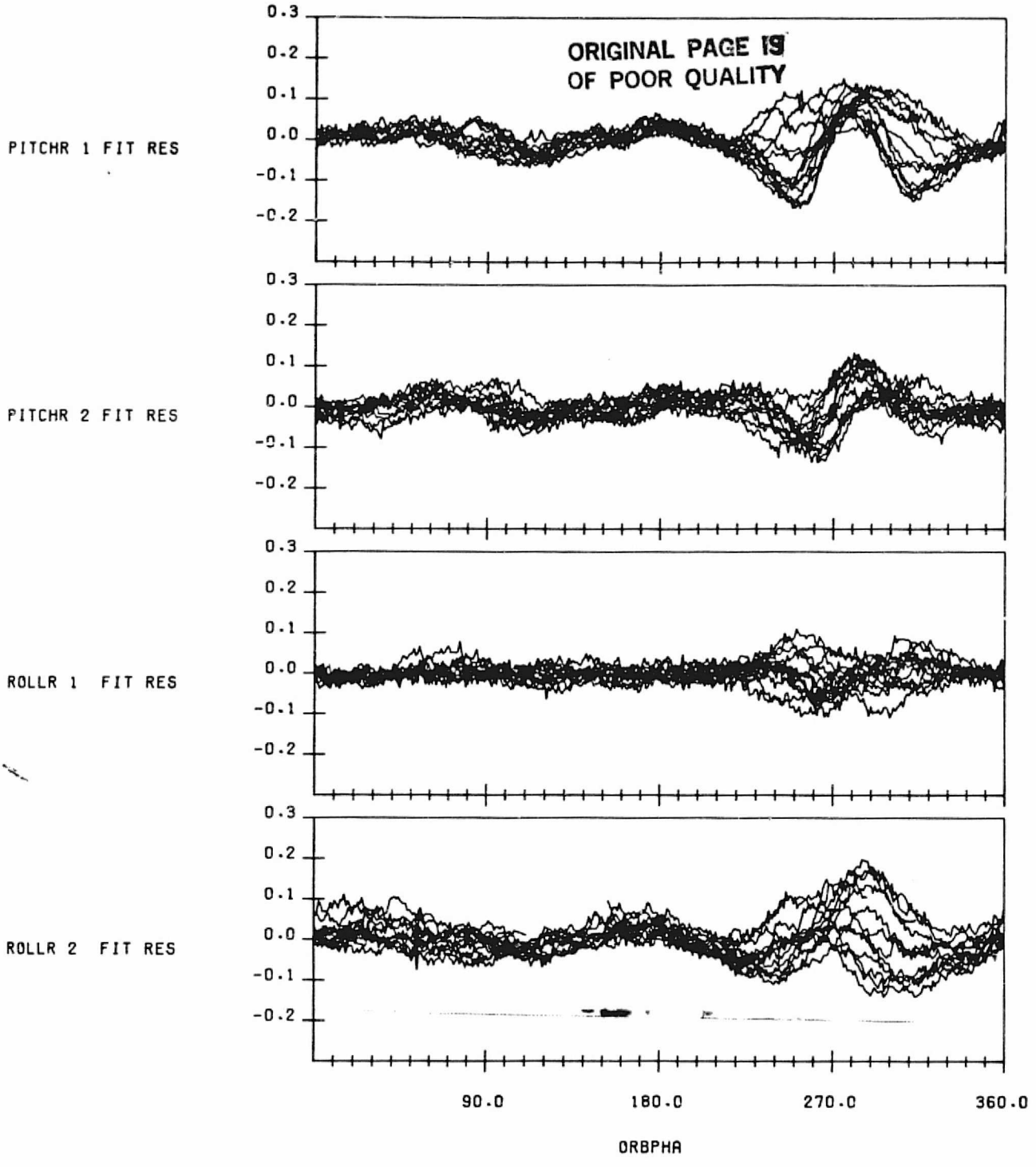

FIGURE G-4. Residual Errors from Second Order Fourier Series Fit to Data Span on September 22-23, 1982

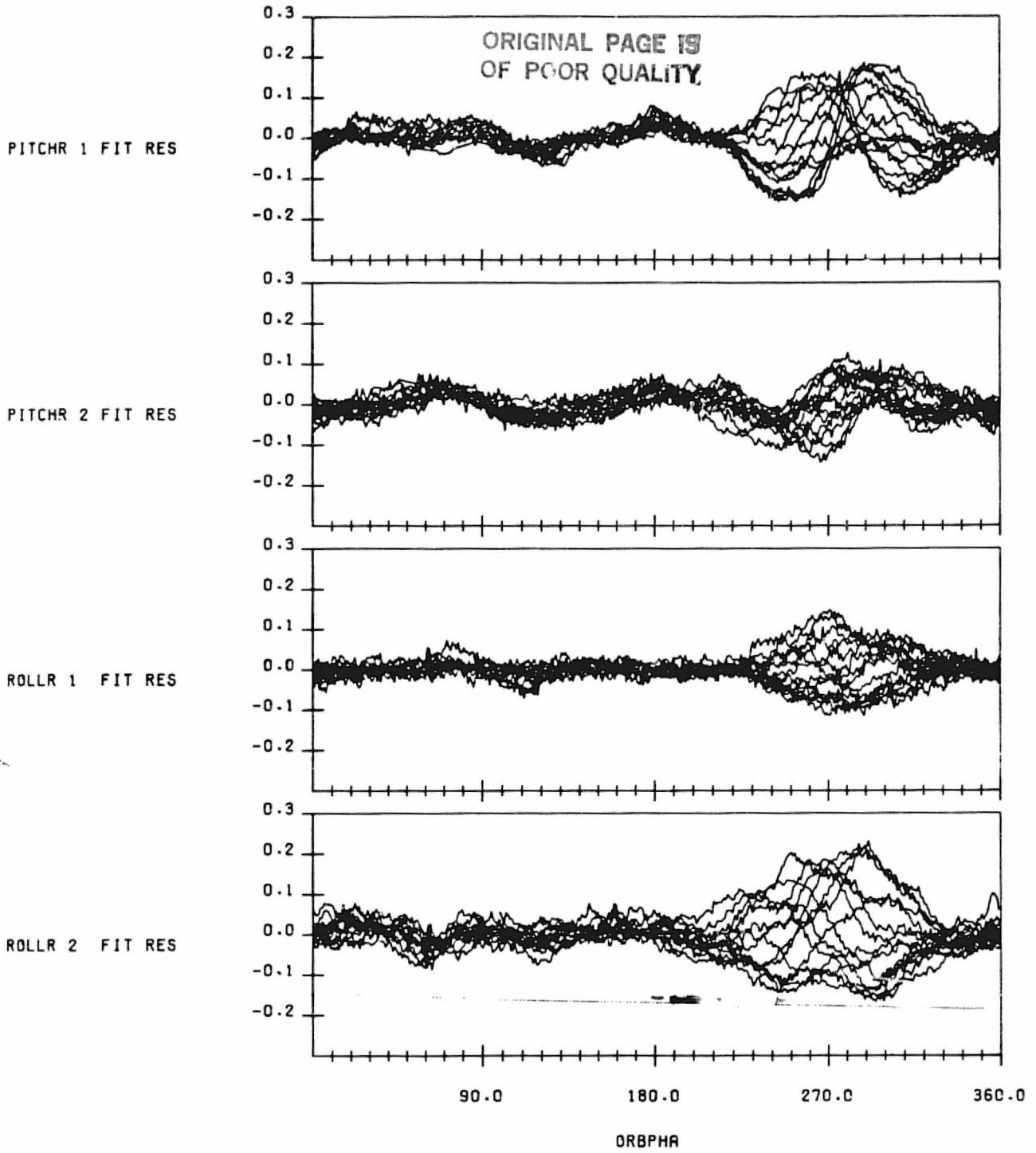

FIGURE G-5. Residual Errors from Second Order Fourier Series Fit to Data Span on October 5-6, 1982

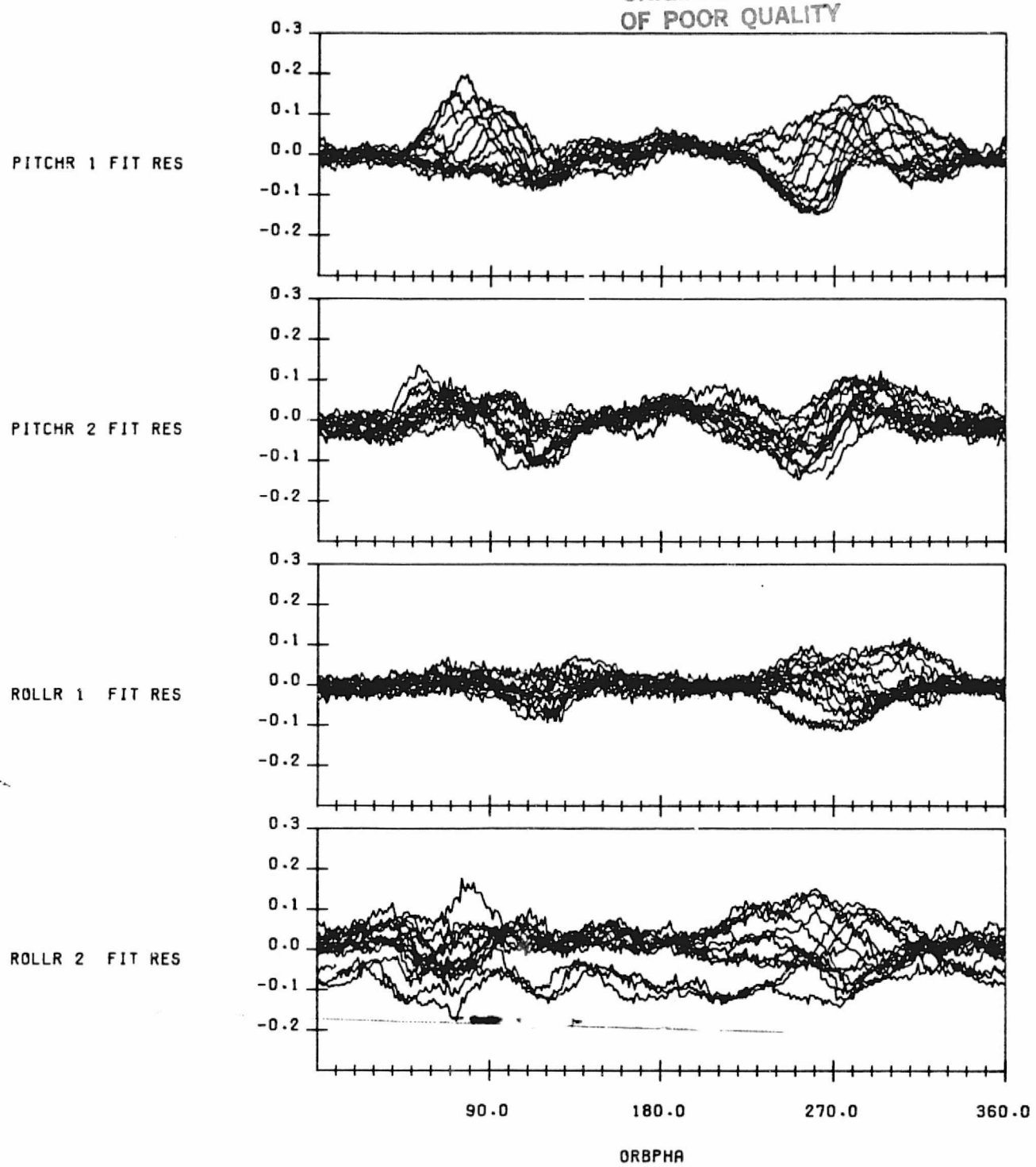

FIGURE G-6. Residual Errors from Second Order Fourier Series Fit to Data Span on October 20-21, 1982

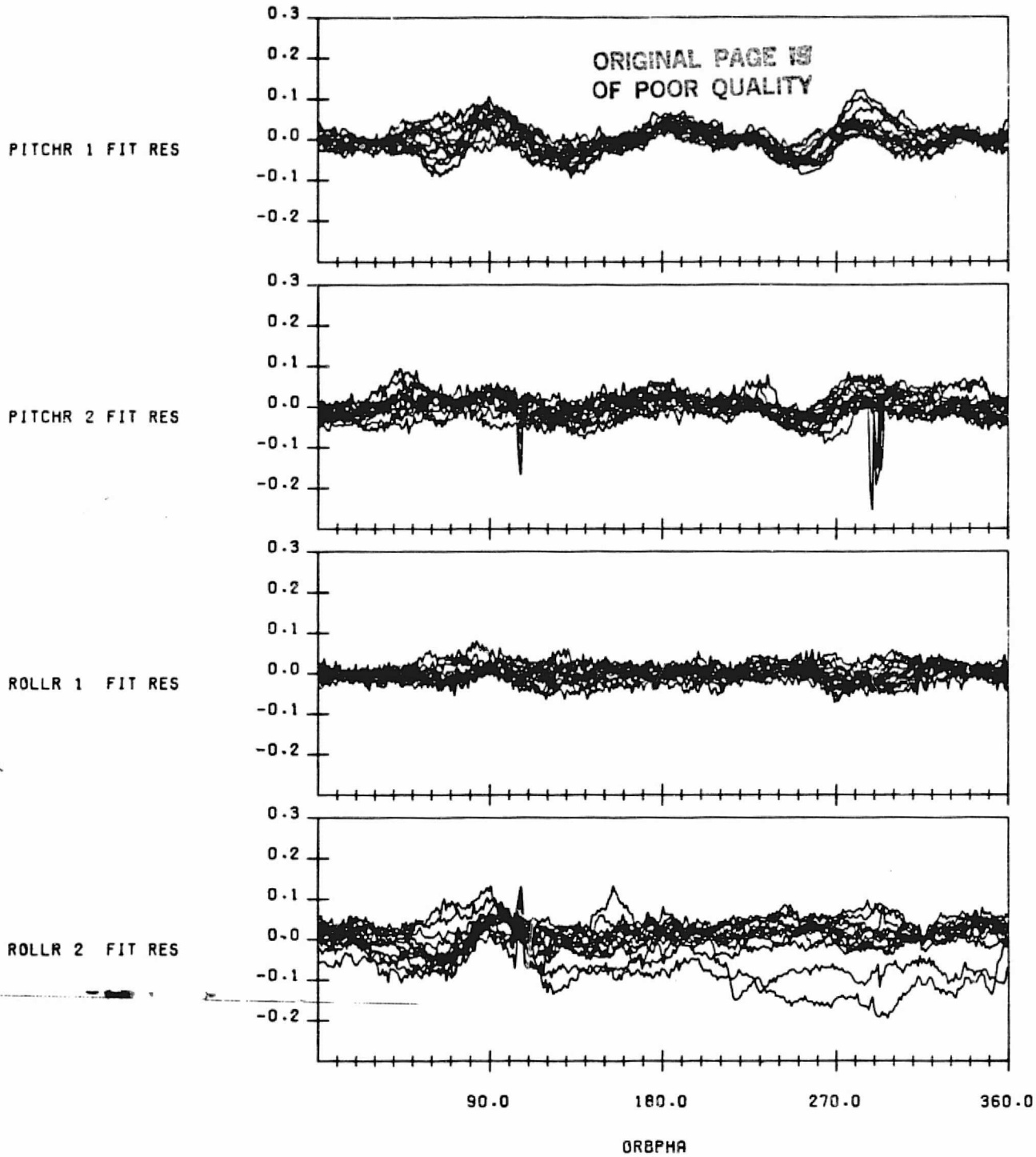

FIGURE G-7. Residual Errors from Second Order Fourier Series Fit to Data Span on November 2-3, 1982

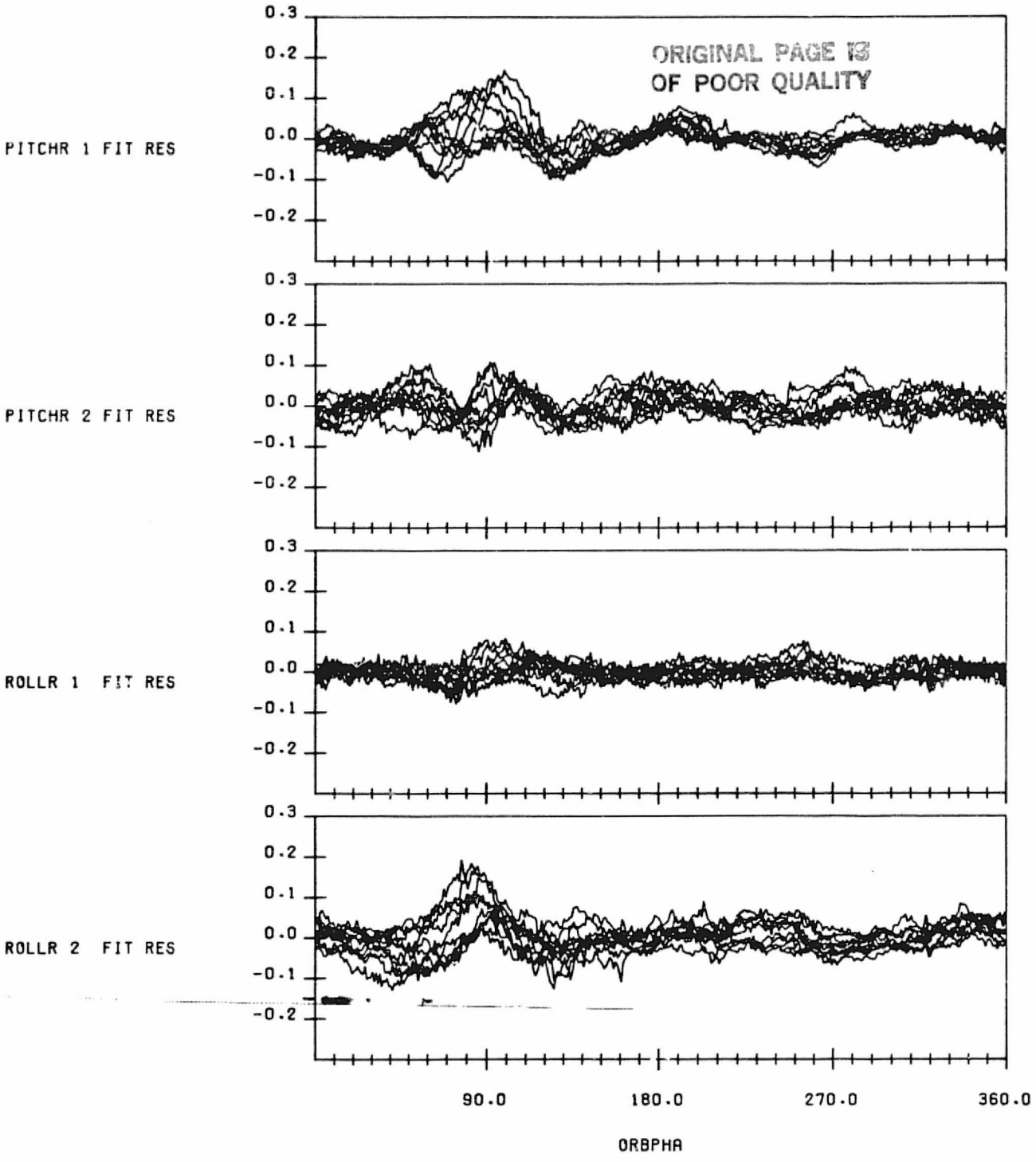

FIGURE G-8. Residual Errors from Second Order Fourier Series Fit to Data Span on November 16, 1982

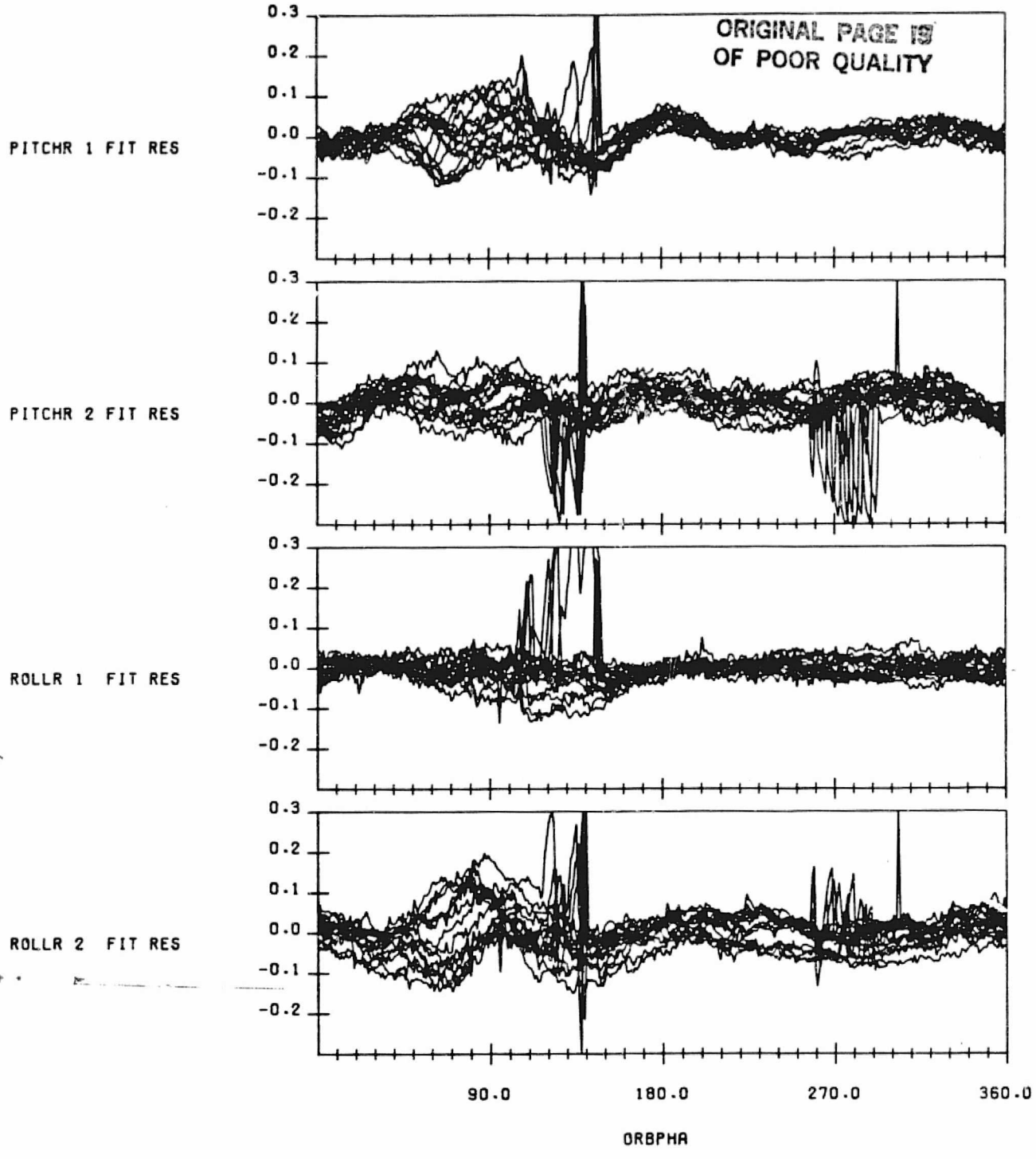

FIGURE G-9. Residual Errors from Second Order Fourier Series Fit to Data Span on December 1-2, 1982

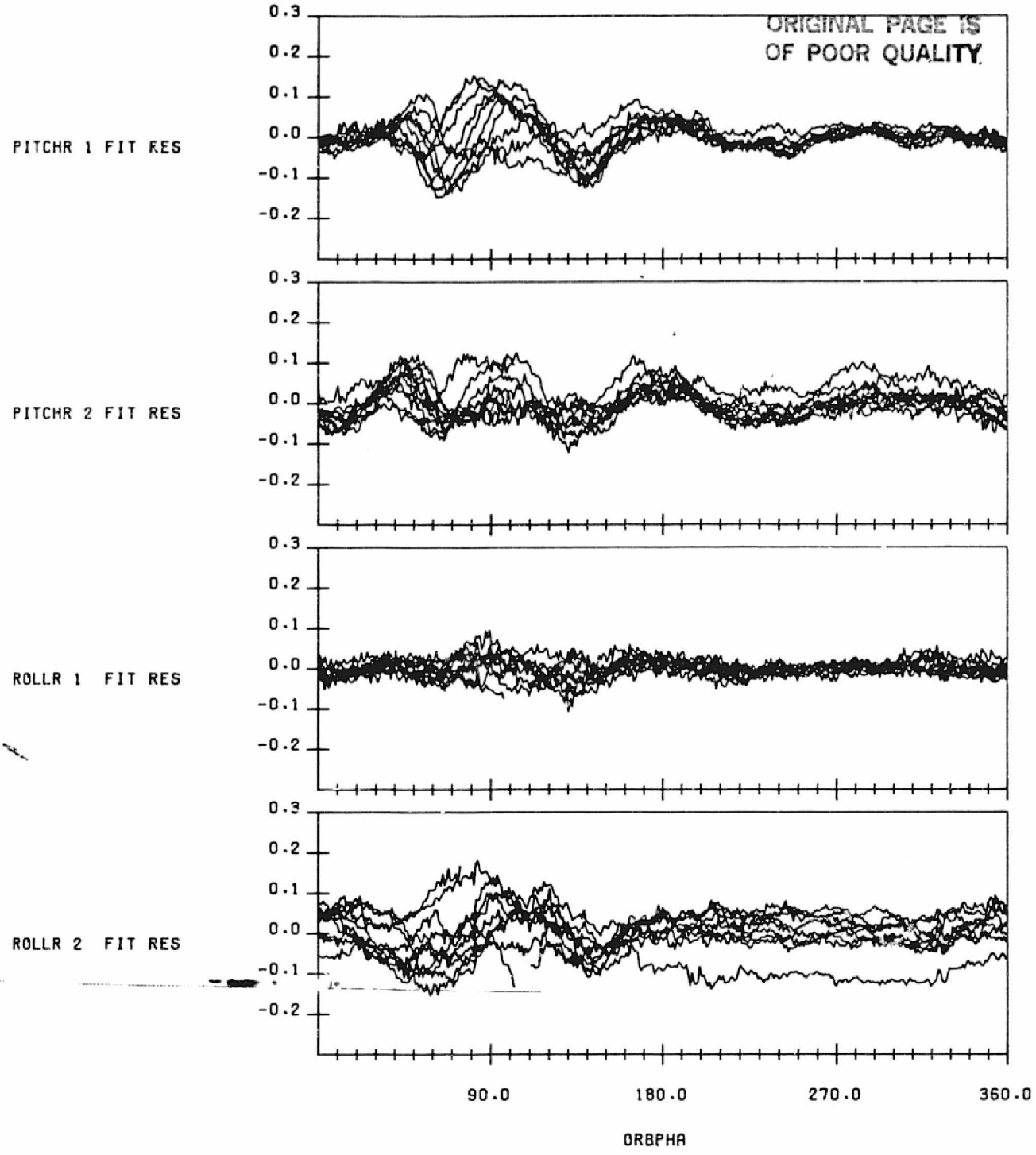

SECOND ORDER FINITE FOURIER SERIES FIT RESIDUALS TO SCANNER
RESIDUAL ERRORS FOR NOMINAL CALIBRATION WITH EARTH OBLATENESS,
OBC ORBIT AND OBC REFERENCE ATTITUDE EFFECTS MODELLED
DATA START TIME:821214.122607064
END TIME:821215.143809812

FIGURE G-10. Residual Errors from Second Order Fourier Series Fit to Data Span on December 14-15, 1982

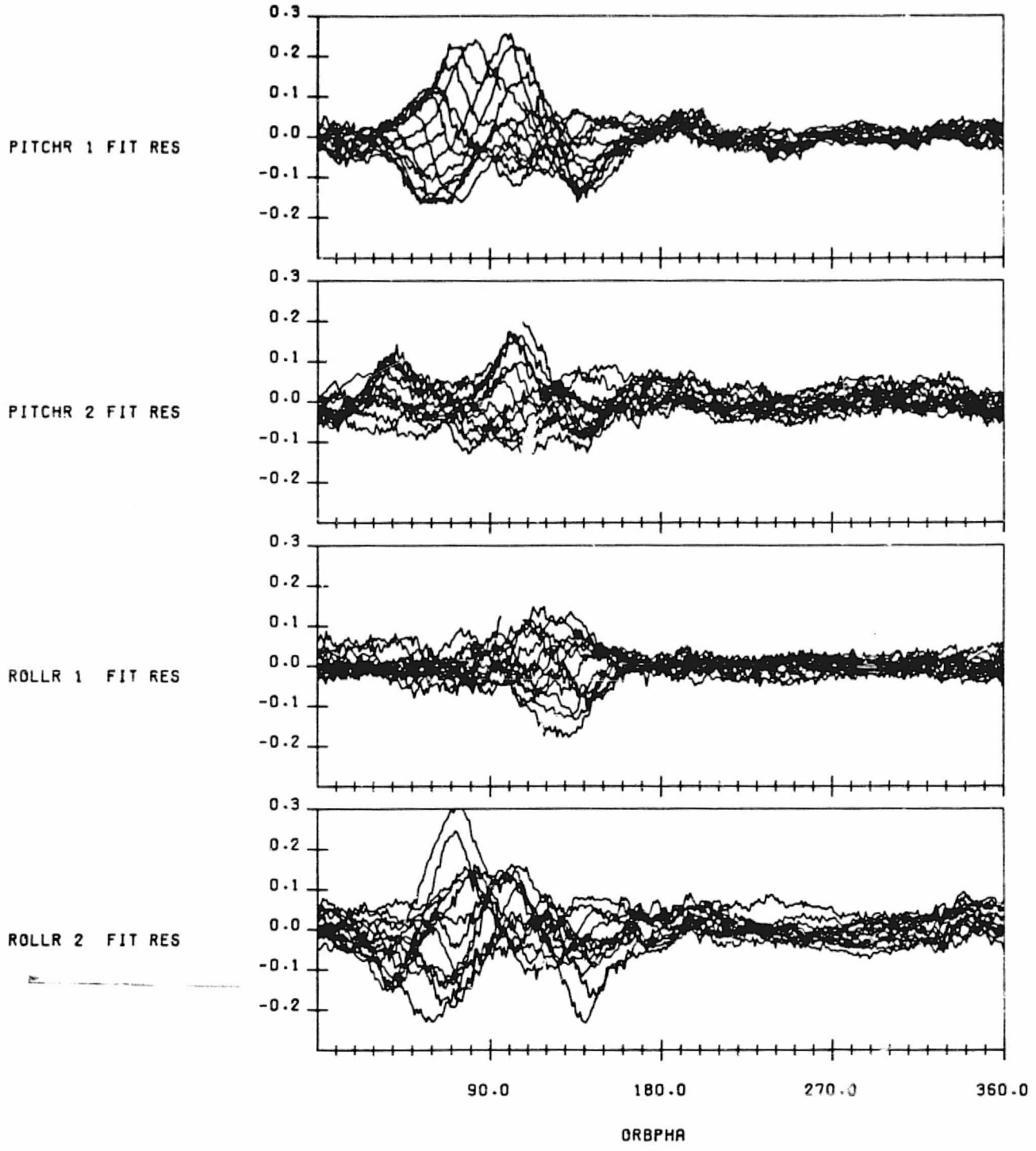

FIGURE G-11. Residual Errors from Second Order Fourier Series Fit to Data Span on December 28-29, 1982

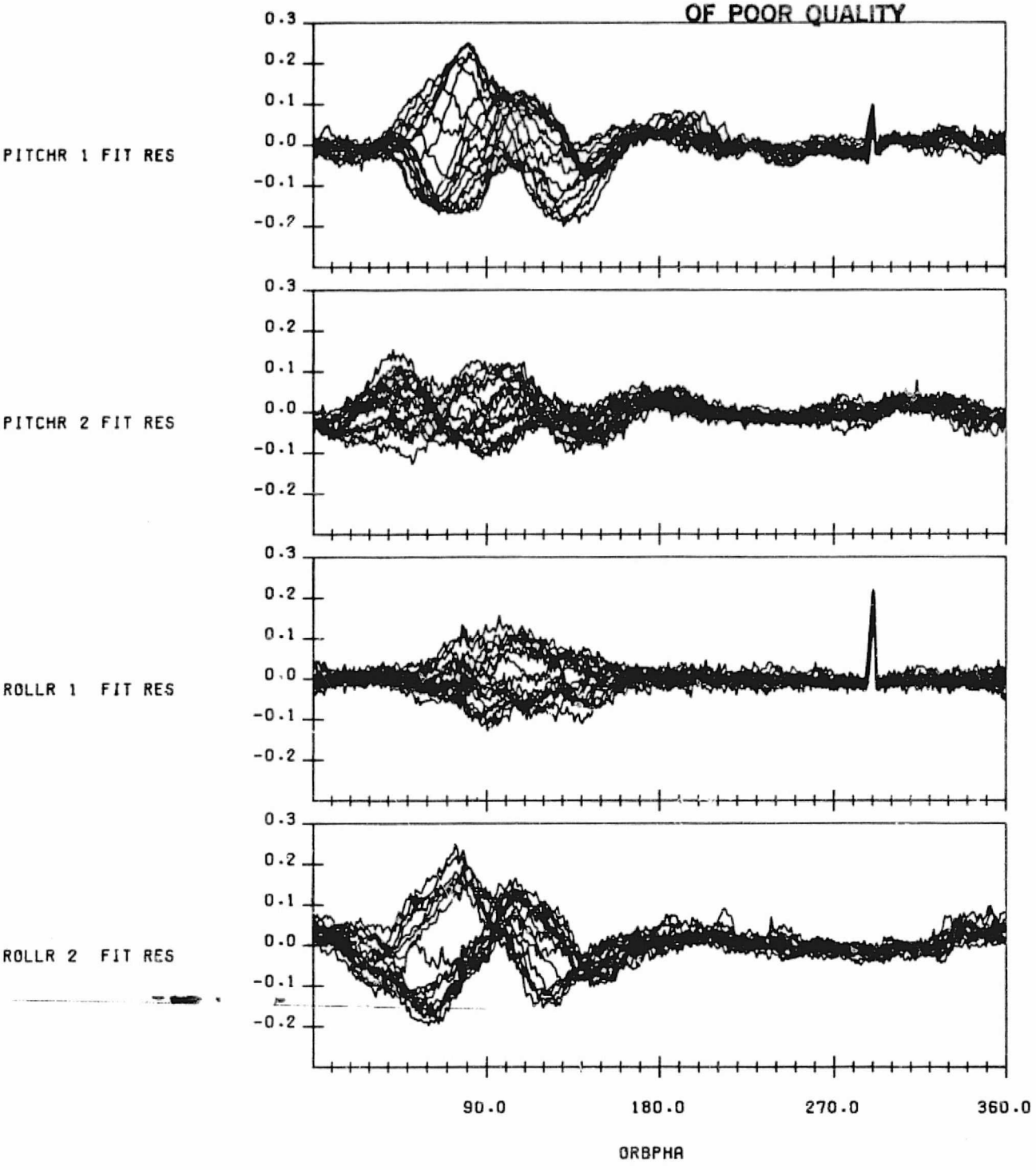

FIGURE G-12. Residual Errors from Second Order Fourier Series Fit to Data Span on January 19-20, 1983

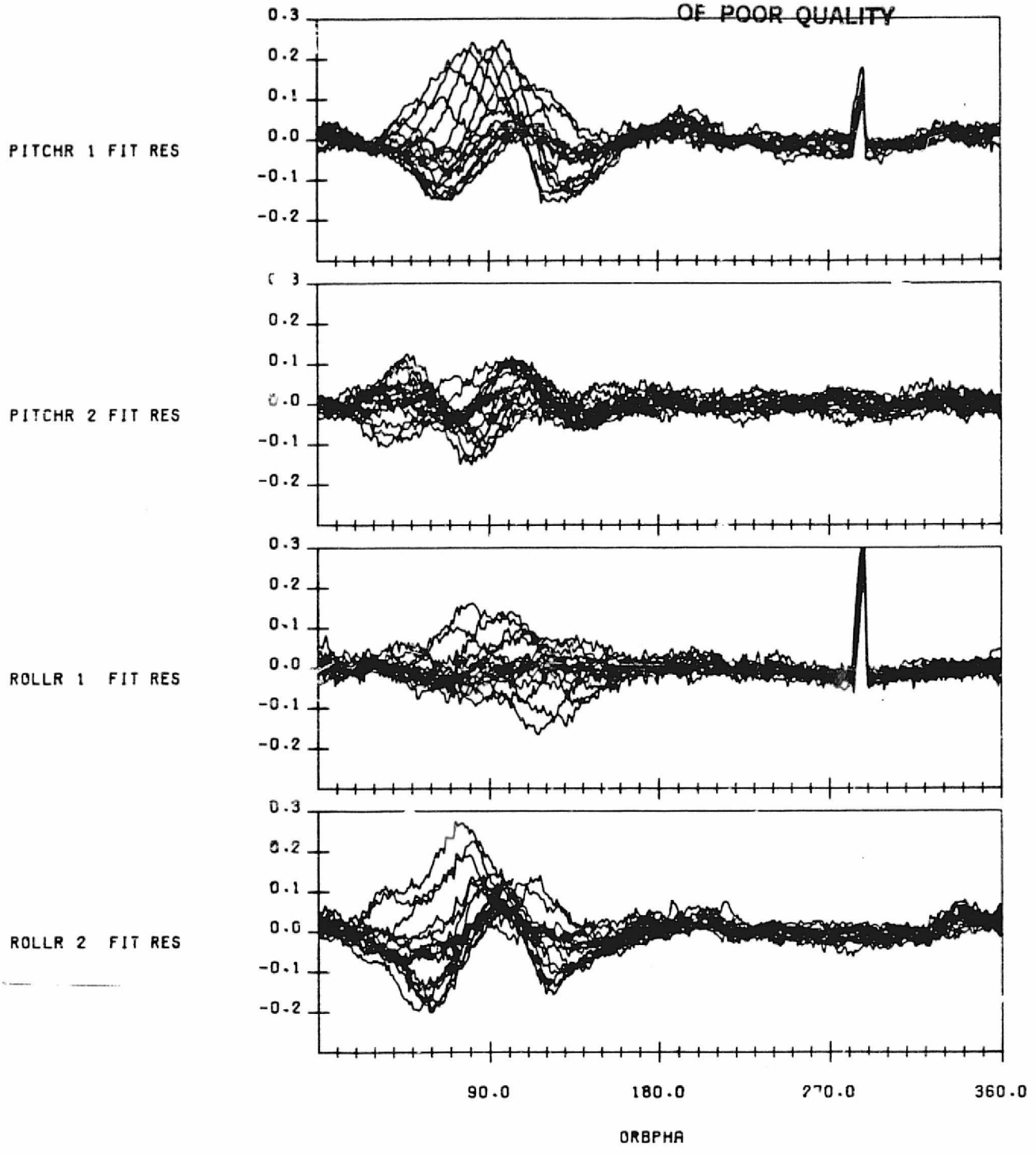

FIGURE G-13. Residual Errors from Second Order Fourier Series Fit to Data Span on February 2-3, 1983

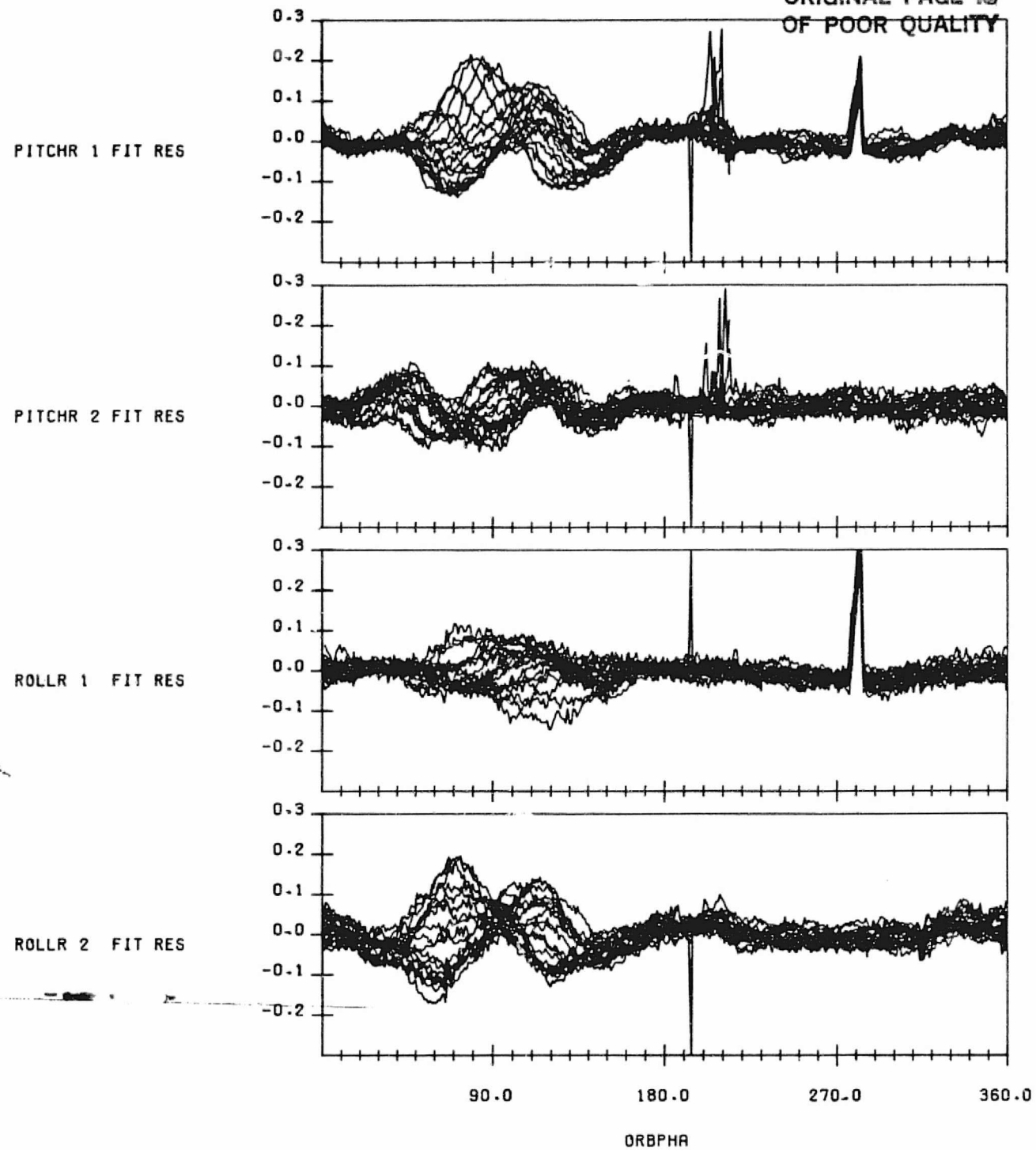

FIGURE G-14. Residual Errors from Second Order Fourier Series Fit to Data Span on February 17-18, 1983

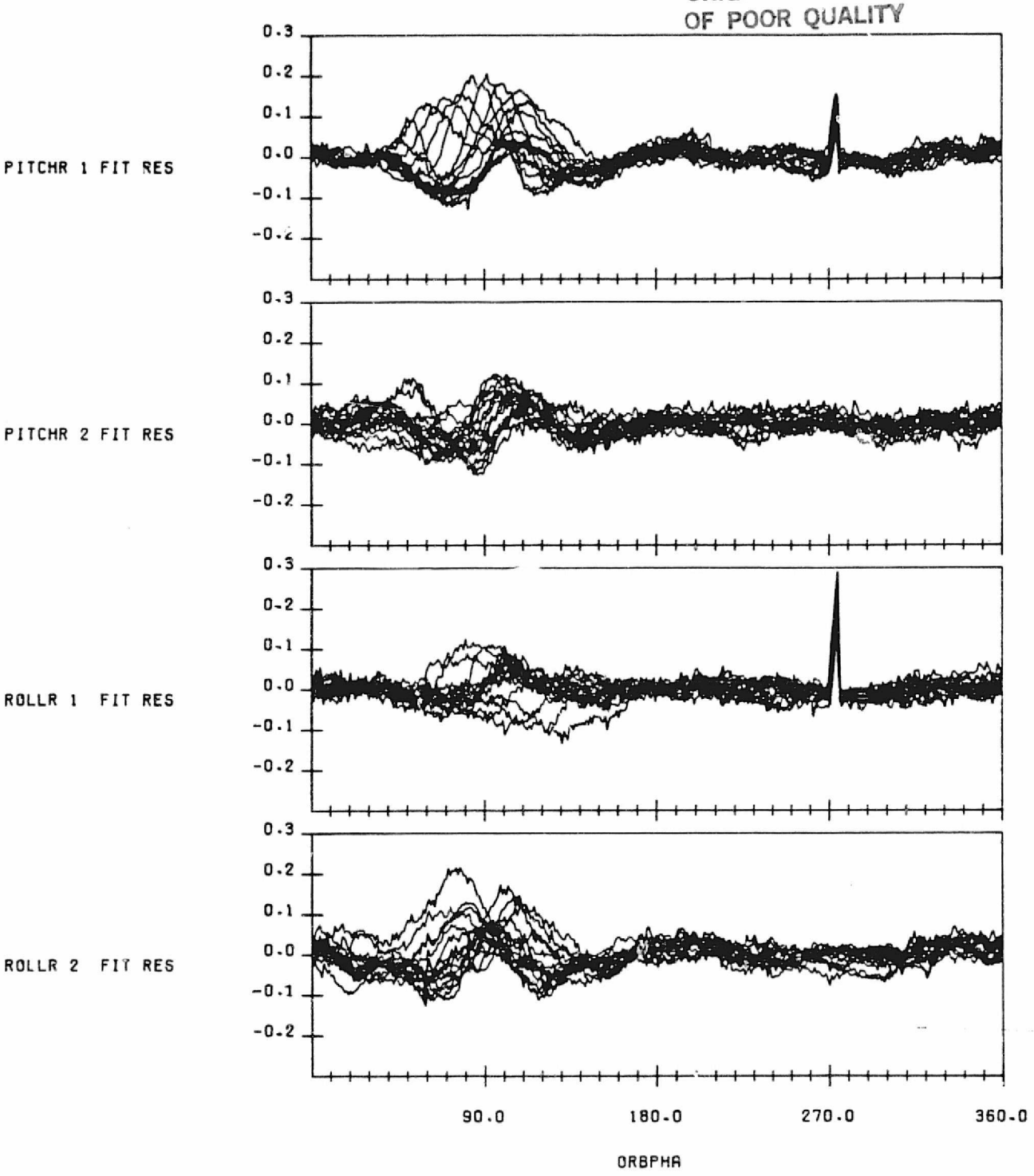

FIGURE G-15. Residual Errors from Second Order Fourier Series Fit to Data Span on March 3-4, 1983

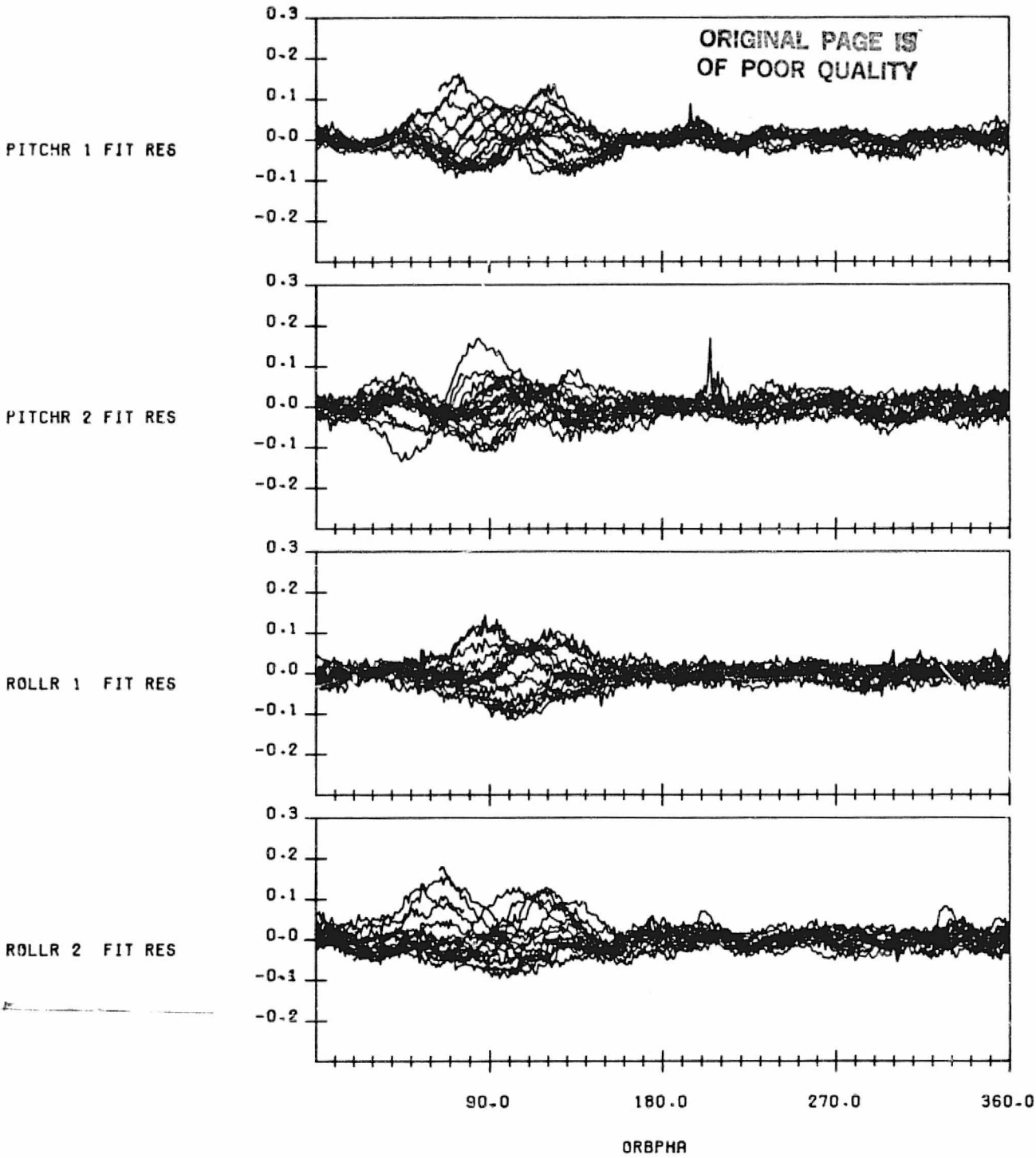

FIGURE G-16. Residual Errors from Second Order Fourier Series Fit to Data Span on March 14-15, 1983

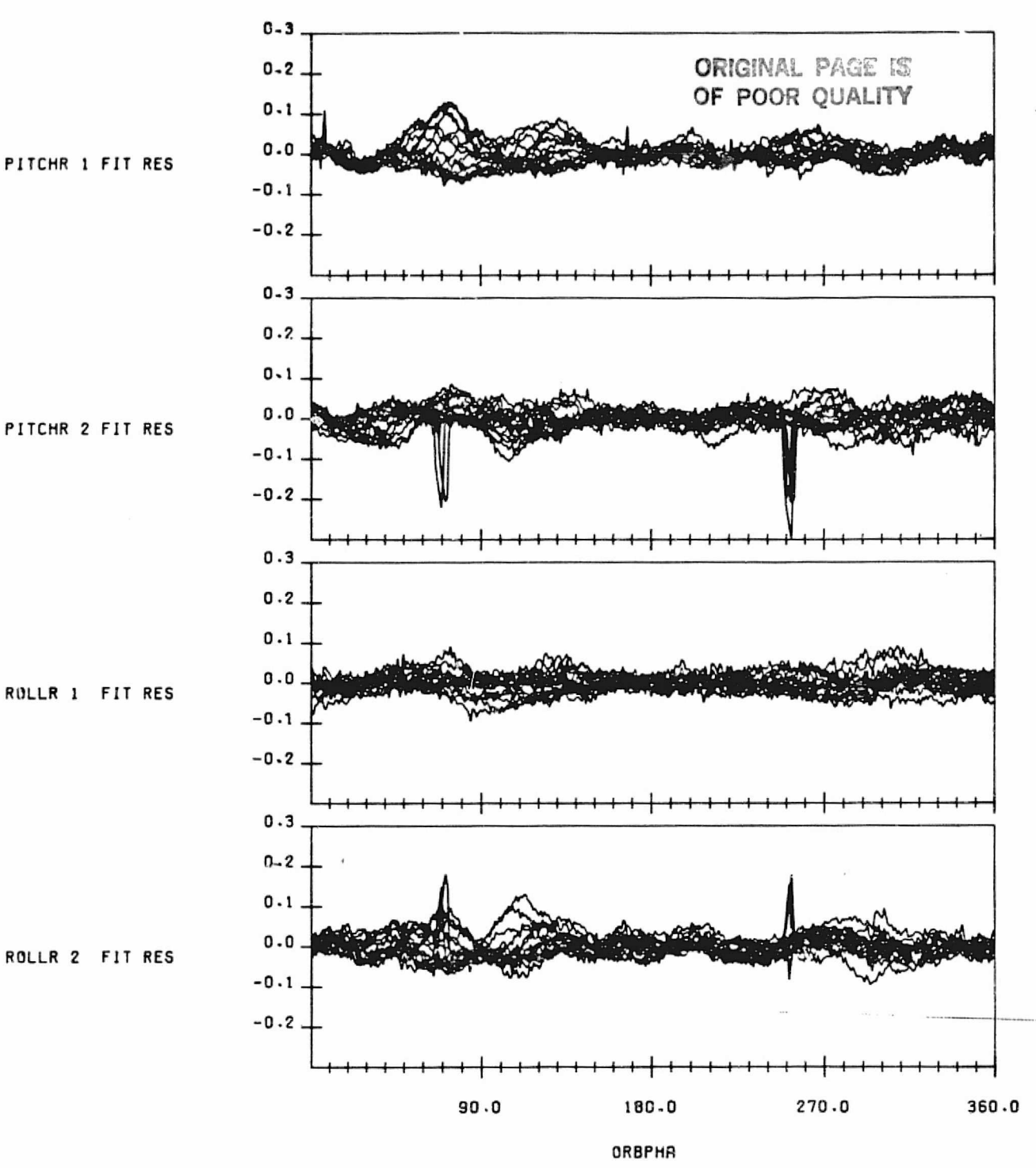

FIGURE G-17. Residual Errors from Second Order Fourier Series Fit to Data Span on March 29-31, 1983

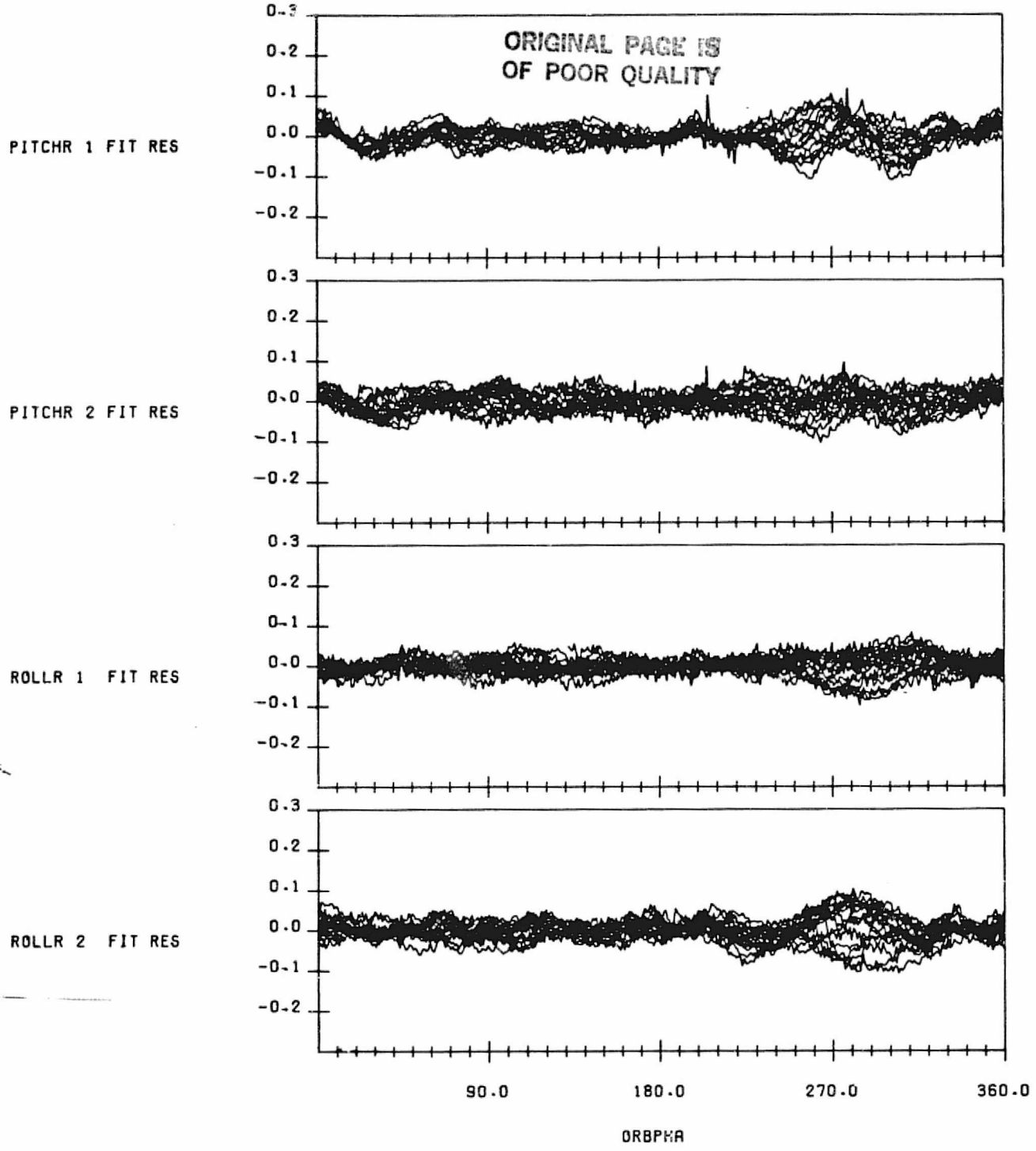

SECOND ORDER FINITE FOURIER SERIES FIT RESIDUALS TO SCANNER
RESIDUAL ERRORS FOR NOMINAL CALIBRATION WITH EARTH OBLATENESS,
OBC ORBIT AND OBC REFERENCE ATTITUDE EFFECTS MODELLED
DATA START TIME:830414.003417145
END TIME=830415.041837625

FIGURE G-18. Residual Errors from Second Order Fourier Series Fit to Data Span on April 14-15, 1983

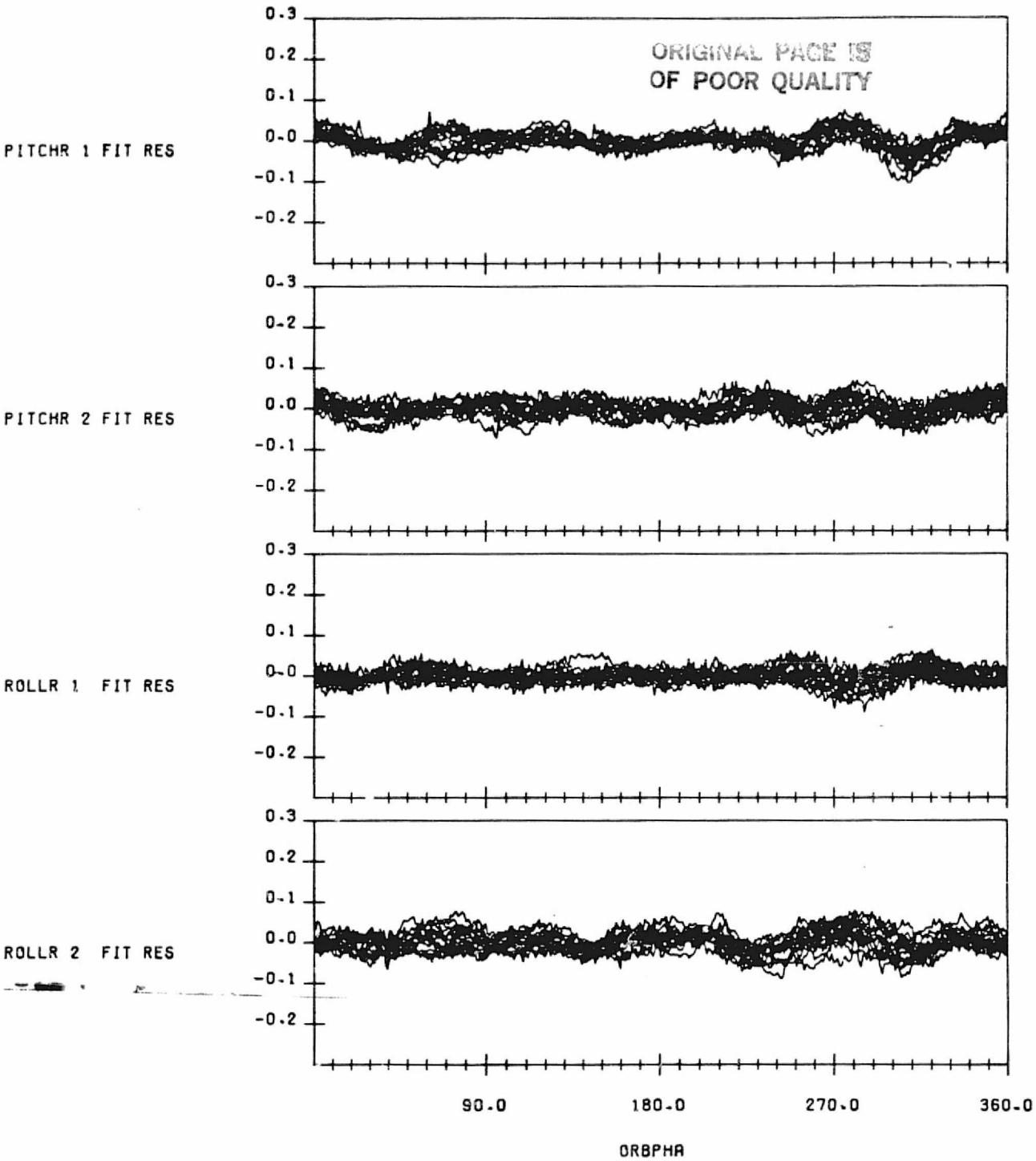

FIGURE G-19. Residual Errors from Second Order Fourier Series Fit to Data Span on April 26-27, 1983

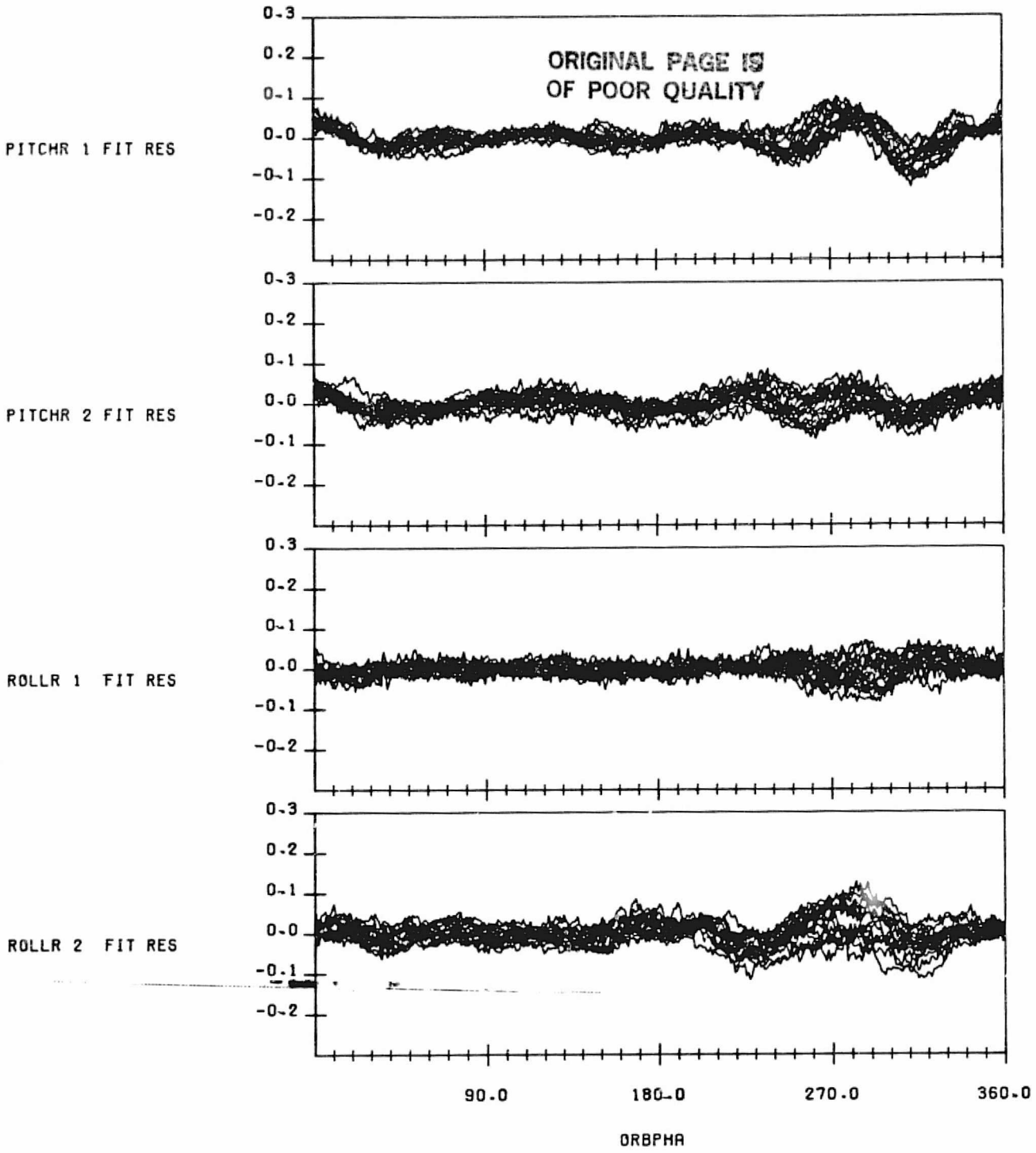

FIGURE G-20. Residual Errors from Second Order Fourier Series Fit to Data Span on May 11-12, 1983

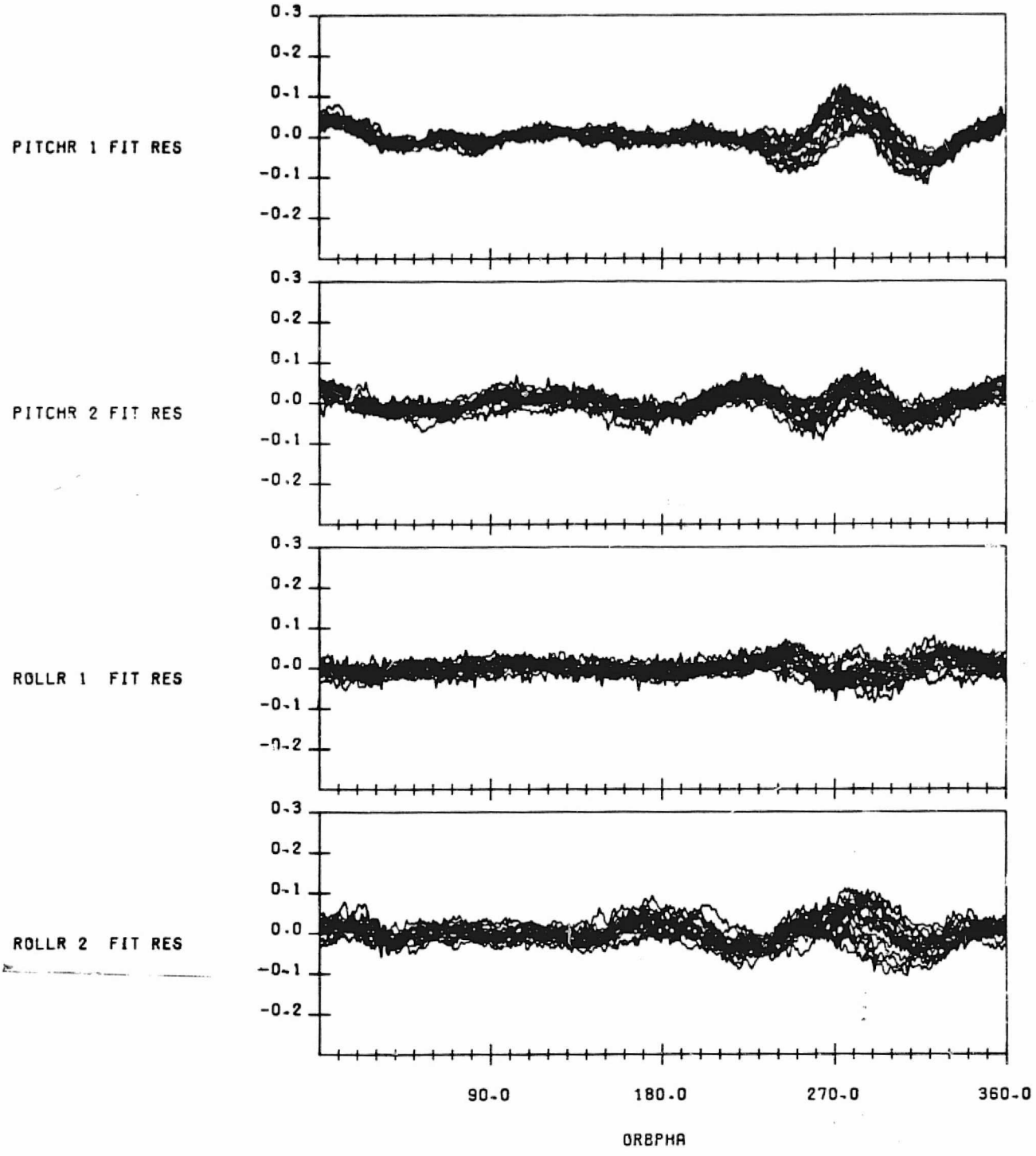

FIGURE G-21. Residual Errors from Second Order Fourier Series Fit to Data Span on May 23-24, 1983

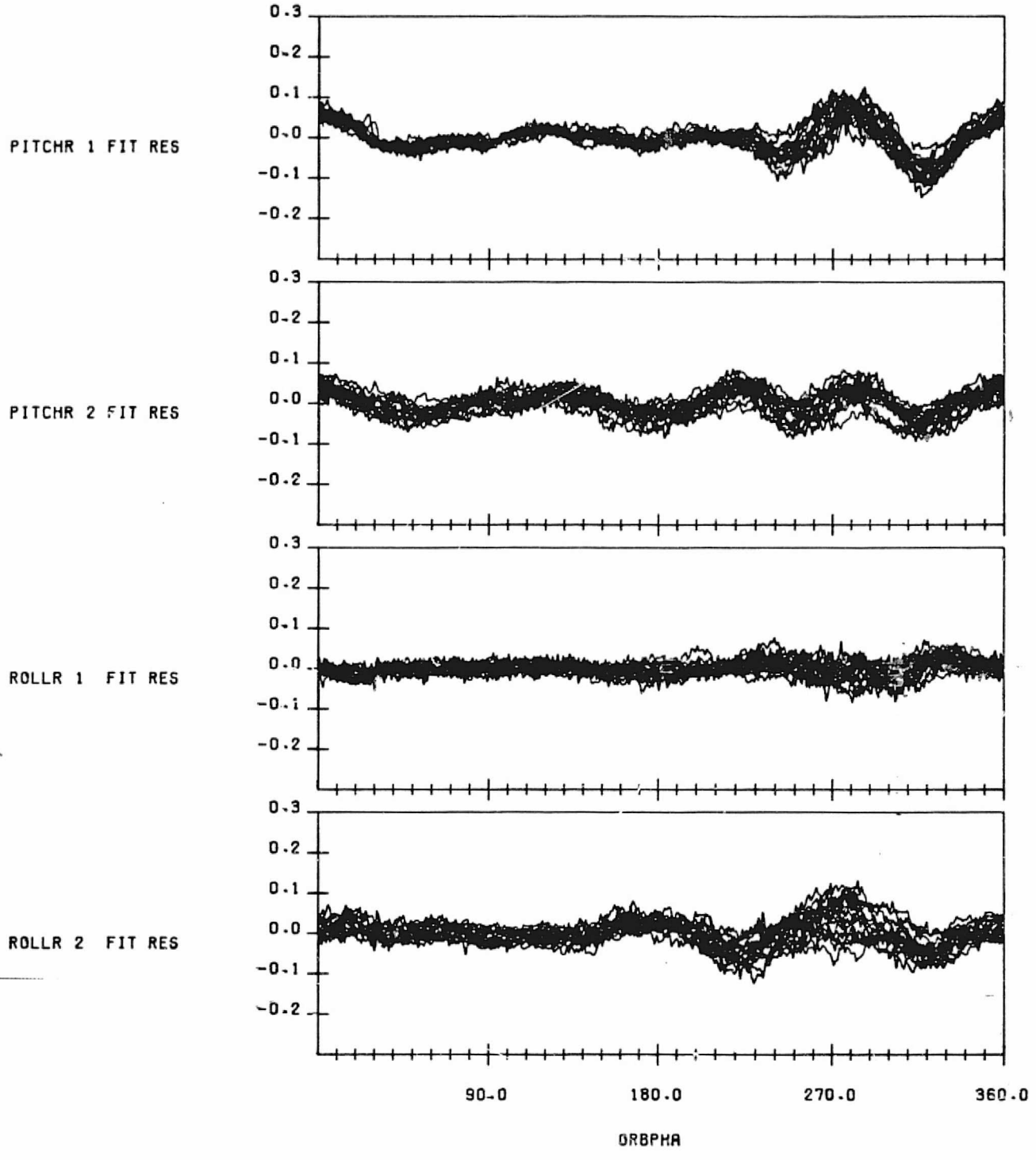

FIGURE G-22. Residual Errors from Second Order Fourier Series Fit to Data Span on June 6-7, 1983

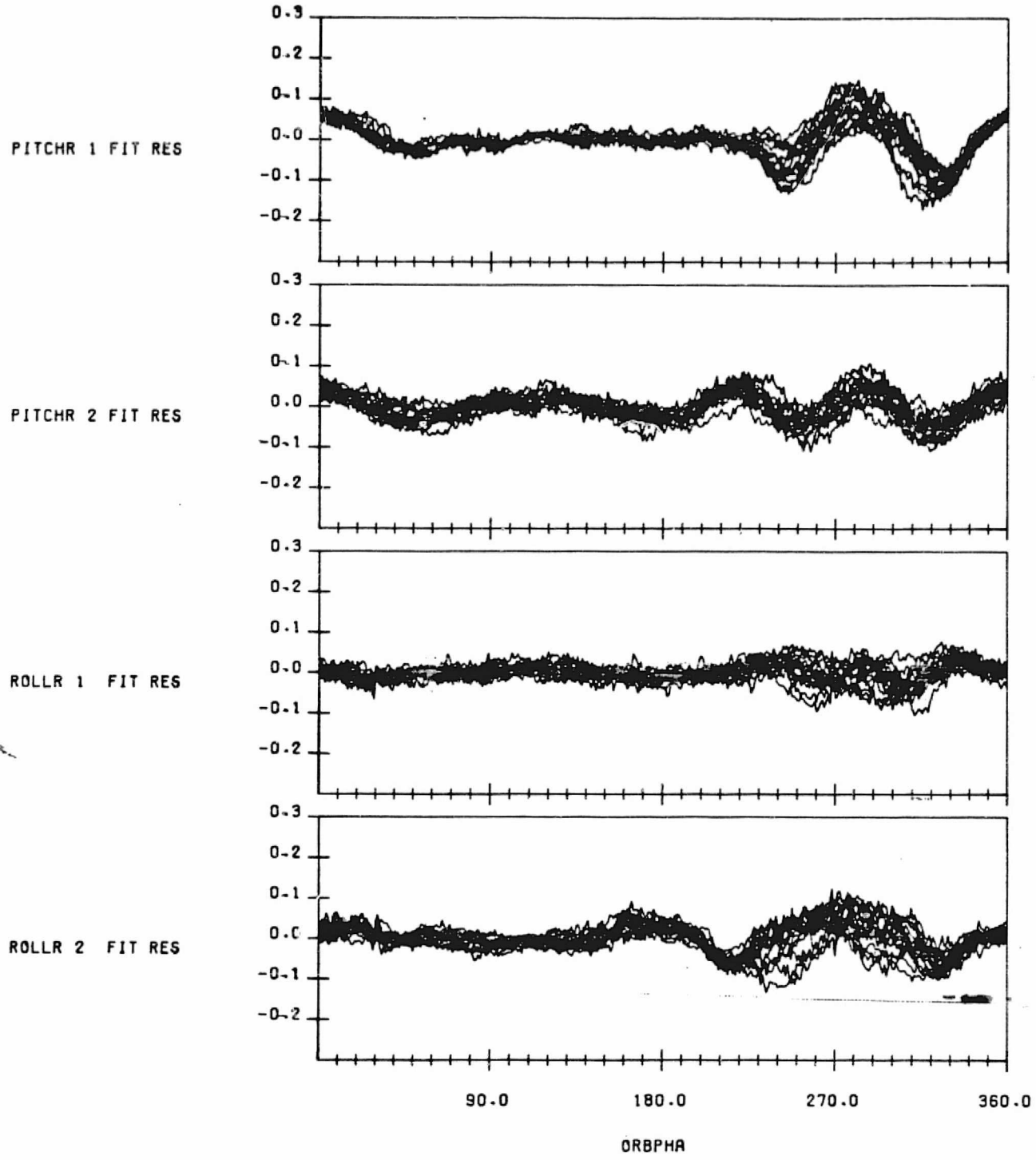

FIGURE G-23. Residual Errors from Second Order Fourier Series Fit to Data Span on June 21-23, 1983

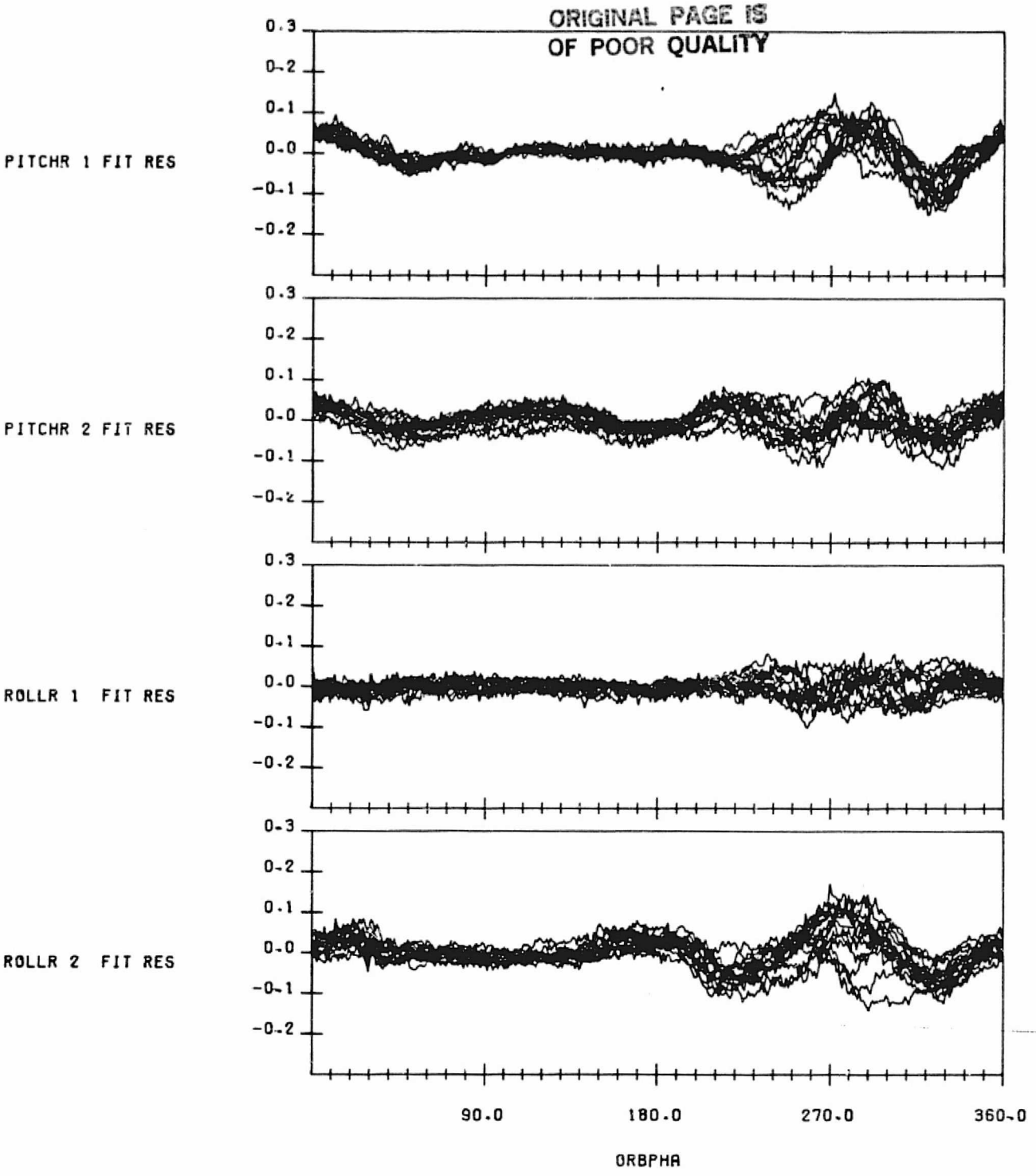

FIGURE G-24. Residual Errors from Second Order Fourier Series Fit to Data Span on July 6-7, 1983

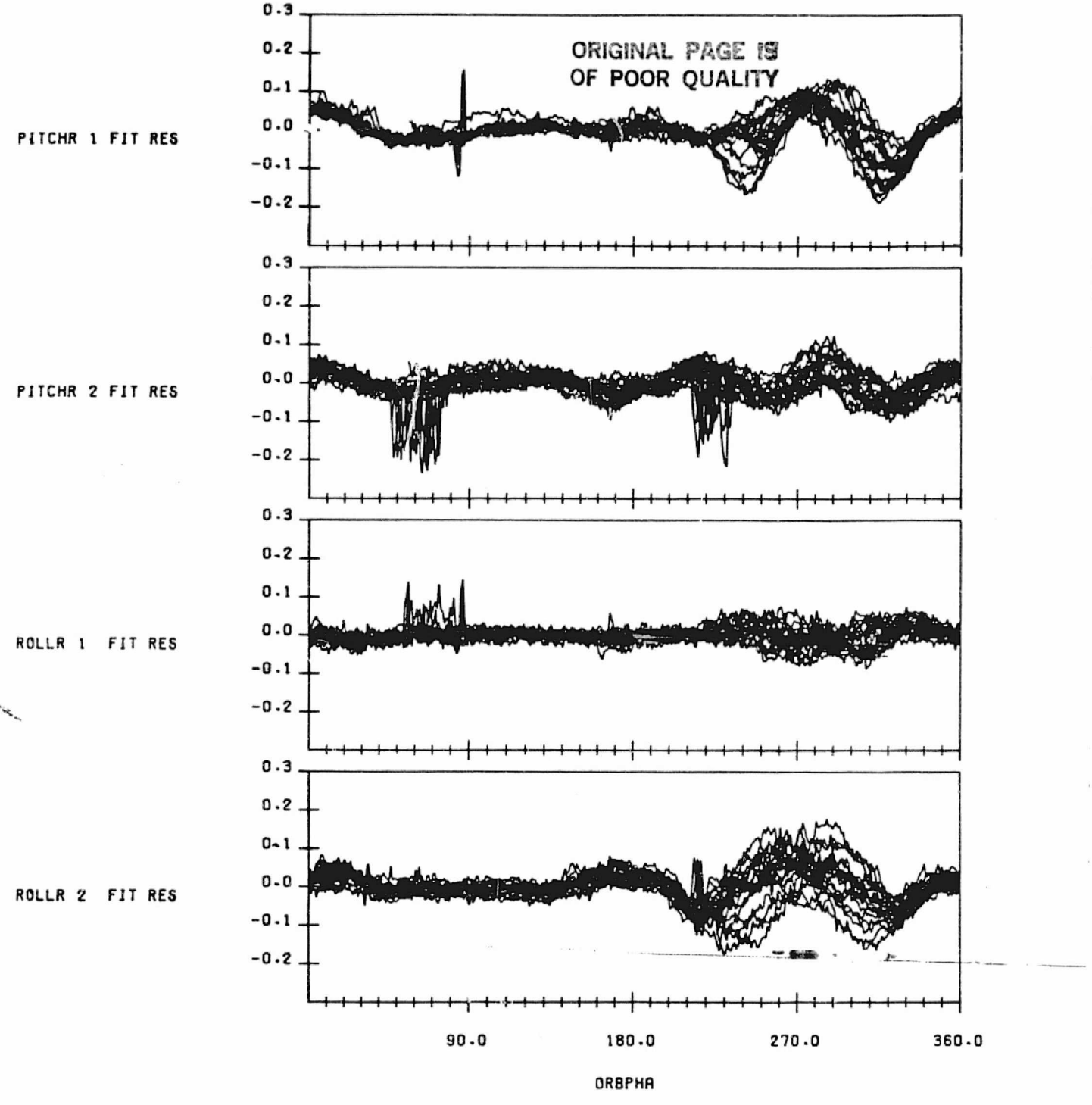

FIGURE G-25. Residual Errors from Second Order Fourier Series Fit to Data Span on July 26-27, 1983

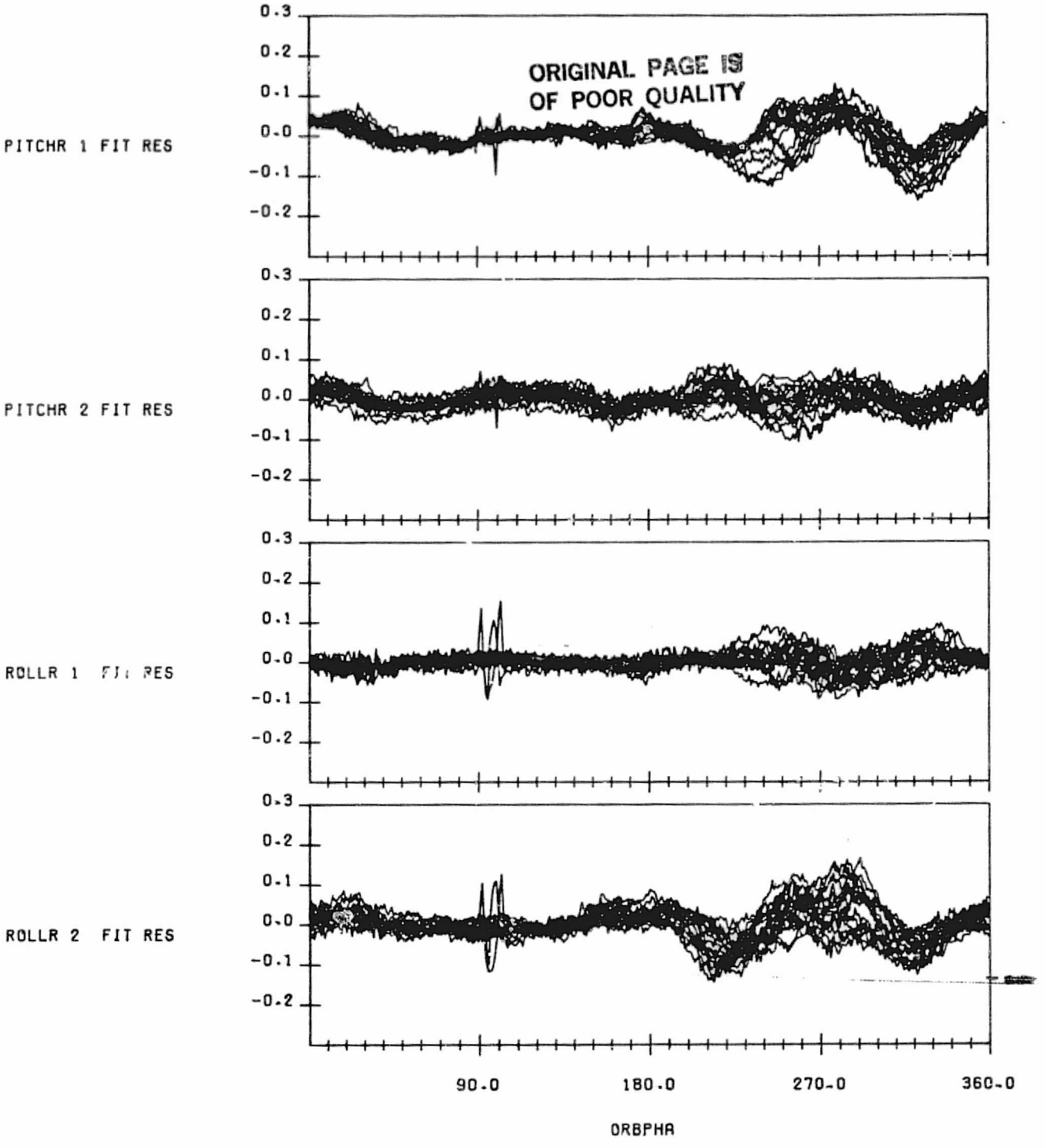

FIGURE G-26. Residual Errors from Second Order Fourier Series Fit to Data Span on August 6-7, 1983

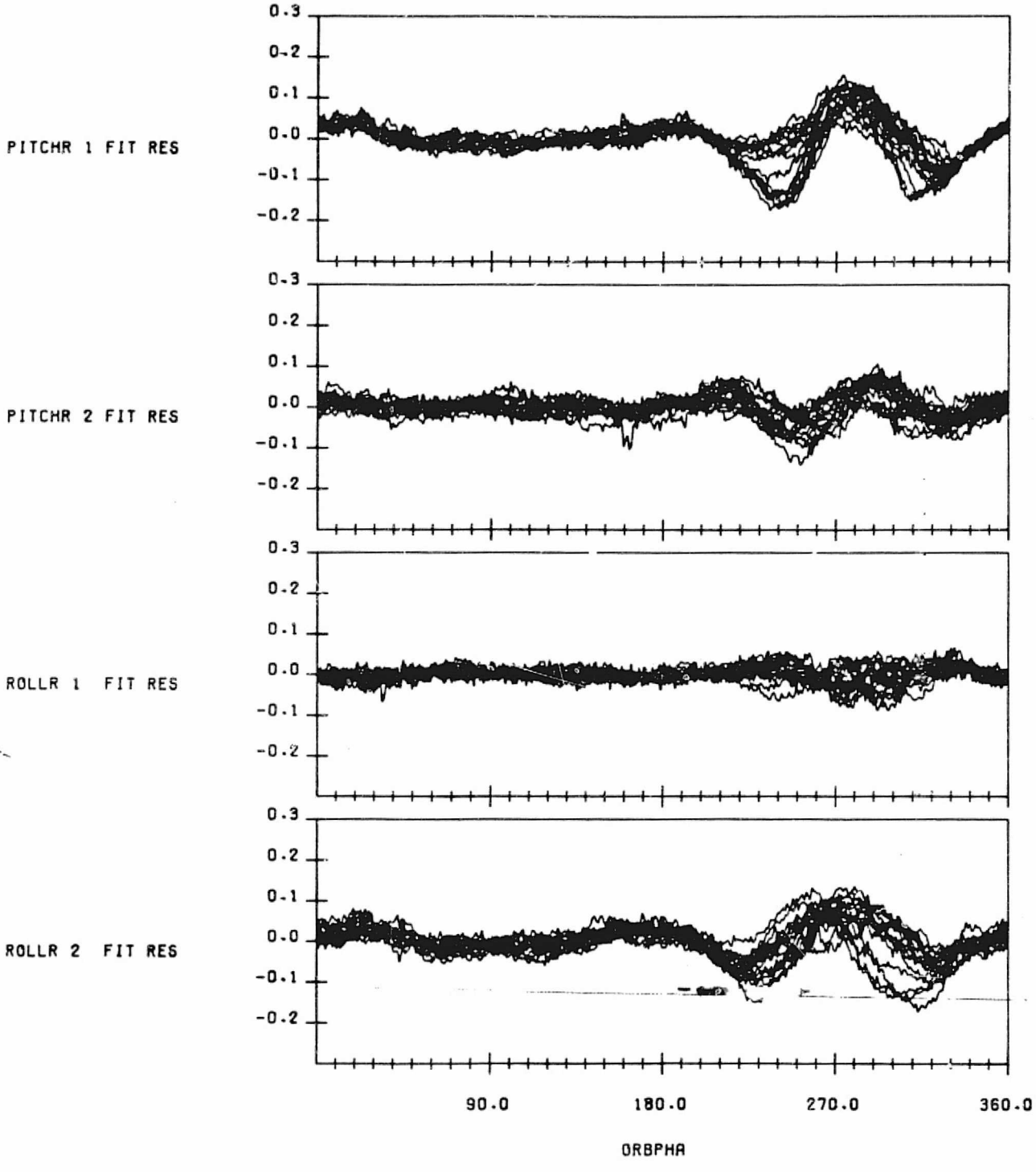

FIGURE G-27. Residual Errors from Second Order Fourier Series Fit to Data Span on August 31 - September 1, 1983

C-5

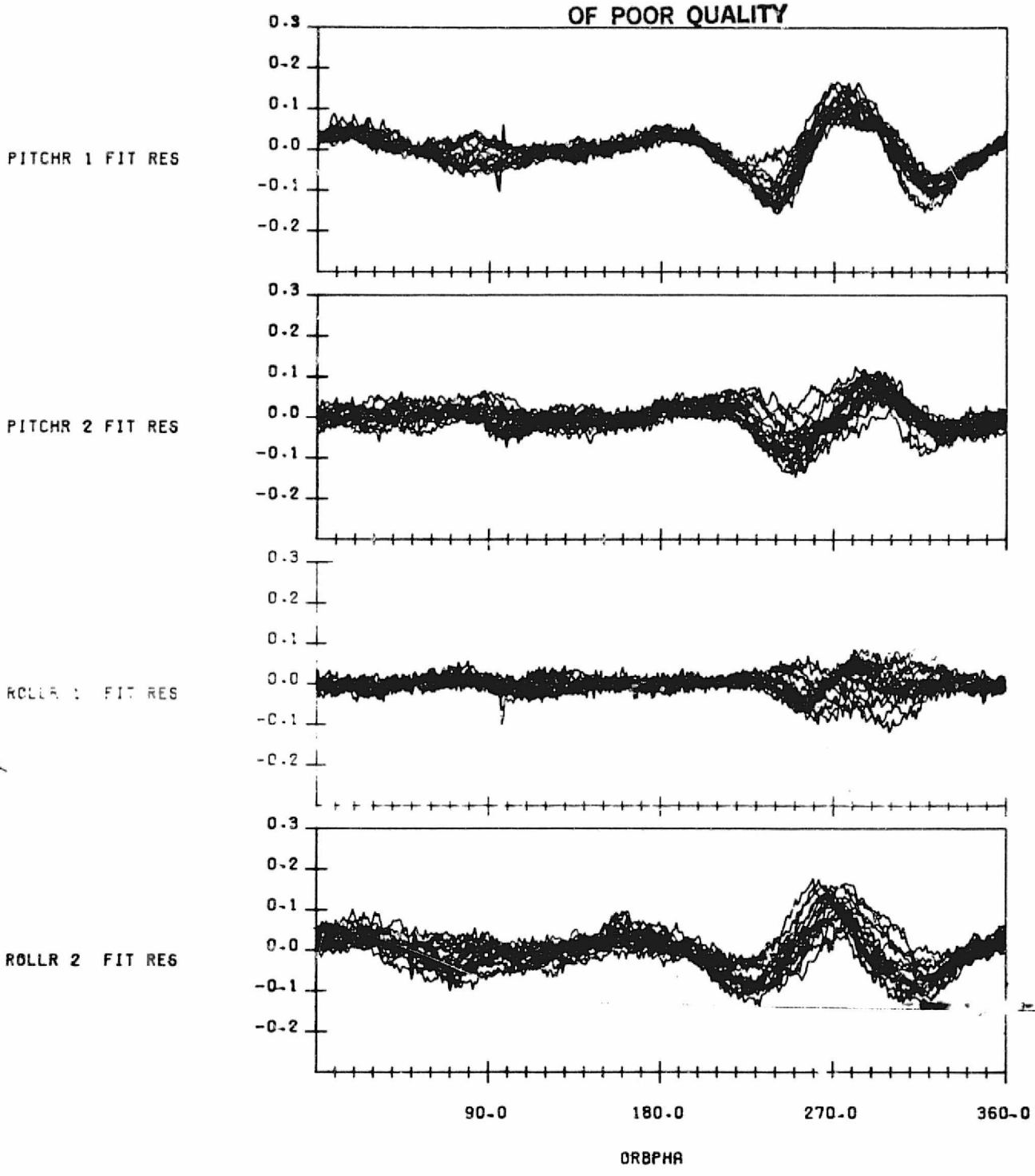

SECOND ORDER FINITE FOURIER SERIES FIT RESIDUALS TO SCANNER
RESIDUAL ERRORS FOR NOMINAL CALIBRATION WITH EARTH OBLATENESS.
OBC ORBIT AND OBC REFERENCE ATTITUDE EFFECTS MODELLED
DATA START TIME:830914.002744703
END TIME:830915.055956878

FIGURE G-28. Residual Errors from Second Order Fourier Series Fit to Data Span on September 14-15, 1983

APPENDIX H - COLD CLOUD EFFECTS ANALYSIS DATA

This appendix presents the basic material required for drawing correlations between errors in the horizon scanner data and cold clouds located on the scanner horizon. Figure H-1 and H-2 show global mapped mozaic infrared photographs of the Earth in the 10 to 12 micron atmospheric window for June 6, 1983. These photographs are from the night (02:30 local time) and day (04:30 local time) portions of the NOAA-7 orbit respectively. The motion of cloud features over 1/2 day is indicated by comparison of these photos. Figure H-3 shows the scanner horizon triggering heights as a function of time throughout the day. Finally, Table H-1 indicates the scanner horizon crossing latitudes and longitudes througout the day.

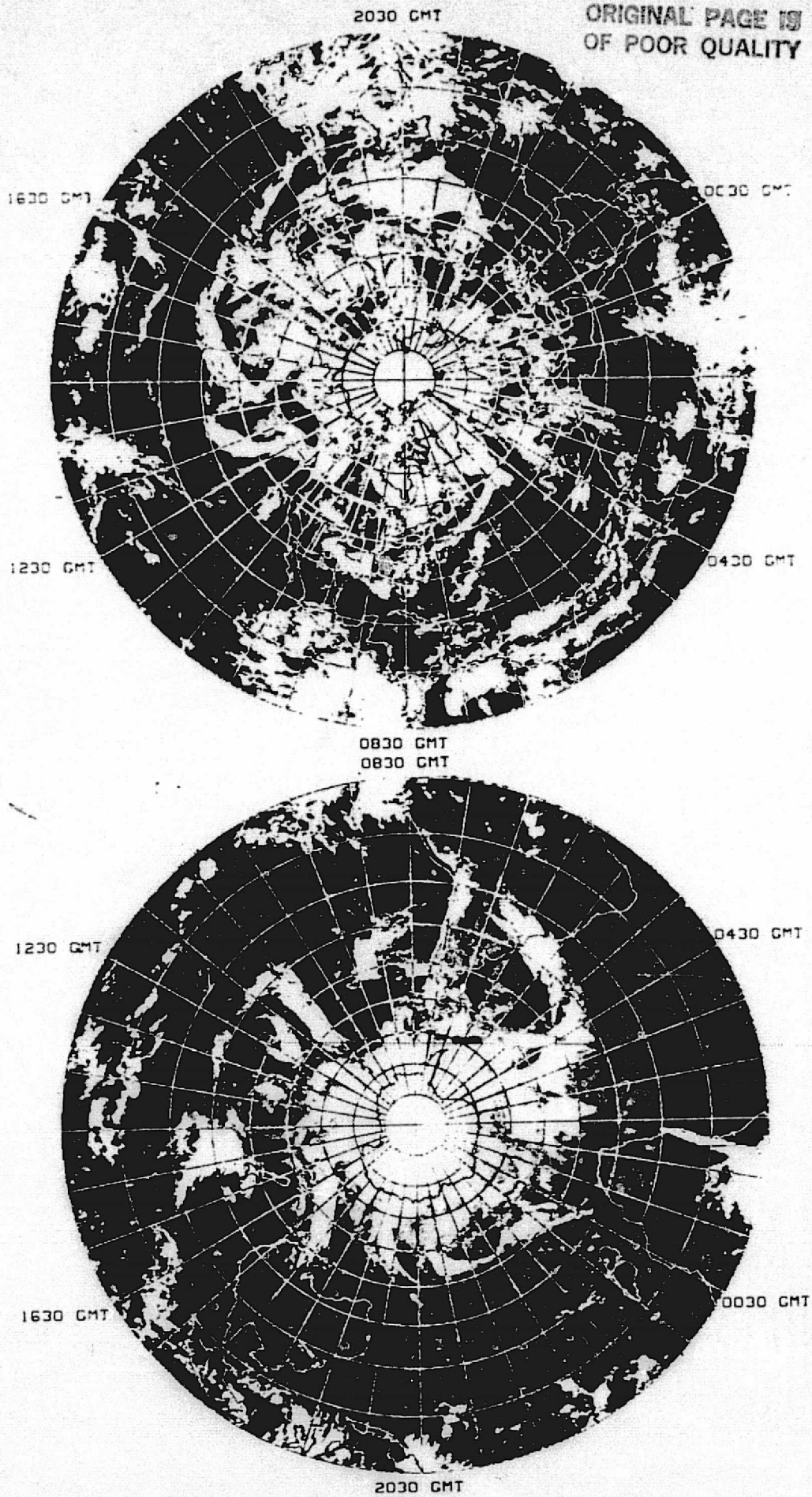

6/ 6/83
0211 - 0200 GMT
02L N-7
IR NGT

NORTHERN
HEMISPHERE

6/ 6/83
0211 - 0200 GMT
02L N-7
IR NGT

SOUTHERN
HEMISPHERE

FIGURE H-1. Earth Infrared Nightime Image on June 6, 1983

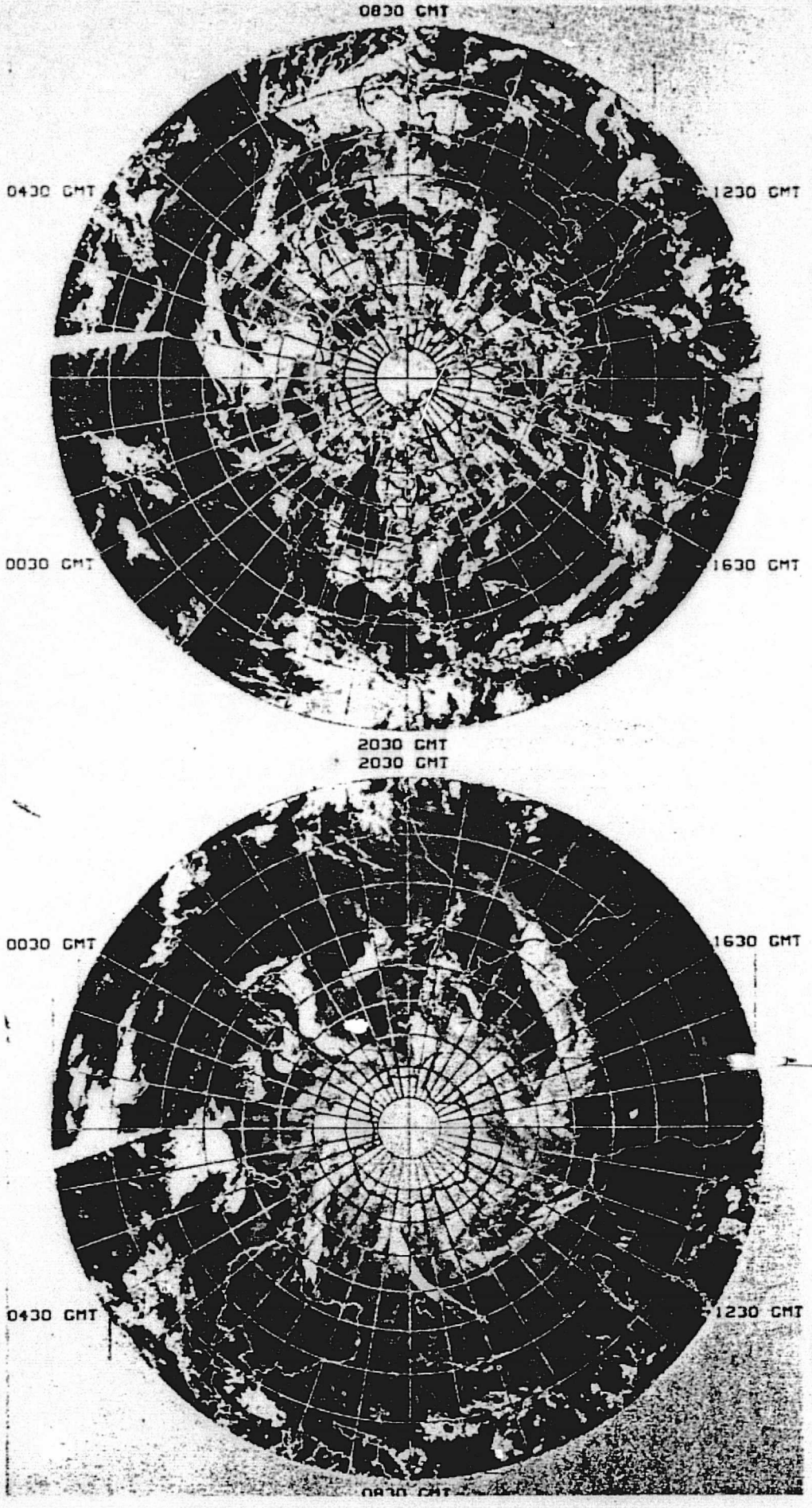

6/ 6/83
0211 - 0200 GMT
14L N-7
IR DAY

NORTHERN
HEMISPHERE

6/ 6/83
0211 - 0200 GMT
14L N-7
IR DAY

SOUTHERN
HEMISPHERE

FIGURE H-2. Earth Infrared Daylight Image on June 6, 1983

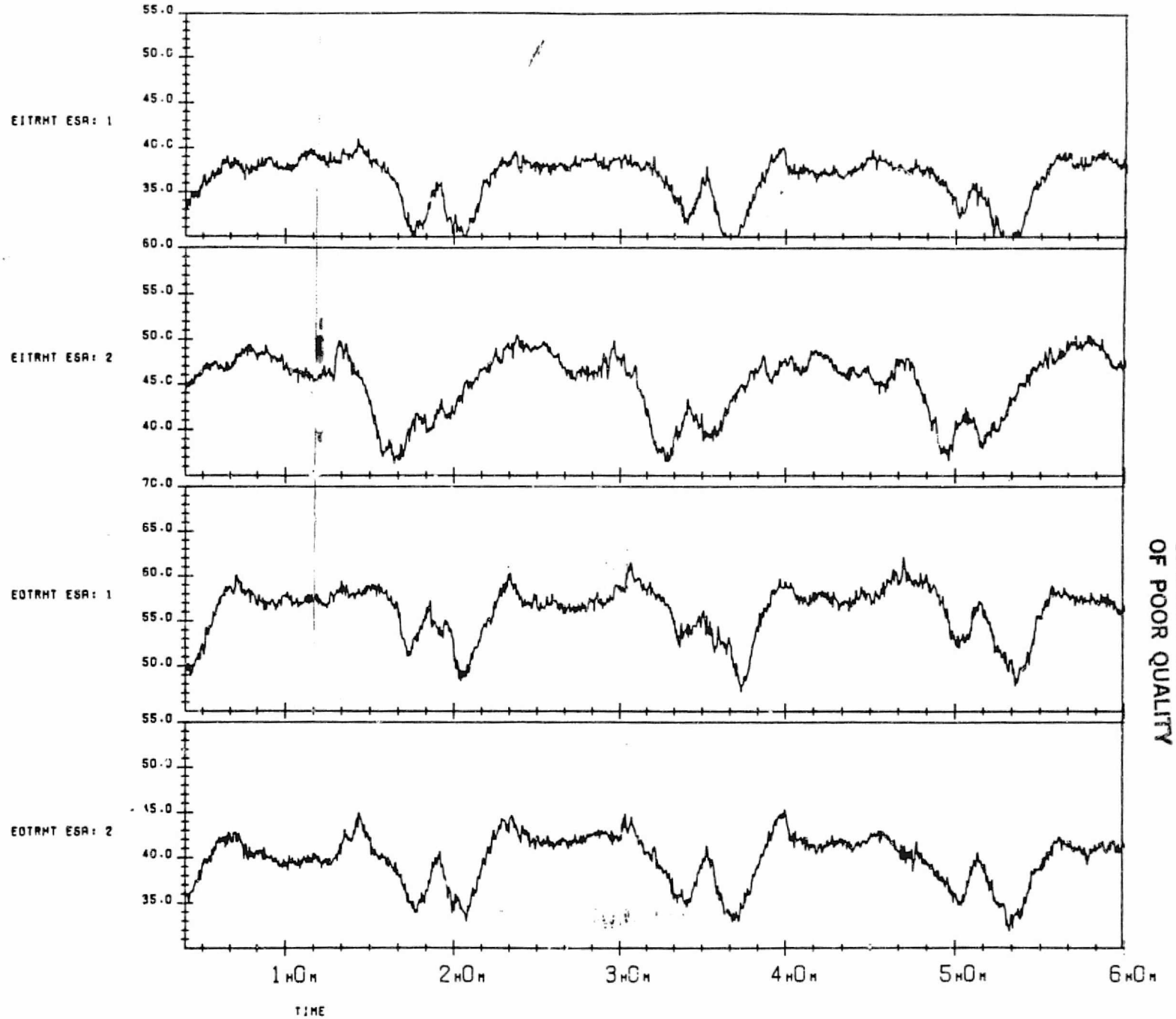

FIGURE H-3. Horizon Triggering Heights as a Function of Time for Data Span on June 6, 1983 (1 of 5)

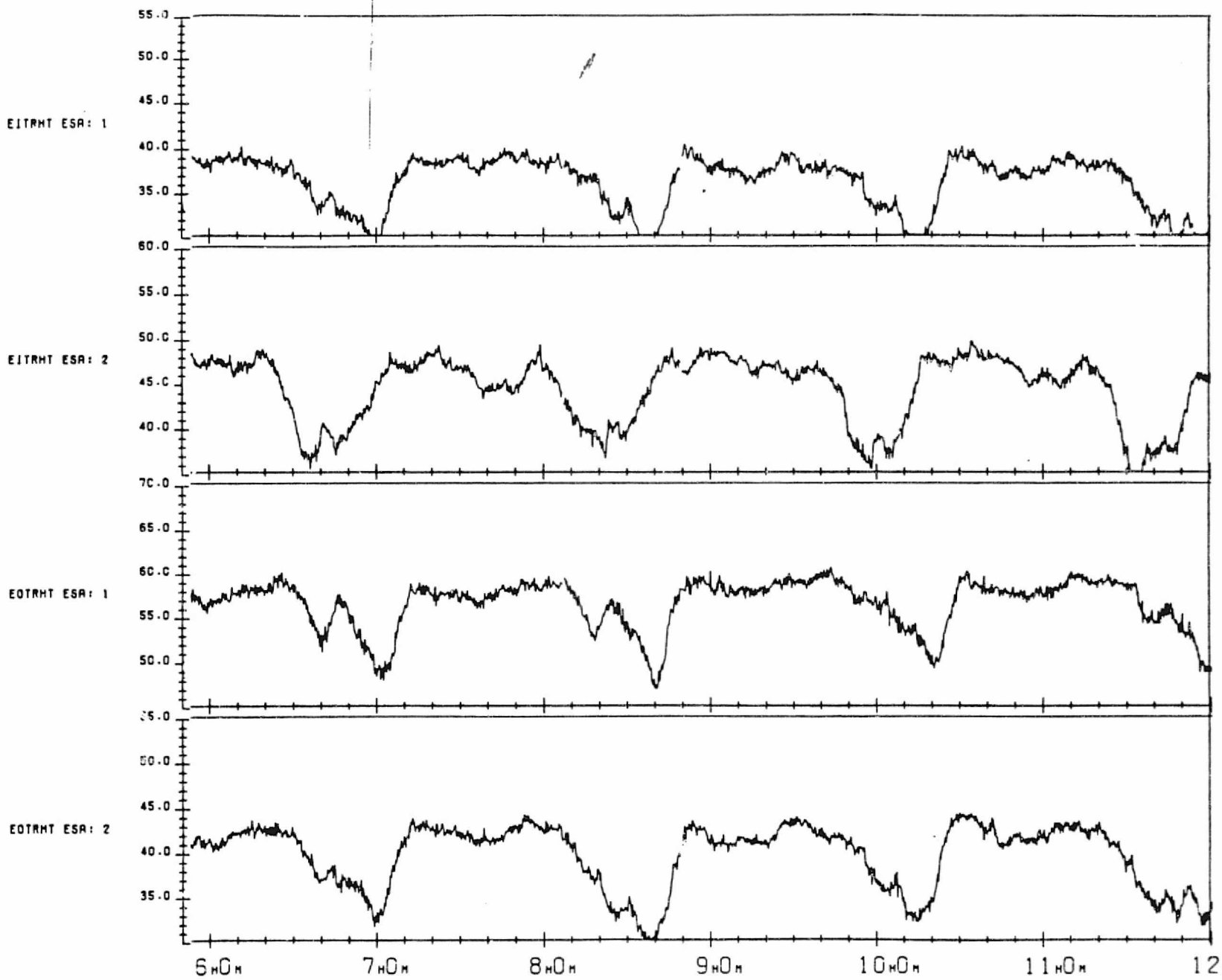

FIGURE H-3. Horizon Triggering Heights as a Function of Time for Data Span on June 6, 1983 (2 of 5)

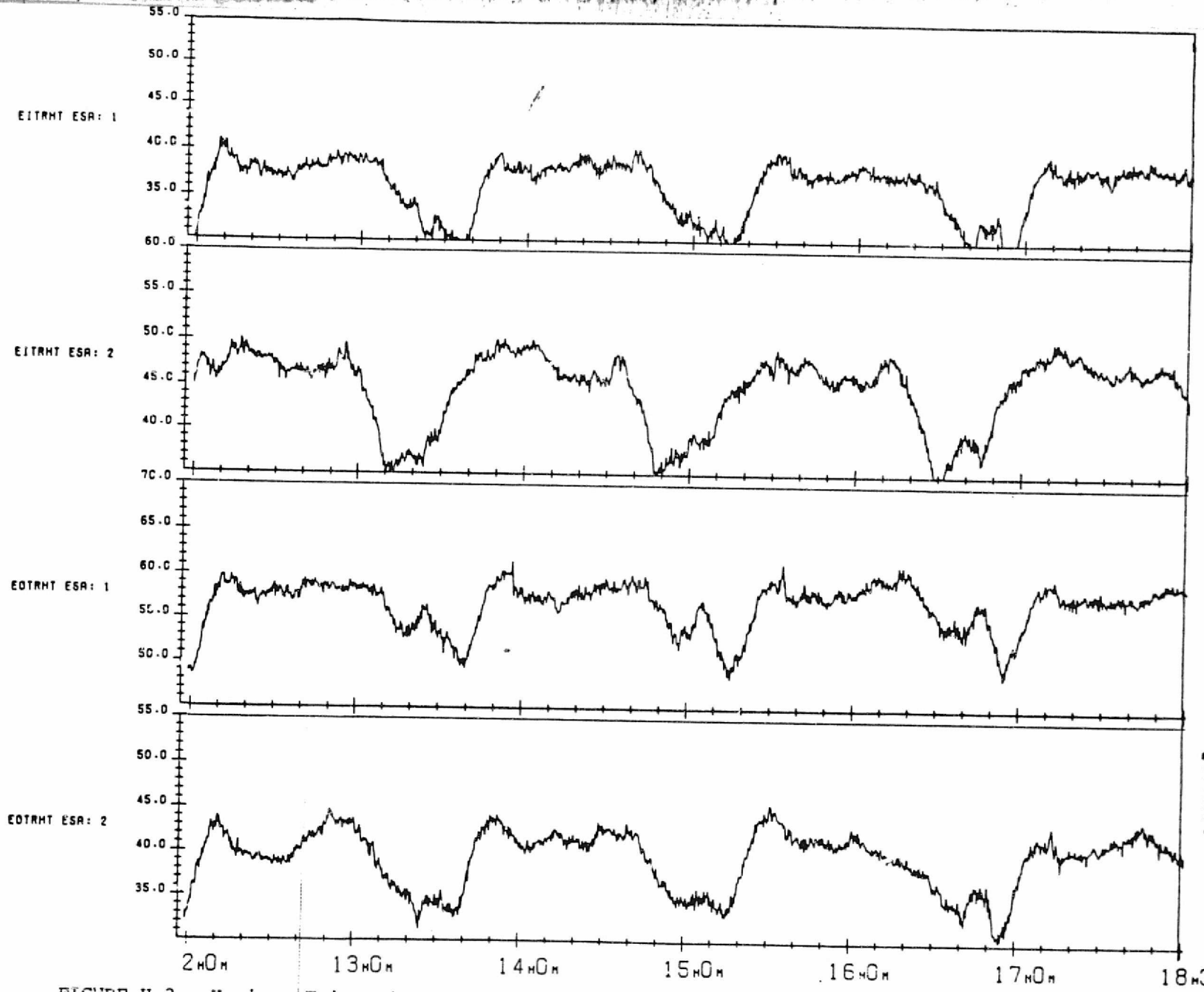

FIGURE H-3. Horizon Triggering Heights as a Function of Time for Data Span on June 6, 1983 (3 of 5)

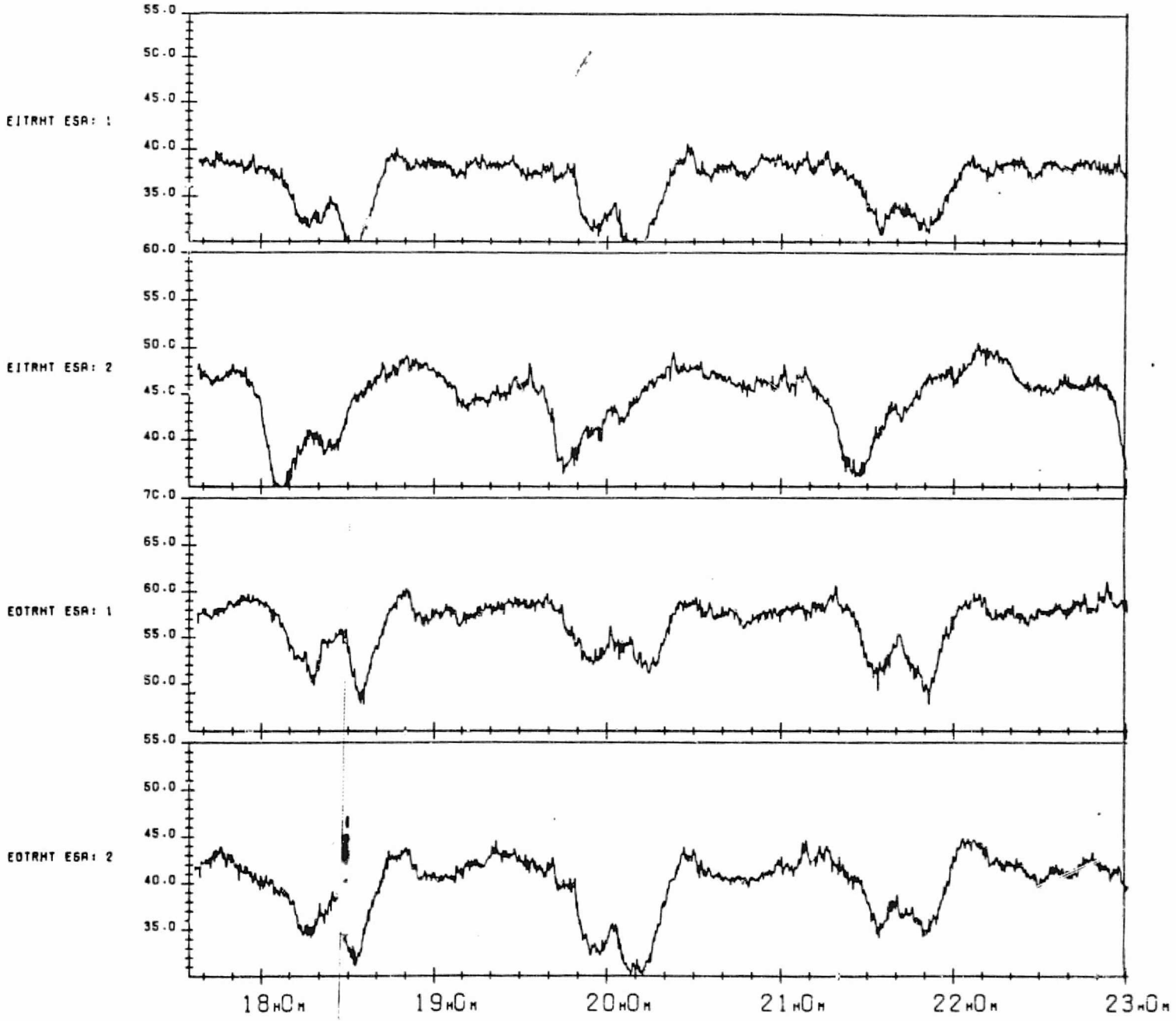

FIGURE H-3. Horizon Triggering Heights as a Function of Time for Data Span on June 6, 1983 (4 of 5)

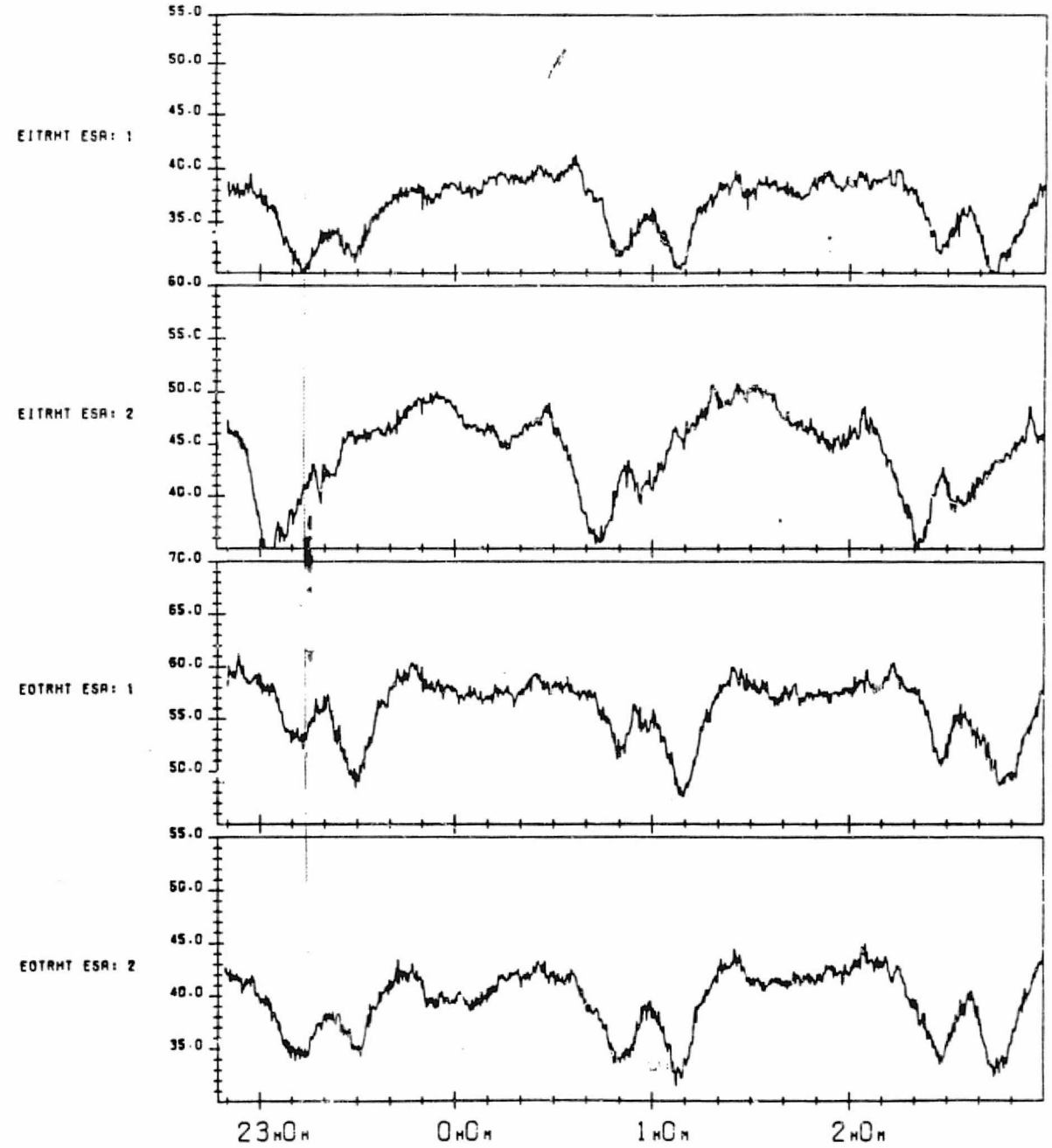

FIGURE H-3. Horizon Triggering Heights as a Function of Time for Data Span on June 6, 1983 (5 of 5)

HORIZON POSITIONS (LATITUDES MEASURED NORTH, NEGATIVE MEANS SOUTH; LONGITUDES MEASURED EAST, NEGATIVE MEANS WEST)

DATE . TIME	SUBSATELLITE		SCANNER 1 EARTH-IN		SCANNER 1 EARTH-OUT		SCANNER 2 EARTH-IN		SCANNER 2 EARTH-OUT	
YYMMDD.HHMMSS	LATITUDE	LONGITUDE	LATITUDE	LONGITUDE	LATITUDE	LONGITUDE	LATITUDE	LONGITUDE	LATITUDE	LONGITUDE
830606.002538	-43.87	-33.77	-48.58	1.54	-57.78	-65.11	-17.52	-20.86	-52.86	0.66
830606.002749	-33.06	-35.10	-42.50	-5.21	-50.49	-62.51	-10.13	-23.20	-46.64	-6.84
830606.003000	-25.22	-38.14	-35.96	-10.56	-43.08	-61.23	-2.66	-25.15	-39.95	-12.54
830606.003211	-17.37	-40.00	-29.10	-14.79	-35.59	-60.78	4.88	-26.80	-32.94	-16.98
830606.003423	-9.51	-41.75	-22.03	-18.21	-28.06	-60.89	12.46	-28.16	-25.72	-20.52
830606.003634	-1.64	-43.44	-14.91	-21.00	-20.53	-61.44	20.08	-29.25	-18.36	-23.42
830606.003845	6.23	-45.13	-7.49	-23.30	-13.00	-62.35	27.73	-30.07	-10.89	-25.82
830606.004056	14.10	-46.95	-0.08	-25.20	-5.50	-63.60	35.38	-30.55	-3.36	-27.83
830606.004307	21.97	-48.66	7.37	-26.73	1.95	-65.19	43.04	-30.60	4.21	-29.52
830606.004518	29.83	-50.51	14.86	-27.93	9.34	-67.14	50.66	-30.05	11.82	-30.91
830606.004729	37.68	-52.81	22.37	-28.80	16.64	-69.51	58.24	-28.51	19.45	-32.03
830606.004940	45.50	-55.40	29.87	-29.30	23.82	-72.40	65.67	-25.12	27.07	-32.88
830606.005151	53.27	-58.66	37.35	-29.34	30.83	-75.94	72.80	-17.69	34.70	-33.39
830606.005402	60.95	-63.11	44.80	-29.79	37.62	-80.36	79.01	0.64	42.31	-33.50
830606.005613	68.45	-70.04	52.18	-27.35	44.07	-85.97	81.83	44.27	49.90	-33.03
830606.005824	75.47	-83.00	59.42	-24.46	50.03	-93.20	78.45	85.17	57.43	-31.63
830606.010035	80.85	-113.31	66.39	-18.92	55.24	-102.65	72.11	101.72	64.84	-28.54
830606.010246	80.90	-145.85	72.74	-7.93	59.33	-114.87	64.97	108.53	72.00	-21.83
830606.010458	75.58	-163.38	77.49	14.56	61.78	-129.87	57.56	111.66	78.37	-5.55
830606.010709	68.57	150.26	78.42	50.31	62.18	-146.42	50.03	113.08	81.83	34.95
830606.010920	61.08	143.27	74.82	78.79	60.43	-162.22	42.45	113.57	79.10	79.01
830606.011131	53.39	139.79	68.57	93.26	56.57	-175.52	34.84	113.48	72.91	97.62
830606.011342	45.62	135.52	62.05	100.40	51.99	174.06	27.21	112.97	65.78	105.14
830606.011553	37.80	132.92	54.95	104.10	46.24	166.09	19.55	112.13	58.34	108.56
830606.011804	29.95	130.72	47.48	105.99	39.92	159.95	11.95	111.01	50.77	110.13
830606.012015	22.09	128.76	40.02	106.94	33.22	155.14	4.35	109.62	43.14	110.70
830606.012226	14.22	126.93	32.52	106.99	26.26	151.31	-3.23	107.94	35.48	110.65
830606.012437	6.35	125.23	25.00	106.65	19.12	148.21	-10.77	105.94	27.82	110.17
830606.012648	-1.53	123.54	17.49	105.91	11.86	145.67	-18.23	103.55	20.17	109.38
830606.012859	-9.40	121.84	10.01	104.83	4.52	143.58	-25.60	100.66	12.55	108.27
830606.013110	-17.27	120.10	2.56	103.42	-2.88	141.87	-32.83	97.12	4.96	106.90
830606.013321	-25.12	118.24	-4.83	101.67	-10.31	140.50	-39.85	92.70	-2.58	105.26
830606.013533	-32.96	116.20	-12.14	99.56	-17.76	139.47	-46.55	87.03	-10.05	103.30
830606.013744	-40.77	113.88	-19.34	96.97	-25.22	138.77	-52.78	79.55	-17.44	100.98
830606.013955	-48.55	111.08	-26.41	93.84	-32.67	138.48	-58.24	69.51	-24.73	98.19
830606.014206	-56.27	107.45	-33.28	89.99	-40.09	138.67	-62.50	56.08	-31.88	96.78
830606.014417	-63.96	102.28	-39.90	85.19	-47.45	139.55	-64.94	39.15	-38.83	96.56
830606.014628	-71.20	93.75	-46.13	79.06	-54.73	141.49	-65.04	20.54	-45.50	85.17
830606.014839	-77.91	76.35	-51.80	71.15	-61.83	145.19	-62.75	3.44	-51.74	78.14
830606.015050	-81.71	35.41	-56.62	60.59	-69.57	152.28	-58.69	-10.19	-57.31	68.74
830606.015301	-79.33	-12.78	-60.16	47.76	-74.46	166.28	-53.36	-20.46	-61.80	56.06
830606.015512	-73.15	-34.88	-61.94	32.24	-78.12	-166.31	-47.27	-28.06	-64.63	39.85
830606.015723	-65.94	-45.03	-61.52	15.57	-77.42	-131.20	-40.70	-33.84	-65.21	21.35
830606.015934	-58.39	-50.87	-59.26	0.90	-72.87	-108.17	-33.82	-38.35	-63.39	3.68
830606.020145	-50.70	-54.82	-55.25	-11.39	-66.61	-96.89	-26.72	-41.95	-59.57	-10.77
830606.020356	-42.94	-57.80	-50.10	-20.94	-59.68	-90.85	-19.47	-44.89	-54.39	-21.67
830606.020609	-35.14	-60.24	-44.17	-28.25	-52.44	-87.77	-12.10	-47.34	-48.35	-29.78
830606.020819	-27.31	-62.34	-37.74	-33.95	-45.05	-86.20	-4.65	-49.39	-41.77	-35.89
830606.021030	-19.46	-64.24	-30.96	-38.48	-37.56	-85.56	2.87	-51.11	-34.83	-40.62
830606.021241	-11.60	-66.01	-23.93	-42.09	-30.06	-85.54	10.44	-52.55	-27.65	-44.38
830606.021452	-3.73	-67.72	-16.75	-45.04	-22.53	-85.98	18.05	-53.71	-20.33	-47.43
830606.021703	4.14	-69.40	-9.44	-47.46	-15.00	-86.80	25.69	-54.60	-12.89	-49.95
830606.021914	12.01	-71.11	-2.05	-49.45	-7.50	-87.98	33.35	-55.18	-5.37	-52.05
830606.022125	19.88	-72.89	5.40	-51.07	-0.03	-89.45	41.01	-55.37	2.20	-53.81
830606.022336	27.75	-74.79	12.87	-52.37	7.38	-91.30	48.64	-55.00	9.80	-55.29
830606.022547	35.59	-76.92	20.37	-53.32	14.70	-93.53	56.24	-53.78	17.42	-56.48
830606.022758	43.42	-79.38	27.87	-53.93	21.92	-96.29	63.71	-51.00	25.05	-57.40
830606.023009	51.21	-82.42	35.36	-54.10	28.99	-99.65	70.95	-45.02	32.67	-58.01
830606.023220	58.92	-86.48	42.83	-53.73	35.84	-103.81	77.53	-30.81	40.29	-58.24
830606.023431	65.48	-92.54	50.22	-52.56	42.39	-109.06	81.67	5.55	47.88	-57.95
830606.023659	74.54	-105.24	58.41	-49.71	49.23	-116.78	79.20	38.53	56.37	-56.82
830606.023926	83.79	-137.32	66.28	-43.75	55.17	-127.20	72.22	76.84	64.73	-53.33
830606.024137	80.96	170.17	72.65	-32.89	59.27	-139.37	65.08	83.74	71.88	-46.71
830606.024349	75.59	138.25	77.43	-10.64	61.76	-154.33	57.68	85.99	78.28	-30.67
830606.024615	67.77	124.58	78.22	29.45	62.09	-172.94	49.21	86.45	81.84	16.02
830606.024827	60.24	117.97	74.25	56.20	60.12	171.47	41.62	88.86	78.52	57.31
830606.025038	52.55	113.56	68.16	69.57	56.39	158.49	34.00	89.71	72.16	74.06
830606.025249	44.77	110.49	61.28	76.21	51.40	148.37	26.38	88.17	64.95	80.93
830606.025500	36.95	107.94	54.05	79.65	45.58	140.62	18.75	87.30	57.52	84.08
830606.025711	29.10	105.77	46.55	81.41	39.21	134.65	11.12	86.15	49.94	85.51
830606.025922	21.24	103.83	39.21	82.16	32.47	129.96	3.52	84.73	42.31	85.99
830606.030133	13.36	102.04	31.70	82.25	25.49	125.22	-4.06	83.02	34.65	85.89
830606.030345	5.49	100.32	24.19	81.86	18.34	123.19	-11.58	80.98	26.99	85.37
830606.030556	-2.39	98.64	16.68	81.08	11.07	120.70	-19.04	78.54	19.34	84.53
830606.030807	-10.25	96.94	9.29	79.97	3.72	118.56	-26.40	75.59	11.72	83.41

TABLE H-1. Scanner Horizon Positions for Data Span on June 6, 1983 (1 of 10)

HORIZON POSITIONS (LATITUDES MEASURED NORTH, NEGATIVE MEANS SOUTH; LONGITUDES MEASURED EAST, NEGATIVE MEANS WEST)

DATE , TIME	SUBSATELLITE		SCANNER 1				SCANNER 2			
			EARTH-IN		EARTH-OUT		EARTH-IN		EARTH-OUT	
YYMMDD.HHMMSS	LATITUDE	LONGITUDE	LATITUDE	LONGITUDE	LATITUDE	LONGITUDE	LATITUDE	LONGITUDE	LATITUDE	LONGITUDE
830606.031015	-19.12	95.18	1.76	78.53	-3.56	116.99	-33.60	71.97	4.14	82.02
830606.031229	-25.97	93.31	-5.62	76.74	-11.12	115.66	-40.59	67.43	-3.39	80.34
830606.031440	-33.81	91.25	-12.92	74.56	-19.57	114.06	-47.26	61.59	-10.36	78.35
830606.031651	-41.52	88.88	-20.11	71.94	-26.03	114.00	-53.41	53.85	-18.24	75.98
830606.031902	-49.39	86.01	-27.16	68.74	-33.47	113.75	-58.77	43.50	-25.91	73.13
830606.032113	-57.10	82.27	-34.01	64.80	-40.59	114.01	-62.86	29.69	-32.64	69.65
830606.032324	-64.68	76.85	-40.59	59.56	-45.25	114.99	-65.07	12.44	-39.57	65.32
830606.032535	-71.97	67.74	-46.78	53.58	-55.51	117.07	-64.90	-5.16	-46.20	59.78
830606.032746	-79.43	48.67	-52.37	45.44	-52.58	121.03	-62.41	-22.94	-52.38	52.53
830606.032957	-81.75	4.65	-57.07	34.21	-69.27	128.68	-58.15	-35.14	-57.86	42.84
830606.033209	-78.77	-40.97	-60.44	21.46	-75.00	143.78	-52.73	-46.11	-62.20	29.75
830606.033423	-72.40	-61.06	-62.01	5.74	-78.28	172.78	-46.58	-53.45	-64.81	13.19
830606.033631	-65.13	-70.52	-61.46	-10.58	-77.07	-152.68	-39.97	-58.11	-65.13	-5.39
830606.033842	-57.56	-76.08	-58.89	-25.30	-72.25	-131.22	-33.06	-63.50	-63.06	-22.79
830606.034053	-49.86	-79.20	-54.74	-37.27	-65.89	-120.57	-25.94	-67.02	-59.07	-36.83
830606.034304	-42.10	-82.81	-49.49	-46.56	-56.90	-115.13	-18.65	-69.90	-53.78	-47.39
830606.034531	-33.31	-85.45	-42.71	-54.47	-50.73	-112.02	-10.37	-72.57	-46.86	-56.08
830606.034742	-25.48	-87.52	-36.18	-59.85	-43.31	-110.70	-2.90	-74.54	-40.17	-61.82
830606.034953	-17.53	-89.38	-29.33	-64.12	-35.83	-110.23	4.63	-76.19	-33.17	-66.30
830606.035205	-9.76	-91.13	-22.27	-67.56	-28.30	-110.33	12.21	-77.56	-25.96	-69.87
830606.035416	-1.99	-92.83	-15.05	-70.37	-20.77	-110.86	19.83	-78.67	-18.59	-72.78
830606.035627	5.98	-94.51	-7.72	-72.68	-13.24	-111.76	27.48	-79.49	-11.13	-75.19
830606.035854	14.83	-96.45	0.61	-74.80	-4.81	-113.17	36.09	-80.02	-2.66	-77.44
830606.040105	22.70	-98.27	8.07	-76.30	2.64	-114.79	43.75	-80.03	4.92	-79.10
830606.040316	33.56	-100.24	15.53	-77.48	10.03	-116.78	51.35	-79.37	12.52	-80.48
830606.040544	39.38	-102.77	24.06	-78.38	18.21	-119.53	59.87	-77.41	21.11	-81.68
830606.040755	47.19	-105.48	31.50	-78.79	25.36	-122.55	67.26	-73.41	28.74	-82.46
830606.041006	54.95	-108.93	38.98	-78.72	32.34	-126.26	74.27	-64.48	36.36	-82.89
830606.041217	62.61	-113.75	46.42	-78.00	39.06	-130.90	80.07	-41.81	43.97	-82.89
830606.041428	70.04	-121.57	53.77	-76.30	45.42	-136.82	81.58	6.15	51.55	-82.25
830606.041639	76.87	-136.91	60.97	-72.97	51.24	-144.45	77.20	40.81	59.06	-80.57
830606.041850	81.47	-173.49	67.84	-66.57	56.25	-154.50	70.59	54.25	66.43	-76.93
830606.042101	80.05	135.47	73.97	-55.71	60.02	-167.35	63.37	59.99	73.48	-68.89
830606.042312	74.13	110.17	78.10	-27.81	62.06	177.15	55.92	62.64	79.50	-48.78
830606.042523	66.96	98.96	77.96	8.43	61.98	160.56	48.38	63.81	81.76	-2.94
830606.042734	59.41	92.70	73.65	33.45	59.79	145.20	40.79	64.15	77.90	35.29
830606.043002	50.73	88.12	66.60	46.52	55.32	131.16	32.22	63.99	70.52	51.48
830606.043213	42.94	85.13	59.61	52.50	50.10	121.65	24.59	63.27	63.26	57.17
830606.043424	35.11	82.69	52.35	55.46	44.13	114.37	16.96	62.33	55.76	59.81
830606.043724	24.31	79.85	42.14	57.24	35.14	106.95	6.49	60.60	45.30	61.17
830606.043935	16.44	78.01	34.64	57.56	28.25	102.87	-1.10	59.00	37.65	61.27
830606.044146	8.57	76.27	27.13	57.34	21.15	99.58	-8.65	57.10	29.99	60.90
830606.044357	0.70	74.57	19.62	56.71	13.93	96.90	-16.13	54.82	22.36	60.18
830606.044625	-8.16	72.67	11.19	55.58	5.68	94.44	-24.45	51.71	13.75	59.01
830606.044836	-16.03	70.94	3.74	54.22	-1.70	92.68	-31.70	48.29	6.18	57.69
830606.045047	-23.88	69.10	-3.66	52.53	-9.13	91.26	-38.76	44.92	-1.39	56.10
830606.045255	-31.72	67.10	-10.98	50.46	-16.58	90.17	-45.52	38.50	-8.87	54.19
830606.045509	-39.54	64.93	-18.20	47.97	-24.04	89.42	-51.80	31.43	-16.28	51.93
830606.045720	-47.32	62.12	-25.29	44.93	-31.49	89.06	-57.44	21.85	-23.58	49.22
830606.045931	-55.05	58.66	-32.21	41.21	-38.91	89.17	-61.93	9.00	-30.75	45.93
830606.050142	-62.67	53.82	-38.87	36.58	-46.29	89.92	-64.70	-7.43	-37.74	41.86
830606.050354	-70.07	46.03	-45.17	30.70	-53.58	91.65	-65.19	-25.97	-44.46	36.69
830606.050605	-76.86	30.74	-50.95	23.11	-60.72	95.01	-63.28	-43.50	-50.78	29.98
830606.050815	-81.46	-5.53	-55.92	13.24	-67.54	101.36	-59.43	-57.73	-56.48	20.97
830606.051043	-79.50	-61.08	-00.06	-1.20	-74.28	116.18	-53.55	-69.61	-61.67	7.10
830606.051254	-73.35	-83.84	-61.92	-16.65	-79.06	143.09	-47.49	-77.28	-64.57	-9.00
830606.051505	-66.19	-94.22	-61.67	-33.04	-77.52	178.30	-40.93	-83.12	-65.23	-27.47
830606.051715	-59.65	-100.15	-59.36	-48.08	-73.07	-158.16	-34.05	-87.66	-63.48	-45.22
830606.051927	-50.96	-104.15	-55.41	-60.47	-66.84	-146.40	-26.96	-91.28	-59.73	-60.79
830606.052138	-43.20	-107.16	-50.29	-70.11	-59.92	-140.43	-19.72	-94.24	-54.59	-70.80
830606.052350	-35.40	-109.61	-44.39	-77.52	-52.68	-137.29	-12.36	-96.70	-48.87	-78.99
830606.052601	-27.57	-111.72	-37.96	-83.26	-45.30	-135.08	-4.91	-98.75	-41.99	-85.16
830606.052812	-19.72	-113.62	-31.18	-87.79	-37.83	-135.01	2.61	-100.50	-35.06	-89.93
830606.053023	-11.86	-115.39	-24.17	-91.43	-30.31	-134.97	10.18	-101.95	-27.89	-93.71
830606.053234	-3.99	-117.10	-16.99	-94.39	-22.78	-135.40	17.80	-103.12	-20.57	-96.78
830606.053445	3.88	-118.78	-9.68	-96.83	-15.25	-136.20	25.43	-104.02	-13.13	-99.32
830606.053656	11.75	-120.49	-2.30	-98.84	-7.74	-137.35	33.09	-104.61	-5.62	-101.43
830606.053907	19.62	-122.27	5.14	-100.47	-0.27	-138.83	40.75	-104.81	1.95	-103.21
830606.054118	27.49	-124.17	12.62	-101.77	7.14	-140.67	48.39	-104.45	9.55	-104.69
830606.054329	35.34	-126.28	20.13	-102.74	14.47	-142.90	55.99	-103.28	17.18	-105.98
830606.054540	43.16	-128.73	27.63	-103.35	21.69	-145.63	63.47	-100.98	24.80	-106.82
830606.054751	50.95	-131.75	35.12	-103.55	28.76	-148.96	70.72	-96.75	32.43	-107.44
830606.055002	58.67	-135.76	42.58	-103.19	35.62	-153.09	77.34	-90.97	40.05	-107.65
830606.055213	66.24	-141.73	49.99	-102.05	42.19	-159.30	81.62	-85.55	47.64	-107.40
830606.055425	73.46	-152.23	57.28	-99.55	48.32	-166.99	79.96	2.03	55.19	-106.33

TABLE H-1. Scanner Horizon Positions for Data Span on June 6, 1983 (2 of 10)

HORIZON POSITIONS (LATITUDES MEASURED NORTH, NEGATIVE MEANS SOUTH; LONGITUDES MEASURED EAST, NEGATIVE MEANS WEST)

DATE . TIME	SUBSATELLITE		SCANNER 1				SCANNER 2			
			EARTH-IN		EARTH-OUT		EARTH-IN		EARTH-OUT	
YYMMDD.HHMMSS	LATITUDE	LONGITUDE	LATITUDE	LONGITUDE	LATITUDE	LONGITUDE	LATITUDE	LONGITUDE	LATITUDE	LONGITUDE
830606.055635	79.58	-175.41	64.35	-95.12	53.79	-173.71	74.13	24.14	62.65	-103.87
830606.055847	81.64	135.11	70.95	-86.21	58.26	174.94	67.14	32.85	59.91	-98.58
830606.060053	77.45	95.68	76.35	-67.96	61.25	160.70	59.75	36.80	76.61	-86.28
830606.060309	73.74	79.07	78.67	-34.92	62.29	144.80	52.25	38.62	91.36	-54.37
830606.060520	53.34	70.84	76.24	-2.16	61.16	128.13	44.71	39.34	80.48	-5.28
830606.060731	55.70	65.80	70.78	15.81	58.09	113.99	37.11	39.39	74.91	19.63
830606.060942	47.95	62.25	64.14	24.58	53.55	102.74	29.49	38.99	67.96	29.33
830606.061153	40.14	59.48	57.03	29.07	48.03	94.10	21.66	38.24	60.59	33.63
830606.061404	32.30	57.18	49.70	31.40	41.85	87.47	14.23	37.21	53.05	35.63
830606.061615	24.44	55.15	42.27	32.50	35.25	82.31	6.62	35.90	45.43	36.44
830606.061826	16.57	53.32	34.77	32.84	28.36	78.21	-0.97	34.31	37.78	36.55
830606.062037	8.70	51.57	27.26	32.63	21.27	74.91	-8.52	32.41	30.12	36.19
830606.062249	0.83	49.88	19.78	32.00	14.05	72.22	-16.01	30.14	22.47	35.47
830606.062460	-7.05	48.19	12.25	31.00	5.73	70.01	-23.41	27.41	14.83	34.46
830606.062711	-14.91	46.47	4.79	29.71	-0.56	68.19	-30.69	24.09	7.23	33.17
830606.062922	-22.77	44.65	-2.62	28.07	-8.08	66.72	-37.77	19.97	-0.32	31.62
830606.063133	-30.61	42.68	-9.95	26.06	-15.53	65.59	-44.59	14.71	-7.81	29.76
830606.063344	-38.43	40.45	-17.19	23.63	-22.98	64.79	-50.98	7.85	-15.23	27.55
830606.063555	-46.22	37.82	-24.30	20.68	-30.43	64.36	-56.71	-1.33	-22.55	24.91
830606.063806	-53.96	34.49	-31.24	17.07	-37.86	64.40	-61.38	-13.68	-29.75	21.72
830606.064017	-61.60	29.91	-37.94	12.58	-45.25	65.04	-64.46	-29.64	-36.76	17.77
830606.064229	-69.05	22.70	-44.31	6.90	-52.56	66.61	-65.27	-48.06	-43.53	12.78
830606.064439	-75.97	9.01	-50.17	-0.42	-59.72	69.66	-63.68	-65.91	-49.92	6.30
830606.064650	-81.08	-23.19	-55.28	-9.93	-66.80	75.45	-60.07	-80.67	-55.72	-2.32
830606.064901	-80.66	-75.38	-59.25	-22.20	-72.83	86.76	-55.06	-91.88	-60.89	-13.95
830606.065112	-75.19	-104.29	-61.62	-37.08	-77.39	109.68	-49.10	-100.16	-53.99	-29.10
830606.065324	-68.15	-116.78	-61.94	-53.44	-78.14	144.74	-42.72	-106.43	-65.30	-47.20
830606.065535	-60.68	-123.54	-60.16	-69.03	-74.50	172.30	-35.91	-111.27	-[illegible]17	-65.46
830606.065746	-53.02	-127.93	-56.00	-82.17	-68.59	-173.49	-29.87	-115.11	-60.85	-80.99
830606.065957	-45.25	-131.14	-51.75	-92.50	-61.80	-166.38	-21.66	-118.23	-56.06	-92.91
830606.070209	-37.48	-133.71	-46.02	-100.45	-54.63	-162.66	-14.33	-120.81	-50.24	-101.76
830606.070419	-29.66	224.10	-39.71	253.41	-47.28	199.28	-6.90	237.03	-43.76	251.81
830606.070630	-21.81	222.15	-33.01	248.59	-39.82	200.17	0.60	235.21	-36.93	246.91
830606.070841	-13.96	220.35	-26.06	244.74	-32.31	200.35	8.16	233.69	-29.82	242.50
830606.071052	-6.09	218.63	-18.91	241.62	-24.78	200.04	15.76	232.44	-22.53	239.26
830606.071302	1.78	216.94	-11.64	239.05	-17.25	199.33	23.40	231.46	-15.12	236.59
830606.071514	9.65	215.25	-4.27	236.94	-9.73	198.26	31.05	230.79	-7.62	234.37
830606.071725	17.53	213.49	3.16	235.21	-2.25	196.87	38.71	230.48	-0.07	232.51
830606.071936	25.39	211.63	10.63	233.82	5.18	195.13	46.35	230.66	7.53	230.98
830606.072147	33.25	209.58	18.14	232.77	12.52	193.02	53.98	231.56	15.15	229.69
830606.072359	41.08	207.24	25.63	232.05	19.78	190.43	61.49	233.77	22.77	228.68
830606.072610	48.89	204.40	33.13	231.73	26.90	187.27	68.83	238.49	30.40	227.97
830606.072821	56.63	200.72	40.60	231.93	33.82	183.38	75.69	249.29	38.02	227.62
830606.073032	64.25	195.42	48.03	232.82	40.48	178.49	80.92	277.24	45.62	227.[illegible]
830606.073243	71.60	186.57	55.35	234.80	46.74	172.24	81.01	326.88	53.19	228.86
830606.073454	78.16	168.21	62.50	238.64	52.41	164.12	75.86	-4.54	60.68	230.56
830606.073705	81.77	125.26	69.27	246.06	57.19	153.52	59.05	5.50	68.01	234.86
830606.073916	78.97	79.42	75.11	261.11	60.63	140.03	61.76	11.31	74.93	244.55
830606.074127	72.63	57.58	78.50	290.43	62.23	124.11	54.29	13.55	80.46	269.43
830606.074338	65.34	47.88	77.29	325.83	61.67	107.61	46.73	14.50	81.36	318.59
830606.074549	57.75	42.23	72.40	347.50	59.07	92.76	39.14	14.70	78.61	-9.84
830606.074800	50.02	38.37	65.97	-1.92	54.88	80.73	31.52	14.41	69.87	2.78
830606.075011	42.22	35.44	58.95	3.42	49.57	71.45	23.90	13.75	62.57	8.07
830606.075222	34.39	33.04	51.67	6.20	43.55	64.35	16.26	12.79	55.06	10.52
830606.075434	26.54	30.96	44.25	7.58	37.34	58.84	8.64	11.55	47.46	11.59
830606.075645	18.67	29.07	36.77	8.09	30.21	54.49	1.05	10.04	39.82	11.85
830606.075856	10.80	27.31	29.26	8.01	23.17	51.01	-6.52	8.23	32.16	11.60
830606.080107	2.92	25.61	21.74	7.48	15.98	48.16	-14.02	5.06	24.50	10.97
830606.080319	-4.95	23.92	14.24	6.59	8.68	45.83	-21.45	3.47	16.86	10.03
830606.080602	-14.79	21.77	4.91	5.01	-0.54	43.49	-30.57	-0.57	7.36	8.48
830606.080845	-24.61	19.48	-4.34	2.91	-9.82	41.70	-39.40	-5.87	-2.08	6.49
830606.081057	-32.44	17.48	-11.65	0.91	-17.27	40.65	-46.13	-11.45	-9.56	4.56
830606.081309	-40.26	15.16	-18.86	-1.74	-24.73	39.93	-52.39	341.22	-16.96	2.26
830606.081519	-49.04	12.39	-25.94	-4.82	-32.18	39.60	-57.91	331.37	-24.25	-0.50
830606.081730	-55.76	8.94	-32.83	-8.62	-39.60	39.76	-62.27	319.19	-31.41	-3.35
830606.081941	-63.37	3.91	-39.47	-13.35	-46.97	40.59	-64.85	301.46	-38.37	-6.02
830606.082152	-70.73	-4.40	-45.73	-19.37	-54.25	42.43	-65.13	282.89	-45.06	-13.30
830606.082403	-77.42	339.13	-51.44	332.95	-61.37	45.98	-62.9[illegible]	265.59	-51.34	339.78
830606.082614	-81.63	300.13	-56.33	322.75	-68.14	52.74	-59.00	251.70	-56.97	330.55
830606.082825	-79.66	250.63	-59.97	309.82	-74.11	66.10	-53.74	241.24	-[illegible]54	318.11
830606.083053	-72.74	225.43	-61.98	292.39	-78.22	96.86	-46.90	232.57	-64.73	299.91
830606.083335	-63.63	213.99	-61.09	272.11	-76.32	135.68	-38.61	225.76	-64.89	276.75
830606.083604	-55.07	208.37	-57.69	256.32	-72.28	155.94	-30.75	221.11	-61.94	258.06
830606.083815	-47.34	204.91	-53.14	245.26	-63.65	167.44	-23.59	217.52	-57.46	245.21
830606.084025	-39.56	202.20	-47.61	236.74	-56.56	171.85	-16.29	215.11	-51.86	235.62

TABLE H-1. Scanner Horizon Positions for Data Span on June 6, 1983 (3 of 10)

HORIZON POSITIONS (LATITUDES MEASURED NORTH, NEGATIVE MEANS SOUTH; LONGITUDES MEASURED EAST, NEGATIVE MEANS WEST)

DATE , TIME	SUBSATELLITE		SCANNER 1 EARTH-IN		SCANNER 1 EARTH-OUT		SCANNER 2 EARTH-IN		SCANNER 2 EARTH-OUT	
YYMMDD,HHMMSS	LATITUDE	LONGITUDE	LATITUDE	LONGITUDE	LATITUDE	LONGITUDE	LATITUDE	LONGITUDE	LATITUDE	LONGITUDE
830606.084237	-31.74	199.93	-41.43	230.18	-49.25	179.17	-8.98	217.84	-45.54	225.48
830606.084448	-23.90	197.93	-34.23	225.05	-41.81	175.29	-1.40	210.94	-38.78	223.02
830606.084659	-16.05	196.10	-27.03	220.97	-34.31	175.64	6.15	209.34	-31.73	218.76
830606.084943	-6.22	193.93	-19.03	216.94	-24.90	175.32	15.64	207.74	-22.65	214.58
830606.085211	3.64	192.04	-10.84	214.08	-16.43	174.50	24.23	206.65	-14.30	211.61
830606.085422	10.51	190.34	-3.46	212.01	-8.92	173.41	31.89	206.01	-6.80	209.43
830606.085633	19.39	188.55	3.77	210.32	-1.44	171.95	39.54	205.75	0.76	207.60
830606.085900	27.23	186.45	12.38	208.82	5.90	169.95	48.14	205.07	9.31	205.91
830606.090111	35.08	184.35	19.89	207.84	14.23	167.73	55.74	207.21	16.93	204.71
830606.090322	42.91	181.91	27.39	207.21	21.46	165.02	63.23	209.86	24.55	203.76
830606.090533	50.70	178.91	34.85	207.01	28.54	161.71	70.50	215.53	32.18	203.13
830606.090744	58.42	174.94	42.35	207.34	35.41	157.51	77.14	229.90	39.80	202.87
830606.090956	66.00	169.06	49.75	208.45	41.98	152.44	81.56	263.38	47.40	203.13
830606.091207	73.24	158.79	57.05	210.77	48.13	145.81	80.10	311.44	54.95	204.17
830606.091418	79.42	136.26	64.13	215.24	53.62	137.15	74.35	-25.72	62.41	206.57
830606.091629	81.69	97.43	70.75	223.95	55.13	125.90	67.37	-16.75	69.68	211.73
830606.091840	77.65	47.05	76.21	241.75	61.18	111.75	60.02	-12.73	76.42	223.67
830606.092051	70.97	29.99	78.67	274.43	62.29	95.49	52.53	-10.86	81.28	254.68
830606.092302	63.58	21.60	76.35	307.59	61.23	79.19	44.96	-10.12	80.60	304.01
830606.092513	55.95	16.49	70.98	-34.03	58.21	64.96	37.35	-10.05	75.12	-30.30
830606.092724	48.20	12.90	64.37	-25.07	53.72	53.61	29.73	-10.44	68.19	-20.31
830606.092935	40.39	10.12	57.27	-20.46	48.22	44.90	22.10	-11.17	60.83	-15.90
830606.093146	32.55	7.81	49.94	-18.10	42.06	38.21	14.47	-12.20	53.29	-13.85
830606.093357	24.70	5.78	42.51	-16.96	35.47	33.01	6.86	-13.50	45.68	-13.02
830606.093608	16.83	3.93	35.01	-16.61	29.58	28.89	-0.73	-15.08	38.03	-12.89
830606.093819	8.95	2.18	27.50	-15.80	21.50	25.57	-9.25	-16.97	30.36	-13.24
830606.094031	1.08	0.49	19.98	-17.42	14.28	22.85	-15.77	-19.22	22.71	-13.95
830606.094242	-6.79	-1.20	12.49	-18.39	6.76	20.62	-23.18	-21.93	15.08	-14.95
830606.094453	-14.66	-2.92	5.03	-19.69	-0.42	18.89	-30.46	-25.23	7.48	-16.22
830606.094704	-22.52	-4.74	-2.38	-21.32	-7.84	17.32	-37.55	-29.33	-0.08	-17.77
830606.094915	-30.36	-6.70	-9.72	-23.32	-15.29	15.17	-44.37	-34.54	-7.58	-19.62
830606.095126	-38.18	8.92	-16.96	-25.73	-22.75	15.36	-50.78	-41.34	-15.00	-21.81
830606.095337	-45.98	-11.53	-24.08	-28.66	-30.20	14.92	-56.84	309.56	-22.32	-24.44
830606.095549	-53.71	-14.83	-31.02	-32.25	-37.63	14.94	-61.25	297.33	-29.52	-27.62
830606.095759	-61.36	-19.36	-37.73	-36.71	-45.02	15.56	-64.37	281.48	-36.54	-31.54
830606.100010	-68.81	-26.45	-44.11	-42.34	-52.33	17.09	-65.28	263.10	-43.32	-36.49
830606.100221	-75.77	-39.82	-49.99	310.40	-59.50	20.08	-63.76	245.18	-49.72	-42.91
830606.100432	-80.98	285.86	-55.13	300.97	-66.39	25.75	-60.21	230.30	-55.55	308.55
830606.100643	-83.78	236.59	-59.15	286.79	-72.65	36.81	-55.23	218.99	-60.45	297.03
830606.100854	-75.38	205.85	-61.57	273.98	-77.30	59.26	-49.36	210.63	-63.92	281.99
830606.101105	-68.38	194.06	-61.97	257.64	-78.19	94.20	-42.93	204.51	-65.29	263.95
830606.101317	-60.92	187.19	-60.24	241.98	-74.67	122.23	-36.13	199.42	-64.24	245.64
830606.101529	-53.26	182.75	-56.73	228.76	-68.80	136.76	-29.10	195.55	-61.02	230.00
830606.101739	-45.52	179.51	-51.91	219.34	-62.02	144.02	-21.99	192.41	-56.23	217.98
830606.101950	-37.73	176.92	-46.21	210.33	-54.86	147.82	-14.56	189.82	-50.43	209.04
830606.102201	-29.91	174.72	-39.92	204.14	-47.51	149.80	-7.14	187.65	-44.00	202.34
830606.102412	-22.06	172.77	-33.23	199.29	-40.06	150.71	0.37	185.82	-37.19	197.21
830606.102623	-14.20	170.96	-26.28	195.41	-32.55	150.91	7.92	184.29	-30.05	193.17
830606.102850	-5.36	169.03	-18.24	191.91	-24.08	150.54	16.45	182.59	-21.84	189.54
830606.103102	2.52	167.34	-10.95	189.39	-15.55	149.80	24.11	181.94	-14.42	186.92
830606.103313	10.39	165.88	-3.58	187.32	-9.04	148.70	31.77	181.30	-6.92	184.74
830606.103524	19.25	163.88	3.86	185.62	-1.56	147.28	39.43	181.02	0.64	182.91
830606.103735	26.13	162.01	11.33	184.26	5.86	145.51	47.07	181.26	8.24	181.38
830606.103946	33.98	159.94	18.84	183.24	13.29	143.35	54.68	182.25	15.86	180.14
830606.104157	41.81	157.55	26.33	182.56	20.45	140.71	62.19	184.63	23.48	179.16
830606.104409	49.61	154.66	33.83	182.29	27.55	137.50	69.50	189.71	31.11	178.48
830606.104619	57.34	150.88	41.30	182.53	34.45	133.52	76.29	201.46	38.73	178.16
830606.104830	64.95	145.34	48.71	183.51	41.08	128.52	81.22	231.93	46.33	178.33
830606.105041	72.26	135.96	56.03	185.67	47.29	122.12	80.65	291.36	53.89	179.24
830606.105252	78.68	116.06	63.15	189.70	52.90	113.80	75.27	-52.48	61.37	181.39
830606.105503	81.78	70.57	69.86	197.60	57.57	102.94	68.38	-42.32	68.68	186.01
830606.105718	79.46	26.15	75.56	213.71	60.86	89.19	61.07	-37.84	75.53	196.54
830606.105925	71.97	6.94	78.60	244.43	62.27	73.12	53.59	-35.76	80.83	223.75
830606.110137	64.64	-2.20	76.95	279.09	61.51	56.68	46.02	-34.87	81.10	273.36
830606.110348	57.03	-7.63	71.84	299.40	58.74	42.07	38.42	-34.74	76.02	-57.30
830606.110559	49.29	-11.37	65.33	-50.71	54.42	30.32	30.90	-35.08	69.20	-48.98
830606.110810	41.49	-14.24	58.28	-45.68	49.04	21.27	23.17	-35.77	61.87	-41.06
830606.111021	33.66	-16.61	50.98	-43.07	42.98	14.33	15.55	-36.76	54.36	-38.78
830606.111232	25.80	-18.67	43.55	-41.79	36.42	8.95	7.93	-38.02	46.75	-37.80
830606.111443	17.93	-20.54	36.07	-41.34	29.57	4.69	0.34	-39.56	39.10	-37.60
830606.111654	10.06	-22.30	28.55	-41.47	22.51	1.27	-7.22	-41.40	31.44	-37.89
830606.111905	2.19	-23.99	21.04	-42.03	15.30	-1.52	-14.72	-43.60	23.78	-38.55
830606.112115	-5.69	-25.68	13.54	-42.95	7.99	-3.81	-22.14	-46.24	16.15	-39.51
830606.112327	-13.55	-27.40	6.07	-44.20	0.62	-5.69	-29.44	-49.45	8.54	-40.75
830606.112538	-21.41	-29.19	-1.34	-45.79	-5.90	-7.22	-36.57	-53.41	0.98	-42.26

TABLE H-1. Scanner Horizon Positions for Data Span on June 6, 1983 (4 of 10)

HORIZON POSITIONS (LATITUDES MEASURED NORTH, NEGATIVE MEANS SOUTH; LONGITUDES MEASURED EAST, NEGATIVE MEANS WEST)

DATE , TIME	SUBSATELLITE		SCANNER 1				SCANNER 2			
			EARTH-IN		EARTH-OUT		EARTH-IN		EARTH-OUT	
YYMMDD.HHMMSS	LATITUDE	LONGITUDE	LATITUDE	LONGITUDE	LATITUDE	LONGITUDE	LATITUDE	LONGITUDE	LATITUDE	LONGITUDE
830606.112749	-29.26	-31.13	-8.69	-47.73	-14.24	-8.41	-43.43	-59.44	-6.53	-44.06
830606.113001	-37.09	-33.31	-15.95	-50.09	-21.70	-9.27	-49.91	-64.99	-13.96	-46.20
830606.113212	-44.89	-35.85	-23.09	-52.93	-29.15	-9.76	-55.75	299.29	-21.30	-48.76
830606.113423	-52.53	-39.03	-30.06	-56.42	-35.59	-9.82	-60.67	274.55	-28.52	-51.85
830606.113634	-60.29	-43.34	-36.81	-60.74	-43.98	-9.29	-64.05	259.19	-35.57	-55.65
830606.113845	-67.78	-49.93	-43.24	-66.19	-51.31	-7.92	-65.30	241.02	-42.39	-60.43
830606.114056	-74.84	-61.98	-49.21	286.82	-58.51	-5.18	-64.11	222.83	-48.85	-66.62
830606.114307	-81.47	270.36	-54.47	277.73	-65.45	0.00	-60.80	207.46	-54.79	255.19
830606.114519	-81.23	218.47	-58.67	265.95	-71.94	10.03	-55.99	195.66	-59.84	274.13
830606.114729	-76.29	184.87	-61.35	251.48	-76.81	30.47	-50.22	186.94	-63.54	259.99
830606.114940	-69.41	170.64	-62.04	235.22	-79.37	64.46	-43.86	180.38	-65.24	241.65
830606.115151	-61.95	163.24	-60.60	219.34	-75.35	94.51	-37.10	175.31	-64.53	223.36
830606.115402	-54.34	158.56	-57.31	205.72	-69.70	110.56	-30.10	171.33	-61.58	207.26
830606.115613	-46.61	155.19	-52.55	194.92	-63.01	115.54	-22.91	168.10	-56.97	194.74
830606.115824	-38.83	152.53	-47.05	186.61	-55.88	122.70	-15.60	165.43	-51.29	185.42
830606.120036	-31.01	150.29	-40.83	180.20	-48.85	124.87	-8.18	163.21	-44.93	178.46
830606.120247	-23.17	148.31	-34.19	175.15	-41.11	125.90	-0.69	161.34	-38.14	173.14
830606.120458	-15.31	146.49	-27.27	171.19	-33.61	126.19	6.86	159.77	-31.06	168.96
830606.120709	-7.44	144.76	-20.15	167.95	-25.98	125.96	14.46	158.47	-23.79	165.61
830606.120920	0.43	143.07	-12.90	165.30	-18.55	125.31	22.08	157.45	-16.40	162.85
830606.121131	8.30	141.38	-5.55	163.11	-11.03	124.30	29.73	156.72	-8.92	160.56
830606.121342	16.17	139.64	1.87	161.32	-3.34	122.97	37.39	156.34	-1.37	158.64
830606.121553	24.04	137.80	9.34	159.87	3.90	121.29	45.04	156.42	6.21	157.04
830606.121804	31.90	135.79	16.83	158.75	11.27	119.24	52.66	157.19	13.83	155.72
830606.122015	39.73	133.51	24.34	157.98	18.54	116.74	60.20	159.10	21.45	154.67
830606.122226	47.54	130.77	31.84	157.59	25.68	113.70	67.59	163.24	29.08	153.91
830606.122437	55.30	127.27	39.32	157.69	32.64	109.95	74.57	172.51	36.71	153.48
830606.122648	62.95	122.34	46.75	158.44	39.35	105.25	80.26	196.19	44.31	153.51
830606.122859	70.36	114.35	54.10	160.19	45.69	99.27	81.45	244.74	51.89	154.18
830606.123111	77.14	98.44	61.29	163.62	51.48	91.51	76.93	-81.87	59.39	155.93
830606.123322	81.56	60.57	68.14	170.22	56.44	81.38	70.28	-68.96	66.76	159.70
830606.123533	79.83	10.17	74.21	183.51	60.15	68.39	63.04	-63.45	73.79	166.05
830606.123744	73.92	-14.13	78.21	210.12	62.10	52.80	55.58	-60.88	79.72	189.08
830606.123955	65.63	-25.00	77.84	246.31	61.92	36.22	48.04	-59.76	81.71	235.80
830606.124206	59.07	-31.12	73.40	270.62	59.65	20.96	40.45	-59.45	77.64	272.73
830606.124417	51.36	-35.21	67.14	-77.42	55.69	8.43	32.83	-59.67	71.09	-72.81
830606.124628	43.57	-38.26	60.18	-71.43	50.55	-1.29	25.20	-60.27	63.85	-66.74
830606.124839	35.74	-40.74	52.93	-68.32	44.63	-8.73	17.58	-61.19	56.36	-63.94
830606.125050	27.89	-42.87	45.53	-66.75	38.19	-14.47	9.95	-62.38	48.77	-62.69
830606.125318	19.04	-45.01	37.12	-66.08	30.54	-19.49	1.40	-64.04	40.18	-62.31
830606.125522	11.17	-46.77	29.61	-66.14	23.51	-23.01	-6.16	-65.84	32.51	-62.54
830606.125740	3.29	-48.48	22.09	-66.65	16.32	-25.88	-13.67	-67.99	24.86	-63.16
830606.125951	-4.58	-50.16	14.59	-67.52	9.02	-28.24	-21.10	-70.56	17.22	-64.08
830606.130202	-12.45	-51.87	7.12	-68.73	1.66	-30.17	-28.42	-73.67	9.61	-65.23
830606.130413	-20.31	-53.66	-0.31	-70.27	-5.78	-31.74	-35.58	-77.52	2.04	-66.75
830606.130624	-28.16	-55.57	-7.67	-72.16	-13.20	-32.98	-42.49	-82.38	-5.48	-68.51
830606.130835	-35.99	-57.70	-14.94	-74.45	-20.65	-33.89	-49.03	-88.67	-12.92	-70.60
830606.131045	-43.79	-60.19	-22.09	-77.22	-29.11	-34.44	-55.01	262.96	-20.28	-73.09
830606.131257	-51.55	-63.25	-29.09	-80.61	-35.55	-34.56	-60.07	251.69	-27.52	-76.10
830606.131508	-59.23	-67.35	-35.88	-84.79	-42.95	-34.13	-63.69	236.84	-34.59	-79.79
830606.131719	-66.75	-73.50	-42.36	-90.06	-50.29	-32.90	-65.27	218.93	-41.45	-84.41
830606.131933	-73.90	-84.43	-48.40	263.19	-57.51	-30.40	-64.42	200.54	-47.97	-90.36
830606.132142	-77.86	291.19	-53.78	254.43	-64.50	-25.66	-61.37	186.67	-53.99	261.77
830606.132353	-81.55	200.95	-58.15	243.06	-70.99	-15.55	-56.74	172.39	-59.20	251.17
830606.132604	-77.16	163.24	-61.08	228.94	-76.26	1.99	-51.08	163.30	-63.13	237.15
830606.132815	-70.42	147.35	-62.07	212.82	-78.44	34.60	-44.78	156.47	-65.15	219.75
830606.133026	-63.04	139.34	-60.93	196.75	-75.98	66.48	-38.07	151.24	-64.78	201.18
830606.133237	-55.43	134.40	-57.87	182.75	-70.57	84.20	-31.09	147.12	-62.11	184.60
830606.133449	-47.70	130.89	-53.37	171.50	-63.99	92.98	-23.93	143.79	-57.70	171.57
830606.133659	-39.92	128.15	-47.88	162.93	-56.90	97.53	-16.63	141.06	-52.14	161.85
830606.133910	-32.11	125.87	-41.73	156.29	-49.59	99.93	-9.23	138.77	-45.85	154.61
830606.134121	-24.27	123.86	-35.14	151.10	-42.16	101.09	-1.75	135.86	-39.11	149.09
830606.134332	-16.42	122.01	-28.26	146.98	-34.67	101.46	5.80	135.25	-32.07	144.78
830606.134543	-8.55	120.27	-21.17	143.65	-27.14	101.29	13.39	133.92	-24.83	141.32
830606.134754	-0.68	118.58	-13.93	140.92	-19.61	100.70	21.01	132.86	-17.45	138.49
830606.135005	7.19	116.90	-6.59	138.67	-12.09	99.74	28.66	132.08	-9.98	136.14
830606.135217	15.06	115.17	0.82	136.83	-4.59	98.45	36.31	131.65	-2.44	134.18
830606.135429	22.93	113.35	8.29	135.34	2.85	96.83	43.97	131.65	5.14	132.53
830606.135639	30.79	111.37	15.76	134.16	10.24	94.82	51.57	132.34	12.74	131.15
830606.135850	38.63	109.13	23.28	133.35	17.52	92.40	59.15	134.01	20.37	130.08
830606.140101	46.44	106.49	30.78	132.90	24.68	89.44	66.56	137.73	28.00	129.27
830606.140312	54.21	103.11	38.26	132.92	31.67	85.80	73.63	145.95	35.63	128.80
830606.140523	61.98	98.45	45.70	133.57	38.42	81.26	79.62	166.59	43.24	128.75
830606.140734	69.34	91.05	53.07	135.15	44.82	75.49	81.73	212.41	50.82	129.32
830606.140945	75.26	75.94	60.28	138.28	50.71	68.02	77.77	250.39	58.34	130.87

TABLE H-1. Scanner Horizon Positions for Data Span on June 6, 1983 (5 of 10)

HORIZON POSITIONS (LATITUDES MEASURED NORTH, NEGATIVE MEANS SOUTH; LONGITUDES MEASURED EAST, NEGATIVE MEANS WEST)

DATE . TIME	SUBSATELLITE		SCANNER 1				SCANNER 2			
			EARTH-IN		EARTH-OUT		EARTH-IN		EARTH-OUT	
YYMMDD.HHMMSS	LATITUDE	LONGITUDE	LATITUDE	LONGITUDE	LATITUDE	LONGITUDE	LATITUDE	LONGITUDE	LATITUDE	LONGITUDE
830606.141155	81.23	43.13	67.20	144.28	55.81	55.26	71.26	-94.95	65.73	134.26
830606.141407	80.45	-8.95	73.44	156.28	59.72	45.68	54.07	-85.71	72.83	141.68
830606.141618	74.78	-36.58	77.85	180.66	61.95	30.40	56.34	-85.85	79.02	150.00
830606.141829	67.68	-48.58	78.19	216.84	62.08	13.81	49.11	-84.59	81.63	203.66
830606.142041	60.15	-55.14	74.17	243.39	60.09	-1.75	41.52	-84.15	78.44	244.58
830606.142252	52.45	-59.43	68.07	-103.37	55.33	-14.70	33.91	-84.34	72.07	-98.87
830606.142503	44.67	-62.60	61.19	-96.79	51.33	-24.79	26.28	-84.59	64.89	-92.07
830606.142714	35.85	-65.14	53.97	-93.37	45.50	-32.51	18.65	-85.76	57.43	-88.94
830606.142925	29.00	-67.30	46.58	-91.63	39.12	-38.47	11.03	-85.91	49.85	-87.53
830606.143136	21.14	-69.24	39.11	-90.89	32.38	-43.14	3.42	-88.34	42.21	-87.06
830606.143347	13.26	-71.03	31.61	-90.80	25.40	-46.87	-4.15	-90.05	34.55	-87.17
830606.143559	5.39	-72.75	24.09	-91.20	18.25	-49.90	-11.68	-92.10	26.89	-87.69
830606.143809	-2.45	-74.43	16.58	-91.98	10.98	-52.38	-19.14	-94.55	19.25	-88.53
830606.144020	-10.36	-76.13	9.10	-93.10	3.63	-54.41	-26.49	-97.50	11.63	-89.66
830606.144231	-18.22	-77.89	1.66	-94.55	-3.78	-56.08	-33.70	-101.13	4.05	-91.05
830606.144442	-25.07	-79.76	-5.71	-96.34	-11.21	-57.40	-40.65	-105.65	-3.48	-92.73
830606.144653	-33.91	-81.83	-13.01	-98.51	-18.67	-58.40	-47.34	-111.54	-10.95	-94.73
830606.144904	-41.72	-84.20	-20.20	-101.15	-26.12	-59.05	-53.49	240.72	-18.33	-97.10
830606.145116	-49.49	-87.08	-27.25	-104.36	-33.57	-59.29	-58.83	230.30	-25.60	-99.96
830606.145327	-57.19	-90.84	-34.10	-108.31	-40.98	-59.03	-62.91	216.43	-32.73	-103.45
830606.145538	-64.77	-96.28	-40.67	-113.25	-48.34	-58.04	-65.08	199.16	-39.65	-107.79
830606.145749	-72.06	-105.46	-46.85	240.44	-55.60	-55.95	-64.88	180.57	-46.28	-113.34
830606.145960	-78.50	235.26	-52.43	232.28	-62.67	-51.95	-62.37	163.83	-52.45	239.38
830606.150211	-81.79	190.90	-57.12	221.71	-69.35	-44.23	-58.09	150.65	-57.92	229.65
830606.150422	-78.70	145.61	-60.45	208.24	-75.06	-28.99	-52.65	140.74	-62.24	216.53
830606.150633	-72.31	125.73	-62.02	192.49	-78.30	0.17	-46.50	133.39	-64.83	199.91
830606.150844	-65.04	116.34	-61.44	176.17	-77.03	34.63	-39.89	127.78	-65.12	181.33
830606.151112	-56.51	110.26	-58.41	159.84	-71.43	57.67	-32.09	122.93	-62.61	162.02
830606.151323	-48.80	106.61	-54.08	148.25	-64.95	67.35	-24.95	119.50	-58.41	148.47
830606.151534	-41.03	103.78	-48.70	139.30	-57.92	72.33	-17.67	116.69	-52.98	138.34
830606.151745	-33.22	101.45	-42.63	132.41	-50.64	74.95	-10.28	114.36	-46.78	130.79
830606.151956	-25.38	99.40	-36.10	127.04	-43.22	76.25	-2.81	112.39	-40.09	125.07
830606.152207	-17.53	97.54	-29.25	122.79	-35.73	76.72	4.73	110.74	-33.08	120.61
830606.152418	-9.67	95.79	-22.18	119.36	-28.21	76.62	12.31	109.37	-25.88	117.04
830606.152629	-1.80	94.10	-14.96	116.55	-20.67	76.06	19.93	108.27	-18.50	114.14
830606.152840	6.08	92.41	-7.63	114.25	-13.15	75.17	27.58	107.45	-11.04	111.73
830606.153051	13.95	90.69	-0.23	112.35	-5.65	73.93	35.23	106.95	-3.51	109.71
830606.153302	21.82	88.99	7.22	110.80	1.80	72.36	42.88	106.90	4.06	108.02
830606.153513	29.68	86.94	14.71	109.60	9.19	70.41	50.51	107.45	11.67	106.62
830606.153724	37.52	84.75	22.21	108.73	16.49	68.05	58.08	109.96	19.29	105.50
830606.153935	45.34	82.17	29.72	108.22	23.68	65.18	65.52	112.30	26.92	104.65
830606.154147	53.11	78.93	37.20	108.17	30.69	61.65	72.65	119.61	34.55	104.12
830606.154358	60.80	74.51	44.65	108.71	37.48	57.25	79.90	137.59	42.16	104.01
830606.154609	68.30	67.66	52.03	110.13	43.94	51.68	91.83	180.73	49.74	104.47
830606.154820	75.34	54.89	59.27	112.98	49.91	44.48	78.56	222.16	57.27	105.65
830606.155031	80.78	25.11	66.25	118.45	55.15	35.09	72.24	-120.97	64.69	108.89
830606.155242	80.97	-27.41	72.62	129.29	59.26	22.93	65.11	-114.05	71.85	115.50
830606.155453	75.71	-58.73	77.42	151.47	61.76	7.98	57.70	-110.87	78.25	131.47
830606.155704	68.72	-72.06	78.45	187.08	62.20	-8.56	50.18	-109.43	81.81	171.37
830606.155915	61.23	-79.11	74.92	215.87	60.49	-24.40	42.60	-108.93	79.20	215.89
830606.160126	53.55	-83.63	69.01	-129.45	56.98	-37.78	34.99	-109.01	73.05	-125.11
830606.160337	45.78	-86.92	62.19	-122.20	52.10	-48.24	27.36	-109.52	65.93	-117.46
830606.160548	37.98	-89.53	55.00	-118.46	46.37	-56.25	19.73	-110.34	58.50	-113.98
830606.160759	30.12	-91.73	47.64	-116.53	40.05	-62.43	12.11	-111.46	50.93	-112.39
830606.161010	22.25	-93.70	40.18	-115.67	33.35	-67.25	4.50	-112.84	43.30	-111.80
830606.161222	14.38	-95.51	32.68	-115.50	26.40	-71.11	-3.08	-114.51	35.64	-111.84
830606.161433	6.51	-97.23	25.18	-115.84	19.27	-74.22	-10.61	-115.51	27.98	-112.31
830606.161644	-1.37	-98.92	17.65	-116.57	12.01	-76.77	-18.08	-115.89	20.33	-113.11
830606.161855	-9.24	-100.61	10.16	-117.64	4.67	-78.87	-25.45	-121.77	12.71	-114.20
830606.162106	-17.10	-102.38	2.72	-119.04	-2.72	-80.59	-32.69	-125.29	5.12	-115.58
830606.162317	-24.96	-104.21	-4.67	-120.78	-10.16	-81.96	-39.71	-129.69	-2.42	-117.19
830606.162528	-32.80	-106.24	-11.98	-122.90	-17.61	-83.00	-46.42	-135.33	-9.89	-119.16
830606.162739	-40.61	-108.56	-19.19	-125.46	-25.06	-83.70	-52.65	217.24	-17.29	-121.46
830606.162950	-48.39	-111.35	-26.26	-128.58	-32.51	-84.01	-58.14	207.26	-24.58	-124.24
830606.163201	-56.10	-114.95	-33.14	-132.41	-39.93	-83.83	-62.43	193.91	-31.73	-127.62
830606.163412	-63.71	-120.07	-39.76	-137.20	-47.30	-82.96	-64.91	177.05	-38.68	-131.63
830606.163623	-71.06	-128.50	-46.01	-143.28	-54.58	-81.06	-65.06	155.44	-45.36	-137.18
830606.163834	-77.69	214.41	-51.69	208.85	-61.68	-77.40	-62.95	141.25	-51.61	215.82
830606.164045	-81.89	174.08	-56.53	195.65	-68.43	-70.41	-58.78	127.57	-57.20	206.48
830606.164257	-79.44	125.44	-60.10	185.58	-74.35	-56.62	-53.49	117.24	-61.72	193.97
830606.164508	-73.30	102.92	-61.93	170.09	-75.08	-29.54	-47.41	109.59	-64.60	177.73
830606.164719	-66.09	92.63	-61.65	153.71	-77.49	5.64	-40.85	103.77	-65.23	159.24
830606.164930	-59.55	86.74	-59.33	138.69	-72.99	28.39	-33.97	99.24	-63.45	141.53
830606.165141	-50.97	82.76	-55.36	126.35	-66.75	40.65	-26.87	95.62	-59.67	127.00
830606.165352	-43.11	79.76	-50.22	116.74	-59.83	46.57	-19.62	92.67	-54.52	116.03

TABLE H-1. Scanner Horizon Positions for Data Spans on June 6, 1983 (6 of 10)

HORIZON POSITIONS (LATITUDES MEASURED NORTH, NEGATIVE MEANS SOUTH; LONGITUDES MEASURED EAST, NEGATIVE MEANS WEST)

DATE . TIME	SUBSATELLITE		SCANNER 1				SCANNER 2			
			EARTH-IN		EARTH-OUT		EARTH-IN		EARTH-OUT	
YYMMDD.HHMMSS	LATITUDE	LONGITUDE	LATITUDE	LONGITUDE	LATITUDE	LONGITUDE	LATITUDE	LONGITUDE	LATITUDE	LONGITUDE
830606.165603	-35.30	77.31	-44.30	109.35	-52.60	49.59	-12.26	90.22	-48.49	107.87
830606.165814	-27.47	75.20	-37.88	103.63	-45.21	51.29	-4.81	88.16	-41.91	101.73
830606.170025	-19.62	73.31	-31.10	99.11	-37.73	51.94	2.71	85.43	-34.97	96.97
830606.170236	-11.76	71.53	-24.05	95.48	-30.22	51.97	10.25	84.99	-27.81	93.20
830606.170504	-2.91	69.62	-15.99	92.19	-21.74	51.46	19.85	83.69	-19.55	89.79
830606.170715	4.96	67.93	-8.68	89.92	-14.22	50.60	28.49	82.83	-12.11	87.32
830606.170925	12.83	66.22	-1.28	87.87	-6.71	49.41	34.15	82.29	-4.58	85.25
830606.171137	20.70	64.43	6.15	86.25	0.75	47.98	41.80	82.16	2.99	83.52
830606.171349	28.56	62.50	13.65	85.02	8.15	45.99	49.43	82.60	10.59	82.08
830606.171559	36.41	60.35	21.15	84.11	15.46	43.70	57.02	83.94	19.21	80.92
830606.171810	44.23	57.94	28.65	83.54	22.67	40.90	64.48	86.94	25.84	80.03
830606.172021	52.01	54.72	36.14	83.42	29.71	37.47	71.68	93.44	33.47	79.45
830606.172232	59.72	50.52	43.60	83.96	36.54	33.21	78.13	109.13	41.08	79.27
830606.172443	67.26	44.14	50.99	85.13	43.05	27.83	81.79	148.45	48.67	79.64
830606.172654	74.40	32.61	58.26	87.73	49.10	20.89	79.30	193.41	56.21	80.85
830606.172905	80.21	6.40	65.28	92.72	54.46	11.85	73.21	-147.24	63.65	83.58
830606.173117	81.39	-45.17	71.78	102.52	59.76	0.11	56.15	-139.45	70.87	89.48
830606.173328	76.62	-80.55	76.90	122.63	61.52	-14.49	38.76	-135.91	77.44	103.44
830606.173539	69.75	-95.41	78.61	157.15	62.27	-30.93	31.25	-134.28	81.65	139.29
830606.173750	62.31	-103.03	75.62	188.05	60.85	-47.00	43.67	-133.67	79.88	180.63
830606.174001	54.65	-107.80	69.92	-155.56	57.55	-60.77	36.07	-133.69	74.00	-151.55
830606.174212	46.88	-111.2[illegible]	63.19	-147.68	52.85	-71.64	28.44	-134.14	66.96	-142.93
830606.174423	39.07	-113.91	56.04	-143.57	47.22	-79.97	20.82	-134.93	59.56	-139.05
830606.174634	31.23	-116.16	48.69	-141.45	40.97	-86.37	13.19	-136.01	52.01	-137.26
830606.174845	23.37	-118.15	41.24	-140.46	34.32	-91.36	5.58	-137.35	44.39	-136.56
830606.175056	15.50	-119.98	33.74	-140.21	27.40	-95.33	-2.01	-138.98	36.73	-136.53
830606.175307	7.62	-121.71	26.23	-140.48	20.29	-98.54	-9.55	-140.93	29.07	-136.94
830606.175519	-0.25	-123.40	18.72	-141.16	13.05	-101.16	-17.03	-143.25	21.42	-137.70
830606.175729	-8.12	-125.09	11.22	-142.19	5.72	-103.32	-24.42	-146.05	13.79	-138.75
830606.175940	-15.99	-126.83	3.77	-143.54	-1.67	-105.09	-31.67	-149.46	6.19	-140.07
830606.180152	-23.84	-128.66	-3.63	-145.24	-9.10	-106.51	-38.73	-153.72	-1.35	-141.67
830606.180403	-31.69	-130.66	-10.95	-147.30	-16.55	-107.60	-45.49	-159.16	-8.84	-143.57
830606.180614	-39.50	-132.93	-18.17	-149.79	-24.01	-108.35	-51.81	193.70	-16.25	-145.63
830606.180825	-47.29	-135.64	-25.27	-152.82	-31.46	-108.72	-57.42	184.14	-23.55	-148.54
830606.181036	-55.02	-139.09	-32.18	-156.54	-38.88	-108.61	-61.91	171.30	-30.73	-151.83
830606.181247	-62.64	-143.93	-38.84	-161.17	-46.26	-107.86	-64.69	154.89	-37.71	-155.90
830606.181459	-70.04	-151.70	-45.15	-167.05	-53.55	-106.14	-65.19	136.34	-44.44	-161.06
830606.181709	-75.54	-166.93	-50.93	185.37	-60.69	-102.80	-63.29	110.80	-50.76	-167.79
830606.181920	-81.45	155.92	-55.90	175.51	-67.51	-96.46	-59.45	109.54	-56.46	183.24
830606.182131	-80.10	105.91	-59.69	162.86	-73.59	-83.95	-54.29	93.79	-61.16	171.14
830606.182342	-74.28	80.34	-61.79	147.67	-77.77	-59.03	-48.31	85.82	-64.31	155.49
830606.182553	-67.14	69.01	-61.82	131.28	-77.86	-23.64	-41.80	79.79	-65.29	137.18
830606.182804	-59.63	62.70	-59.77	115.95	-73.77	1.84	-34.96	75.10	-63.84	119.16
830606.183015	-51.96	58.53	-56.00	103.29	-67.69	14.73	-27.59	71.37	-60.31	104.12
830606.183227	-44.21	55.42	-51.00	93.23	-60.83	21.22	-20.66	68.33	-55.31	92.67
830606.183439	-36.41	52.91	-45.18	85.56	-53.63	24.64	-13.11	65.82	-49.38	84.17
830606.183649	-28.58	50.77	-38.81	79.64	-46.26	25.40	-5.87	63.71	-42.86	77.78
830606.183950	-20.74	48.58	-32.07	74.97	-38.80	27.17	1.64	61.93	-35.97	72.86
830606.184111	-12.89	47.06	-25.08	71.23	-31.29	27.28	9.21	60.45	-28.83	68.97
830606.184322	-5.01	45.34	-17.92	68.19	-23.75	26.91	16.81	59.24	-21.52	65.81
830606.184533	2.95	43.65	-10.64	65.69	-16.22	26.14	24.45	58.30	-14.10	63.22
830606.184744	10.73	41.96	-3.26	63.63	-8.71	25.04	32.10	57.67	-6.59	61.05
830606.184955	18.60	40.20	4.17	61.94	-1.23	23.60	39.76	57.42	0.96	59.23
830606.185205	26.47	38.31	11.65	60.60	6.18	21.81	47.40	57.69	8.56	57.71
830606.185417	34.32	36.23	19.16	59.60	13.52	19.64	55.01	58.72	16.19	56.45
830606.185628	42.15	33.93	26.65	58.93	20.76	16.98	62.51	61.18	23.81	55.51
830606.185839	49.95	30.91	34.15	58.65	27.85	13.74	69.81	66.44	31.44	54.85
830606.190050	57.67	27.06	41.62	58.96	34.75	9.72	76.55	78.66	39.06	54.55
830606.190302	65.27	21.44	49.03	59.97	41.35	4.68	81.34	110.34	46.66	54.75
830606.190513	72.56	11.80	56.34	62.14	47.55	-1.50	80.51	159.47	54.21	55.70
830606.190724	79.92	-8.86	63.45	66.33	53.12	-10.22	74.99	-175.44	61.69	57.92
830606.190935	81.77	-55.47	70.14	74.48	57.75	-21.20	68.07	-155.66	68.98	62.70
830606.191146	79.22	-98.69	75.77	91.10	60.97	-35.08	60.75	-161.33	75.81	73.64
830606.191357	71.67	-117.20	78.64	122.44	62.25	-51.21	53.26	-159.31	80.98	101.99
830606.191609	64.32	-126.10	76.78	156.58	61.43	-67.61	45.70	-158.48	80.95	151.65
830606.191819	56.70	-131.43	71.59	176.38	58.58	-82.11	38.10	-158.36	75.75	179.83
830606.192030	48.96	-135.12	65.34	-174.02	54.21	-93.74	30.47	-158.71	68.89	-159.28
830606.192241	41.15	-137.96	57.97	-169.14	48.79	-102.59	22.85	-159.41	61.55	-164.53
830606.192452	33.32	-140.31	50.66	-166.59	42.68	-109.54	15.22	-160.41	54.03	-162.32
830606.192703	25.46	-142.36	43.23	-165.36	36.12	-114.87	7.60	-161.69	46.42	-161.39
830606.192914	17.59	-144.23	35.74	-164.94	29.26	-119.08	0.01	-163.24	38.77	-161.21
830606.193125	9.72	-145.98	28.23	-165.09	22.19	-122.47	-7.55	-165.09	31.11	-161.52
830606.193337	1.84	-147.68	20.71	-165.57	14.98	-125.24	-15.05	-167.31	23.45	-162.19
830606.193548	-5.03	-149.36	13.21	-166.61	7.67	-127.51	-22.46	-169.97	15.81	-163.17
830606.193759	-13.90	-151.09	5.75	-167.87	0.30	-129.37	-29.76	-173.21	8.21	-164.42

TABLE H-1. Scanner Horizon Positions for Data Span on June 6, 1983 (7 of 10)

HORIZON POSITIONS (LATITUDES MEASURED NORTH, NEGATIVE MEANS SOUTH; LONGITUDES MEASURED EAST, NEGATIVE MEANS WEST)

DATE , TIME	SUBSATELLITE		SCANNER 1				SCANNER 2			
			EARTH-IN		EARTH-OUT		EARTH-IN		EARTH-OUT	
YYMMDD.HHMMSS	LATITUDE	LONGITUDE	LATITUDE	LONGITUDE	LATITUDE	LONGITUDE	LATITUDE	LONGITUDE	LATITUDE	LONGITUDE
830606.194010	-21.76	52.88	-1.67	-169.47	-7.12	-130.58	-36.87	-177.21	0.65	-165.94
830606.194221	-29.60	54.83	-9.01	-171.43	-14.57	-132.06	-43.73	177.70	-6.85	-167.75
830606.194432	-37.43	57.02	-16.26	-173.80	-22.03	-132.91	-50.18	171.04	-14.28	-169.91
830606.194643	-45.22	59.58	-23.39	-176.68	-29.48	-133.38	-56.02	162.24	-21.62	-172.49
830606.194854	-52.97	62.80	-30.36	179.80	-36.91	-133.42	-60.86	150.35	-28.93	-175.61
830606.195105	-60.63	67.17	-37.10	175.44	-44.30	-132.86	-64.16	134.84	-35.87	-179.45
830606.195315	-68.10	73.91	-43.51	169.93	-51.62	-131.44	-65.30	116.59	-42.68	175.72
830606.195527	-75.13	173.65	-49.45	162.86	-58.91	-128.63	-64.01	98.48	-49.13	169.46
830606.195739	-80.64	144.90	-54.58	153.67	-65.74	-123.29	-60.62	83.25	-55.02	161.17
830606.195949	-81.10	92.75	-58.82	141.77	-72.09	-112.96	-55.76	71.61	-60.03	149.97
830606.200201	-76.01	60.38	-61.42	127.19	-76.97	-91.92	-49.96	63.01	-63.66	135.28
830606.200412	-69.09	46.62	-62.02	110.90	-78.32	-57.59	-43.57	56.52	-65.26	117.44
830606.200623	-61.65	39.39	-60.50	95.10	-75.14	-28.15	-36.80	51.52	-64.45	99.02
830606.200834	-54.01	34.79	-57.14	81.59	-69.42	-12.59	-29.79	47.57	-61.41	83.04
830606.201045	-46.28	31.46	-52.43	70.91	-62.70	-4.83	-22.60	44.37	-56.75	70.67
830606.201256	-38.49	28.82	-46.79	62.69	-55.57	-0.79	-15.27	41.72	-51.02	61.47
830606.201507	-30.67	25.59	-40.54	55.35	-48.24	1.33	-7.85	39.51	-44.64	54.60
830606.201718	-22.83	24.62	-33.89	51.39	-40.79	2.32	-0.36	37.65	-37.83	49.34
830606.201929	-14.97	22.80	-26.96	47.43	-33.29	2.59	7.19	36.09	-30.75	45.20
830606.202140	-7.11	21.07	-19.84	44.22	-25.76	2.33	14.79	34.81	-23.48	41.67
830606.202351	0.76	19.39	-12.58	41.59	-18.23	1.56	22.42	33.50	-16.08	39.14
830606.202602	8.64	17.69	-5.23	39.42	-10.71	0.05	30.07	33.09	-8.59	36.87
830606.202813	15.51	15.95	2.19	37.69	-3.22	-0.71	37.72	32.72	-1.05	34.96
830606.203024	24.38	14.11	9.66	36.21	4.22	-2.40	45.37	32.83	6.54	33.37
830606.203235	32.23	12.09	17.16	35.11	11.58	-4.47	52.99	33.63	14.16	32.06
830606.203447	40.07	9.79	24.56	34.35	18.85	-5.99	60.52	35.61	21.78	31.02
830606.203658	47.88	7.03	32.16	33.98	25.98	-10.06	67.90	39.89	29.41	30.27
830606.203909	55.63	3.49	39.64	34.10	32.94	-13.84	74.85	49.52	37.03	29.87
830606.204120	63.27	-1.53	47.07	34.88	39.63	-18.58	80.44	74.20	44.64	29.91
830606.204331	70.57	-9.73	54.41	36.69	45.95	-24.63	81.38	123.20	52.21	30.62
830606.204542	77.40	-26.20	61.59	40.22	51.72	-32.48	76.67	155.37	59.71	32.43
830606.204753	81.63	-55.36	68.43	47.01	56.63	-42.73	69.97	167.75	67.07	36.32
830606.205004	79.62	-115.00	74.45	60.72	60.28	-55.84	62.72	173.11	74.38	45.00
830606.205215	73.53	-138.38	78.30	88.03	62.14	-71.52	55.26	175.58	79.93	66.94
830606.205426	66.31	-148.94	77.72	124.10	61.87	-88.09	47.72	176.66	81.64	114.41
830606.205637	58.74	-154.94	73.15	147.74	59.51	-103.25	40.12	176.94	77.39	150.08
830606.205848	51.02	-159.96	66.85	159.33	55.49	-115.65	32.50	176.70	70.78	163.97
830606.210059	43.23	-161.99	59.88	165.14	50.30	-125.26	24.85	176.09	63.53	169.83
830606.210311	35.40	-164.44	52.62	168.17	44.35	-132.62	17.25	175.16	56.09	172.94
830606.210522	27.55	-166.56	45.21	169.69	37.90	-138.30	9.63	173.96	48.44	173.73
830606.210733	19.69	-168.46	37.73	170.29	31.11	-142.78	2.03	172.48	40.80	174.08
830606.210944	11.81	-170.24	30.22	170.28	24.09	-146.36	-5.54	170.71	33.14	173.89
830606.211155	3.94	-171.95	22.70	169.80	16.91	-149.28	-13.06	168.60	25.48	173.30
830606.211406	-3.94	-173.63	15.20	168.96	9.62	-151.67	-20.50	166.09	17.34	172.40
830606.211617	-11.81	-175.34	7.72	167.77	2.26	-153.64	-27.83	163.00	10.22	171.22
830606.211829	-19.67	-177.11	0.30	166.27	-5.15	-155.24	-35.00	159.22	2.65	169.78
830606.212039	-27.52	-179.02	-7.07	164.41	-12.59	-156.50	-41.94	154.46	-4.87	168.04
830606.212250	-35.35	179.87	-14.35	162.15	-20.05	-157.44	-48.51	148.30	-12.32	165.98
830606.212501	-43.16	178.42	-21.51	159.42	-27.50	-158.02	-54.54	140.13	-19.68	163.52
830606.212712	-50.92	176.42	-28.53	156.09	-34.94	-158.18	-59.69	129.13	-26.93	160.56
830606.212923	-58.61	169.43	-35.34	151.98	-42.35	-157.80	-63.46	114.58	-34.02	156.94
830606.213134	-66.15	163.51	-41.85	146.81	-49.69	-156.65	-65.23	96.84	-40.90	152.40
830606.213345	-73.34	153.16	-47.93	140.20	-56.92	-154.28	-64.55	78.36	-47.46	146.57
830606.213557	-79.47	130.50	-53.38	131.62	-63.94	-149.78	-61.69	62.21	-53.52	138.89
830606.213808	-81.68	81.74	-57.85	120.49	-70.50	-141.15	-57.16	49.65	-59.81	128.55
830606.214019	-77.65	41.53	-60.91	106.58	-75.91	-123.66	-51.56	40.33	-62.87	114.82
830606.214230	-71.00	24.63	-62.07	90.56	-78.43	-92.00	-45.31	33.35	-65.07	97.65
830606.214441	-63.65	16.24	-61.10	74.40	-76.33	-59.18	-38.03	28.01	-64.90	79.06
830606.214652	-56.05	11.13	-58.19	60.19	-71.07	-40.43	-31.67	23.82	-62.40	62.22
830606.214903	-49.34	7.54	-53.78	45.77	-64.54	-31.14	-24.52	20.44	-58.11	48.90
830606.215114	-40.55	4.75	-48.35	39.95	-57.49	-26.34	-17.23	17.66	-52.62	38.94
830606.215325	-32.75	2.43	-42.25	33.17	-50.20	-23.82	-9.93	15.34	-46.38	31.52
830606.215536	-24.91	0.41	-35.69	27.88	-42.78	-22.58	-2.36	13.40	-39.67	25.89
830606.215747	-17.06	-1.45	-29.52	23.68	-35.29	-22.15	5.15	11.76	-32.65	21.49
830606.215958	-9.19	-3.19	-21.75	20.29	-27.76	-22.28	12.77	10.41	-25.42	17.97
830606.220209	-1.33	-4.89	-14.52	17.52	-20.23	-22.94	20.39	9.32	-18.06	15.10
830606.220421	6.55	-6.57	-7.19	15.23	-12.70	-23.77	25.03	8.53	-10.59	12.71
830606.220632	14.42	-8.30	0.22	13.36	-5.20	-25.04	35.69	8.05	-3.06	10.72
830606.220843	22.29	-10.11	7.67	11.83	2.25	-26.64	43.34	8.03	4.52	9.04
830606.221054	30.15	-12.07	15.16	10.64	9.64	-28.60	50.96	8.62	12.12	7.65
830606.221305	37.99	-14.28	22.67	9.80	16.93	-30.99	58.54	10.20	19.76	6.55
830606.221516	45.81	-16.90	30.17	9.31	24.10	-33.90	65.96	13.70	27.38	5.72
830606.221727	53.58	-20.19	37.66	9.29	31.11	-37.48	73.09	21.37	35.01	5.22
830606.221938	61.26	-24.71	45.10	9.87	37.88	-41.93	79.22	42.43	42.62	5.13
830606.222149	68.74	-31.78	52.48	11.36	44.32	-47.59	81.81	85.02	50.21	5.63

TABLE H-1. Scanner Horizon Positions for Data Span on June 6, 1983 (8 of 10)

HORIZON POSITIONS (LATITUDES MEASURED NORTH, NEGATIVE MEANS SOUTH; LONGITUDES MEASURED EAST, NEGATIVE MEANS WEST)

DATE . TIME	SUBSATELLITE		SCANNER 1				SCANNER 2			
			EARTH-IN		EARTH-OUT		EARTH-IN		EARTH-OUT	
YYMMDD.HHMMSS	LATITUDE	LONGITUDE	LATITUDE	LONGITUDE	LATITUDE	LONGITUDE	LATITUDE	LONGITUDE	LATITUDE	LONGITUDE
830605.222403	75.74	-45.15	59.71	14.32	50.26	-54.91	79.23	124.93	57.73	7.07
830606.222611	80.98	-76.55	66.66	20.01	55.43	-64.46	71.83	140.75	65.14	10.26
830606.222819	80.27	-134.35	73.69	33.41	59.86	-78.54	53.75	147.46	73.13	18.55
830606.223053	74.49	-160.91	77.98	58.50	62.00	-93.93	56.32	150.62	79.25	37.69
830606.223301	67.35	-172.55	78.10	94.76	62.03	-110.53	48.78	151.85	81.82	82.41
830606.223512	59.81	-178.97	73.94	120.61	59.95	-126.00	41.19	152.22	78.20	122.13
830606.223723	52.11	176.81	67.79	133.44	56.13	-138.82	33.57	152.04	71.76	137.90
830606.223934	44.33	173.58	60.58	139.82	51.09	-148.79	25.95	151.47	64.56	144.54
830606.224145	36.50	171.16	53.64	143.14	45.22	-156.42	18.32	150.59	57.09	147.55
830606.224356	28.65	169.00	46.25	144.52	39.83	-162.31	10.69	149.43	49.51	148.91
830606.224607	20.79	167.07	38.75	145.53	32.08	-166.93	3.09	147.99	41.87	149.35
830606.224819	12.91	165.28	31.27	145.59	25.08	-170.63	-4.49	146.26	34.21	149.22
830606.225029	5.04	163.57	23.76	145.17	17.92	-173.63	-12.01	144.20	26.55	148.68
830606.225241	-2.84	161.86	16.25	144.38	10.65	-176.05	-19.46	141.73	18.91	147.82
830606.225452	-10.71	160.18	8.77	143.24	3.29	-178.11	-26.81	138.75	11.29	146.68
830606.225703	-18.57	158.42	1.33	141.78	-4.11	-179.76	-34.01	135.08	3.71	145.27
830606.225914	-26.42	156.59	-6.04	139.97	-11.55	178.93	-40.98	130.48	-3.82	143.58
830606.230126	-34.26	154.46	-13.34	137.77	-19.00	177.95	-47.62	124.55	-11.28	141.57
830606.230336	-42.07	151.07	-20.52	135.11	-26.46	177.32	-53.74	116.70	-18.66	139.17
830606.230547	-49.93	146.16	-27.56	131.88	-33.90	177.09	-59.04	106.15	-25.92	136.29
830606.230759	-57.53	140.35	-34.40	127.89	-41.31	177.39	-63.04	92.12	-33.04	132.77
830606.231009	-65.10	133.60	-40.96	122.89	-48.67	178.41	-65.12	74.73	-39.95	128.38
830606.231223	-72.37	130.35	-47.11	116.51	-55.92	-179.43	-64.91	56.15	-46.56	122.76
830606.231431	-79.74	110.31	-52.66	108.25	-62.98	-175.32	-62.21	39.55	-52.71	115.39
830606.231642	-81.75	84.79	-57.30	97.55	-69.63	-167.40	-57.87	26.52	-58.14	105.52
830606.231853	-79.45	60.70	-60.58	83.97	-75.27	-151.63	-52.39	16.76	-62.39	92.25
830606.232104	-71.99	41.57	-62.04	68.15	-78.35	-121.83	-46.21	9.50	-64.89	75.30
830606.232316	-64.70	27.56	-61.36	51.87	-76.87	-97.70	-39.58	3.96	-65.07	56.91
830606.232527	-57.13	-12.99	-58.69	37.30	-71.91	-67.05	-32.66	-0.37	-62.88	39.67
830606.232738	-49.42	-16.74	-54.47	25.48	-65.50	-56.82	-25.53	-3.85	-58.79	25.83
830606.232949	-41.55	-19.61	-49.16	16.33	-58.50	-51.57	-18.25	-6.71	-53.44	15.44
830606.233160	-33.64	-21.98	-43.13	9.30	-51.23	-48.80	-10.87	-9.08	-47.29	7.72
830606.233411	-26.01	-24.04	-36.63	3.93	-43.82	-47.42	-3.41	-11.07	-40.63	1.87
830606.233622	-19.16	-25.92	-29.80	-0.51	-36.34	-46.89	4.12	-12.74	-33.65	-2.67
830606.233833	-10.30	-27.67	-22.75	-4.00	-28.82	-46.96	11.70	-14.14	-26.45	-6.30
830606.234044	-2.43	-29.37	-15.54	-6.85	-21.28	-47.47	19.32	-15.26	-19.10	-9.25
830606.234255	5.44	-31.06	-8.22	-9.19	-13.76	-48.34	26.96	-16.10	-11.64	-11.70
830606.234505	13.31	-32.77	-0.53	-11.12	-6.25	-49.56	34.61	-16.62	-4.12	-13.74
830606.234717	21.18	-34.57	6.63	-12.69	1.20	-51.11	42.27	-16.72	3.45	-15.46
830606.234928	29.05	-36.51	14.11	-13.93	8.60	-53.02	49.90	-16.24	11.06	-16.89
830606.235139	36.89	-38.67	21.62	-14.83	15.91	-55.34	57.48	-14.83	18.68	-18.03
830606.235351	44.71	-41.22	29.12	-15.37	23.11	-58.18	64.93	-11.69	26.31	-18.91
830606.235602	52.49	-44.39	36.61	-15.46	30.14	-61.65	72.11	-4.85	33.94	-19.46
830606.235913	60.19	-48.69	44.04	-14.98	36.95	-65.97	79.47	11.79	41.55	-19.61
830607.000024	67.71	-55.26	51.45	-13.85	43.44	-71.44	81.44	52.83	49.14	-19.21
830607.000235	74.81	-67.31	58.70	-10.94	49.46	-78.49	78.92	96.34	56.68	-17.93
830607.000446	80.47	-95.03	65.71	-5.76	54.77	-87.69	72.80	114.58	64.11	-15.07
830607.000657	81.22	-147.17	72.15	4.48	58.98	-99.61	65.70	121.97	71.30	-8.88
830607.000908	76.23	179.26	77.15	24.49	61.63	-114.37	58.31	125.35	77.81	5.92
830607.001119	69.30	165.10	78.56	60.58	62.24	-130.86	50.79	126.90	81.75	43.61
830607.001330	61.83	157.73	75.32	90.60	60.69	-146.84	43.21	127.46	79.60	89.86
830607.001541	54.16	153.07	69.52	106.15	57.29	-160.42	35.60	127.41	73.59	110.37
830607.001752	46.40	149.71	62.75	113.79	52.52	-171.12	27.97	126.94	66.51	118.54
830607.002029	37.60	146.76	54.67	118.07	46.09	179.81	19.39	126.01	58.15	122.53
830607.002231	29.76	144.57	47.29	119.93	39.75	173.71	11.76	124.89	50.58	124.06
830607.002442	21.89	142.61	39.83	120.75	33.04	168.93	4.16	123.49	42.94	124.61
830607.002653	14.02	140.81	32.33	120.89	26.08	165.12	-3.42	121.80	35.29	124.54
830607.002904	5.15	139.08	24.81	120.54	18.94	162.04	-10.96	119.79	27.63	124.06
830607.003115	-1.73	137.40	17.30	119.75	11.69	159.50	-18.43	117.39	19.97	123.23
830607.003325	-9.60	135.70	9.82	118.70	4.33	157.43	-25.79	114.48	12.36	122.14
830607.003537	-17.47	133.95	2.37	117.28	-3.07	155.73	-33.01	110.92	4.77	120.77
830607.003749	-25.32	132.09	-5.01	115.52	-10.50	154.38	-40.02	106.42	-2.77	119.12
830607.003959	-33.16	130.05	-12.32	113.39	-17.96	153.35	-46.71	100.76	-10.24	117.15
830607.004210	-40.97	127.71	-19.52	110.90	-25.41	152.66	-52.92	93.23	-17.63	114.82
830607.004422	-48.75	126.90	-26.58	107.65	-32.86	152.38	-58.36	83.11	-24.91	112.01
830607.004633	-56.46	121.25	-33.45	103.78	-40.27	152.59	-62.58	69.59	-32.05	108.59
830607.004844	-64.05	116.02	-40.06	98.94	-47.64	153.49	-64.97	52.59	-39.00	104.34
830607.005055	-71.38	107.36	-46.29	92.79	-54.91	155.46	-65.01	33.98	-45.66	98.92
830607.005305	-77.96	89.58	-51.93	84.82	-62.00	159.22	-62.70	16.95	-51.88	91.83
830607.005517	-81.74	47.92	-56.72	74.51	-68.74	166.46	-59.55	3.42	-57.44	82.38
830607.005729	-79.20	0.30	-60.22	61.30	-74.58	-179.32	-53.21	-6.77	-61.89	69.60
830607.005939	-72.99	-21.32	-61.96	45.73	-78.16	-151.54	-47.11	-14.32	-64.67	53.30
830607.010150	-65.75	-31.30	-61.59	29.37	-77.34	-116.54	-40.53	-20.07	-65.20	34.79
830607.010401	-58.20	-37.08	-59.17	14.46	-72.73	-93.88	-33.64	-24.55	-63.31	17.18
830607.010612	-50.51	-41.00	-55.13	2.25	-65.45	-82.59	-26.54	-27.13	-59.45	2.83

TABLE H-1. Scanner Horizon Positions for Data Span on June 6, 1983 (9 of 10)

HORIZON POSITIONS (LATITUDES MEASURED NORTH, NEGATIVE MEANS SOUTH; LONGITUDES MEASURED EAST, NEGATIVE MEANS WEST)

DATE , TIME	SUBSATELLITE		SCANNER 1				SCANNER 2			
			EARTH-IN		EARTH-OUT		EARTH-IN		EARTH-OUT	
YYMMDD.HHMMSS	LATITUDE	LONGITUDE	LATITUDE	LONGITUDE	LATITUDE	LONGITUDE	LATITUDE	LONGITUDE	LATITUDE	LONGITUDE
830607.010823	-42.75	-43.97	-49.96	-7.24	-59.50	-76.84	-19.28	-31.06	-54.25	-8.00
830607.011034	-34.94	-46.39	-44.02	-14.54	-52.26	-73.81	-11.92	-33.69	-48.19	-16.05
830607.011245	-27.11	-49.49	-37.57	-20.20	-44.87	-72.25	-4.46	-35.53	-41.50	-22.12
830607.011457	-19.26	-50.38	-30.78	-24.58	-37.39	-71.65	3.06	-37.25	-34.65	-26.82
830607.011708	-11.40	-52.15	-23.76	-29.27	-29.88	-71.64	10.63	-38.59	-27.48	-30.56
830607.011919	-3.54	-53.86	-16.57	-31.20	-22.34	-72.09	18.24	-39.84	-20.14	-33.59
830607.012130	4.33	-55.54	-9.26	-33.61	-14.82	-72.92	25.95	-40.72	-12.70	-36.10
830607.012341	12.21	-57.25	-1.87	-35.59	-7.31	-74.09	33.54	-41.29	-5.18	-38.20
830607.012552	20.08	-59.03	5.57	-37.21	0.16	-75.59	41.19	-41.46	2.38	-39.96
830607.012803	27.94	-60.94	13.05	-38.49	7.56	-77.45	48.83	-41.08	9.99	-41.42
830607.013014	35.79	-63.07	20.56	-39.44	14.88	-79.71	56.42	-39.83	17.61	-42.60
830607.013225	43.61	-65.55	28.06	-40.03	22.10	-82.47	63.90	-37.00	25.24	-43.52
830607.013436	51.40	-68.61	35.55	-40.20	29.16	-85.84	71.13	-30.91	32.86	-44.12
830607.013647	59.11	-72.70	43.01	-39.81	36.01	-90.02	77.68	-18.36	40.48	-44.34
830607.013853	66.57	-78.84	50.41	-38.62	42.55	-95.30	81.71	20.73	48.07	-44.03
830607.014109	73.96	-89.75	57.69	-36.15	49.65	-102.10	79.69	67.30	55.62	-42.90
830607.014321	79.86	-114.16	64.75	-31.42	54.07	-110.98	73.75	88.21	63.07	-40.33
830607.014532	81.55	-164.64	71.30	-22.16	58.47	-122.47	66.72	96.53	70.31	-34.80
830607.014743	77.11	157.64	76.59	-3.14	61.37	-136.86	59.36	100.29	76.97	-21.83
830607.014954	73.33	141.80	78.66	30.58	62.29	-153.23	51.85	102.03	81.50	11.74
830607.015205	62.90	133.83	75.99	52.62	61.03	-169.41	44.28	102.70	80.24	50.26
830607.015416	55.25	128.91	70.42	79.85	57.86	176.60	36.67	102.72	74.53	83.81
830607.015627	47.50	125.41	63.74	85.27	53.26	165.51	29.05	102.30	67.54	93.03
830607.015839	39.69	122.58	56.61	92.52	47.69	157.00	21.42	101.54	60.15	97.14
830607.020049	31.85	120.40	49.27	94.93	41.48	150.47	13.79	100.49	52.60	99.05
830607.020300	23.99	118.39	41.83	95.89	34.86	145.38	6.18	99.16	44.98	99.81
830607.020511	16.12	116.56	34.33	96.18	27.95	141.34	-1.41	97.56	37.33	99.88
830607.020722	8.24	114.92	26.92	95.95	20.85	138.08	-8.96	95.64	29.67	99.50
830607.020933	0.37	113.13	19.30	95.30	13.62	135.42	-16.44	93.36	22.02	98.76
830607.021144	-7.50	111.44	11.81	94.30	6.30	133.23	-23.84	90.59	14.39	97.74
830607.021356	-15.37	109.71	4.35	92.97	-1.09	131.43	-31.10	87.23	6.79	96.44
830607.021607	-23.23	107.88	-3.05	91.31	-8.52	129.99	-38.18	83.04	-0.76	94.87
830607.021815	-31.07	105.90	-10.38	89.28	-15.97	128.87	-44.97	77.71	-8.25	92.99
830607.022029	-38.89	103.65	-17.61	86.82	-23.43	128.09	-51.33	70.73	-15.67	90.76
830607.022240	-46.68	100.99	-24.72	83.83	-30.88	127.69	-57.01	61.39	-22.98	88.09
830607.022451	-54.41	97.61	-31.64	80.18	-38.30	127.75	-61.61	48.84	-30.17	84.85
830607.022702	-62.05	92.92	-38.33	75.62	-45.68	128.45	-64.55	32.68	-37.17	80.85
830607.022913	-69.47	85.48	-44.37	69.86	-52.99	130.08	-65.24	14.20	-43.92	75.79
830607.023124	-76.35	71.16	-50.50	62.43	-60.14	133.25	-63.52	-3.54	-50.28	69.20
830607.023335	-81.25	37.29	-55.55	52.77	-66.99	139.27	-59.50	-18.05	-56.04	60.43
830607.023545	-80.43	-14.55	-59.44	40.34	-73.16	151.07	-54.73	-29.10	-60.84	48.60
830607.023757	-74.79	-41.97	-61.70	25.33	-77.56	174.86	-48.79	-37.23	-64.14	33.24
830607.024008	-67.72	-53.95	-61.90	8.95	-78.03	-149.89	-42.32	-43.40	-65.30	15.04
830607.024219	-60.23	-60.50	-59.99	-6.53	-74.19	-123.22	-35.50	-49.15	-64.03	-3.12
830607.024431	-52.57	-64.80	-56.34	-19.51	-68.21	-109.59	-28.45	-51.97	-60.64	-18.44
830607.024642	-44.82	-67.97	-51.43	-29.68	-61.39	-102.75	-21.23	-55.05	-55.74	-30.15
830607.024853	-37.02	-70.51	-45.66	-37.51	-54.20	-99.16	-13.89	-57.60	-49.87	-38.85
830607.025104	-29.20	-72.68	-39.33	-43.55	-46.84	-97.30	-6.46	-59.74	-43.39	-45.38
830607.025315	-21.35	-74.61	-32.62	-48.31	-39.39	-96.47	1.05	-61.54	-36.53	-50.40
830607.025526	-13.50	-76.41	-25.65	-52.11	-31.88	-96.32	8.61	-63.04	-29.40	-54.36
830607.025737	-5.63	-78.13	-18.49	-55.20	-24.35	-96.65	16.21	-64.25	-22.10	-57.57
830607.025948	2.24	-79.91	-11.21	-57.73	-16.82	-97.39	23.85	-65.23	-14.69	-60.20

TABLE H-1. Scanner Horizon Positions for Data Span on June 6, 1983 (10 of 10)

REFERENCES

1. S. Bilanow, L. Chen, "Landsat-D Conical Scanner Evaluation Plan," General Software Corporation, GSC-TR8203, March 1982.

2. S. Bilanow, L. Chen, I. Kulikov, "Landsat-D Conical Scanner Mathematical Modeling," General Software Corporation, GSC-TR8202, February, 1982.

3. S. Bilanow, L. Chen, W. Davis, J. Stanley, "Landsat-4 Horizon Scanner Performance Evaluation Preliminary Report," General Software Corporation, GSC-TR8305, April, 1983.

4. S. Bilanow, L. Chen, "Landsat-4 Horizon Scanner Flight Performance," AAS/AIAA Astrodynamics Specialist Conference, paper 83-320, August 22-25, 1983.

5. Ithaco, Inc., "Conical Earth Sensor (Advertising Flyer)," Ithaco Inc. IPS 0006, July 1979.

6. W. Richmond, "Landsat-D Specification for the Earth Sensor Assembly, Revision A," General Electric SVS-10148, May 8, 1981.

7. S. Bilanow, K. Cumella, I. Kulikov, "The Conical Scanner Evaluation System Design," General Software Corporation, GSC-TR8306, May, 1982.

8. A. Gilmore et. al., "Landsat-D Flight Segment Operations Manual, Appendix A Coefficients/Calibration Data", General Electric Company, SVS-10266/3A, June 1982.

9. A. Das, R. Quinn, "In-Flight Attitude Determination Performance of the Landsat-4 Spacecraft," General Electric Space Division, U-1D50-LSD-1421, March 18, 1983.

10. D. Strafella, Personal Communication, Goddard Space Flight Center, April and December, 1983.

11. S. Bilanow, et. al., "Evaluation of the Horizon Radiance Data Base (HRDB)," General Software Corporation, GSC-TR8307, September 1983.

12. S. Singhal, "Horizon Radiance Data Base: Generation and Data Description," Computer Sciences Corporation, CSC/TM-82/6118, July 9, 1982.

13. R. Nieman, "User's Guide to RAOBS Climatology Programs", Computer Sciences Corporation, CSC/TM-77/6138, 1977.

14. F. Kneizys et. al., "Atmospheric Transmittance/Radiance: Computer Code LOWTRAN 5", Air Force Geophysics Laboratory, Report AFGL-TR-80-0067, February 21, 1980.

15. S. Fritz, S.D. Soules, "Planetary Variations of Stratospheric Temperatures", Monthly Weather Review, July 1972.

16. S. Bilanow, M. Phenneger, "The Response of the Seasat and Magsat Infrared Horizon Scanners to Cold Clouds", Fifth Annual Flight Mechanics/Estimation Theory Symposium," NASA CP 2152, October 1980.

17. Vaughn Selby, Personal Communication, Ithaco Inc., November, 1982.

18. Walt Richmond, Personal Communication, General Electric Company Space Systems Division, November, 1982.

19. P. Leary, "Landsat-D ESA Noise Test Data", Ithaco Inc., Report 92334, July 22, 1982.

20. J. Stanley, S. Bilanow, "Landsat-4 Horizon Scanner Full Orbit Averages," General Software Corporation, GSC-TR8308, November 1983.

21. R. Quinn, Personal Communication, General Electric Company Space Systems Division, March 2, 1983.